

---

Identification and characterization of substances  
interfering with steroid metabolizing enzymes and  
retinoic acid-related orphan receptor  $\gamma$ t activity

---

**Inauguraldissertation**

zur

Erlangung der Würde eines Doktors der Philosophie

vorgelegt der

Philosophisch-Naturwissenschaftlichen Fakultät

der Universität Basel

von

Manuel Gregor Robert Kley

2024

Genehmigt von der Philosophisch-Naturwissenschaftlichen Fakultät

auf Antrag von

Erstbetreuer: Prof. Dr. Alex Odermatt,

Zweitbetreuer: Prof. Dr. Jörg Huwyler,

Externer Experte: Prof. Dr. Michael Arand

Basel, der 17.09.2024

---

Dekan  
Prof. Dr. Marcel Mayor

## Table of contents

<b>Table of contents</b> .....	3
<b>List of abbreviations</b> .....	5
<b>1. Summary</b> .....	7
<b>2. Introduction</b> .....	10
2.1 Steroid hormones.....	10
2.1.1 Mineralocorticoids.....	11
2.1.2 Glucocorticoids .....	12
2.1.3 Androgens .....	14
2.2 Hydroxysteroid dehydrogenases .....	16
2.3 Steroidogenesis.....	17
2.3.1 Backdoor pathway of dihydrotestosterone biosynthesis.....	20
2.4 Steroid hormone receptors.....	22
2.4.1 Mineralocorticoid receptor .....	23
2.4.2 Glucocorticoid receptor .....	25
2.4.3 Androgen Receptor.....	26
2.5 Retinoic acid-related orphan receptors.....	27
2.6 Endocrine disrupting chemicals .....	29
2.6.1 Azole antifungals.....	29
2.6.2 Parabens .....	30
2.6.3 UV-filters .....	31
<b>3. General aims of this thesis</b> .....	33
<b>4. Project 1: <i>In vitro</i> assessment of 11<math>\beta</math>-hydroxysteroid dehydrogenase activity and species-specific inhibition of HSD11B2 by azole antifungals</b> .....	35
4.1 Introduction .....	35
4.2 Published article: Species-specific differences in the inhibition of 11 $\beta$ -hydroxysteroid dehydrogenase 2 by itraconazole and posaconazole .....	39
4.3 Published article: <i>In vitro</i> methods to assess 11 $\beta$ -hydroxysteroid dehydrogenase type 1 activity .....	56
4.4 Published article: <i>In vitro</i> methods to assess 11 $\beta$ -hydroxysteroid dehydrogenase type 2 activity .....	102
4.5 Discussion .....	137
<b>5. Project 2: Potential antiandrogenic effects of parabens and benzophenone-type UV-filters inhibiting 3<math>\alpha</math>-hydroxysteroid dehydrogenases</b> .....	139
5.1 Introduction .....	139
5.2 Published article: Potential antiandrogenic effects of parabens and benzophenone-type UV-filters by inhibition of 3 $\alpha$ -hydroxysteroid dehydrogenases .....	142
5.3 Discussion .....	166
<b>6. Project 3: Activation of retinoic acid-related orphan receptor <math>\gamma</math>(t) by parabens and benzophenone UV-filters</b> .....	170

6.1 Introduction .....	170
6.2. Published article: Activation of retinoic acid-related orphan receptor $\gamma(t)$ by parabens and benzophenone UV-filters .....	172
6.3 Discussion .....	188
<b>7. Additional project 4: Assessment of novel mutations in <i>HSD17B3</i> gene.....</b>	<b>191</b>
7.1 Introduction .....	191
7.2 Published article: Molecular mechanisms underlying the defects of two novel mutations in the <i>HSD17B3</i> gene found in the Tunisian population.....	193
7.3 Discussion .....	210
<b>8. Conclusion.....</b>	<b>212</b>
<b>9. Acknowledgements.....</b>	<b>213</b>
9.1 Additional mentioning.....	213
<b>10. References .....</b>	<b>214</b>

## List of abbreviations

3 $\alpha$ -adiol	3 $\alpha$ -androstane-1,2-diol
3 $\alpha$ -HSD	3 $\alpha$ -hydroxysteroid dehydrogenase
4-MBC	4-methylbenzylidene camphor
5 $\alpha$ -DHP	5 $\alpha$ -dihydroprogesterone
11 $\beta$ -HSDs	11 $\beta$ -hydroxysteroid dehydrogenases
17OH-allopregnanolone	17 $\alpha$ -hydroxyallopregnanolone
17OH-DHP	17 $\alpha$ -hydroxydihydroprogesterone
17OH-pregnenolone	17 $\alpha$ -hydroxypregnenolone
17OH-progesterone	17 $\alpha$ -hydroxyprogesterone
ACE	Angiotensin-converting enzyme
ACTH	Adrenocorticotrophic hormone
ADT	Androgen deprivation therapy
AIS	Androgen insensitivity syndrome
AKRs	Aldo-keto reductases
AKR1C1	Aldo-keto reductase family 1 member C1
AKR1C2	Aldo-keto reductase family 1 member C2
AKR1C3	Aldo-keto reductase family 1 member C3
AKR1C4	Aldo-keto reductase family 1 member C4
AME	Apparent mineralocorticoid excess
AMH	Anti-Müllerian hormone
AP	Accessory proteins
AR	Androgen receptor
ARE	Androgen response element
AT1-R	Angiotensin II type 1 receptor
BP	Benzophenone
CAIS	Complete androgen insensitivity syndrome
CRH	Corticotropin releasing hormone
CRPC	Castration-resistant prostate cancer
CSF	Cerebrospinal fluid
CYP	Cytochrome P450
CYP11A1	Cholesterol side-chain cleavage enzyme (P450 <sub>sc</sub> )
CYP11B1	11 $\beta$ -hydroxylase
CYP11B2	Aldosterone synthase
CYP17A1	17 $\alpha$ -hydroxylase/17,20-lyase
CYP19	Aromatase
CYP21A2	21-hydroxylase
DBD	DNA-binding domain
DHEA	Dehydroepiandrosterone
DHRS9	Dehydrogenase/reductase SDR family member 9
DHT	5 $\alpha$ -dihydrotestosterone
DSD	Disorders of sexual development
EDCs	Endocrine disrupting chemicals
ER	Endoplasmic reticulum
ERE	Estrogen response element
FSH	Follicle-stimulating hormone
GABA <sub>A</sub>	$\gamma$ -aminobutyric acid type A
GnRH	Gonadotropin-releasing-hormone
GR	Glucocorticoid receptor

H6PD	Hexose-6-phosphate dehydrogenase
HPA	Hypothalamic-pituitary-adrenal
HPG	Hypothalamus-pituitary-gonadal
HRE	Hormone response elements
HSDs	Hydroxysteroid dehydrogenases
HSD3B1	3 $\beta$ -hydroxysteroid dehydrogenase type 1
HSD3B2	3 $\beta$ -hydroxysteroid dehydrogenase type 2
HSD11B1	11 $\beta$ -hydroxysteroid dehydrogenase type 1
HSD11B2	11 $\beta$ -hydroxysteroid dehydrogenase type 2
HSD17B2	17 $\beta$ -hydroxysteroid dehydrogenase type 2
HSD17B3	17 $\beta$ -hydroxysteroid dehydrogenase type 3
HSD17B6	17 $\beta$ -hydroxysteroid dehydrogenase type 6
HSD17B10	17 $\beta$ -hydroxysteroid dehydrogenases type 10
IL	Interleukin
ILC3	Type 3 innate lymphoid cells
LBD	Ligand binding domain
LH	Luteinizing hormone
MAIS	Mild Androgen insensitivity syndrome
MR	Mineralocorticoid receptor
NADH/NAD <sup>+</sup>	Nicotinamide adenine dinucleotides
NADPH/NADP <sup>+</sup>	Nicotinamide adenine dinucleotide phosphates
NTD	N-terminal transactivation domain
PAIS	Partial androgen insensitivity syndrome
PBTK	Physiological based toxicokinetic
PTSD	Posttraumatic stress disorder
RAAS	Renin-angiotensin-aldosterone system
RDH5	Retinol dehydrogenase type 5
RDH16	Retinol dehydrogenase type 16
ROR	Retinoic acid-related orphan receptor
ROR $\gamma$	Retinoic acid-related orphan receptor $\gamma$
ROR $\gamma$ t	Retinoic acid-related orphan receptor $\gamma$ t
RORE	ROR response element
SAR	Structure-activity relationship
SDR	Short-chain dehydrogenase/reductase
SHR	Steroid hormone receptors
SOX9	SRY-Box Transcription Factor 9
SRD5A1	Steroid 5 $\alpha$ -reductase type 1
SRD5A2	Steroid 5 $\alpha$ -reductase type 2
SRY	Sex-determining region Y protein
StAR	Steroidogenic acute regulatory
Th17	T helper 17 cells
VCaP	Vertebral cancer of the prostate

## 1. Summary

Steroid hormones regulate a wide range of physiological processes by activating nuclear receptors, which then act as transcription factors to control the expression of their target genes. Toxicological safety assessments of chemicals to which humans may be exposed also include a section on endocrine assessments, which often focus on direct effects on the nuclear receptors of the sex steroid hormones, namely the androgen and the estrogen receptors. The effects of chemicals on pre-receptor control, which includes the biosynthesis of the steroid hormones themselves, as well as on other nuclear receptors such as the immunomodulating retinoic acid-related orphan receptor  $\gamma$  (ROR $\gamma$ ) activity have been investigated insufficiently so far. This thesis aims to identify and characterize substances that interfere with steroid metabolizing enzymes and ROR $\gamma$  activity. We have addressed this goal in three different projects, which are focusing on different areas of endocrinology.

The steroidogenic enzyme 11 $\beta$ -hydroxysteroid dehydrogenase type 2 (HSD11B2), is involved in the pre-receptor control of the mineralocorticoid receptor (MR) by inactivating 11-hydroxylated glucocorticoids, that can bind and activate the MR. This ensures the receptors specificity for its natural ligand, aldosterone. Inhibition of HSD11B2 can lead to pseudohyperaldosteronism, an effect that has also been described in clinical case studies with patients treated with the azole antifungals itraconazole and posaconazole. In the first project, we assessed species-specific susceptibility towards azole fungicide-dependent HSD11B2 inhibition. The results of this investigation provided a possible explanation, why this adverse drug effect was missed during clinical trials. The human HSD11B2 homolog was strongly inhibited by both azole fungicides, while the rat enzyme was only moderately inhibited. Mouse and zebrafish homologs were only weakly inhibited. Using predictions based on homology modeling of HSD11B2 and analysis of chimeric enzyme variants, we were able to identify the C-terminal region and the amino acid residues at positions 170 and 172 as relevant structural elements that are partly responsible for the species-specific differences between the mouse and human homologs. This study highlights that such species-specific differences in the inhibition of steroidogenic enzymes by chemicals may be relevant for toxicological investigations and should therefore be considered in future studies. As an extension of this project, we summarized the methods used for the analysis of the enzymatic activity of HSD11B2 together with further assessment possibilities for the *in vitro* enzyme activity determination of HSD11B2 and 11 $\beta$ -hydroxysteroid dehydrogenase type 1 (HSD11B1) in two chapters for the book series 'Methods in Enzymology'. HSD11B1 catalyzes the reverse reaction of HSD11B2, reducing 11-keto glucocorticoids to their active 11 $\beta$ -hydroxy forms.

Parabens and UV-filters are used as additives in body care products and cosmetics to increase their shelf life. These compounds have been measured in various human matrices, including fetal samples, and are known to have antiandrogenic effects by blocking androgen receptor (AR) activity. To date, the influence of these chemicals on the pre-receptor control of AR, specifically the androgen biosynthesis, is poorly understood.  $3\alpha$ -hydroxysteroid dehydrogenases ( $3\alpha$ -HSD) are steroidogenic enzymes that can catalyze one of the last two synthesis steps in the backdoor pathway of the most potent androgen,  $5\alpha$ -dihydrotestosterone (DHT). Androgen mediated AR activation is required for normal male genitalia formation during embryogenesis.

In the second project, we investigated the effects of parabens and UV-filters on the enzymatic activity of different  $3\alpha$ -HSDs that can produce DHT in the backdoor pathway using a novel, radiometric enzyme activity assay. We have identified several parabens and benzophenone-type UV-filters as the first inhibitors of the  $3\alpha$ -HSD  $17\beta$ -hydroxysteroid dehydrogenase type 6 (HSD17B6) with  $IC_{50}$  values in the mid- and high nanomolar range. Said identified inhibitors were analyzed for their structure-activity relationship using a novel HSD17B6 homology model, which highlighted the importance of the 4-hydroxylated phenyl head group present in both substance classes. The addition of a methyl group to the 4-hydroxy group resulted in a loss of inhibitory capacity in 4-methoxylated benzophenones, as it prevented the formation of a hydrogen bond with the amide group of the cofactor nicotinamide adenine dinucleotide ( $NAD^+$ ) in the binding pocket of the homology model.

Parabens and UV-filters, like many other chemicals, have so far mainly been investigated for their direct effects on the androgen and estrogen receptors.  $ROR\gamma t$  is involved in immune response regulation and is essential for the differentiation of T helper 17 cells and their expression of pro-inflammatory interleukins. Excessive activation of  $ROR\gamma t$  has been associated with inflammatory and autoimmune diseases such as psoriasis.

In the third project, we evaluated the effect of parabens and UV-filters on  $ROR\gamma t$  activity using a previously established tetracycline-inducible reporter gene assay in Chinese hamster ovary cells. We identified hexylparaben, benzylparaben and benzophenone-10 as potent  $ROR\gamma t$  agonists with  $EC_{50}$  values within the higher nanomolar and lower micromolar range. Those  $ROR\gamma t$  agonists were also able to enhance pro-inflammatory cytokine expression in a mouse EL4 T-lymphocyte model. Together with structurally similar chemicals which we identified by virtual screening of a cosmetics database, the chemicals identified as  $ROR\gamma t$  agonists in this study showed additive effects on the receptor activity when assessed as mixtures.



Additional experiments are required to determine whether parabens and UV filters can reach the concentrations described in the second and third projects to exert potential antiandrogenic effects in organs expressing HSD17B6, or possibly aggravate existing inflammatory and autoimmune diseases through the additional ROR $\gamma$ t activation.

As an additional, fourth project, we examined three case studies of Tunisian patients diagnosed with 17 $\beta$ -hydroxysteroid dehydrogenase type 3 (HSD17B3) deficiencies for their underlying molecular causes. HSD17B3 is a steroidogenic enzyme that is exclusively expressed in the testes and catalyzes the last enzymatic step of testosterone synthesis. Testosterone, a potent androgen, is essential for normal male sexual development. Pathogenic mutations in the *HSD17B3* gene can lead to undervirilization of the male sexual organs due to insufficient testosterone production during embryogenesis, which is why HSD17B3 deficiencies are classified as 46,XY disorders of sexual development. Genetic analysis of the three patients revealed in one patient the first homozygous mutation in the catalytic tetrad of HSD17B3, p.K202M, for which we were able to show a complete loss of function using a radiometric enzyme activity assay. The second patient was a compound heterozygote with a paternally inherited, already characterized, inactive truncation mutation p.C206X and a maternally inherited splice site mutation (c.490 -6 T > C) for which we could show by means of a splicing assay that the mutation causes skipping of exon 7 during mRNA splicing which presumably results in a truncated and inactive enzyme. The last patient turned out to have a homozygous p.C206X mutation of HSD17B3. Consanguineous marriages can promote the emergence and establishment of deleterious mutations such as the ones identified in this project. This study highlights the importance of genetic counseling and the sensitization of medical personnel towards HSD17B3 deficiencies.

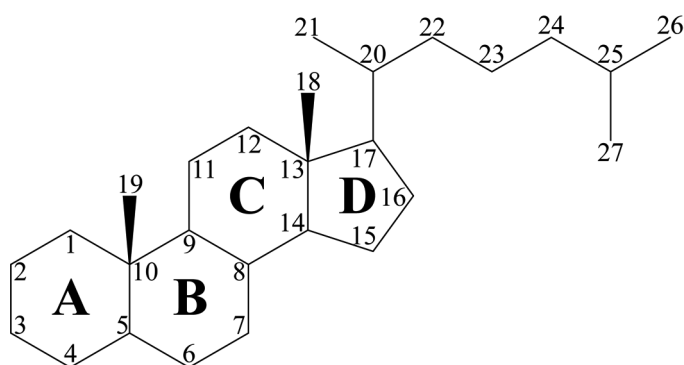
The projects conducted in this thesis address relevant limitations of endocrine studies that are part of safety assessments of chemicals. By assessing species-specific inhibition of HSD11B2 by azole fungicides, and identifying parabens and UV-filters as modulators of HSD17B6 and ROR $\gamma$ t activities, we have created a foundation for further research. The methods and homology models described in the respective projects of this thesis may prove to be valuable tools for future studies.

## 2. Introduction

### 2.1 Steroid hormones

Steroid hormones regulate a plethora of essential physiological processes in body homeostasis, growth, development and reproduction. They play key roles in metabolism, blood pressure regulation, inflammatory processes and immune functions, the maintenance of pregnancies as well as the development of primary and secondary sexual characteristics. [1-6].

Steroid hormones act as signaling molecules that bind to their target receptors in the respective target tissue [7]. This binding causes a conformational change, which leads to dimerization of the receptor and, if the receptor was initially not within the nucleus, to a translocation from the cytoplasm to the nucleus. Within the nucleus, such a steroid hormone receptor complex often binds, along with additional coregulators, to its respective hormone response elements (HRE) in the promoter regions of target genes, modulating their gene expression (reviewed in [1, 8, 9]). Structurally, steroid hormones consist of a sterane scaffold with four intact ring systems (Figure 1): three cyclohexane rings (A, B, C) and one cyclopentane ring (D) [10]. Substitutions of hydrogen moieties of the sterane scaffold to functional groups ensure the specific binding properties of the respective steroid hormones to their corresponding receptors. Steroid hormones are categorized into five groups, mineralocorticoids, glucocorticoids, androgens, estrogens and progestogens [1]. Since the focus of this doctoral thesis lays mainly on glucocorticoids, androgens and partly mineralocorticoids, the role of estrogens and progestogens will not be addressed in detail.



**Figure 1. Structure and nomenclature of steroids** (adapted from [10]). Steroids have a sterane scaffold with four rings (A-D). Carbon moieties are numbered according to the presented structure.

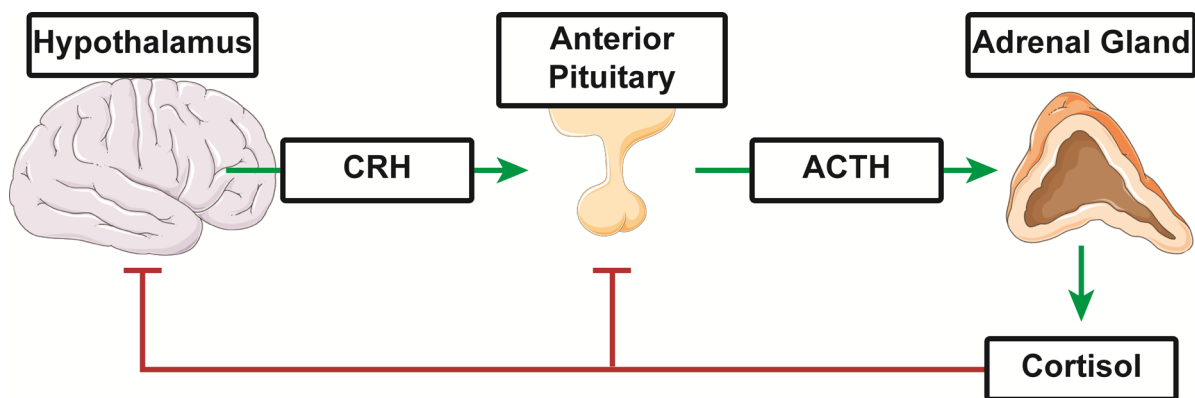
### 2.1.1 Mineralocorticoids

The main physiological mineralocorticoid in terrestrial vertebrates is aldosterone, which regulates salt and water balance by activating the mineralocorticoid receptor (MR) [11]. Aldosterone is produced primarily in the adrenal cortex and promotes the transcription of ion transporters in the distal convoluted tubules and cortical collecting ducts of the kidney, as well as in the colonic mucosa in the large intestine, which reabsorb sodium ions. This causes an increase in passive water uptake, which leads to an indirect increase in blood volume and blood pressure [12]. Corticosterone, another mineralocorticoid, can also bind and activate the MR with a similar affinity [13]. Increased levels of mineralocorticoids in humans is one of the most common causes of secondary hypertension. Accordingly, overproduction of mineralocorticoids, known as primary aldosteronism, caused by, for example, adenomas or hyperplasia of the adrenal glands, can result in an increase in blood pressure and associated cardiovascular morbidities, including stroke, non-fatal myocardial infarction, atrial fibrillation and heart failure (reviewed in [14]). Primary hypoaldosteronism on the other hand is usually caused by a genetic defect or an inhibition of a steroidogenic enzyme involved in the aldosterone synthesis, which leads to insufficient synthesis of aldosterone in the adrenal glands. Deficiency of aldosterone leads to an electrolyte imbalance, which can result in hypovolemia, salt wasting and low blood pressure in affected individuals (reviewed in [15]).

### 2.1.2 Glucocorticoids

Cortisol is the most important glucocorticoid in humans and is essential for survival. Cortisol is synthesized in humans by the adrenal cortex in a circadian manner, with highest levels in the early morning that decline during the day [16]. In contrast to cortisol in humans, corticosterone acts as the main glucocorticoid in mice, rats and birds [11, 17]. Glucocorticoids bind and activate the glucocorticoid receptor (GR), which plays an important role in a variety of processes in the body, including glucose metabolism, immune and stress response, development, growth, reproduction, cardiovascular function as well as cognitive functions (extensively reviewed in [18, 19]).

Glucocorticoid secretion in mammals and in birds is controlled by the hypothalamic-pituitary-adrenal (HPA) axis (Figure 2). The hypothalamus secretes corticotropin releasing hormone (CRH) as a result of internal or external signals, which stimulates the synthesis and secretion of the adrenocorticotropic hormone (ACTH) in the pituitary gland. ACTH stimulates production and secretion of glucocorticoids in the adrenal cortex, e.g. cortisol in humans and corticosterone in rats, mice and birds. This triggers GR activation within the body, leading to inhibition of both CRH and ACTH release from the hypothalamus, and pituitary gland, respectively, creating a negative feedback loop (reviewed in [20, 21]).



**Figure 2. The hypothalamic-pituitary-adrenal axis regulates glucocorticoid levels in humans** (adapted from Burford et al., 2017 [22]). Hypothalamic corticotropin releasing hormone (CRH) stimulates adrenocorticotropic hormone (ACTH) secretion and production, which triggers adrenal glucocorticoid, e.g. cortisol biosynthesis, and release. A negative feedback loop mediated by cortisol inhibits CRH and ACTH release. Stimulatory and generative processes are depicted by green arrows, while inhibitory actions are indicated by red arrows.

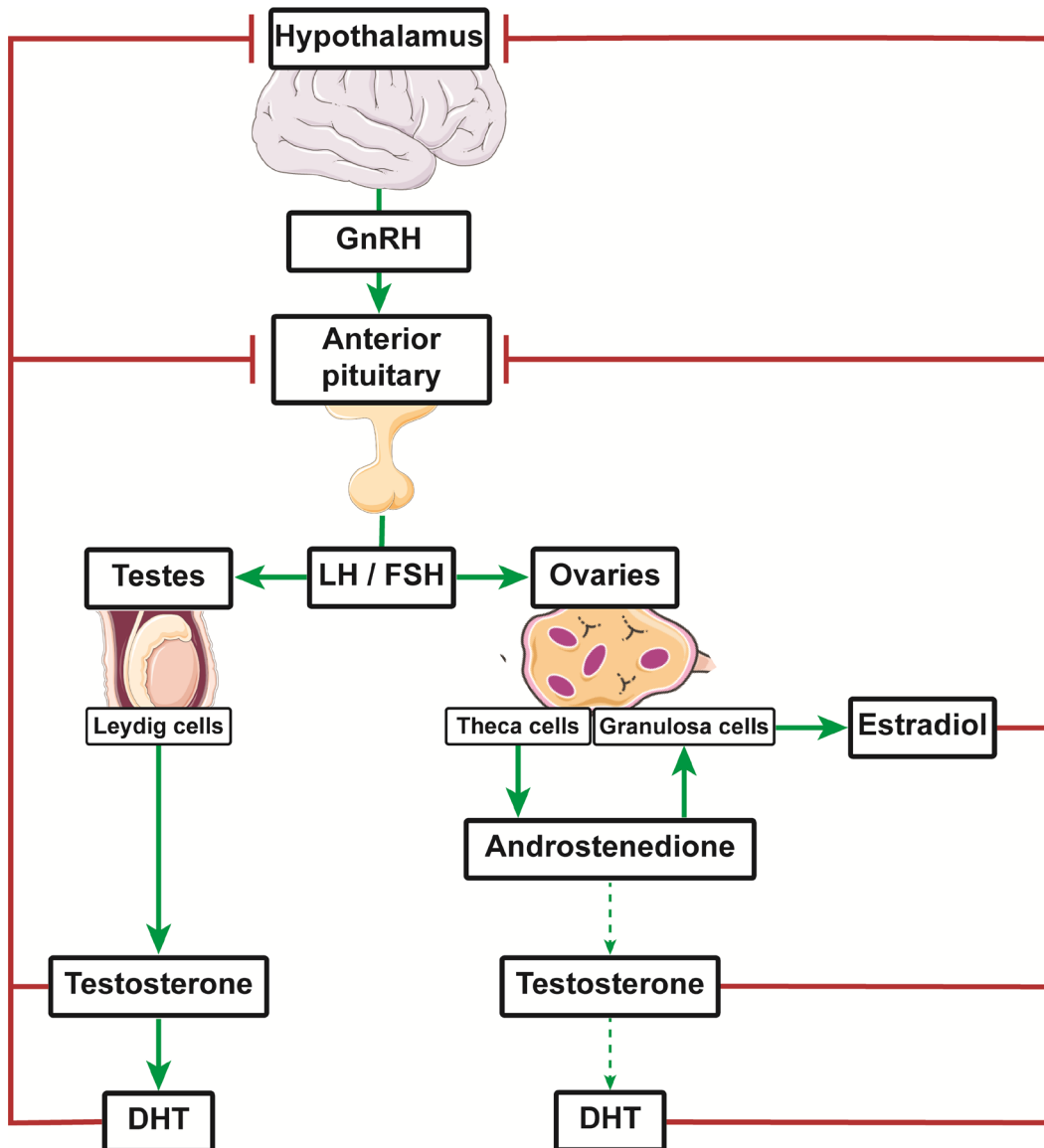
Abnormal glucocorticoid levels in the human body cause a variety of symptoms in affected patients. Too low glucocorticoid levels may arise from adrenal insufficiency which is either caused by destruction of the adrenal glands or disruption of the HPA axis, for instance by tumors in the pituitary gland or the hypothalamus. Destruction of the adrenal glands may be caused by viral or bacterial infections, adrenal metastases or Addison's disease, an autoimmune condition that targets the adrenal glands. Adrenal insufficiency and Addison's disease present with a wide range of symptoms, including weight loss, fatigue, low blood pressure and low sugar levels and can be diagnosed by measuring serum ACTH and adrenal hormone levels in the blood and urine (reviewed in [23]).

Excess cortisol can be caused by adenomas in the pituitary gland or in the adrenal cortex and causes the so called Cushing's disease. Pituitary adenomas can increase the secretion of ACTH and thus stimulate cortisol synthesis and secretion [24]. Symptomatic manifestations of Cushing's include central obesity, hypertension, diabetes, osteoporosis and increased susceptibility to infections [25]. Cushing's disease can be diagnosed measuring ACTH and cortisol levels in serum or free cortisol levels in urine [26].

Due to their anti-inflammatory and immunosuppressive effects, artificial and natural glucocorticoids are used as treatments for many immune diseases and chronic inflammations, including asthma, rheumatoid arthritis, inflammatory bowel disease, multiple sclerosis and psoriasis [27, 28]. However, excessive and chronic treatment with glucocorticoids can cause Cushing's syndrome which shows the same symptomatic manifestations as Cushing's disease [24, 29].

### 2.1.3 Androgens

Androgens are produced and secreted from male testes, female ovaries and the adrenal glands, where they travel via the bloodstream to their target tissues either exerting their biological effect through binding and activating the androgen receptor (AR) or by serving as a substrate for intermediate steroid metabolism [30]. Androgens are essential for normal male development, physiology and reproduction, and are required for *in utero* male sexual differentiation, the formation of secondary male sexual characteristics during puberty and the maturation of spermatozoa in the testes [31, 32]. Dehydroepiandrosterone (DHEA), androstenedione, 5 $\alpha$ -androstenedione, 3 $\alpha$ -androsterone and 3 $\alpha$ -androstenediol can be considered weak intermediate androgens that bind to the AR, but only with low affinity [33-37]. These intermediate steroids can be metabolically converted to the highly active human main androgen, testosterone, and its five- to tenfold more potent, reduced version 5 $\alpha$ -dihydrotestosterone (DHT) [38, 39]. Active androgens are involved in the regulation of growth-associated processes of bones, hair, skin, muscles and the prostate. They may serve as precursors for estrogen biosynthesis in the gonads and in the periphery in both sexes [40, 41]. Gonadal androgen production in adults is controlled by the hypothalamus-pituitary-gonadal (HPG) axis (Figure 3). The hypothalamus secretes the gonadotropin-releasing-hormone (GnRH) that triggers production and secretion of follicle-stimulating hormone (FSH) and luteinizing hormone (LH), which in turn stimulate androgen production in the gonads. In the male gonads, testosterone is synthesized in the Leydig cells which is then further converted to DHT in extragonadal tissue, e.g. the prostate and the skin. Female ovarian theca cells produce mainly androstenedione, which is mostly metabolized to estradiol in the ovarian granulosa cells or also converted in small amounts to testosterone and DHT in the periphery [40, 42-46]. Systemic testosterone and DHT as well as estradiol inhibit GnRH, FSH and LH secretion by the hypothalamus and the pituitary gland [47, 48]. The human adrenal glands produce weakly active steroids, such as dehydroepiandrosterone, androstenediol and androstenedione, providing a pool of precursors for peripheral conversion to testosterone, DHT and estrogens [49]. Although the regulation of adrenal androgen synthesis is not very well understood, the inhibition of ACTH excretion and biosynthesis in the HPA axis through glucocorticoids remains the most accepted primary mediator of adrenal steroid production [50].



**Figure 3. The hypothalamus-pituitary-gonadal axis regulates gonadal androgen (and estrogen) production** (simplified from Naamneh et al., 2022 [43]). Hypothalamic gonadotropin releasing hormone (GnRH) stimulates pituitary production and secretion of luteinizing hormone (LH) and follicle-stimulating hormone (FSH), resulting in gonadal production of androgens. Testicular Leydig cells produce testosterone, which can be converted extratesticularly to 5 $\alpha$ -dihydrotestosterone (DHT). Ovarian theca cells produce androstenedione, of which the largest part is converted to estradiol in the ovarian granulosa cells. Small amounts of androstenedione secreted by the ovaries may also be converted in peripheral tissues to testosterone and DHT. Testosterone, DHT and estradiol inhibit GnRH, FSH and LH secretion as negative feedback loop. Generative and stimulatory processes are depicted by green arrows, while inhibitory actions are indicated by red arrows.

Excessive, as well as insufficient or absent androgen synthesis during intrauterine development can lead to disorders of sexual development (DSD) in both sexes, which may manifest with ambiguous genitalia at birth [51-53]. Additional adverse effects may arise at any stage of life on other organ systems including muscles, bones, brain, and the cardiovascular system [54, 55].

Excessively high androgen levels in genetically female individuals are in most cases caused by congenital adrenal hyperplasia and can lead to virilized genitalia. In most cases, an interruption in the glucocorticoid synthesis pathway, for example due to a mutation of one of the steroidogenic enzymes involved, leads to the complete or partial loss of the negative feedback loop on the HPA axis (Figure 2 in chapter 2.1.2), and overall increased adrenal hormone production, including androgens (reviewed in [51]). Androgen accumulation in genetically female individuals may also occur through interruption in estrogen synthesis whereby androgen precursor steroids such as androstenedione accumulate and are then converted to more active androgens such as testosterone and DHT instead [56]. Extremely low androgen levels in genetically male individuals can be caused by disruption in androgen biosynthesis through mutation or potentially the inhibition of involved steroidogenic enzymes. Affected individuals exhibit varying degrees of undervirilization at birth, depending on the severity of the condition [57]. The correct diagnosis of DSD is often difficult, as the patients may present with typical male or female genitalia and no other obvious symptoms at birth. Measurements of systemic steroids, along with genetic analyses of the enzymes involved in androgen synthesis and the androgen receptor, can provide clinical insight into which step of androgen signaling may be impaired (reviewed extensively in [58]).

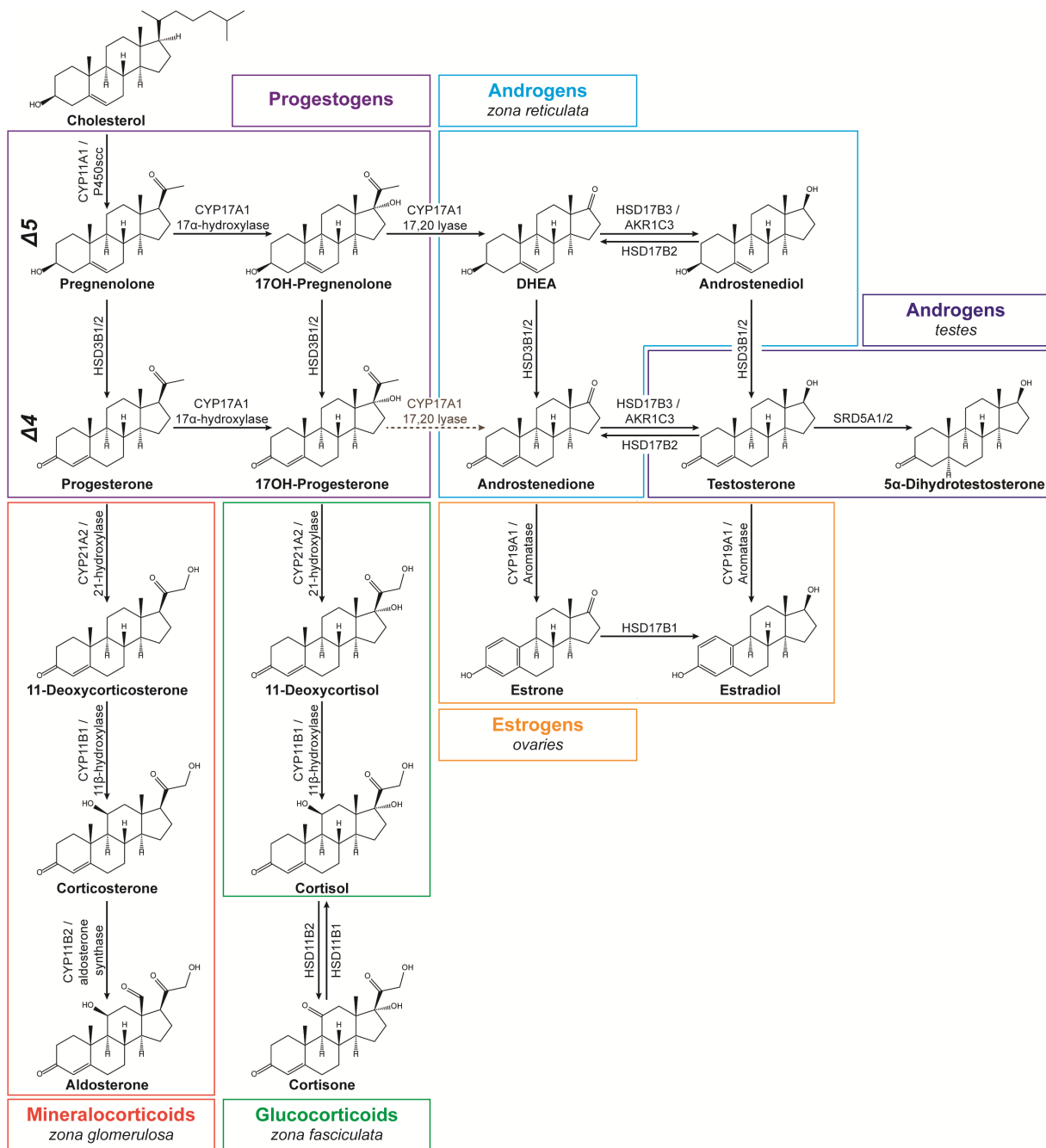
## 2.2 Hydroxysteroid dehydrogenases

Biosynthesis of steroids is mediated by steroidogenic enzymes from mostly two enzyme classes, the hydroxysteroid dehydrogenases (HSDs) and the cytochrome P450 (CYP) enzymes [59]. HSDs can be further subdivided into aldo-keto reductases (AKRs) and short-chain dehydrogenase/reductases (SDRs) [60]. Both subfamilies of HSDs, SDRs and AKRs require nicotinamide adenine dinucleotides (NADH/NAD<sup>+</sup>) or nicotinamide adenine dinucleotide phosphates (NADPH/NADP<sup>+</sup>) as cofactors to catalyze reductive or oxidative reaction steps of steroidogenesis [61, 62]. The four most relevant members of the human AKR superfamily required for human steroidogenesis, aldo-keto reductase family 1 member C1 to C4 (AKR1C1- AKR1C4) share a sequence identity of over 86% and contain a characteristic ( $\alpha/\beta$ )<sub>8</sub> barrel protein fold [63]. SDRs have sequence identities below 30%, yet they all contain the Rossmann fold, which is essential for cofactor binding, along with a conserved catalytic tetrad composed of asparagine, serine, tyrosine, and lysine residues. [64-66]. The Rossmann-fold is a super-secondary structure of alternating  $\beta$ -strands and  $\alpha$ -helices where the  $\beta$ -strands form a central  $\beta$ -sheet. There can be up to seven  $\beta$ -strands in one sheet [67, 68].



### 2.3 Steroidogenesis

Steroidogenesis occurs not only in primary steroidogenic organs like the adrenal cortex, gonads, and placenta, but also in other tissues such as the liver, adipose tissue, prostate, and skin. Many enzymatic steps are redundant and can be catalyzed by multiple enzymes in different tissues. Since these processes have already been thoroughly reviewed elsewhere [69], only a brief overview of steroidogenesis is given here (Figure 4). *De novo* steroidogenesis starts with the import of cholesterol into the inner mitochondrial membrane by the steroidogenic acute regulatory (StAR) protein, where it is converted to pregnenolone by the cholesterol side-chain cleavage enzyme (CYP11A1/P450<sub>scc</sub>) [70]. Pregnenolone can then be converted to progesterone in the endoplasmic reticulum (ER) by 3 $\beta$ -hydroxysteroid dehydrogenase type 1 (HSD3B1) and -type 2 (HSD3B2) [71-74]. Progesterone can then be further converted by the ER resident 21-hydroxylase (CYP21A2) to 11-deoxycorticosterone, and by both mitochondrial 11 $\beta$ -hydroxylase (CYP11B1) and aldosterone synthase (CYP11B2) to corticosterone and aldosterone, respectively [75-77]. In adult humans, this mineralocorticoid synthesis occurs in the adrenal zona glomerulosa, which lacks 17 $\alpha$ -hydroxylase (CYP17A1) activity, thereby channeling pregnenolone into the mineralocorticoid synthesis pathway [69, 78].



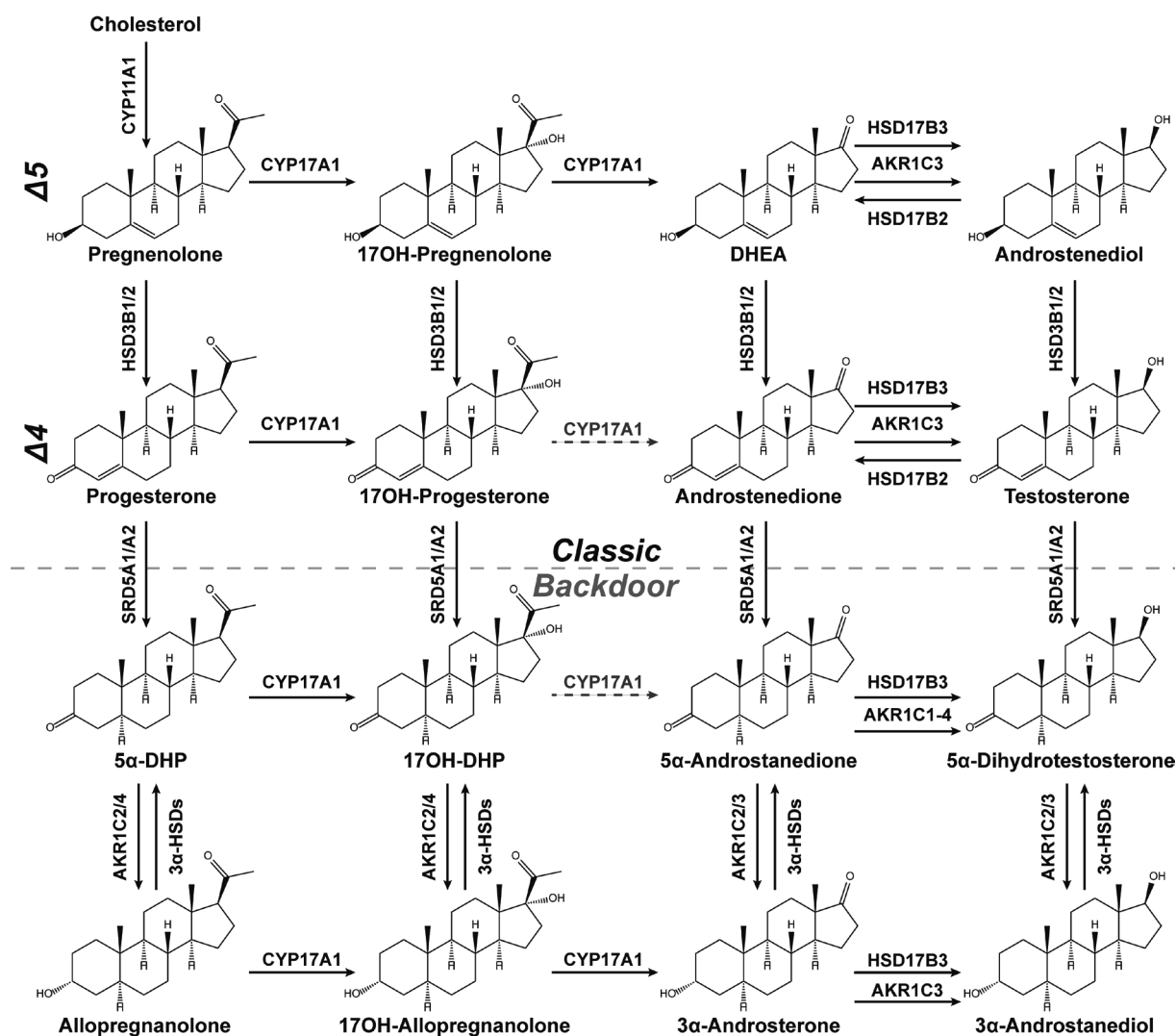
**Figure 4. Human adrenal and gonadal steroidogenic biosynthesis pathways** (adapted from Miller and Auchus et al., 2011 [69]). The displayed steroids are categorized into five groups, progestogens (purple), mineralocorticoids (red), glucocorticoids (green), androgens (blue) and estrogens (orange). Mineralocorticoids and glucocorticoids are synthesized exclusively within the zona glomerulosa and the zona fasciculata of the adrenal cortex, respectively. Androgens can be produced in the zona reticulata of the adrenal cortex (light blue) and the testes (dark blue) while estrogens can be generated within the ovaries. Black arrows represent reactions catalyzed by one or several steroidogenic enzymes. The dotted grey arrow represents the poor conversion of 17 $\alpha$ -hydroxyprogesterone (17OH-progesterone) to androstenedione in humans, in which the  $\Delta^5$ -pathway of androgen synthesis is preferred. Abbreviations: DHEA, dehydroepiandrosterone; 17OH-pregnenolone, 17 $\alpha$ -hydroxypregnenolone.

Progesterone can also be converted to  $17\alpha$ -hydroxyprogesterone by the  $17\alpha$ -hydroxylase activity of  $17\alpha$ -hydroxylase/ $17,20$ -lyase (CYP17A1), which can then be converted by CYP21A2 to 11-deoxycortisol and further to the main human glucocorticoid cortisol by CYP11B1 [69]. Cortisol synthesis takes place in the zona fasciculata of the adrenal cortex [79]. Interestingly, mice, rats, birds, reptiles, and amphibians do not possess  $17\alpha$ -hydroxylase activity in the adrenal cortex which is why corticosterone acts as the main biological glucocorticoid instead of cortisol [11, 17]. Additionally, both  $17\alpha$ -hydroxypregnenolone and  $17\alpha$ -hydroxyprogesterone can be converted by the  $17,20$  lyase activity of CYP17A1 to the weakly active androgens DHEA and androstenedione, respectively. Human  $17,20$ -lyase activity is about 50 times more efficient for the conversion of  $17\alpha$ -hydroxypregnenolone to DHEA than for the conversion of  $17\alpha$ -hydroxyprogesterone to androstenedione, which is why the  $\Delta 5$ -pathway of androgen synthesis is preferred in humans [80-82]. Cytochrome b5 acts in this reaction as an allosteric effector of CYP17A1 to augment its  $17,20$  lyase activity [80, 81]. Interestingly, mouse and rat  $17,20$ -lyases accept both  $17\alpha$ -hydroxypregnenolone and  $17\alpha$ -hydroxyprogesterone as substrates, but favor the  $\Delta 4$ - pathway over  $17\alpha$ -hydroxyprogesterone [83-85]. The synthesis of those two weak androgens takes place not only in the zona reticularis of the adrenal cortex but also in the Leydig cells in the testicles, and in the theca cells of the ovaries [86-88]. DHEA and androstenedione can both be further converted to androstenediol and testosterone. This conversion is mediated in the testicles through the ER resident  $17\beta$ -hydroxysteroid dehydrogenase type 3 (HSD17B3) [89]. Cytosolic AKR1C3, which is expressed in various tissues including prostate, ovary, liver, skeletal muscle as well as adrenal and mammary glands, has been shown to catalyze the same reactions [90-92]. Testosterone can be further converted to the most potent human androgen, DHT, by the two ER resident isoforms of  $5\alpha$ -ketoreductases, steroid  $5\alpha$ -reductase type 1 (SRD5A1) and steroid  $5\alpha$ -reductase type 2 (SRD5A2) [93]. While SRD5A1 is expressed in liver and nongenital skin, SRD5A2 is found in prostate, epididymis, seminal vesicle and genital skin [94]. Estrogens such as estrone and estradiol can be produced from androstenedione or testosterone in the ER by the enzyme aromatase (CYP19) [95, 96]. Inactivation and reactivation of steroids allows a further level of regulation of the total amount of steroids in the body. Examples include the reverse reaction of HSD17B3 that is catalyzed by  $17\beta$ -hydroxysteroid dehydrogenase type 2 (HSD17B2), where the active testosterone is oxidized back to the weak androgen androstenedione and the  $11\beta$ -hydroxysteroid dehydrogenase type 2 (HSD11B2)-dependent inactivation of cortisol and the corresponding reactivation by  $11\beta$ -hydroxysteroid dehydrogenase type 1 (HSD11B1) [97-99].

### 2.3.1 Backdoor pathway of dihydrotestosterone biosynthesis

In addition to the so-called classical pathway of DHT synthesis, there is an additional biosynthesis pathway for DHT, the so-called backdoor pathway, which was, although originally discovered in marsupials, also described in human fetal testes as well as in mouse testes [100-102]. The classic synthesis pathway via DHEA, androstenedione and testosterone is bypassed and instead progesterone and  $17\alpha$ -hydroxyprogesterone may be  $5\alpha$ -reduced to  $5\alpha$ -dihydroprogesterone ( $5\alpha$ -DHP) and  $17\alpha$ -hydroxydihydroprogesterone (17OH-DHP) by SRD5A1 or SRD5A2 (Figure 5). Similar to  $17\alpha$ -hydroxyprogesterone, 17OH-DHP is a poor substrate for the 17,20 lyase activity of CYP17A1 [82, 103]. An additional  $3\alpha$ -reduction of  $5\alpha$ -DHP and 17OH-DHP mediated by AKR1C2 or AKR1C4 results in allopregnanolone and  $17\alpha$ -hydroxyallopregnanolone, respectively. CYP17A1 then converts those intermediate steroids to  $3\alpha$ -androsterone. DHT can be synthesized from  $3\alpha$ -androsterone in two additional steps, a  $3\alpha$ -oxidation that can be catalyzed by a  $3\alpha$ -hydroxysteroid dehydrogenase ( $3\alpha$ -HSD) and a  $17\beta$ -reduction by either HSD17B3 or AKR1C3, respectively. Depending on the order in which the reactions take place,  $5\alpha$ -androstenedione or  $3\alpha$ -androstenediol ( $3\alpha$ -adiol) act as intermediate products [102, 104].

Measurements of plasma steroid concentrations and tissue expression levels of enzymes involved in the backdoor pathway in second trimester male fetuses indicate that backdoor androgens are likely to originate from placental progesterone. Progesterone is then presumably converted to  $3\alpha$ -androsterone in non-gonadal tissues such as the placenta, liver and adrenals via  $5\alpha$ -DHP, allopregnanolone and  $17\alpha$ -hydroxyallopregnanolone, respectively.  $3\alpha$ -androsterone has been identified as the major circulating backdoor androgen in male fetuses. The final enzymatic conversion steps of  $3\alpha$ -androsterone to DHT presumably occur in the target tissues themselves, acting in a para- or autocrine fashion, since no circulatory DHT could be measured in human fetuses [105].

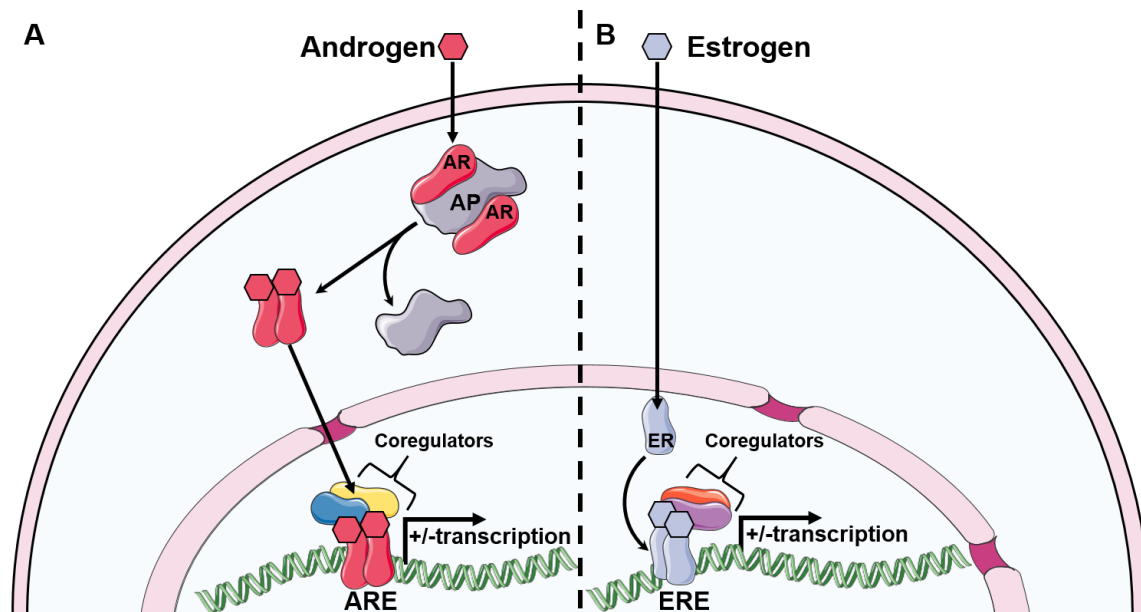


**Figure 5. The classic and backdoor pathways of 5 $\alpha$ -dihydrotestosterone biosynthesis** (adapted from O'Shaughnessy et al., 2019 [105]). Cholesterol cleavage through CYP11A1 produces pregnenolone. In the classical pathway of 5 $\alpha$ -dihydrotestosterone (DHT) biosynthesis, pregnenolone may be converted by CYP17A1 to 17 $\alpha$ -hydroxypregnenolone (17OH-pregnenolone) and dehydroepiandrosterone (DHEA), which can then be further converted to testosterone in two additional enzymatic steps, via either androstenedione or androstenediol as intermediate steroids. Testosterone is subsequently 5 $\alpha$ -reduced to DHT. Alternatively, in the backdoor pathway of DHT synthesis, pregnenolone is converted to progesterone through HSD3B1/2 activity, which is then further 5 $\alpha$ - and 3 $\alpha$ - reduced to allopregnanolone. This intermediate is subsequently converted by CYP17A1 to 17 $\alpha$ -hydroxyallopregnanolone (17OH-allopregnanolone) and 3 $\alpha$ -androsterone. 3 $\alpha$ -androsterone can be converted to DHT in two enzymatic steps, a 17 $\beta$ -reduction through one of the four AKR1C enzymes or HSD17B3 and a 3 $\alpha$ -oxidation catalyzed by a 3 $\alpha$ -HSD. Black arrows represent reactions catalyzed by one or several steroidogenic enzymes. The dotted grey arrows represent the poor conversion of 17 $\alpha$ -hydroxyprogesterone (17OH-progesterone) and 17 $\alpha$ -hydroxydihydroprogesterone (17OH-DHP) by CYP17A1. Abbreviation: 5 $\alpha$ -DHP, 5 $\alpha$ -dihydroprogesterone.

## 2.4 Steroid hormone receptors

Steroid hormone receptors (SHR) belong to the nuclear receptor superfamily and act as ligand-dependent transcription factors [106]. SHRs are involved in the regulation of various important physiological processes within the body, including development, growth, homeostasis, immune regulation, and reproduction. Those regulatory actions are mediated in a tissue specific manner by different members of the SHRs which include androgen-, estrogen-, progesterone-, as well as glucocorticoid- and mineralocorticoid receptors [1]. The SHRs are modular and share structural similarities amongst each other. Mainly, they are composed of three functional domains, the N-terminal transactivation domain (NTD), the DNA-binding domain (DBD), and the C-terminal ligand binding domain (LBD) [107].

SHRs mediate their transcriptional activity by binding to their corresponding steroid hormones [7]. Inactive SHRs may locate within the cytosol or the nucleus and can be associated with accessory proteins (Figure 6) [108]. Binding of a steroid to the LBD leads to dissociation of the accessory proteins and allows dimerization of the SHR [109]. Such a steroid-SHR complex is able to translocate to the nucleus (if it was not already localized within the nucleus) where it associates with additional coregulators and binds with its DBD to site-specific DNA sequences within the promotor regions of target genes, the so called hormone response elements [110, 111]. This complex process leads to either up or downregulation of the respective gene expression, depending on the cellular context and expressed coregulators [112].



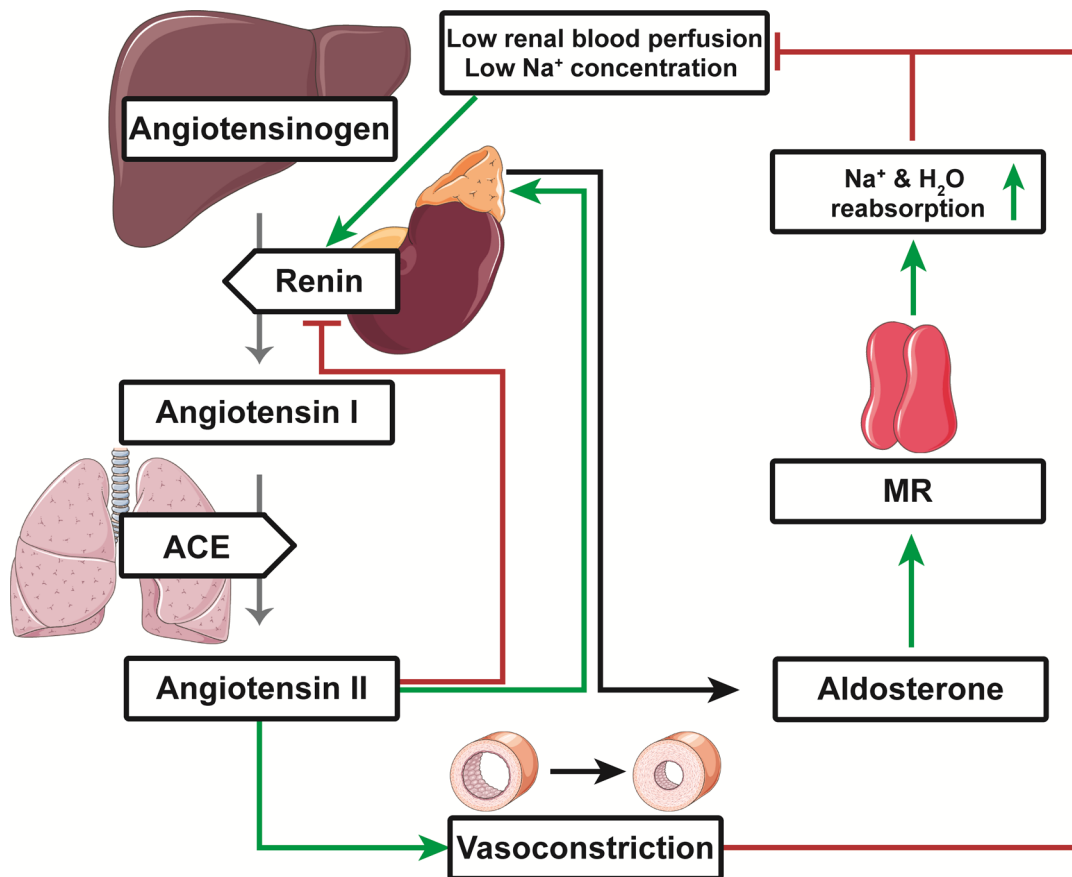
**Figure 6. Classical steroid hormone receptor signaling demonstrated on the example of the androgen and the estrogen receptor** (adapted from Levin & Hammes, 2016 [113]). **(A)** The androgen receptor (AR) is primarily located in the cytosol as monomers and bound to accessory proteins (AP). Binding of androgens to the cytoplasmic AR monomers leads to the release of accessory proteins, AR dimerization and nuclear translocation of the AR-androgen complex. **(B)** The estrogen receptor (ER) is mostly localized within the nucleus as a monomer. Binding of estrogens to the nuclear ER leads to dimerization of the ER. **(A, B)** Both receptor-hormone complexes bind to their specific steroid response elements, the androgen- and the estrogen response element (ARE, ERE) and modulate together with nuclear coregulators gene transcription of their respective target genes.

#### 2.4.1 Mineralocorticoid receptor

The mineralocorticoid receptor (MR) is highly expressed in the epithelial cells in the distal convoluted tubule and cortical collecting duct of the kidney, the ducts of salivary and sweat glands, as well as in colonic mucosa cells [114-117]. MR is activated by the mineralocorticoids aldosterone and corticosterone as well as by the glucocorticoid cortisol, with similar affinities [13]. MR regulates salt and water homeostasis by stimulating the expression of ion transporters such as the epithelial sodium channel and the basolateral sodium/potassium-ATPase, resulting in transepithelial sodium and water absorption, and potassium excretion (reviewed in [12, 118]).

Mineralocorticoid receptor activity is tightly regulated by the renin-angiotensin-aldosterone system (RAAS) (Figure 7). Low renal blood perfusion or low sodium concentration in the blood triggers the release of the protease renin from the kidneys into the bloodstream, which enzymatically cleaves the hepatically secreted angiotensinogen to angiotensin I. Angiotensin I is further cleaved to angiotensin II by the angiotensin-converting enzyme (ACE) in the lungs. Angiotensin II stimulates aldosterone secretion in the adrenal cortex and

simultaneously inhibits renal renin production through activation of the angiotensin II type 1 receptor (AT1-R). Angiotensin II additionally acts as a potent vasoconstrictor, increasing blood pressure and thus perfusion. The aldosterone-mediated activation of the MR increases uptake of sodium and water in the gut and kidneys, resulting in an increase in sodium concentration as well as an elevation in blood pressure, which increases renal perfusion (extensively reviewed in [119, 120]).



**Figure 7. Simplified depiction of the renin-angiotensin-aldosterone system (RAAS)** (adapted from Triebel & Castrop, 2024 [121]). If either the renal perfusion or the sodium (Na<sup>+</sup>) concentration within the blood is low, the kidneys release the protease renin into the blood where it cleaves hepatic angiotensinogen to angiotensin I. After subsequent cleavage of angiotensin I by the pulmonary angiotensin-converting enzyme (ACE), angiotensin II is formed. Angiotensin II inhibits renal renin production, stimulates aldosterone secretion from the adrenal cortex and triggers vasoconstriction which leads to an increase in blood pressure. Aldosterone-mediated activation of the mineralocorticoid receptor (MR) increases sodium and water uptake in the kidneys and gut, leading to a higher blood (Na<sup>+</sup>) concentration and higher blood pressure, i.e. increased renal perfusion. Stimulatory processes are depicted by green arrows, inhibitory actions are indicated by red arrows, and enzymatic reactions are symbolized by grey arrows.



The aldosterone specificity of MR activation in the kidneys and colon is ensured by continuous enzymatic inactivation of corticosterone and cortisol through the co-expression of HSD11B2. This enzyme oxidizes the hydroxyl group at the C-11 of corticosterone and cortisol, converting them to their biologically inactive 11-keto forms [122, 123].

Disruption of this gatekeeping function, whether through inhibition or mutation of HSD11B2, results in cortisol-mediated over-activation of the MR, a condition described as apparent mineralocorticoid excess (AME) syndrome. This syndrome is characterized by hypertension, low renin and aldosterone levels, hypokalemia, and hypernatremia in affected individuals. [124-128].

Heterozygous loss-of-function mutations of MR lead to pseudohypoaldosteronism, as the mutated receptor variant is resistant to aldosterone. Infants with this condition present with dehydration and salt wasting, hyperkalemia and elevated plasma aldosterone and renin levels [129, 130]. MR is also expressed in several non-epithelial tissues, including the heart, blood vessels, adipose tissue, and the brain, as well as in macrophages and was suggested to be involved in fibrosis, heart disease, inflammation, as well as modulation of neuronal cell viability and brain function (extensively reviewed in [131, 132]).

#### 2.4.2 Glucocorticoid receptor

The glucocorticoid receptor (GR) is expressed in almost every vertebrate cell and regulates a wide array of genes that are involved in glucose metabolism, immune and stress response, development, growth, reproduction, and cardiovascular function [18, 19, 133]. In certain cell types, up to 20% of all genes are regulated via the GR [134]. The outcome of GR activation through glucocorticoids is strongly dependent on the cellular context, i.e. cell-specific allosteric signals, other transcription factors and coregulators and may lead to either induction or repression of target genes in the nucleus [135-137]. Post-translational modifications such as phosphorylation, ubiquitination, SUMOylation and acetylation have been shown to influence the binding behavior and add another layer of GR activity regulation [138-141]. GR activity is essential for survival after birth [142]. Accordingly, glucocorticoid resistance as a result of mutations in the GR is usually only partial or occurs in a tissue-specific manner. Glucocorticoid resistances are often referred to as Chrousos syndrome [143-145]. Decreased GR activity in the hypothalamus and pituitary gland leads to loss of the negative feedback loops of the HPA axis, which ultimately leads to increased ACTH release and stimulation of hormone production in the adrenal glands, including glucocorticoids, androgens and mineralocorticoids. Affected individuals present with elevated cortisol and ACTH levels in their blood, but do not show any

of the typical symptoms of Cushing's syndrome [143]. The symptoms of the disease are rather characterized by the mineralocorticoid and androgen excesses, which can cause symptoms such as hypertension, hypernatremia, hypokalemia as well as hirsutism, acne and infertility, respectively [146].

Tissue-specific glucocorticoid resistance has also been associated with autoimmune, allergic or inflammatory diseases, among others. The underlying condition may lead to direct GR modification or influence coregulator composition and availability, altering the affinity of the GR to its target genes (reviewed in detail in [147]). Glucocorticoid resistance substantially complicates glucocorticoid treatment of such inflammatory diseases.

### 2.4.3 Androgen Receptor

The androgen receptor (AR) is expressed in a variety of tissues and cell types and is involved in many essential biological regulatory processes, including male development and homeostasis, as well as the cardiovascular, reproductive, and immune systems [148]. In humans, the AR gene is located on the X chromosome resulting in only one copy in genetically male individuals. The AR acts either as an activator or repressor of its target genes according to coregulators present in the respective cell context [149]. Posttranslational modifications of the AR include phosphorylation, ubiquitination, methylation, acetylation, and SUMOylation, which can influence its transcriptional activity, subcellular localization and stability [150].

Congenital loss of function mutations of the AR in patients with XY karyotype can lead to resistance to androgens, which is referred to as androgen insensitivity syndrome (AIS). AR activity is essential for normal human male development *in utero*, in particular for the normal development of the external male sex organs. AIS affected patients may exhibit a wide range of undervirilization at birth, depending on the residual AR activity [151]. Accordingly, AIS is also categorized as a DSD, similarly as insufficient or interrupted androgen production due to mutations in the required steroidogenic enzymes [152].

In the case of complete androgen insensitivity syndrome (CAIS), affected patients may already present with a female external phenotype at birth, but with a blind-ended vagina, absent uterus and undescended testes instead of ovaries [153]. Lack of AR activity may also prevent the development of secondary male sexual characteristics during puberty, such as the growth of axillary and pubic hair in affected patients [154]. Lack of androgen response rather than elevated estrogen levels has been the suggested reason for development of female secondary sexual characteristics in affected patients [155]. CAIS affected individuals also present with primary amenorrhea at the onset of puberty due to lack of female internal organs [156]. There

are also milder degrees of undervirilization in patients known as partial androgen insensitivity syndrome (PAIS) who present with ambiguous genitalia at birth or mild AIS (MAIS) which is only associated with infertility in men (extensively reviewed in [154, 157, 158]).

AR signaling also plays an essential role in the growth and development of the prostate, which is especially important for the onset and progression of prostate cancer. Prostate cancer is one of the most common cancers in men and depends on AR activity to maintain its growth and survival [159]. Consequently, androgen deprivation therapy (ADT) is used in the treatment of prostate cancer to limit its growth. ADT may include surgical removal of the testes, the main source of androgens in men, direct chemical inhibition of AR activity, chemical inhibition of steroidogenic enzymes involved in the androgen biosynthesis or blocking of the HPG axis with GnRH agonists [160, 161]. However, prostate cancer can become castration resistant through various mechanisms of AR signaling modification, such as AR overexpression or expression of constitutively active AR splice variants without ligand binding domain, to name a few. Further adaptations of ARs in castration-resistant prostate cancer (CRPC) have been summarized elsewhere [162].

## 2.5 Retinoic acid-related orphan receptors

The retinoic acid-related orphan receptors (ROR) are a subfamily of the nuclear receptor superfamily which consists of three members, ROR $\alpha$ , ROR $\beta$  and ROR $\gamma$ . These receptors exert different regulatory functions in the body, which are also mediated by cell type-specific expressed isoforms of the respective receptor types [163]. RORs display the typical modular nuclear receptor structure and feature a DBD, a LBD as well as a hinge domain that connects the two other domains with each other [1, 164]. The DBD recognizes and binds to the so-called ROR response elements (ROREs) [165-167]. Originally, these receptors were referred to as so-called orphan receptors, as their natural ligands had not been identified or characterized well enough [168]. In contrast to hormone receptors, RORs bind to their target sequence as monomers and are constitutively active, meaning that they are able to activate gene expression of target genes independently of ligands, together with other coregulators (reviewed in [163, 169]). Ligands may however act as agonists or inverse agonists and increase or decrease ROR transcriptional activity [170]. In addition, the activity and stability of the various RORs can also be modulated by post-translational modifications such as phosphorylation, acetylation, ubiquitination and SUMOylation [171-173].

A total of four human isoforms of ROR $\alpha$  are known which are expressed in a wide variety of tissues, including the brain, kidney, lung, liver, testis, muscle and adipose tissue (reviewed

in [163, 174]). Studies with ROR $\alpha$  KO mice have revealed important roles of ROR $\alpha$  in the regulation of the circadian rhythm, cerebral development and bone tissue formation [175, 176]. ROR $\alpha$  has been found to bind to a number of sterols and oxysterols, including cholesterol, 7-dehydrocholesterol as well as 25- and 27-hydroxycholesterol which may be considered as possible physiological ligands [177-179].

ROR $\beta$  is only expressed in certain regions of the central nervous system and in the retina (reviewed in [163]). ROR $\beta$  KO mice showed retinal degeneration and abnormalities in their circadian rhythm, suggesting a role for ROR $\beta$  in its regulation as well [180, 181]. Natural ligands for ROR $\beta$  include retinoids such as all-trans retinoic acid [182].

ROR $\gamma$  has two isoforms, the complete transcript and its 21 amino acid shorter isoform, ROR $\gamma$ t, which share the same DNA and ligand binding domains [183-185]. The tissue expression pattern of ROR $\gamma$  largely coincides with that of ROR $\alpha$ , as it is also expressed in kidney, liver, skeletal muscle and adipose tissue, but additionally includes the mammary glands and thymus. ROR $\gamma$  has been shown to regulate glucose and lipid metabolism as well as the circadian rhythm [165, 186, 187]. ROR $\gamma$ t is only expressed in a variety of immune cells, including type 3 innate lymphoid cells (ILC3) and T helper 17 (Th17) cells [188, 189]. ROR $\gamma$ t has been shown to be essential for the differentiation of naïve CD4<sup>+</sup> T cells into Th17 cells, and also regulates their production of pro-inflammatory cytokines such as interleukin (IL) 17A, IL17F and IL22 [188]. Mouse KO mutants of ROR $\gamma$  showed resistance to the development of Th17-dependent inflammation in autoimmune disease models, such as psoriasis or multiple sclerosis, which is why ROR $\gamma$ t has been regarded as potential pharmaceutical target [188, 190, 191]. Naturally occurring ligands of both ROR $\gamma$  isoforms include various oxysterols such as 7 $\beta$ , 25- or 7 $\beta$ , 27-dihydroxycholesterol as well as their 7-keto forms [174, 179, 192-194]. From here on, statements that relate to both ROR $\gamma$  isoforms, are referred to as ROR $\gamma$ (t).

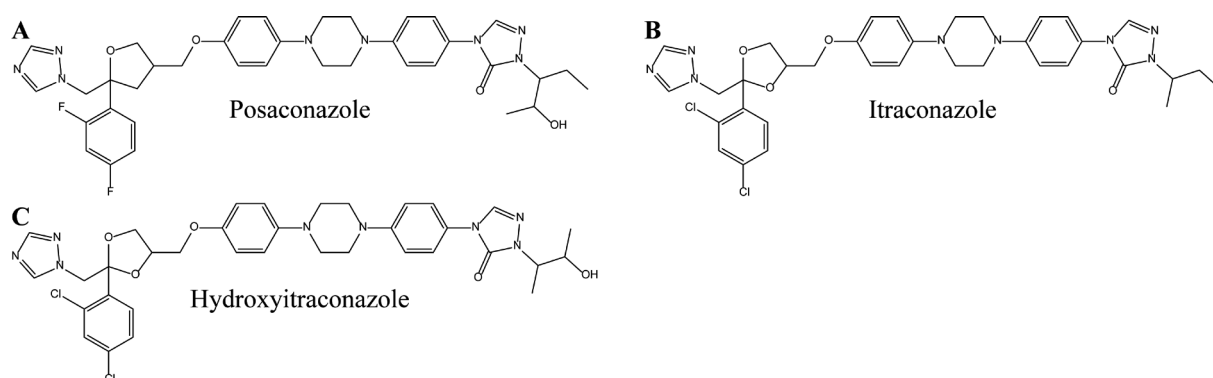
## 2.6 Endocrine disrupting chemicals

Xenobiotics are compounds that do not naturally occur or cannot be produced within an organism. Certain xenobiotics can display adverse health effects in living organisms after exposure, such as environmental toxins, pesticides and carcinogens or drugs with undesirable side effects. Xenobiotics that alter the functions of the endocrine system, either by themselves or in mixtures, in such a way that they trigger adverse health effects in an organism or its offspring, are known as endocrine disrupting chemicals (EDCs) [195]. In recent years, these ECDs have increasingly become the focus of scientific research and are to some extent the subject of extensive public debate [196].

### 2.6.1 Azole antifungals

Azole antifungals are used topically and systemically in the treatment of fungal infections, where they act as inhibitors of the fungal cytochrome P-450-dependent lanosterol 14 $\alpha$ -demethylase which catalyzes the essential conversion of lanosterol to ergosterol, a major component of the plasma membrane of fungi (reviewed in [197]). Examples of these azole antifungals are itraconazole and posaconazole, which are used to treat various fungal diseases such as oropharyngeal candidiasis and aspergillosis (Figure 8) [198-200]. Itraconazole is metabolized in humans to hydroxyitraconazole which itself has similar antifungal activity to its parent compound [201, 202].

Although they are generally well tolerated, azole antifungals can cause side effects, including headache, dizziness and fatigue for posaconazole and heartburn, nausea, vomiting and diarrhea for itraconazole [203, 204]. Interestingly, pseudohyperaldosteronism with symptoms like hypertension, hypokalemia, and hypernatremia can also occur during systemic treatment with these azole antifungals, and has been reported in various case reports [205-211].

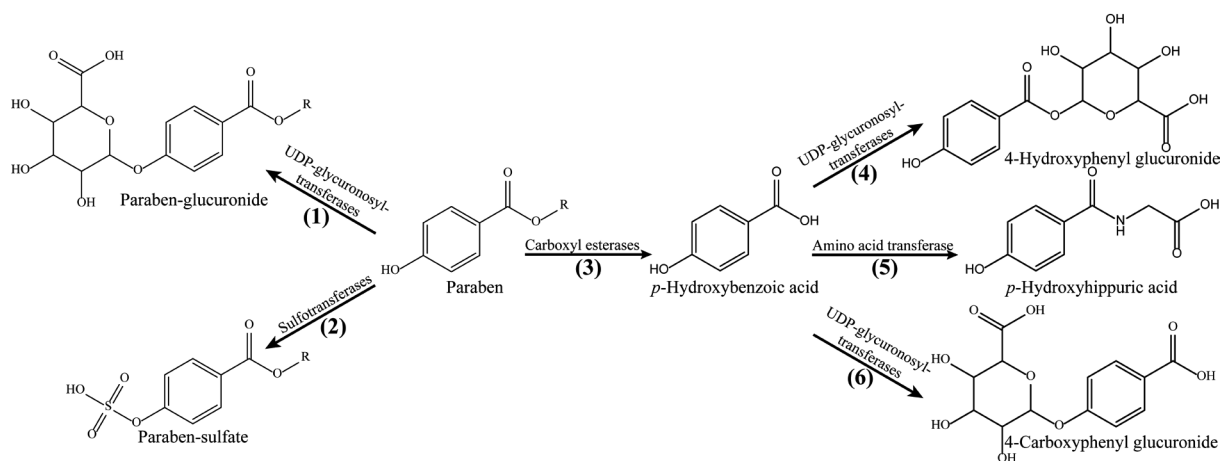


**Figure 8. Chemical structures of azole antifungals that can cause pseudohyperaldosteronism.** Displayed are posaconazole (A), itraconazole (B) and its main metabolite, hydroxyitraconazole (C).

## 2.6.2 Parabens

Parabens are esters of *p*-hydroxybenzoic acid that are added to cosmetics, food and body care products for their anti-bacterial and anti-fungal properties [212]. These preservative properties help to improve product stability and thus extend shelf life [213, 214]. Parabens are mainly absorbed into the body via the gastrointestinal tract and the skin and have been detected in various human matrices, including urine, blood serum, breast milk, but also fetal cord serum and placental tissue [215-217]. This suggests not only systemic exposure but also prenatal exposure. Parabens are continuously metabolized by carboxylesterases in the skin and liver *p*-hydroxybenzoic acid and alcohols (Figure 9) [218-220]. Parabens and their main metabolite *p*-hydroxybenzoic acid are also conjugated with glucuronide, glycine and sulfate to increase their solubility for renal excretion [214, 221-223].

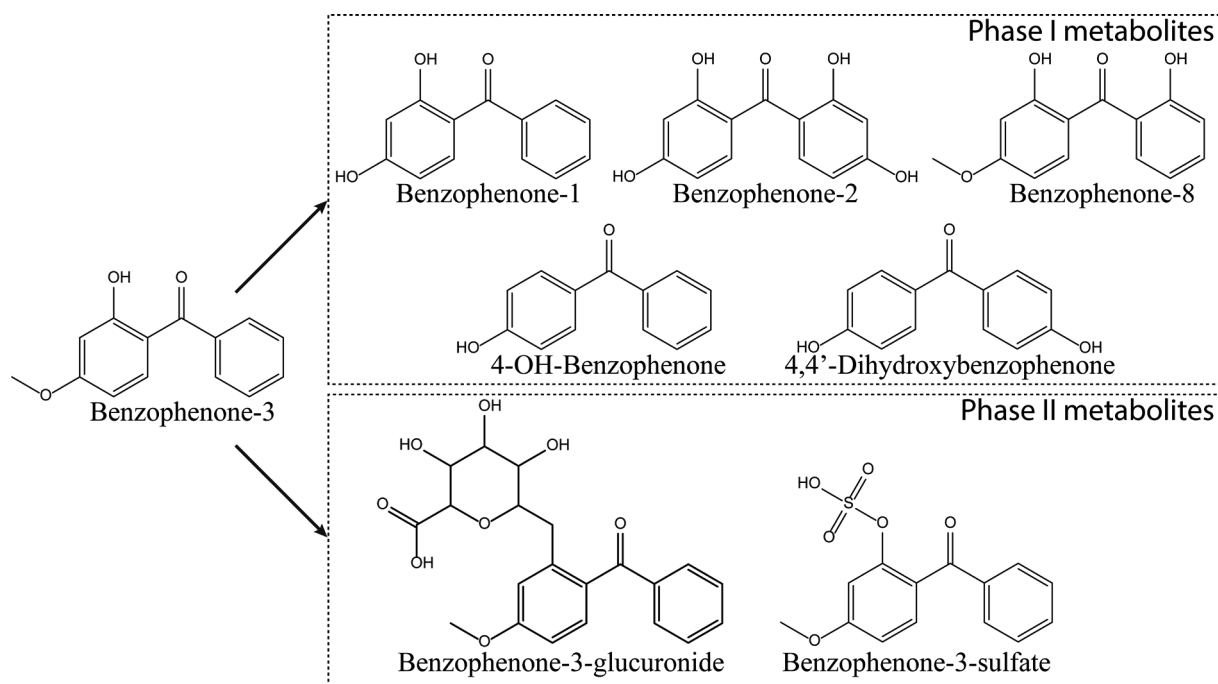
To date, parabens are not considered carcinogenic, even at higher concentrations, as various animal experiments have shown, but they have long been subject to criticism for their endocrine disrupting properties [224]. Those compounds have been shown to possess estrogenic and antiandrogenic properties in various *in vitro* and *in vivo* experiments by acting on estrogen and androgen receptors [225-228]. These antiandrogenic effects are suspected to have a negative impact on the human reproductive potential, since lower testosterone levels as well as a reduction of testicular volume and sperm quality have been observed in paraben treated male rats [228-231]. Accordingly, the usage of parabens has been heavily restricted in the EU [232].



**Figure 9. Human paraben metabolism** (adapted from Abbas et al., 2010 and Lester et al., 2021 [222, 233]). Parabens can either be directly conjugated to glucuronide (1) or sulfate (2) or hydrolyzed to *p*-hydroxybenzoic acid and an alcohol rest within the skin or the liver (3). *p*-Hydroxybenzoic acid can be further conjugated to glucuronide (4, 6) or glycine (5) to increase its solubility for efficient renal excretion.

### 2.6.3 UV-filters

UV-filters are used as additives in cosmetics, body care products as well as plastics and textiles to protect products against UV radiation, increasing their overall stability, and contributing to odor- and color preservation [228, 234-237]. Some UV-filters, including avobenzone and benzophenone (BP)-3, may also be used as active UV-absorbing ingredients in sunscreens [238, 239]. Similar to parabens, UV-filters are mainly absorbed via skin penetration after topical application or by ingestion [240, 241]. Accordingly, those UV-filters have been measured in numerous human matrices, including urine, blood serum, seminal fluid and breast milk. In addition, UV-filters have also been measured in placental tissue, fetal cord serum, blood serum and amniotic fluid, suggesting trans-placental transport and prenatal exposure [242]. Benzophenone-type UV-filters such as BP-3 can penetrate the skin efficiently due to their small molecule size [241]. Similar to parabens, these benzophenone-type UV-filters are readily conjugated in the liver to glucuronide and sulfate for rapid urinary excretion (Figure 10) [243]. BP-3, which can be used as active ingredient in sun screens was shown to be metabolized into other UV-filters in humans, including BP-1, -2 and -8 as well as 4-hydroxy- and 4,4'-dihydroxy-BP, resulting in mixtures of different metabolites after exposure (reviewed in [242]). The usage of benzophenone-type UV-filters is extensively debated due to their endocrine disrupting properties. Several benzophenone-type UV-filters were found to exert antiandrogenic and estrogenic effects *in vitro* through direct interaction with the androgen and estrogen receptors, respectively [244-249]. Possible endocrine-disrupting properties of UV-filters on the androgen and estrogen receptors have also been shown in several animal studies [228, 250-252]. To date, BP-3 exposure has only been associated with smaller testicular volume and lower testosterone levels in adolescent boys, while BP-2 was associated with diminished sperm quality in men [253-255]. However, a clear mode-of-action explaining these observations has not been identified yet.



**Figure 10. Human metabolism of benzophenone-3** (adapted from Wang & Kannan, 2013 and Watanabe et al., 2015 [243, 249]). Benzophenone (BP)-3 has been shown to be metabolized into other UV-filters, including BP-1, -2, and -8, as well as 4-hydroxy- and 4,4'-dihydroxy-BP. Additionally, BP-3 may be conjugated to glucuronide and sulfate for efficient urinary excretion.



### 3. General aims of this thesis

Throughout their lives, humans are exposed to thousands of xenobiotics. New synthetic chemicals are registered every year, whether in industry, agriculture, pharmaceuticals or consumer products, to which humans can potentially be exposed. Accordingly, it is also important to ensure that chemical compounds are safe for the user. However, safety assessments of new compounds require extensive investigation and time-consuming laboratory work, which may include both *in vitro* screening and *in vivo* experimentation. In the field of endocrinology, these tests are often limited to the direct effects of a test substance on the sex steroid hormone receptors, the estrogen and androgen receptors. Possible negative influences of xenobiotics on the highly complex process of steroidogenesis involving numerous steroid metabolizing enzymes in different tissues and cell types as well as effects on other important nuclear receptors such as ROR $\gamma$ (t) have often been neglected. The use of animal studies for safety assessment adds another layer of complexity, namely the transferability of results from animal studies to a possible outcome in the human organism. Species-specific differences in steroidogenesis or steroidogenic enzymes can complicate the proper safety assessment of certain chemicals.

In order to address some of these safety assessment challenges, we have carried out three projects with the ultimate objective of identifying and characterizing substances that interfere with steroid metabolizing enzymes or ROR $\gamma$ (t) activity. In an additional, fourth project, we investigated possible molecular mechanisms of two novel mutations in the *HSD17B3* gene that were identified in two Tunisian patients with 46,XY DSD.

Each of the projects will be introduced and discussed in more detail in the following chapters. As the different projects appear to be rather far apart from each other in terms of their individual subject areas, the reader shall at this point receive a rough overview of all the projects covered in this thesis with the respective underlying goals.

As mentioned in the introduction, the steroidogenic enzyme HSD11B2 inactivates glucocorticoids in the kidneys and colon and therefore prevents excessive activation of the MR, which is essential for salt and water homeostasis. Several previous studies have found that certain patients treated with the azole antifungals posaconazole and itraconazole developed a form of pseudohyperaldosteronism, the AME syndrome, indicating an inhibition of HSD11B2 activity that was not detected during preclinical investigations.

In the first project (Chapter 4), we therefore investigated possible species-specific differences in the inhibition of human, mouse, rat, and zebrafish homologs of HSD11B2 by the azole antifungals posaconazole and itraconazole. We also assessed structure-activity relationships (SAR) between the different HSD11B2 homologs and these two azole antifungals

to facilitate future investigations on possible species-specific inhibition of HSD11B2. Robust and reproducible *in vitro* methodology is required to assess the activity of steroidogenic enzymes such as HSD11B2. In this regard, we also authored two chapters in the book series 'Methods in Enzymology', detailing experimental approaches for the effective and concise analysis of the enzymatic activities of HSD11B2 and its isozyme HSD11B1, which converts inactive 11-ketoglucocorticoids to their active 11 $\beta$ -hydroxylated forms.

Commercially used parabens and UV-filters have so far mainly been investigated for their endocrine effects on the AR and the estrogen receptor, leading to the discovery of their endocrine disrupting capacities that exert antiandrogenic effects by direct AR inhibition. Their influence on androgen biosynthesis, in particular the backdoor pathway of DHT synthesis, has not yet been investigated.

In the second project (Chapter 5), we therefore aimed to elucidate the potential antiandrogenic effects of parabens and UV-filters through inhibition of 3 $\alpha$ -HSDs in the backdoor pathway of DHT synthesis. We also investigated possible SARs between identified inhibitors and the respective targeted 3 $\alpha$ -HSD using *in silico* modeling of the enzyme and docking simulations.

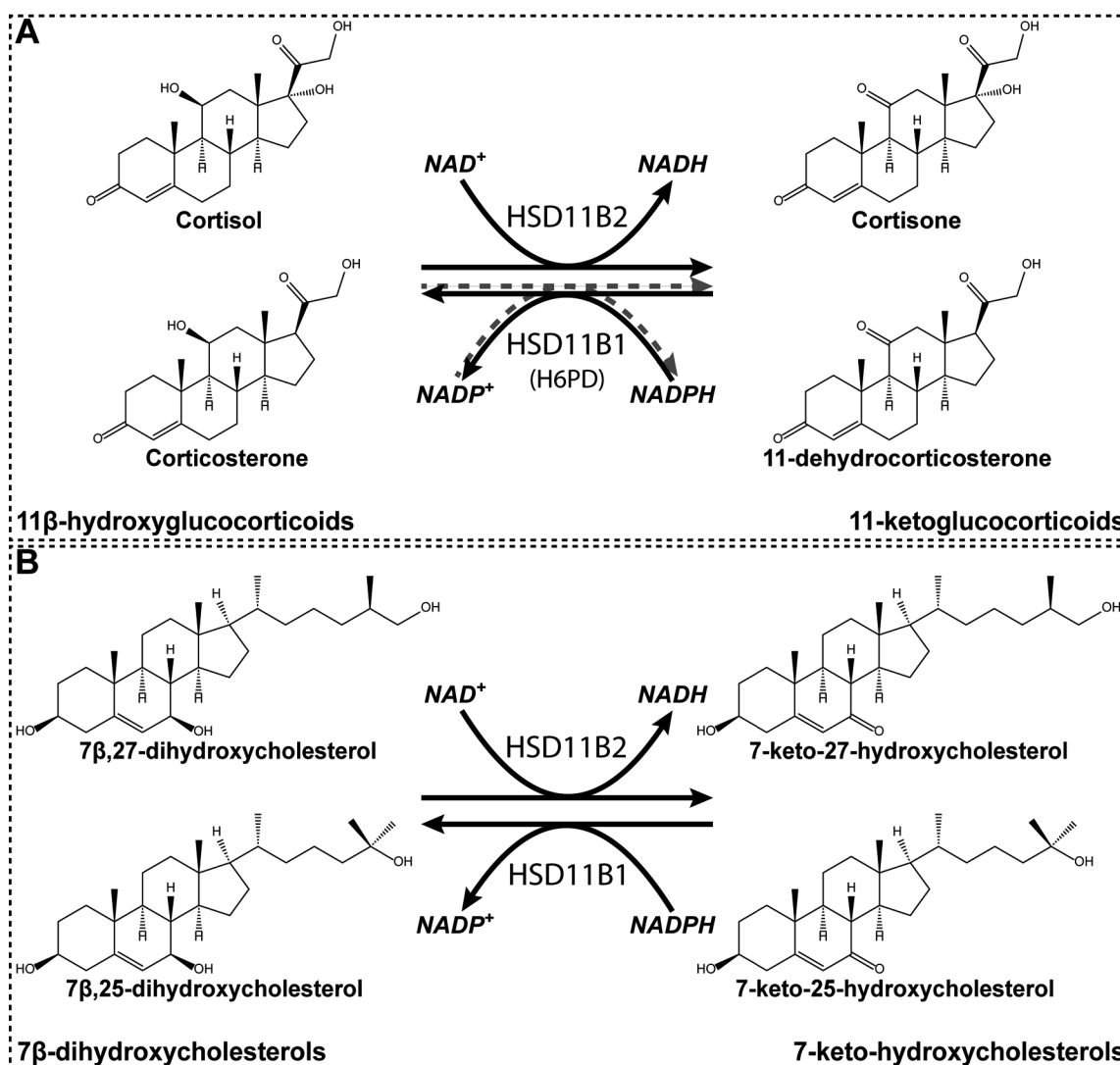
ROR $\gamma$  and its isoform ROR $\gamma$ t are nuclear receptors that play an important role in metabolism and in the regulation of inflammatory processes. So far, however, they have hardly been investigated as potential targets of xenobiotics in safety assessments. In the third project (Chapter 6), we investigated the effects of parabens and UV-filters on the transcriptional activity of ROR $\gamma$  and ROR $\gamma$ t. We applied *in silico* methods to identify additional substances from a cosmetics database that potentially modulate the transcriptional activity of ROR $\gamma$ (t).

In an additional, fourth project (Chapter 7), we investigated the underlying defects of two novel mutations in the *HSD17B3* gene that were identified in two Tunisian patients with 46,XY DSD. The enzyme transcribed from this gene, HSD17B3, catalyzes the conversion of androstenedione to testosterone in the classical pathway of androgen synthesis, which is essential for the normal fetal development of male genitalia.

## **4. Project 1: *In vitro* assessment of 11 $\beta$ -hydroxysteroid dehydrogenase activity and species-specific inhibition of HSD11B2 by azole antifungals**

### 4.1 Introduction

11 $\beta$ -hydroxysteroid dehydrogenases (11 $\beta$ -HSDs) belong to the SDR superfamily and catalyze the interconversion of 11 $\beta$ -glucocorticoids and their inactive 11-keto forms (Figure 11A). 11 $\beta$ -hydroxysteroid dehydrogenase type 1 (HSD11B1) catalyzes the NADPH-dependent reduction and thus the activation of cortisone and 11-dehydrocorticosterone to cortisol and corticosterone, respectively, while 11 $\beta$ -hydroxysteroid dehydrogenase type 2 (HSD11B2) catalyzes the reverse reactions using NAD<sup>+</sup> as cofactor [98, 256, 257]. *In vitro* activity assays with HSD11B1 revealed an oxidase activity, when the enzyme was provided with NADP<sup>+</sup> as cofactor [99]. Both glucocorticoid metabolizing enzymes are located in the ER membrane, with HSD11B1 having a luminal active site and the active site of HSD11B2 facing the cytosol [257]. There is strong evidence for functional coupling between HSD11B1 and hexose-6-phosphate dehydrogenase (H6PD), an enzyme of the pentose phosphate pathway that generates NADPH in the ER lumen [258, 259]. *In vivo*, NADPH generation by H6PD specifies the reaction direction of HSD11B1 by providing the necessary cofactor for the cortisone activation [260-262]. Besides regulation of the active glucocorticoid levels, both isozymes are able to interconvert oxysterols (Figure 11B) [263, 264]. HSD11B1 additionally accepts 11-oxo and 7-oxo-steroids as substrates and seems to play an important role in the detoxification of non-steroidal compounds [265-268].



**Figure 11. Enzymatic interconversion of (A) glucocorticoids and (B) oxysterols by HSD11B1 and HSD11B2.** HSD11B2 catalyzes the  $\text{NAD}^+$ -dependent oxidation of  $11\beta$ -hydroxyglucocorticoids and  $7\beta$ -dihydroxycholesterols. *In vitro*, HSD11B1 is able to catalyze the reduction of 11-ketoglucocorticoids as well as the oxidation of  $11\beta$ -hydroxyglucocorticoids (dashed grey arrows), depending on which cofactor is provided in the reaction. In most human tissues HSD11B1 acts predominantly as an oxoreductase due to the presence of hexose-6-phosphate dehydrogenase (H6PD), which produces the cofactor NADPH. HSD11B1 has also been shown to reduce 7-keto-hydroxycholesterols to  $7\beta$ -dihydroxycholesterols.

HSD11B1 is widely expressed within the body, especially in metabolically active tissues such as liver, adipose tissue, brain and skeletal muscle [266, 269-271]. Physiological HSD11B1 activity provides active glucocorticoids required for GR activation while elevated activity of HSD11B1 has been observed in patients with diabetes and in adipose tissue of obese people, among others [131, 272, 273]. In addition, elevated cortisol levels have been associated with Alzheimer's disease [274, 275]. Based on these observations and promising results in

corresponding animal models, HSD11B1 was identified as a therapeutic target for which specific inhibitors have been developed (extensively reviewed in [276]).

HSD11B2 is predominantly expressed in tissues that also co-express the mineralocorticoid receptor such as the renal distal tubules or the cortical collecting ducts and distal colon (extensively reviewed in [131] and [277]). Cortisol, one of the enzyme's substrates, does not only bind to and activates the GR but also activates the MR with a similar affinity [13, 278, 279]. MR regulates the transcription of genes involved in ion and water transport (reviewed in [131]). Since physiological cortisol levels are about 1000 times higher than aldosterone, the main ligand of MR, HSD11B2 activity serves as a gatekeeping mechanism that ensures aldosterone-specific MR activation [122, 123]. Inhibition or homozygous pathological mutations of HSD11B2 may lead to an unspecific activation of the MR through cortisol, resulting in the AME syndrome (Subchapter 2.4.1).

HSD11B2 activity also plays an important role during pregnancy, where placental HSD11B2 reduces the maternal cortisol concentrations that may reach the fetus [280, 281]. Elevated fetal cortisol exposure during pregnancy caused by HSD11B2 inhibition may result in metabolic or neurological implications, such as poorer memory, lower intelligence quotients and an overall higher probability for hyperactivity and attention deficit disorders [282-284]. Certain xenobiotics such as glycyrrhetic acid, a natural compound of licorice, have been shown to potently inhibit HSD11B2, resulting in elevated blood pressure [285, 286]. Since the placental HSD11B2 protects the fetus from the relatively high cortisol concentrations of the mother, licorice consumption during pregnancy is not recommended [284]. These consequences illustrate the importance of knowing whether certain substances, e.g. xenobiotics such as environmental compounds or drugs to which humans are exposed to, can inhibit HSD11B2 activity.

In order to identify potential inhibitors for HSD11B1 and HSD11B2, robust experimental methods that can reliably quantify the activity of both 11 $\beta$ -HSD isoforms are required. Accordingly, we compiled two chapters for the book series 'Methods in Enzymology', in which we described in detail the various *in vitro* methods for HSD11B1 and HSD11B2 that have been established and optimized in our laboratory, including radiometric enzyme activity assays. We placed particular emphasis on providing the reader with a comprehensive overview of the described *in vitro* methods and included a decision tree to facilitate the selection of the optimal method to cover certain aspects of the enzyme activity of both 11 $\beta$ -HSD isoforms. Advantages and disadvantages of the described methods were included as well as subchapters for troubleshooting during the respective method establishment.

Even if novel drugs successfully pass the preclinical and clinical phases and are finally approved, patient treatment may still lead to adverse drug effects. Such effects have also been observed in patients treated with azole antifungals such as itraconazole and posaconazole which manifested in the form of an acquired AME syndrome [205-211]. An additional study then finally revealed that both azole antifungals as well as the metabolite of itraconazole, hydroxyitraconazole, potently inhibit human HSD11B2 activity with  $IC_{50}$  values in the nanomolar range and thus likely caused the observed AME syndrome in the affected patients. However, this study also demonstrated that the tested compounds inhibited the mouse and rat homologs of HSD11B2 to a lesser extent [287].

This led to the question whether this apparent species-specific difference in HSD11B2 inhibition may have been the reason why the described adverse drug effects have not been observed in preclinical studies. We therefore investigated the inhibitory capacities of posaconazole, itraconazole and its main metabolite hydroxyitraconazole on the enzymatic activity of HSD11B2 from different species. This included HSD11B2 homologs of model organisms used in preclinical trials, namely rat, mouse and zebrafish that we compared to the findings of the already characterized human variant. All three compounds analyzed were confirmed to potently inhibit human HSD11B2 with  $IC_{50}$  values in the nanomolar range. The rat HSD11B2 was comparatively moderately inhibited by the tested compounds but the mouse and zebrafish homologs were barely inhibited at the examined concentrations. We then identified enzyme domains and amino acid residues of the human and mouse HSD11B2 homologs that may be responsible for this species-specific inhibition by azole antifungals. Molecular modeling allowed us to generate a novel HSD11B2 homology model with which we then assessed the species-specific SAR between the mouse and human HSD11B2 and the tested azole antifungals.

## 4.2 Published article: Species-specific differences in the inhibition of 11 $\beta$ -hydroxysteroid dehydrogenase 2 by itraconazole and posaconazole

Silvia G Inderbinen<sup>a</sup>, Michael Zogg<sup>a</sup>, Manuel Kley<sup>a</sup>, Martin Smieško<sup>b</sup>, Alex Odermatt<sup>a,\*</sup>

<sup>a</sup> Swiss Centre for Applied Human Toxicology and Division of Molecular and Systems Toxicology, Department of Pharmaceutical Sciences, University of Basel, Klingelbergstrasse 50, Basel 4056, Switzerland.

<sup>b</sup> Computational Pharmacy, Department of Pharmaceutical Sciences, University of Basel, Klingelbergstrasse 61, Basel 4056, Switzerland.

\* Corresponding author. e-mail address: alex.odermatt@unibas.ch

### Published article

**Personal contribution:** Completion of several additional experiments for the manuscript revision.

**Aims:** Investigate the inhibitory capacities of posaconazole, itraconazole and its main metabolite hydroxyitraconazole on the enzymatic activity of human, rat, mouse and zebrafish HSD11B2 homologs.

**Conclusion:** Compared to the human HSD11B2 homolog which was potently inhibited by all three compounds with nanomolar IC<sub>50</sub> values, the rat homolog was only weakly inhibited. The mouse and zebrafish homologs were barely inhibited at the examined concentrations. Different C-termini and amino acid residues at positions 170 and 172 are at least partially responsible for the species-specific differences in the inhibition of human and mouse HSD11B2 through the assessed azole antifungals.



## Species-specific differences in the inhibition of 11 $\beta$ -hydroxysteroid dehydrogenase 2 by itraconazole and posaconazole

Silvia G. Inderbinen<sup>a</sup>, Michael Zogg<sup>a</sup>, Manuel Kley<sup>a</sup>, Martin Smieško<sup>b</sup>, Alex Odermatt<sup>a,\*</sup>

<sup>a</sup> Swiss Centre for Applied Human Toxicology and Division of Molecular and Systems Toxicology, Department of Pharmaceutical Sciences, University of Basel, Klingelbergstrasse 50, Basel 4056, Switzerland

<sup>b</sup> Computational Pharmacy, Department of Pharmaceutical Sciences, University of Basel, Klingelbergstrasse 61, Basel 4056, Switzerland

### ARTICLE INFO

#### Keywords:

Glucocorticoid  
Pseudohyperaldosteronism  
Hypertension  
11beta-Hydroxysteroid Dehydrogenase  
Azole Fungicide  
Species Difference

### ABSTRACT

11 $\beta$ -hydroxysteroid dehydrogenase 2 (11 $\beta$ -HSD2) converts active 11 $\beta$ -hydroxyglucocorticoids to their inactive 11-keto forms, thereby preventing inappropriate mineralocorticoid receptor activation by glucocorticoids. Disruption of 11 $\beta$ -HSD2 activity by genetic defects or inhibitors causes the syndrome of apparent mineralocorticoid excess (AME), characterized by hypokalemia, hypernatremia and hypertension. Recently, the azole antifungals itraconazole and posaconazole were identified to potently inhibit human 11 $\beta$ -HSD2, and several case studies described patients with acquired AME. To begin to understand why this adverse drug effect was missed during preclinical investigations, the inhibitory potential of itraconazole, its main metabolite hydroxyitraconazole (OHI) and posaconazole against 11 $\beta$ -HSD2 from human and three commonly used experimental animals was assessed. Whilst human 11 $\beta$ -HSD2 was potently inhibited by all three compounds (IC<sub>50</sub> values in the nanomolar range), the rat enzyme was moderately inhibited (1.5- to 6-fold higher IC<sub>50</sub> values compared to human), and mouse and zebrafish 11 $\beta$ -HSD2 were very weakly inhibited (IC<sub>50</sub> values above 7  $\mu$ M). Sequence alignment and application of newly generated homology models for human and mouse 11 $\beta$ -HSD2 revealed significant differences in the C-terminal region and the substrate binding pocket. Exchange of the C-terminus and substitution of residues Leu170,Ile172 in mouse 11 $\beta$ -HSD2 by the corresponding residues His170,Glu172 of the human enzyme resulted in a gain of sensitivity to itraconazole and posaconazole, resembling human 11 $\beta$ -HSD2. The results provide an explanation for the observed species-specific 11 $\beta$ -HSD2 inhibition by the studied azole antifungals. The obtained structure-activity relationship information should facilitate future assessments of 11 $\beta$ -HSD2 inhibitors and aid choosing adequate animal models for efficacy and safety studies.

### 1. Introduction

11 $\beta$ -hydroxysteroid dehydrogenase type 2 (11 $\beta$ -HSD2) catalyzes the oxidation of potent 11 $\beta$ -hydroxyglucocorticoids (cortisol in human and fish, corticosterone in rodents) to inactive 11-ketoglucocorticoids (cortisone in human and fish, 11-dehydrocorticosterone in rodents). In mineralocorticoid target tissues such as kidney, colon, salivary and sweat glands, 11 $\beta$ -HSD2 has a gate-keeper function to regulate the access of cortisol to mineralocorticoid receptors (MR), thereby allowing specificity of aldosterone to activate MR (Edwards et al. 1988; Funder et al. 1988; Odermatt and Kratschmar 2012). By this mechanism, 11 $\beta$ -HSD2 has an important role in the regulation of the electrolyte balance.

Loss of function mutations in the gene encoding 11 $\beta$ -HSD2 lead to the syndrome of apparent mineralocorticoid excess (AME), caused by excessive MR activation by cortisol (Mune et al. 1995; Wilson et al. 1995; White et al. 1997). These patients suffer from pseudohyperaldosteronism with hypokalemia, hypernatremia, water retention and hypertension, with typically low renin and aldosterone levels along with increased plasma and urinary cortisol to cortisone ratios. Acquired forms of AME can be caused by the excessive consumption of licorice, containing the potent 11 $\beta$ -HSD inhibitor glycyrrhetic acid (GA) (reviewed in (Ferrari 2010)), and, as more recently reported, by the systemically administered azole antifungals posaconazole and itraconazole (Thompson et al., 2017; Barton et al. 2018; Boughton et al. 2018;

**Abbreviations:** 11 $\beta$ -HSD2, 11 $\beta$ -hydroxysteroid dehydrogenase type 2; AME, Apparent mineralocorticoid excess; C-terminal, Carboxy-terminal; GA, Glycyrrhetic acid; MR, Mineralocorticoid receptors; OHI, Hydroxyitraconazole; WT, Wild type.

\* Corresponding author.

*E-mail address:* Alex.Odermatt@unibas.ch (A. Odermatt).

<https://doi.org/10.1016/j.taap.2020.115387>

Received 22 October 2020; Received in revised form 11 December 2020; Accepted 23 December 2020

Available online 31 December 2020

0041-008X/© 2020 The Author(s). Published by Elsevier Inc. This is an open access article under the CC BY license (<http://creativecommons.org/licenses/by/4.0/>).



Hoffmann et al. 2018; Wassermann et al. 2018; Thompson et al., 2019).

11 $\beta$ -HSD2 is also highly expressed in the placenta, where it exerts a barrier function to protect the developing fetus from high maternal cortisol concentrations (Albiston et al. 1994; Stewart et al. 1995). Inhibition of placental 11 $\beta$ -HSD2 is associated with intra-uterine growth restriction and results in an increased risk for cardio-metabolic diseases in later life of the off-spring (Edwards et al. 1993; Lindsay et al. 1996; Seckl et al. 2000; Odermatt 2004). Given its important physiological functions, it is crucial to identify exogenous substances inhibiting 11 $\beta$ -HSD2 that might cause adverse health effects in human. Furthermore, 11 $\beta$ -HSD2 was recently found to be involved in oxysterol metabolism, with possible roles in the regulation of the immune system and in the control of cancer cell properties (Voisin et al. 2017; Raleigh et al. 2018; Beck et al. 2019a; Beck et al. 2019b). However, whether a disturbance of these functions contributes to the observed adverse health effects upon inhibition of 11 $\beta$ -HSD2 remains unknown.

Animal models are widely applied for efficacy and safety studies during the development and testing of novel drugs. However, the fact that the itraconazole- and posaconazole-induced pseudohyperaldosteronism remained undetected in preclinical investigations emphasizes the importance to understand species-specific differences as well as caution when trying to extrapolate findings from animal studies to human. The most frequently used animal species for preclinical toxicological studies is the rat, whereas the mouse is most widely used for mechanistic investigations, including transgenic lines. Additionally, the importance of zebrafish has gained considerable attraction due to the low cost and because experiments with larvae during the first 96 h are not considered as animal experiment (Planchart et al. 2016; Wrighton et al. 2019).

Rather few studies addressed species-specific differences in 11 $\beta$ -HSD2 so far. Nevertheless, *in vitro* studies showed potent inhibitory effects of the anabolic androgenic steroid fluoxymesterone (Fürstenberger et al. 2012) and of dithiocarbamates (Meyer et al. 2012) against human but not rodent or zebrafish 11 $\beta$ -HSD2, respectively. Furthermore, itraconazole and posaconazole were shown to be potent inhibitors of recombinant human 11 $\beta$ -HSD2 in *in vitro* experiments (Beck et al. 2017), whereas measurements performed in whole rat and mouse kidney homogenates suggested much weaker inhibitory effects in these species. However, in whole renal homogenates the compounds could have been metabolized and therefore no longer able to inhibit 11 $\beta$ -HSD2 activity, thus requiring a direct comparison of inhibitory effects on recombinant enzymes determined in the same cellular background. Nevertheless, no significant adverse effects were observed after inspection of endocrine parameters in preclinical rat studies following exposure to itraconazole (Van Cauteren et al. 1987). This suggests that due to species-differences rodents may not serve as suitable surrogate models to study effects on 11 $\beta$ -HSD2 in human.

The present study aimed to compare inhibitory potencies of posaconazole, itraconazole and its main metabolite hydroxyitraconazole (OHI) towards recombinant human, rat, mouse and zebrafish 11 $\beta$ -HSD2. A more detailed comparison then focused on the human and mouse enzyme. For this purpose, new homology models, molecular docking calculations as well as site-directed mutagenesis and enzyme activity assays with chimeric proteins were applied to elucidate the structure-function relationships of the species-specific differences in the mechanism of inhibition by the azole antifungals.

## 2. Material and methods

### 2.1. Chemicals and reagents

[1,2,6,7-<sup>3</sup>H]-cortisol was obtained from Perkin-Elmer (Boston, MA, USA) and hydroxyitraconazole (OHI) from Carbosynth (Berkshire, UK). All other chemicals were from Sigma-Aldrich (Buchs, Switzerland) if not stated otherwise.

### 2.2. Cell culture

Human embryonic kidney-293 cells (HEK-293) were purchased from ATCC (Manassas, VA, USA). Cells were cultured in Dulbecco's modified Eagle medium (DMEM) supplemented with 4.5 g/L glucose, 10% fetal bovine serum (S1810-500, Biowest, Nuaille, France), 100 U/mL penicillin, 0.1 mg/mL streptomycin, 10 mM HEPES buffer (pH 7.4) and 1% MEM non-essential amino acids (Bio Concept, Allschwil, Switzerland) at standard conditions (37 °C and humidified 5% CO<sub>2</sub>).

### 2.3. Molecular cloning

All chimeric proteins were designed to bear a C-terminal Flag-tag (DYKDDDDK) and were cloned into the pcDNA3.1 vector (Invitrogen, Carlsbad, CA, USA) (schematic overview of the chimera in Fig. 3). The chimera A (human 11 $\beta$ -HSD2 with mouse C-terminus), B (mouse 11 $\beta$ -HSD2 with human C-terminus), C (human 11 $\beta$ -HSD2 with mouse cassette) and D (mouse 11 $\beta$ -HSD2 with human cassette) were generated by a sequence overlap extension approach based on the human (Odermatt et al. 1999) or mouse 11 $\beta$ -HSD2 cDNA (NM\_008289.2 in pcDNA3.1 from GenScript, Piscataway Township, NJ, USA). The fragments were amplified with complementary overhangs of the cassette corresponding to residues 268–277 for human (5'-GAGTCAGTGA-GAAACGTGGGTCAGTGGGAA-3') and mouse 11 $\beta$ -HSD2 (5'-GATGCAGTGACTAATGTGAACCTCTGGGAG-3') (oligonucleotide primers used for amplification are shown in Suppl. Table 1). The two purified fragments containing the complementary overhangs were supplied in an equimolar ratio, followed by a PCR reaction using primers at the 5' and 3' end of the entire sequence for amplification. PCR reactions were carried out using iProof™ High-Fidelity DNA polymerase (Bio-rad, Hercules, CA, USA). The final PCR product was digested with Hind-III HF and Kpn-I HF (New England Biolabs, NEB, Ipswich, MA, USA) and ligated into pcDNA3 by T4 ligase (NEB).

Chimera E (human 11 $\beta$ -HSD2 with His170Leu, Glu172Ile) and G (chimera A with His170Leu, Glu172Ile) were obtained by site directed mutagenesis using Pfu polymerase (NEB) and TaKaRa PrimeSTAR GXL polymerase (Takara Bio Inc., Kusatsu, Japan). Oligonucleotide primers were designed to achieve a circular nicked PCR-product. Template DNA was removed by a Dpn I digest (NEB), and the PCR product was transformed into competent bacterial cells for amplification. Chimera F (mouse 11 $\beta$ -HSD2 bearing mutations Leu170His, Ile172Glu) and H (chimera B with mutations Leu170His, Ile172Glu) were generated utilizing iProof™ High-Fidelity DNA polymerase, resulting in a linear unphosphorylated PCR-product. To facilitate re-circularization, the 5'-ends were phosphorylated by T4 polynucleotide kinase (NEB) prior to ligation by T4 ligase. After Dpn I digest, the clones were transformed into competent bacterial cells. Sequences were verified by Sanger sequencing (Microsynth, Balgach, Switzerland).

### 2.4. Determination of the inhibition of wild type and mutant 11 $\beta$ -HSD2 activity by azole antifungals

HEK-293 cells ( $2 \times 10^6$  cells per 10 cm cell culture dish) were incubated for 24 h and transiently transfected with plasmids encoding mouse (NM\_008289.2), rat (NM\_017081.2) or zebrafish 11 $\beta$ -HSD2 (NM\_212720.2), or with chimera A-H, using the calcium precipitation method. All constructs were C-terminally flag epitope tagged and cloned into pcDNA3. At 48 h post-transfection, the cells were washed with PBS, collected in 2 mL ice-cold PBS per 10 cm dish, aliquoted (200  $\mu$ L or 400  $\mu$ L) and centrifuged at 4 °C for 4 min at  $16,000 \times g$ . Subsequently, supernatants were discarded, pellets shock-frozen and stored at  $-80$  °C. For the analysis of human 11 $\beta$ -HSD2 activity, HEK-293 cells stably expressing 11 $\beta$ -HSD2 (AT8 clone) were utilized as described earlier (Inderbinen et al., 2020). Cell pellets were suspended in 400  $\mu$ L TS2 buffer (NaCl 100 mM, EGTA 1 mM, EDTA 1 mM, MgCl<sub>2</sub> 1 mM, sucrose 250 mM, Tris-HCl 20 mM, pH 7.4) and lysed by sonication (UP50H

sonicator, Hielscher Ultrasonics). Conditions for each batch of cell pellets were optimized to reach 20–30% substrate to product conversion rate. Lysates were incubated with test substances or vehicle control (DMSO), 50 nM cortisol (containing 10 nCi of [1,2,6,7-<sup>3</sup>H] cortisol) and 500  $\mu$ M NAD<sup>+</sup> in a total volume of 22  $\mu$ L TS2 buffer at 37 °C. The DMSO concentration was kept below 1.2%. At this concentration the solvent did not affect enzyme activity. After 10 min (human, chimera B) or 20 min (mouse, rat, zebrafish, chimera A, C, D, E, F and H), reactions were stopped by adding excess amounts of unlabeled cortisone and cortisol in methanol (1:1, 2 mM each). Samples were separated by thin-layer chromatography (mobile phase chloroform/methanol; 9:1), dissolved in scintillation cocktail (IRGASAFE Plus, Zinsser Analytic, Frankfurt am Main, Germany) and radioactivity was measured by liquid scintillation counting (Packard, Connecticut, USA). Experiments were repeated at least three times independently and data were normalized to vehicle control.

### 2.5. Homology model and docking

As there is no crystal structure of 11 $\beta$ -HSD2 available to date, the modeling study aiming at explaining the mechanism of inhibition of the human and mouse enzyme variants was initiated with homology modeling using the SwissModel homology modeling platform (<https://swissmodel.expasy.org>). The primary FASTA sequence of human 11 $\beta$ -HSD2 was used as input to the SwissModel web-server. Up to thirty homology models were built based on templates identified by sequence similarity to existing proteins.

Eight homology models were built using template structures of 17 $\beta$ -HSD1 (various PDB IDs), twenty models were based on the template structure of 11 $\beta$ -HSD1 (various PDB IDs), one model on the template structure of 3-oxoacyl-[acyl-carrier-protein] reductase (PDB ID: 3u9l) and finally one on the template structure of a putative short chain dehydrogenase (PDB ID: 5u4s).

Visual inspection of eight models based on template structures of 17 $\beta$ -HSD1 yielded no satisfactory model with respect to the placement of both the substrate and cofactor NAD<sup>+</sup> and the dehydrogenation reaction that the enzyme is supposed to catalyze (at position 11). The assumed pose of the cofactor within the active site was found to interfere with backbone elements of the built homology models, rendering them unsuitable for further processing. This is in contrast with a previous study that, however, used a complex multi-step refinement and optimization procedure to obtain a valid putative model (Yau et al. 2017).

Therefore, we focused on twenty homology models based on the template structure of 11 $\beta$ -HSD1, *i.e.* the closest relative in this enzyme family. Their Global Model Quality Estimation (GMQE) scores did not differ substantially from those of the 17 $\beta$ -HSD1 based models (0.40 vs 0.44 for the best scored models). Both cofactor (NAD<sup>+</sup>) and substrate (cortisol) poses were reconstructed by a rigid body transfer and subsequent structure modification from the 11 $\beta$ -HSD1 structure with the PDB ID 1y5r (cofactor, NADPH; ligand, corticosterone) after protein alignment. Most of the 11 $\beta$ -HSD-based models did not show any unfavorable steric backbone clashes with the assumed cofactor pose and allowed placing of the natural substrate into the active site. In analogy to human 11 $\beta$ -HSD2 models, we built thirty homology models using the mouse FASTA sequence. For both species, homology models based on guinea pig 11 $\beta$ -HSD1 (PDB ID: 3g49) revealed the most reliable models that were utilized for further investigations.

The structure-activity relationships-conform binding modes of the natural substrate cortisol at both human and mouse homology models were found by manual docking. As mentioned earlier, the corticosterone pose relative to the nicotinamide moiety of NAD<sup>+</sup> and key catalytic residues Tyr232 and Ser219, as it occurs in homologous 11 $\beta$ -HSD1 structure with PDB ID 1y5r, was used as a reference starting point. The 17 $\alpha$ -hydroxy group was added, turning corticosterone to cortisol, and together with the hydroxymethylcarbonyl group at position 17 $\beta$  oriented for the most optimal interaction with the nearby backbone,

cofactor and side-chain (in this order of preference) H-bond donors and acceptors. As the C-terminal part of 11 $\beta$ -HSD2 interacting with azole fungicides could not be sufficiently resolved in homology modeling, only the 1-(butan-2-yl)-4-phenyl-4,5-dihydro-1H-1,2,4-triazol-5-one part of itraconazole responsible for the sensitivity towards 11 $\beta$ -HSD2 was manually docked. The binding mode was constructed by satisfying the carbonyl H-bond acceptor with a properly directional hydrogen bond donor from Tyr232 while paying attention to minimizing the steric clashes with the other residues in the active site. The manual docking was performed in Maestro modeling environment (Maestro, version 10.4, Schrödinger, LLC, New York, NY, 2015). Protein Preparation Wizard minimizer routine with OPLS\_2005 force field was used to relax manually constructed protein-ligand complexes and Maestro was used for visualization (Sastry et al. 2013).

### 2.6. Statistical analysis

Data were analyzed using two-way ANOVA with Bonferroni's *post hoc* tests in the GraphPad Prism 5 software. Values represent mean  $\pm$  SD.

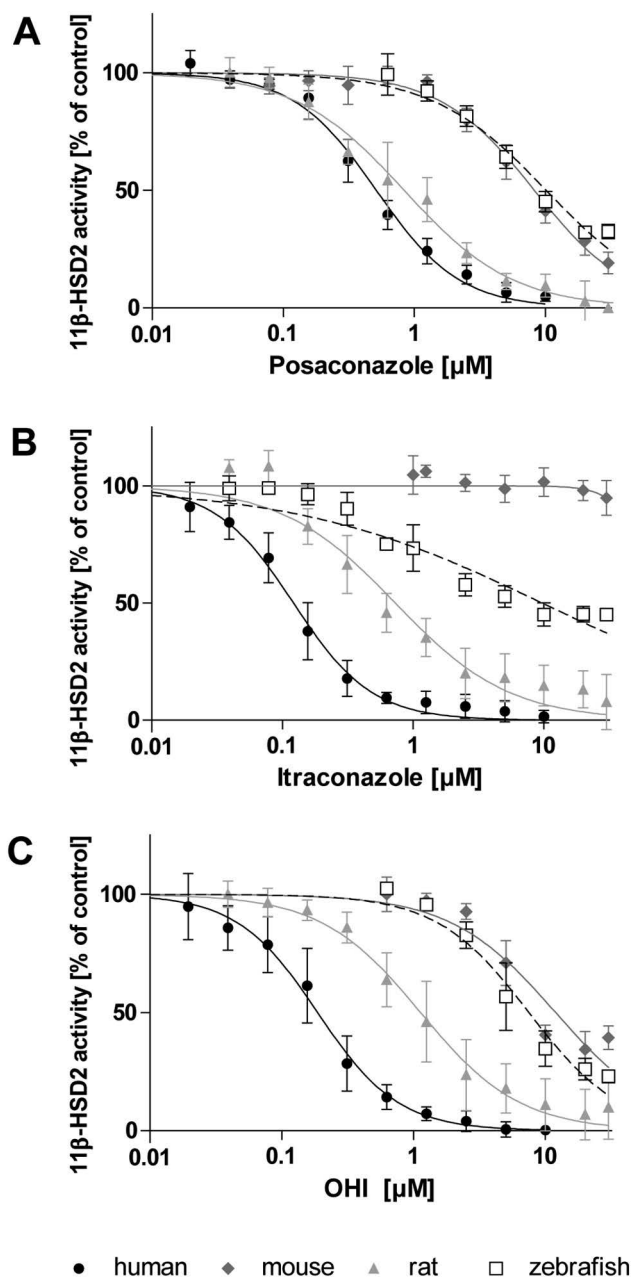
## 3. Results

### 3.1. Species-specific differences in the inhibition of 11 $\beta$ -HSD2 by posaconazole, itraconazole and OHI

The posaconazole-, itraconazole- and OHI-dependent inhibition of cortisol oxidation by 11 $\beta$ -HSD2 from the four different species human, mouse, rat and zebrafish was determined in lysates of HEK-293 cells expressing recombinant enzyme (Fig. 1, Table 1). Itraconazole, OHI and posaconazole potently inhibited the human enzyme, with IC<sub>50</sub> values of 121  $\pm$  30, 187  $\pm$  56 and 512  $\pm$  79 nM, respectively. Itraconazole and OHI were approximately 6-fold less active towards the rat enzyme, whereas posaconazole was only 1.6-fold less active. In contrast, all three azole antifungals showed only very weak inhibitory effects towards mouse and zebrafish 11 $\beta$ -HSD2, with IC<sub>50</sub> values above 7  $\mu$ M.

### 3.2. Comparison of human, mouse, rat and zebrafish 11 $\beta$ -HSD2 protein sequences

To begin to understand which regions of the sequence are responsible for the observed species-specific differences in 11 $\beta$ -HSD2 inhibition by the azole antifungals, the protein sequences of human, mouse, rat and zebrafish 11 $\beta$ -HSD2 were aligned (Fig. 2). The justbio (justbio.com) alignment tool was utilized to analyze protein sequences (human: NP\_000187.3; mouse: NP\_032315.2; rat: NP\_058777.1; zebrafish: NP\_997885). The catalytic triad Ser219, Tyr232 and Lys236, the cofactor-binding site in the Rossmann-fold (Gly89-X-X-X-Gly93-X-Gly95) and most of the  $\alpha$ -helices and  $\beta$ -sheets are conserved among the four species. As expected, human 11 $\beta$ -HSD2 shares higher sequence similarities with mouse and rat enzymes than with that of the zebrafish. Significant differences were detected in the C-terminal regions. The mouse enzyme is 19 amino acids shorter than its human counterpart, while the rat C-terminus is more similar to that of the human enzyme. Thus, we hypothesized that the variable C-terminal region could be responsible for the differences in the inhibition of human and mouse 11 $\beta$ -HSD2 by the investigated azole fungicides. Previous predictions using rigid homology models of the human and mouse enzyme suggested a different orientation of Trp276 that would cause steric hindrance in the mouse enzyme and prevent binding of posaconazole, itraconazole and OHI (Beck et al. 2017). Additionally, Arg279 was proposed to stabilize the binding of itraconazole and OHI in the human enzyme but not in mouse 11 $\beta$ -HSD2, where this residue did not seem to form interactions with the investigated azole fungicides (Beck et al. 2017; Beck et al. 2020a). Interestingly, Trp276 and Arg279 are both conserved in human and mouse 11 $\beta$ -HSD2. Nevertheless, a closer inspection of the sequence upstream of these two amino acids led to the



**Fig. 1.** Inhibition of human, mouse, rat and zebrafish 11β-HSD2 activity. Lysates of HEK-293 cells expressing recombinant 11β-HSD2 of the respective species were incubated for 10 min (human) or 20 min (mouse, rat, zebrafish) in the presence of 50 nM cortisol, 500 μM NAD<sup>+</sup> and increasing concentrations of posaconazole (A), itraconazole (B) or OHI (C). Substrate conversion was normalized to that of the vehicle control (DMSO; 0.3% for posaconazole, 0.6% for itraconazole and 1.2% for OHI). Inhibition curves were fitted and analyzed by non-linear regression. Data shown are from at least three independent experiments and represent mean ± SD.

hypothesis that the rather bulky amino acids Arg271 and Gln275 in human compared to Thr271 and Leu275 in mouse 11β-HSD2 might result in a different orientation of Trp276 and Arg279 in the two species. Thus, in a next step, the species difference between human and mouse 11β-HSD2 was investigated by site-directed mutagenesis and generation of chimeric proteins.

**Table 1**

IC<sub>50</sub> values for human, mouse, rat and zebrafish 11β-HSD2 of posaconazole, itraconazole and OHI. 11β-HSD2 activity was determined in lysates of HEK-293 cells expressing the recombinant enzyme of the respective species. The conversion of cortisol to cortisone was measured in the presence of increasing concentrations of inhibitor. Inhibition curves were fitted and analyzed by non-linear regression. Data were normalized to vehicle control and represent mean ± SD of at least three independent experiments. \* % remaining activity at the highest concentration of 30 μM.

	Inhibition of 11β-HSD2 activity: IC <sub>50</sub> [μM]			
	Human	Mouse	Rat	Zebrafish
Posaconazole	0.512 ± 0.079	8.21 ± 0.56	0.835 ± 0.142	10.1 ± 0.5
Itraconazole	0.121 ± 0.030	(95%)*	0.729 ± 0.592	9.80 ± 1.96
OHI	0.187 ± 0.056	11.9 ± 2.5	1.13 ± 0.96	7.48 ± 1.68

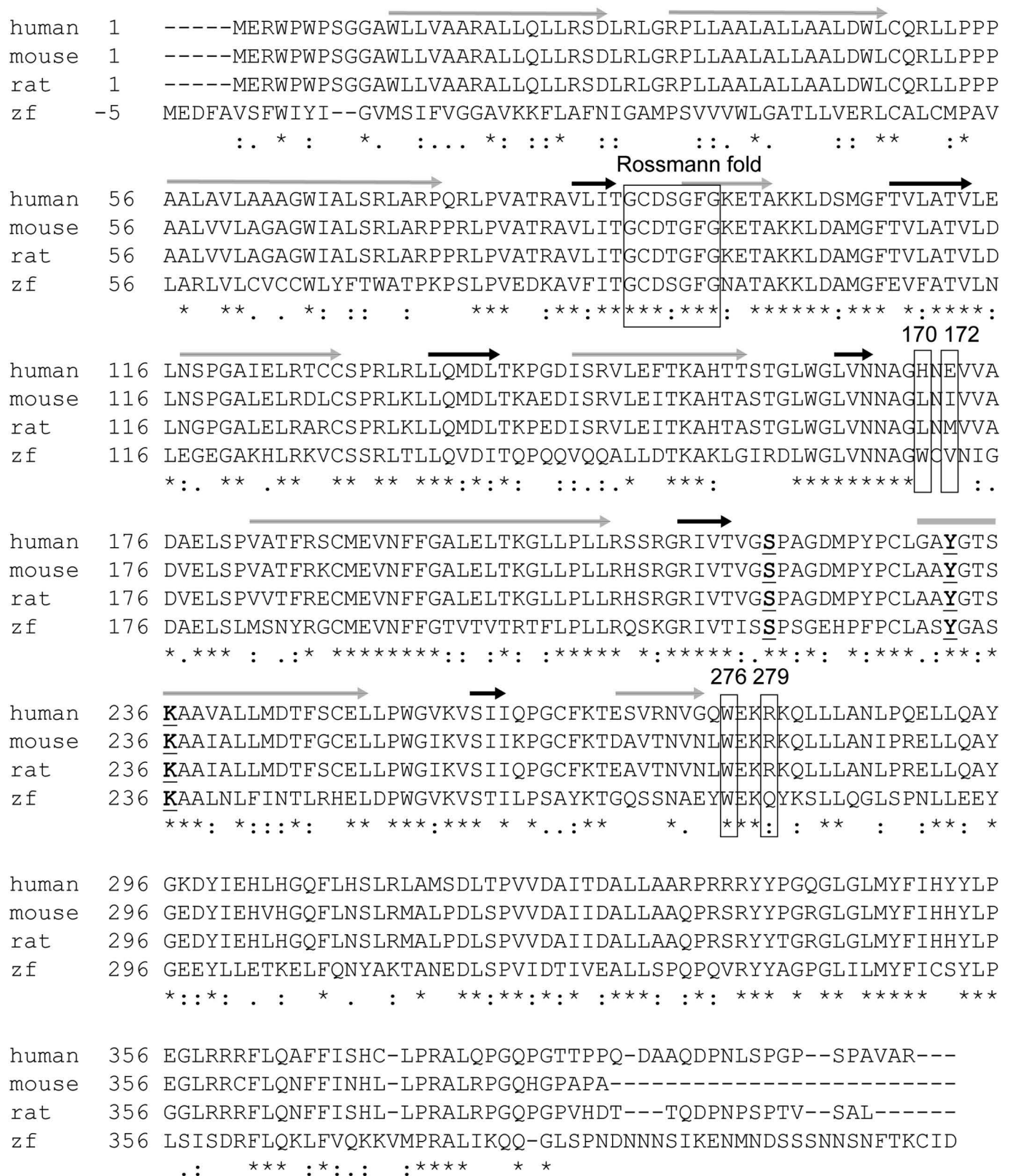
### 3.3. The role of the C-terminal region and of residues 268–277 on the inhibition of human and mouse 11β-HSD2 by azole fungicides

Four different chimera were constructed to investigate the role of the C-terminus in the different response of human and mouse 11β-HSD2 to the azole antifungals (Fig. 3A). Chimera A contains the sequence of human 11β-HSD2 up to residue 268, followed by the mouse C-terminus. Chimera B represents the complementary construct with the mouse sequence up to position 268, followed by the human C-terminus. To investigate the impact of the amino acids 268–277 on the orientation of Trp276 and Arg279, this cassette of 8 amino acids was exchanged between human and mouse, resulting in chimera C (human enzyme with the mouse cassette) and D (mouse enzyme with the human cassette). These chimeric proteins were expressed similar to the wild type enzymes and able to convert cortisol to cortisone (Suppl. Fig. 1).

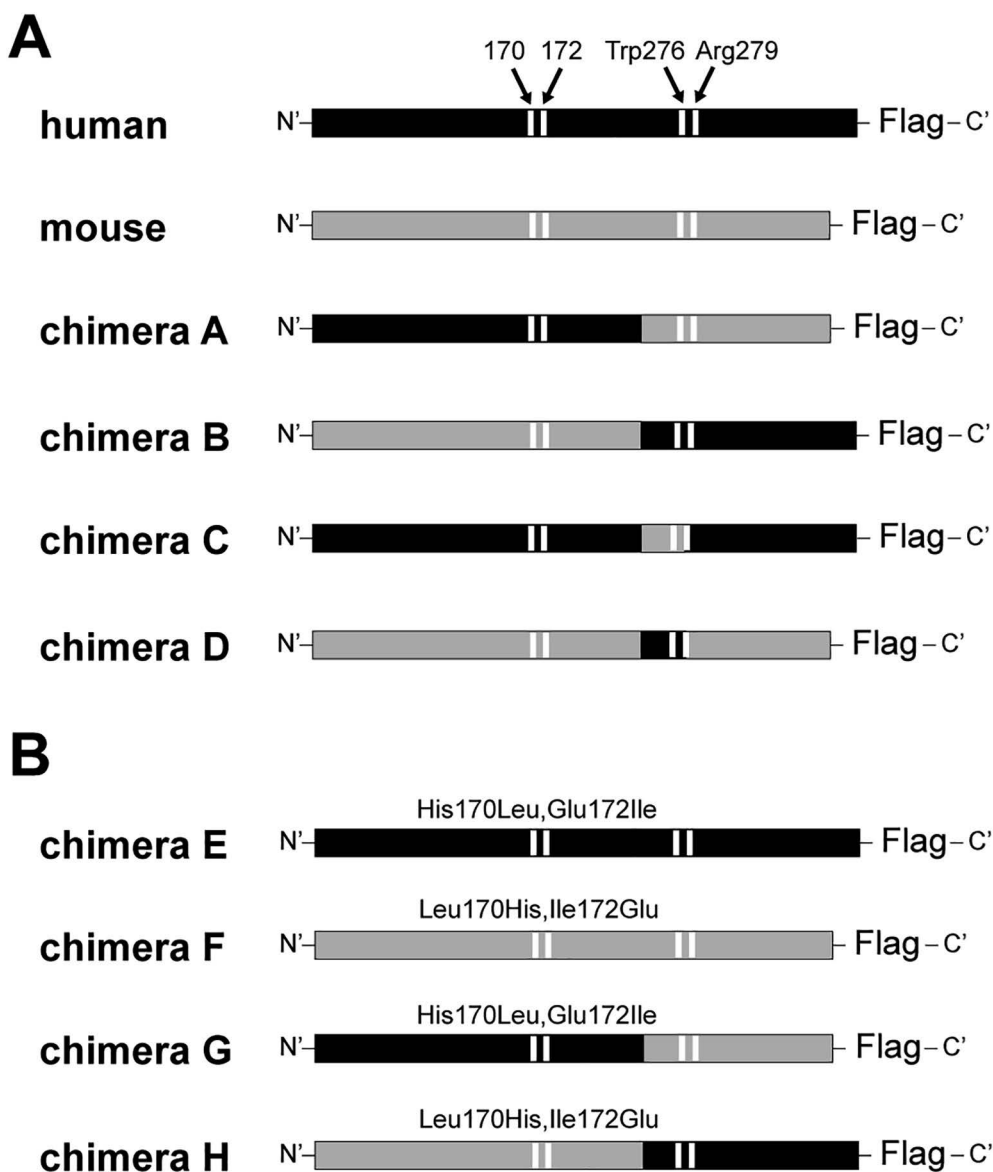
We hypothesized that chimera A and C would show a loss of inhibition by the azole fungicides compared to human 11β-HSD2 and that chimera B and D would show a gain of inhibitory effect compared to the mouse enzyme. Therefore, lysates of HEK-293 cells expressing the respective protein were subjected to enzyme activity assays in the absence and presence of 1 μM or 10 μM of the indicated azole fungicide (Fig. 4). Substitution of the human C-terminal region by that of the mouse enzyme in chimera A significantly decreased the inhibitory effect of the tested azole fungicides (Fig. 4). The analogous substitution, *i.e.* mouse enzyme bearing the human C-terminal region (chimera B), resulted in a trend to increased sensitivity towards itraconazole but not towards posaconazole or OHI (Figure 4). Substitution of the human sequence upstream of Trp276 by the corresponding mouse cassette (chimera C) as well as the analogous exchange in the mouse enzyme (chimera D) did not affect the azole fungicide-mediated inhibition (data not shown).

### 3.4. Use of homology models to study differences between human and mouse 11β-HSD2

Due to the limitations of previously used rigid homology models, more flexible models of human and mouse 11β-HSD2 were developed to study further species-specific differences. The new models both predicted comparable hydrogen bonds between Ser219 and Tyr232 with the C11-hydroxyl on cortisol and the cofactor, essential for catalytic activity (Fig. 5, Video 1 and Video 2). Additionally, Tyr226 forms a hydrogen bond with the C3-carbonyl on cortisol, and the C21-hydroxyl on cortisol forms a hydrogen bond with NAD<sup>+</sup> in both species. Predicted differences include hydrogen bonds between Gln342 and the C3-carbonyl on cortisol as well as between NAD<sup>+</sup> and Ser269 in human 11β-HSD2 that are both absent in the mouse enzyme. Furthermore, Ser269 forms a hydrogen bond with the C17-hydroxyl on cortisol, while the mouse enzyme has an alanine at this position. Notably, the new models predicted differences in the orientation and interactions of the loop consisting of residues 168–180 that are lining the active site. A



**Fig. 2.** Alignment of human, mouse, rat and zebrafish 11 $\beta$ -HSD2 protein sequences. Symbols are coded as followed: grey arrow,  $\alpha$ -helix; black arrow,  $\beta$ -sheets; rectangles, cofactor-binding site in the Rossmann-fold, and positions 170, 172, 276 and 279; underlined and bold letter, active site; (\*), fully conserved residues; (:), residues with considerably similar properties; (.), residues with moderately similar properties.



**Fig. 3.** Schematic representation of the cloned 11 $\beta$ -HSD2 mutants. Human sequence is indicated in black, mouse sequence in grey and the positions 170, 172, 276 and 279 are represented by white bars. All sequences were cloned into pcDNA3 and carry a C-terminal FLAG-tag.

closer look in human 11 $\beta$ -HSD2 on the binding site region in the vicinity of the steroid substrate D-ring, dictating selectivity to cortisol, indicated that the loop portion around histidine residue 170 (His170) could be responsible for interspecies differences in the enzyme selectivity. Optimization of a human homology model built on the guinea pig 11 $\beta$ -HSD1 (PDB ID: 3g49) template showed that His170 offers an ideal hydrogen bonding interaction to the cortisol C20 carbonyl (Fig. 5A, Video 1). Due to the particular pKa properties of His170, it may also provide positive charge for compensating the negative charge of the cofactor's phosphate groups. Furthermore, the human 11 $\beta$ -HSD2 model bears a charged glutamic acid at position 172 (Glu172) in close proximity to His170. Even though Glu172 is not directly involved in substrate binding, it may influence the structure of the protein considerably due to its charge and positioning preference towards the solvent. Interestingly, Glu172 was proposed earlier to interact with Leu179 and disruption of the stabilization of a flexible turn in the AME causing mutant Leu179Arg may contribute to the observed loss of function (Yau et al. 2017).

In contrast, the active site loop (residues 168–180) of mouse 11 $\beta$ -HSD2 contains more lipophilic residues (Leu170, Ile172) compared to the human structure (Fig. 5B, Video 2). These two lipophilic residues

were predicted to hide from the solvent into the interior of the active site cavity, causing substantial reshaping of the backbone path in the area critical for substrate binding and slightly limiting the accessibility of the pocket. This still allowed binding of endogenous substances like cortisol, but bulky compounds like itraconazole, OHI and posaconazole (Suppl. Fig. 2) may experience less favorable interactions in the mouse compared to the human enzyme. For the reasons described above, we aimed to investigate to which extent the residues at position 170 and 172 are involved in the observed species-dependent 11 $\beta$ -HSD2 inhibition by the studied azole antifungals.

### 3.5. Effect of residues at positions 170 and 172 on the inhibition of human and mouse 11 $\beta$ -HSD2 by azole fungicides

To test the relevance of the residues at positions 170 and 172 for the azole fungicide-dependent inhibition of human 11 $\beta$ -HSD2, His170 and Glu172 were mutated to the respective residues in mouse 11 $\beta$ -HSD2 (Leu170, Ile172) in human wild type 11 $\beta$ -HSD2 (chimera E) or in the human enzyme bearing the mouse C-terminal region (chimera G) (Fig. 3B). The analogous exchange in mouse wild type (chimera F) and

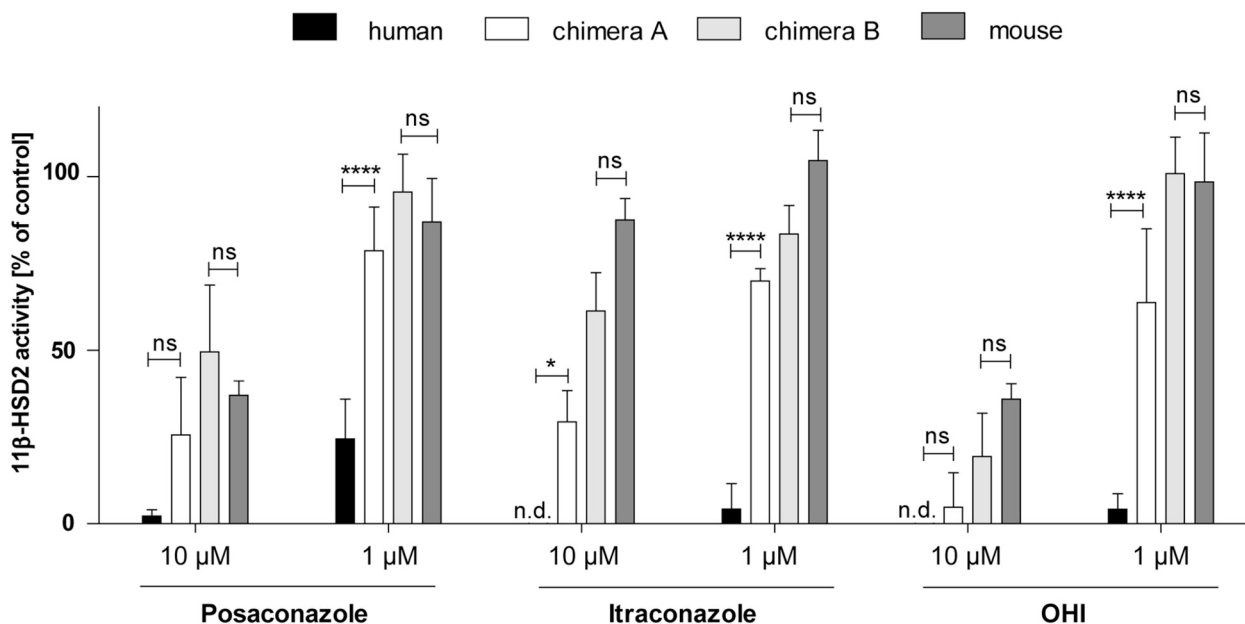


Fig. 4. Effect of the substitution of the C-terminal region of human and mouse 11 $\beta$ -HSD2 on azole fungicide-mediated inhibition. Lysates of HEK-293 cells expressing the indicated 11 $\beta$ -HSD2 construct were incubated for 10 min (human, chimera B) or 20 min (mouse, chimera A) with 50 nM cortisol, 500  $\mu$ M NAD<sup>+</sup> and 1  $\mu$ M or 10  $\mu$ M of test substances. Substrate conversion was normalized to vehicle control (0.4% DMSO). Data from three independent experiments represent mean  $\pm$  SD. Two-way ANOVA with Bonferroni's *post hoc* test, *p* values: \* < 0.05, \*\*\*\* < 0.0001 and ns (not significant), n.d. (not detected).

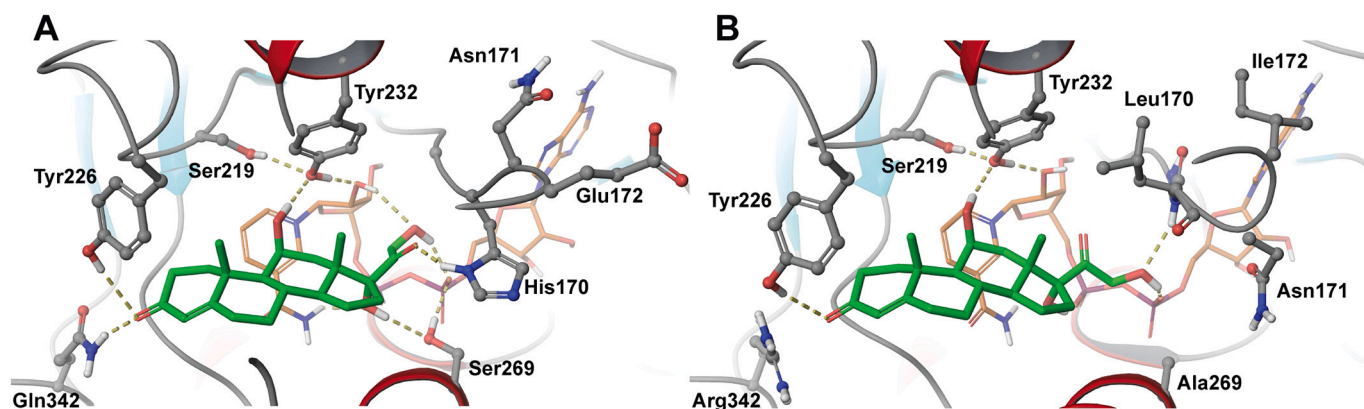


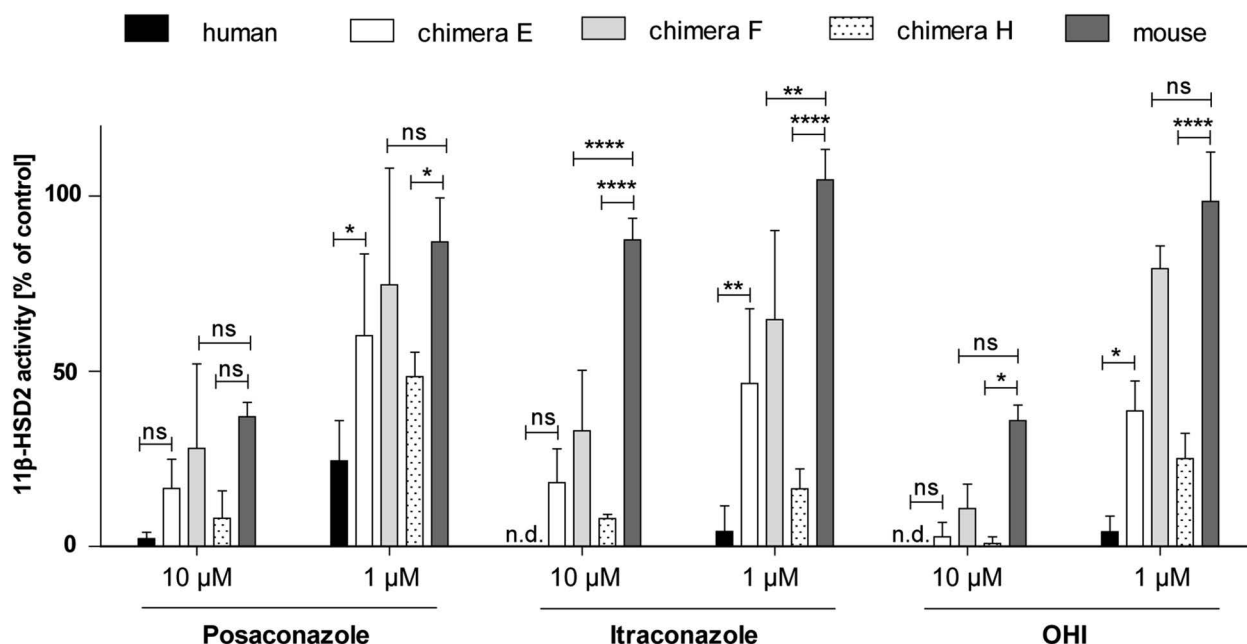
Fig. 5. Predicted binding of cortisol (green) and NAD<sup>+</sup> (orange) to 11 $\beta$ -HSD2. A) human and B) mouse 11 $\beta$ -HSD2 homology models. Dashed yellow lines indicate relevant hydrogen bond interactions (fulfilling directionality and distance criteria <2.8 Å) for protein-ligand binding. (For interpretation of the references to colour in this figure legend, the reader is referred to the web version of this article.)

mouse 11 $\beta$ -HSD2 bearing the human C-terminus (chimera H) were constructed as well. The chimeric enzymes were well expressed and active in intact HEK-293 cells, except of chimera G that seemed to be unstable as indicated by its reduced expression following detection by western blot and based on the loss of enzyme activity in assays using lysates of HEK-293 cells transiently expressing chimera G (Supp. Fig. 1).

Human 11 $\beta$ -HSD2 with the substitution His170Leu, Glu172Ile (chimera E) displayed significantly decreased inhibition by the three azole fungicides tested at 1  $\mu$ M (Fig. 6). The analogous mutation Leu170His, Ile172Glu in the murine enzyme (chimera F) significantly increased and tended to increase the sensitivity towards itraconazole and OHI, respectively. In contrast, chimera F and mouse 11 $\beta$ -HSD2 were similarly inhibited by posaconazole. Importantly, replacing the C-terminal region in the mouse sequence by that from human and introducing substitutions Leu170His, Ile172Glu (chimera H) changed the inhibition pattern for the three azole antifungals almost to that of the human enzyme (Fig. 6). Unfortunately, the combination of replacing the C-terminus of the human enzyme by that of the mouse and introducing

substitutions His170Leu, Glu172Ile (chimera G), was not stable and could thus not be tested.

Next, concentration-dependence curves were determined for the most potent 11 $\beta$ -HSD2 inhibitor, itraconazole (Fig. 7). Whilst an IC<sub>50</sub> of itraconazole for human 11 $\beta$ -HSD2 of 121  $\pm$  30 nM was obtained, a more than 15-fold weaker inhibition (2.17  $\pm$  1.66  $\mu$ M) was determined for chimera E carrying the His170Leu, Glu172Ile substitution (Table 2). Exchange of the human C-terminus by that of the mouse (chimera A) decreased the inhibitory potency of itraconazole by a factor of 30 (IC<sub>50</sub> value of 3.55  $\pm$  1.81  $\mu$ M). The combination of C-terminus exchange and His170Leu, Glu172Ile substitution could not be assessed due to the instability of chimera G. The murine enzyme showed a residual activity of about 95% at the highest itraconazole concentration tested (30  $\mu$ M) and an IC<sub>50</sub> value could not be determined. Regarding mouse 11 $\beta$ -HSD2, a gain of sensitivity towards inhibitory effect of itraconazole could be observed by replacing the C-terminal region by that from human (chimera B, 58% residual enzyme activity at 30  $\mu$ M) or by introducing the substitution Leu170His, Ile172Glu (chimera F) (IC<sub>50</sub> value of 6.34  $\pm$



**Fig. 6.** Comparison of the posaconazole-, itraconazole- and OHI-dependent inhibition of human and mouse 11 $\beta$ -HSD2 with that of chimera E, F and H. Lysates of HEK-293 cells expressing recombinant 11 $\beta$ -HSD2 of the indicated species or the respective chimera were incubated for 10 min (human) or 20 min (mouse, chimeras) with 50 nM cortisol, 500  $\mu$ M NAD<sup>+</sup> and 1  $\mu$ M or 10  $\mu$ M of the test compounds. Substrate conversion was normalized to that of the vehicle control (0.4% DMSO). Data represent mean  $\pm$  SD from three independent experiments. Data were analyzed by two-way ANOVA with Bonferroni's *post hoc* test. *P* values: \* < 0.05, \*\* < 0.01, \*\*\*\* < 0.0001 and ns (not significant), n.d. (not detected).

3.83  $\mu$ M). Most importantly, exchange of the mouse C-terminus by that of the human enzyme in combination with the substitution Leu170His, Ile172Glu (chimera H), displayed a humanized phenotype, with an IC<sub>50</sub> value of 561  $\pm$  85 nM. Similar results were found for posaconazole (Fig. 7 and Table 2): the IC<sub>50</sub> for chimera B and F were about two and three times lower than for the mouse enzyme, respectively. Substitution Leu170His, Ile172Glu in combination with the introduction of the human C-terminus (chimera H) further reduced the IC<sub>50</sub>. Moreover, posaconazole was about three times less effective to inhibit chimera E and approximately 7-fold less potent to inhibit chimera A compared to the human enzyme.

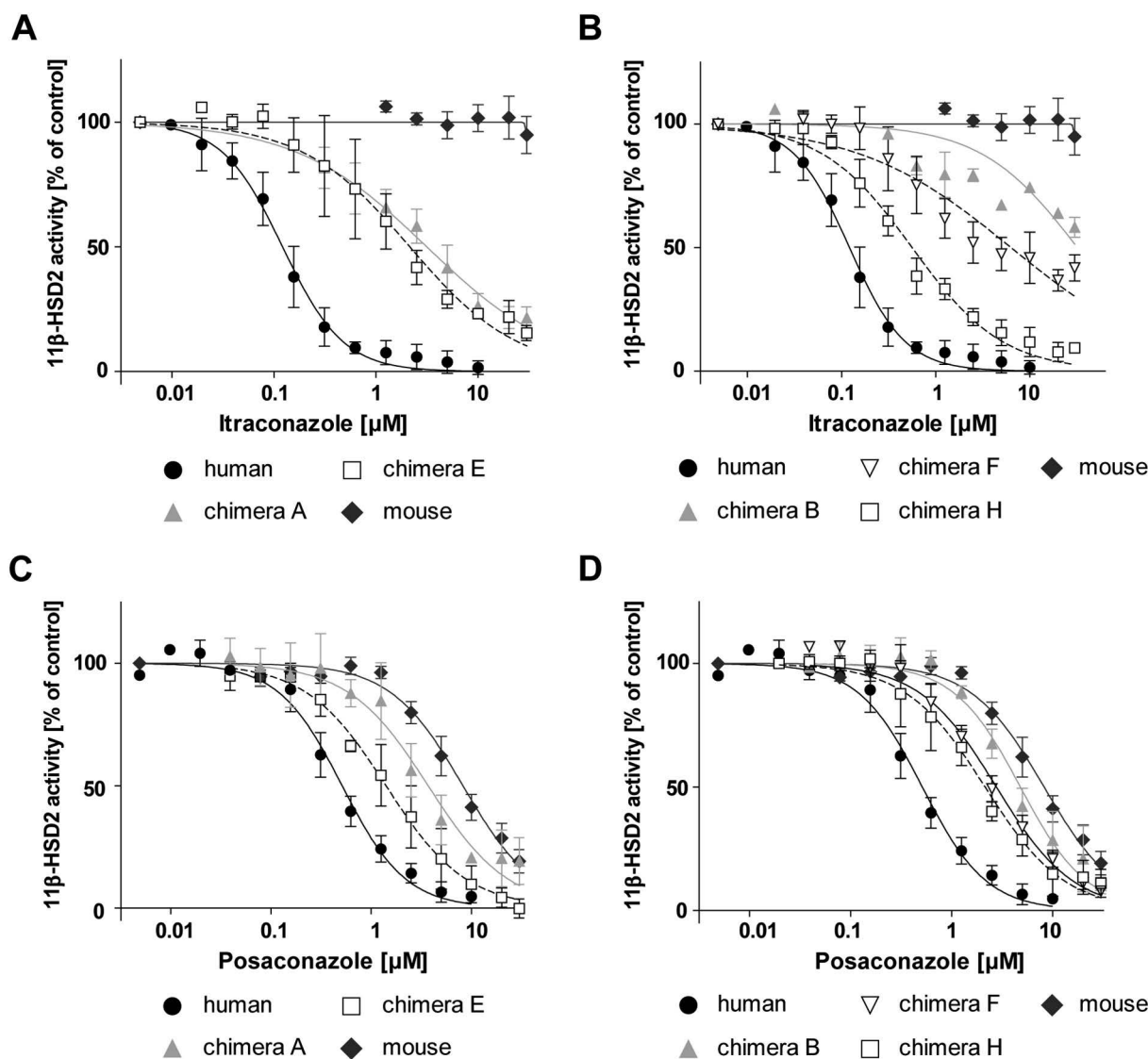
#### 4. Discussion

Recent clinical studies and case reports evidenced that the systemically used azole antifungals posaconazole and itraconazole can cause pseudohyperaldosteronism (reviewed in (Beck et al. 2020b)). Two distinct mechanisms were proposed, namely inhibition of the adrenal cortisol synthesis by CYP11B1, which seems to be the predominant mechanism for posaconazole (Barton et al. 2018; Boughton et al. 2018; Kuriakose et al. 2018; Beck et al. 2020a), and inhibition of cortisol inactivation by 11 $\beta$ -HSD2 in the kidney and colon, which seems to be the predominant mode-of-action for itraconazole (Hoffmann et al. 2018; Beck et al. 2020b). These adverse effects have only recently been recognized in patients, mainly in those reaching high serum drug levels, and they have remained unrecognized in preclinical investigations.

The present study revealed considerable species-specific differences in the inhibition of 11 $\beta$ -HSD2 by posaconazole, itraconazole and its main metabolite OHI. Regarding posaconazole, a very moderate difference of only 1.6-fold lower inhibitory activity was found against rat compared to human 11 $\beta$ -HSD2, in line with a previous estimation based on a comparison of human recombinant enzyme with whole rat kidney homogenate (Beck et al. 2017). Earlier toxicological studies in rats on the safety of posaconazole reported effects at high dose that were related to inhibition of steroid hormone synthesis; however, no information was provided on the underlying mechanism and typical symptoms of

pseudohyperaldosteronism were not declared (European Medicines Agency 2019). Compared to posaconazole, itraconazole is a more potent inhibitor of human 11 $\beta$ -HSD2 (Beck et al. 2017). However, both itraconazole and its major metabolite OHI only moderately inhibited rat 11 $\beta$ -HSD2, in line with the previous preliminary assessment comparing human recombinant enzyme with whole rat kidney homogenate (Beck et al. 2017). This earlier experiment could not exclude a degradation of itraconazole and OHI by renal drug metabolizing enzymes, thus the present comparison of recombinant enzymes of the different species in an identical cellular background was needed. Interestingly, preclinical repeated-dose toxicity studies in rats assessing the safety of itraconazole did not detect any significant alterations of endocrine parameters (Van Cauteren et al. 1987). The lower sensitivity of rat compared to human 11 $\beta$ -HSD2 towards posaconazole and itraconazole may explain, at least in part, why pseudohyperaldosteronism as an adverse drug reaction has not been recognized in rodent preclinical studies. However, the difference in the inhibitory potency, especially of posaconazole, between rat and human 11 $\beta$ -HSD2 is very moderate and the reason why preclinical studies in rats did not reveal more pronounced effects on blood pressure and blood electrolytes are not fully understood. Further research should evaluate inter-individual as well as inter-species drug bioavailability. Regarding posaconazole, a recent study reported pseudohyperaldosteronism in only 20–25% of treated patients that also reached high serum concentrations (Nguyen et al. 2020). If rats exhibit a higher capacity to metabolize posaconazole and itraconazole than humans or if they have increased activity of efflux proteins, sufficiently high drug levels to inhibit 11 $\beta$ -HSD2 may not be reached in this species at the site of the target, *i.e.* kidney and adrenals. Both posaconazole and itraconazole also inhibit human CYP11B1 and CYP11B2; however, their inhibitory effects towards the rat enzymes remains to be determined. A lower inhibitory activity of these two azole antifungals towards rat CYP11B1 could also contribute to a lower risk for pseudohyperaldosteronism.

Blood pressure and blood electrolyte are usually measured in pre-clinical and clinical studies. If altered, pseudohyperaldosteronism could be detected by determination of serum renin and aldosterone. In case of low renin and aldosterone, further steroid analysis is indicated.



**Fig. 7.** Concentration-dependent inhibition of 11 $\beta$ -HSD2 variants by itraconazole and posaconazole. Lysates of HEK-293 cells expressing recombinant 11 $\beta$ -HSD2 of the indicated species or the respective chimera were incubated for 10 min (human, chimera B) or 20 min (mouse, chimera A, E, F, H) with 50 nM radiolabeled cortisol, 500  $\mu$ M NAD<sup>+</sup> and increasing concentrations of itraconazole (A, B) and posaconazole (C, D). Substrate conversion was normalized to that of the vehicle control (0.6% DMSO for itraconazole and 0.3% DMSO for posaconazole). Data from three independent experiments are shown as mean  $\pm$  SD.

**Table 2**

IC<sub>50</sub> values for human and mouse 11 $\beta$ -HSD2 as well as for chimera A, B, E, F and H for itraconazole and posaconazole. 11 $\beta$ -HSD2 activity was determined in lysates of HEK-293 cells expressing the indicated 11 $\beta$ -HSD2 variant, measuring the conversion of cortisol to cortisone in presence of increasing concentrations of inhibitor. Inhibition curves were fitted and analyzed by non-linear regression. Data were normalized to vehicle control and represent mean  $\pm$  SD of at three independent experiments. \* % remaining activity at highest concentration of 30  $\mu$ M.

		IC <sub>50</sub> [ $\mu$ M]	
		Itraconazole	Posaconazole
Human		0.121 $\pm$ 0.030	0.512 $\pm$ 0.079
Mouse		(95%)*	8.212 $\pm$ 0.557
Chimera	A	3.55 $\pm$ 1.81	3.78 $\pm$ 1.58
	B	(58%)*	4.80 $\pm$ 1.66
	E	2.17 $\pm$ 1.66	1.40 $\pm$ 0.45
	F	6.34 $\pm$ 3.83	2.77 $\pm$ 0.38
	H	0.561 $\pm$ 0.085	2.30 $\pm$ 0.61

Increased serum and urinary ratios of active to inactive glucocorticoids are indicative of 11 $\beta$ -HSD2 inhibition and elevated 11-deoxycortisol and 11-deoxycorticosterone of CYP11B1 inhibition (Beck et al. 2020b).

An additional safety concern represents the disruption of the 11 $\beta$ -HSD2-mediated placental glucocorticoid barrier between mother and fetus. Inhibition of placental 11 $\beta$ -HSD2 can lead to elevated fetal exposure to cortisol, affecting fetal programming. An observational study in pregnant Finnish woman, assessing the effect of licorice intake (containing the potent 11 $\beta$ -HSD2 inhibitor GA) on pregnancy duration and health of the children, detected shorter gestation times, reduced birth weight, as well as an increased HPA axis activity and behavioral disturbances in the childhood (Strandberg et al. 2002; R  ikk  nen et al. 2009; R  ikk  nen et al. 2010). However, the use of azole antifungals is not indicated during pregnancy.

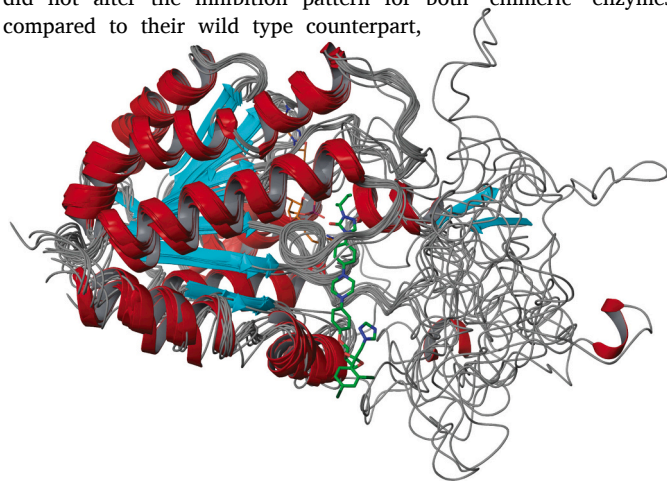
Importantly, the present study demonstrates that posaconazole and itraconazole (including OHI) are very weak inhibitors of mouse and zebrafish 11 $\beta$ -HSD2, with IC<sub>50</sub> values above 7  $\mu$ M. Whilst the mouse represents the most widely used species for mechanistic investigations, including transgene lines, the zebrafish is a frequently used model organism that gained increasing interest due to the low cost and the fact



that experiments with larvae are not considered as animal experiments (Planchart et al. 2016; Wrighton et al. 2019). Thus, mechanisms and possible consequences for human of 11 $\beta$ -HSD2 inhibition by these azole antifungals cannot be studied in these two species. Furthermore, as the concentrations of azole antifungals in the environment were reported to be in the picomolar range (Assress et al. 2019); the risk that itraconazole and posaconazole from wastewater affect fish health via 11 $\beta$ -HSD2 inhibition is negligible. Nevertheless, CYP11B1/2 that are also targets of posaconazole and itraconazole in human remain to be investigated as targets of these drugs in fish as well as in rodents (Beck et al. 2020a). This study emphasizes a cautious approach when trying to extrapolate findings from animal models to human. Species differences need to be taken into account when using animals as disease models or when investigating alternative 11 $\beta$ -HSD2 substrates, environmental inhibitors or potential therapeutic inhibitors.

To begin to understand the species-specific differences in the inhibition of 11 $\beta$ -HSD2 by the investigated azole antifungals, molecular modeling and chimeric enzymes with residue substitutions between human and mouse sequences were applied. As no 11 $\beta$ -HSD2 crystal structure is available to date, homology models were built for the human and mouse enzyme, based on human and guinea-pig 11 $\beta$ -HSD1 crystal structures, similar to previously reported models (Yamaguchi et al. 2011a; Yamaguchi et al. 2011b). In contrast to a recently reported model based on 17 $\beta$ -HSD1 structure (Yau et al. 2017), our attempts failed to find a suitable binding pose of cortisol allowing electron transfer to NAD<sup>+</sup> in 11 $\beta$ -HSD2 models derived from 17 $\beta$ -HSD1 structures. Furthermore, as shown in Fig. 8, superposition of 20 human homology models revealed the highly flexible C-terminal region for which no suitable structural prediction could be made due to the low similarity with any to-date crystallized protein. This emphasizes the uniqueness of the 11 $\beta$ -HSD2 C-terminal region compared to other short-chain dehydrogenase/reductase enzymes.

The roles of Trp276 and Arg279, suggested previously to be involved in the different response of human and mouse 11 $\beta$ -HSD2 to itraconazole and posaconazole (Beck et al. 2017), are difficult to predict by using homology models. Nevertheless, the influence of the non-conserved eight amino-acid long sequence located upstream of Trp276 was investigated by exchanging this cassette between human and mouse 11 $\beta$ -HSD2, followed by analysis of inhibitory effects. The observation that the exchange of this sequence did not alter the inhibition pattern for both chimeric enzymes compared to their wild type counterpart,



**Fig. 8.** Superposition of 20 human 11 $\beta$ -HSD2 homology models. Alpha helices are represented in red and beta sheets as arrows in turquoise. Itraconazole (green) and the cofactor NAD<sup>+</sup> (orange) were docked into the binding pocket. The high variability of the predicted C-terminal region is indicated by the unstructured grey lines. (For interpretation of the references to colour in this figure legend, the reader is referred to the web version of this article.)

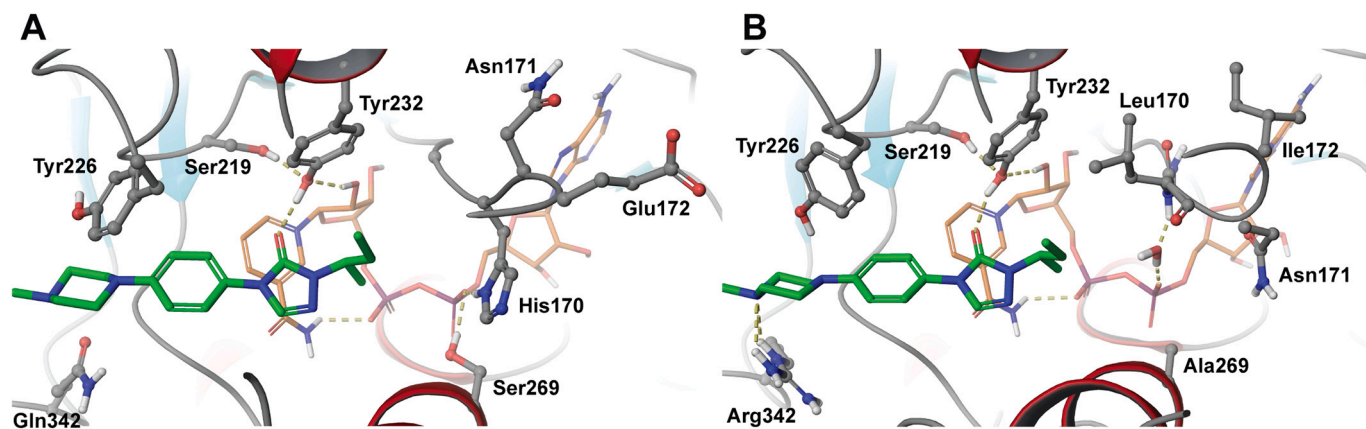
suggests that a different positioning of Trp276 and Arg279 is not responsible for the observed species differences towards posaconazole and itraconazole. Alternatively, the substituted residues may not alter the different orientations of Trp276 and Arg279 in human and mouse 11 $\beta$ -HSD2.

Nevertheless, the C-terminal region had a partial effect on the species-specific inhibition of 11 $\beta$ -HSD2 by the studied azole antifungals. Itraconazole, its metabolite OHI and posaconazole have a prolonged rigid shape composed of consecutive rings, whereby the extended moiety of the molecule is oriented into the binding pocket to compete with the substrate and the rest of the molecule faces the C-terminal region of the enzyme (approximately 60% of the structure). In order to elucidate how such large rigid molecules can interact with residues in the C-terminal region, crystal structures with the cofactor and either cortisol or the respective inhibitor will be needed.

Besides the C-terminus, the active site loop comprising residues 168–180 was found to be responsible for part of the differences in the azole fungicide-mediated inhibition of 11 $\beta$ -HSD2 between human and mouse. The weak inhibition of mouse 11 $\beta$ -HSD2 by these compounds suggests that the lipophilic residues Leu170 and Ile172 at the analogous position of His170 and Glu172 in the human enzyme might cause steric hindrance, preventing the binding at this particular site. The homology model of mouse 11 $\beta$ -HSD2 can accommodate endogenous substrates like cortisol, but the bulky terminal groups of itraconazole and posaconazole are predicted to experience less favorable interactions compared to the human enzyme (Fig. 9, Video 3 and Video 4). In the human model, residue Glu172 is charged and expected to be oriented towards the solvent, leaving more room for bulky lipophilic ligands, while the amphiphilic character of histidine can be exploited. Substitution of Ile172 by glutamate in the mouse enzyme might induce conformational changes by reorientation of Glu172 to the solvent, thus increasing the size of the binding cavity, which consequently allows inhibition by the studied azole antifungals. Indeed, if the two residues 170 and 172 were mutated in the human enzyme to those present in mouse (chimera E), a substantial drop of inhibitory potency of itraconazole, OHI and posaconazole was seen. On the other hand, increased inhibition was observed, when the amino acids at position 170 and 172 in the mouse enzyme were changed to those in the human enzyme (chimera F).

Interestingly, a synergistic gain of inhibitory effect of itraconazole was observed when the mouse enzyme was mutated to bear the human C-terminal region and the Leu170His,Ile172Glu substitution. This chimeric enzyme represented the inhibitory pattern of human 11 $\beta$ -HSD2, indicating that both, residues in close proximity of the substrate and cofactor as well as residues in the C-terminal region, are involved in the potent inhibition by itraconazole. Interestingly, an interaction of the backbone of Asn171 with Arg279 located in the C-terminal region was proposed earlier to be important for the activity of the human enzyme (Yau et al. 2017). Asn171 was also proposed earlier to stabilize the binding of substrates (Fürstenberger et al. 2012) or of amino acids that interact with the pyrophosphate moiety of the cofactor (Arnold et al. 2003). Itraconazole and posaconazole might disturb such interactions and consequently inhibit human 11 $\beta$ -HSD2 activity. Whether mutation of the rat enzyme, or the zebrafish enzyme that is less conserved, at these positions leads to a humanized phenotype remains to be investigated.

In conclusion, the present study revealed significant species-specific differences in the inhibition of 11 $\beta$ -HSD2 by the azole antifungals itraconazole and posaconazole that have been missed in preclinical studies using rodents and that would also not be detected using zebrafish as an animal model. Predictions based on homology modeling and analysis of chimeric enzymes showed that substitution of Leu170,Ile172 in mouse 11 $\beta$ -HSD2 by the corresponding residues of the human enzyme, *i.e.* His170,Glu172, along with the exchange of the C-terminal region resulted in a gain of sensitivity towards inhibitory effect of these azole antifungals to resemble the pattern observed for the human enzyme. The derived structure-activity relationship information should facilitate follow-on studies to assess drugs with the potential to cause 11 $\beta$ -HSD2-



**Fig. 9.** Itraconazole (green) and NAD<sup>+</sup> (orange) docked into 11 $\beta$ -HSD2. A) human 11 $\beta$ -HSD2 and B) mouse 11 $\beta$ -HSD2 homology models. Hydrogen bond interactions (fulfilling directionality and distance criteria <2.8 Å) are depicted by yellow dashed lines. (For interpretation of the references to colour in this figure legend, the reader is referred to the web version of this article.)

dependent pseudohyperaldosteronism, and it should also be useful for the design of 11 $\beta$ -HSD2 inhibitors for specific therapeutic application and selection of adequate experimental animal models. In order to improve modeling-based predictions, mature artificial intelligence algorithms like AlphaFold capable of predicting the fold as well as crystal structures of 11 $\beta$ -HSD2 from different species in the presence of cofactor and substrate or inhibitor will be needed.

Supplementary data to this article can be found online at <https://doi.org/10.1016/j.taap.2020.115387>.

#### Declaration of Competing Interest

SGI, MZ, MS and AO declare no conflict of interest.

#### Acknowledgement

This work was supported by the Swiss Centre for Applied Human Toxicology (SCAHT).

#### References

- Albiston, A.L., Obeyesekere, V.R., Smith, R.E., Krozowski, Z.S., 1994. Cloning and tissue distribution of the human 11 beta-hydroxysteroid dehydrogenase type 2 enzyme. *Mol. Cell. Endocrinol.* 105, R11–R17.
- Arnold, P., Tam, S., Yan, L., Baker, M.E., Frey, F.J., Odermatt, A., 2003. Glutamate-115 renders specificity of human 11beta-hydroxysteroid dehydrogenase type 2 for the cofactor NAD<sup>+</sup>. *Mol. Cell. Endocrinol.* 201, 177–187.
- Assess, H.A., Nyoni, H., Mamba, B.B., Msagati, T.A.M., 2019. Target quantification of azole antifungals and retrospective screening of other emerging pollutants in wastewater effluent using UHPLC-QTOF-MS. *Environ. Pollut.* 253, 655–666.
- Barton, K., Davis, T.K., Marshall, B., Elward, A., White, N.H., 2018. Posaconazole-induced hypertension and hypokalemia due to inhibition of the 11 $\beta$ -hydroxylase enzyme. *Clin. Kidney J.* 11, 691–693.
- Beck, K.R., Bächler, M., Vuorinen, A., Wagner, S., Akram, M., Griesser, U., Temml, V., Klusonova, P., Yamaguchi, H., Schuster, D., Odermatt, A., 2017. Inhibition of 11 $\beta$ -hydroxysteroid dehydrogenase 2 by the fungicides itraconazole and posaconazole. *Biochem. Pharmacol.* 130, 93–103.
- Beck, K.R., Inderbinen, S.G., Kanagaratnam, S., Kratschmar, D.V., Jetten, A.M., Yamaguchi, H., Odermatt, A., 2019a. 11 $\beta$ -Hydroxysteroid dehydrogenases control access of 7 $\beta$ ,27-dihydroxycholesterol to retinoid-related orphan receptor  $\gamma$ . *J. Lipid Res.* 60, 1535–1546.
- Beck, K.R., Kanagaratnam, S., Kratschmar, D.V., Birk, J., Yamaguchi, H., Sailer, A.W., Seuwen, K., Odermatt, A., 2019b. Enzymatic interconversion of the oxysterols 7 $\beta$ ,25-dihydroxycholesterol and 7-keto,25-hydroxycholesterol by 11 $\beta$ -hydroxysteroid dehydrogenase type 1 and 2. *J. Steroid Biochem. Mol. Biol.* 190, 19–28.
- Beck, K.R., Telisman, L., van Koppen, C.J., Thompson 3rd, G.R., Odermatt, A., 2020a. Molecular mechanisms of posaconazole- and itraconazole-induced pseudohyperaldosteronism and assessment of other systemically used azole antifungals. *J. Steroid Biochem. Mol. Biol.* 199, 105605.
- Beck, K.R., Thompson 3rd, G.R., Odermatt, A., 2020b. Drug-induced endocrine blood pressure elevation. *Pharmacol. Res.* 154, 104311.
- Boughton, C., Taylor, D., Ghataore, L., Taylor, N., Whitelaw, B.C., 2018. Mineralocorticoid hypertension and hypokalaemia induced by posaconazole. *Endocrinol Diabetes Metab Case Rep* 2018.
- Edwards, C.R., Stewart, P.M., Burt, D., Brett, L., McIntyre, M.A., Sutanto, W.S., de Kloet, E.R., Monder, C., 1988. Localisation of 11 beta-hydroxysteroid dehydrogenase—tissue specific protector of the mineralocorticoid receptor. *Lancet* 2, 986–989.
- Edwards, C.R., Benediktsson, R., Lindsay, R.S., Seckl, J.R., 1993. Dysfunction of placental glucocorticoid barrier: link between fetal environment and adult hypertension? *Lancet* 341, 355–357.
- European Medicines Agency, 2019. Noxafil, INN-posaconazole, Summary of Product Characteristics. [https://www.ema.europa.eu/en/documents/product-information/noxafil-epar-product-information\\_en.pdf](https://www.ema.europa.eu/en/documents/product-information/noxafil-epar-product-information_en.pdf) (accessed 4 August 2020).
- Ferrari, P., 2010. The role of 11 $\beta$ -hydroxysteroid dehydrogenase type 2 in human hypertension. *Biochim. Biophys. Acta* 1802, 1178–1187.
- Funder, J.W., Pearce, P.T., Smith, R., Smith, A.I., 1988. Mineralocorticoid action: target tissue specificity is enzyme, not receptor, mediated. *Science* 242, 583–585.
- Fürstemberger, C., Vuorinen, A., Da Cunha, T., Kratschmar, D.V., Saugy, M., Schuster, Odermatt, A., 2012. The anabolic androgenic steroid fluoxymesterone inhibits 11 $\beta$ -hydroxysteroid dehydrogenase 2-dependent glucocorticoid inactivation. *Toxicol. Sci.* 126, 353–361.
- Hoffmann, W.J., McHardy, I., Thompson 3rd, G.R., 2018. Itraconazole induced hypertension and hypokalemia: mechanistic evaluation. *Mycoses* 61, 337–339.
- Inderbinen, S.G., Engeli, R.T., Rohrer, S.R., Di Renzo, E., Aengenheister, L., Buerki-Thurnherr, T., Odermatt, A., 2020. Tributyltin and triphenyltin induce 11 $\beta$ -hydroxysteroid dehydrogenase 2 expression and activity through activation of retinoid X receptor  $\alpha$ . *Toxicol. Lett.* 322, 39–49.
- Kuriakose, K., Nesbitt, W.J., Greene, M., Harris, B., 2018. Posaconazole-Induced Pseudohyperaldosteronism. *Antimicrob. Agents Chemother.* 62.
- Lindsay, R.S., Lindsay, R.M., Waddell, B.J., Seckl, J.R., 1996. Prenatal glucocorticoid exposure leads to offspring hyperglycaemia in the rat: studies with the 11 beta-hydroxysteroid dehydrogenase inhibitor carbenoxolone. *Diabetologia* 39, 1299–1305.
- Meyer, A., Strajhar, P., Murer, C., Da Cunha, T., Odermatt, A., 2012. Species-specific differences in the inhibition of human and zebrafish 11 $\beta$ -hydroxysteroid dehydrogenase 2 by thiram and organotin. *Toxicology* 301, 72–78.
- Mune, T., Rogerson, F.M., Nikkilä, H., Agarwal, A.K., White, P.C., 1995. Human hypertension caused by mutations in the kidney isozyme of 11 beta-hydroxysteroid dehydrogenase. *Nat. Genet.* 10, 394–399.
- Nguyen, M.H., Davis, M.R., Wittenberg, R., McHardy, I., Baddley, J.W., Young, B.Y., Odermatt, A., Thompson, G.R., 2020. Posaconazole serum drug levels associated with Pseudohyperaldosteronism. *Clin. Infect. Dis.* 70, 2593–2598.
- Odermatt, A., 2004. Corticosteroid-dependent hypertension: environmental influences. *Swiss Med. Wkly.* 134, 4–13.
- Odermatt, A., Kratschmar, D.V., 2012. Tissue-specific modulation of mineralocorticoid receptor function by 11 $\beta$ -hydroxysteroid dehydrogenases: an overview. *Mol. Cell. Endocrinol.* 350, 168–186.
- Odermatt, A., Arnold, P., Stauffer, A., Frey, B.M., Frey, F.J., 1999. The N-terminal anchor sequences of 11beta-hydroxysteroid dehydrogenases determine their orientation in the endoplasmic reticulum membrane. *J. Biol. Chem.* 274, 28762–28770.
- Planchart, A., Mattingly, C.J., Allen, D., Ceger, P., Casey, W., Hinton, D., Kanungo, J., Kullman, S.W., Tal, T., Bondesson, M., Burgess, S.M., Sullivan, C., Kim, C., Behl, M., Padilla, S., Reif, D.M., Tanguay, R.L., Hamm, J., 2016. Advancing toxicology research using in vivo high throughput toxicology with small fish models. *Altex* 33, 435–452.
- Räikkönen, K., Pesonen, A.K., Heinonen, K., Lahti, J., Komi, N., Eriksson, J.G., Seckl, J.R., Järvenpää, A.L., Strandberg, T.E., 2009. Maternal licorice consumption and detrimental cognitive and psychiatric outcomes in children. *Am. J. Epidemiol.* 170, 1137–1146.
- Räikkönen, K., Seckl, J.R., Heinonen, K., Pyhälä, R., Feldt, K., Jones, A., Pesonen, A.K., Phillips, D.L., Lahti, J., Järvenpää, A.L., Eriksson, J.G., Matthews, K.A., Strandberg, T.E., Kajantie, E., 2010. Maternal prenatal licorice consumption alters

- hypothalamic-pituitary-adrenocortical axis function in children. *Psychoneuroendocrinology* 35, 1587–1593.
- Raleigh, D.R., Sever, N., Choksi, P.K., Sigg, M.A., Hines, K.M., Thompson, B.M., Elnatan, D., Jaishankar, P., Bisignano, P., Garcia-Gonzalo, F.R., Krup, A.L., Eberl, M., Byrne, E.F.X., Siebold, C., Wong, S.Y., Renslo, A.R., Grabe, M., McDonald, J.G., Xu, L., Beachy, P.A., Reiter, J.F., 2018. Cilia-associated Oxysterols activate smoothened. *Mol. Cell* 72, 316–327.
- Sastry, G.M., Adzhigirey, M., Day, T., Annabhimoju, R., Sherman, W., 2013. Protein and ligand preparation: parameters, protocols, and influence on virtual screening enrichments. *J. Comput. Aided Mol. Des.* 27, 221–234.
- Seckl, J.R., Cleasby, M., Nyirenda, M.J., 2000. Glucocorticoids, 11beta-hydroxysteroid dehydrogenase, and fetal programming. *Kidney Int.* 57, 1412–1417.
- Stewart, P.M., Rogerson, F.M., Mason, J.I., 1995. Type 2 11 beta-hydroxysteroid dehydrogenase messenger ribonucleic acid and activity in human placenta and fetal membranes: its relationship to birth weight and putative role in fetal adrenal steroidogenesis. *J. Clin. Endocrinol. Metab.* 80, 885–890.
- Strandberg, T.E., Andersson, S., Järvenpää, A.L., McKeigue, P.M., 2002. Preterm birth and licorice consumption during pregnancy. *Am. J. Epidemiol.* 156, 803–805.
- Thompson 3rd, G.R., Chang, D., Wittenberg, R.R., McHardy, L., Semrad, A., 2017. In Vivo 11β-Hydroxysteroid Dehydrogenase Inhibition in Posaconazole-Induced Hypertension and Hypokalemia. *Antimicrob Agents Chemother* 61.
- Thompson 3rd, G.R., Beck, K.R., Patt, M., Kratschmar, D.V., Odermatt, A., 2019. Posaconazole-Induced Hypertension Due to Inhibition of 11β-Hydroxylase and 11β-Hydroxysteroid Dehydrogenase 2. *J Endocr Soc* 3, 1361–1366.
- Van Cauteren, H., Heykants, J., De Coster, R., Cauwenbergh, G., 1987. Itraconazole: pharmacologic studies in animals and humans. *Rev. Infect. Dis.* 9 (Suppl. 1), S43–S46.
- Voisin, M., de Medina, P., Mallinger, A., Dalenc, F., Huc-Claustre, E., Leignadier, J., Serhan, N., Soules, R., Ségala, G., Mougel, A., Noguier, E., Mhamdi, L., Bacquié, E., Iuliano, L., Zerbinati, C., Lacroix-Triki, M., Chaltiel, L., Filleron, T., Cavallès, V., Al Saati, T., Rochaix, P., Duprez-Paumier, R., Franchet, C., Ligat, L., Lopez, F., Record, M., Poirot, M., Silvente-Poirot, S., 2017. Identification of a tumor-promoter cholesterol metabolite in human breast cancers acting through the glucocorticoid receptor. *Proc. Natl. Acad. Sci. U. S. A.* 114, E9346–E9355.
- Wassermann, T., Reimer, E.K., McKinnon, M., Stock, W., 2018. Refractory Hypokalemia from syndrome of apparent mineralocorticoid excess on low-dose Posaconazole. *Antimicrob. Agents Chemother.* 62.
- White, P.C., Mune, T., Agarwal, A.K., 1997. 11 beta-Hydroxysteroid dehydrogenase and the syndrome of apparent mineralocorticoid excess. *Endocr. Rev.* 18, 135–156.
- Wilson, R.C., Harbison, M.D., Krozowski, Z.S., Funder, J.W., Shackleton, C.H., Hanauske-Abel, H.M., Wei, J.Q., Hertecant, J., Moran, A., Neiberger, R.E., et al., 1995. Several homozygous mutations in the gene for 11 beta-hydroxysteroid dehydrogenase type 2 in patients with apparent mineralocorticoid excess. *J. Clin. Endocrinol. Metab.* 80, 3145–3150.
- Wrighton, P.J., Oderberg, I.M., Goessling, W., 2019. There is something fishy about liver Cancer: Zebrafish models of hepatocellular carcinoma. *Cell Mol Gastroenterol Hepatol* 8, 347–363.
- Yamaguchi, H., Akitaya, T., Kidachi, Y., Kamiie, K., Noshita, T., Umetsu, H., Ryoyama, K., 2011a. Mouse 11β-hydroxysteroid dehydrogenase type 2 for human application: homology modeling, structural analysis and ligand-receptor interaction. *Cancer Inform* 10, 287–295.
- Yamaguchi, H., Akitaya, T., Yu, T., Kidachi, Y., Kamiie, K., Noshita, T., Umetsu, H., Ryoyama, K., 2011b. Homology modeling and structural analysis of 11β-hydroxysteroid dehydrogenase type 2. *Eur. J. Med. Chem.* 46, 1325–1330.
- Yau, M., Haider, S., Khattab, A., Ling, C., Mathew, M., Zaidi, S., Bloch, M., Patel, M., Ewert, S., Abdullah, W., Toygar, A., Mudryi, V., Al Badi, M., Alzubdi, M., Wilson, R. C., Al Azkawi, H.S., Ozdemir, H.N., Abu-Amer, W., Hertecant, J., Razzaghy-Azar, M., Funder, J.W., Al Senani, A., Sun, L., Kim, S.M., Yuen, T., Zaidi, M., New, M.I., 2017. Clinical, genetic, and structural basis of apparent mineralocorticoid excess due to 11β-hydroxysteroid dehydrogenase type 2 deficiency. *Proc. Natl. Acad. Sci. U. S. A.* 114, E11248–E11256.

# 1 Supplementary Information

## Supplementary Table 1. Oligonucleotide primer sequences for the chimeric expression constructs.

Primer name	Primer sequence (5' to 3')
Human fw (5')	TAAGCAA <u>AAGCTT</u> ACCATGGAGCGCTGGC
Mouse insert human rev	CTCCCAGAGGTTACATTAGTCACTGCATCTGTCTTGAAGCAGCCAG
Mouse insert mouse fw	GATGCAGTGAATAATGTGAACC
Mouse rev (3')	TGCTTAGG <u>TACCTT</u> ACTTATCGTCGTCATCCTTGTAATC
Mouse fw (5')	TAAGCAA <u>AAGCTT</u> ACCATGGAGCGCTG
Human insert mouse rev	TTCCCACTGACCCACGTTTCTCACTGACTCTGTCTTGAAGCAGCCAG
Human insert human fw	GAGTCAGTGAGAAACGTGG
Human rev (3')	TGCTTAGG <u>TACCTT</u> ACTTGTGCATCGTCGTCCTTG
Chimera E/G fw	CTCGTCAACAACGCAGGCctcaatcGTAGTTGCTGATGCGGAGC
Chimera E/G rev	GCTCCGCATCAGCAACTACgatattgagGCCTGCGTTGTTGACGAG
Chimera F/H fw	tgaaGTAGTGGCTGACGTGGAA
Chimera F/H rev	ttgtgGCCAGCGTTGTTAACCAG

Underlined sequence: site for molecular cloning, small font: site of mutation

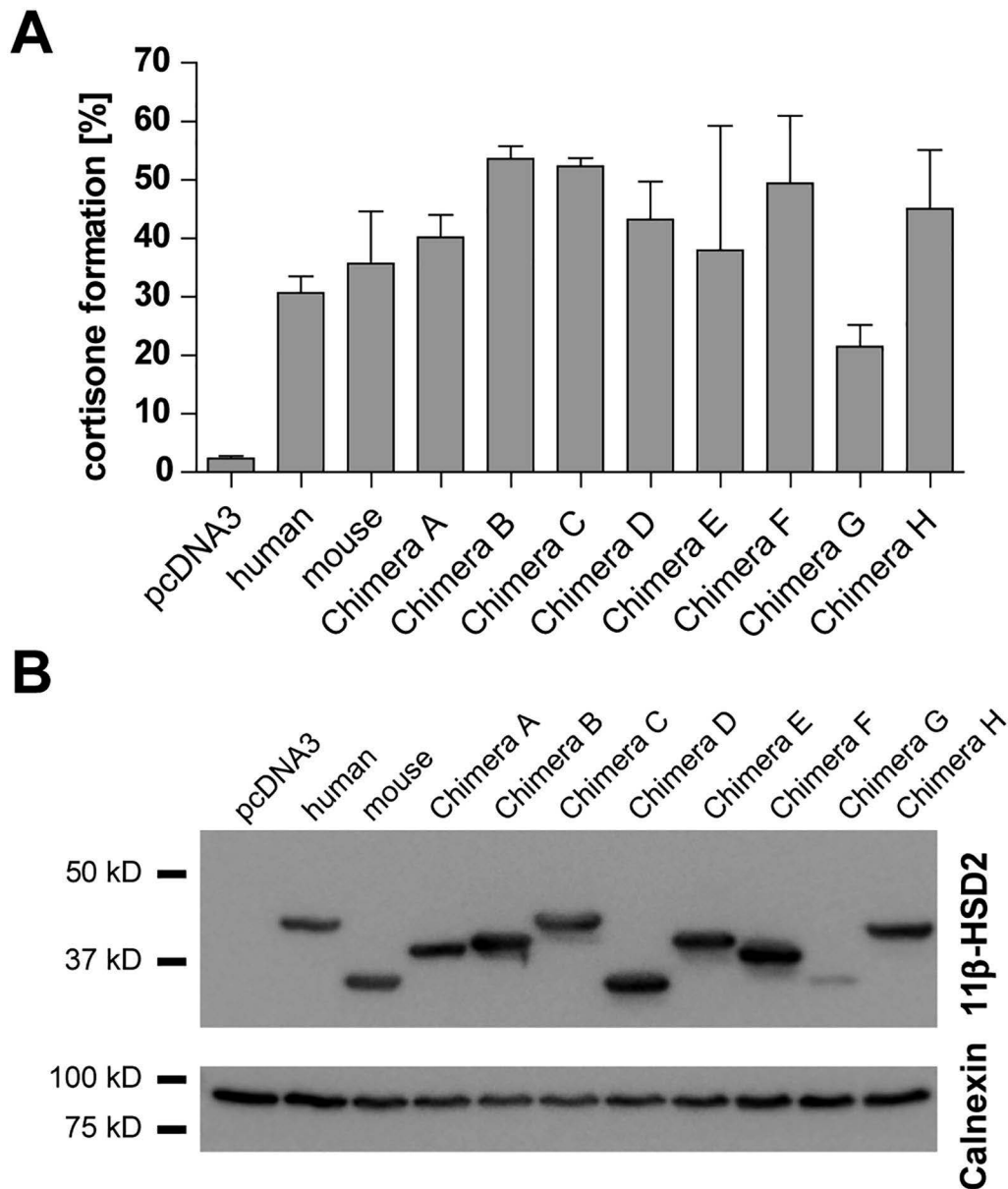
### 1.1 Expression and activity of wild type and mutant 11 $\beta$ -HSD2 enzymes

To determine whether the constructed chimera are active, HEK-293 cells were seeded and transfected as described in the main methods section. To compare the activity of the chimera with that of the human enzyme, a batch of cells was transfected according to the same procedure with the plasmid encoding C-terminally Flag-tagged human 11 $\beta$ -HSD2 (AT8 clone, (Odermatt *et al.*, 1999)). As a control, cells transfected with the empty vector pcDNA3 were utilized. At 48 h post-transfection cells were transferred to poly-L-lysine coated 96 well plates (40'000 cells per well) and incubated for another 24 h. The next day, the medium was replaced with charcoal stripped serum-free medium containing 50 nM cortisol (including 10 nCi of [1,2,6,7-<sup>3</sup>H] cortisol) and cells were incubated for 1 h at 37°C. Reactions were stopped

and analyzed as described above. Enzyme activity was determined as percentage of the conversion of the initially supplied 50 nM cortisol per 40'000 cells. Experiments were carried out two times independently each in duplicates.

## **1.2 Determination of the expression of wild type and mutant 11 $\beta$ -HSD2 enzymes**

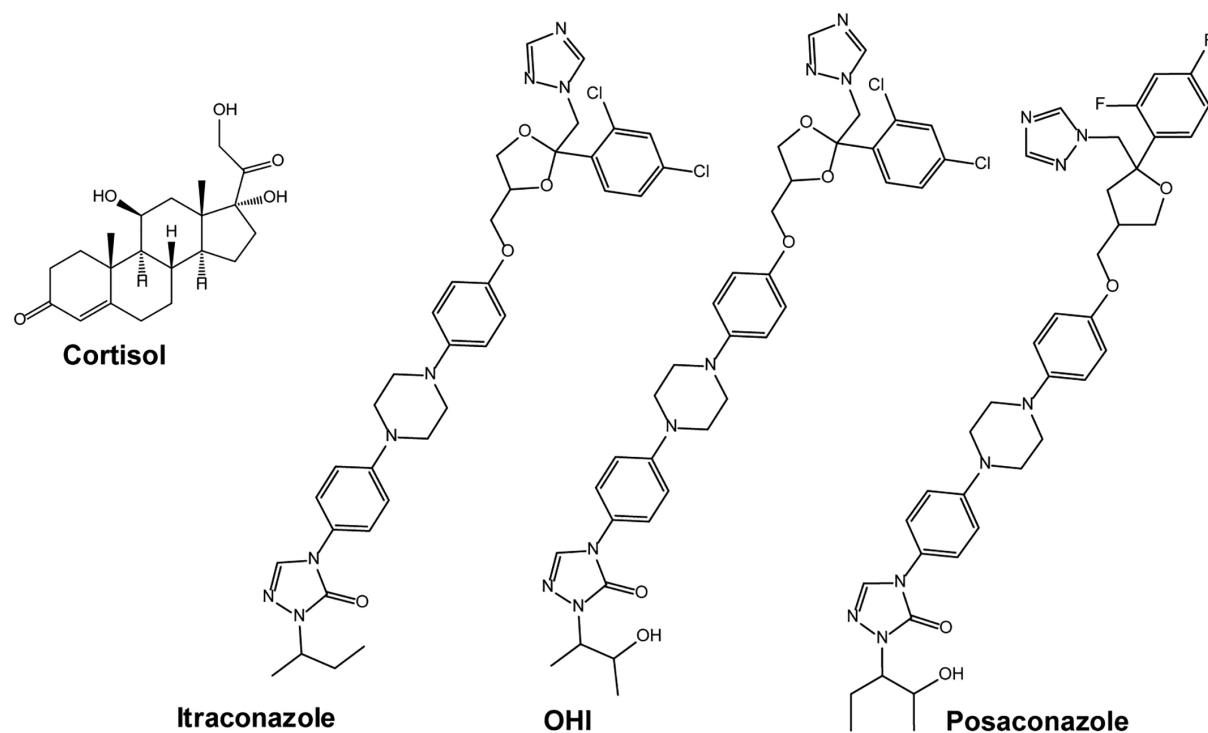
To determine expression of the chimera, cells were seeded and transfected as described in the main section. At 48 h after transfection cells were lysed in RIPA buffer (Sigma-Aldrich) containing protease inhibitor cocktail (Roche, Basel, Switzerland). The samples were processed as described previously (Inderbinen *et al.*, 2020). Antibodies were diluted in 5% defatted milk blocking solution at the following final concentrations: calnexin 0.125  $\mu$ g/mL (SAB4503258, Sigma-Aldrich), anti-FLAG M2 0.125  $\mu$ g/mL (Sigma-Aldrich), anti-mouse IgG HRP conjugated secondary antibody 1-2.75 $\mu$ g/mL (A0168, Sigma-Aldrich) and anti-rabbit IgG HRP conjugated secondary antibody 1:5'000 (7074, Cell signaling, Danvers, MA, USA). Immobilon Western Chemiluminescent HRP substrate kit (Millipore Corporation, Billerica, MA, USA) and Fujifilm ImageQuant<sup>TM</sup> LAS-4000 (GE Healthcare, Glattbrugg, Switzerland) were used for detection of the protein bands.



**Supplementary Fig. 1. Enzymatic activity of wild type and mutant 11 $\beta$ -HSD2 (A).** At 48 h post-transfection of HEK-293 cells with expression plasmids for wild type 11 $\beta$ -HSD2, chimera A-H and pcDNA3 vector control, cells were seeded (40'000 cells per well of a 96-well plate) and incubated for another 24 h. Enzymatic activity was determined by measuring of conversion of cortisol to cortisone after 1 h at 37°C. Enzyme activity is presented as cortisone formation [%] from the initially supplied 50 nM cortisol. Results show mean  $\pm$  SD of two independent experiments each performed in duplicate.

**Western blot of wild type and mutant 11 $\beta$ -HSD2 enzymes (B).** HEK-293 cells were transiently transfected with plasmids for wild type 11 $\beta$ -HSD2, chimera A-H and pcDNA3 vector control. At 48 h post-transfection cells were lysed and equal amounts of protein were separated by SDS-PAGE and blotted onto Immobilon®-P membranes. An anti-FLAG

antibody was utilized to detect the C-terminally FLAG-tagged proteins and detection of calnexin served as a loading control. One representative western blot is shown.



**Supplementary Fig. 2. Chemical structures of cortisol and the anti-fungal agents used in this study.**

### 4.3 Published article: *In vitro* methods to assess 11 $\beta$ -hydroxysteroid dehydrogenase type 1 activity

Manuel Kley<sup>a,b</sup>, Seraina O. Moser<sup>a,b</sup>, Denise V. Winter<sup>a</sup>, and Alex Odermatt<sup>a,b,\*</sup>

<sup>a</sup> Division of Molecular and Systems Toxicology, Department of Pharmaceutical Sciences, University of Basel, Basel, Switzerland

<sup>b</sup> Swiss Centre for Applied Human Toxicology, Department of Pharmaceutical Sciences, University of Basel, Basel, Switzerland

\* Corresponding author. e-mail address: alex.odermatt@unibas.ch

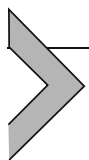
Published article

**Personal contribution:** Drafting and revision of the manuscript except subchapter 8. Illustration of the whole chapter.

**Aims:** Providing an overview of the current *in vitro* methodology with in-depth descriptions of a variety of established *in vitro* methods to assess HSD11B1 activity.

**Conclusion:** The detailed protocols described in this chapter may be used to identify novel potentially therapeutic inhibitors of HSD11B1 or to assess further roles of HSD11B1 in human and animal physiology.





# *In vitro* methods to assess 11 $\beta$ -hydroxysteroid dehydrogenase type 1 activity

Manuel Kley<sup>a,b</sup>, Seraina O. Moser<sup>a,b</sup>, Denise V. Winter<sup>a</sup>, and Alex Odermatt<sup>a,b,\*</sup>

<sup>a</sup>Division of Molecular and Systems Toxicology, Department of Pharmaceutical Sciences, University of Basel, Basel, Switzerland

<sup>b</sup>Swiss Centre for Applied Human Toxicology, Department of Pharmaceutical Sciences, University of Basel, Basel, Switzerland

\*Corresponding author. e-mail address: alex.odermatt@unibas.ch

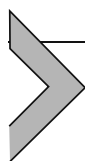
## Contents

1. Introduction	122
2. Historical context of <i>in vitro</i> 11 $\beta$ -HSD1 enzyme activity assays	124
3. Project- and resource-based choice of 11 $\beta$ -HSD1 activity assay	128
4. 11 $\beta$ -HSD1 enzyme activity assay using whole cell lysates	128
4.1 Transfection and overexpression of 11 $\beta$ -HSD1 in HEK-293 cells	129
4.2 Preparation of cell pellets	132
4.3 Radiometric enzyme activity assay (oxoreductase/dehydrogenase)	133
4.4 TLC separation of radiolabeled steroids and liquid scintillation counting	137
4.5 Expected outcomes	139
4.6 Data analysis of 11 $\beta$ -HSD1 enzyme activity assays	139
4.7 Advantages and limitations of the whole cell lysate activity assay	139
4.8 Optimization and troubleshooting	140
5. 11 $\beta$ -HSD1 enzyme activity assay using microsomal preparations	140
5.1 Microsomal preparation from cultured cells	141
5.2 Advantages and limitations of microsomal preparations from transfected cells	144
5.3 Preparation of microsomes from tissue samples	145
5.4 Advantages and limitations of using microsomal preparations from tissue samples for 11 $\beta$ -HSD1 activity measurements	148
5.5 Optimization and troubleshooting	149
6. Enzyme activity assay using purified 11 $\beta$ -HSD1	149
6.1 Advantages and limitations of using purified 11 $\beta$ -HSD1	150
7. 11 $\beta$ -HSD1 activity assay in intact cells	150
7.1 Radiometric activity assay using intact cells	151
7.2 Data analysis of 11 $\beta$ -HSD1 activity from intact cell-based assays	154
7.3 Advantages and limitations of intact cell-based activity assays	155
7.4 Optimization and troubleshooting	155

8. Alternative quantification methods	156
8.1 Quantification using HPLC-DAD, GC-MS or LC-MS	156
8.2 Advantages and limitations of using HPLC, GC-MS or LC-MS	157
8.3 Quantification using ELISA kits	157
8.4 Advantages and limitations of ELISA kits	158
9. Safety considerations and standards of the described methods	158
10. Concluding remarks	158
Acknowledgments	159
References	159

## Abstract

11 $\beta$ -Hydroxysteroid dehydrogenase type 1 (11 $\beta$ -HSD1) converts inactive 11-keto-glucocorticoids to their active 11 $\beta$ -hydroxylated forms. It also catalyzes the oxoreduction of other endogenous and exogenous substrates. The ubiquitously expressed 11 $\beta$ -HSD1 shows high levels in liver and other metabolically active tissues such as brain and adipose tissue. Pharmacological inhibition of 11 $\beta$ -HSD1 was found to ameliorate adverse metabolic effects of elevated glucocorticoids in rodents and humans, improve wound healing and delay skin aging, and enhance memory and cognition in rodent Alzheimer's disease models. Thus, there is an interest to develop 11 $\beta$ -HSD1 inhibitors for therapeutic purposes. This chapter describes in vitro methods to assess 11 $\beta$ -HSD1 enzyme activity for different purposes, be it in disease models, for the assessment of the kinetics of novel substrates or for the screening and characterization of inhibitors. 11 $\beta$ -HSD1 protein expression and preparations of the different biological samples are discussed first, followed by a description of a well-established and easily adaptable 11 $\beta$ -HSD1 enzyme activity assay. Finally, different readout methods are shortly described. This chapter should provide the reader with a toolbox of methods to assess 11 $\beta$ -HSD1 activity with instructions in the form of a decision tree for the choice and implementation of an appropriate enzyme activity assay.



## 1. Introduction

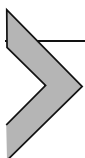
11 $\beta$ -Hydroxysteroid dehydrogenase type 1 (11 $\beta$ -HSD1) is a short-chain dehydrogenase/reductase (SDR26C1) located at the membrane of the endoplasmic reticulum (ER) with its active site facing the luminal space (Mziaut, Korza, Hand, Gerard, & Ozols, 1999; Odermatt, Arnold, Stauffer, Frey, & Frey, 1999). Human 11 $\beta$ -HSD1 is ubiquitously expressed with high expression in liver but also in other metabolically active tissues such as adipose tissue, skeletal muscle and brain (do Nascimento et al., 2015; Odermatt & Kratschmar, 2012; Whorwood, Donovan, Flanagan, Phillips, & Byrne, 2002; Wyrwoll, Holmes, & Seckl, 2011). In the presence of hexose-6-phosphate dehydrogenase (H6PD) that provides the NADPH

cofactor, 11 $\beta$ -HSD1 reduces the 11-keto group of inactive cortisone to produce the potent 11 $\beta$ -hydroxysteroid cortisol. By doing so it regulates the occupancy of the glucocorticoid receptor (GR) and in some tissues the mineralocorticoid receptor (MR). Purified 11 $\beta$ -HSD1 and lysates expressing recombinant 11 $\beta$ -HSD1 show both oxoreductase and oxidase activity, depending on whether NADP<sup>+</sup> or NADPH is supplied to the reaction (Agarwal, Monder, Eckstein, & White, 1989; Agarwal, Mune, Monder, & White, 1994). In most human tissues 11 $\beta$ -HSD1 acts predominantly as an oxoreductase, due to its coexpression with H6PD that catalyzes the first two steps of the ER-luminal pentose phosphate pathway and generates NADPH (Atanasov, Nashev, Schweizer, Frick, & Odermatt, 2004; Banhegyi, Benedetti, Fulceri, & Senesi, 2004). In a few specific cell types such as renal interstitial cells and immortalized proximal tubular cells (Brem et al., 2010), some cell types of the vasculature (Morris, Souness, Latif, Hardy, & Brem, 2004), and in some immune cells, 11 $\beta$ -HSD1 seems to act as a dehydrogenase to regulate the access of glucocorticoids to the GR. Besides its role in glucocorticoid activation, 11 $\beta$ -HSD1 accepts several other endogenous and exogenous substrates, including 11-oxo and 7-oxo steroids and oxysterols but also several carbonyl containing xenobiotics (Beck, Inderbinen, et al., 2019; Beck, Kanagaratnam, et al., 2019; Hult et al., 2004; Odermatt & Klusonova, 2015; Odermatt et al., 2011; Schweizer, Zurcher, Balazs, Dick, & Odermatt, 2004).

11 $\beta$ -HSD1 has been associated with a number of diseases, including mental illnesses, osteoporosis, metabolic disease and diabetes, as well as inflammatory disorders (Barnes, 2011; Gathercole et al., 2013; Gomez-Sanchez & Gomez-Sanchez, 2021; Kadmiel & Cidlowski, 2013; Odermatt & Kratschmar, 2012). Elevated expression and activity of 11 $\beta$ -HSD1 was observed in adipose tissue of obese individuals as well as in type 2 diabetes patients (Gathercole et al., 2013; Paulmyer-Lacroix, Boullu, Oliver, Alessi, & Grino, 2002; Rask et al., 2001; Shukla et al., 2019). These observations are supported by studies in mice where an overexpression of 11 $\beta$ -HSD1 specifically in adipose tissue led to visceral obesity and a phenotype resembling the metabolic syndrome while overexpression in liver resulted in insulin resistance, dyslipidemia and hypertension (Masuzaki et al., 2001; Paterson et al., 2004). Global 11 $\beta$ -HSD1 knockout suppressed the weight gain in high-fat fed mice and systemic 11 $\beta$ -HSD1 inhibition enhanced insulin sensitivity and lowered blood glucose levels in diabetic mice (Alberts et al., 2003; Morton et al., 2004). Furthermore, elevated plasma cortisol levels have been linked to Alzheimer's disease and may contribute

to its pathogenesis (Csernansky et al., 2006; Peskind, Wilkinson, Petrie, Schellenberg, & Raskind, 2001). Inhibition of 11 $\beta$ -HSD1 in Alzheimer's disease rodent models resulted in improved memory and cognition after short-term treatment and prevented cognitive decline after chronic treatment (Mohler et al., 2011; Sooy et al., 2015). These observations have led to the development of new 11 $\beta$ -HSD1 inhibitors to treat metabolic syndrome and type 2 diabetes or Alzheimer's disease, some of which have been tested clinically. However, to date none of the inhibitors tested have made it beyond phase II clinical trials, mainly because they did not meet the primary endpoints or the effects were not superior to existing therapies. For further information on 11 $\beta$ -HSD1 inhibitors in different clinical trials, we refer to a recent review (Gregory et al., 2020).

Despite these drawbacks 11 $\beta$ -HSD1 still represents a promising pharmacological target. Recent evidence indicates beneficial effects of 11 $\beta$ -HSD1 inhibition in fatty liver disease (Lee et al., 2022; Stefan et al., 2014; Yadav et al., 2022), intra-cranial hypertension (Hardy et al., 2021; Markey et al., 2020), skin aging (Boudon et al., 2017; Kim et al., 2021; Tiganescu et al., 2013), wound healing (Ajjan et al., 2022; Terao et al., 2011; Tiganescu et al., 2013; Tiganescu et al., 2018; Youm et al., 2013), ameliorating adverse effects of glucocorticoid therapy (Othonos et al., 2023), or for targeting the tumor micro-environment (Han et al., 2021; Saito et al., 2020). Thus, the assessment of 11 $\beta$ -HSD1 enzyme activity is needed for different purposes. This chapter describes various in vitro assays that allow assessing 11 $\beta$ -HSD1 enzyme activity in tissue samples from patients or animal disease models but also after overexpression in cultured cells for larger scale screenings in order to identify novel therapeutic inhibitors.

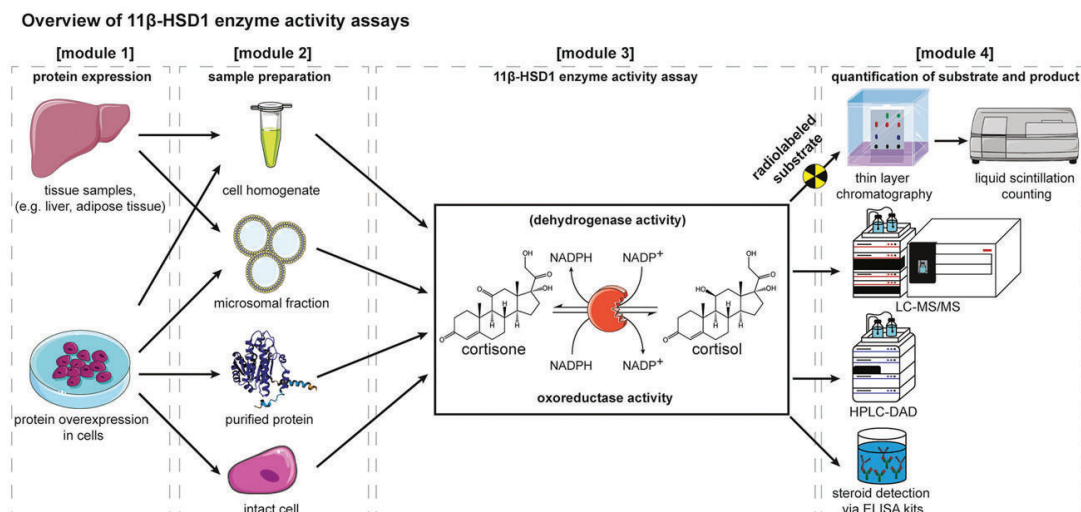


## **2. Historical context of in vitro 11 $\beta$ -HSD1 enzyme activity assays**

Early studies showed the interconversion of the 11-keto and 11 $\beta$ -hydroxyl groups on glucocorticoids by reactions that went in opposite directions and that the 11 $\beta$ -hydroxysteroids were responsible for the anti-inflammatory activity (Burton, Keutmann, Waterhouse, & Schuler, 1953; Bush & Mahesh, 1959; Bush, 1956; Hench, Slocumb, Polley, & Kendal, 1950; Sarett, 1959). Subsequently, 11 $\beta$ -HSD activity was detected in microsomal fractions of various human and animal tissues, revealing species

differences as well as differences in the net reaction direction in distinct organs, based on which it was concluded that two distinct 11 $\beta$ -HSD enzymes must exist (Monder & Shackleton, 1984). This was confirmed by the cloning of 11 $\beta$ -HSD1 which catalyzed both the oxoreduction and oxidation of glucocorticoids (Agarwal et al., 1989; Tannin, Agarwal, Monder, New, & White, 1991) and 11 $\beta$ -HSD2 which acted as a dehydrogenase (Agarwal et al., 1994; Albiston, Obeyesekere, Smith, & Krozowski, 1994). The available 11 $\beta$ -HSD1 cDNA allowed overexpression of the enzyme in cell lines devoid of background activity, which facilitated the development of activity assays. Upon lysis of cells expressing 11 $\beta$ -HSD1 the dehydrogenase activity could readily be measured whilst the oxoreductase activity declined after cell lysis, with a ten-fold increase in  $K_m$  for its substrate but without affecting  $V_{max}$  (Schweizer, Atanasov, Frey, & Odermatt, 2003). The loss of 11 $\beta$ -HSD1 oxoreductase activity could be attenuated by the coexpression of H6PD, which provides cofactor NADPH (Atanasov et al., 2004; Banhegyi et al., 2004). Significant progress was made in the purification of functional 11 $\beta$ -HSD1 (Agarwal, Tusie-Luna, Monder, & White, 1990; Maser & Bannenberg, 1994; Nobel, Dunas, & Abrahmsen, 2002; Shafqat et al., 2003), which resulted in its crystal structure and in complex with inhibitors (reviewed in Ref. Thomas & Potter, 2011).

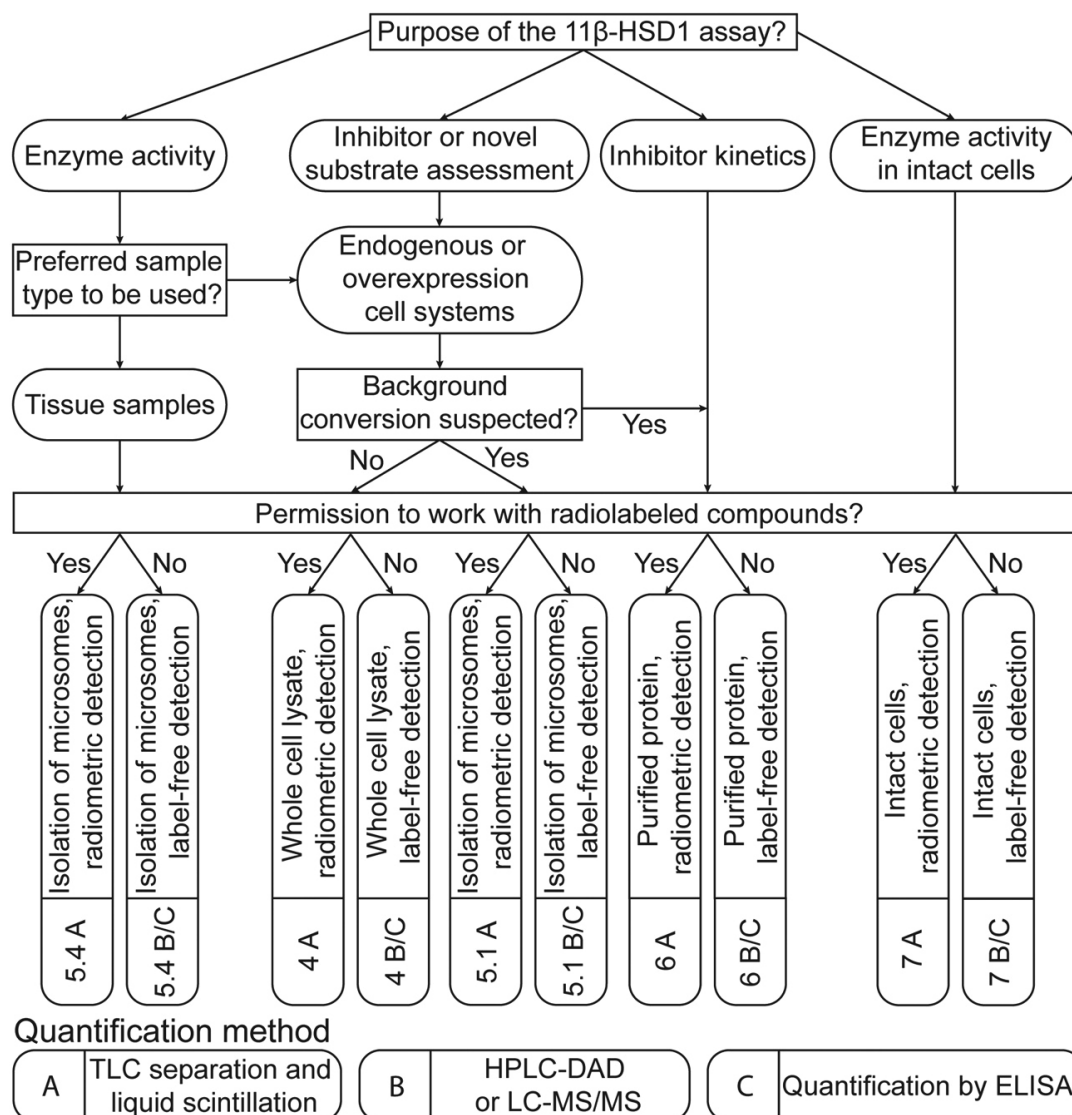
The in vitro 11 $\beta$ -HSD1 activity assays now described are modular in design (see Fig. 1). The first module covers protein expression, which can be achieved by overexpressing 11 $\beta$ -HSD1 cDNA in cultured cells or by collecting tissue samples endogenously expressing the protein (Fig. 1, module 1). The second step includes the preparation of the 11 $\beta$ -HSD1 expressing samples. Homogenates of 11 $\beta$ -HSD1 expressing tissues or microsomal preparations thereof can be used. Alternatively, cells endogenously expressing 11 $\beta$ -HSD1 or overexpressing the enzyme after transfection can be used, followed by preparation of whole cell lysates or microsomal fractions. 11 $\beta$ -HSD1 may be purified from these sources (Fig. 1, module 2). The third step describes the enzyme activity assays. The 11 $\beta$ -HSD1 reaction direction (oxidative or reductive) is determined in the presence of an excess of the respective cofactor (Fig. 1, module 3). The substrate and product may be directly quantified or a radiolabeled tracer may be added to the substrate to facilitate the quantification of product formation. The method for quantification of the substrate and product depends on the setup of the previously performed reaction. If a radiolabeled tracer was included, liquid scintillation counting will be applied, if not,



**Fig. 1 Overview of 11 $\beta$ -HSD1 activity assays.** Methods described in this chapter to investigate 11 $\beta$ -HSD1 enzyme activity are presented schematically and divided into four modules reflecting the general procedure of an enzyme activity assay: protein expression; sample preparation; enzyme activity assay; and quantification of substrate and product. 11 $\beta$ -HSD1, either from an endogenous tissue sample or after overexpression is prepared by cell lysis and optionally microsomal preparation or purification. Alternatively, enzyme activity may be assessed in intact cells. Both 11 $\beta$ -HSD1 oxoreductase and dehydrogenase activities can be assessed. Depending on whether a radioactive tracer has been used for the substrate or not, the substrate conversion can be determined using either thin-layer chromatography (TLC) and liquid scintillation counting or liquid chromatography-mass spectrometry (LC-MS), high-performance liquid chromatography and diode array detection (HPLC-DAD) and enzyme-linked immunosorbent assay (ELISA).

separation of substrate and product can be achieved by high-performance liquid chromatography (HPLC) with subsequent quantification by UV measurement (HPLC-DAD) or mass spectrometry (LC-MS). Alternatively, antibody based detection with enzyme-linked immunosorbent assay (ELISA) (Fig. 1, module 4) can be used.

Each module contains different options, which can be selected depending on the purpose of the 11 $\beta$ -HSD1 activity assay and the available laboratory equipment. This chapter is built around a rapid enzyme activity assay using whole cell lysates and a radiolabeled tracer, i.e. tritiated cortisol or cortisone, for quantification. Other approaches mentioned above are described as alternative protocols and each of those have different advantages and disadvantages, which are listed at the end of the respective section. To help the reader choose a suitable 11 $\beta$ -HSD1 in vitro assay – based on research purpose and available laboratory equipment – a decision tree is included in Fig. 2.



**Fig. 2 Decision tree to select a suitable 11 $\beta$ -HSD1 activity assay.** Depending on the research purpose, a suitable assay format can be chosen. Comparing 11 $\beta$ -HSD1 activity in physiological situations and disease models may require the use of tissue samples. Due to the presence of many potentially interfering proteins in tissue homogenates, the preparation of microsomes is indicated to enrich the enzyme and reduce the background. When characterizing inhibitors, whole cell lysates, microsomal preparations or purified enzyme from endogenous or overexpressing cell systems may be applied depending on the degree of observed background conversion of the substrate. Inhibitor kinetics may be measured using purified 11 $\beta$ -HSD1. If the impact of components in the medium or the influence of other proteins on 11 $\beta$ -HSD1 activity is studied, intact cells allowing coexpression of proteins of interest may be the method of choice. The quantification method for substrate and product depends on whether a radiolabeled tracer is used in the reaction. The number and letter(s) in the box below the recommended enzyme activity assay correspond to the number of the subchapter, where the method is described and the respective quantification method (s) that may be used.



### **3. Project- and resource-based choice of 11 $\beta$ -HSD1 activity assay**

Assessment of 11 $\beta$ -HSD1 activity in complex matrices such as tissue samples may require enzyme enrichment to reduce background and remove possible contaminants that might interfere with the enzyme activity or cofactor consumption. This can be achieved by the preparation of microsomes from tissues, for example from liver and adipose tissue. Microsomal preparation from cells overexpressing 11 $\beta$ -HSD1 may be used when studying potentially novel substrates. Alternatively, to fully exclude interfering enzymes, purified 11 $\beta$ -HSD1 may be used. Purification of the enzyme to homogeneity is laborious. However, purified 11 $\beta$ -HSD1 is required to determine exact enzyme kinetic parameters such as  $K_m$  and  $K_i$  for substrates and inhibitors, respectively. For the identification and characterization of inhibitors, especially for relative comparisons of the potency of compounds, the use of easy accessible whole lysates of 11 $\beta$ -HSD1 overexpressing cells is a rapid and low cost option, bypassing the time-consuming and demanding purification. For the investigation of the impact of other enzymes or specific nutrient conditions on 11 $\beta$ -HSD1 activity, intact cell systems may be advantageous. Depending on its coexpression with H6PD, for example in hepatocytes, adipocytes and macrophages, primarily the oxoreductase activity can be measured. The substrate to product conversion can be quantified by different methods after chromatographic separation (TLC, HPLC, GC), either using a radiolabeled substrate followed by scintillation counting or by label-free UV-detection and mass spectrometry (MS) or antibody-based detection kits.



### **4. 11 $\beta$ -HSD1 enzyme activity assay using whole cell lysates**

This section describes a time- and cost-efficient 11 $\beta$ -HSD1 activity assay using whole cell lysates for the identification of inhibitors. Pellets from cells overexpressing the enzyme are prepared and frozen for storage, followed by lysis prior to starting the enzymatic reaction. The assay can be performed in the presence of a radiolabeled tracer of the substrate, followed by substrate and product separation by thin-layer chromatography (TLC) and analysis of product formation by liquid scintillation counting. The oxoreductase activity is performed in the presence of NADPH while NADP<sup>+</sup> is used to assess the dehydrogenase activity. Label-free detection methods are generally less



sensitive and larger reaction volumes may be required to keep the reaction parameters (substrate, cofactor, enzyme concentrations) constant and obtain sufficient amounts of formed product that exceeds the limit of quantification of HPLC-DAD and LC-MS-based methods or of antibody-based quantification methods. These alternative quantification methods and their advantages and disadvantages are described in Section 8.

Enzyme assays using whole cell lysates are considered as “quick and dirty” methods due to the presence of many other enzymes and metabolites that could potentially interfere with the enzymatic reaction. Thus, it is important to choose a cell system for overexpression of 11 $\beta$ -HSD1 that exhibits a very low background of enzymes metabolizing either the substrate or the product. Cell lines fulfilling these criteria include, for example, HEK-293, COS-1 or -7, and CV-1 (Low, Chapman, Edwards, & Seckl, 1994; Mercer, Obeyesekere, Smith, & Krozowski, 1993; Odermatt et al., 1999; Warriar, Page, & Govindan, 1994).

## **4.1 Transfection and overexpression of 11 $\beta$ -HSD1 in HEK-293 cells**

### **4.1.1 Equipment**

- Cell incubator
- Sterile filter 0.2  $\mu$ M (Filtropur S 0.2, Sarstedt, Nümbrecht, Germany)
- Nano drop spectrophotometer (NanoDrop<sup>TM</sup> OneC, Thermo Fisher Scientific, Waltham, MA, USA)
- Centrifuge (5810 R, Eppendorf, Hamburg, Germany)

### **4.1.2 Cell line**

- Human Embryonic Kidney-293 cells (HEK-293, ATCC (CRL-1573), Manassas, VA, USA)

### **4.1.3 Plasmids**

- Human *HSD11B1* cDNA with a C-terminal FLAG-tag in a pcDNA3.1 backbone (Odermatt et al., 1999)

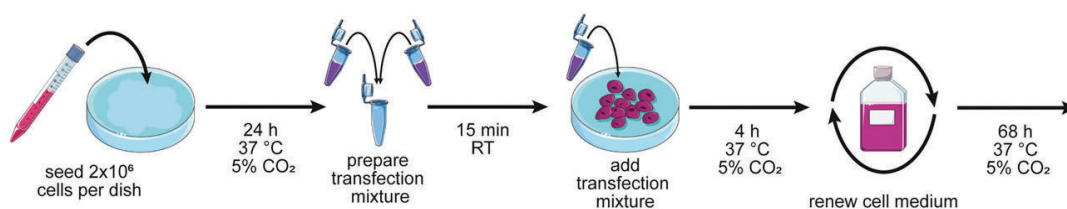
### **4.1.4 Buffers and media for 11 $\beta$ -HSD1 overexpression**

All chemicals and reagents were purchased from Sigma-Aldrich (St. Louis, MO, USA) if not stated otherwise.

- **Complete HEK-293 medium** (Dulbecco's Modified Eagle Medium, high glucose 4.5 g/L and 584 mg/L L-glutamine (D5796) supplemented with 10% fetal bovine serum (FBS, heat inactivated prior to use for 20 min at 58 °C, Biowest, Nuaille, France), 100 U/mL penicillin, 100 mg/mL streptomycin (Life Technologies, Grand Island, NY, USA), 10 mM HEPES buffer pH 7.4 (Life Technologies), and 1% MEM non-essential amino acid solution)
- **2x BEST solution** (275 mM NaCl, 1.5 mM Na<sub>2</sub>HPO<sub>4</sub>, 50 mM BES (N,N-Bis(2-hydroxyethyl)-2-aminoethanesulfonic acid), pH 7.0 adjusted at 37 °C, sterile filtrated with 0.2 µm filter, store at 4 °C)
- **CaCl<sub>2</sub> solution** (2 M, sterile filtrated with 0.2 µm filter, store at 4 °C)
- **PBS** (137 mM NaCl, 2.7 mM KCl, 10.1 mM Na<sub>2</sub>HPO<sub>4</sub>, 1.8 mM KH<sub>2</sub>PO<sub>4</sub>, pH 7.4, store at 4 °C)

#### 4.1.5 Procedure

1. Seed  $2 \times 10^6$  HEK-293 cells in a total volume of 10 mL complete HEK-293 medium per 10 cm culture dish and incubate for 24 h at 37 °C, 5% CO<sub>2</sub>. (see Fig. 3 for an overview of the procedure; see Note a.)
2. Prepare transfection (calcium phosphate precipitation) by pre-warming sterile H<sub>2</sub>O, CaCl<sub>2</sub>, and 2 × BEST solution at 37 °C. (see Note b.)
3. Transfer 8 µg of the plasmid containing *HSD11B1* into a 1.5 mL plastic tube. Add PCR grade H<sub>2</sub>O to a total volume of 437.5 µL.
4. Add 62.5 µL CaCl<sub>2</sub> solution dropwise to the DNA solution.
5. Prepare 500 µL of 2 × BEST solution in a new plastic tube and transfer the prepared DNA CaCl<sub>2</sub> mixture dropwise into the prepared 2 × BEST solution.



**Fig. 3 Schematic overview of the transfection procedure for 11β-HSD1 over-expression in cultured HEK-293 cells.** Cells are seeded and transfected on the next day using the calcium phosphate precipitation method. The medium is renewed after 4 h and the transfected cells are incubated for a total of 72 h.

6. Invert the plastic tube once and incubate the transfection mix at room temperature (RT) for 15 min
7. Pipet the transfection mix (1000  $\mu$ L) dropwise onto the medium of the prepared HEK-293 cell suspension and then sway the dish slightly. (see Note c.)
8. Incubate the cells for 4 h at 37  $^{\circ}$ C, 5% CO<sub>2</sub>, then exchange the medium with fresh complete HEK-293 medium.
9. Incubate the cells for 48 h; then proceed with the protocol for the cell pellet preparation. (see Note d.)

#### 4.1.6 Notes

- a. One 10 cm dish will produce 10 cell pellets. Production of larger homogenous batches of transfected cell pellets is recommended which can be obtained by transfecting several 10 cm dishes. When using a different cell line than HEK-293, the background conversion of the substrates cortisol and cortisone should be assessed first in non-transfected cells.
- b. An additional transfection with an empty plasmid backbone as a negative control is recommended while establishing the method. The pellets should be treated as those transfected with 11 $\beta$ -HSD1. A transfection efficiency of 20–30% should be obtained using the calcium phosphate precipitation method. Other cell lines or transfection methods and kits may be used for 11 $\beta$ -HSD1 overexpression.
- c. For better consistency between different transfections, prepare a slight excess of the transfection mix to consider tip retention volumes.
- d. Before performing the assay, overexpression of 11 $\beta$ -HSD1 by the cells should be confirmed by Western blotting (WB). Establishment of a cell line stably expressing 11 $\beta$ -HSD1 is recommended to maximize time and cost efficiency and enhance reproducibility. For this purpose, HEK-293 cells are transfected as described above with a pcDNA3 plasmid backbone containing *HSD11B1* cDNA and a neomycin resistance gene (*neoR*). Selection is performed by culturing cells in complete HEK-293 medium containing G-418 sulfate (Geneticin). Alternatively, HEK-293 cells are transduced with the lentiviral vector pLenti-PGK-GFP-Puro, where the green-fluorescence protein (GFP) sequence was replaced by *HSD11B1* cDNA and subsequently selected using puromycin.

## 4.2 Preparation of cell pellets

### 4.2.1 Equipment

- Centrifuge with cooling function (5424 R, Eppendorf, Hamburg, Germany)
- Plastic tube 15 mL (Sarstedt)
- Cell scraper (Sarstedt)
- Liquid nitrogen or dry ice

### 4.2.2 Buffers and solutions

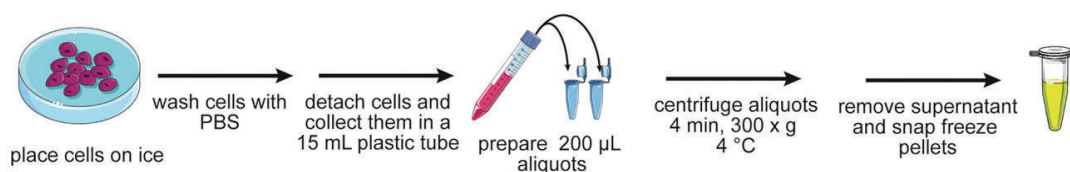
- PBS

### 4.2.3 Procedure

1. Pre-cool the centrifuge to 4 °C, prepare an ice box and 8 mL of ice-cold PBS per 10 cm culture dish (see Fig. 4).
2. Remove the transfected culture dish(es) from the incubator and place them immediately on ice.

**Critical: For the following steps, the samples need to be kept on ice.**

1. Remove the media and wash the cells with 5 mL ice-cold PBS. Keep the culture dishes on ice. (see Note a.)
2. Add 2 mL of ice-cold PBS to each dish. Detach the cells by pipetting the PBS directly onto the cells. Tilt the dish and scrape the remaining cells to one site. Suspend the cells by pipetting up and down 10 times per dish. (see Note b.)
3. Pool the scraped cells (if more than one 10 cm dish was transfected with the same plasmid) into a 15 mL plastic tube and carefully mix the cells by inverting the tube (until homogenous).
4. Pipet 200  $\mu$ L aliquots of cell suspension into 1.5 mL plastic tubes. Sway the cells in the 15 mL plastic tube slightly before pipetting an aliquot.



**Fig. 4 Schematic overview of the preparation of cell pellets for 11 $\beta$ -HSD1 activity assays.** The harvested cells should be kept on ice during the entire procedure. The cells should be immediately washed, aliquoted and frozen.

5. Centrifuge the aliquots at 4 °C for 4 min at 300g.
6. Carefully remove the supernatants and immediately snap freeze the pellets in the plastic tubes in liquid nitrogen or freeze the pellets for 15 min on dry ice. Store pellets at –80 °C. (see Note c.)  
Breakpoint: The experiment can be paused here and continued when it convenes.

#### 4.2.4 Notes

- a. HEK-293 cells detach easily from culture dishes, wash carefully.
- b. Cell scraping or trypsinization and subsequent trypsin inactivation may be required if another cell line is used that is more adherent to the culture dish.
- c. The 11 $\beta$ -HSD1 protein within the prepared pellet retains its activity for up to one year when stored at –80 °C. Nevertheless, enzymatic activity should be examined after prolonged storage of pellets prior to starting an experiment. The cell lysate dilution factor described in subchapter 4.3, Note b. may be reassessed for older batches of cell pellets.

### 4.3 Radiometric enzyme activity assay (oxoreductase/dehydrogenase)

#### 4.3.1 Equipment

- Sonicator (UP50H, Hielscher Ultrasonics, Teltow, Germany)
- Vortex (TX4 Digital IR Vortex Mixer, Velp Scientifica<sup>TM</sup>, Usmate, Italy)
- Thermoshaker with 96-well plate attachment (Thermomixer comfort, Eppendorf)

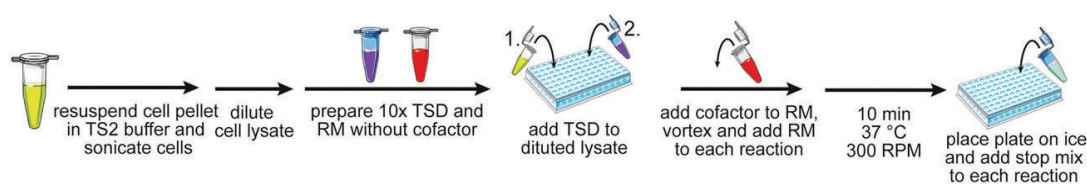
#### 4.3.2 Buffers and solutions

- **TS2 buffer** (100 mM NaCl, 1 mM EGTA, 1 mM EDTA, 1 mM MgCl<sub>2</sub>, 250 mM sucrose, 20 mM Tris-HCl, pH 7.4, store at 4 °C)
- **[1,2,6,7-<sup>3</sup>H] labeled cortisone or cortisol stock solutions** ~4  $\mu$ M (dilute <sup>3</sup>H-cortisone or <sup>3</sup>H-cortisol (American Radiolabeled Chemicals, Saint Louis, Missouri, USA) with ethanol if needed, store at –20 °C)
- **Unlabeled cortisone or cortisol stock solutions** 10 mM in DMSO (store at –20 °C)

- **NADPH or NADP<sup>+</sup> stock solutions** 25 mM in H<sub>2</sub>O (store 20  $\mu$ L aliquots at  $-80$  °C, up to one month)
- **Stop mix** (2 mM cortisol, 2 mM cortisone in methanol, store at 4 °C, see Note d.)
- **Test substance stocks** 10 mM in DMSO or methanol (verify solubility!), store at  $-20$  °C

#### 4.3.3 Procedure

1. Preheat a thermoshaker to 37 °C and prepare a 1% solvent control solution (TS2 buffer either with DMSO or methanol, depending on the solvent used to dissolve the test compounds) and prepare a dilution series of test substances in their corresponding solvent. The addition of the 1% solvent control solution to a reaction will result in a 1:10 dilution, reaching a total solvent concentration of 0.1%. Store the diluted solution on ice. (see Fig. 5 for an overview of the procedure; see Note a.)
2. Dilute each prepared test substance concentration 1:100 in TS2 buffer, reaching 10  $\times$  of the concentration to be assessed in the assay. The final addition of the test substance dilution to the enzyme assay will result in a 1:10 dilution. Store the diluted solutions on ice. (see Note a.)
3. Depending on the 11 $\beta$ -HSD1 reaction direction to be assessed, prepare a 50  $\mu$ M unlabeled cortisone or cortisol working solution by diluting the 10 mM stock 1:200 in TS2 buffer. Store it on ice.



**Fig. 5 Schematic overview of the radiometric 11 $\beta$ -HSD1 activity assay.** The thawed and diluted cell pellet (yellow plastic tube) is kept on ice until starting the enzyme reaction. Test substance dilutions (TSD, purple plastic tube) are added to the diluted cell lysate in a 96-well plate. After adding the cofactor to the reaction mix (RM, red plastic tube), the enzyme reaction takes place in a thermoshaker at 37 °C for 10 min, shaking at 300 rpm. The reaction is stopped by placing the 96-well plate containing the reactions immediately on ice and by adding the stop mix (green plastic tube).

4. For an enzyme activity assay, resuspend an aliquot of the prepared 11 $\beta$ -HSD1 pellets stored in the  $-80^{\circ}\text{C}$  freezer in 400  $\mu\text{L}$  ice-cold TS2 buffer ( $4^{\circ}\text{C}$ ) by pipetting up and down, then mix the suspension well at 300 rpm. Keep the cell suspension on ice. (see Note b.)  
**Critical: Keep the thawed cell pellets on ice whenever possible and immediately proceed with the subsequent protocol steps.**
5. Lyse the cells by sonication with 10 pulses (0.3 cycles, 20% amplitude) of the UP50H sonicator. Mix well at 300 rpm. Store the lysate on ice.
6. Dilute the lysate in ice-cold TS2 buffer to achieve 20–30% substrate conversion after 10 min (see Note b.), mix well at 300 rpm. Store the diluted lysate on ice.
7. Prepare a 96-well PCR plate, label it and place it on ice. All reactions may be carried out in technical duplicates. Include two wells for solvent control samples and two wells as background samples.
8. Add 10  $\mu\text{L}$  of the diluted cell lysate per reaction in the 96-well PCR plate on ice (except for the prepared wells for the background samples).
9. Prepare two background samples by adding ice-cold 12.2  $\mu\text{L}$  TS2 buffer into 2 wells.
10. Add 2.2  $\mu\text{L}$  of 1% solvent control solution into the two prepared solvent control wells and 2.2  $\mu\text{L}$  of the diluted test substance solutions into their corresponding wells.
11. Prepare the reaction mixture according to Table 1. Thaw one cofactor aliquot and add the corresponding amount to the reaction mixture immediately before pipetting the reaction mixture to the prepared samples. (see Note c.)
12. Add 10  $\mu\text{L}$  of reaction mix to every well, including background and solvent control wells.
13. Incubate the 96-well plate for 10 min with 300 rpm shaking at  $37^{\circ}\text{C}$  in the preheated thermoshaker.
14. Put the 96-well plate immediately on ice and quickly add 10  $\mu\text{L}$  of stop mix to every well to stop the enzyme reaction. (Optional: mix by pipetting in each well up and down once). Keep the 96-well plate on ice until loading the samples onto the TLC plate. (see Note d.)

**Table 1** Preparation of reaction mix for 25 reactions (oxidoreductase/dehydrogenase activity).

Oxoreductase activity Buffer/solution	Dehydrogenase activity Buffer/solution	Amount to add	Final concentration per reaction and well
TS2 buffer	TS2 buffer	260 $\mu\text{L}$	—
$^3\text{H}$ -cortisone [ $\sim 4 \mu\text{M}$ ]	$^3\text{H}$ -cortisol [ $\sim 4 \mu\text{M}$ ]	1.5 $\mu\text{L}$	10 nM
Unlabeled cortisone working solution [50 $\mu\text{M}$ ]	Unlabeled cortisol working solution [50 $\mu\text{M}$ ]	2.3 $\mu\text{L}$	190 nM
NADPH [25 mM]	NADP <sup>+</sup> [25 mM]	12.3 $\mu\text{L}$	500 $\mu\text{M}$

This Table lists end concentrations as well as the respective amounts of buffer, substrate and cofactor solutions to be added to the reaction mix for the radiometric enzyme activity assay. The amount of prepared reaction mix considers dead volumes of pipet tips.

#### 4.3.4 Notes

- a. The total amount of solvent in the enzyme reaction should be maximally 1% to ensure the integrity of 11 $\beta$ -HSD1 during the reaction.
- b. The dilution factor of the cell pellet suspension depends on the transfection efficiency and size of the prepared cell pellet and needs to be determined for each prepared homogenous cell pellet batch prior to assessing test substances. For this, a dilution series of the resuspended cell pellet is assessed adding 2.2  $\mu\text{L}$  of the 1% solvent control solution to each dilution of the cell pellet, except for the background sample where 12.2  $\mu\text{L}$  TS2 buffer is added. We recommend diluting the cell lysate in a range between 1:2–1:10 in TS2 buffer. If another cell line than HEK-293 was transfected initially, the lysis protocol as well as the dilution range may vary.
- c. The remaining cofactor should not be reused after thawing.
- d. The stop mix consists of methanol and 2 mM each of unlabeled cortisone and cortisol to be able to detect the steroid spots after TLC separation under the UV light. Both steroids absorb in the UV spectrum (254 nm) and will be visible as dark spots on the silica plate that is emitting green fluorescence under UV light due to the presence of the UV254 indicator in the TLC silica coating. Methanol denatures 11 $\beta$ -HSD1 and thus stops the reaction.



## 4.4 TLC separation of radiolabeled steroids and liquid scintillation counting

### 4.4.1 Equipment

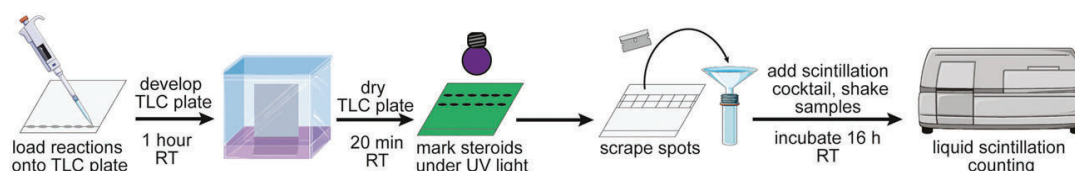
- Fume hood
- TLC developing chamber (Sigma-Aldrich, St. Louis, Missouri, USA)
- UV-illuminator (UV-Cabinet II, CAMAG Muttenz, Switzerland)
- Liquid scintillation counter (2900 TR Tricarb Liquid, PerkinElmer, Waltham, MA, USA)
- 20  $\times$  20 cm pre-coated glass TLC-plates (SIL G-25 UV254 TLC plates, Macherey-Nagel, Düren, Germany, see Note c.)
- 20  $\times$  20 cm piece of filter paper
- Mini-Vial 6 mL with caps (Sarstedt)
- Single edge razor blade
- Plastic funnel
- Plastic collection tray

### 4.4.2 Buffers and solutions

- **TLC mobile phase** (chloroform: methanol; 8:1, e.g. 80 mL chloroform and 10 mL methanol)
- **Scintillation cocktail** IRGASAFE Plus (Zinsser Analytic, Eschborn, Germany)

### 4.4.3 Procedure

**Critical:** The following steps should be performed in a fume hood. Wear proper protection such as lab coat, gloves, and for step 7–9 an FFP2 face mask and safety goggles (see Fig. 6).



**Fig. 6 Schematic overview of TLC separation of glucocorticoids and subsequent liquid scintillation counting.** Steroids from samples of the radiometric enzyme activity assay are separated by TLC. Steroids are visualized under the UV light, collected by scraping and the contained radiolabeled tracers are quantified by liquid scintillation counting. All steps may be performed at room temperature (RT).

1. Prepare the TLC chamber with a  $20 \times 20$  cm filter paper in a fume hood. Pour the TLC mobile phase into the chamber, let the filter paper get soaked and the chamber saturated for at least 30 min
2. Prepare TLC plates by marking an “origin” line 2.5 cm above the lower edge with a pencil, where the samples will be loaded onto the plate.
3. Pipet each reaction of the 96-well plate up and down 4 times, then load  $10 \mu\text{L}$  onto the prepared TLC plate. Report the order of the samples. (see Note a.)
4. Develop the TLC plate for 45–60 min in the TLC chamber and mark the running front (front should reach at least  $2/3$  of the total distance to the top edge of the TLC plate).
5. Dry the TLC plate for 20 min  
Breakpoint: The experiment can be paused here and continued when it convenes.
6. Visualize the steroids under the UV light (dark spots on green fluorescent TLC plate) and draw a square grid with a pencil encasing the spots. Cortisone ( $R_f = 0.5$ ) runs farther on the TLC plate than cortisol ( $R_f = 0.39$ ). Label the samples. (see Note b.)
7. In the fume hood, scrape each individual spot from the TLC plate with a razor blade and a funnel into a  $\beta$ -counter tube (Mini-Vial, 6 mL). Arrange the tubes in a defined order. (see Note c.)
8. Add 2 mL scintillation cocktail to every tube, close the tubes tightly with their lids and label your samples on the lid.
9. Incubate for 16 h (overnight).
10. Measure the samples in the liquid scintillation counter.

#### 4.4.4 Notes

- a. Load not more than 14 spots per  $20 \times 20$  cm plate to achieve a good horizontal resolution of the single steroid spots on the plate. To optimize the sample throughput per plate, after drawing the origin line onto the plate, the TLC coating on the glass plate may be scratched perpendicular to the origin line with a hypodermic needle and a ruler, dividing the plate into vertical 1 cm lanes. The outer lanes should not be loaded. The 96-well plate containing the rest of the samples ( $\sim 20 \mu\text{L}$ ) can be sealed and stored at  $4^\circ\text{C}$ . In case of any mistake during TLC separation or scraping of the steroid spots, the TLC can be re-run with those backup samples.

- b. The areas containing a single spot should be of comparable size, since the silica coating may interfere with the liquid scintillation readout.
- c. Alternatively, polyester TLC plates with the same silica coating may be used and the steroid spots can be excised instead of scratched from the plate. Hold the scissors at an angle during cutting to prevent flaking of the silica coating. The TLC coating not containing the steroid spots should be collected in a tray for radioactive waste.

#### 4.5 Expected outcomes

The sum of the counts for substrate and product from liquid scintillation measurements should be similar between different reactions, independent of the measurement unit, when the same reaction mix was applied. A total count of a minimum of 2000 disintegrations per min (DPM) or 1000 counts per min (CPM) is recommended per sample in order to minimize electrostatic artefacts. Substrate conversion is calculated by dividing the counts for the product by the total counts. The background, determined in samples containing only TS2 buffer and the reaction mix, is subtracted and should be below 10%. Substrate conversion for the solvent control should reach 20–30% after background correction.

#### 4.6 Data analysis of 11 $\beta$ -HSD1 enzyme activity assays

The total conversion of substrate to product is calculated by dividing the counts for the product by the total counts (sum of counts for product and substrate). The background samples are needed to determine the percentage of radiolabeled product initially present in the reaction mix due to prolonged storage and compound instability. This background is subtracted from all values of the reactions. The conversion obtained for a treated sample is normalized to that of the solvent control, yielding a fold change of 11 $\beta$ -HSD1 enzyme activity.

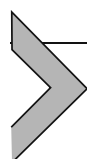
#### 4.7 Advantages and limitations of the whole cell lysate activity assay

Advantages	Limitations
Low cost of calcium phosphate precipitation	Moderate transfection efficiency by calcium phosphate precipitation (20–30%)
Overexpression in cultured eukaryotic cells allows coexpression of 11 $\beta$ -HSD1 with other proteins such as H6PD	Presence of metabolites and other enzymes in the cell lysate may affect 11 $\beta$ -HSD1 activity
High protein stability of 11 $\beta$ -HSD1 in cell pellets at $-80^{\circ}\text{C}$ (retains enzyme activity for up to 1 year)	Enzyme concentration unknown, only apparent $K_m$ and $V_{max}$ can be determined

Direct access of inhibitors to 11 $\beta$ -HSD1 in the lysate (allows identification of novel inhibitors/scaffolds)	Inhibitors unable to enter a cell or highly cytotoxic chemicals are not excluded
High sensitivity of liquid scintillation counting, allows use of nanomolar substrate range at low reaction volume, requires low amount of biological material	Not suitable for upscaling for high throughput screening (HTS)

## 4.8 Optimization and troubleshooting

Problem	Possible solutions
The lysate shows no enzyme activity	<ol style="list-style-type: none"> <li>1. Prepare a fresh pellet batch (frozen pellet might be too old or degraded due to unintentional thawing)</li> <li>2. Confirm 11<math>\beta</math>-HSD1 expression by Western blotting</li> <li>3. Check the percentage of total solvent per reaction</li> <li>4. Test a wider range of lysate dilutions to reach optimal substrate conversion</li> <li>5. Assess enzyme activity after prolonged reaction time (e. g. 20 min, 30 min, ...)</li> <li>6. Use HEK-293 to overexpress 11<math>\beta</math>-HSD1 (if not previously implemented)</li> </ol>
Cortisone and cortisol spots after TLC separation are not on a horizontal line	<ol style="list-style-type: none"> <li>1. Increase the time for saturation of the TLC chamber</li> <li>2. Close the lid of the chamber immediately after placing the TLC plate in the chamber</li> <li>3. Replace solvent</li> </ol>
Total counts between samples are not consistent	<ol style="list-style-type: none"> <li>1. Mix the assay samples well before loading them onto the TLC plate by pipetting up and down</li> <li>2. Make sure to apply the whole volume in the tip of the pipette onto the TLC plate</li> <li>3. Make sure to excise spots exactly and to add in the correct scintillation vial</li> </ol>
Too high/too small readout after scintillation counting	<ol style="list-style-type: none"> <li>1. Adjust the concentration of the radioactive tracer</li> </ol>



## 5. 11 $\beta$ -HSD1 enzyme activity assay using microsomal preparations

This section describes the preparation of microsomal fractions from cultured cells expressing 11 $\beta$ -HSD1 and from tissue samples of disease

models. The use of microsomal fractions reduces cellular background due to an enrichment of 11 $\beta$ -HSD1, which is important when analyzing 11 $\beta$ -HSD1 activity in cell types with rather low expression, in disease models, or if testing for alternative substrates.

## 5.1 Microsomal preparation from cultured cells

This section describes the preparation of microsomes from cells overexpressing 11 $\beta$ -HSD1 that may be used in the radiometric enzyme activity assay (see Section 4.3). We recommend to use a cell line stably overexpressing 11 $\beta$ -HSD1, which is less laborious than the use of transiently transfected HEK-293 cells. The protocol can be adapted if other cell lines or transfection methods are used. The enrichment of 11 $\beta$ -HSD1 in microsomal fractions and removal of cytoplasmic and mitochondrial enzymes can facilitate the discovery and assessment of new substrates. To investigate a potentially new 11 $\beta$ -HSD1 substrate, the compound of interest together with the appropriate cofactor are used instead of cortisol or cortisone in the enzyme activity assay. Microsomal preparations from untransfected cells not expressing 11 $\beta$ -HSD1 or the use of a selective inhibitor serve as control to exclude interference by other enzymes. For quantification by scintillation counting a radiolabeled compound has to be used. If a radiolabeled substrate is not commercially available, substrate and product can be separated chromatographically (HPLC, GC) and quantified by UV-detection (DAD) or mass spectrometry (MS). In general, radioactive quantification is more sensitive than UV-detection and mass spectrometry; thus, reaction volume, substrate concentration and amount of microsomes need to be established experimentally. Examples for enzyme activity assays in the absence of a radiolabeled substrate to assess new 11 $\beta$ -HSD1 substrates using microsomal preparations or whole cell lysates have been reported elsewhere (Beck, Inderbinen, et al., 2019; Beck, Kanagaratnam, et al., 2019; Hult et al., 2004; Meyer, Vuorinen, Zielinska, Da Cunha, et al., 2013; Meyer, Vuorinen, Zielinska, Strajhar, et al., 2013; Odermatt et al., 2011; Schweizer et al., 2004) (see also chapter “*In vitro* methods for 11 $\beta$ -hydroxysteroid dehydrogenase type 2 activity assessment”).

### 5.1.1 Equipment

- Plastic tube 15 mL (Sarstedt)
- Cell scraper (Sarstedt)
- Dounce homogenizer (Thermo Fisher Scientific)
- Branson tip sonicator (Thermo Fisher Scientific)
- Centrifuge with cooling function (5424 R, Eppendorf)

- Ultracentrifuge, pre-cooled at 4 °C (Optima™ MAX-XP Ultracentrifuge, Beckman Coulter, Brea, California, USA)
- Swinging-Bucket Rotor for Ultracentrifuge, pre-cooled at 4 °C (TLS-55, Beckman Coulter)
- Ultracentrifuge tubes (Polypropylene Centrifuge Tubes 11 × 34 mm, Beckman Coulter)
- Liquid nitrogen or dry ice

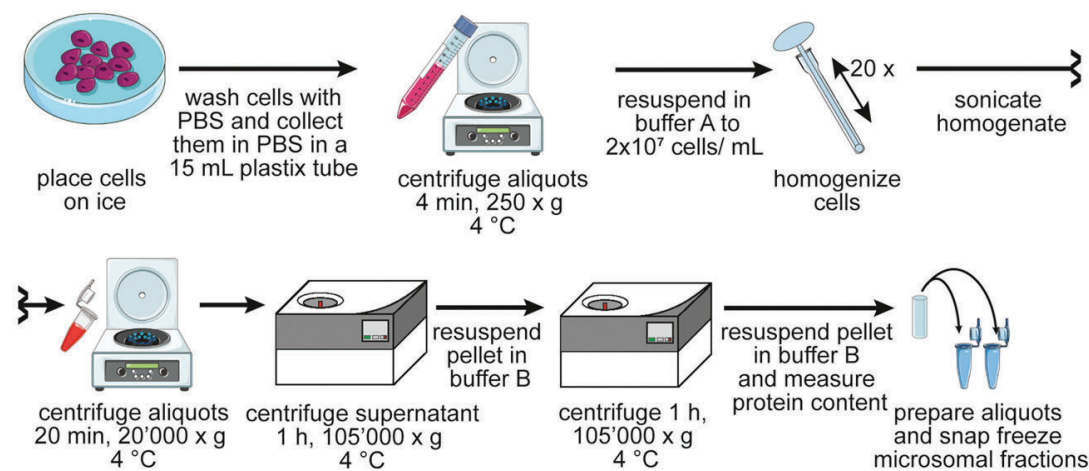
### 5.1.2 Buffers, media, and kits

- PBS
- Buffer A (50 mM Tris, 1 mM EDTA, 100 mM NaCl, pH 7.5, store at 4 °C)
- Buffer B (20 mM Tris, 1 mM EDTA, 10% glycerol, pH 7.5, store at 4 °C)
- RIPA buffer (store at 4 °C)
- Pierce™ BCA Protein Assay Kit (Thermo Fisher Scientific)

### 5.1.3 Procedure

1. Prepare at least four 10 cm culture dishes of 11 $\beta$ -HSD1 transfected HEK-293 cells according to subchapter 4.1 and culture the transfected cells until they reach confluence (see Fig. 7).
2. Pre-cool the centrifuge to 4 °C, prepare a big ice box and 5 mL of ice-cold PBS per culture dish.
3. Remove the prepared culture dishes from the incubator and immediately place them on ice.

**Critical: All subsequent steps should be performed at 4 °C**



**Fig. 7 Schematic overview of microsomal preparation of cells overexpressing 11 $\beta$ -HSD1.** After collection and homogenization of transfected cells, the microsomal fraction is isolated by several centrifugation steps and aliquoted after resuspension.

4. Aspirate the medium from the cells and wash carefully with 3 mL ice-cold PBS per dish.
5. Aspirate the PBS, add 1 mL ice-cold PBS to each dish and use the cell scraper to detach the cells. Pool the cells in a 15 mL plastic tube.
6. Centrifuge the cells at 4 °C for 4 min at 150g, aspirate the supernatant and resuspend the pellet to a final concentration of  $\sim 2 \times 10^7$  cells/mL in ice-cold buffer A. Then transfer the cell suspension to a Dounce homogenizer. (see Note a.)
7. Homogenize the cells with a total of 20 pestle passes. Store the homogenizer containing the cell homogenate for 10 s on ice after every fifth stroke.
8. Transfer the homogenate to a 15 mL plastic tube and sonicate twice on ice for 30 s at 10% amplitude. (see Note b.)
9. Centrifuge the homogenate at 4 °C for 20 min at 20'000g to pellet nuclei and mitochondria and transfer the supernatant into ultracentrifuge tubes. Equilibrate the tubes by adding buffer A.
10. Run the samples in the ultracentrifuge at 4 °C for 1 h at 105'000g.
11. After centrifugation, resuspend the pellet in buffer B using the same volume loaded previously to the ultracentrifuge tubes. Resuspend by scraping the bottom of the ultracentrifuge tube while pipetting the microsomal fraction up and down. Avoid foaming. Equilibrate the tubes with buffer B. (see Note c.)
12. Repeat the ultracentrifugation step.
13. Carefully remove the supernatant, resuspend the barely visible pellet in 60  $\mu$ L buffer B per initially used 10 cm dish of transfected cells. (see Note c.)
14. Transfer the suspension into a 1.5 mL plastic tube and homogenize large microsomes by pipetting the microsomal fraction up and down with a 100  $\mu$ L pipette tip. Store the microsomal fraction on ice.
15. Measure the protein concentration with the BCA Protein Assay Kit. It is recommended to dilute an aliquot of the prepared microsomes at least 1:6 in RIPA buffer before determining the protein concentration according to the manufacturer's protocol. (see Note d.)
16. Split the microsomal fraction into aliquots and snap freeze the aliquots in liquid nitrogen or freeze them for 10 min on dry ice. Store the aliquots at  $-80$  °C. (see Note e.)  
Breakpoint: The experiment can be paused here and continued when it convenes.
17. Use one aliquot of microsomes for an enzyme activity assay as described in subchapter 4.3 instead of a diluted cell lysate. Dilute the

microsomes by adding TS2 buffer and use it directly to start a reaction, without additional sonication. (see Note f.)

### 5.1.4 Notes

- a. Confluent 10 cm culture dishes contain up to  $1 \times 10^7$  HEK-293 cells per dish.
- b. Avoid heating during sonication of the homogenate.
- c. The microsomal fraction often sticks to the pipette tip during resuspension. It is therefore recommended to cut the end of a 100  $\mu$ L tip horizontally approx. 0.5 cm above its narrow end; use this modified tip for resuspension. The microsomes after resuspension have a turbid but homogenous appearance.
- d. The dilution factor may vary if another cell type or transfection method is used to overexpress 11 $\beta$ -HSD1.
- e. It is recommended to initially use 20  $\mu$ L aliquots of microsomes, which may be optimized, depending on the total dilution factor needed to achieve a substrate conversion of 20–30% after a 10 min reaction time and the number of reactions to be performed in an experiment.
- f. The activity and dilution factor for the microsomal preparation depends on the transfection efficiency, the cell type used and the quality of the preparation. Determine the dilution factor by assessing a dilution series of the microsomal fraction as described in subchapter 4.3, Note b. for cell lysate. Determine the total amount of microsomal protein used per reaction to have a benchmark for dilution for further experiments.

## 5.2 Advantages and limitations of microsomal preparations from transfected cells

Advantages	Limitations
Assessment of new 11 $\beta$ -HSD1 substrates by removing other enzymes and lowering cellular background is facilitated	Microsomal preparations are time-consuming
Enrichment of 11 $\beta$ -HSD1, high levels after overexpression of the enzyme	<ol style="list-style-type: none"> <li>1. Partial loss of enzyme activity during homogenization and centrifugation is possible</li> <li>2. Only apparent <math>K_m</math> and <math>V_{max}</math> of 11<math>\beta</math>-HSD1 can be determined (protein is not purified)</li> </ol>



Overexpression in cultured cells allows comparison of 11 $\beta$ -HSD1 homologs from different species and coexpression with other enzymes such as H6PD	Upon disruption of the cell, interactions with other proteins may be impaired (i.e., H6PD)
---	--

### 5.2.1 Optimization and troubleshooting

Problem	Possible solutions
Lack of enzyme activity of the microsomal fraction	<ol style="list-style-type: none"> <li>1. Confirm 11<math>\beta</math>-HSD1 expression in HEK-293 cells and its enrichment after preparation of microsomes</li> <li>2. Check the percentage of total solvent per reaction</li> <li>3. Assess enzyme activity after prolonged reaction time (e.g. 20 min, 30 min, ...)</li> <li>4. If not previously implemented: use HEK-293 cells for overexpression of 11<math>\beta</math>-HSD1</li> <li>5. Confirm 11<math>\beta</math>-HSD1 activity in whole cell lysate</li> <li>6. Prepare microsomes using only one ultracentrifugation step</li> </ol>
11 $\beta$ -HSD1 is degraded during preparation of microsomes (confirmed by Western blotting)	<ol style="list-style-type: none"> <li>1. Include 1 <math>\times</math> cOmplete, Mini Protease Inhibitor Cocktail (Roche, Rotkreuz, Switzerland) in buffer A and B to prevent protein degradation</li> <li>2. Ensure constant cooling of the samples during microsomal preparation</li> </ol>
Observed mass balance between novel substrate and its product before and after the reaction is not fulfilled	<ol style="list-style-type: none"> <li>1. Examine substrate conversion in microsomes of non-transfected cells to exclude other interfering enzymes</li> <li>2. Repeat the microsomal preparation with another cell line</li> </ol>

See Section 4.8 for further optimization of the enzyme reaction or TLC separation.

### 5.3 Preparation of microsomes from tissue samples

This section describes the isolation of microsomes from tissue samples to assess 11 $\beta$ -HSD1 activity. Tissue samples can be obtained from human biopsies or experimental animals. Tissues consist of different cell types embedded in an extracellular matrix; thus, the heterogeneity of the sample material has to be kept in mind when preparing the samples. The isolation of the microsomal fraction results in an enrichment of 11 $\beta$ -HSD1 and removal of cytoplasmic and mitochondrial enzymes.

### 5.3.1 Equipment

- Potter-Elvehjem homogenizer (Thermo Fisher Scientific)
- Overhead stirrer (R50, CAT, Ballrechten-Dottingen, Germany)
- Branson tip sonicator (Model 250 CE, Thermo Fisher Scientific)
- Centrifuge with cooling function, pre-cooled at 4 °C (5424 R, Eppendorf)
- Ultracentrifuge, pre-cooled at 4 °C (Optima™ MAX-XP Ultracentrifuge, Beckman Coulter)
- Swinging-Bucket Rotor for ultracentrifuge, pre-cooled at 4 °C (TLS-55, Beckman Coulter)
- Ultracentrifuge tubes (Polypropylene centrifuge tubes 11 × 34 mm, Beckman Coulter)
- Liquid nitrogen or dry ice

### 5.3.2 Buffers, media, and kits

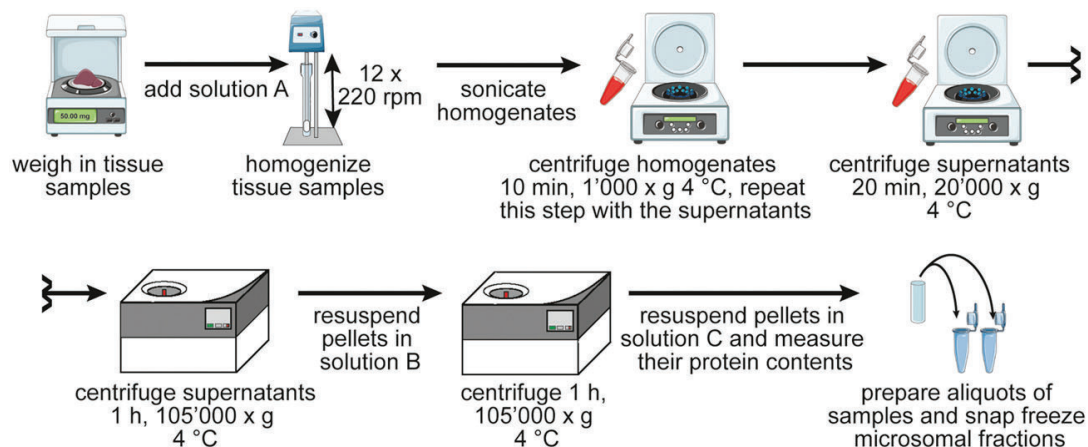
- **Solution A** freshly prepared prior to use (10 mM imidazole, 0.3 M sucrose, pH 7.0, supplemented with 1% of 7x cOmplete, Mini Protease Inhibitor Cocktail (Roche), store at 4 °C)
- **Solution B** freshly prepared prior to use (20 mM Tris-maleate, 0.6 M KCl, 0.3 M sucrose, pH 7.0, supplemented with 1% of 7x cOmplete, Mini Protease Inhibitor Cocktail (Roche), store at 4 °C)
- **Solution C** freshly prepared prior to use (10 mM Tris-maleate, 0.15 M KCl, 0.25 M sucrose, pH 7.0 supplemented with 1% of 7x cOmplete, Mini Protease Inhibitor Cocktail (Roche), store at 4 °C)
- **RIPA buffer**
- **Pierce™ BCA Protein Assay Kit** (Thermo Fisher Scientific)

### 5.3.3 Procedure

1. Place weighted fresh or frozen organ pieces into the Potter-Elvehjem homogenizer and add 2 mL ice-cold solution A per 100 mg tissue. (see Fig. 8 for an overview of the procedure; see Note a.)

**Critical: Keep the tissue samples and homogenates on ice whenever possible and immediately perform the subsequent protocol steps.**

2. Using the overhead stirrer under rotation at 220 rpm, homogenize the samples by moving the cylindrical glass tube 10–12 times up and down the pestle and transfer the homogenates to 2 mL plastic tubes.
3. Sonicate the homogenate with 5 pulses (output 2, duty cycle 20) of the Branson tip sonicator. (see Note b.)



**Fig. 8 Schematic overview of the preparation of microsomes from tissues expressing 11 $\beta$ -HSD1.** After collection, homogenization and sonication of tissue, the microsomal fraction is purified by several centrifugation steps and aliquoted after resuspension.

4. Centrifuge the samples at 4 °C for 10 min at 1000g, to pellet the nuclear fractions, then transfer the supernatants to new plastic tubes. Repeat this step.
5. Centrifuge the supernatants at 4 °C for 20 min at 20,000g to pellet the mitochondrial fractions, then transfer the supernatants to ultracentrifugation tubes. Equilibrate the tubes by adding solution A.
6. Run the ultracentrifuge at 4 °C for 1 h at 105,000g.
7. Discard the supernatants and resuspend the pellets in 0.5 mL of solution B per 100 mg initial tissue weight. Equilibrate the tubes by adding solution B. (see Note c.)
8. Wash the microsomes by centrifugation at 4 °C for 1 h at 105,000g.
9. Discard the supernatants and resuspend the pellets in 0.2 mL of solution C per 100 mg initial tissue weight and transfer the suspensions to 1.5 mL plastic tubes. (see Note c.)
10. Spin the samples at 4 °C for 5 s at maximal speed to remove debris, transfer the supernatants containing the microsomes to new plastic tubes.
11. Homogenize the microsomes by pipetting the microsomal fraction up and down with a 100  $\mu$ L pipette tip. Store the microsomal fractions on ice.
12. Measure the protein concentration of the microsomal fractions using the BCA Protein Assay Kit. It is recommended to dilute an aliquot of the prepared microsomes before determining the protein concentrations according to the manufacturer.
13. Split the microsomal fractions into aliquots and snap freeze the aliquots in liquid nitrogen or freeze them for 10 min on dry ice. Store the aliquots at  $-80$  °C. (see Note d.)

Breakpoint: The experiment can be paused here and continued when it convenes.

14. Use one aliquot of microsomal fraction in the enzymatic activity assay described in subchapter 4.3 instead of diluted cell lysate. Dilute the microsomal fraction by adding TS2 buffer and use it directly for a reaction without additional sonication. (see Note e.)

### 5.3.4 Notes

- a. When comparing microsomes from tissues of different animals, make sure to consistently use the same parts of a tissue, e.g. the same lobe of the liver, or a symmetrically cut half of a kidney, or a whole organ grinded and mixed well before taking comparable amounts for microsomal preparation. This helps optimizing the reproducibility between samples of different individuals.
- b. Avoid heating during sonication of the homogenate.
- c. The microsomal preparation often sticks to the pipette tip during the resuspension step. It is therefore recommended to cut a 100  $\mu\text{L}$  pipette tip horizontally approx. 0.5 cm above its narrow end and using this modified tip for resuspension. The microsomal fraction after resuspension looks turbid but homogenous.
- d. It is recommended to use aliquots of 20  $\mu\text{L}$ . This can be adjusted depending on the dilution factor needed to reach a total substrate conversion of 20–30% after 10 min of reaction time and the number of reactions to be performed.
- e. Determine this dilution factor by assessing a dilution series of the microsomal preparation as described in subchapter 4.3, Note b. for cell lysates. Determine the total amount of microsomal protein used per reaction to have a benchmark for dilution for further microsomal preparations.

## 5.4 Advantages and limitations of using microsomal preparations from tissue samples for 11 $\beta$ -HSD1 activity measurements

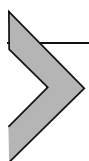
Advantages	Limitations
Allows comparison of 11 $\beta$ -HSD1 activity in tissue biopsies from different human cohorts or from experimental animals (–disease models)	<ol style="list-style-type: none"> <li>1. Time-consuming process</li> <li>2. Possible bias due to different composition of the tissue (fibrotic tissue, lipid accumulation)</li> <li>3. Partial loss of enzyme activity during homogenization and centrifugation is possible</li> </ol>

Enrichment of 11 $\beta$ -HSD1 through microsomal preparation	<ol style="list-style-type: none"> <li>1. Only apparent <math>K_m</math> and <math>V_{max}</math> of 11<math>\beta</math>-HSD1 can be determined (protein is not purified)</li> <li>2. Most tissues exhibit lower 11<math>\beta</math>-HSD1 levels than microsomal preparations from overexpressing cells</li> </ol>
---	--

## 5.5 Optimization and troubleshooting

Problem	Possible solutions
The microsomal preparation shows no enzyme activity	<ol style="list-style-type: none"> <li>1. Confirm 11<math>\beta</math>-HSD1 expression in the tissue sample and its enrichment after microsomal preparation</li> <li>2. Check the percentage of total solvent per reaction</li> <li>3. Assess enzyme activity after prolonged reaction time (e.g. 20 min, 30 min, ...)</li> <li>4. Prepare microsomes with only one ultracentrifugation step</li> <li>5. If degradation during tissue storage cannot be excluded, repeat with a new tissue sample</li> </ol>
11 $\beta$ -HSD1 is degraded during microsomal preparation (confirmed by Western blotting)	<ol style="list-style-type: none"> <li>1. Use 1 <math>\times</math> cOmplete, Mini Protease Inhibitor Cocktail (Roche) in solutions A to C instead of only 1%</li> <li>2. Ensure constant cooling of the samples during microsomal preparation</li> </ol>

See Section 4.8 for further optimization of the enzyme reaction or TLC separation.



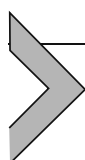
## 6. Enzyme activity assay using purified 11 $\beta$ -HSD1

Assessment of accurate kinetic parameters including  $K_m$  for a particular substrate and elucidation of the exact mechanism of action of an inhibitor requires using pure protein. 11 $\beta$ -HSD1 is an integral protein of the ER-membrane with a luminal orientation and its topology is important for the interaction with H6PD, supplying cofactor NADPH and coupling glucocorticoid activation to glucose metabolism (Atanasov et al., 2008; Mziaut et al., 1999; Odermatt et al., 1999). Thus, removal of 11 $\beta$ -HSD1 from the ER-membrane and purification to homogeneity is a challenge, and during early attempts of purification the biologically important oxoreductase function of the enzyme was at least partially lost (Bush, Hunter, & Meigs, 1968; Lakshmi & Monder, 1985). Later,

successful purification of 11 $\beta$ -HSD1 was achieved by using an N-terminally His<sub>6</sub>-tagged protein and nickel columns as well as optimized detergent conditions (Nobel et al., 2002; Shafqat et al., 2003). Both, the full-length protein and a modified soluble version lacking the N-terminal transmembrane domain retained their enzyme activity for glucocorticoids and 7-ketocholesterol after purification (Hult et al., 2004). The detailed description of 11 $\beta$ -HSD1 purification is out of the scope of this chapter and we refer to excellent earlier studies (Nobel et al., 2002; Shafqat et al., 2003).

## 6.1 Advantages and limitations of using purified 11 $\beta$ -HSD1

Advantages	Limitations
Determination of accurate $K_m$ and $V_{max}$ for different 11 $\beta$ -HSD1 substrates	Time-consuming and expensive process
Determination of $K_I$ for inhibitors	Partial or complete loss of enzyme activity during purification cannot be excluded
Possibility of co-crystallization and obtaining structural information	Each batch of purified protein requires verification of purity; conditions when using ligands might need to be adapted
Suitable for HTS and read-outs using antibody-based detection	



## 7. 11 $\beta$ -HSD1 activity assay in intact cells

11 $\beta$ -HSD1 enzyme activity can also be measured in intact cells. Measurements in intact cells do not require addition of exogenous NADPH because the hydrophilic cofactor cannot freely permeate cellular membranes. Cofactor concentration and other parameters such as ionic strength are in a physiological context. If cells expressing H6PD are used, NADPH is regenerated in the ER-lumen and mainly the 11 $\beta$ -HSD1 oxoreductase activity is measurable. Despite a lower total enzyme activity in intact cell systems, the time of incubation can be chosen considerably longer than in cell-free assays. Intact cell assays may be used for the identification of alternative substrates, if a prolonged incubation time is required due to a specific experimental setup or for the characterization of a selected inhibitor. Access of inhibitors to 11 $\beta$ -HSD1 in an intact cell system or the absence or presence of other proteins such as H6PD may also be

addressed. Because chemicals do not have direct access to the 11 $\beta$ -HSD1 ligand binding pocket due to the membrane barrier and access may be restricted by efflux transporters, intact cell systems are not an ideal choice for inhibitor screening purposes.

## 7.1 Radiometric activity assay using intact cells

### 7.1.1 Equipment

- Sterile filter 0.2  $\mu$ M (Filtropur S 0.2, Sarstedt, Nümbrecht, Germany)
- Cell incubator
- Rolling mixer (RM5, CAT)
- Centrifuge (5810 R, Eppendorf)
- See-saw wave rocker (SSL4, Witec AG, Sursee, Switzerland)
- Plastic tubes 15 mL (Sarstedt)
- **Pre-coated 96-well cell culture plates** (dilute 0.1% Poly L-Lysin solution in PBS to 0.05%, add 20  $\mu$ L thereof to each well of a 96-well plate and sway on the see-saw wave rocker for 1 h at RT. Wash the plate three times with 100  $\mu$ L PBS, remove PBS and store in sealed plastic bag at 4  $^{\circ}$ C up to a year)

### 7.1.2 Cell line

- Human Embryonic Kidney-293 cells (HEK-293, ATCC)

### 7.1.3 Plasmids

- C-terminally FLAG-tagged human *HSD11B1* in a pcDNA3.1 backbone (Odermatt et al., 1999)
- Optional cotransfection to increase 11 $\beta$ -HSD1 activity: c-myc-tagged human *H6PD* in a pcDNA3 backbone (Atanasov et al., 2004)

### 7.1.4 Buffers and media

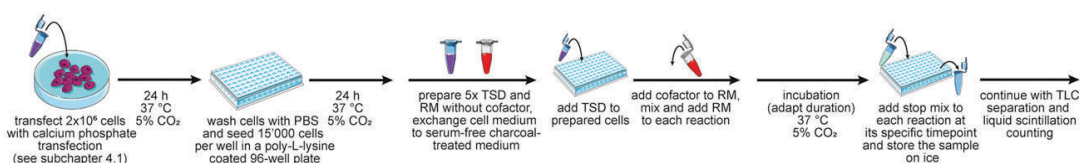
- PBS
- Complete HEK-293 medium
- Serum-free HEK-293 medium (complete HEK-293 medium without FBS)
- Serum-free, charcoal treated HEK-293 medium (Add 0.2 g of charcoal to 50 mL serum-free HEK-293 medium in a 50 mL plastic tube, wrap it in aluminum foil and put it on the rolling mixer for 1 h. Pellet the charcoal

by centrifugation at 2'000g for 4 min, decant the medium into a new 50 mL plastic tube and repeat the charcoal treatment. Sterile filtrate the medium using a 0.2 µm filter and store it at 4 °C)

- Trypsin-EDTA solution (Sigma-Aldrich)
  - [1,2,6,7-<sup>3</sup>H]-labeled cortisone stock solution ~4 µM (dilute <sup>3</sup>H-cortisone (American Radiolabeled Chemicals) with ethanol if needed, store at -20 °C)
  - Unlabeled cortisone stock solution 10 mM in DMSO (store at -20 °C)
  - Stop mix (2 mM cortisol, 2 mM cortisone in methanol, store at 4 °C, see subchapter 4.3 Note d.)
  - Test substance stocks 10 mM in DMSO or methanol (store at -20 °C)
- See Section 4.1 for transfection and overexpression of 11β-HSD1 in HEK-293 cells.

### 7.1.5 Procedure

1. Transfect  $2 \times 10^6$  HEK-293 cells with a plasmid for overexpression of 11β-HSD1 using the calcium phosphate precipitation method described in the subchapter 4.1. (see Fig. 9 for an overview of the procedure; see Note a.)
2. After 24 h of transfection, wash the cells carefully with 5 mL PBS per 10 cm culture dish and detach them using 1 mL trypsin-EDTA solution for 5 min in the incubator under standard conditions.
3. Add 4 mL of complete HEK-293 medium to the detached cells and mix them carefully by pipetting up and down. Transfer the cells to a 10 mL plastic tube.



**Fig. 9 Schematic overview of the radiometric 11β-HSD1 activity assay in intact cells.** Cells are transfected for overexpression of 11β HSD1. Subsequently, the cells are seeded in a 96-well plate and allowed to adhere. After changing to serum-free medium, test substance dilutions (TSD, purple plastic tube) are added to the cells. After adding the cofactor to the reaction mix (RM, red plastic tube), the cells are incubated under standard conditions for different time periods to reach a total substrate conversion of 20–30%. At each time point, the reactions are stopped by adding the stop mix (green plastic tube). Quantification of substrate and product of the samples is performed by TLC separation and scintillation counting.



4. Pellet the cells at 200g for 4 min, discard the supernatant and resuspend the cells in 5 mL fresh complete HEK-293 medium.
5. Seed 15'000 cells per well in a total volume of 100  $\mu$ L complete HEK-293 medium into a poly-L-lysine coated 96-well plate. Include technical duplicates for each condition assessed. Include two solvent control wells as well as two empty wells as background samples per assessment time point. Incubate the cells for an additional 24 h under standard conditions.
6. Prepare 0.5% solvent control solution (either 0.5% DMSO or 0.5% methanol), in charcoal treated serum-free HEK-293 medium, depending on solvent used for the test substance stocks.
7. Dilute the test substance stock solutions first in the respective solvent (DMSO or methanol), then 1:200 in serum-free charcoal treated HEK-293 medium, reaching 5  $\times$  of the concentration to be assessed with a total solvent content equal to 0.5% (the final addition of the test substance dilution to the reaction mixture will result in a 1:5 dilution). (see Note b.)

**Critical: Perform the subsequent steps immediately.**

1. Aspirate the medium from the transfected cells and add 30  $\mu$ L of charcoal treated, serum-free HEK-293 medium to each well. Use 40  $\mu$ L thereof for the prepared empty background samples.
2. Add 10  $\mu$ L of the prepared test substance dilutions or the 0.5% solvent control to the respective wells.
3. Dilute the 10 mM unlabeled cortisone stock solution 1:100 in charcoal treated, serum-free HEK-293 medium to reach a 100  $\mu$ M working dilution.
4. Prepare the reaction mix according to Table 2 and quickly add 10  $\mu$ L of reaction mix to each prepared well, including solvent control and background wells.
5. Incubate the cells under standard conditions for different time periods (5 min; 10 min; 20 min; 40 min; etc.) to find the optimal substrate conversion of 20–30% for the solvent control. (see Note c.)
6. To stop a reaction at a specific time point, add 20  $\mu$ L of stop mix and transfer the entire sample into a 1.5 mL plastic tube and store at 4  $^{\circ}$ C.
7. Continue with the TLC separation and liquid scintillation protocol as described in subchapter 4.4, load a total of 20  $\mu$ L per sample onto the TLC plate instead of 10  $\mu$ L.

### 7.1.6 Notes

- a. Other cell types transfected by different techniques or cells endogenously expressing 11 $\beta$ -HSD1 may also be used. However, it should be

**Table 2** Preparation of reaction mix for 25 reactions (oxoreductase activity of 11 $\beta$ -HSD1).

Buffer/solution	Amount to add	Final concentration per reaction and well
Serum-free charcoal treated HEK-293 medium	270 $\mu$ L	
<sup>3</sup> H-cortisone [ $\sim$ 4 $\mu$ M]	1.7 $\mu$ L	5 nM
Unlabeled cortisone working solution [100 $\mu$ M] in serum-free charcoal treated HEK-293 medium	2.7 $\mu$ L	195 nM

This Table lists final concentrations and the respective volumes of medium and substrate solutions for the reaction mix for the radiometric enzyme activity assay in intact cells. The amount of prepared reaction mix considers dead volumes of pipet tips.

noted that other cell systems may show different sensitivity to solvents and cytotoxicity towards test substances.

- b. The final solvent concentration in the experiment should be kept low in order to avoid a negative impact on cell viability. A total solvent concentration up to 0.2% (DMSO, methanol, ethanol) is usually well tolerated by HEK-293 cells.
- c. It is advisable to perform cell viability assays, such as the XTT assay, using the same total solvent and inhibitor concentration in the media and incubation time as for the treatments in the activity assay. For treatment times longer than 8 h consider using regular HEK-293 medium containing serum. Take into account that the test substances might bind to serum proteins in the medium.

## 7.2 Data analysis of 11 $\beta$ -HSD1 activity from intact cell-based assays

To calculate the 11 $\beta$ -HSD1-dependent conversion of cortisone to cortisol by the cells, the counts for the product after liquid scintillation measurements are divided by the total counts (sum of counts for product and substrate). The background counts obtained from controls with cells not expressing 11 $\beta$ -HSD1 or from samples in the absence of cells are subtracted from the values of the reactions. The conversion obtained for a treated sample is normalized to that of the solvent control, yielding a fold change of 11 $\beta$ -HSD1 enzyme activity.

### 7.3 Advantages and limitations of intact cell-based activity assays

<b>Advantages</b>	<b>Limitations</b>
Activity measurements in intact cells allow investigating effects of factors on enzyme reaction direction	The fact that this assay is a closed system without a flux of metabolites needs to be kept in mind
Allows comparison of 11 $\beta$ -HSD1 homologs from different species in an identical background	Species-specificity of proteins and other factors influencing 11 $\beta$ -HSD1 activity are not considered
No direct access of inhibitors due to cell membrane barriers	Specificity of transport proteins is highly cell-type dependent
Cells endogenously expressing 11 $\beta$ -HSD1 can be employed	1. Prolonged incubation time needed 2. Low throughput
Effects on 11 $\beta$ -HSD1 expression can be assessed	Restricted to mechanistic studies

### 7.4 Optimization and troubleshooting

<b>Problem</b>	<b>Possible solutions</b>
1. Inefficient conversion of cortisone by transfected cells	1. Confirm 11 $\beta$ -HSD1 expression by Western blotting
2. Inefficient conversion of cortisone by cell model endogenously expressing 11 $\beta$ -HSD1	2. Check the percentage of final solvent concentration in the reaction
	3. Cotransfect cells with H6PD
	4. Choose prolonged incubation time
	5. Use HEK-293 to overexpress 11 $\beta$ -HSD1 (if not previously implemented)
	6. Verify expression of 11 $\beta$ -HSD1 and H6PD in endogenous cell system by Western blotting
	7. Test for absence of 11 $\beta$ -HSD2 expression
	8. Increase the incubation time, up to 8 h
	9. Verify that total counts are not substantially decreasing over time (indicating the presence of other metabolizing enzymes)
	10. Consider limited access of the test-compound
	11. Consider transporter activity

See Section 4.8 for further optimization of the enzyme reaction or TLC separation.



## 8. Alternative quantification methods

Besides using radiolabeled tracers of the substrate and scintillation counting as a readout, there are other methods to measure 11 $\beta$ -HSD1 enzyme activity. Cortisol and cortisone can be directly quantified after the reaction using either mass spectrometry (MS) or UV-detection with previous separation by liquid- or gas-chromatography. Additionally, 11 $\beta$ -HSD1 activity can be assessed by antibody-based quantification of cortisol and cortisone formation.

### 8.1 Quantification using HPLC-DAD, GC-MS or LC-MS

Cortisone and cortisol both absorb light in the UV spectrum and thus allow their detection by a diode array detector (DAD) after HPLC separation (HPLC-DAD), which has been applied in early studies using different sample types such as serum, saliva and urine (Jenner & Richards, 1985; Turpeinen & Hamalainen, 2013). With the development of mass spectrometry the sensitivity and specificity for substrate and product detection was increased, allowing quantification of cortisone and cortisol at very low limits of detections through GC-MS and LC-MS methods (Arioli et al., 2022; Fariha et al., 2022; Lee et al., 2014; Shackleton, 1993). The chromatographic separation of analytes by liquid or gas chromatography with subsequent detection using mass spectrometry or UV-measurement can also be used to quantify other substrate/product pairs of 11 $\beta$ -HSD1, including prednisone/prednisolone (Cooper et al., 2003; Escher, Meyer, Vishwanath, Frey, & Frey, 1995), 11keto-androstenedione/11 $\beta$ -hydroxyandrostenedione and 11keto-testosterone/11 $\beta$ -hydroxytestosterone (Gent, du Toit, Bloem, & Swart, 2019), 7-ketocholesterol/11 $\beta$ -hydroxycholesterol (Hult et al., 2004; Schweizer et al., 2004; Song, Chen, Dean, Redinger, & Prough, 1998), and 7 $\alpha$ -oxo-lithocholic acid/ursodeoxycholic acid (Odermatt et al., 2011).

The establishment and sensitivity of a quantification method using HPLC-DAD and GC-MS or LC-MS is dependent on the available equipment and requires appropriate analytical expertise. When using HPLC-DAD, GC-MS or LC-MS methods, the conditions described for the radiometric enzyme activity assay (see previous Sections) need to be adapted. For example, a larger reaction volume or an initially higher substrate concentration and/or performing an additional extraction step to remove salts or proteins from the sample matrix might be needed to achieve an optimal readout. (see also Chapter on 11 $\beta$ -HSD2).

## 8.2 Advantages and limitations of using HPLC, GC-MS or LC-MS

Advantages	Limitations
No radiotracers or scintillation counter needed, no special laboratory for work with radiolabeled compounds required, no radioactive waste disposal	<ol style="list-style-type: none"> <li>1. Expensive equipment</li> <li>2. Professional expertise required</li> </ol>
Simultaneous detection and identification of several substrate/product pairs as well as formed metabolites possible	<ol style="list-style-type: none"> <li>1. Method development is time consuming</li> <li>2. Moderate limit of quantification, larger amounts of biological material required</li> </ol>
Not limited to cortisone/cortisol, applicable for the detection of novel 11 $\beta$ -HSD1 substrates	<ol style="list-style-type: none"> <li>1. Laborious sample preparation might be required to avoid instrument break down and/or enhance sensitivity</li> <li>2. Limited suitability for HTS of novel 11<math>\beta</math>-HSD1 inhibitors</li> </ol>
HPLC: relatively easy to use; usually label-free quantification	<ol style="list-style-type: none"> <li>1. HPLC requires solubility of the screening compounds within the specific method</li> <li>2. Limited sensitivity requires larger sample amount/volume</li> </ol>
LC-MS: high sensitivity and specificity; usually label-free quantification; sensitivity can be further enhanced by derivatization	<ol style="list-style-type: none"> <li>1. Requirement for pure standards, ideally deuterized standards; time-consuming method validation</li> </ol>
GC-MS: sensitivity can be enhanced after specific derivatization of the desired substrate/product pair.	<ol style="list-style-type: none"> <li>1. GC-MS: need for derivatization; time-consuming method validation</li> </ol>

## 8.3 Quantification using ELISA kits

Commercially available kits for cortisol or cortisone detection (i.e. from Thermo Fisher Scientific, or Roche) may be used to measure product formation in the enzyme assay. These kits are usually based on the competitive ELISA principle and contain an internal standard for concentration determination. The reaction conditions need to be optimized first to obtain sufficient amounts of product, in the range of the calibration curve of the respective kit. Parameters to be checked include concentration or expression level of 11 $\beta$ -HSD1, total reaction volume, initial substrate concentration, reaction time and cross-reactivity of the antibody. Furthermore, it is not recommended to terminate the enzyme reaction using solvent as this could interfere with the antibody used in the ELISA detection kit. The reactions can be terminated by heat denaturation of the protein instead.

## 8.4 Advantages and limitations of ELISA kits

Advantages	Limitations
Time efficiency	Requires adaptation of the activity assay protocol
Kit-based assay with well-adapted and -explained procedures, normal plate reader for analysis, no specialized instrumentation required, suitable for HTS of novel 11 $\beta$ -HSD1 inhibitors	Cross reactivity of detection antibodies between cortisol and cortisone vary depending on the kit that is used
Higher sensitivity of antibody-based detection than HPLC-DAD	Might require microsomal preparation or enzyme purification due to cross-reactivity of antibodies with other substances of unknown identity in the matrix
Routine procedure easy to transfer between laboratories	May require validation in complex matrices by preparing standard curves in the same matrix and by spiking of individual samples to verify detection

## 9. Safety considerations and standards of the described methods

Handling of HEK-293 cells requires biosafety level 1 standard (BSL-1). We recommend adhering to the guidelines and safety precautions of your institution regarding the handling of tritiated compounds. Tritiated compounds should neither be ingested nor inhaled. TLC separation and scraping of the silica plates should always be conducted in a fume hood. The fumes of the mobile phase of the TLC are hazardous. While scraping TLC plates, wear gloves, a lab coat, safety glasses and a FFP2 mask to prevent ingestion or inhalation of silica dust containing radiolabeled steroids. Silica dust is toxic when inhaled.

## 10. Concluding remarks

Small molecules selectively inhibiting 11 $\beta$ -HSD1 and thereby lowering the production of cortisol are still of interest due to its potential value for the treatment of metabolic complications, osteoporosis, wound healing or inflammatory diseases. In addition, 11 $\beta$ -HSD1 enzyme activity measurements are of interest for the characterization of animal models of

metabolic and inflammatory disease and ultimately to study such disease in human. The modular structure of this chapter is built around the radio-metric whole cell lysate 11 $\beta$ -HSD1 activity assay. The decision tree at the beginning of the chapter should help planning of the experiments and answer specific predefined questions on research involving 11 $\beta$ -HSD1 activity. The detailed protocols and their advantages and limitations provide an overview of the currently practiced in vitro activity assays that may be used to investigate physiological roles of 11 $\beta$ -HSD1 or identify novel potential therapeutic inhibitors.

## Acknowledgments

We thank Tania Jetzer for proofreading and suggestions. We acknowledge Servier Medical Art (smart.servier.com) and AlphaFold Protein Structure Data Base (alphafold.ebi.ac.uk) (Jumper et al., 2021; Varadi et al., 2022) for providing elements used in the Figures of this chapter.

## References

- Agarwal, A. K., Monder, C., Eckstein, B., & White, P. C. (1989). Cloning and expression of rat cDNA encoding corticosteroid 11 beta-dehydrogenase. *The Journal of Biological Chemistry*, 264(32), 18939–18943. Retrieved from <https://www.ncbi.nlm.nih.gov/pubmed/2808402>.
- Agarwal, A. K., Mune, T., Monder, C., & White, P. C. (1994). NAD(+)-dependent isoform of 11 beta-hydroxysteroid dehydrogenase. Cloning and characterization of cDNA from sheep kidney. *The Journal of Biological Chemistry*, 269(42), 25959–25962. Retrieved from <https://www.ncbi.nlm.nih.gov/pubmed/7929304>.
- Agarwal, A. K., Tusie-Luna, M. T., Monder, C., & White, P. C. (1990). Expression of 11 beta-hydroxysteroid dehydrogenase using recombinant vaccinia virus. *Molecular Endocrinology (Baltimore, Md.)*, 4(12), 1827–1832. <https://doi.org/10.1210/mend-4-12-1827>
- Ajjan, R. A., Hensor, E. M. A., Del Galdo, F., Shams, K., Abbas, A., Fairclough, R. J., ... Tiganescu, A. (2022). Oral 11beta-HSD1 inhibitor AZD4017 improves wound healing and skin integrity in adults with type 2 diabetes mellitus: a pilot randomized controlled trial. *European Journal of Endocrinology/European Federation of Endocrine Societies*, 186(4), 441–455. <https://doi.org/10.1530/EJE-21-1197>
- Alberts, P., Nilsson, C., Selen, G., Engblom, L. O., Edling, N. H., Norling, S., ... Abrahamson, L. B. (2003). Selective inhibition of 11 beta-hydroxysteroid dehydrogenase type 1 improves hepatic insulin sensitivity in hyperglycemic mice strains. *Endocrinology*, 144(11), 4755–4762. <https://doi.org/10.1210/en.2003-0344>
- Albiston, A. L., Obeyesekere, V. R., Smith, R. E., & Krozowski, Z. S. (1994). Cloning and tissue distribution of the human 11 beta-hydroxysteroid dehydrogenase type 2 enzyme. *Molecular and Cellular Endocrinology*, 105(2), R11–R17. [https://doi.org/10.1016/0303-7207\(94\)90176-7](https://doi.org/10.1016/0303-7207(94)90176-7)
- Arioli, F., Gamberini, M. C., Pavlovic, R., Di Cesare, F., Draghi, S., Bussei, G., ... Fidani, M. (2022). Quantification of cortisol and its metabolites in human urine by LC-MS(n): Applications in clinical diagnosis and anti-doping control. *Analytical and Bioanalytical Chemistry*, 414(23), 6841–6853. <https://doi.org/10.1007/s00216-022-04249-3>

- Atanasov, A. G., Nashev, L. G., Gelman, L., Legeza, B., Sack, R., Portmann, R., & Odermatt, A. (2008). Direct protein-protein interaction of 11beta-hydroxysteroid dehydrogenase type 1 and hexose-6-phosphate dehydrogenase in the endoplasmic reticulum lumen. *Biochimica et Biophysica Acta*, 1783(8), 1536–1543. <https://doi.org/10.1016/j.bbamcr.2008.03.001>
- Atanasov, A. G., Nashev, L. G., Schweizer, R. A., Frick, C., & Odermatt, A. (2004). Hexose-6-phosphate dehydrogenase determines the reaction direction of 11beta-hydroxysteroid dehydrogenase type 1 as an oxoreductase. *FEBS Letters*, 571(1–3), 129–133. <https://doi.org/10.1016/j.febslet.2004.06.065>
- Banhegyi, G., Benedetti, A., Fulceri, R., & Senesi, S. (2004). Cooperativity between 11beta-hydroxysteroid dehydrogenase type 1 and hexose-6-phosphate dehydrogenase in the lumen of the endoplasmic reticulum. *The Journal of Biological Chemistry*, 279(26), 27017–27021. <https://doi.org/10.1074/jbc.M404159200>
- Barnes, P. J. (2011). Glucocorticosteroids: Current and future directions. *British Journal of Pharmacology*, 163(1), 29–43. <https://doi.org/10.1111/j.1476-5381.2010.01199.x>
- Beck, K. R., Inderbilen, S. G., Kanagaratnam, S., Kratschmar, D. V., Jetten, A. M., Yamaguchi, H., & Odermatt, A. (2019). 11beta-Hydroxysteroid dehydrogenases control access of 7beta,27-dihydroxycholesterol to retinoid-related orphan receptor gamma. *Journal of Lipid Research*, 60(9), 1535–1546. <https://doi.org/10.1194/jlr.M092908>
- Beck, K. R., Kanagaratnam, S., Kratschmar, D. V., Birk, J., Yamaguchi, H., Sailer, A. W., ... Odermatt, A. (2019). Enzymatic interconversion of the oxysterols 7beta,25-dihydroxycholesterol and 7-keto,25-hydroxycholesterol by 11beta-hydroxysteroid dehydrogenase type 1 and 2. *The Journal of Steroid Biochemistry and Molecular Biology*, 190, 19–28. <https://doi.org/10.1016/j.jsbmb.2019.03.011>
- Boudon, S. M., Vuorinen, A., Geotti-Bianchini, P., Wandeler, E., Kratschmar, D. V., Heidl, M., ... Odermatt, A. (2017). Novel 11beta-hydroxysteroid dehydrogenase 1 inhibitors reduce cortisol levels in keratinocytes and improve dermal collagen content in human ex vivo skin after exposure to cortisone and UV. *PLoS One*, 12(2), e0171079. <https://doi.org/10.1371/journal.pone.0171079>
- Brem, A. S., Morris, D. J., Ge, Y., Dworkin, L., Tolbert, E., & Gong, R. (2010). Direct fibrogenic effects of aldosterone on normotensive kidney: An effect modified by 11beta-HSD activity. *American Journal of Physiology. Renal Physiology*, 298(5), F1178–F1187. <https://doi.org/10.1152/ajprenal.00532.2009>
- Burton, R. B., Keutmann, E. H., Waterhouse, C., & Schuler, E. A. (1953). The conversion of cortisone acetate to other alphaketolic steroids. *The Journal of Clinical Endocrinology and Metabolism*, 13(1), 48–63. <https://doi.org/10.1210/jcem-13-1-48>
- Bush, I. E. (1956). The 11-oxygen function in steroid metabolism. *Experientia*, 12(9), 325–331. <https://doi.org/10.1007/BF02165330>
- Bush, I. E., Hunter, S. A., & Meigs, R. A. (1968). Metabolism of 11-oxygenated steroids. Metabolism in vitro by preparations of liver. *The Biochemical Journal*, 107(2), 239–258. <https://doi.org/10.1042/bj1070239>
- Bush, I. E., & Mahesh, V. B. (1959). Metabolism of 11-oxygenated steroids. 1. Influence of the A/B ring junction on the reduction of 11-oxo groups. *The Biochemical Journal*, 71(4), 705–717. <https://doi.org/10.1042/bj0710705>
- Cooper, M. S., Blumsohn, A., Goddard, P. E., Bartlett, W. A., Shackleton, C. H., Eastell, R., ... Stewart, P. M. (2003). 11beta-hydroxysteroid dehydrogenase type 1 activity predicts the effects of glucocorticoids on bone. *The Journal of Clinical Endocrinology and Metabolism*, 88(8), 3874–3877. <https://doi.org/10.1210/jc.2003-022025>
- Csernansky, J. G., Dong, H., Fagan, A. M., Wang, L., Xiong, C., Holtzman, D. M., & Morris, J. C. (2006). Plasma cortisol and progression of dementia in subjects with Alzheimer-type dementia. *The American Journal of Psychiatry*, 163(12), 2164–2169. <https://doi.org/10.1176/ajp.2006.163.12.2164>



- do Nascimento, F. V., Piccoli, V., Beer, M. A., von Frankenberg, A. D., Crispim, D., & Gerchman, F. (2015). Association of HSD11B1 polymorphic variants and adipose tissue gene expression with metabolic syndrome, obesity and type 2 diabetes mellitus: a systematic review. *Diabetol Metab Syndr*, 7, 38. <https://doi.org/10.1186/s13098-015-0036-1>
- Escher, G., Meyer, K. V., Vishwanath, B. S., Frey, B. M., & Frey, F. J. (1995). Furosemide inhibits 11 beta-hydroxysteroid dehydrogenase in vitro and in vivo. *Endocrinology*, 136(4), 1759–1765. <https://doi.org/10.1210/endo.136.4.7895688>
- Fariha, R., Jabrah, M., Hill, C., Spooner, A., Deshpande, P., & Tripathi, A. (2022). Simultaneous detection of salivary cortisol and cortisone using an automated high-throughput sample preparation method for LC-MS/MS. *SLAS Technology*, 27(4), 237–246. <https://doi.org/10.1016/j.slast.2022.01.006>
- Gathercole, L. L., Lavery, G. G., Morgan, S. A., Cooper, M. S., Sinclair, A. J., Tomlinson, J. W., & Stewart, P. M. (2013). 11beta-Hydroxysteroid dehydrogenase 1: Translational and therapeutic aspects. *Endocrine Reviews*, 34(4), 525–555. <https://doi.org/10.1210/er.2012-1050>
- Gent, R., du Toit, T., Bloem, L. M., & Swart, A. C. (2019). The 11beta-hydroxysteroid dehydrogenase isoforms: Pivotal catalytic activities yield potent C11-oxy C(19) steroids with 11betaHSD2 favouring 11-ketotestosterone, 11-ketoandrostenedione and 11-ketoprogesterone biosynthesis. *The Journal of Steroid Biochemistry and Molecular Biology*, 189, 116–126. <https://doi.org/10.1016/j.jsbmb.2019.02.013>
- Gomez-Sanchez, E. P., & Gomez-Sanchez, C. E. (2021). 11beta-hydroxysteroid dehydrogenases: A growing multi-tasking family. *Molecular and Cellular Endocrinology*, 526, 111210. <https://doi.org/10.1016/j.mce.2021.111210>
- Gregory, S., Hill, D., Grey, B., Ketelbey, W., Miller, T., Muniz-Terrera, G., & Ritchie, C. W. (2020). 11beta-hydroxysteroid dehydrogenase type 1 inhibitor use in human disease—a systematic review and narrative synthesis. *Metabolism: Clinical and Experimental*, 108, 154246. <https://doi.org/10.1016/j.metabol.2020.154246>
- Han, D., Yu, Z., Zhang, H., Liu, H., Wang, B., & Qian, D. (2021). Microenvironment-associated gene HSD11B1 may serve as a prognostic biomarker in clear cell renal cell carcinoma: A study based on TCGA, RT-qPCR, Western blotting, and immunohistochemistry. *Bioengineered*, 12(2), 10891–10904. <https://doi.org/10.1080/21655979.2021.1994908>
- Hardy, R. S., Botfield, H., Markey, K., Mitchell, J. L., Alimajstorovic, Z., Westgate, C. S. J., ... Sinclair, A. J. (2021). 11betaHSD1 inhibition with AZD4017 improves lipid profiles and lean muscle mass in idiopathic intracranial hypertension. *The Journal of Clinical Endocrinology and Metabolism*, 106(1), 174–187. <https://doi.org/10.1210/clinem/dgaa766>
- Hench, P. S., Slocumb, C. H., Polley, H. F., & Kendal, E. C. (1950). Effect of cortisone and pituitary adrenocorticotrophic hormone (ACTH) on rheumatic diseases. *Journal of the American Medical Association*, 144(16), 1327–1335. <https://doi.org/10.1001/jama.1950.02920160001001>
- Hult, M., Elleby, B., Shafqat, N., Svensson, S., Rane, A., Jornvall, H., ... Oppermann, U. (2004). Human and rodent type 1 11beta-hydroxysteroid dehydrogenases are 7beta-hydroxycholesterol dehydrogenases involved in oxysterol metabolism. *Cellular and Molecular Life Sciences: CMLS*, 61(7–8), 992–999. <https://doi.org/10.1007/s00018-003-3476-y>
- Jenner, D. A., & Richards, J. (1985). Determination of cortisol and cortisone in urine using high-performance liquid chromatography with UV detection. *Journal of Pharmaceutical and Biomedical Analysis*, 3(3), 251–257. [https://doi.org/10.1016/0731-7085\(85\)80030-3](https://doi.org/10.1016/0731-7085(85)80030-3)
- Jumper, J., Evans, R., Pritzel, A., Green, T., Figurnov, M., Ronneberger, O., ... Hassabis, D. (2021). Highly accurate protein structure prediction with AlphaFold. *Nature*, 596(7873), 583–589. <https://doi.org/10.1038/s41586-021-03819-2>
- Kadmiel, M., & Cidlowski, J. A. (2013). Glucocorticoid receptor signaling in health and disease. *Trends in Pharmacological Sciences*, 34(9), 518–530. <https://doi.org/10.1016/j.tips.2013.07.003>

- Kim, B. J., Lee, N. R., Lee, C. H., Lee, Y. B., Choe, S. J., Lee, S., ... Choi, E. H. (2021). Increased expression of 11beta-hydroxysteroid dehydrogenase type 1 contributes to epidermal permeability barrier dysfunction in aged skin. *International Journal of Molecular Sciences*, 22(11), <https://doi.org/10.3390/ijms22115750>
- Lakshmi, V., & Monder, C. (1985). Extraction of 11 beta-hydroxysteroid dehydrogenase from rat liver microsomes by detergents. *Journal of Steroid Biochemistry*, 22(3), 331–340. [https://doi.org/10.1016/0022-4731\(85\)90435-2](https://doi.org/10.1016/0022-4731(85)90435-2)
- Lee, S., Lim, H. S., Shin, H. J., Kim, S. A., Park, J., Kim, H. C., ... Kim, Y. J. (2014). Simultaneous determination of cortisol and cortisone from human serum by liquid chromatography-tandem mass spectrometry. *Journal of Analytical Methods in Chemistry*, 2014, 787483. <https://doi.org/10.1155/2014/787483>
- Lee, S. Y., Kim, S., Choi, I., Song, Y., Kim, N., Ryu, H. C., ... Seo, H. R. (2022). Inhibition of 11beta-hydroxysteroid dehydrogenase 1 relieves fibrosis through depolarizing of hepatic stellate cell in NASH. *Cell Death Disease*, 13(11), 1011. <https://doi.org/10.1038/s41419-022-05452-x>
- Low, S. C., Chapman, K. E., Edwards, C. R., & Seckl, J. R. (1994). 'Liver-type' 11 beta-hydroxysteroid dehydrogenase cDNA encodes reductase but not dehydrogenase activity in intact mammalian COS-7 cells. *Journal of Molecular Endocrinology*, 13(2), 167–174. <https://doi.org/10.1677/jme.0.0130167>
- Markey, K., Mitchell, J., Botfield, H., Ottridge, R. S., Matthews, T., Krishnan, A., ... Sinclair, A. J. (2020). 11beta-Hydroxysteroid dehydrogenase type 1 inhibition in idiopathic intracranial hypertension: A double-blind randomized controlled trial. *Brain Communications*, 2(1), fcz050. <https://doi.org/10.1093/braincomms/fcz050>
- Maser, E., & Bannenberg, G. (1994). The purification of 11 beta-hydroxysteroid dehydrogenase from mouse liver microsomes. *The Journal of Steroid Biochemistry and Molecular Biology*, 48(2–3), 257–263. [https://doi.org/10.1016/0960-0760\(94\)90153-8](https://doi.org/10.1016/0960-0760(94)90153-8)
- Masuzaki, H., Paterson, J., Shinyama, H., Morton, N. M., Mullins, J. J., Seckl, J. R., & Flier, J. S. (2001). A transgenic model of visceral obesity and the metabolic syndrome. *Science (New York, N. Y.)*, 294(5549), 2166–2170. <https://doi.org/10.1126/science.1066285>
- Mercer, W., Obeyesekere, V., Smith, R., & Krozowski, Z. (1993). Characterization of 11 beta-HSD1B gene expression and enzymatic activity. *Molecular and Cellular Endocrinology*, 92(2), 247–251. [https://doi.org/10.1016/0303-7207\(93\)90015-c](https://doi.org/10.1016/0303-7207(93)90015-c)
- Meyer, A., Vuorinen, A., Zielinska, A. E., Da Cunha, T., Strajhar, P., Lavery, G. G., ... Odermatt, A. (2013). Carbonyl reduction of triadimefon by human and rodent 11beta-hydroxysteroid dehydrogenase 1. *Biochemical Pharmacology*, 85(9), 1370–1378. <https://doi.org/10.1016/j.bcp.2013.02.014>
- Meyer, A., Vuorinen, A., Zielinska, A. E., Strajhar, P., Lavery, G. G., Schuster, D., & Odermatt, A. (2013). Formation of threohydrobupropion from bupropion is dependent on 11beta-hydroxysteroid dehydrogenase 1. *Drug Metabolism and Disposition: The Biological Fate of Chemicals*, 41(9), 1671–1678. <https://doi.org/10.1124/dmd.113.052936>
- Mohler, E. G., Browman, K. E., Roderwald, V. A., Cronin, E. A., Markosyan, S., Scott Bitner, R., ... Rueter, L. E. (2011). Acute inhibition of 11beta-hydroxysteroid dehydrogenase type-1 improves memory in rodent models of cognition. *The Journal of Neuroscience*, 31(14), 5406–5413. <https://doi.org/10.1523/JNEUROSCI.4046-10.2011>
- Monder, C., & Shackleton, C. H. (1984). 11 beta-Hydroxysteroid dehydrogenase: Fact or fancy? *Steroids*, 44(5), 383–417. [https://doi.org/10.1016/s0039-128x\(84\)80001-x](https://doi.org/10.1016/s0039-128x(84)80001-x)
- Morris, D. J., Souness, G. W., Latif, S. A., Hardy, M. P., & Brem, A. S. (2004). Effect of chenodeoxycholic acid on 11beta-hydroxysteroid dehydrogenase in various target tissues. *Metabolism: Clinical and Experimental*, 53(6), 811–816. <https://doi.org/10.1016/j.metabol.2003.12.027>
- Morton, N. M., Paterson, J. M., Masuzaki, H., Holmes, M. C., Staels, B., Fievet, C., ... Seckl, J. R. (2004). Novel adipose tissue-mediated resistance to diet-induced visceral

- obesity in 11 beta-hydroxysteroid dehydrogenase type 1-deficient mice. *Diabetes*, 53(4), 931–938. <https://doi.org/10.2337/diabetes.53.4.931>
- Mziaut, H., Korza, G., Hand, A. R., Gerard, C., & Ozols, J. (1999). Targeting proteins to the lumen of endoplasmic reticulum using N-terminal domains of 11beta-hydroxysteroid dehydrogenase and the 50-kDa esterase. *The Journal of Biological Chemistry*, 274(20), 14122–14129. <https://doi.org/10.1074/jbc.274.20.14122>
- Nobel, C. S., Dunas, F., & Abrahmsen, L. B. (2002). Purification of full-length recombinant human and rat type 1 11beta-hydroxysteroid dehydrogenases with retained oxidoreductase activities. *Protein Expression and Purification*, 26(3), 349–356. [https://doi.org/10.1016/s1046-5928\(02\)00547-8](https://doi.org/10.1016/s1046-5928(02)00547-8)
- Odermatt, A., Arnold, P., Stauffer, A., Frey, B. M., & Frey, F. J. (1999). The N-terminal anchor sequences of 11beta-hydroxysteroid dehydrogenases determine their orientation in the endoplasmic reticulum membrane. *The Journal of Biological Chemistry*, 274(40), 28762–28770. <https://doi.org/10.1074/jbc.274.40.28762>
- Odermatt, A., Da Cunha, T., Penno, C. A., Chandsawangbhuwana, C., Reichert, C., Wolf, A., ... Baker, M. E. (2011). Hepatic reduction of the secondary bile acid 7-oxolithocholic acid is mediated by 11beta-hydroxysteroid dehydrogenase 1. *The Biochemical Journal*, 436(3), 621–629. <https://doi.org/10.1042/BJ20110022>
- Odermatt, A., & Klusonova, P. (2015). 11beta-Hydroxysteroid dehydrogenase 1: Regeneration of active glucocorticoids is only part of the story. *The Journal of Steroid Biochemistry and Molecular Biology*, 151, 85–92. <https://doi.org/10.1016/j.jsbmb.2014.08.011>
- Odermatt, A., & Kratschmar, D. V. (2012). Tissue-specific modulation of mineralocorticoid receptor function by 11beta-hydroxysteroid dehydrogenases: An overview. *Molecular and Cellular Endocrinology*, 350(2), 168–186. <https://doi.org/10.1016/j.mce.2011.07.020>
- Othonos, N., Pofi, R., Arvaniti, A., White, S., Bonaventura, I., Nikolaou, N., ... Tomlinson, J. W. (2023). 11beta-HSD1 inhibition in men mitigates prednisolone-induced adverse effects in a proof-of-concept randomised double-blind placebo-controlled trial. *Nature Communications*, 14(1), 1025. <https://doi.org/10.1038/s41467-023-36541-w>
- Paterson, J. M., Morton, N. M., Fievet, C., Kenyon, C. J., Holmes, M. C., Staels, B., ... Mullins, J. J. (2004). Metabolic syndrome without obesity: Hepatic overexpression of 11beta-hydroxysteroid dehydrogenase type 1 in transgenic mice. *Proceedings of the National Academy of Sciences of the United States of America*, 101(18), 7088–7093. <https://doi.org/10.1073/pnas.0305524101>
- Paulmyer-Lacroix, O., Boullu, S., Oliver, C., Alessi, M. C., & Grino, M. (2002). Expression of the mRNA coding for 11beta-hydroxysteroid dehydrogenase type 1 in adipose tissue from obese patients: An in situ hybridization study. *The Journal of Clinical Endocrinology and Metabolism*, 87(6), 2701–2705. <https://doi.org/10.1210/jcem.87.6.8614>
- Peskind, E. R., Wilkinson, C. W., Petrie, E. C., Schellenberg, G. D., & Raskind, M. A. (2001). Increased CSF cortisol in AD is a function of APOE genotype. *Neurology*, 56(8), 1094–1098. <https://doi.org/10.1212/wnl.56.8.1094>
- Rask, E., Olsson, T., Soderberg, S., Andrew, R., Livingstone, D. E., Johnson, O., & Walker, B. R. (2001). Tissue-specific dysregulation of cortisol metabolism in human obesity. *The Journal of Clinical Endocrinology and Metabolism*, 86(3), 1418–1421. <https://doi.org/10.1210/jcem.86.3.7453>
- Saito, R., Miki, Y., Abe, T., Miyauchi, E., Abe, J., Nanamiya, R., ... Sasano, H. (2020). 11beta hydroxysteroid dehydrogenase 1: A new marker for predicting response to immune-checkpoint blockade therapy in non-small-cell lung carcinoma. *British Journal of Cancer*, 123(1), 61–71. <https://doi.org/10.1038/s41416-020-0837-3>
- Sarett, L. H. (1959). Some aspects of the evolution of anti-inflammatory steroids. *Annals of the New York Academy of Sciences*, 82, 802–808. <https://doi.org/10.1111/j.1749-6632.1960.tb44961.x>

- Schweizer, R. A., Atanasov, A. G., Frey, B. M., & Odermatt, A. (2003). A rapid screening assay for inhibitors of 11beta-hydroxysteroid dehydrogenases (11beta-HSD): flavanone selectively inhibits 11beta-HSD1 reductase activity. *Molecular and Cellular Endocrinology*, 212(1–2), 41–49. <https://doi.org/10.1016/j.mce.2003.09.027>
- Schweizer, R. A., Zurcher, M., Balazs, Z., Dick, B., & Odermatt, A. (2004). Rapid hepatic metabolism of 7-ketocholesterol by 11beta-hydroxysteroid dehydrogenase type 1: Species-specific differences between the rat, human, and hamster enzyme. *The Journal of Biological Chemistry*, 279(18), 18415–18424. <https://doi.org/10.1074/jbc.M313615200>
- Shackleton, C. H. (1993). Mass spectrometry in the diagnosis of steroid-related disorders and in hypertension research. *The Journal of Steroid Biochemistry and Molecular Biology*, 45(1–3), 127–140. [https://doi.org/10.1016/0960-0760\(93\)90132-g](https://doi.org/10.1016/0960-0760(93)90132-g)
- Shafqat, N., Elleby, B., Svensson, S., Shafqat, J., Jornvall, H., Abrahmsen, L., & Oppermann, U. (2003). Comparative enzymology of 11 beta-hydroxysteroid dehydrogenase type 1 from glucocorticoid resistant (Guinea pig) versus sensitive (human) species. *The Journal of Biological Chemistry*, 278(3), 2030–2035. <https://doi.org/10.1074/jbc.M210135200>
- Shukla, R., Basu, A. K., Mandal, B., Mukhopadhyay, P., Maity, A., Chakraborty, S., & Devrabhai, P. K. (2019). 11beta Hydroxysteroid dehydrogenase – 1 activity in type 2 diabetes mellitus: A comparative study. *BMC Endocrine Disorders*, 19(1), 15. <https://doi.org/10.1186/s12902-019-0344-9>
- Song, W., Chen, J., Dean, W. L., Redinger, R. N., & Prough, R. A. (1998). Purification and characterization of hamster liver microsomal 7alpha-hydroxycholesterol dehydrogenase. Similarity to type I 11beta-hydroxysteroid dehydrogenase. *The Journal of Biological Chemistry*, 273(26), 16223–16228. <https://doi.org/10.1074/jbc.273.26.16223>
- Sooy, K., Noble, J., McBride, A., Binnie, M., Yau, J. L., Seckl, J. R., ... Webster, S. P. (2015). Cognitive and disease-modifying effects of 11beta-hydroxysteroid dehydrogenase type 1 inhibition in male Tg2576 mice, a model of Alzheimer's disease. *Endocrinology*, 156(12), 4592–4603. <https://doi.org/10.1210/en.2015-1395>
- Stefan, N., Ramsauer, M., Jordan, P., Nowotny, B., Kantartzis, K., Machann, J., ... Furst-Recktenwald, S. (2014). Inhibition of 11beta-HSD1 with RO5093151 for non-alcoholic fatty liver disease: A multicentre, randomised, double-blind, placebo-controlled trial. *Lancet Diabetes Endocrinology*, 2(5), 406–416. [https://doi.org/10.1016/S2213-8587\(13\)70170-0](https://doi.org/10.1016/S2213-8587(13)70170-0)
- Tannin, G. M., Agarwal, A. K., Monder, C., New, M. I., & White, P. C. (1991). The human gene for 11 beta-hydroxysteroid dehydrogenase. Structure, tissue distribution, and chromosomal localization. *Journal of Biological Chemistry*, 266(25), 16653–16658. Retrieved from <https://www.ncbi.nlm.nih.gov/pubmed/1885595>.
- Terao, M., Murota, H., Kimura, A., Kato, A., Ishikawa, A., Igawa, K., ... Katayama, I. (2011). 11beta-Hydroxysteroid dehydrogenase-1 is a novel regulator of skin homeostasis and a candidate target for promoting tissue repair. *PLoS One*, 6(9), e25039. <https://doi.org/10.1371/journal.pone.0025039>
- Thomas, M. P., & Potter, B. V. (2011). Crystal structures of 11beta-hydroxysteroid dehydrogenase type 1 and their use in drug discovery. *Future Medicinal Chemistry*, 3(3), 367–390. <https://doi.org/10.4155/fmc.10.282>
- Tiganescu, A., Hupe, M., Uchida, Y., Mauro, T., Elias, P. M., & Holleran, W. M. (2018). Topical 11beta-hydroxysteroid dehydrogenase type 1 inhibition corrects cutaneous features of systemic glucocorticoid excess in female mice. *Endocrinology*, 159(1), 547–556. <https://doi.org/10.1210/en.2017-00607>
- Tiganescu, A., Tahrani, A. A., Morgan, S. A., Otranto, M., Desmouliere, A., Abrahams, L., ... Stewart, P. M. (2013). 11beta-Hydroxysteroid dehydrogenase blockade prevents age-induced skin structure and function defects. *The Journal of Clinical Investigation*, 123(7), 3051–3060. <https://doi.org/10.1172/JCI64162>

- Turpeinen, U., & Hamalainen, E. (2013). Determination of cortisol in serum, saliva and urine. *Best Practice & Research. Clinical Endocrinology & Metabolism*, 27(6), 795–801. <https://doi.org/10.1016/j.beem.2013.10.008>
- Varadi, M., Anyango, S., Deshpande, M., Nair, S., Natassia, C., Yordanova, G., ... Velankar, S. (2022). AlphaFold Protein Structure Database: Massively expanding the structural coverage of protein-sequence space with high-accuracy models. *Nucleic Acids Research*, 50(D1), D439–D444. <https://doi.org/10.1093/nar/gkab1061>
- Warriar, N., Page, N., & Govindan, M. V. (1994). Transcription activation of mouse mammary tumor virus-chloramphenicol acetyltransferase: A model to study the metabolism of cortisol. *Biochemistry*, 33(43), 12837–12843. <https://doi.org/10.1021/bi00209a015>
- Whorwood, C. B., Donovan, S. J., Flanagan, D., Phillips, D. I., & Byrne, C. D. (2002). Increased glucocorticoid receptor expression in human skeletal muscle cells may contribute to the pathogenesis of the metabolic syndrome. *Diabetes*, 51(4), 1066–1075. <https://doi.org/10.2337/diabetes.51.4.1066>
- Wyrwoll, C. S., Holmes, M. C., & Seckl, J. R. (2011). 11beta-hydroxysteroid dehydrogenases and the brain: From zero to hero, a decade of progress. *Frontiers in Neuroendocrinology*, 32(3), 265–286. <https://doi.org/10.1016/j.yfrne.2010.12.001>
- Yadav, Y., Dunagan, K., Khot, R., Venkatesh, S. K., Port, J., Galderisi, A., ... Basu, R. (2022). Inhibition of 11beta-Hydroxysteroid dehydrogenase-1 with AZD4017 in patients with nonalcoholic steatohepatitis or nonalcoholic fatty liver disease: A randomized, double-blind, placebo-controlled, phase II study. *Diabetes, Obesity & Metabolism*, 24(5), 881–890. <https://doi.org/10.1111/dom.14646>
- Youm, J. K., Park, K., Uchida, Y., Chan, A., Mauro, T. M., Holleran, W. M., & Elias, P. M. (2013). Local blockade of glucocorticoid activation reverses stress- and glucocorticoid-induced delays in cutaneous wound healing. *Wound Repair and Regeneration: Official Publication of the Wound Healing Society [and] the European Tissue Repair Society*, 21(5), 715–722. <https://doi.org/10.1111/wrr.12083>

#### 4.4 Published article: *In vitro* methods to assess 11 $\beta$ -hydroxysteroid dehydrogenase type 2 activity

Manuel Kley<sup>a,b</sup>, Seraina O. Moser<sup>a,b</sup>, Denise V. Winter<sup>a</sup>, and Alex Odermatt<sup>a,b,\*</sup>

<sup>a</sup> Division of Molecular and Systems Toxicology, Department of Pharmaceutical Sciences, University of Basel, Basel, Switzerland

<sup>b</sup> Swiss Centre for Applied Human Toxicology, Department of Pharmaceutical Sciences, University of Basel, Basel, Switzerland

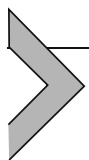
\* Corresponding author. e-mail address: alex.odermatt@unibas.ch

Published article

**Personal contribution:** Drafting and revision of the manuscript except subchapters 3.4 to 3.7. Illustration of the whole chapter.

**Aims:** Providing an overview of the current *in vitro* methodology to assess HSD11B2 activity with stepwise experimental procedures including optimization and troubleshooting sections.

**Conclusion:** This chapter describes various *in vitro* methods, including cell-based models and usage of animal tissue samples that allow assessment of novel roles of HSD11B2 in human physiology as well as the identification of xenobiotics that inhibit HSD11B2.



# *In vitro* methods to assess 11 $\beta$ -hydroxysteroid dehydrogenase type 2 activity

Manuel Kley<sup>a,b</sup>, Seraina O. Moser<sup>a,b</sup>, Denise V. Winter<sup>a</sup>, and  
Alex Odermatt<sup>a,b,\*</sup>

<sup>a</sup>Division of Molecular and Systems Toxicology, Department of Pharmaceutical Sciences, University of Basel, Basel, Switzerland

<sup>b</sup>Swiss Centre for Applied Human Toxicology, Department of Pharmaceutical Sciences, University of Basel, Basel, Switzerland

\*Corresponding author. e-mail address: alex.odermatt@unibas.ch

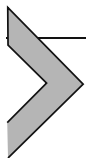
## Contents

1. Introduction	168
2. Overview of <i>in vitro</i> 11 $\beta$ -HSD2 activity assays	170
3. Whole cell lysate enzyme activity assay using LC-MS/MS for quantification	172
3.1 Transfection of HEK-293 cells and overexpression of 11 $\beta$ -HSD2 from different species	172
3.2 Preparation of cell pellets	172
3.3 Enzyme activity assay	173
3.4 Product and substrate quantification by LC-MS/MS	177
3.5 Qualitative analysis	179
3.6 Quantitative analysis and expected experimental outcome	183
3.7 Optimization and troubleshooting	184
4. 11 $\beta$ -HSD2 activity assay using tissue homogenates	185
4.1 Preparation of placenta tissue for 11 $\beta$ -HSD2 activity assay	185
4.2 Radiometric enzyme activity assay	186
4.3 TLC separation of radiolabeled steroids and liquid scintillation counting	189
4.4 Expected outcomes of 11 $\beta$ -HSD2 enzyme activity assay and data analysis	189
4.5 Optimization and troubleshooting	190
5. Alternative methods to assess 11 $\beta$ -HSD2 activity	190
5.1 11 $\beta$ -HSD2 activity assays using microsomal preparations	191
5.2 11 $\beta$ -HSD2 activity assay using intact cells	191
5.3 Alternative quantification methods	192
6. Project and resource based choice of 11 $\beta$ -HSD2 activity assays	194
7. Biomarkers to assess 11 $\beta$ -HSD2 activity in preclinical and clinical studies	194
8. Safety considerations and standards of the described methods	196
9. Concluding remarks	196

Acknowledgments	197
References	197

## Abstract

11 $\beta$ -Hydroxysteroid dehydrogenase type 2 (11 $\beta$ -HSD2) converts active 11 $\beta$ -hydroxyglucocorticoids to their inactive 11-keto forms, fine-tuning the activation of mineralocorticoid and glucocorticoid receptors. 11 $\beta$ -HSD2 is expressed in mineralocorticoid target tissues such as renal distal tubules and cortical collecting ducts, and distal colon, but also in placenta where it acts as a barrier to reduce the amount of maternal glucocorticoids that reach the fetus. Disruption of 11 $\beta$ -HSD2 activity by genetic defects or inhibitors causes the syndrome of apparent mineralocorticoid excess (AME), characterized by hypernatremia, hypokalemia and hypertension. Secondary hypertension due to 11 $\beta$ -HSD2 inhibition has been observed upon consumption of excessive amounts of licorice and in patients treated with theazole fungicides posaconazole and itraconazole. Furthermore, inhibition of 11 $\beta$ -HSD2 during pregnancy with elevated exposure of the fetus to cortisol can cause neurological complications with a lower intelligence quotient, higher odds of attention deficit and hyperactivity disorder as well as metabolic reprogramming with an increased risk of cardio-metabolic disease in adulthood. This chapter describes *in vitro* methods for the determination of 11 $\beta$ -HSD2 activity that can be applied to identify inhibitors that may cause secondary hypertension and characterize the enzyme's activity in disease models. The included decision tree and the list of methods with their advantages and disadvantages aim to enable the reader to select and apply an *in vitro* method suitable for the scientific question and the equipment available in the respective laboratory.



## 1. Introduction

11 $\beta$ -Hydroxysteroid dehydrogenase 2 (11 $\beta$ -HSD2) is an endoplasmic reticulum (ER) membrane anchored enzyme with its active site facing the cytosol that catalyzes the oxidation of active 11 $\beta$ -hydroxyglucocorticoids such as cortisol or corticosterone to their inactive keto-forms (Odermatt, Arnold, Stauffer, Frey, & Frey, 1999). Together with 11 $\beta$ -HSD1, which catalyzes the opposite reaction, 11 $\beta$ -HSD2 regulates the tissue- and cell-specific concentration of active glucocorticoids (Brown, Chapman, Edwards, & Seckl, 1993; Odermatt & Kratschmar 2012; Tannin, Agarwal, Monder, New, & White, 1991). The active 11 $\beta$ -hydroxyglucocorticoid cortisol not only binds to and activates the glucocorticoid receptor (GR) but also the mineralocorticoid receptor (MR), which controls the expression of genes involved in ion- and water transport (Arriza et al., 1987; Hollenberg et al., 1985). The MR has a similar binding affinity for cortisol and aldosterone; however, cortisol is present in plasma



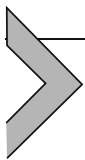
at a 1000-fold higher concentration than aldosterone. In mineralocorticoid target tissues, including renal distal tubules and cortical collecting ducts, 11 $\beta$ -HSD2 inactivates cortisol and renders access of aldosterone to the MR (Edwards et al., 1988; Funder, Pearce, Smith, & Smith, 1988).

Deleterious, homozygous mutations of 11 $\beta$ -HSD2 cause apparent mineralocorticoid excess (AME) by excessive cortisol-dependent MR activation, characterized by sodium retention, hypokalemia and severe hypertension (Ferrari, 2010; Mune, Rogerson, Nikkila, Agarwal, & White, 1995; White, Mune, & Agarwal, 1997). A similar form of AME is caused by the ingestion of excessive amounts of licorice, containing the potent 11 $\beta$ -HSD2 inhibitor glycyrrhetic acid (GA) (Farese, Biglieri, Shackleton, Irony, & Gomez-Fontes, 1991; Ferrari, 2010; Stewart et al., 1987). Moreover, the systemically applied azole antifungal drugs itraconazole and posaconazole cause acquired hypertension and hypokalemia, in part by their potent inhibition of 11 $\beta$ -HSD2 (Beck & Odermatt, 2021; Beck et al., 2017; Hoffmann, McHardy, & Thompson, 2018; 2018; Nguyen et al., 2020; Thompson, Beck, Patt, Kratschmar, & Odermatt, 2019; Kuriakose et al., 2018). This adverse effect of posaconazole and itraconazole was not observed during preclinical drug development, which may be explained by species-specific differences in their inhibitory capacity towards 11 $\beta$ -HSD2, with potent inhibition of human but weak or moderate inhibitory effects towards rodent and zebrafish enzymes (Inderbinen, Zogg, Kley, Smiesko, & Odermatt, 2021). The availability of robust activity assays allowing at least medium throughput screening for enzymes from different species could help preventing such adverse effects by detecting such liabilities in early drug development.

Moreover, 11 $\beta$ -HSD2 has an important role in the placenta. Its expression can be detected as early as 3 weeks post-conception and it acts as a barrier to reduce the amount of maternal glucocorticoids that reach the fetus (Benediktsson, Calder, Edwards, & Seckl, 1997; Murphy, 1981; Salvante, Milano, Kliman, & Nepomnaschy, 2017). Inhibition of 11 $\beta$ -HSD2 during pregnancy leads to a reprogramming of fetal development with an elevated risk for metabolic diseases later in life (Seckl, Benediktsson, Lindsay, & Brown, 1995; Stewart, Whorwood, & Mason, 1995). In this respect, the consumption of licorice is strongly discouraged during pregnancy because the inhibition of placental 11 $\beta$ -HSD2 leads to an increased fetal cortisol exposure, which may cause neurological implications such as lower intelligence quotients, poorer memory and higher odds of attention deficit and hyperactivity disorder later in life (Raikkonen et al., 2017). Thus, an exposure to 11 $\beta$ -HSD2 inhibitors has to be avoided especially during pregnancy.

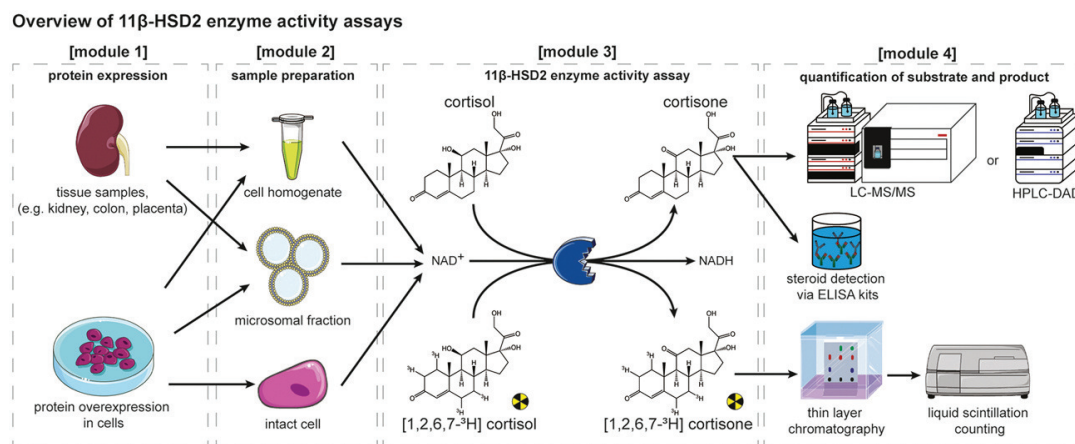
Recently, 11 $\beta$ -HSD2 was shown to convert the oxysterols 7 $\beta$ ,27-dihydroxycholesterol (7 $\beta$ 27OHC) and 7 $\beta$ 25OHC to 7-keto,27-hydroxycholesterol (7k27OHC) and 7k25OHC, respectively (Beck, Inderbinen, et al., 2019; Beck, Kanagaratnam, et al., 2019). Thereby it regulates the activities of retinoic acid-related orphan receptor gamma t (ROR $\gamma$ t) and G-protein coupled receptor EBI-2, which play important roles in the regulation of immune cell functions (Hannedouche et al., 2011; Jetten & Cook, 2020; Miossec & Kolls, 2012; Soroosh et al., 2014). Interestingly, the apparent affinities of 11 $\beta$ -HSD2 for these oxysterols are equal to or higher than those for the glucocorticoids, suggesting a role of 11 $\beta$ -HSD2 in immunomodulation (Beck, Inderbinen, et al., 2019; Beck, Kanagaratnam, et al., 2019; Hannedouche et al., 2011; Soroosh et al., 2014).

This chapter describes *in vitro* methods to assess 11 $\beta$ -HSD2 activity, based on tissue samples with endogenous expression or on samples of cultured cells overexpressing the enzyme. Some parts of the methods have already been described in detail in the chapter “*In vitro* methods to assess 11 $\beta$ -hydroxysteroid dehydrogenase type 1 activity”; therefore, the reader will be referred to the corresponding section, if applicable, and deviations are highlighted.



## 2. Overview of *in vitro* 11 $\beta$ -HSD2 activity assays

*In vitro* 11 $\beta$ -HSD2 activity assays can be divided into four steps, or modules. (1) Protein expression, which is achieved by collecting tissue samples (kidney, colon, placenta) with endogenous expression or by overexpressing recombinant protein in cultured cells (see Fig. 1, module 1). (2) 11 $\beta$ -HSD2 expressing samples are prepared by cell lysis and optionally by enrichment through microsomal preparation (Fig. 1, module 2). Microsomal preparation may be necessary when assessing novel substrates interferes with the novel substrate or its product. To the best of our knowledge, 11 $\beta$ -HSD2 has not yet been successfully purified in a fully functional state, and its activity was lost when isolating it from the ER membrane (Brown, Chapman, Murad, Edwards, & Seckl, 1996). 11 $\beta$ -HSD2 activity may also be assessed in intact cells expressing endogenous 11 $\beta$ -HSD2 or after overexpression. (3) After sample preparation, an enzyme activity assay is conducted to assess 11 $\beta$ -HSD2 dehydrogenase activity (Fig. 1, module 3). The reaction can be performed using cofactor NAD<sup>+</sup> in combination with either label-free substrate or by including

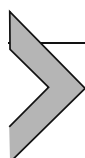


**Fig. 1** Overview of 11 $\beta$ -HSD2 activity assays. Methods described in this chapter to assess 11 $\beta$ -HSD2 activity are presented schematically and grouped into four modules, reflecting the general process required to perform an enzyme activity assay: protein expression; sample preparation; enzyme activity assay and quantification of substrate and product. 11 $\beta$ -HSD2, either from a tissue sample with endogenous expression or after overexpression of recombinant enzyme in cultured cells is prepared by lysis of cells and optionally enriched by preparation of microsomal fraction. Alternatively, 11 $\beta$ -HSD2 activity can be measured in intact cells. 11 $\beta$ -HSD2 activity can be quantified using liquid chromatography and tandem mass spectrometry (LC-MS/MS), high-performance liquid chromatography and diode array detection (HPLC-DAD), enzyme-linked immunosorbent assay (ELISA), or thin-layer chromatography (TLC) followed by liquid scintillation counting when using a radioactive tracer.

radiolabeled cortisol as tracer, requiring quantification by liquid scintillation counting (Fig. 1, module 4). (4) If label-free cortisol is used, the substrate conversion by 11 $\beta$ -HSD2 can be measured after separation by liquid chromatography by tandem mass spectrometry (LC-MS/MS) or UV-detection (HPLC-DAD), or directly by enzyme-linked immunosorbent assay (ELISA) quantification (Fig. 1, module 4). Each module contains different options to address different tasks concerning 11 $\beta$ -HSD2 activity.

This chapter focuses on two enzyme activity assays, the first based on whole lysates of cells overexpressing 11 $\beta$ -HSD2 and quantification of substrate and product by liquid chromatography and tandem mass spectrometry (LC-MS/MS). The second assay utilizes placenta homogenates endogenously expressing 11 $\beta$ -HSD2 and tritiated cortisol as radiolabeled tracer for quantification. The other methods mentioned above are shortly described as alternative protocols in sections 5 and 6. Reference will be made to the chapter “*In vitro* methods to assess 11 $\beta$ -hydroxysteroid dehydrogenase type 1 activity” where appropriate and where these methods are described in detail. A decision tree and an overview table on

advantages and limitations to all methods described in this chapter are included in section 7 to help the reader choosing the appropriate  $11\beta$ -HSD2 activity assay.



### **3. Whole cell lysate enzyme activity assay using LC-MS/MS for quantification**

This section describes an  $11\beta$ -HSD2 activity assay using whole cell lysates that can be used to screen inhibitors. By overexpressing different homologs of  $11\beta$ -HSD2 in cultured cells, species-specific differences of inhibitors can be assessed. For this purpose, the respective homolog is overexpressed in cultured cells, which are then pelleted and frozen for storage. After lysis of the cell pellets, the enzyme assay is carried out, followed by steroid extraction and subsequent quantification of substrate and product by LC-MS/MS. Since whole cell lysates are used in this experiment, it is important to exclude background  $11$ -oxoreductase or dehydrogenase activity in the cell line used for expression of recombinant  $11\beta$ -HSD2. A recommended cell line devoid of endogenous  $11\beta$ -HSD expression is HEK-293 (Odermatt et al., 1999; Schweizer, Atanasov, Frey, & Odermatt, 2003). Instead of using LC-MS/MS, product and substrate concentrations can be measured using HPLC with UV-detectors (HPLC-DAD) or steroid specific ELISA kits (see Section 5.3). Alternatively, adding a radiolabeled tracer can facilitate the relative quantification of enzyme activity (see Section 4) and allow reducing the reaction volume due to the high sensitivity of radioactive detection by liquid scintillation counting.

#### **3.1 Transfection of HEK-293 cells and overexpression of $11\beta$ -HSD2 from different species**

Calcium phosphate precipitation represents a low cost transfection method and can be applied as described in subchapter 4.1 of the chapter “*In vitro* methods to assess  $11\beta$ -hydroxysteroid dehydrogenase type 1 activity”. Various species of *HSD11B2* in a pcDNA3.1 backbone can be used instead of *HSD11B1* as described earlier (Meyer, Strajhar, Murer, Da Cunha, & Odermatt, 2012; Odermatt et al., 1999).

#### **3.2 Preparation of cell pellets**

The preparation of cell pellets can be conducted as described in chapter “*In vitro* methods to assess  $11\beta$ -hydroxysteroid dehydrogenase type 1 activity”,

subchapter 4.2 by preparing 400  $\mu$ L aliquots instead of 200  $\mu$ L aliquots before spinning down the cells and snap freezing them.

### 3.3 Enzyme activity assay

#### 3.3.1 Equipment

- Sonicator (UP50H, Hielscher Ultrasonics, Teltow, Germany)
- Vortex (TX4 Digital IR Vortex Mixer, Velp Scientifica<sup>TM</sup>, Usmate, Italy)
- Thermoshaker for 1.5 mL plastic tubes (Thermomixer comfort, Eppendorf, Hamburg, Germany)
- Evaporator (Genevac, SP Scientific, Warminster, PA, USA)

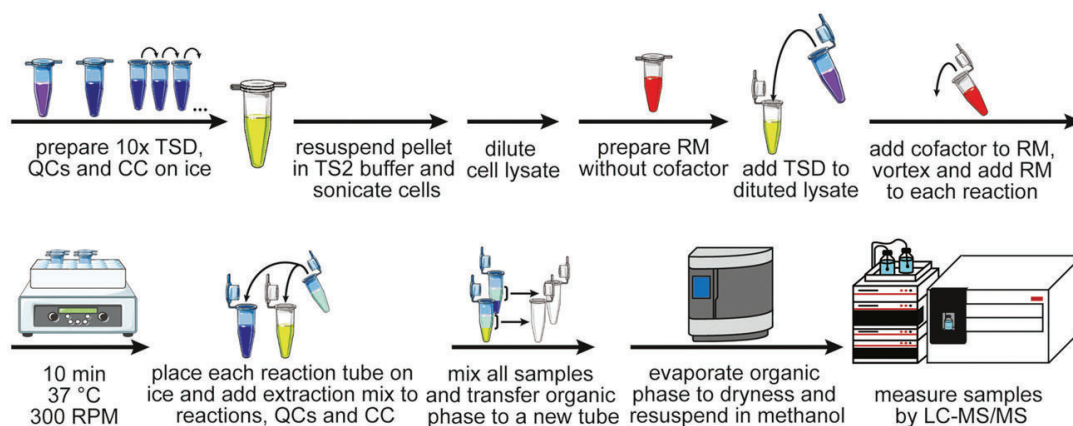
#### 3.3.2 Buffers and solutions

All chemicals and reagents were purchased from Sigma-Aldrich (St. Louis, MO, USA) if not stated otherwise. The solvents and steroids used in subchapters 3.3 and 3.4 were purchased at the highest purity available (HPLC grade).

- **TS2 buffer** (100 mM NaCl, 1 mM EGTA, 1 mM EDTA, 1 mM MgCl<sub>2</sub>, 250 mM sucrose, 20 mM Tris-HCl, pH 7.4, store at 4 °C)
- **Cortisol stock solution 1** 10 mM in methanol (store at -20 °C)
- **Cortisol stock solution 2** 1 mg/mL in methanol (store at -20 °C)
- **Cortisone stock solution** 1 mg/mL in methanol (store at -20 °C)
- **Cortisol-D4 stock solution** 1 mg/mL in methanol (store at -20 °C)
- **Cortisone-D2 stock solution** 1 mg/mL in methanol (store at -20 °C)
- **NAD<sup>+</sup> stock solution** 25 mM in H<sub>2</sub>O (store 60  $\mu$ L aliquots at -80 °C, up to 6 months)
- **Extraction mix** freshly prepared prior to use (D4-cortisol and D2-cortisone (both 10–30 ng/mL, Steraloids Newport, RI, USA) in ethyl acetate) (see Note a.)
- Test substance stocks 10 mM in methanol (verify solubility and store at -20 °C)

#### 3.3.3 Procedure

1. Preheat a thermoshaker to 37 °C and prepare a 1% solvent control solution (TS2 buffer with 1% methanol) and prepare a dilution series of test substances in methanol (see Fig. 2).
2. Dilute each prepared test substance concentration 1:100 in TS2 buffer, reaching 10x of the concentration to be assessed in the assay. The final



**Fig. 2** Schematic overview of the  $11\beta$ -HSD2 activity assay with label-free substrate and subsequent LC-MS/MS quantification. Prior to the experiment, test substance dilutions (TSD, purple solution), quality control samples (QC, blue solution) and the calibrators (CC, blue solution) are prepared on ice. The thawed and diluted cell lysate (yellow solution) is kept on ice until the start of the enzyme reaction, meanwhile the reaction mix (RM, red solution) is prepared without the cofactor. Test substance dilutions (TSD, purple solution) are added to the diluted cell lysate prepared in 1.5 mL plastic tubes. After adding cofactor to the reaction mix, the enzyme reaction takes place in a thermoshaker at 37 °C for 10 min, shaking at 300 rpm. The reaction is stopped by placing the tubes containing the reactions immediately on ice. The extraction mix (green solution) is added to the reactions as well as to the prepared quality control and calibration curve samples. After mixing all samples, the organic phases are transferred to new plastic tubes. The samples are evaporated to dryness, resuspended in methanol and quantified by LC-MS/MS.

addition of the test substance dilution to the enzyme reaction will result in a 1:10 dilution. Store the diluted solutions on ice. (see Note b.)

3. Prepare a 20  $\mu$ M label-free cortisol working solution by diluting the 10 mM stock 1:500 in TS2 buffer and keep on ice.
4. Prepare additional cortisol and cortisone working solutions by diluting both 1 mg/mL glucocorticoid stocks 1:25 in HPLC grade methanol, then mix both glucocorticoids working solutions to equal parts and dilute this solution mix 1:1000 in TS2 buffer. Prepare a ten-point calibration curve using this spiked mix as highest level (20 ng/mL) of the calibration curve by diluting this calibrator solution in 1:2 steps in TS2 buffer containing 0.1% HPLC grade methanol. Prepare a 500  $\mu$ L aliquot of each calibrator and store on ice. Prepare three additional samples with known glucocorticoid concentrations of the mixed glucocorticoid working solutions, containing a total of 0.1% of solvent, which will be used as quality controls. Store them on ice. The

**Table 1** Preparation of reaction mix for 10 enzyme reactions.

Buffer/solution	Amount to add	final concentration per reaction and well
TS2 buffer	2.5 mL	—
Label-free cortisol, working solution [20 $\mu$ M]	13.1 $\mu$ L	50 nM
NAD <sup>+</sup> [25 mM]	104.7 $\mu$ L	500 $\mu$ M

This table lists end concentrations as well as the respective amounts of buffer, substrate and cofactor solutions to add to the reaction mix for the enzyme activity assay.

calibrator aliquots and the quality controls are to be treated as the reaction samples from step 14 onwards.

5. For an enzyme activity assay, resuspend at least one aliquot of the prepared 11 $\beta$ -HSD2 cell pellets stored at  $-80$  °C in 400  $\mu$ L ice-cold TS2 buffer (4 °C) by pipetting up and down, then mix the suspension well at 300 rpm. Keep all suspensions on ice. (see Note c.)
6. **Critical: Keep the thawed cell pellets on ice and immediately proceed with the subsequent protocol steps.**
7. Lyse the suspended cells by sonication with 10 pulses (0.3 cycles, 20% amplitude) of the UP50H sonicator. Mix well at 300 rpm. Store the lysates on ice.
8. Dilute the lysate in ice-cold TS2 buffer to achieve 20–30% substrate conversion after 10 min (see Note d.), mix well at 300 rpm. Store the diluted lysate on ice.
9. Prepare per reaction one 1.5 mL plastic tube, label it and place it on ice. Include one plastic tube each for solvent control and background sample.
10. Add 200  $\mu$ L of the diluted cell lysate per prepared plastic tube except for the background control where 250  $\mu$ L ice-cold TS2 buffer is prepared instead.
11. Add 50  $\mu$ L of 1% solvent control solution and 50  $\mu$ L of the diluted test substance solutions into their corresponding plastic tubes.
12. Prepare the reaction mixture according to Table 1. Thaw the corresponding amount of cofactor aliquots on ice and add the cofactor to the reaction mixture right before pipetting the reaction mixture to the prepared samples (see Note e.).

13. Add 250  $\mu\text{L}$  of reaction mix to every prepared plastic tube, including background and solvent control tubes.
14. Incubate the plastic tubes for 10 min at 37  $^{\circ}\text{C}$  with 300 rpm shaking in the preheated thermoshaker.
15. Place the tubes from the thermoshaker immediately on ice and add to each reaction tube as well as each quality control and calibrator aliquot 1 mL of extraction mix. Mix all the samples at 300 rpm.
16. Transfer the organic phase of each sample to a new plastic tube and evaporate the samples to dryness.
17. Reconstitute the samples in at least 25  $\mu\text{L}$  HPLC grade methanol (see Note f.).

### 3.3.4 Notes

1. The required amount of deuterated internal controls per mL extraction mix depends on the sensitivity of the instrument used and must be established experimentally first.
2. The total amount of solvent within the enzyme reaction should always be kept below a maximum of 1% to make sure that 11 $\beta$ -HSD2 activity is sustained during the reaction. Higher amounts of solvent within the reaction may inactivate the enzyme.
3. Since these reactions must be carried out with relatively high volumes so that the substrate and product can be successfully detected by LC-MS/MS after the reaction, a larger quantity of diluted cell lysate is also required. Several pellets may have to be thawed and pooled at this step.
4. The dilution factor of the resuspended cell pellet depends on initial cell density and transfection efficiency before harvesting the cells. This factor needs to be determined for each batch of cell pellets before assessing test substances. For this, a dilution series of the cell lysate is assessed, adding 50  $\mu\text{L}$  of the 1% solvent control solution to 200  $\mu\text{L}$  of each dilution of the cell pellet, except for the background sample where 250  $\mu\text{L}$  TS2 buffer is used instead. Proceed from step 11 onwards as described in the protocol above. If cell lines other than HEK-293 are used, the lysis protocol as well as the dilution range may vary.
5. The remaining cofactor should not be reused after thawing.
6. The resuspension volume may have to be adjusted depending on the sensitivity of the detection equipment and the used injection volume of the LC-MS/MS.



## 3.4 Product and substrate quantification by LC-MS/MS

### 3.4.1 Equipment

- Agilent 1290 Infinity II Serie high speed pump, with active seal wash, power range 1300 bar and 5 mL/min (Agilent Technologies, Santa Clara, CA, USA)
- Agilent 6495B Serie Triple Quadrupole mass spectrometer equipped with a JetStream electrospray ionization interface (Agilent Technologies)
- 1290 Infinity Multisampler, 1300 bar, 2  $\times$  54-vial container (Agilent Technologies), needle flush port, 40  $\mu$ L metering device and 20  $\mu$ L loop.
- InfinityLab Sample Thermostat (4–40  $^{\circ}$ C) (Agilent Technologies)
- Multi Column Thermostat (4–110  $^{\circ}$ C), 6-column selector 1300 bar (Agilent Technologies)
- Software: Data acquisition and qualitative and quantitative analysis MassHunter (Version B.10.0. Build 10.0.27, Agilent Technologies)
- High Vacuum MS40 Pumps (Agilent Technologies)
- Nitrogen Generator System GeniusXE 70 (Peak Scientific, Scotland, UK)
- Milli-Q<sup>®</sup> Direct Water Purification System equipped with EDS-Pak<sup>®</sup> Polisher (Merck, Darmstadt Germany)
- ACQUITY UPLC BEH C18 Column, 130  $\text{Å}$ , 1.7  $\mu$ m, 2.1 mm  $\times$  150 mm (Waters, Milford, MA, USA)

### 3.4.2 Solutions

- Ultra-pure water, 0.2  $\mu$ m filtered with final removal of potential endocrine disruptors (Milli-Q, Merck)
- Acetonitrile (Biosolve, Valkenswaard, Netherlands)
- Methanol (Acros Organics, Geel, Belgium)
- 2-Propanol (Merck)
- Formic acid (Merck)
- Solvent A: 95% Water: Acetonitrile, 0.1% formic acid (v/v/v)
- Solvent B: 95% Acetonitrile: Water, 0.1% formic acid (v/v/v)
- Seal wash solution: 50% 2-Propanol: Water (v/v)
- Needle flush solution: 75% Methanol: Water (v/v)
- Sample resuspensions prepared after the enzyme activity assay (described in subchapter 3.3)

### 3.4.3 Procedure

This procedure is applicable for the separation and quantification of the  $11\beta$ -HSD2 substrate-product pair cortisol and cortisone, which are major glucocorticoids in human and zebrafish (Pippal, Cheung, Yao, Brennan, & Fuller, 2011). Although  $11\beta$ -HSD2 homologs of mice and rats are also capable of converting cortisol to cortisone, corticosterone and  $11$ -dehydrocorticosterone are the main glucocorticoids in rodents. This LC-MS/MS separation and quantification method can be used to quantify both glucocorticoid pairs, if needed. The hydroxysteroids exhibit higher retention times than their oxosteroid counterparts under reversed phase conditions.

1. Prepare mobile phases, needle flush- and seal wash solution.
2. Load acquisition method and equilibrate instrument temperatures and pressures for 30 min
3. Parameters: gas temperature 290 °C, gas flow 14 L/min, nebulizer 20 psi, sheath gas heater 300 °C, sheath gas flow 11 L/min, capillary voltage 4000 V, charging 1500 V. IonFunnel settings: high pressure radio frequency (POS) 200 V, Low Pressure radio frequency (POS) 110 V.
4. Confirm system stability and absence of any contamination within a blank measurement by injecting 5  $\mu$ L HPLC grade methanol, which was used previously for sample resuspension.
5. Confirm system stability and mobile phase integrity with the measurement of one of the mid-range calibrator samples; confirm expected retention time (RT) for all analytes and corresponding internal standards.
6. Exclude carry over within an additional blank measurement.
7. Equip auto sampler after stabilization to 4 °C (optional).
8. Control LC-MS/MS system for possible leaks.
9. Check column backpressure.
10. Write an automated worklist on the program starting with the three quality controls first, followed by randomized samples and calibrators and finally the three quality controls again. Start the worklist.
11. Start automated process according to the following specifications: sample injection (5  $\mu$ L injection volume, speed 100  $\mu$ L/min) with needle wash (10 s).
12. Steroids are separated at a total flow rate of 0.63 mL/min, with a linear gradient from 25%–70% solvent B over a time of 10 min. The column is subsequently flushed with 100% solvent B for 2 min at the same flow rate, followed by column re-equilibration with solvent A to start column conditioning for 1.5 min before injecting the next sample.

13. Multiple-reaction monitoring (MRM) is performed for analyte precursor and corresponding quantifier and qualifier transitions with positive ionization (see Table 2).
14. Load acquired data into quantitative data analysis software and quantify analyte amount according to the prepared calibration curve and quality controls.

### 3.5 Qualitative analysis

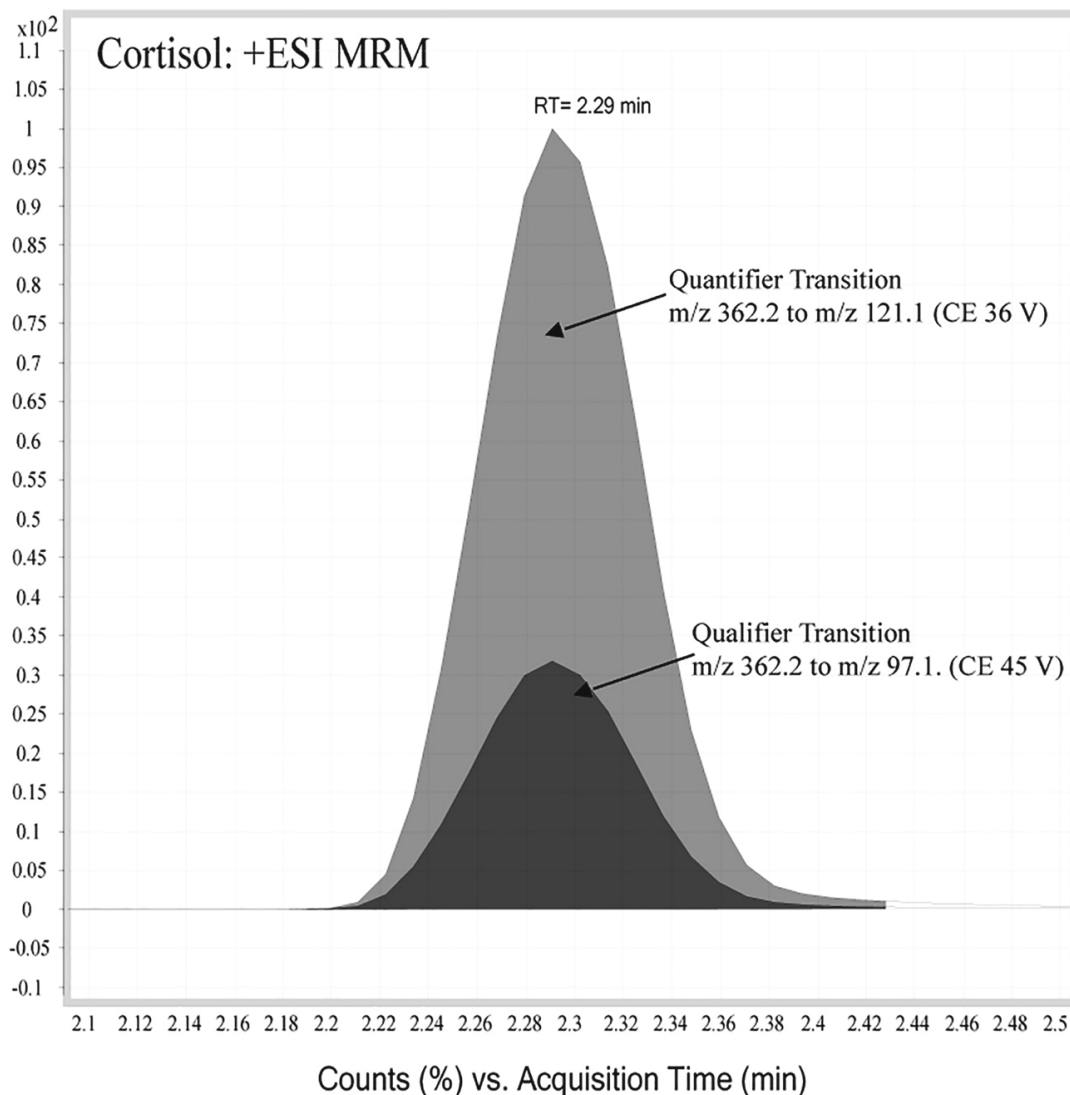
Each analyte is measured by the mass to charge ratio ( $m/z$ ) within a process called multiple reaction monitoring (MRM). A compound is characterized by the specific retention time (RT), the mass to charge ratio ( $m/z$ ) of the precursor ion and at least two specific mass fragments. These mass fragments are products from the collision-induced decay (CID) of the precursor ion. The decay of the precursor ion by a certain collision energy (CE) is reproducible, yielding stable amounts of product ions in the samples, calibrators and quality controls. The decay of a precursor ion to its product is referred to as transition. The transition with the higher abundance (counts) is defined as quantifier, while the transition with the lower abundance will be defined as qualifier (Fig. 3).

MRM measurements enable the use of the ratio of these two specific mass fragments (area under the curve quantifier/area under the curve qualifier) as an additional compound characteristic and thus, contribute to compound identity. The abundance of the quantifier transitions is visualized as the single compound peak and the response is used for further calculations of concentration while the ratio of both transitions confirms compound integrity. Accurate peaks are recorded by repeated measurement over the entire peak width, in general, 18 counts or measure points during the elution of the peak at its specific RT. Moreover, an acceptable peak shape is defined by peak symmetry for the baseline-separated peak. Symmetry of the peak depends on the chromatographic condition such as column type, particle size, flow rate, type of the mobile phase, gradient condition and temperatures. In order to be considered as detected or quantified, any analyte signal has to be greater than the response measured for the sample matrix under the given chromatographic condition (noise). The ratio of specific signal to its noise (signal to noise ratio, SNR) is used as quality criteria for every measured transition. As a lower limit of quantification (LLOQ) the SNR should be  $\geq 10$  (noise algorithm root mean square (RMS), with noise multiplier of 5). As a lower limit of detection (LLOD), the SNR should be  $\geq 3$ . The physicochemical properties of

**Table 2** LC-MS/MS detection parameters for glucocorticoids.

<b>Compound</b>	<b>Precursor (m/z)</b>	<b>Quantifier (m/z)</b>	<b>CID (V)</b>	<b>Qualifier (m/z)</b>	<b>CID (V)</b>
Cortisol	363.2	121.1	36	97.1	45
Cortisol-D4	367.2	125.1	32	101.1	45
Cortisone	361.2	163.2	24	90.9	60
Cortisone-D2	363.2	165.2	36	123.1	12
Corticosterone	347.2	329.2	9	121.2	25
Corticosterone-D8	355.2	125.1	25	114.0	32
11-Dehydrocorticosterone	345.2	120.9	25	90.9	60

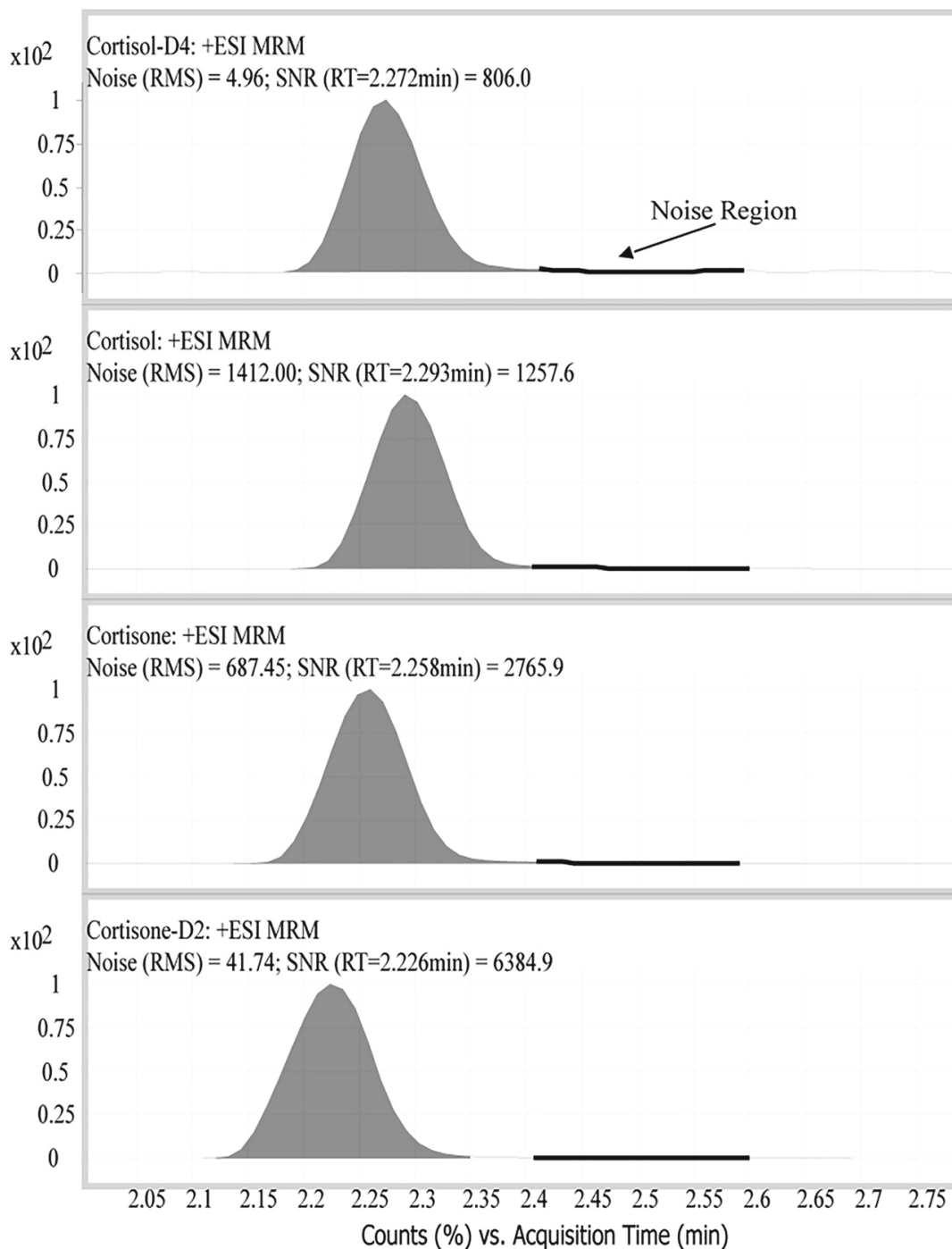
This table lists all relevant analytes to assess 11 $\beta$ -HSD2 activity in humans, rodents and zebrafish, with their corresponding transitions and collision induced energies (CID).



**Fig. 3** Electrospray ionization multiple reaction monitoring of cortisol. Chromatogram of cortisol at 2.29 min depicted as overlay of quantifier ( $m/z$  121.1) and qualifier transition ( $m/z$  97.1) of the precursor ion ( $m/z$  363.2) derived from collision induced decay at 36 V and 45 V.

deuterated standards (ISTD) are considered to be equal to the analyte of interest. The ISTD will therefore elute at similar to equal RT and have equal susceptibility to any ion disturbing influence during the measurement (Fig. 4).

The inclusion of a known and constant quantity of a deuterated ISTD for the analyte of interest at the earliest possible time-point prior sample extraction is used to monitor analytic problems within the given sample matrix and variations within the extraction process. Thereby the calculated ratio of ISTD quantifier and qualifier transitions (ISTD response) enables normalization of the sample response. Response factors (RF) for the

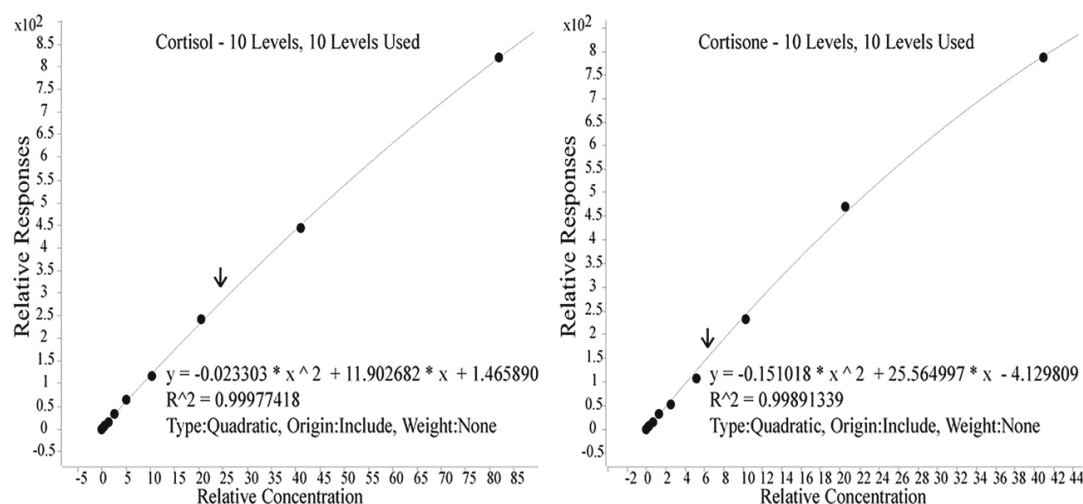


**Fig. 4** Retention times, peak shapes and noise ratios of analytes and ISTD. Chromatograms of cortisol (2.25 min), cortisone (2.23 min) and their corresponding deuterated ISTDs cortisol-D4 (2.24 min) and cortisone-D2 (2.23 min).

quantifier to qualifier ions as well as the overall RF of analyte to its corresponding ISTD should yield 80–120% accuracy. For the data analysis a relative RT derivation of less than 10% for any measured analyte and ISTD from calibrators and quality controls measured within the same run should be met.

### 3.6 Quantitative analysis and expected experimental outcome

All calibrators and quality controls are prepared in the same matrix as the samples and measured within the same analytic run. Prior to the experiment the absence of the analyte of interest within the matrix is controlled. In order to quantify an unknown sample, ten calibration samples are prepared by serial dilution with known concentrations. One of the calibrators represents the matrix blank, this sample contains the ISTD but no analyte concentration. The calibration concentrations are designed regarding the expected maximal and minimal analyte concentration within the experiment. The accuracy for calibrator samples are calculated as variation (%) from the known nominal concentration. All calibrators should reach an accuracy of 80–100%. In order to define the precision of an analytic run, quality control samples with known concentrations at three different concentration levels over the entire calibration range (low, middle and high) might be prepared as three independent replicates. The precision can be calculated as variation from the nominal concentration at the given concentration level. If quality controls are used all quality controls have to reach 80–100% accuracy to the nominal concentration to be considered for precision calculations. At least seven out of ten calibrators should fit all mentioned criteria to be included in the calibration curve. As quality control for the applied calibration curve fitting, the  $R^2$  of the calibration curve should be greater than 0.998 (Fig. 5).



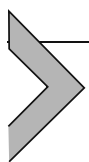
**Fig. 5** Calibration curves for cortisol and cortisone. Relative sample response of cortisol over its relative concentration depicted as calibration curve derived from 10 calibrators. The arrow represents an unknown sample response, which can be calculated by the resulting equation of the calibration curve.

Analyte concentrations with a  $\text{SNR} \leq 10$  are considered as not reliably quantifiable. In case of experimentally expected low product concentrations that cannot be quantified, such as complete  $11\beta$ -HSD2 inhibition, the value  $\text{LLOD}/2$  can be introduced as constant value for statistic calculations. To determine  $11\beta$ -HSD2 activity, the respective product/substrate ratio is calculated, corrected for the measured background conversion and normalized to the background-corrected solvent control. The background, determined in the sample containing only TS2 buffer and the reaction mix, is subtracted and should be below 10%. Substrate conversion for the solvent control, after background-correction, should reach 20–30%.

### 3.7 Optimization and troubleshooting

<b>Problem</b>	<b>Possible solutions</b>
The lysate shows no enzyme activity	<ul style="list-style-type: none"> <li>– Confirm <math>11\beta</math>-HSD2 expression by Western blotting</li> <li>– Check the total solvent percentage per reaction</li> <li>– Test a wider range of lysate dilutions to reach optimal substrate conversion</li> <li>– Assess enzyme activity after prolonged reaction time (e. g. 20 min, 30 min, ...)</li> <li>– Overexpress <math>11\beta</math>-HSD2 in a suitable cell model such as HEK-293 (if not previously used)</li> </ul>
Peaks of different compounds are not well separated	<ul style="list-style-type: none"> <li>– Change to another type of analytical column</li> <li>– Optimize separation conditions such as gradient, solvent composition and flow rate.</li> </ul>
Internal standards differ between samples	<ul style="list-style-type: none"> <li>– Ensure accurate and reproducible extraction</li> <li>– Confirm steroid solubility/sample integrity</li> <li>– Exclude ion suppression/ion enhancement (matrix effect)</li> </ul>
Readout in the solvent control after LC-MS/MS measurement is below the limit of quantification	<ul style="list-style-type: none"> <li>– Adjust substrate concentration</li> <li>– Enhance measuring sensitivity by modification of LC-MS/MS detection:</li> <li>– Enhance injection volume (background signal will change as well)</li> <li>– Optimize sample preparation to purify analytes and remove contaminations</li> <li>– Select better transitions for quantification</li> <li>– Optimize source parameters such as temperature, gas flow and voltage</li> </ul>





## 4. 11 $\beta$ -HSD2 activity assay using tissue homogenates

This section describes an assay using homogenates of tissues endogenously expressing 11 $\beta$ -HSD2 such as placenta. Besides assessing the activity in a given tissue, the inhibitory potency of xenobiotics potentially disrupting the important barrier function of 11 $\beta$ -HSD2 in the placenta can also be determined by this assay. After homogenization and subsequent dilution, the enzyme reaction is performed in the presence of a radiolabeled tracer of the substrate, followed by subsequent separation of substrate and product by thin-layer chromatography (TLC) and quantification of product formation using liquid scintillation counting. Tissues other than placenta that express endogenous levels of 11 $\beta$ -HSD2 can be used, *i.e.* colon and kidney. An enrichment of 11 $\beta$ -HSD2 can be achieved by the preparation of microsomes, which can help removing factors that might interfere with the enzyme activity measurement (see section 5).

### 4.1 Preparation of placenta tissue for 11 $\beta$ -HSD2 activity assay

#### 4.1.1 Equipment

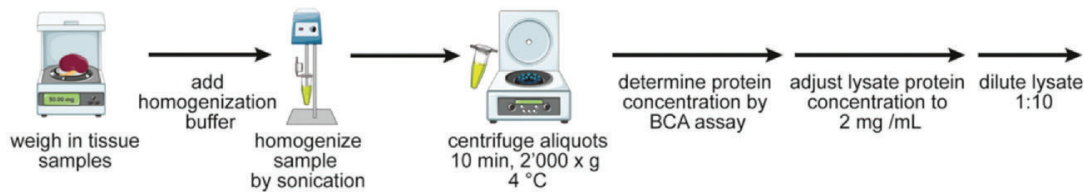
- Ultrasonic homogenizer (Omni Sonic Ruptor 400, Kennesaw, GA, USA)
- Centrifuge with cooling function, pre-cooled at 4 °C (5424 R, Eppendorf)

#### 4.1.2 Buffers, media, and kits

- **Homogenization buffer** (250 mM sucrose, 10 mM HEPES, pH: 7.4, store at 4 °C)
- **Reaction buffer** (300 mM NaCl, 1 mM EDTA, 10% glycerol, 20 mM Tris-HCl, pH 7.7, store at 4 °C)
- **Pierce™ BCA Protein Assay Kit** (Thermo Fisher Scientific, Waltham, MA, USA)

#### 4.1.3 Procedure

1. Place weighted, snap frozen placental tissue into a 1.5 mL plastic tube, add 900  $\mu$ L ice-cold homogenization buffer per 100 mg tissue and homogenize the placental tissue on ice with the ultrasonic homogenizer (power level 3, pulser set to 40)(see Fig. 6). (see Note a.)



**Fig. 6** Schematic overview of whole tissue samples expressing 11 $\beta$ -HSD2. After weighing in the tissue sample and the subsequent homogenization of the tissue by sonication, the samples are centrifuged, pellets discarded and the total protein content in the supernatant is measured. Subsequently, the samples are diluted to a final protein concentration of 0.2 mg/mL.

2. **Critical: Keep the tissue sample and homogenate on ice and immediately proceed with the further protocol steps.**
3. Centrifuge the homogenate at 4 °C for 10 min at 2000  $\times$  g to pellet the nuclear fraction and cellular debris.
4. Transfer the supernatant to a new tube and measure the protein concentration with the BCA Protein Assay Kit according to the manufacturer's protocol.
5. Dilute the homogenates to a concentration of 2 mg/mL with homogenization buffer and further dilute 1:10 in reaction buffer.

#### 4.1.4 Notes

1. To enhance the reproducibility and comparability between samples from different individuals, isolate comparable parts from the respective tissues. Use 50–100 mg of snap frozen placental tissue.

## 4.2 Radiometric enzyme activity assay

This assay may be used to assess 11 $\beta$ -HSD2 activity in homogenates from tissues of treated and untreated, healthy and diseased, or wild-type and genetically modified organisms, or to investigate 11 $\beta$ -HSD2 inhibition by xenobiotics. Alternatively, whole lysates prepared from cells overexpressing recombinant 11 $\beta$ -HSD2 (see section 3) may be applied.

### 4.2.1 Equipment

- Vortex (TX4 Digital IR Vortex Mixer, Velp Scientifica<sup>TM</sup>)
- Thermoshaker with 96-well plate attachment (Thermomixer comfort, Eppendorf)

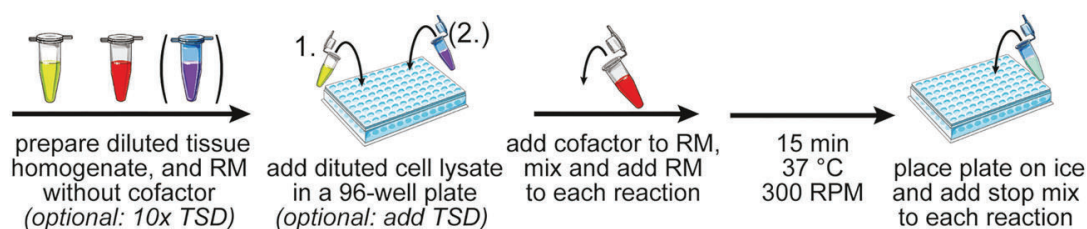
#### 4.2.2 Buffers and solutions

- **Reaction buffer** (300 mM NaCl, 1 mM EDTA, 10% glycerol, 20 mM Tris-HCl, pH 7.7, store at 4 °C)
- **[1,2,6,7-<sup>3</sup>H] labeled cortisol stock solution** ~4  $\mu$ M (dilute <sup>3</sup>H-cortisol (American Radiolabeled Chemicals, Saint Louis, Missouri, USA) with ethanol after determination of the actual concentration of radiolabeled cortisol in the purchased stock, store at -20 °C)
- **Label-free cortisol stock solution** 10 mM in DMSO (store at -20 °C)
- **NAD<sup>+</sup> stock solution** 25 mM in H<sub>2</sub>O (store 20  $\mu$ L aliquots at -80 °C, up to six months)
- **Stop mix** (2 mM cortisol, 2 mM cortisone in methanol, store at 4 °C, see Note d.)
- **Test substance stocks** 10 mM in DMSO or methanol (store at -20 °C)

#### 4.2.3 Procedure

**Critical: Steps 2, 3 and 8 are optional if 11 $\beta$ -HSD2 inhibition by xenobiotics is assessed. Follow instructions in *brackets ()* and *italic* for inhibitor assessment protocol.** (see Fig. 7)

1. Preheat a thermoshaker at 37 °C.
2. *Prepare a 1% solvent control solution (reaction buffer either with DMSO or methanol, depending on the solvent used to dissolve the test compounds) and prepare a dilution series of test substances in the corresponding solvent. The addition of the 1% solvent control solution to a reaction will result in a 1:10 dilution, resulting in a final solvent concentration of 0.1%. Store the diluted solution on ice. (see Note a.)*



**Fig. 7** Schematic overview of the radiometric 11 $\beta$ -HSD2 activity assay. The diluted tissue homogenate (yellow solution) is kept on ice until the start of the enzyme reaction. Tissue homogenate (and optionally test substance dilutions (TSD, purple solution)) are added to a 96-well plate. After addition of the cofactor to the reaction mix, the enzyme reaction takes place in a thermoshaker at 37 °C for 15 min, shaking at 300 rpm. The reaction is stopped by placing the 96-well plate containing the reactions on ice immediately after and by addition of the stop mix (green solution).

3. Dilute each prepared test substance concentration 1:100 in reaction buffer, reaching 10x of the concentration to be assessed in the assay. The final addition of the test substance dilution to the enzyme assay will result in a 1:10 dilution. Store the diluted solutions on ice. (see Note a.)
4. Prepare a 20  $\mu\text{M}$  label-free cortisol working solution by diluting the 10 mM stock 1:500 in reaction buffer and keep on ice.
5. Prepare a 96-well PCR plate, label it and place it on ice. All reactions should be carried out in technical duplicates. Include two wells as background samples (and two wells for solvent control samples).
6. Add 10  $\mu\text{L}$  of the prepared and diluted 11 $\beta$ -HSD2 placenta homogenate per well in the 96-well PCR plate on ice (except for the prepared background sample wells).
7. Prepare the two background samples by adding 10  $\mu\text{L}$  (12.2  $\mu\text{L}$ ) ice-cold reaction buffer into two wells.
8. (Add 2.2  $\mu\text{L}$  of 1% solvent control solution in the two solvent control wells and 2.2  $\mu\text{L}$  of the diluted test substance solutions into their corresponding wells.)
9. Prepare the reaction mixture according to Table 3 (use column in brackets and italic for the inhibitor assessment protocol). Thaw one cofactor aliquot and add the corresponding amount to the reaction mixture immediately before pipetting the reaction mixture to the prepared samples. (see Note b.)
10. Add 10  $\mu\text{L}$  of reaction mix to every well, including background (and solvent control) wells.

**Table 3** Preparation of reaction mix for 25 enzyme reactions.

Buffer/solution	Amount to add	(Amount to add)	Final concentration per reaction well
Reaction buffer	260 $\mu\text{L}$	(260 $\mu\text{L}$ )	—
$^3\text{H}$ -cortisol [~4 $\mu\text{M}$ ]	1.4 $\mu\text{L}$	(1.5 $\mu\text{L}$ )	10 nM
Label-free cortisol working solution [20 $\mu\text{M}$ ]	1.1 $\mu\text{L}$	(1.2 $\mu\text{L}$ )	40 nM
$\text{NAD}^+$ [25 mM]	10.9 $\mu\text{L}$	(12.2 $\mu\text{L}$ )	500 $\mu\text{M}$

This table lists end concentrations as well as the respective amounts of buffer, substrate and cofactor solutions to add to the reaction mix for the radiometric enzyme activity assay. Amounts used in radiometric assay for inhibitor screening are included in italic and brackets.

11. Incubate the 96-well plate for 15 min with 300 rpm shaking at 37 °C in the preheated thermoshaker. (Note c.)
12. Place the 96-well plate immediately on ice and add 10  $\mu$ L of stop mix in every well to stop the enzyme reaction. (Optional: mix by pipetting in each well up and down once.) Keep the 96-well plate on ice until loading of the samples onto the TLC plate. (see Note d.)

#### 4.2.4 Notes

1. The final solvent concentration in the enzyme reaction should be maximally 1% to assure the integrity of 11 $\beta$ -HSD2.
2. The aliquot of the cofactor should not be reused after thawing.
3. The activity of the placenta homogenate depends on the expression level in the tissue and proper handling during sampling and preparation. 11 $\beta$ -HSD2 is not expressed in every placental cell type and its expression depends on the developmental stage of the placenta. The experimental outcome can vary between different tissue pieces and the assay conditions may need to be adapted.
4. The stop mix consists of methanol, which is added to denature 11 $\beta$ -HSD2 and terminate the enzyme reaction. An excess of label-free cortisone and cortisol is added with the stop mix to visualize the steroid spots after TLC separation under the UV light. Both steroids absorb light within the UV spectrum and are visible as dark spots on the UV254 indicator containing silica plate that is emitting green fluorescent light under UV.

### 4.3 TLC separation of radiolabeled steroids and liquid scintillation counting

TLC separation of substrate and product can be conducted as described in chapter “*In vitro* methods to assess 11 $\beta$ -hydroxysteroid dehydrogenase type 1 activity”, section 4.4.

### 4.4 Expected outcomes of 11 $\beta$ -HSD2 enzyme activity assay and data analysis

The expected outcomes for the quantification using liquid scintillation counting are described in chapter “*In vitro* methods to assess 11 $\beta$ -hydroxysteroid dehydrogenase type 1 activity”, section 4.5. The 11 $\beta$ -HSD2 activity determined from tissue samples may be expressed as nanomol of substrate

converted per microgram of protein per minute ( $\text{nmol} \times \mu\text{g}^{-1} \times \text{min}^{-1}$ ) by entering the percentage of substrate conversion obtained after background correction in the formula below.

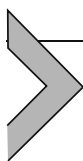
$$\frac{\text{substrate concentration (nM)} * \text{substrate conversion (\%)} * \text{reaction volume (\mu L)}}{100 * \text{reaction time (min)} * \text{protein amount in reaction (\mu g)}}$$

Use this equation to calculate the 11 $\beta$ -HSD2 activity from tissue homogenates in nanomol per  $\mu\text{g}$  of total protein per minute. The background-corrected substrate conversion percentile should be entered. The parameters: substrate concentration, reaction volume, protein amount and reaction time that are used in this protocol amount to 50 nM, 20  $\mu\text{L}$ , 2  $\mu\text{g}$  and 15 min, respectively.

The quantification of the relative inhibitor potency using tissue lysates is performed exactly as described in chapter “*In vitro* methods to assess 11 $\beta$ -hydroxysteroid dehydrogenase type 1 activity”, subchapter 4.6, by normalization of the background-corrected percentile substrate conversion to the solvent control.

## 4.5 Optimization and troubleshooting

Problem	Possible solutions
The tissue homogenate shows no enzyme activity	<ul style="list-style-type: none"> <li>– Confirm the expression of 11<math>\beta</math>-HSD2 in the tissue sample by RT-PCR or Western blotting</li> <li>– Check the percentage of total solvent concentration per reaction</li> <li>– Assess enzyme activity using prolonged reaction time (e. g. 20 min, 30 min, ...)</li> <li>– Use higher amounts of total protein of the tissue homogenate</li> </ul>
11 $\beta$ -HSD2 is degraded during preparation (confirmed by Western blotting)	<ul style="list-style-type: none"> <li>– Add 1x cOmplete, Mini Protease Inhibitor Cocktail (Roche, Basel, Switzerland) in the homogenization buffer</li> <li>– Ensure constant cooling of the samples during tissue preparation</li> </ul>
See chapter “ <i>In vitro</i> methods to assess 11 $\beta$ -hydroxysteroid dehydrogenase type 1 activity”, section 4.8 for further optimization of the separation of steroids by TLC.	



## 5. Alternative methods to assess 11 $\beta$ -HSD2 activity

In addition to the use of whole cell lysates or tissue homogenates, microsomal preparations to enrich 11 $\beta$ -HSD2 or intact cells

representing a more physiological system can be used for enzyme activity measurements. Besides LC-MS/MS quantification or liquid scintillation counting, cortisol and cortisone can also be quantified by other detection methods such as HPLC-DAD or ELISA. This subchapter focuses on presenting alternative options to assess 11 $\beta$ -HSD2 activity. Each of the methods mentioned in this subchapter is described in more detail in chapter “*In vitro* methods to assess 11 $\beta$ -hydroxysteroid dehydrogenase type 1 activity” and are similar or identical to implement for 11 $\beta$ -HSD2. Where possible, the chapter on 11 $\beta$ -HSD1 is referred to or the differences when assessing 11 $\beta$ -HSD2 activity are mentioned here.

### 5.1 11 $\beta$ -HSD2 activity assays using microsomal preparations

Isolation of the microsomal fraction from tissue samples or cultured cells with endogenous 11 $\beta$ -HSD2 expression or overexpressing the enzyme represent ways to enrich the enzyme, which may be required to reduce the presence of interfering factors such as other metabolizing enzymes or inhibitory substances. Enzyme enrichment is especially useful when investigating potentially novel 11 $\beta$ -HSD2 substrates. Enzyme assays using microsomal preparations can be performed using label-free substrate or in the presence of radiolabeled tracers with the corresponding analytical method. The experimental procedure for the preparation of microsomes from either cultured cells or tissue samples can be carried out as described in subchapter 5 of “*In vitro* methods to assess 11 $\beta$ -hydroxysteroid dehydrogenase type 1 activity” with the only difference that tissues express 11 $\beta$ -HSD2 and cells are transfected with a plasmid containing a *HSD11B2* cDNA for overexpression.

### 5.2 11 $\beta$ -HSD2 activity assay using intact cells

11 $\beta$ -HSD2 activity can also be measured in intact cell systems that endogenously express the enzyme or after transfection. No cofactor needs to be added to the reaction because NAD<sup>+</sup> cannot freely permeate cellular membranes and is available within the cell. For overexpression, a cell system not expressing glucocorticoid metabolizing enzymes, such as HEK-293 cells, is recommended. Intact cell systems are not ideal for assessing kinetic properties and comparing the potency of different inhibitors, including structure-activity-relationship analyses, due to cellular membranes and differences in the access of substances to the enzyme’s ligand binding pocket. However, they are

**Table 4** Preparation of reaction mix for 25 reactions.

Buffer/solution	Amount to add	Final concentration per reaction well
Serum-free charcoal treated HEK-293 medium	260 $\mu$ L	—
$^3$ H-cortisol [ $\sim 4 \mu$ M]	3.3 $\mu$ L	10 nM
Label-free cortisol working solution [ $20 \mu$ M] in serum-free charcoal treated HEK-293 medium	2.7 $\mu$ L	40 nM

This table lists final concentrations and the respective volumes of medium and substrate solutions to add to the reaction mix for the radiometric enzyme activity assay in intact cells.

useful to study the consequences of identified modulators in a more physiological context. Moreover, the influence of other proteins upon cotransfection and the impact of nutrients in the culture medium can be studied in intact cells.

The experimental procedure for activity measurements in intact cells may be carried out as described in Section 7 of “*In vitro* methods to assess  $11\beta$ -hydroxysteroid dehydrogenase type 1 activity” by transfecting a plasmid containing the *HSD11B2* cDNA instead of *HSD11B1*. The reaction mix used to assess  $11\beta$ -HSD2 activity is depicted below in Table 4.

### 5.2.1 Solutions required to prepare the reaction mix

- **Serum-free charcoal treated HEK-293 medium** (described in Section 7.1 of “*In vitro* methods to assess  $11\beta$ -hydroxysteroid dehydrogenase type 1 activity”)
- **[1,2,6,7- $^3$ H] labeled cortisol stock solution**  $\sim 4 \mu$ M (dilute  $^3$ H-cortisol (American Radiolabeled Chemicals) with ethanol, store at  $-20 \text{ }^\circ\text{C}$ )
- **Unlabeled cortisol stock solution** 10 mM in DMSO (store at  $-20 \text{ }^\circ\text{C}$ )

### 5.3 Alternative quantification methods

Alternative methods for quantification of cortisol and cortisone include measurements by HPLC coupled to a UV-detector or antibody-based



Advantages and limitations of the methods described in this chapter


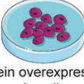



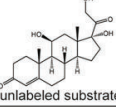
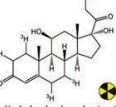
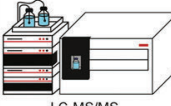



	Advantages	Limitations
protein expression	 <p>tissue samples, (e.g. kidney, colon, placenta)</p>	<ul style="list-style-type: none"> <li>- allows comparison of 11β-HSD2 activity in tissue biopsies from different human cohorts or from experimental animals (disease models)</li> <li>- lower 11β-HSD2 levels compared to overexpressing cells</li> <li>- presence of metabolites and other enzymes within tissue lysate may impair 11β-HSD2 activity</li> <li>- only apparent Km and Vmax of 11β-HSD2 can be determined in samples</li> <li>- high variability between different tissue samples possible</li> <li>- inhibitors may be metabolized by enzymes present in the tissue homogenate</li> <li>- not every tissue is suitable for direct 11β-HSD2 activity assessment, microsomal preparation may be required</li> </ul>
	 <p>protein overexpression in cells</p>	<ul style="list-style-type: none"> <li>- low cost of calcium phosphate precipitation</li> <li>- high enzyme levels after overexpression of the enzyme</li> <li>- overexpression in cultured cells allows comparison of 11β-HSD2 homologs from different species</li> <li>- moderate transfection efficiency by calcium phosphate precipitation (20-30%)</li> </ul>
sample preparation	 <p>cell homogenate</p>	<ul style="list-style-type: none"> <li>- direct access of inhibitors to 11β-HSD2 in the lysate (allows identification of novel inhibitors/scaffolds)</li> <li>- high protein stability of 11β-HSD2 within cell pellets at -80 °C (retains enzymatic activity for up to 1 year)</li> <li>- only apparent Km and Vmax can be determined</li> <li>- presence of metabolites and other enzymes in the cell lysate may affect 11β-HSD2 activity</li> <li>- inhibitors that would not enter the cell or highly cytotoxic chemicals are not eliminated and inhibit 11β-HSD2 as well</li> <li>- enzyme concentration is unknown</li> </ul>
	 <p>microsomal fraction</p>	<ul style="list-style-type: none"> <li>- enrichment of 11β-HSD2</li> <li>- assessment of new 11β-HSD2 substrates by removing other enzymes and lowering cellular background is facilitated</li> <li>- only apparent Km and Vmax of 11β-HSD2 can be determined</li> <li>- microsome preparations are time-consuming</li> <li>- partial loss of enzyme activity during homogenization and centrifugation is possible</li> </ul>
	 <p>intact cell</p>	<ul style="list-style-type: none"> <li>- no direct access of inhibitors due to cell membrane barriers</li> <li>- cells endogenously expressing 11β-HSD2 can be employed</li> <li>- allows comparison of 11β-HSD2 homologs from different species in an identical background</li> <li>- effects on 11β-HSD2 expression can be assessed</li> <li>- prolonged incubation time needed</li> <li>- low throughput, restricted to mechanistic studies</li> <li>- species-specificity of proteins and other factors influencing 11β-HSD2 activity are not considered</li> <li>- specificity of transport proteins is highly cell-type dependent</li> <li>- the fact that this assay is a closed system without a flux of metabolites needs to be kept in mind</li> </ul>
enzyme activity assay type	 <p>unlabeled substrate</p>	<ul style="list-style-type: none"> <li>- no radiotracers needed</li> <li>- no special laboratory required</li> <li>- no radioactive waste disposal</li> <li>- time consuming substrate/product extraction prior to measurement may be required</li> <li>- larger reaction volumes and enzyme amounts required for reactions</li> </ul>
	 <p>radiolabeled substrate</p>	<ul style="list-style-type: none"> <li>- high sensitivity of liquid scintillation counting</li> <li>- allows use of nanomolar substrate range and low reaction volume</li> <li>- requires low amount of biological material</li> <li>- not suitable for upscaling for high throughput screening (HTS)</li> <li>- requires radiotracers</li> <li>- special laboratory required</li> <li>- radioactive waste disposal</li> </ul>
quantification of substrate and product	 <p>LC-MS/MS</p>	<ul style="list-style-type: none"> <li>- not limited to cortisone/cortisol substrate pair, applicable for the detection of novel 11β-HSD2 substrates</li> <li>- option to combine several substrate/product pairs in one method</li> <li>- LC-MS/MS is a rather expensive detection method</li> <li>- time consuming substrate/product extraction prior to measurement may be required</li> <li>- LC-MS/MS handling requires experience</li> <li>- requires the establishment and validation of the method on own instrument</li> <li>- interference of high salt concentrations and poorly soluble substances with separation of steroids</li> <li>- limited suitability for HTS of novel 11β-HSD2 inhibitors</li> </ul>
	 <p>HPLC-DAD</p>	<ul style="list-style-type: none"> <li>- not limited to cortisone/cortisol, applicable for the detection of novel 11β-HSD2 substrates</li> <li>- option to combine several substrate/product pairs in one method</li> <li>- moderate limit of quantification for HPLC-DAD, larger amounts of biological material required</li> <li>- time consuming substrate/product extraction prior to measurement may be required</li> <li>- professional expertise required</li> <li>- requires the establishment and validation of the method on own instrument</li> <li>- limited suitability for HTS of novel 11β-HSD2 inhibitors</li> </ul>
	 <p>ELISA kits</p>	<ul style="list-style-type: none"> <li>- time efficiency</li> <li>- suitable for HTS of novel 11β-HSD2 inhibitors</li> <li>- requires adaptation of the activity assay protocol</li> <li>- cross reactivity of detection antibodies between cortisol and cortisone vary depending on the kit that is used</li> <li>- might require microsome preparation due to cross-reactivity of antibodies with metabolites in the cellular background</li> </ul>
	 <p>liquid scintillation counting</p>	<ul style="list-style-type: none"> <li>- high sensitivity of liquid scintillation counting</li> <li>- allows use of nanomolar substrate range and low reaction volume</li> <li>- requires low amount of biological material</li> <li>- not suitable for upscaling for high throughput screening (HTS)</li> <li>- requires radiotracers</li> <li>- special laboratory required</li> <li>- radioactive waste disposal</li> </ul>


Fig. 8 Advantages and limitations of the methods described in this chapter. The plethora of methods described in this chapter are grouped according to the modules mentioned in section 2: protein expression, sample preparation, enzyme activity assay type and quantification of substrate and product, allowing a direct comparison of different methods within each module.

methods such as ELISA. The advantages and disadvantages of these methods are listed in Fig. 8 and further described in Section 8 of the chapter “In vitro methods to assess 11β-hydroxysteroid dehydrogenase type 1 activity”.



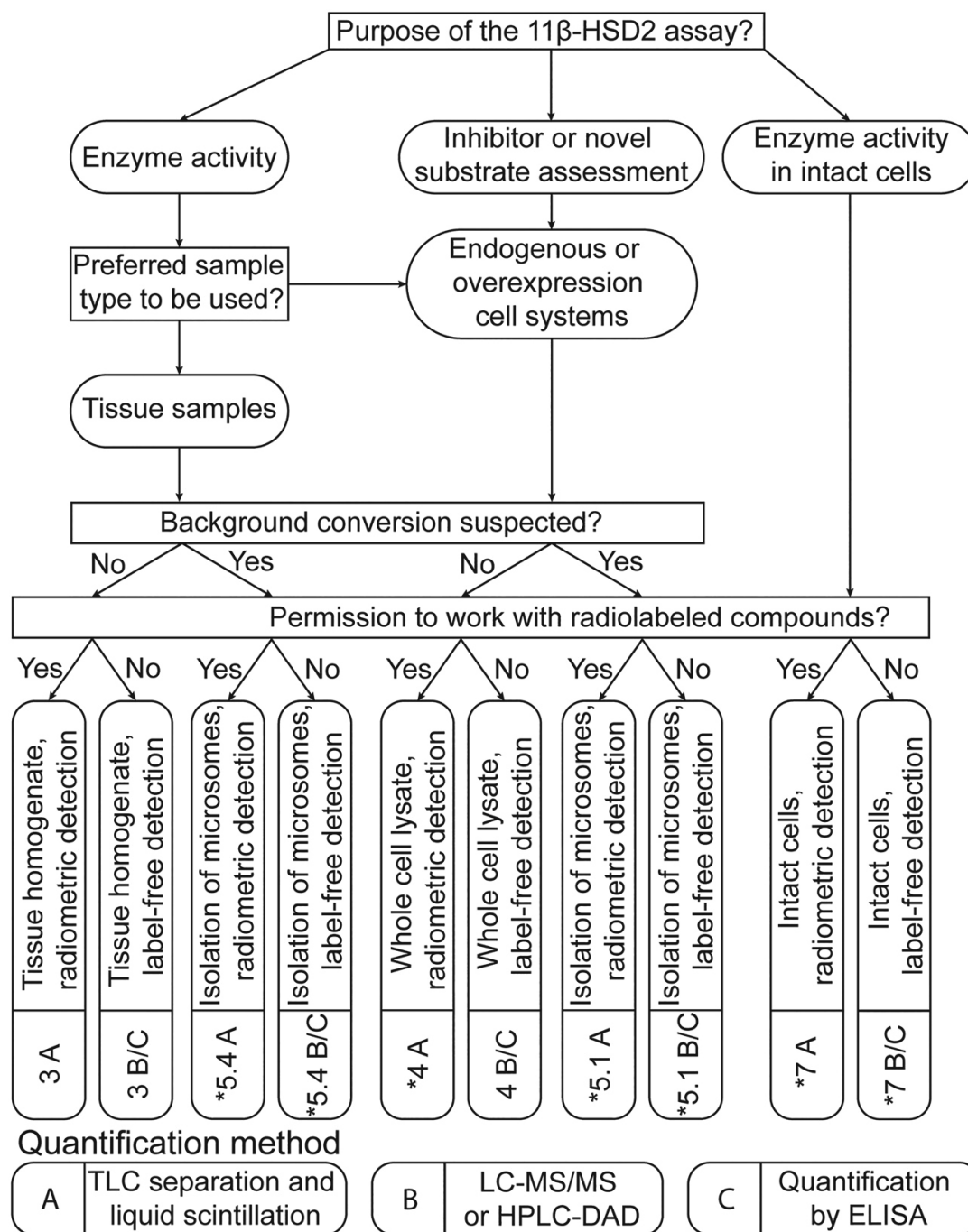
## 6. Project and resource based choice of 11 $\beta$ -HSD2 activity assays

The decision tree shown in Fig. 9 should assist the reader in selecting an 11 $\beta$ -HSD2 assay suitable for the research question and available equipment. Assessment of 11 $\beta$ -HSD2 activity in tissues with endogenous expression, such as placenta, kidney and colon, may be either conducted using whole tissue homogenates or microsomal preparations to enrich the enzyme and remove factors that could interfere with the reaction. Microsomal preparations from cells overexpressing 11 $\beta$ -HSD2 may be useful to study potentially novel substrates to avoid interference by other metabolizing enzymes. The use of whole lysates of cells overexpressing 11 $\beta$ -HSD2 represents a cost and time saving method for the screening and characterization of inhibitors. The inhibitory capacity of xenobiotics and the influence of other enzymes and natural ligands can be assessed also in intact cells, either expressing endogenous levels or after overexpression of 11 $\beta$ -HSD2. Each assay may either be performed using label-free substrate, followed by quantification using HPLC-DAD, LC-MS/MS and ELISA, or by using radiolabeled cortisol as a tracer followed by liquid scintillation counting. Each of the methods described in this chapter has advantages and limitations, summarized in Fig. 8, allowing direct comparison between different procedures and facilitating the choice of the method.



## 7. Biomarkers to assess 11 $\beta$ -HSD2 activity in preclinical and clinical studies

The activity of 11 $\beta$ -HSD2 can be indirectly assessed by measuring the ratio of active to inactive glucocorticoid metabolites in blood samples (plasma, serum) or in urine samples (ideally 24-hour urine) of preclinical and clinical studies. A lack of 11 $\beta$ -HSD2 activity due to genetic defects in patients can be detected by an increased plasma or serum cortisol to cortisone ratio, which is mainly due to a decreased cortisone concentration as a result of feedback regulation (Carvajal et al., 2018). Similarly, an increased corticosterone to 11-dehydrocorticosterone ratio with decreased 11-dehydrocorticosterone in plasma or serum is seen in mice with genetic defects in 11 $\beta$ -HSD2 (Bailey et al., 2011). In human urine, the ratio of free cortisol to cortisone and the ratio of the reduced glucocorticoid metabolites (5 $\alpha$ -tetrahydrocortisol + 5 $\beta$ -tetrahydrocortisol)/5 $\beta$ -tetrahydrocortisone are



**Fig. 9** Decision tree to choose a suitable 11β-HSD2 activity assay. The assay format should be chosen depending on the research purpose. 11β-HSD2 from tissue samples may be required if disease models or certain inhibitors are investigated. Depending on potentially interfering metabolites or other enzymes in the homogenate, microsomal isolation might be necessary to reduce cellular background. For inhibitor characterization or novel substrate assessment, which are best performed in lysates of endogenously or overexpressing cell systems, microsomal preparation is indicated if background conversion of the substrate or interference by other enzymes is suspected. The inhibitory potential of test compounds or the influence of other enzymes and natural ligands on 11β-HSD2 can also be assessed in intact cells. The choice of the substrate and product quantification method depends on whether radiolabeled (Continued)

markers of 11 $\beta$ -HSD2 activity (Mantero et al., 1996; Palermo, Delitala, Mantero, Stewart, & Shackleton, 2001; Wilson et al., 1995). For the same determination in rodent models the ratios of corticosterone to 11-dehydrocorticosterone and their respective metabolites (5 $\alpha$ -tetrahydrocorticosterone + 5 $\beta$ -tetrahydrocorticosterone)/ 5 $\beta$ -tetrahydro-11-dehydrocorticosterone can be assessed instead. These biomarkers of 11 $\beta$ -HSD2 activity can also be used to detect enzyme inhibition by compounds in food such as glycyrrhetic acid or drugs such as the anti-fungals itraconazole and posaconazole that can cause secondary hypertension (Farese et al., 1991; Morris, Brem, & Odermatt, 2021; Stewart et al., 1987; Thompson et al., 2019).

---



## 8. Safety considerations and standards of the described methods

Handling of HEK-293 cells requires a cell culture laboratory of Biosafety Level 1 standards (BSL-1). We recommend adhering to the safety precautions at your workplace regarding the handling of tritiated compounds. Tritiated compounds should neither be ingested nor inhaled. Separation of steroids by TLC and scraping the TLC plates should always be performed in a fume hood. The fumes of the mobile phase of the TLC are hazardous. While scraping TLC plates, wear gloves, a lab coat, safety goggles and a FFP2 mask to prevent ingestion or inhalation of the radiolabeled steroids in the silica dust. Silica dust is hazardous and inhalation must be avoided.

---



## 9. Concluding remarks

11 $\beta$ -HSD2 exerts essential protective functions. It prevents an unintentional activation of the mineralocorticoid receptor by glucocorticoids in the distal tubules and cortical collecting ducts of the kidney, and on the other hand, it acts as an enzymatic barrier in the placenta to reduce the amount of active glucocorticoids that reach the fetus. Inhibition of

---

**Fig. 9—Cont'd** cortisol is included in the reaction. The number and letter(s) in the box below the recommended enzyme activity assay correspond to the number of the subchapter where the method is described and the associated quantification method, respectively. Sections marked with an asterisk are described in the previous chapter, "In vitro methods to assess 11 $\beta$ -hydroxysteroid dehydrogenase type 1 activity". Additions or changes to the methods are described here in section 5.

11 $\beta$ -HSD2 is detrimental, as it can cause secondary hypertension and hypokalemia. In addition, an increased exposure of a fetus to cortisol due to a diminished 11 $\beta$ -HSD2 activity can cause cardio-metabolic disturbances and neurological impairments later in life. This chapter provides the reader with *in vitro* methods that can be used to identify and characterize xenobiotics inhibiting 11 $\beta$ -HSD2 as well as to assess the activity of this enzyme in cell-based models and in tissues from animal experiments.

## Acknowledgments

We would like to thank Ms Tania Jetzer for proofreading this chapter. We acknowledge Servier Medical Art (smart.servier.com) and AlphaFold Protein Structure Data Base (alphafold.ebi.ac.uk) (Jumper et al., 2021; Varadi et al., 2022) for providing elements used in the Figures of this chapter.

## References

- Arriza, J. L., Weinberger, C., Cerelli, G., Glaser, T. M., Handelin, B. L., Housman, D. E., & Evans, R. M. (1987). Cloning of human mineralocorticoid receptor complementary DNA: Structural and functional kinship with the glucocorticoid receptor. *Science (New York, N. Y.)*, *237*(4812), 268–275. <https://doi.org/10.1126/science.3037703>
- Beck, K. R., Bachler, M., Vuorinen, A., Wagner, S., Akram, M., Griesser, U., & Odermatt, A. (2017). Inhibition of 11beta-hydroxysteroid dehydrogenase 2 by the fungicides itraconazole and posaconazole. *Biochemical Pharmacology*, *130*, 93–103. <https://doi.org/10.1016/j.bcp.2017.01.010>
- Bailey, M. A., Craigie, E., Livingstone, D. E. W., Kotelevtsev, Y. V., Al-Dujaili, E. A. S., Kenyon, C. J., & Mullins, J. J. (2011). Hsd11b2 haploinsufficiency in mice causes salt sensitivity of blood pressure. *Hypertension*, *57*(3), 515–520. <https://doi.org/10.1161/HYPERTENSIONAHA.110.163782>
- Benediktsson, R., Calder, A. A., Edwards, C. R., & Seckl, J. R. (1997). Placental 11 beta-hydroxysteroid dehydrogenase: A key regulator of fetal glucocorticoid exposure. *Clinical Endocrinology (Oxford)*, *46*(2), 161–166. <https://doi.org/10.1046/j.1365-2265.1997.1230939.x>
- Brown, R. W., Chapman, K. E., Edwards, C. R., & Seckl, J. R. (1993). Human placental 11 beta-hydroxysteroid dehydrogenase: Evidence for and partial purification of a distinct NAD-dependent isoform. *Endocrinology*, *132*(6), 2614–2621. <https://doi.org/10.1210/endo.132.6.8504762>
- Brown, R. W., Chapman, K. E., Murad, P., Edwards, C. R., & Seckl, J. R. (1996). Purification of 11 beta-hydroxysteroid dehydrogenase type 2 from human placenta utilizing a novel affinity labelling technique (Pt 3) *The Biochemical Journal*, *313*(Pt 3), 997–1005. <https://doi.org/10.1042/bj3130997>
- Beck, K. R., Inderbilen, S. G., Kanagaratnam, S., Kratschmar, D. V., Jetten, A. M., Yamaguchi, H., & Odermatt, A. (2019). 11beta-Hydroxysteroid dehydrogenases control access of 7beta,27-dihydroxycholesterol to retinoid-related orphan receptor gamma. *Journal of Lipid Research*, *60*(9), 1535–1546. <https://doi.org/10.1194/jlr.M092908>
- Beck, K. R., Kanagaratnam, S., Kratschmar, D. V., Birk, J., Yamaguchi, H., Sailer, A. W., & Odermatt, A. (2019). Enzymatic interconversion of the oxysterols 7beta,25-dihydroxycholesterol and 7-keto,25-hydroxycholesterol by 11beta-hydroxysteroid dehydrogenase type 1 and 2. *The Journal of Steroid Biochemistry and Molecular Biology*, *190*, 19–28. <https://doi.org/10.1016/j.jsbmb.2019.03.011>

- Beck, K. R., & Odermatt, A. (2021). Antifungal therapy with azoles and the syndrome of acquired mineralocorticoid excess. *Molecular and Cellular Endocrinology*, 524, 111168. <https://doi.org/10.1016/j.mce.2021.111168>
- Carvajal, C. A., Tapia-Castillo, A., Valdivia, C. P., Allende, F., Solari, S., Lagos, C. F., & Fardella, C. E. (2018). Serum cortisol and cortisone as potential biomarkers of partial 11beta-hydroxysteroid dehydrogenase type 2 deficiency. *American Journal of Hypertension: Journal of the American Society of Hypertension*, 31(8), 910–918. <https://doi.org/10.1093/ajh/hpy051>
- Edwards, C. R., Stewart, P. M., Burt, D., Brett, L., McIntyre, M. A., Sutanto, W. S., & Monder, C. (1988). Localisation of 11 beta-hydroxysteroid dehydrogenase—Tissue specific protector of the mineralocorticoid receptor. *Lancet*, 2(8618), 986–989. [https://doi.org/10.1016/s0140-6736\(88\)90742-8](https://doi.org/10.1016/s0140-6736(88)90742-8)
- Farese, R. V., Jr., Biglieri, E. G., Shackleton, C. H., Irony, I., & Gomez-Fontes, R. (1991). Licorice-induced hypermineralocorticoidism. *The New England Journal of Medicine*, 325(17), 1223–1227. <https://doi.org/10.1056/NEJM199110243251706>
- Ferrari, P. (2010). The role of 11beta-hydroxysteroid dehydrogenase type 2 in human hypertension. *Biochimica et Biophysica Acta*, 1802(12), 1178–1187. <https://doi.org/10.1016/j.bbadis.2009.10.017>
- Funder, J. W., Pearce, P. T., Smith, R., & Smith, A. I. (1988). Mineralocorticoid action: Target tissue specificity is enzyme, not receptor, mediated. *Science (New York, N. Y.)*, 242(4878), 583–585. <https://doi.org/10.1126/science.2845584>
- Hoffmann, W. J., McHardy, I., & Thompson, G. R., 3rd (2018). Itraconazole induced hypertension and hypokalemia: Mechanistic evaluation. *Mycoses*, 61(5), 337–339. <https://doi.org/10.1111/myc.12749>
- Hollenberg, S. M., Weinberger, C., Ong, E. S., Cerelli, G., Oro, A., Lebo, R., & Evans, R. M. (1985). Primary structure and expression of a functional human glucocorticoid receptor cDNA. *Nature*, 318(6047), 635–641. <https://doi.org/10.1038/318635a0>
- Hannedouche, S., Zhang, J., Yi, T., Shen, W., Nguyen, D., Pereira, J. P., & Sailer, A. W. (2011). Oxysterols direct immune cell migration via EBI2. *Nature*, 475(7357), 524–527. <https://doi.org/10.1038/nature10280>
- Inderbinen, S. G., Zogg, M., Kley, M., Smiesko, M., & Odermatt, A. (2021). Species-specific differences in the inhibition of 11beta-hydroxysteroid dehydrogenase 2 by itraconazole and posaconazole. *Toxicology and Applied Pharmacology*, 412, 115387. <https://doi.org/10.1016/j.taap.2020.115387>
- Jetten, A. M., & Cook, D. N. (2020). (Inverse) Agonists of retinoic acid-related orphan receptor gamma: Regulation of immune responses, inflammation, and autoimmune disease. *Annual Review of Pharmacology and Toxicology*, 60, 371–390. <https://doi.org/10.1146/annurev-pharmtox-010919-023711>
- Jumper, J., Evans, R., Pritzel, A., Green, T., Figurnov, M., Ronneberger, O., & Hassabis, D. (2021). Highly accurate protein structure prediction with AlphaFold. *Nature*, 596(7873), 583–589. <https://doi.org/10.1038/s41586-021-03819-2>
- Kuriakose, K., Nesbitt, W. J., Greene, M., & Harris, B. (2018). Posaconazole-Induced Pseudohyperaldosteronism. *Antimicrobial Agents and Chemotherapy*, 62(5), <https://doi.org/10.1128/AAC.0213>
- Morris, D. J., Brem, A. S., & Odermatt, A. (2021). Modulation of 11beta-hydroxysteroid dehydrogenase functions by the cloud of endogenous metabolites in a local micro-environment: The glycyrrhetic acid-like factor (GALF) hypothesis. *The Journal of Steroid Biochemistry and Molecular Biology*, 214, 105988. <https://doi.org/10.1016/j.jsbmb.2021.105988>
- Mantero, F., Palermo, M., Petrelli, M. D., Tedde, R., Stewart, P. M., & Shackleton, C. H. (1996). Apparent mineralocorticoid excess: Type I and type II. *Steroids*, 61(4), 193–196. [https://doi.org/10.1016/0039-128x\(96\)00012-8](https://doi.org/10.1016/0039-128x(96)00012-8)

- Meyer, A., Strajhar, P., Murer, C., Da Cunha, T., & Odermatt, A. (2012). Species-specific differences in the inhibition of human and zebrafish 11 $\beta$ -hydroxysteroid dehydrogenase 2 by thiram and organotins. *Toxicology*, *301*(1–3), 72–78. <https://doi.org/10.1016/j.tox.2012.07.001>
- Miossec, P., & Kolls, J. K. (2012). Targeting IL-17 and TH17 cells in chronic inflammation. *Nature Reviews. Drug Discovery*, *11*(10), 763–776. <https://doi.org/10.1038/nrd3794>
- Mune, T., Rogerson, F. M., Nikkila, H., Agarwal, A. K., & White, P. C. (1995). Human hypertension caused by mutations in the kidney isozyme of 11  $\beta$ -hydroxysteroid dehydrogenase. *Nature Genetics*, *10*(4), 394–399. <https://doi.org/10.1038/ng0895-394>
- Murphy, B. E. (1981). Ontogeny of cortisol-cortisone interconversion in human tissues: A role for cortisone in human fetal development. *Journal of Steroid Biochemistry*, *14*(9), 811–817. [https://doi.org/10.1016/0022-4731\(81\)90226-0](https://doi.org/10.1016/0022-4731(81)90226-0)
- Nguyen, M. H., Davis, M. R., Wittenberg, R., McHardy, I., Baddley, J. W., Young, B. Y., & Thompson, G. R. (2020). Posaconazole serum drug levels associated with pseudo-hyperaldosteronism. *Clinical Infectious Diseases: An Official Publication of the Infectious Diseases Society of America*, *70*(12), 2593–2598. <https://doi.org/10.1093/cid/ciz741>
- Odermatt, A., Arnold, P., Stauffer, A., Frey, B. M., & Frey, F. J. (1999). The N-terminal anchor sequences of 11 $\beta$ -hydroxysteroid dehydrogenases determine their orientation in the endoplasmic reticulum membrane. *The Journal of Biological Chemistry*, *274*(40), 28762–28770. <https://doi.org/10.1074/jbc.274.40.28762>
- Odermatt, A., & Kratschmar, D. V. (2012). Tissue-specific modulation of mineralocorticoid receptor function by 11 $\beta$ -hydroxysteroid dehydrogenases: an overview. *Molecular and Cellular Endocrinology*, 168–186. <https://doi.org/10.1016/j.mce.2011.07.020>
- Palermo, M., Delitala, G., Mantero, F., Stewart, P. M., & Shackleton, C. H. (2001). Congenital deficiency of 11 $\beta$ -hydroxysteroid dehydrogenase (apparent mineralocorticoid excess syndrome): Diagnostic value of urinary free cortisol and cortisone. *Journal of Endocrinological Investigation*, *24*(1), 17–23. <https://doi.org/10.1007/BF03343803>
- Pippal, J. B., Cheung, C. M., Yao, Y. Z., Brennan, F. E., & Fuller, P. J. (2011). Characterization of the zebrafish (*Danio rerio*) mineralocorticoid receptor. *Molecular and Cellular Endocrinology*, *332*(1–2), 58–66. <https://doi.org/10.1016/j.mce.2010.09.014>
- Raikkonen, K., Martikainen, S., Pesonen, A. K., Lahti, J., Heinonen, K., Pyhala, R., & Kajantie, E. (2017). Maternal licorice consumption during pregnancy and pubertal, cognitive, and psychiatric outcomes in children. *American Journal of Epidemiology*, *185*(5), 317–328. <https://doi.org/10.1093/aje/kww172>
- Schweizer, R. A., Atanasov, A. G., Frey, B. M., & Odermatt, A. (2003). A rapid screening assay for inhibitors of 11 $\beta$ -hydroxysteroid dehydrogenases (11 $\beta$ -HSD): Flavanone selectively inhibits 11 $\beta$ -HSD1 reductase activity. *Molecular and Cellular Endocrinology*, *212*(1–2), 41–49. <https://doi.org/10.1016/j.mce.2003.09.027>
- Seckl, J. R., Benediktsson, R., Lindsay, R. S., & Brown, R. W. (1995). Placental 11  $\beta$ -hydroxysteroid dehydrogenase and the programming of hypertension. *The Journal of Steroid Biochemistry and Molecular Biology*, *55*(5–6), 447–455. [https://doi.org/10.1016/0960-0760\(95\)00193-x](https://doi.org/10.1016/0960-0760(95)00193-x)
- Salvante, K. G., Milano, K., Kliman, H. J., & Nepomnaschy, P. A. (2017). Placental 11  $\beta$ -hydroxysteroid dehydrogenase type 2 (11 $\beta$ -HSD2) expression very early during human pregnancy. *Journal of Developmental Origins of Health and Disease*, *8*(2), 149–154. <https://doi.org/10.1017/S2040174416000611>
- Soroosh, P., Wu, J., Xue, X., Song, J., Sutton, S. W., Sablad, M., & Sun, S. (2014). Oxysterols are agonist ligands of ROR $\gamma$  and drive Th17 cell differentiation. *Proceedings of the National Academy of Sciences of the United States of America*, *111*(33), 12163–12168. <https://doi.org/10.1073/pnas.1322807111>

- Stewart, P. M., Wallace, A. M., Valentino, R., Burt, D., Shackleton, C. H., & Edwards, C. R. (1987). Mineralocorticoid activity of liquorice: 11-Beta-hydroxysteroid dehydrogenase deficiency comes of age. *Lancet*, *2*(8563), 821–824. [https://doi.org/10.1016/s0140-6736\(87\)91014-2](https://doi.org/10.1016/s0140-6736(87)91014-2)
- Stewart, P. M., Whorwood, C. B., & Mason, J. I. (1995). Type 2 11 beta-hydroxysteroid dehydrogenase in foetal and adult life. *The Journal of Steroid Biochemistry and Molecular Biology*, *55*(5–6), 465–471. [https://doi.org/10.1016/0960-0760\(95\)00195-6](https://doi.org/10.1016/0960-0760(95)00195-6)
- Tannin, G. M., Agarwal, A. K., Monder, C., New, M. I., & White, P. C. (1991). The human gene for 11 beta-hydroxysteroid dehydrogenase. Structure, tissue distribution, and chromosomal localization. *The Journal of Biological Chemistry*, *266*(25), 16653–16658. (<https://www.ncbi.nlm.nih.gov/pubmed/1885595>).
- Thompson, G. R., 3rd, Beck, K. R., Patt, M., Kratschmar, D. V., & Odermatt, A. (2019). Posaconazole-induced hypertension due to inhibition of 11beta-hydroxylase and 11beta-hydroxysteroid dehydrogenase 2. *Journal of the Endocrine Society*, *3*(7), 1361–1366. <https://doi.org/10.1210/js.2019-00189>
- Varadi, M., Anyango, S., Deshpande, M., Nair, S., Natassia, C., Yordanova, G., & Velankar, S. (2022). AlphaFold Protein Structure Database: Massively expanding the structural coverage of protein-sequence space with high-accuracy models. *Nucleic Acids Research*, *50*(D1), D439–D444. <https://doi.org/10.1093/nar/gkab1061>
- White, P. C., Mune, T., & Agarwal, A. K. (1997). 11 beta-Hydroxysteroid dehydrogenase and the syndrome of apparent mineralocorticoid excess. *Endocrine Reviews*, *18*(1), 135–156. <https://doi.org/10.1210/edrv.18.1.0288>
- Wilson, R. C., Krozowski, Z. S., Li, K., Obeyesekere, V. R., Razzaghy-Azar, M., Harbison, M. D., & New, M. I. (1995). A mutation in the HSD11B2 gene in a family with apparent mineralocorticoid excess. *The Journal of Clinical Endocrinology and Metabolism*, *80*(7), 2263–2266. <https://doi.org/10.1210/jcem.80.7.7608290>



## 4.5 Discussion

Azole fungicides such as itraconazole and posaconazole are used for the treatment and prevention of fungal diseases. In some patients, however, long-term treatment with these fungicides has triggered adverse drug effects, which manifested themselves in the AME syndrome, which is characterized by similar symptoms as hyperaldosteronism, i.e. hypokalemia, hypernatremia and low renin and aldosterone levels. Although both azole antifungals are able to potently inhibit the human HSD11B2 homolog (with nanomolar IC<sub>50</sub> values), different mechanisms of action for the development of the AME syndrome have been proposed for both assessed azole antifungals in humans. Itraconazole and its metabolite hydroxyitraconazole are thought to act mainly via cortisol accumulation through HSD11B2 inhibition. However, posaconazole preferentially inhibits the 11 $\beta$ -hydroxylase (CYP11B1) activity, leading to accumulation of the mineralocorticoid 11-deoxycorticosterone and 11-deoxycortisol which is further driven by activation of the HPA axis [287, 288].

In this study, we confirmed the previously hypothesized species-specific inhibition of HSD11B2 by the tested azole fungicides using radiometric enzyme activity assays. Indeed, human HSD11B2 is potently inhibited by all three test compounds, itraconazole, hydroxyitraconazole and posaconazole, with nanomolar IC<sub>50</sub> values (0.121  $\mu$ M, 0.187  $\mu$ M, and 0.512  $\mu$ M, respectively). The rat homolog of HSD11B2 is inhibited up to 6 times less compared to the human variant (IC<sub>50</sub> values: 0.729  $\mu$ M, 1.13  $\mu$ M and 0.835  $\mu$ M). The mouse and zebrafish homologs are relatively weakly inhibited by the examined azole antifungals which is illustrated by IC<sub>50</sub> values above 7  $\mu$ M. Furthermore, by cloning different chimeric HSD11B2 variants from the human and mouse homologs, we identified the enzyme regions and amino acid residues responsible for the species-specific differences in HSD11B2 inhibition by itraconazole, hydroxyitraconazole and posaconazole, namely the C-terminal region and amino acid residues 170 and 172. The new homology model of HSD11B2 that we generated was based on 20 different HSD11B2 models and allowed us to draw some conclusions regarding the structure-activity relationship between HSD11B2 and the analyzed azole antifungals. However, this homology model has certain limitations, e.g. it was not possible to determine the optimal binding pose of cortisol that would allow efficient electron transfer to the cofactor NAD<sup>+</sup>. In addition, the relatively unstructured C-terminus, which turned out to be relevant for the species-specific differences in the inhibition of HSD11B2 by the examined azole fungicides, is difficult to predict *in silico*. Thus, resolving the crystal structure of different HSD11B2 homologs would be required to optimize the modeling, but this has not yet been

achieved. A possible difficulty could be that HSD11B2 structure may be stabilized by its embedding in the ER membrane, which would complicate structure resolving. Said possible stabilization through the ER membrane may also explain why purification of this protein was so far not possible without loss of enzymatic activity [289]. A novel strategy would have to be pursued to determine the structure of HSD11B2 anchored in the membrane, such as cryo-electron microscopy that allows effective analysis of transmembrane proteins (methods reviewed in [290]).

Species-specific differences are particularly relevant in translational pharmacology and toxicology. A promising treatment method that has been validated in animal models may prove to be useless or harmful in human medicine. There are many examples of species-specific differences in the field of steroidogenesis. In rodents for instance, corticosterone is the main glucocorticoid, not cortisol [291]. Teleost fish, to which the zebrafish belongs, also use cortisol as their main corticosteroid, but have no HSD11B1 homolog that can reactivate cortisone. As a matter of fact, no 11-ketoreductase activity towards cortisone could be measured in zebrafish [292]. Instead of reactivation, cortisone in zebrafish is metabolized by 20 $\beta$ -hydroxysteroid dehydrogenase type 2 to 20 $\beta$ -hydroxycortisone and is then excreted [293, 294]. Our study highlights another species-specific difference with the inhibition of HSD11B2 by azole antifungals, an important finding that should be considered in future toxicological and clinical studies.

Reliable *in vitro* and *in silico* methods have become increasingly important since the 3R principle (refinement, reduction and replacement) regarding the use of animals in scientific experiments has been implemented in Europe [295, 296]. The two book chapters, in which we described detailed *in vitro* experimental approaches enabling successful analysis of both 11 $\beta$ -HSD isozyme activities, also contribute to the 3R principle. They allow at least medium throughput screening of both enzymes to prevent adverse effects by HSD11B2 inhibition through xenobiotics, including novel drugs, and may also be used to identify new, potentially therapeutic compounds for the inhibition of HSD11B1. Furthermore, the experimental principles described in the book chapters may also be used for the establishment of other enzymatic assays with steroidogenic enzymes.

## **5. Project 2: Potential antiandrogenic effects of parabens and benzophenone-type UV-filters inhibiting 3 $\alpha$ -hydroxysteroid dehydrogenases**

### 5.1 Introduction

Safety assessments in the field of endocrinology are still largely based on the detection of potential endocrine disrupting properties of test substances that act directly on the receptors of sex steroids, the estrogen and androgen receptors. Other mechanisms that may alter those receptors activities, including receptor modifications such as phosphorylation, acetylation or SUMOylation or the regulation of intracellular ligand concentration by steroid biosynthesis and catabolism have been largely neglected. Activation of the AR by testosterone and DHT is essential for the initial development of male reproductive structures during the fetal stage and later plays an important role during adolescence for maturation and growth of the penis, prostate, testicles, and the development of body-, facial- and pubic hair [297]. The biosynthesis of the most potent human androgen, DHT, takes place either via the classic pathway or the so-called backdoor pathway. In the classic pathway, DHT is produced by the reduction of testosterone via one of the 5 $\alpha$ -ketoreductases, SRD5A1 or SRD5A2. In the backdoor pathway, 3 $\alpha$ -androsterone is first formed as the main circulating intermediate steroid from placental progesterone and then converted to DHT in two further enzymatic steps, a 3 $\alpha$ -oxidation and a 17 $\beta$ -reduction (Subchapter 2.3.1).

It appears that not only the classical pathway of DHT synthesis but also the backdoor pathway is relevant for the correct formation of the male reproductive system. Inactivating mutations of the steroidogenic enzymes AKR1C2 and AKR1C4, which act exclusively in the backdoor pathway, can, similarly to mutations of enzymes involved in the classical pathway, result in a 46,XY DSD with undervirilization of male external genitalia in affected patients [102].

3 $\alpha$ -HSDs include 17 $\beta$ -hydroxysteroid dehydrogenases types 6 and 10 (HSD17B6, HSD17B10), dehydrogenase/reductase SDR family member 9 (DHRS9), and retinol dehydrogenases type 5 and 16 (RDH5, RDH16) which are capable of catalyzing one of the last two enzymatic steps in the backdoor pathway, the NAD<sup>+</sup>-dependent 3 $\alpha$ -oxidation of 3 $\alpha$ -androsterone to 5 $\alpha$ -androstenedione or of 3 $\alpha$ -adiol to DHT. However, substrate affinities towards those two steroids may differ between these 3 $\alpha$ -HSDs. They also display different tissue expression patterns in the human body and can convert other substrate classes such as retinoids and the neurosteroid allopregnanolone, indicating a variety of tissue-specific roles for the respective 3 $\alpha$ -HSDs (see Table 1).

	HSD17B6	HSD17B10	DHRS9	RDH5	RDH16
tissue expression pattern	liver	testis	testis	liver	liver
	testis	prostate	brain	testis	epidermis
	prostate	brain	colon,	uterus	
	uterus	ovary	heart	adrenal gland	
	brain	spleen,	epidermis	ovaries	
	adrenal gland	thymus	placenta	spleen	
		colon	trachea	thymus	
			bone marrow	colon	
			spinal cord	heart	
			lung	skeletal muscle	
			lymph nodes	kidneys	
				pancreas	
				small intestine	
				bladder	
				mammary tissue	
			retinal pigment epithelium		
substrates	3 $\alpha$ -androsterone,	3 $\alpha$ -androsterone		3 $\alpha$ -androsterone	3 $\alpha$ -androsterone
	3 $\alpha$ -androstanediol	3 $\alpha$ -androstanediol,	3 $\alpha$ -androstanediol	3 $\alpha$ -androstanediol	3 $\alpha$ -androstanediol
	allopregnanolone	allopregnanolone	allopregnanolone		
	all- <i>trans</i> -retinol				all- <i>trans</i> -retinol
			9-, 11-, 13- <i>cis</i> retinol	13- <i>cis</i> -retinol	

**Table 1. Systematic overview of tissue expression patterns and substrates of 3 $\alpha$ -HSDs.** Depicted are the tissue expression patterns and substrate specificities of the 3 $\alpha$ -HSDs studied in this project, including HSD17B6 [104, 298, 299], HSD17B10 [300-302], DHRS9 [303-305], RDH5 [306-310] and RDH16 [311-313].

To date, there are no known mutations of the 3 $\alpha$ -HSDs described that result in 46,XY DSD with undervirilization of male external genitalia. However, mutations of the RDH5 gene appear to impair the 11-*cis*-retinol conversion to 11-*cis*-retinal in the retinal pigment epithelium, resulting in a delay in the regeneration of cone and rod photopigments. This may lead to stationary night blindness and an accumulation of white spots in the retina of affected individuals [307, 310].

Despite displaying endocrine disrupting properties, parabens and UV-filters are still used as additives in cosmetics and body care products to improve their stability and prolonging their shelf life. Those additives display mild estrogenic and weak antiandrogenic activities acting directly on the estrogen receptor and the AR, with EC<sub>50</sub> or IC<sub>50</sub> values in the micromolar range [225, 314-317]. Paraben and UV-filter uptake have been demonstrated via both the oral route, or through skin penetration after topical application [215, 216, 240, 318, 319]. In addition to other human matrices such as urine and blood serum, these compounds were also measured in amniotic fluid, placental tissue and fetal cord serum, suggesting prenatal exposure in human fetuses (reviewed in [217, 242]). Possible effects of parabens and UV-filters have only been

measured on a fraction of steroidogenic enzymes involved in the classical pathway of DHT synthesis, but so far, no studies have been conducted on enzymes that act exclusively in the backdoor pathway [247, 320]. For this reason, we decided to investigate possible antiandrogenic effects of parabens and UV-filters through inhibition of oxidative 3 $\alpha$ -HSDs in the backdoor pathway. First, we examined HSD17B6, HSD17B10, DHRS9, RDH5 and RDH16 for their respective enzymatic activities. Then we assessed 26 parabens and UV-filters in total on the most active 3 $\alpha$ -HSDs identified, HSD17B6, RDH5 and RDH16. After determining the inhibitory potential of the newly identified inhibitors through their respective IC<sub>50</sub> values, which were found to be in the nanomolar and lower micromolar range, we analyzed the binding mode and the SAR of the identified inhibitors with a novel *in silico* homology model of HSD17B6.

## 5.2 Published article: Potential antiandrogenic effects of parabens and benzophenone-type UV-filters by inhibition of 3 $\alpha$ -hydroxysteroid dehydrogenases

Manuel Kley<sup>a,b</sup>, Simon Stücheli<sup>a</sup>, Pamela Ruffiner<sup>a,b</sup>, Veronika Temml<sup>c</sup>, Stéphanie Boudon<sup>b</sup>, Daniela Schuster<sup>c</sup>, Alex Odermatt<sup>a,b,\*</sup>

<sup>a</sup> Division of Molecular and Systems Toxicology, Department of Pharmaceutical Sciences, University of Basel, Klingelbergstrasse 50, 4056 Basel, Switzerland.

<sup>b</sup> Swiss Centre for Applied Human Toxicology and Department of Pharmaceutical Sciences, University of Basel, Missionsstrasse 64, 4055 Basel, Switzerland.

<sup>c</sup> Institute of Pharmacy, Department of Pharmaceutical and Medicinal Chemistry, Paracelsus Medical University, Strubergasse 21, 5020 Salzburg, Austria

\* Corresponding author. e-mail address: alex.odermatt@unibas.ch

### Published article

**Personal contribution:** Establishment and execution of a novel radiometric *in vitro* enzyme activity assay. Screening of parabens and UV-filters as well as determination of corresponding IC<sub>50</sub> values for HSD17B6 (Figure 4A and B, Supplementary Figure 2). Establishment and execution of HSD17B6 activity assay with AR transactivation readout (Figure 5). Data analysis, as well as drafting and revision of the manuscript.

**Aims:** Assessment of potential antiandrogenic effects exerted by parabens and UV-filters through inhibition of 3 $\alpha$ -HSDs in the backdoor pathway of DHT synthesis.

**Conclusion:** Several parabens and UV-filters potently inhibit HSD17B6 with IC<sub>50</sub> values in the nanomolar range. Generation of a HSD17B6 homology model explained the SAR of the identified inhibitors. Whether these xenobiotics reach high enough concentrations in target tissue to affect male development *in utero*, during adolescence or puberty remains to be determined.



## Potential antiandrogenic effects of parabens and benzophenone-type UV-filters by inhibition of 3 $\alpha$ -hydroxysteroid dehydrogenases

Manuel Kley<sup>a,b</sup>, Simon Stücheli<sup>a,1</sup>, Pamela Ruffiner<sup>a,b</sup>, Veronika Temml<sup>c</sup>, Stéphanie Boudon<sup>b</sup>, Daniela Schuster<sup>c</sup>, Alex Odermatt<sup>a,b,\*</sup>

<sup>a</sup> Division of Molecular and Systems Toxicology, Department of Pharmaceutical Sciences, University of Basel, Klingelbergstrasse 50, Basel 4056, Switzerland

<sup>b</sup> Swiss Centre for Applied Human Toxicology and Department of Pharmaceutical Sciences, University of Basel, Missionsstrasse 64, 4055 Basel, Switzerland

<sup>c</sup> Institute of Pharmacy, Department of Pharmaceutical and Medicinal Chemistry, Paracelsus Medical University, Strubergasse 21, Salzburg 5020, Austria

### ARTICLE INFO

Handling Editor: Dr. Mathieu Vinken

#### Keywords:

3 $\alpha$ -hydroxysteroid dehydrogenase  
17 $\beta$ -hydroxysteroid dehydrogenase  
Backdoor pathway  
Enzyme inhibition  
Paraben  
Benzophenone  
UV-filter  
Homology model  
Endocrine disrupting chemical

### ABSTRACT

Parabens and UV-filters are frequently used additives in cosmetics and body care products that prolong shelf-life. They are assessed for potential endocrine disrupting properties. Antiandrogenic effects of parabens and benzophenone-type UV-filters by blocking androgen receptor (AR) activity have been reported. Effects on local androgen formation received little attention. Local 5 $\alpha$ -dihydrotestosterone (DHT) production with subsequent AR activation is required for male external genitalia formation during embryogenesis. We investigated whether parabens and benzophenone-type UV-filters might cause potential antiandrogenic effects by inhibiting oxidative 3 $\alpha$ -hydroxysteroid dehydrogenases (3 $\alpha$ -HSDs) involved in the backdoor pathway of DHT formation. Five different 3 $\alpha$ -HSDs were assessed for their efficiency to catalyze the 3 $\alpha$ -oxidation reaction to form DHT and activate AR. 17 $\beta$ -hydroxysteroid dehydrogenase type 6 (HSD17B6), retinol dehydrogenases type 5 and 16 were further assessed using a radiometric *in vitro* activity assay to determine the conversion of 5 $\alpha$ -androstane-3 $\alpha$ -ol-17-one to 5 $\alpha$ -androstane-3,17-dione in lysates of overexpressing HEK-293 cells. All parabens tested, except *p*-hydroxybenzoic acid (a main metabolite) inhibited HSD17B6 activity. Hexyl- and heptylparaben, as well as benzophenone (BP)-1 and BP-2, showed the highest inhibitory potencies, with nanomolar IC<sub>50</sub> values. Molecular modeling predicted binding modes for the inhibitory parabens and BPs and provided an explanation for the observed structure-activity-relationship. Our results propose a novel mechanism of antiandrogenic action for commercially used parabens and BP UV-filters by inhibiting HSD17B6 and lowering DHT synthesis. Follow-up studies should assess BP-3 metabolism after topical application and whether the identified inhibitors reach concentrations in liver, testis, or prostate to inhibit HSD17B6, thereby causing antiandrogenic effects.

### 1. Introduction

Parabens and UV-filters are widely used as additives to improve the

stability and shelf-life of cosmetics and various personal care products. Parabens are esters of *p*-hydroxybenzoic acid that are added to products for their antibacterial and antifungal properties, while UV-filters are

**Abbreviations:** 3 $\alpha$ -adiol, 3 $\alpha$ -androstenediol, 5 $\alpha$ -androstane-3 $\alpha$ ,17 $\beta$ -diol; 3 $\alpha$ -androsterone, 5 $\alpha$ -androstane-3 $\alpha$ -ol-17-one; 3 $\alpha$ -HSD, 3 $\alpha$ -hydroxysteroid dehydrogenase; 3-BC, 3-benzylidene camphor; 3 $\beta$ -adiol, 3 $\beta$ -androstenediol, 5 $\alpha$ -androstane-3 $\beta$ ,17 $\beta$ -diol; 3 $\beta$ -epiandrosterone, 5 $\alpha$ -androstane-3 $\beta$ -ol-17-one; 4-MBC, 4-methylbenzylidene camphor; 5 $\alpha$ -adione, 5 $\alpha$ -androstenedione, 5 $\alpha$ -androstane-3,17-dione; 5 $\alpha$ -DHP, 5 $\alpha$ -dihydroprogesterone; 17 $\alpha$ -DHP, 17 $\alpha$ -hydroxydihydroprogesterone; AKR1, aldo-keto reductase family 1; Androstenediol, androst-5-ene-3 $\beta$ ,17 $\beta$ -diol; Androstenedione, androst-4-ene-3,17-dione; AR, androgen receptor; ARE, androgen response element; BP, benzophenone; DHEA, dehydroepiandrosterone; DHRS9, dehydrogenase/reductase SDR family member 9; DHT, 5 $\alpha$ -dihydrotestosterone; DMSO, dimethyl sulfoxide; ER, estrogen receptor; EU, European Union; FDA, Food and Drug Administration; HEK-293 cells, Human Embryonic Kidney-293 cells; HSD3B1/2, 3 $\beta$ -hydroxysteroid dehydrogenases type 1 and 2; HSD17B3, 17 $\beta$ -hydroxysteroid dehydrogenase type 3; HSD17B6, 17 $\beta$ -hydroxysteroid dehydrogenase type 6; HSD17B10, 17 $\beta$ -hydroxysteroid dehydrogenase type 10; RDH5, retinol dehydrogenase type 5; RDH16, retinol dehydrogenase type 16; SCCS, Scientific Committee on Consumer Safety SCCS; SRD5A1/2, steroid 5 $\alpha$ -reductases type 1 and 2; SAR, structure-activity relationship; US, United States.

\* Corresponding author at: Division of Molecular and Systems Toxicology, Department of Pharmaceutical Sciences, University of Basel, Klingelbergstrasse 50, Basel 4056, Switzerland.

E-mail address: [alex.odermatt@unibas.ch](mailto:alex.odermatt@unibas.ch) (A. Odermatt).

<sup>1</sup> Present address: Department of Biomedicine, University of Basel.

<https://doi.org/10.1016/j.tox.2024.153997>

Received 3 August 2024; Received in revised form 2 November 2024; Accepted 8 November 2024

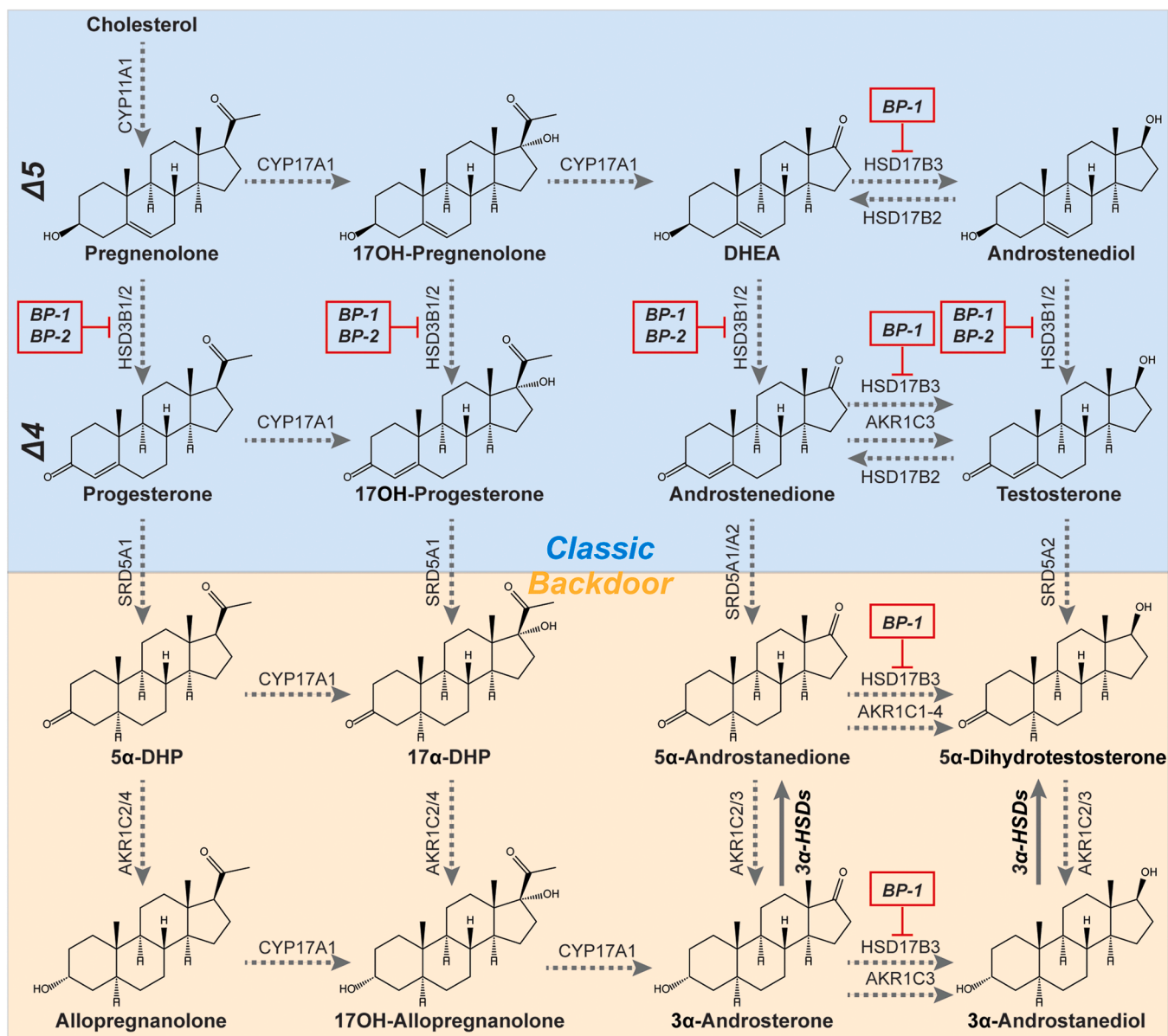
Available online 10 November 2024

0300-483X/© 2024 The Author(s). Published by Elsevier B.V. This is an open access article under the CC BY license (<http://creativecommons.org/licenses/by/4.0/>).

used to protect products against UV radiation, thus preserving stability, color and odor (Bens, 2014; Soni et al., 2005; Soni et al., 2002). In addition, these compounds are also widely used in food packaging, plastics and textiles (Asimakopoulos et al., 2016; Elder R, L., 1984; Lu et al., 2014; Rodríguez-Bernaldo de Quirós et al., 2009; Suzuki et al., 2005; Xue et al., 2017). Some UV-filters, such as benzophenone (BP)-3, avobenzone, and 4-methylbenzylidene camphor (4-MBC) are also found as active ingredients in sunscreens (EC, 2009; FDA, 1999). Parabens and UV-filters were shown to penetrate the skin after topical application or taken up orally, which constitute the main routes of exposure of those compounds (Darbre, 2006; Harvey and Darbre, 2004; Hayden et al.,

1997; Ishiwatari et al., 2007; Janjua et al., 2008b). Both substance classes have been detected systemically in various human matrices, including placental tissue and fetal cord serum, suggesting trans-placental transport and thus prenatal exposure in humans (Mao et al., 2022; Wei et al., 2021).

Numerous *in vitro* and *in vivo* studies suggested that parabens and BP-type UV-filters might cause endocrine disrupting effects, raising safety concerns; in particular, these compounds were found to exert estrogenic and antiandrogenic effects by directly acting on estrogen and androgen receptors (ER and AR) (Chen et al., 2007; Ding et al., 2017; Kolšek et al., 2015; Kunz and Fent, 2006; Ma et al., 2003; Molina-Molina et al., 2008;



**Fig. 1.** Benzophenone-type UV-filters interfere with the human classic and backdoor pathways of dihydrotestosterone synthesis. (Adapted from O'Shaughnessy et al., 2019) Pregnenolone originates from cholesterol cleavage through CYP11A1 and may be converted to 17OH-pregnenolone and DHEA by CYP17A1, following the  $\Delta 5$  pathway through androstenedione or androstenediol to testosterone, which is subsequently 5 $\alpha$ -reduced to 5 $\alpha$ -dihydrotestosterone. Alternatively, pregnenolone is converted to progesterone through HSD3B1/2 activity, which is then stepwise converted along the backdoor pathway to 3 $\alpha$ -androsterone that acts as intermediate steroid. 3 $\alpha$ -androsterone is converted in two enzymatic steps to 5 $\alpha$ -dihydrotestosterone, a 17 $\beta$ -reduction through HSD17B3 or one of the four AKR1C enzymes and a 3 $\alpha$ -oxidation conducted by a 3 $\alpha$ -HSD. Each of the different reaction steps is represented by a gray arrow and is catalyzed by at least one steroidogenic enzyme. Benzophenones-1 and -2 (BP-1 and BP-2) that have been shown to inhibit some of the depicted enzymatic steps are indicated with red boxes. Abbreviations: 3 $\alpha$ -androsterone, 5 $\alpha$ -androstane-3 $\alpha$ -ol-17-one; 3 $\alpha$ -androstanediol, 5 $\alpha$ -androstane-3 $\alpha$ ,17 $\beta$ -diol; 5 $\alpha$ -androstenedione, 5 $\alpha$ -androstane-3,17-dione; androstenediol, androst-5-ene-3 $\beta$ ,17 $\beta$ -diol; androstenedione, androst-4-ene-3,17-dione; DHEA, dehydroepiandrosterone; 5 $\alpha$ -DHP, 5 $\alpha$ -dihydroprogesterone; 17 $\alpha$ -DHP, 17 $\alpha$ -hydroxydihydroprogesterone.



Nashev et al., 2010; Pop et al., 2016; Pugazhendhi et al., 2005; Schlecht et al., 2004; Schreurs et al., 2002; Watanabe et al., 2015; Zhang et al., 2014). Treatment of male rats with parabens or UV-filters resulted in a reduction of testicular volume, a deterioration of sperm quality and lower testosterone levels (Kang et al., 2002; Oishi, 2001, 2002; Suzuki et al., 2005). In humans, BP-3 exposure has been associated with smaller testicular volume and lower testosterone levels (Huang et al., 2020; Scinicariello and Buser, 2016). BP-2 was associated with diminished sperm quality (Buck Louis et al., 2015). However, the mechanism-of-action underlying these observations remains unclear.

The male genital development depends on androgen synthesis and its disruption by xenobiotics causes reproductive toxicity. In the fetal period, androgens and anti-Müllerian hormone are required to form male reproductive structures (Yamada et al., 2006). During adolescence, local 5 $\alpha$ -dihydrotestosterone (DHT) production plays an important role in the growth and maturation of the penis, scrotum, prostate and the development of facial-, body- and pubic hair. (Horton, 1992).

According to the classic pathway, androgens are synthesized in the testes and *zona reticularis* of the adrenal cortex (Miller and Auchus, 2011). The side-chain cleavage enzyme (P450<sub>scc</sub>; CYP11A1) catalyzes the first step, cholesterol to pregnenolone, which is 17 $\alpha$ -hydroxylated and further 17,20-lyased to dehydroepiandrosterone (DHEA) by CYP17A1 (Fig. 1). 3 $\beta$ -Hydroxysteroid dehydrogenase type 2 (HSD3B2) converts DHEA to androstenedione (androst-4-ene-3,17-dione) in the testis and adrenals, but only the testes express 17 $\beta$ -hydroxysteroid dehydrogenase type 3 (HSD17B3) to form testosterone. Testosterone is secreted and converted in genital skin to the more potent androgen DHT by steroid 5 $\alpha$ -reductase type 2 (SRD5A2) (Flück et al., 2003; Miller and Auchus, 2011; Wilson, 2001; Wilson et al., 1993). Loss-of-function mutations in the *HSD17B3* and *SRD5A2* genes and in the classic pathway of androgen synthesis cause disorders of sexual development in genetically male patients with various degrees of undervirilization of the male genitalia (Geissler et al., 1994; SAEZ et al., 1971; Thigpen et al., 1992).

However, increasing evidence shows the involvement of a second pathway, *i.e.* the backdoor pathway of DHT formation that bypasses the usual intermediates DHEA, androstenedione and testosterone (Auchus, 2004). In the backdoor pathway, first described in marsupial mammals (O'Shaughnessy et al., 2019; Renfree et al., 1996; Renfree et al., 1992), progesterone from non-gonadal tissues, mainly the placenta, is converted in fetal tissues by steroid 5 $\alpha$ -reductase type 1 (SRD5A1), reductive 3 $\alpha$ -hydroxysteroid dehydrogenases (3 $\alpha$ -HSDs) from the aldo-keto reductase family 1 (AKR1C2/4) and CYP17A1 to the main intermediate 3 $\alpha$ -androsterone (5 $\alpha$ -androstane-3 $\alpha$ -ol-17-one), which is further metabolized by AKR1C3 or 17 $\beta$ -HSD3 to 3 $\alpha$ -androstanediol (5 $\alpha$ -androstane-3 $\alpha$ ,17 $\beta$ -diol, 3 $\alpha$ -adiol) and in the last step by oxidative 3 $\alpha$ -HSD to DHT (Fig. 1) (Flück et al., 2011; Fukami et al., 2013; Miller and Auchus, 2011; O'Shaughnessy et al., 2019). Genetic mutations in the *ARK1C2* and *AKR1C4* genes cause under-masculinization of the external genitalia in affected male patients, emphasizing the role of the backdoor pathway to synthesize DHT that is needed for virilization of the male fetus (Flück et al., 2011).

Whilst there are studies that identified environmental chemicals inhibiting enzymes of the classic pathway of androgen synthesis, there are none on backdoor pathway enzymes so far. With respect to potential antiandrogenic effects of parabens and UV-filters by acting on steroidogenic enzymes, inhibition of HSD3B1/2 by BP-1 and BP-2, as well as of HSD17B3 by BP-1, has been demonstrated, with IC<sub>50</sub> values in the low micromolar range (Nashev et al., 2010; Wang et al., 2023). Effects of parabens and BP-type UV-filters have not yet been investigated against enzymes of the backdoor pathway of DHT synthesis.

HSD17B6, HSD17B10, retinol dehydrogenases type 5 and 16 (RDH5, RDH16), and dehydrogenase/reductase SDR family member 9 (DHRS9), were all shown to possess oxidative 3 $\alpha$ -HSD activity and to be expressed in human testis and prostate, with the exception of RDH16 that is mainly expressed in liver (Chetyrkin et al., 2001a; Chetyrkin et al., 2001b;

Gough et al., 1998; He et al., 1999; He et al., 2003; Huang and Luu-The, 2000; Wang et al., 1999). All five enzymes are conserved among human, mouse and rat homologs (sharing between 68 % and 84 % amino acid sequence identity) and were shown to catalyze both, the 3 $\alpha$ -oxidation of 3 $\alpha$ -androsterone to 5 $\alpha$ -androstenedione (5 $\alpha$ -androstane-3,17-dione) and the last step of 3 $\alpha$ -androstanediol (5 $\alpha$ -androstane-3 $\alpha$ ,17 $\beta$ -diol, 3 $\alpha$ -adiol) to DHT. Nevertheless, as seen for other SDRs (Arampatzis et al., 2005; Inderbinen et al., 2021), species-specific differences may be assumed for these 3 $\alpha$ -HSDs, but to our knowledge this has not been investigated thoroughly so far.

In this study, we addressed whether parabens and UV-filters potentially exert antiandrogenic effects by inhibiting the oxidative 3 $\alpha$ -HSD enzymes of the backdoor pathway of DHT synthesis. After an initial assessment of the most active 3 $\alpha$ -HSDs, 9 parabens and their main metabolite *p*-hydroxybenzoic acid as well as 16 UV-filters were tested for their inhibitory capacity using a novel radiometric *in vitro* enzyme activity assay. The binding mode of the identified inhibitors was then analyzed using a newly generated *in silico* homology model of HSD17B6 and to elucidate the structure-activity relationship (SAR).

## 2. Materials and methods

### 2.1. Chemicals and reagents

Unlabeled steroids were purchased from Steraloids (Newport, RI, USA), [9,11-<sup>3</sup>H(N)]-3 $\alpha$ -androsterone from American Radiolabeled Chemicals (St. Louis, MO, USA), and all other chemicals from Merck (Darmstadt, Germany) if not stated otherwise. The purity of all tested parabens and UV-filters was equal or greater 95 % (Supplementary Table 1). Dulbecco's Modified Eagle Medium (DMEM) (4.5 g/L glucose, 2 mM L-glutamine), penicillin-streptomycin (10,000 U/mL-10 mg/mL), HEPES buffer, pH 7.4, non-essential amino acid solution (NEAA), and sodium pyruvate solution (100 mM) were purchased from Bioconcept (Allschwil, Switzerland). Minimum Essential Medium (containing Earle's balanced salts and NEAA) was purchased from Merck, fetal bovine serum (FBS, S1810-500) from Biowest (Nuaille, France), Opti-MEM from Gibco (Thermo Fischer Scientific, Waltham, MA, USA), polyethylenimine (PEI, 25 kDa linear) from Polyscience (Warrington, PA, USA), FUGENE® HD transfection reagent from Promega (Madison, WI, USA) and the Tropix kit from Applied Biosystems (Waltham, MA, USA).

### 2.2. Cell culture

Human Embryonic Kidney-293 cells (HEK-293, ATCC, Manassas, VA, USA) were cultured in DMEM supplemented with 10 % FBS, 100 U/mL penicillin, 0.1 mg/mL streptomycin, 10 mM HEPES buffer, pH 7.4, and 1 % MEM NEAA. CV-1 cells (CCL-70, ATCC) were cultured in MEM supplemented with 10 % FBS, 100 U/mL penicillin, 0.1 mg/mL streptomycin, 2 mM L-glutamine, and 1 mM sodium pyruvate. Both cell lines were cultivated under standard conditions (37 °C, 5 % CO<sub>2</sub>) in an incubator (Thermo Fisher Scientific).

### 2.3. Plasmids

Plasmids expressing C-terminally FLAG-tagged RDH5 (NM\_002905), RDH16 (NM\_003708), and DHRS9 (NM\_001142270) in pcDNA3.1 were purchased from GenScript (Piscataway Township, NJ, USA). Plasmids for MMTV-lacZ, pCMV-LUC, and FLAG-tagged HSD17B6 in a pcDNA3.1 backbone were described earlier (Fürstenberger et al., 2012; Satoh et al., 1993; Tsachaki et al., 2015). The FLAG-tagged human AR construct was kindly provided by Dr. J. J. Palvimo (Poukka et al., 2000). FLAG-tagged HSD17B10 was generated by PCR amplification of a donor vector (ID: 2819721) purchased from Biovalley (Nanterre, France) by inserting a FLAG peptide sequence at the C-terminus using oligonucleotide primers downstream of the coding sequence. After PCR amplification, the construct was subcloned between *NotI/NotI* restriction sites into the

pcDNA3.1 vector and verified by sequencing.

#### 2.4. Assessment of AR transcriptional activity in transfected CV-1 cells

CV-1 cells were seeded in 24-well plates at a density of 50'000 cells/500  $\mu$ L culture medium followed by incubation for 18 h. Subsequently, the cells were washed with PBS and the medium was replaced by 500  $\mu$ L Opti-MEM. The cells were transfected with plasmids encoding FLAG-tagged human AR,  $\beta$ -galactosidase expressed under an androgen response element (ARE) (MMTV-lacZ) (160 ng/well each), a constitutively expressed luciferase (10 ng/well), and pcDNA3.1 control vector or either HSD17B6, DHRS9, RDH5, RDH16, HSD17B10 (70 ng/well). The plasmids were mixed with 1200 ng PEI in Opti-MEM, reaching a total volume of 50  $\mu$ L/well. After incubation for 15 min at room temperature (RT), the transfection mixture was added to the cells and 6 h later the supernatant replaced by culture medium. At 22 h post-transfection, the cells were washed once with PBS and once with charcoal treated medium. Subsequently, the cells were incubated in charcoal treated medium containing various concentrations of steroids as indicated. After 24 h, the medium was removed, cells were washed with PBS and lysed with 60  $\mu$ L Tropic lysis solution containing 1 mM dithiothreitol for 5 min at RT, and stored at  $-80^{\circ}\text{C}$  for at least 20 min.

Luciferase activity was determined by injecting 100  $\mu$ L D-luciferin substrate solution [0.56 mM D-luciferin, 63 mM ATP, 0.27 mM CoA, 0.13 mM EDTA, 33.3 mM dithiothreitol, 8 mM  $\text{MgSO}_4$ , 20 mM tricine (pH 7.8)] to 20  $\mu$ L lysate prepared in pure grade white 96-well micro-titration plates (BRAND, Wertheim, Germany) and measuring luminescence on a SpectraMax L Microplate Reader (Molecular Devices, San Jose, CA, USA). The respective  $\beta$ -galactosidase activity was measured with the same plates and device using the Tropic kit. The activity of  $\beta$ -galactosidase was normalized to the respective luciferase activity and subsequently normalized to the DMSO control.

#### 2.5. Radiometric $3\alpha$ -HSD activity assay using lysates of transiently transfected HEK-293 cells

HEK-293 cell were transiently transfected with an expression plasmid for the respective  $3\alpha$ -HSD and lysates were prepared as described recently (Kley et al., 2023), with some modifications. Briefly,  $2 \times 10^6$  HEK-293 cells per 10 cm dish were transfected with 8  $\mu$ g of the respective FLAG-tagged  $3\alpha$ -HSD encoding plasmid using the calcium phosphate precipitation method (Kingston et al., 1987). The cells were harvested 48 h post-transfection in 2 mL ice-cold PBS, then portioned in 200  $\mu$ L aliquots and pelleted for 4 min at  $300 \times g$  at  $4^{\circ}\text{C}$  prior to snap-freezing in liquid nitrogen and storage at  $-80^{\circ}\text{C}$ . For each activity assay, cell pellets were resuspended in 400  $\mu$ L TS2 buffer (100 mM NaCl, 1 mM EGTA, 1 mM EDTA, 1 mM  $\text{MgCl}_2$ , 250 mM sucrose, 20 mM Tris-HCl, pH 7.4) and lysed by sonication (UP50H sonicator, Hielscher Ultrasonics).

Cell lysates were diluted to obtain 20–30 % substrate to product conversion after a 10 min incubation for HSD17B6 and RDH16 and 30 min for RDH5, respectively. Lysates were incubated with 100 nM  $3\alpha$ -androsterone containing 5.55 nCi [9,11- $^3\text{H}(\text{N})$ ]- $3\alpha$ -androsterone, and 500  $\mu$ M  $\text{NAD}^+$  in a total volume of 22.2  $\mu$ L, at  $37^{\circ}\text{C}$  with either DMSO as solvent control or in presence of a test compound at the final concentration indicated. The total solvent concentration was kept constant at 0.1 %. The reactions were stopped by adding 10  $\mu$ L methanol containing 800  $\mu$ M of each, unlabelled  $5\alpha$ -androstanedione,  $3\alpha$ -androsterone and  $3\beta$ -epiandrosterone (5 $\alpha$ -androstane- $3\beta$ -ol-17-one). An amount of 10  $\mu$ L per sample was loaded onto TLC plates (Macherey-Nagel, Oensingen, Switzerland) and steroids were separated using a mobile phase of toluene/acetone at a ratio of 4:1. Substrate and product bands were visualized by spraying the TLC plate with a *p*-anisaldehyde staining solution (anisaldehyde 0.5 % (v/v), acetic acid 10 % (v/v), methanol 84.5 % (v/v), sulphuric acid 5 % (v/v)) using a derivatizer (CAMAG, Muttenz, Switzerland). After drying for 10 min at RT, plates were heated

on a TLC plate heater 3 (CAMAG) to  $110^{\circ}\text{C}$  for 10 min. Visualized steroids were marked, bands excised and analyzed by scintillation counting (Tri-Carb 2900TR liquid scintillation analyzer, Packard, Connecticut), using the IRGASAFE Plus scintillation cocktail (Zinsser Analytic, Eschborn, Germany). Because no epimerase activity could be observed, both epimers were excised together and included in the determination of the conversion rate.

#### 2.6. HSD17B6 activity assay using AR transactivation as readout

HEK-293 cells were seeded in poly-L-lysine coated 24-well plates at a density of 100,000 cells/500  $\mu$ L culture medium and incubated for 18 h. Cells were washed once with PBS and new medium was added, followed by transfection using FuGENE<sup>®</sup> HD reagent. Briefly, plasmids encoding AR and  $\beta$ -galactosidase expressed under an AR response element (MMTV-lacZ) (190 ng/well each) and a constitutively expressed luciferase vector (20 ng/well) were mixed in Opti-MEM with the FuGENE<sup>®</sup> transfection reagent at a reagent to DNA ratio of 3:1, reaching a total transfection mixture volume of 21.2  $\mu$ L/well. After incubation of the mixture for 10 min at RT, cells were transfected and incubated under standard conditions for 22 h. Subsequently, cells were washed with PBS and incubated in charcoal treated medium for 3 h.

As described in Section 2.5, HEK-293 cell lysate (10  $\mu$ L) over-expressing HSD17B6 was incubated with 100 nM  $3\alpha$ -androsterone, 500  $\mu$ M  $\text{NAD}^+$ , and either DMSO as solvent control or 10  $\mu$ M test compound in a total volume of 22.2  $\mu$ L for 10 min at  $37^{\circ}\text{C}$ . The reactions were terminated by heat inactivation for 1 min at  $95^{\circ}\text{C}$ .

The medium of the transfected cells was then replaced with charcoal treated medium (500  $\mu$ L/well) containing a 125-fold dilution of the enzymatic reactions mentioned above, followed by incubation for 24 h. The medium was then removed and cells were washed with PBS and lysed with 60  $\mu$ L Tropic lysis solution containing 1 mM dithiothreitol for 5 min at RT, and stored at  $-80^{\circ}\text{C}$  for at least 20 min. Luciferase and the corresponding galactosidase activity of each sample were measured as described in Section 2.5 using a Cytation 5 reader (BioTek, Winooski, VT, USA).

#### 2.7. Molecular modeling

Initially an AI generated homology model of HSD17B6, AF-O14756-F1-model\_v4, was downloaded from AlphaFold (Jumper et al., 2021; Varadi et al., 2024). However, this model does not contain the cofactor  $\text{NAD}^+$ , which is required for biologic activity and likely also for appropriate ligand binding.

A BLAST search revealed that the photoreceptor dehydrogenase (pdb entry 5ilg for crystal structure) from *Drosophila melanogaster* (Hofmann et al., 2016) shares closest homology with HSD17B6. We aligned the HSD17B6 homology model and 5ilg to determine the location of  $\text{NAD}^+$ , copied it into the homology model and performed an energetic minimization using Schrödinger's maestro suite software (Schrödinger Release 2024-2: Force Fields, Schrödinger, LLC, New York, NY, USA, 2024) with default settings. This construct was then used to dock the paraben derivatives.

GOLD (version 2021, Cambridge Crystallographic Data Centre, Cambridge, UK) was used to conduct a docking simulation (Jones et al., 1997). The binding site was defined in a 12 Å radius around the C3N of  $\text{NAD}^+$ . GoldScore was selected as a scoring function. Energetically minimized starting conformations for all query molecules were generated with OMEGA (OMEGA 5.1.0.0. OpenEye, Cadence Molecular Sciences, Santa Fe, NM, USA. <http://www.eyesopen.com>.) and 10 poses were calculated per ligand in the docking simulation (Hawkins et al., 2010). Interactions were calculated and visualized in Ligandscout (vs. 4.5. Inte:ligand, Vienna, Austria).

## 2.8. Statistical analysis

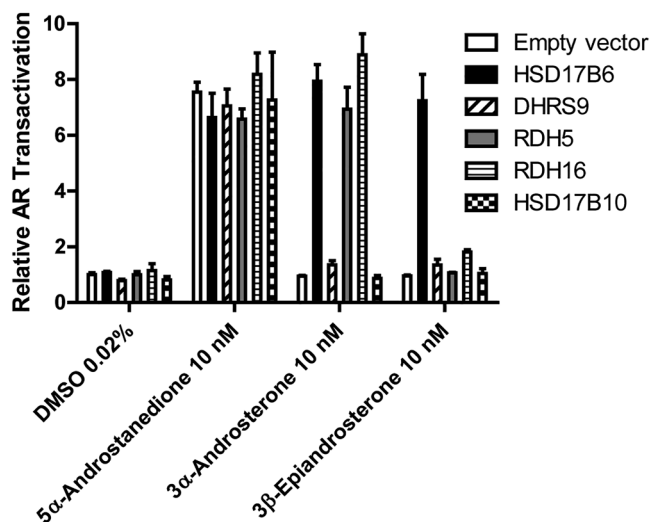
All data were analyzed using GraphPad Prism version 5 for Windows (GraphPad Software, San Diego, California USA, [www.graphpad.com](http://www.graphpad.com)). The transactivation assays were analyzed either by a two-way ANOVA or one-way ANOVA followed by Dunnett's post-hoc test. Enzyme activity assays were analyzed by ANOVA and Dunnett's post-hoc test. Concentration-response curves for estimation of IC<sub>50</sub> values were fitted and analyzed by non-linear regression.

## 3. Results

### 3.1. 3 $\alpha$ -HSDs promote AR transcriptional activity

To identify the 3 $\alpha$ -HSDs with the highest affinities that are relevant in the human backdoor pathway of DHT formation, CV-1 cells were co-transfected with plasmids for AR, an ARE-reporter construct, a transfection control plasmid and either of the previously mentioned 3 $\alpha$ -HSDs. CV-1 cells express endogenous 17-oxoreductase activity (Mohler et al., 2011), likely the AKR1C3 homologue, and they are able to efficiently convert 5 $\alpha$ -androstenedione to DHT and thus activate AR (Fig. 2). At low concentration (10 nM) of 3 $\alpha$ -androsterone, HSD17B6, RDH5 and RDH16, but not DHRS9 and HSD17B10, efficiently formed 5 $\alpha$ -androstenedione, which was then converted by endogenous 17-oxoreductase to DHT to activate AR (Fig. 2). In contrast, only HSD17B6 was able to activate AR when 3 $\beta$ -epiandrosterone was supplied, which can be explained by the 3 $\alpha$ / $\beta$ -epimerase activity of this enzyme (Huang and Luu-The, 2000).

Next, we assessed the concentration-dependent AR activation by 3 $\alpha$ - and 3 $\beta$ -androstenediol (3 $\alpha$ - and 3 $\beta$ -adiol) in the presence of the 3 $\alpha$ -HSDs. Since HSD17B10 showed low 3 $\alpha$ -HSD activity, it was not further analyzed. HSD17B6, RDH5 and RDH16 efficiently converted 3 $\alpha$ -adiol to DHT and activated AR, whilst DHRS9 was much less efficient (Fig. 3). The only enzyme analyzed that exhibited 3-epimerase activity and was able to use 3 $\beta$ -adiol and activate AR in a concentration-dependent manner was HSD17B6 (Suppl. Fig. 1B). When DHT was supplied to the cells expressing the 3 $\alpha$ -HSDs and the reporter construct, a



**Fig. 2.** Relative AR transactivation mediated by HSD17B6, DHRS9, RDH5, RDH16 and HSD17B10. CV-1 cells were transfected with a plasmid encoding the human AR, a luciferase reporter gene construct expressed under an ARE, and a plasmid encoding the indicated 3 $\alpha$ -HSD enzyme or empty pcDNA3.1 control vector and a transfection control. Transfected cells were treated with 10 nM of either 5 $\alpha$ -androstenedione, 3 $\alpha$ -androsterone or 3 $\beta$ -epiandrosterone. AR transactivation was first normalized to the transfection control and then to the vector control sample in the presence of 0.2 % DMSO. Data represent mean  $\pm$  SD from three independent experiments.

concentration-dependent AR activation was observed for all enzymes tested, with very moderate 3-oxoreductase activity observed for HSD17B6 only at the highest concentrations tested (Suppl. Fig. 1). It should be noted that 3 $\alpha$ -adiol and 3 $\beta$ -adiol have weak intrinsic androgenic activity and activated the AR at concentrations of 33 nM and higher (Fig. 3, Suppl. Fig. 1) (Chang et al., 1999). Because DHRS9 exhibited much lower efficiency to metabolize 3 $\alpha$ -adiol and 3 $\alpha$ -androsterone than HSD17B6, RDH5 and RDH16, this enzyme was not further investigated.

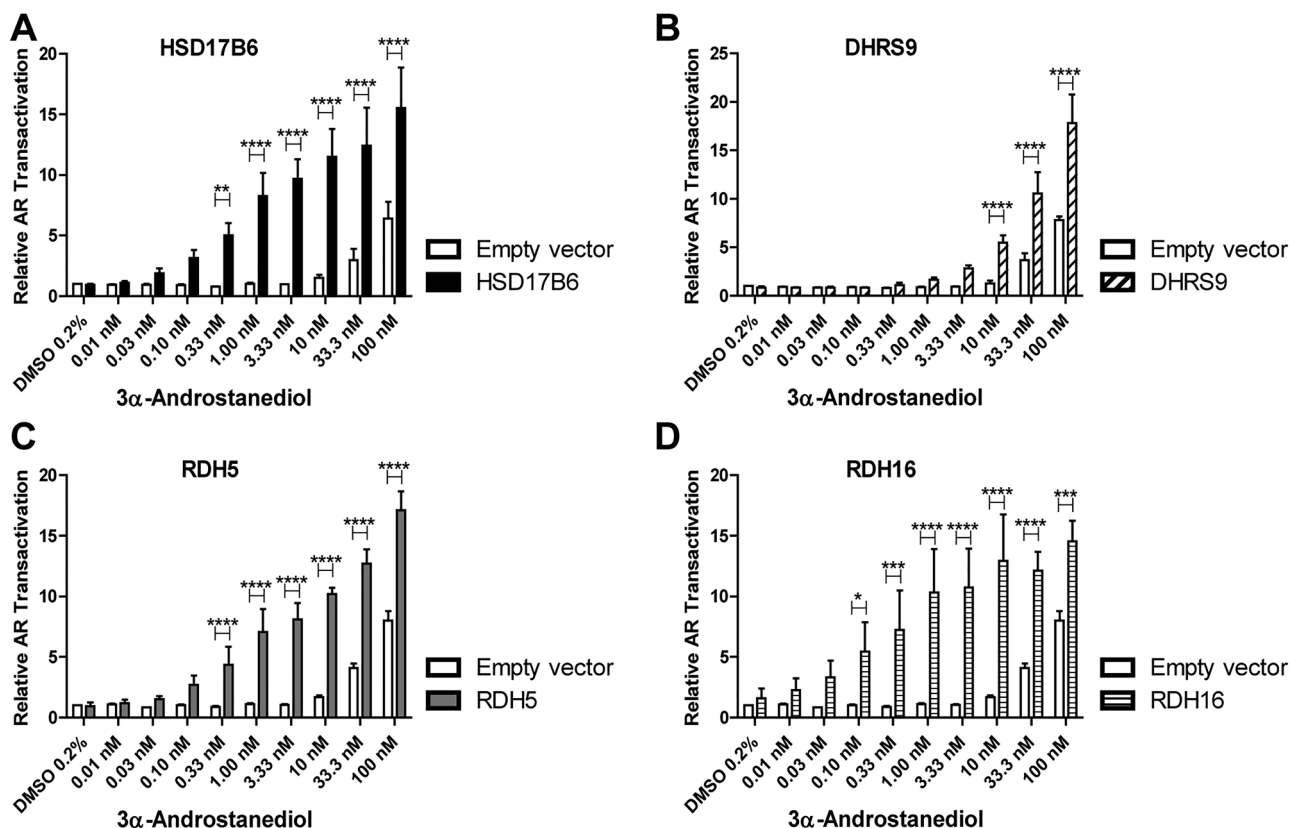
### 3.2. Identification of parabens and BP-type UV-filters inhibiting 3 $\alpha$ -HSDs

First, we established a radiometric *in vitro* enzyme activity assay by incubating whole cell lysates overexpressing the respective enzyme with 3 $\alpha$ -androsterone as substrate. Possible 3 $\alpha$ / $\beta$ -epimerase activity was ruled out by co-quantification of the formation of 3 $\beta$ -epiandrosterone, which could not be detected despite prolonged incubation for 2 h. Relative product formation was adjusted to about 25 % for the vehicle control. Second, initial screening experiments were performed. Except for the main metabolite *p*-hydroxybenzoic acid, all tested parabens were able to inhibit HSD17B6 activity to a certain extent at a concentration of 10  $\mu$ M (Fig. 4A). Among the BP compounds, BP-6 and 4,4'-dihydroxy-BP partially inhibited HSD17B6 at 10  $\mu$ M, while BP-1, BP-2, 4-hydroxy-BP, and 2,4,4'-trihydroxy-BP almost completely inhibited the enzyme at this concentration (Fig. 4B). RDH5 and RDH16 were both significantly inhibited by hexyl- and heptylparaben, but moderately compared to HSD17B6 (Fig. 4A, C and E). The same was observed for RDH5 and HSD17B6 with BP-2, 4-hydroxy-BP, 4,4'-dihydroxy-BP and 2,4,4'-trihydroxy-BP (Fig. 4B, D and F). Additionally, 3-BC and 4-MBC moderately inhibited the 3 $\alpha$ -activity of RDH5 by about 50 % and 60 %, respectively, at the tested concentration of 10  $\mu$ M (Fig. 4D). RDH16 showed no significant inhibition by any of the tested BP-type UV-filters at 10  $\mu$ M (Fig. 4F).

Next, IC<sub>50</sub> values were determined for compounds exhibiting more than 75 % inhibitory activity at a concentration of 10  $\mu$ M. This pre-defined cutoff was reached by some parabens and UV-filters inhibiting HSD17B6. To further assess the inhibitory capacities of hexyl- and heptylparaben against the three examined 3 $\alpha$ -HSDs, their IC<sub>50</sub> values were also determined for RDH5 and RDH16. The examined parabens and BP-type UV-filters showed IC<sub>50</sub> values in the nanomolar range for HSD17B6 (Tables 1 and 2, Suppl. Fig. 2). RDH5 and RDH16 showed IC<sub>50</sub> values for heptyl- and hexylparaben in the low micromolar range (Table 1).

### 3.3. HSD17B6 inhibition by parabens and BP-type UV-filters lowers AR transcriptional activity

The newly established radiometric enzyme activity assay was used to assess the conversion of 3 $\alpha$ -androsterone to 5 $\alpha$ -androstenedione. To test whether these compounds also inhibit the 3 $\alpha$ -oxidation of 3 $\alpha$ -adiol to DHT and thereby exert antiandrogenic effects, a combined assay was performed by first incubating HEK-293 cell lysates overexpressing HSD17B6 with 3 $\alpha$ -adiol as substrate in the absence or presence of parabens or UV-filters, followed by adding a dilution of the reaction mixture to HEK-293 cells transfected with human AR, an AR-responsive reporter gene construct and a transfection control. To exclude a direct effect on the AR of the examined compounds, the AR transcriptional activity was normalized to a control in the absence of enzyme activity reaction mixture. The tested parabens (Fig. 5A) and BP-type UV-filters (Fig. 5B) showed an inhibition pattern similar to that of the enzyme activity screening using 3 $\alpha$ -androsterone as substrate (Fig. 4A and B). With the exception of benzylparaben, all previously identified inhibitors significantly decreased the AR transcriptional activity mediated by HSD17B6.



**Fig. 3.** Concentration-dependent AR transactivation mediated by HSD17B6, DHRS9, RDH5, RDH16 in the presence of 3 $\alpha$ -androstanediol as substrate. CV-1 cells were transfected with plasmids containing genes of the human androgen receptor, a reporter gene construct under the control of an AR-responsive promoter, and either the pcDNA3.1 control vector or HSD17B6 (A), DHRS9 (B), RDH5 (C) or RDH16 (D), and a transfection control. Transfected cells were treated with increasing concentrations of 3 $\alpha$ -androstanediol. AR transactivation was first normalized to the transfection control and subsequently to the vector control sample in the presence of 0.2% DMSO. Data represent mean  $\pm$  SD from three independent experiments. Statistical analysis was performed by two-way ANOVA. Significant statistical differences between tested enzyme and control vector are indicated. P values: \*\*\*\* < 0.0001, \*\*\* < 0.001, \*\* < 0.01, \* < 0.05.

### 3.4. Structure-activity relationship of parabens and UV-filters inhibiting HSD17B6

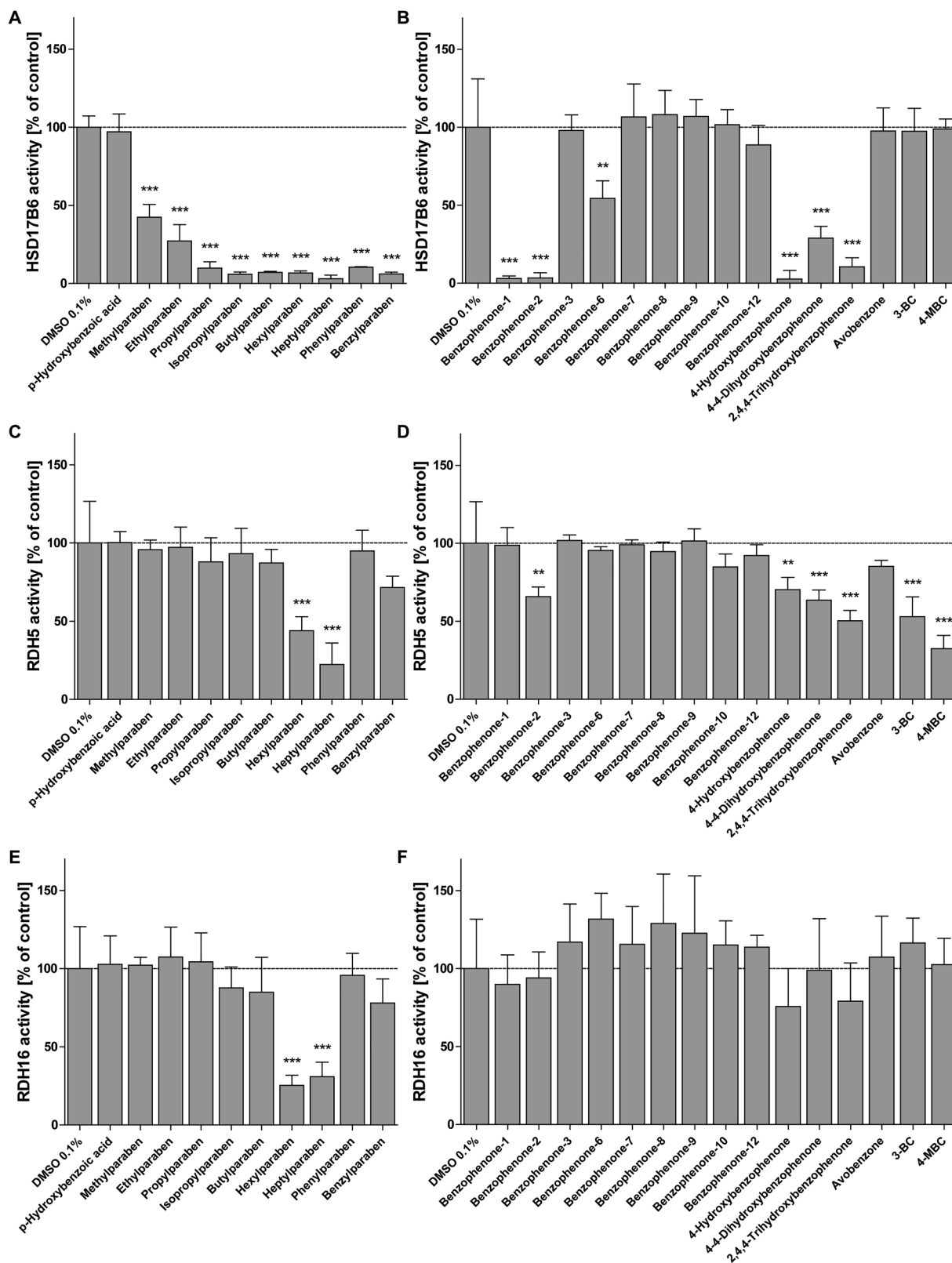
A homology model of HSD17B6 was generated to assess the binding mode and SAR of the identified inhibitors. An initial BLAST search revealed highest homology to photoreceptor dehydrogenase of *D. melanogaster*, of which a crystal structure with bound cofactor NAD<sup>+</sup> was available (PDB entry 5ilg, published in (Hofmann et al., 2016)). The HSD17B6 structure predicted by AlphaFold was superimposed with the crystal structure of the *D. melanogaster* protein to determine the cofactor binding site, and an energetic minimization was performed in Schrödinger's maestro suite software. To validate and optimize the docking workflow, an initial docking was performed with the HSD17B6 substrates 3 $\alpha$ -adiol and 3 $\alpha$ -androsterone, confirming correct substrate placement and orientation in the binding pocket with the 3 $\alpha$ -hydroxyl group in the vicinity of NAD<sup>+</sup>, enabling the catalytic reaction (Suppl. Fig. 3). The successful definition of the binding pocket was then used to dock all investigated compounds into the HSD17B6 homology model with bound cofactor. This predicted an interaction of the 4-hydroxy group of parabens with the amide group of NAD<sup>+</sup> and a possible  $\pi$ -stacking of the aromatic ring of Tyr208 with the paraben head group (Fig. 6). Linear parabens appear to be able to additionally form interactions with the hydrophobic channel leading to the binding pocket, which could be a possible explanation for the observed IC<sub>50</sub> values, which are inversely proportional to the length of the aliphatic, linear residual group of the parabens (Figs. 6A and 6B, Table 1). Isopropyl paraben, with a branched alkyl, also interacts with Tyr208 and NAD<sup>+</sup> (Fig. 6C). However, the more bulky benzyl group of benzylparaben leads

to a tilt in the binding phenyl moiety, and a loss of the  $\pi$ -stacking interaction between its aromatic ring and Tyr208 while the hydrogen bond to NAD<sup>+</sup> is retained, providing a possible explanation for the slightly higher IC<sub>50</sub> values of structures with bulkier substituents (Fig. 6D, Table 1).

With regard to the BP-type UV-filters, only those with a 4-hydroxy group, similar to the head group of parabens, may be able to form a hydrogen bond with the amide group of NAD<sup>+</sup>. Again,  $\pi$ -stacking interaction involving the aromatic ring of Tyr208 may stabilize the binding of 4-hydroxylated BPs in the binding pocket of HSD17B6 (Fig. 7A, C and D). A second hydrogen bond with Cys257 and the 2-hydroxy group on BP-1 and the 4-hydroxy group on BP-2, respectively (Fig. 7A/B) does not seem to be crucial for bioactivity but could explain the more potent activity of these two compounds. If the critical 4-hydroxy group is substituted by another group, as it is the case in 4-methoxylated BPs, (BP-3, -8 and -10), the respective compounds are no longer able to form the hydrogen bond with NAD<sup>+</sup> (Fig. 7E to G). In addition, they are not stabilized through the  $\pi$ -stacking interaction with Tyr208 or an interaction with Cys257, resulting in a loss of their affinity to bind HSD17B6 and thus their inhibitory potential.

## 4. Discussion

Various rodent *in vivo* studies provided evidence for endocrine-disrupting properties of parabens and UV-filters, with antiandrogenic effects observed for several parabens and the UV-filter BP-3 at the highest concentration tested, respectively, indicated by reduced sperm count, impaired sperm quality, reduced testis, epididymis and prostate



**Fig. 4.** Identification of parabens and UV-filters inhibiting HSD17B6, RDH5 or RDH16. Paraben- and UV-filter-mediated inhibition of (A, B) HSD17B6, (C, D) RDH5 and (E, F) RDH16. Lysates of HEK-293 cells expressing one of the three examined  $3\alpha$ -HSDs were incubated for 10 min (HSD17B6, RDH16) or 30 min (RDH5) at 37°C in the presence of 100 nM  $3\alpha$ -androsterone, containing 5.55 nCi of [9,11- $^3$ H(N)]- $3\alpha$ -androsterone, 500  $\mu$ M NAD<sup>+</sup> and 10  $\mu$ M test compounds or vehicle control. Percentage of total conversion of  $3\alpha$ -androsterone to  $5\alpha$ -androstenedione was analyzed by TLC separation of both steroids, on-plate derivatization and scintillation counting. Substrate conversion was normalized to vehicle control (0.1 % DMSO). Data represent mean  $\pm$  SD from three independent experiments. Statistical analysis was performed by one-way ANOVA followed by the Dunnett's post-hoc test. Significant statistical differences between test compounds and vehicle control are indicated. P values: \* $<0.05$ , \*\* $<0.01$ , \*\*\* $<0.001$ .

**Table 1**

IC<sub>50</sub> values for HSD17B6, RDH5 and RDH16 of the assessed parabens. Enzyme activity was determined in lysates of HEK-293 cells expressing the indicated enzyme. The conversion of 3 $\alpha$ -androsterone to 5 $\alpha$ -androstenedione was measured in the presence of increasing paraben concentrations. Total substrate conversion was normalized to vehicle control and inhibition curves were fitted and analyzed by non-linear regression. Data represent mean  $\pm$  SD of three independent experiments. NA; not assessed.

Inhibition of 3 $\alpha$ -HSD activity by parabens: IC <sub>50</sub> values (mean $\pm$ SD)			
Paraben	HSD17B6	RDH5	RDH16
Heptylparaben	77 $\pm$ 79 nM	8.0 $\pm$ 3.0 $\mu$ M	3.4 $\pm$ 0.4 $\mu$ M
Hexylparaben	133 $\pm$ 61 nM	9.0 $\pm$ 0.8 $\mu$ M	4.0 $\pm$ 0.7 $\mu$ M
Butylparaben	339 $\pm$ 204 nM	NA	NA
Propylparaben	523 $\pm$ 102 nM	NA	NA
Isopropylparaben	345 $\pm$ 87 nM	NA	NA
Benzylparaben	328 $\pm$ 128 nM	NA	NA
Phenylparaben	570 $\pm$ 224 nM	NA	NA

**Table 2**

IC<sub>50</sub> values for HSD17B6 of benzophenone-1, benzophenone-2, 4-hydroxy- and 2,4,4'-trihydroxybenzophenone. Enzyme activity was determined in lysates of HEK-293 cells expressing HSD17B6. The conversion of 3 $\alpha$ -androsterone to 5 $\alpha$ -androstenedione was measured in the presence of increasing UV-filter concentrations. Total substrate conversion was normalized to vehicle control and inhibition curves were fitted and analyzed by non-linear regression. Data represent mean  $\pm$  SD of three independent experiments.

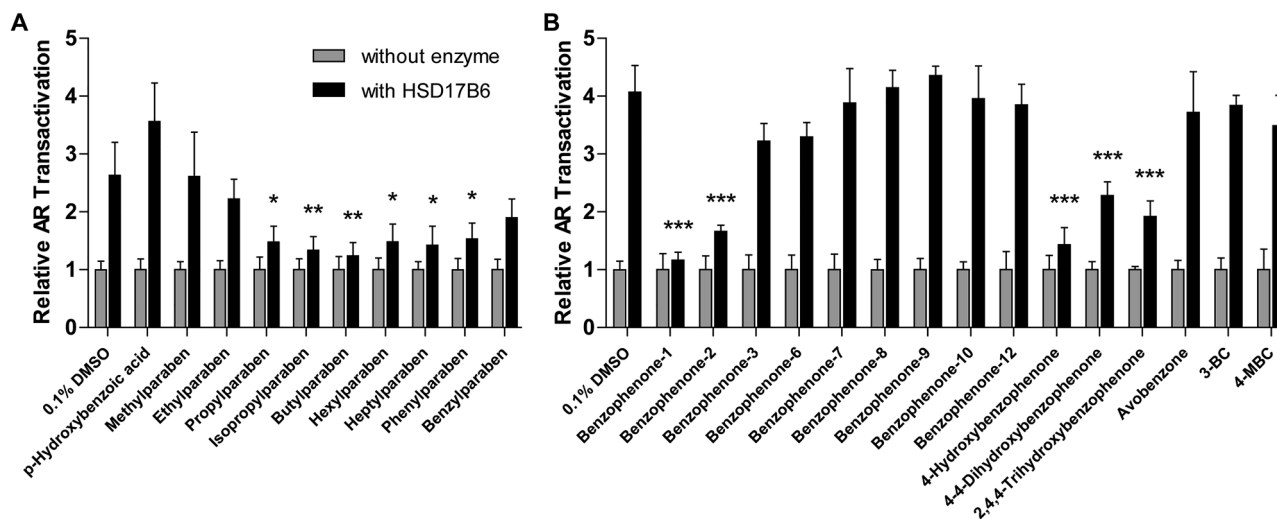
Inhibition of HSD17B6 activity: IC <sub>50</sub> values (mean $\pm$ SD)	
Benzophenone-type UV-filter	HSD17B6
Benzophenone-1	87 $\pm$ 41 nM
Benzophenone-2	161 $\pm$ 80 nM
4-hydroxybenzophenone	232 $\pm$ 55 nM
2,4,4'-trihydroxybenzophenone	287 $\pm$ 181 nM

weights, lower serum testosterone levels and shortened anogenital distance in the offspring of treated dams (Boberg et al., 2016; Guerra et al., 2017; Hoberman et al., 2008; Kang et al., 2002; Nakamura et al., 2015; Nakamura et al., 2018; Oishi, 2001, 2002; Yang et al., 2016; Zhang et al., 2014). AR activity is essential for spermatogenesis, as demonstrated by

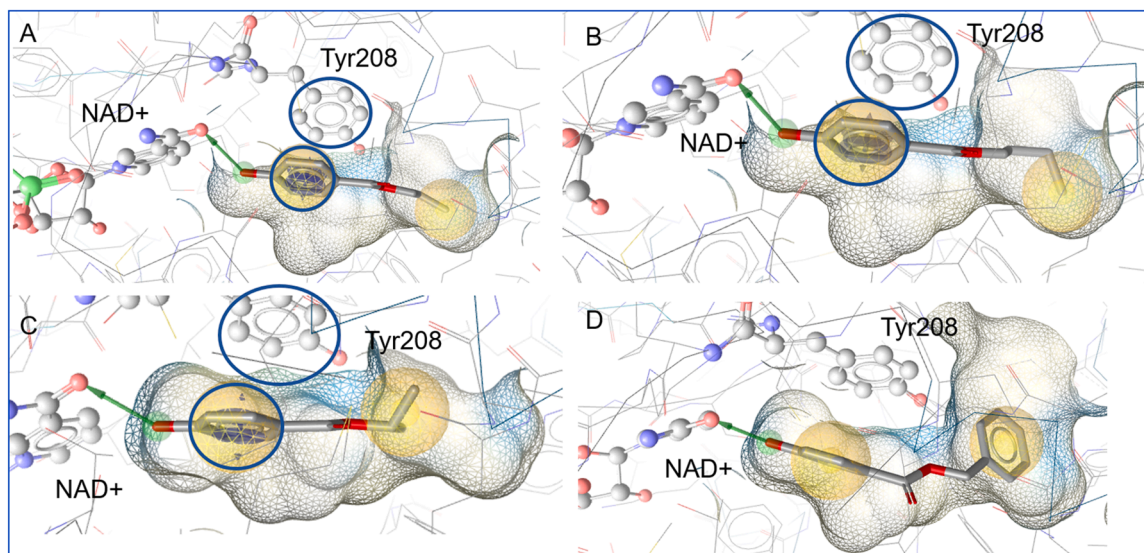
mouse models using Sertoli- and Leydig cell-specific AR ablation and by several studies on rats exposed to the respective compounds (Desai et al., 2022; O'Hara and Smith, 2015; Sharpe et al., 1990; Wang et al., 2009; Zhu et al., 2000). So far, the observed antiandrogenic effects of parabens and UV-filters were mainly assigned to direct AR inhibition, based on *in vitro* experiments reporting IC<sub>50</sub> values in the micromolar range (Berger et al., 2015; Chen et al., 2007; Darbre and Harvey, 2008; Ding et al., 2017; Kolšek et al., 2015; Kunz and Fent, 2006; Ma et al., 2003; Molina-Molina et al., 2008; Mustieles et al., 2023; Nashev et al., 2010; Pop et al., 2016; Watanabe et al., 2015). However, other mechanisms by which these chemicals can alter AR, including pre-receptor control of intracellular ligand concentration, receptor modification such as phosphorylation, acetylation or SUMOylation, as well as androgen biosynthesis and catabolism, have been largely neglected so far.

In this study, we addressed whether parabens and UV-filters potentially exert antiandrogenic effects by inhibiting the oxidative 3 $\alpha$ -HSD activity of the backdoor pathway of DHT generation. Our results revealed that several of these chemicals inhibit HSD17B6 with IC<sub>50</sub> values in the nanomolar range, thus at an order of magnitude lower concentrations than those observed in experiments on AR. To our knowledge, the parabens and UV-filters described in this study represent the first HSD17B6 inhibitors identified. An inhibition of androgen synthesis and AR signaling, for instance due to impaired oxidative 3 $\alpha$ -HSD activity and DHT formation, is particularly critical during the sensitive prenatal period of male sexual development. Whether human exposure levels of the active parabens and UV-filters identified in this study reach high enough concentrations to inhibit HSD17B6 in target tissues requires further investigations.

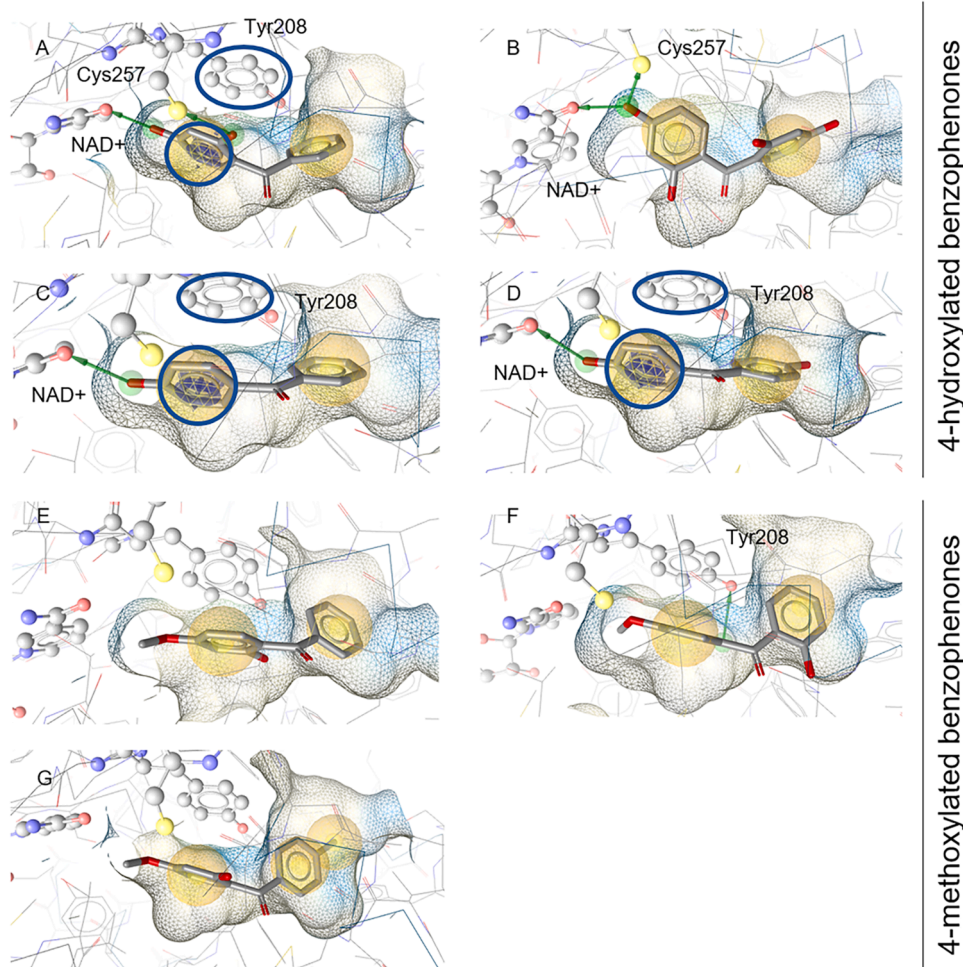
Due to potential endocrine disrupting properties and widespread human exposure, the use of parabens in cosmetics has been regulated in the European Union (EU) (Supplementary Table 2). The use of parabens with a linear alkyl group has been restricted to  $\leq$  1 %, alone or as mixtures. The Scientific Committee on Consumer Safety (SCCS) decided to prohibit the use of parabens with branched and phenol residue groups (e.g. isopropyl-, isobutyl-, pentyl-, benzyl- and phenylparaben) in cosmetic products in the EU due to a lack of data submitted by the industry for the reassessment of the safety evaluation (Commission, 2014). In the United States (US) parabens in cosmetics are so far not regulated by the Food and Drug Administration (FDA).



**Fig. 5.** Parabens and UV-filters inhibit HSD17B6 and decrease AR transcriptional activity. Inhibition of AR transcriptional activity by inhibition of HSD17B6 activity by (A) parabens and (B) BP-type UV-filters. Either lysates of HEK-293 cells expressing HSD17B6 or enzyme-free reaction buffer were incubated for 10 min at 37°C in the presence of 100 nM 3 $\alpha$ -androstenediol and 500  $\mu$ M NAD<sup>+</sup> with either 10  $\mu$ M test compound or vehicle control. After termination, the reactions were diluted in steroid-free medium and applied to HEK-293 cells transfected with AR, a AR responsive reporter gene and a transfection control. AR transactivation was first normalized to the internal transfection control and then to the corresponding HSD17B6 negative control. Data represent mean  $\pm$  SD from three independent experiments. Statistical analysis was performed by one-way ANOVA followed by the Dunnett's post-hoc test. Significant differences between normalized test compounds and vehicle control are indicated. P values: \* $<$ 0.05, \*\* $<$ 0.01, \*\*\* $<$ 0.001.



**Fig. 6.** Binding poses of parabens predicted by the HSD17B6 homology model. Predicted docking poses of (A) propylparaben, (B) butylparaben, (C) isopropylparaben and (D) benzylparaben in the binding site of the HSD17B6 homology model. Yellow spheres represent hydrophobic interactions, the blue ring marks  $\pi$ -stacking interactions and the green arrow indicate a hydrogen bond donor interaction.



**Fig. 7.** Binding poses of benzophenones predicted by the HSD17B6 homology model. Predicted docking poses of active inhibitors (A) benzophenone-1, (B) benzophenone-2, (C) 4-hydroxybenzophenone, (D) 4,4'-dihydroxybenzophenone, and the inactive compounds (E) benzophenone-3, (F) benzophenone-8 and (G) benzophenone-10 in the binding site of the homology model of HSD17B6. Green arrows indicate a hydrogen bond donor interaction, yellow spheres represent hydrophobic interactions and the blue rings mark  $\pi$ -stacking interactions.

The present study revealed a correlation of the length of the linear aliphatic side-chain of the tested parabens with their HSD17B6 inhibitory capacity. This SAR may be explained by additional interactions of the longer aliphatic side-chain with residues of the hydrophobic substrate binding pocket of the enzyme. Methyl- and propylparaben are most frequently used, followed by ethyl- and butylparaben, and these compounds have been detected in human urine, serum, fetal cord plasma, amniotic fluid and breast milk, indicating fetal exposure (reviewed in (Wei et al., 2021)). Parabens with longer side-chains, including hexyl- and heptylparaben, are used to a lesser extent due to their limited solubility. Additionally, the ability of parabens to penetrate the skin declines with increasing length or degree of branching of the ester alkyl side chain (Andersen, 2008; El Hussein et al., 2007). Thus, the systemic exposure of humans to longer-chain parabens such as hexyl- and heptylparaben is assumed to be rather low, although there are currently no biomonitoring data available on these compounds.

Parabens are efficiently metabolized in liver and skin by carboxylesterases (Harville et al., 2007; Jewell et al., 2007; Ozaki et al., 2013), resulting in an alcohol and *p*-hydroxybenzoic acid that did not inhibit HSD17B6, RDH5 and RDH16. All parabens including *p*-hydroxybenzoic acid can be conjugated by glucuronide and sulfate, allowing rapid elimination by urinary excretion, resulting in a relatively short half-life (Abbas et al., 2010; Soni et al., 2005; Ye et al., 2006). Additionally, *p*-hydroxybenzoic acid can be conjugated to glycine through amino acid transferases, generating *p*-hydroxyhippuric acid, which represents the main metabolite of parabens in humans (approximately 60 % of total paraben after oral administration) (Abbas et al., 2010; Moos et al., 2016). Various pharmacokinetic studies of methyl-, ethyl-, propyl- and butylparaben in rodents and humans revealed that due to the extensive metabolism only a small fraction of the administered dose is detectable as free, unconjugated parental compound in serum and urine, regardless of the administration route, e.g. dermal, subcutaneous or oral (Aubert et al., 2012; Gazin et al., 2013; Janjua et al., 2008a; Janjua et al., 2007; Moos et al., 2016; Shin et al., 2023; Shin et al., 2019; Ye et al., 2006).

Maximal reported serum levels of free, unconjugated parabens after dermal application of a mixture of methyl-, ethyl- and propylparaben (at 0.26, 0.26 and 0.28 %, respectively) in a human pharmacokinetic study reached mid nanomolar concentrations in approximately 5 h (Supplementary Table 3) (Shin et al., 2023). The measured parabens were not completely eliminated after 48 h, indicating a reservoir function of the skin (Shin et al., 2023) or subcutaneous fat. Application of 2 % butylparaben (as part of a mixture of butylparaben, diethyl- and dibutylphthalate, 2 % each) resulted in a serum concentration of free, unconjugated butylparaben of almost 700 nM within 3 h (Supplementary Table 3) (Janjua et al., 2007). Butylparaben could still be detected in the serum 24 h after administration (90 nM). It should be noted that the amounts of propyl- and butylparaben applied in the test creams in these studies were twice and more than ten times higher, respectively, than the maximum amounts permitted in cosmetic products in the EU (Supplementary Table 2). Therefore, peak serum concentrations after dermal application of European cosmetic products containing parabens are assumed to be below their respective IC<sub>50</sub> values for HSD17B6.

Methyl-, ethyl-, propyl- and butylparaben have been detected in several biomonitoring studies worldwide in urine samples with measured maximum values up to the mid-micromolar range, indicating extensive human exposure (reviewed in (Wei et al., 2021)). Reported concentrations in the medium to high nanomolar range in maternal serum, fetal cord plasma and amniotic fluid indicate potential fetal exposure (Assens et al., 2019; Pycke et al., 2015; Shekhar et al., 2017). Of note, in most of those biomonitoring studies, the total exposure of the parental parabens and their glucuronidated and/or sulfated conjugates were quantified without an assessment of the unconjugated parent compound, which does not fully reflect the actual exposure to bioactive parabens.

To address this issue, physiologically-based pharmacokinetic (PBPK)

models for methyl-, propyl-, and butylparaben have been developed, integrating plasma time-course kinetics from several rat and human studies with *in vitro* metabolism data (Aubert et al., 2012; Campbell et al., 2015). Estimations of free human plasma concentrations were made based on measured urinary paraben levels from biomonitoring studies. Under the assumption of a constant paraben intake, model predictions based on urinary paraben levels reported in the large biomonitoring dataset from the US National Health and Nutrition Examination Survey (NHANES, collection period 2009–2010) suggested maximum plasma concentrations in the low nanomolar range, thus below the IC<sub>50</sub> values of parabens against HSD17B6 observed in the present study. Of note, the SCCS has not considered any of these models for safety assessments due to limitations, including an approximately 4-fold overestimation of peak plasma levels and the use of the same dataset for both PBPK model calibration and validation (Bernauer et al., 2023b).

Human tissue-specific concentrations of free paraben have been measured in breast and adipose tissues (Supplementary Table 4) (Artacho-Cordón et al., 2019; Barr et al., 2012; Darbre et al., 2004; Downs et al., 2023; Wang et al., 2015). Assuming average tissue densities (breast 0.98 mL/g (Chan et al., 2019), adipose tissue 0.92 mL/g (Farvid et al., 2005)), median and mean concentrations of free, unconjugated methyl-, ethyl-, propyl-, and butylparaben reached the upper nanomolar range in breast tissue, which overlaps with the respective inhibitory activities of propyl- and butylparaben against HSD17B6. Methyl-, ethyl- and propylparaben reached concentrations in the micromolar range in normal breast tissue, with even higher levels in breast tumors, suggesting bioaccumulation that is more pronounced in cancerous compared to normal tissue. Paraben concentrations in adipose tissue were considerably lower, with maximal levels in the mid to high nanomolar range. To date, it remains unclear whether unconjugated parabens also accumulate in subcutaneous fat or in fat-rich tissues expressing 3 $\alpha$ -HSDs such as liver, testis and prostate.

Hepatic UDP-glucuronosyltransferases and carboxylesterases, which are involved in paraben metabolism, show age-dependent expression patterns, and remain at low levels up to 1 year of age (Boberg et al., 2016; Miyagi and Collier, 2011; Neumann et al., 2016). As a result, newborns and infants are assumed to display higher internal levels and prolonged half-life of unmetabolized parabens compared to adults, a fact that needs to be considered in risk assessment. It remains to be elucidated to which extent the maternal metabolism protects the unborn fetus from paraben exposure and whether unconjugated parabens reach concentrations in 3 $\alpha$ -HSD expressing tissues to cause antiandrogenic effects in male fetuses or later on during childhood and adolescence.

The UV-filters covered in this study are allowed in cosmetics and sunscreens only in small quantities in the US and EU, with the exception of 4-MBC, avobenzene and BP-3 (Supplementary Table 2) (Commission, 2022; FDA, 1999). 4-MBC was recently banned for the use in all cosmetic products and sunscreens in the EU due to its impact on thyroid and estrogen action and remains unapproved by the FDA as a UV-filter in sunscreens (Bernauer et al., 2023a; Commission, 2024). The weak inhibition of RDH5 observed for 4-MBC makes it unlikely that this compound exerts antiandrogenic effects and disrupt male fetal development through this mechanism. Peak serum concentrations of 78.6 nM were observed in humans after topical application of sunscreen containing 10 % 4-MBC, while concentrations within breast tissue were reported up to 110 nM (Barr et al., 2018; Janjua et al., 2004), which are around 100 times lower than the concentration applied to inhibit 70 % of RDH5 activity in our *in vitro* assay. To our knowledge, there are currently no studies demonstrating prenatal exposure to 4-MBC in humans, such as its presence in fetal serum, amniotic fluid or placenta samples. However, 4-MBC was detected in human breast milk, indicating exposure during post-natal development (Schlumpf, 2008). Bioaccumulation of 4-MBC cannot be completely ruled out (Janjua et al., 2008b; Janjua et al., 2004); however, it appears unlikely that 4-MBC reaches micromolar concentrations in the target tissues to achieve an antiandrogenic effect



by inhibiting RDH5.

Avobenzone can be used as a UV-filter in sunscreens up to 5 % in the EU and 3 % in the US; however, it did not inhibit any of the analyzed 3 $\alpha$ -HSDs. BP-3 is permitted in sunscreens up to 6 % in both the EU and US. Although BP-3 did not inhibit the investigated 3 $\alpha$ -HSDs, its well-known metabolites BP-1, BP-2 and 4-hydroxy-BP (Jeon et al., 2008; Okereke et al., 1993; Sarveiya et al., 2004; Watanabe et al., 2015) potently inhibited HSD17B6, with IC<sub>50</sub> values in the mid nanomolar range. 4, 4'-dihydroxy-BP, another known BP-3 metabolite that was shown to cause estrogenic effects *in vitro* and *in vivo*, weakly inhibited HSD17B6 by about 70 % at 10  $\mu$ M (Molins-Delgado et al., 2018; Suzuki et al., 2005).

A homology model of HSD17B6 was used for docking of these metabolites, predicting the formation of a hydrogen bond of the respective 4-hydroxy groups with the cofactor NAD<sup>+</sup> in the active site of the enzyme. Binding of these inhibitors may be further stabilized by  $\pi$ -stacking of the aromatic ring of the p-hydroxybenzoic acid with the side chain of Tyr208 of HSD17B6 and additionally by a second hydrogen bond of the 2-hydroxy group on BP-1 and 4-hydroxy group on BP-2, respectively, with Cys257 of HSD17B6. The methyl group of BP-3, BP-8, and BP-10, which covers the 4-hydroxy group, prevents this hydrogen bond formation, which reduces the affinity to the binding pocket of the enzyme, explaining why they did not inhibit HSD17B6.

Several earlier *in vitro* and *in vivo* experiments showed that BP-1, BP-2, BP-3 and 4-hydroxy-BP directly inhibit AR transcriptional activity (reviewed in (Krause et al., 2012; Kunz and Fent, 2006; Suzuki et al., 2005)). In addition, BP-1 and BP-2 have been shown to inhibit steroidogenic enzymes such as HSD3B1, HSD3B2 and HSD17B3 (Nashev et al., 2010; Wang et al., 2023). However, the IC<sub>50</sub> values reported for UV-filters against AR and the assessed steroidogenic enzymes were in the low to mid micromolar range.

Dermal application of a cream containing 10 % BP-3 to human subjects highlighted sex differences in the uptake and peak plasma levels of the UV-filter (Janjua et al., 2008b). BP-3 reached a peak plasma level of 0.82  $\mu$ M after 4 h in female and 1.04  $\mu$ M after 3 h in male subjects. The measured serum concentration ranges were 0.12–1.72  $\mu$ M and 0.11–3.49  $\mu$ M respectively, suggesting not only sex-specific differences in BP-3 uptake but also considerable interindividual differences within sexes.

A more recent toxicokinetic study with human volunteers showed that a whole body application of cream with 4 % BP-3 resulted in peak plasma levels of 0.41  $\mu$ M after a one-day application and over 1  $\mu$ M (1.13  $\mu$ M) after a four-day application (Matta et al., 2020). Again, a relatively large range of serum concentrations was observed, 0.20–0.78  $\mu$ M and 0.58–2.18  $\mu$ M, respectively. BP-3 metabolites have not been quantified in either study, thus their contribution after topical application to antiandrogenic effects remains to be assessed. For BP-1, the main metabolite of BP-3, maximum values in the medium nanomolar range were measured in blood (52  $\mu$ g/L ~ 228 nM) and semen (90  $\mu$ g/L ~ 394 nM) as part of biomonitoring studies (Janjua et al., 2008b; Kim and Choi, 2014; Okereke et al., 1993; Song et al., 2020; Vela-Soria et al., 2011; Watanabe et al., 2015), which overlaps with its inhibitory activity on HSD17B6 seen in the present study. Mean BP-3 concentrations in adipose and normal breast tissue were found to be in the low to mid nanomolar range (Supplementary Table 5) (Artacho-Cordón et al., 2019; Barr et al., 2012; Wang et al., 2015). However, maximum values were in the high nanomolar range for breast tissue and in the mid micromolar range for adipose tissue. Unfortunately, the BP-3 metabolites BP-1, BP-2 and 4-hydroxy-BP were not quantified in these studies.

Another BP-type UV-filter, 2,4,4'-trihydroxy-BP, that potently inhibited HSD17B6 activity in our study, with an IC<sub>50</sub> value in the nanomolar range, is mainly used as UV-stabilizer in plastics for food packaging materials and in small amounts in printing inks (Bradley et al., 2013), which limits human exposure. Whether 2,4,4'-trihydroxy-BP and BP-3 metabolites after topical application reach high enough

concentrations in target tissues expressing HSD17B6, such as liver, testis and prostate requires further research.

The role of the backdoor pathway the fetal male sexual development is still not fully understood. For example, no pathogenic mutations of the 3 $\alpha$ -HSDs investigated in this work have been described so far that are linked to a disorder of sexual development. It cannot be ruled out that the redundancy of 3 $\alpha$ -HSDs in the testes and prostate prevents a clear phenotype by mutations in only one of the relevant genes. The assessment of the relative contribution to the antiandrogenic effects of parabens and UV-filters through AR or the respective DHT synthesizing enzyme of the backdoor pathway requires further studies, ideally in human primary cell models, organoids of the respective tissue, or induced pluripotent stem cells expressing the respective proteins.

## 5. Conclusions

This study reports the first xenobiotics inhibiting HSD17B6, a key oxidative 3 $\alpha$ -HSD of the backdoor pathway of DHT generation, representing a novel mechanism by which the identified parabens and BP-type UV-filters with IC<sub>50</sub> values in the nanomolar range may exert antiandrogenic effects. A newly generated HSD17B6 homology model provides an explanation for the SAR of the identified inhibitors. Based on the allowed concentration in sunscreens and cosmetics in the EU and US, as well as available human biomonitoring and toxicokinetic information, the active parabens and UV-filters identified in the present study might cause antiandrogenic effects in the general population. While medium to high nanomolar concentrations of parabens were reported in maternal serum, fetal cord plasma and amniotic fluid, the extent of the fetal exposure and whether unconjugated parabens reach relevant concentrations in target tissues to exert antiandrogenic effects in male fetuses or later on during childhood and adolescence requires further research. Our study proposes to further consider the backdoor pathway of DHT synthesis as a mechanism by which EDCs may cause antiandrogenic effects to disturb male sexual development. To test a large number of chemicals in more advanced test systems, animal-free New Approach Methods (NAMs) should be established for safety assessment.

## CRedit authorship contribution statement

**Simon Stücheli:** Writing – review & editing, Investigation, Formal analysis, Data curation. **Manuel Kley:** Writing – review & editing, Writing – original draft, Visualization, Validation, Investigation, Formal analysis, Data curation. **Pamela Ruffiner:** Writing – review & editing, Investigation, Formal analysis, Data curation. **Alex Odermatt:** Writing – review & editing, Writing – original draft, Supervision, Resources, Project administration, Funding acquisition, Conceptualization. **Daniela Schuster:** Writing – review & editing, Supervision, Software, Resources. **Veronika Temml:** Writing – review & editing, Writing – original draft, Visualization, Investigation, Formal analysis, Data curation. **Stéphanie Boudon:** Writing – review & editing.

## Declaration of Competing Interest

The authors declare the following financial interests/personal relationships which may be considered as potential competing interests Alex Odermatt reports financial support was provided by Swiss Centre for Applied Human Toxicology. Alex Odermatt reports a relationship with Swiss National Science Foundation that includes: funding grants.

## Acknowledgement

This work was supported by a grant from the Swiss Centre for Applied Human Toxicology: SCAHT-GL 21-06.

## Appendix A. Supporting information

Supplementary data associated with this article can be found in the online version at doi:10.1016/j.tox.2024.153997.

### Data availability

Data will be made available on request.

### References

- Abbas, S., Greige-Gerges, H., Karam, N., Piet, M.-H., Netter, P., Magdalou, J., 2010. Metabolism of parabens (4-Hydroxybenzoic Acid Esters) by hepatic esterases and UDP-Glucuronosyltransferases in man. *Drug Metab. Pharmacokinet.* 25, 568–577.
- Andersen, F.A., 2008. Final amended report on the safety assessment of methylparaben, ethylparaben, propylparaben, isopropylparaben, butylparaben, isobutylparaben, and benzylparaben as used in cosmetic products. *Int. J. Toxicol.* 27, 1–82.
- Arampatzis, S., Kadereit, B., Schuster, D., Balazs, Z., Schweizer, R.A., Frey, F.J., Langer, T., Odermatt, A., 2005. Comparative enzymology of 11 $\beta$ -hydroxysteroid dehydrogenase type 1 from six species. *J. Mol. Endocrinol.* 35, 89–101.
- Artacho-Cordón, F., Ríos-Arrabal, S., León, J., Frederiksen, H., Sáenz, J.M., Martín-Omedo, P., Fernández, M.F., Olea, N., Arrebola, J.P., 2019. Adipose tissue concentrations of non-persistent environmental phenols and local redox balance in adults from Southern Spain. *Environ. Int.* 133, 105118.
- Asimakopoulos, A.G., Elangovan, M., Kannan, K., 2016. Migration of parabens, bisphenols, benzophenone-type UV filters, triclosan, and triclocarban from teethers and its implications for infant exposure. *Environ. Sci. Technol.* 50, 13539–13547.
- Assens, M., Frederiksen, H., Petersen, J.H., Larsen, T., Skakkebaek, N.E., Juul, A., Andersson, A.M., Main, K.M., 2019. Variations in repeated serum concentrations of UV filters, phthalates, phenols and parabens during pregnancy. *Environ. Int.* 123, 318–324.
- Aubert, N., Ameller, T., Legrand, J.J., 2012. Systemic exposure to parabens: pharmacokinetics, tissue distribution, excretion balance and plasma metabolites of [14C]-methyl-, propyl- and butylparaben in rats after oral, topical or subcutaneous administration. *Food Chem. Toxicol.* 50, 445–454.
- Auchus, R.J., 2004. The backdoor pathway to dihydrotestosterone. *Trends Endocrinol. Metab.* 15, 432–438.
- Barr, L., Alamer, M., Darbre, P.D., 2018. Measurement of concentrations of four chemical ultraviolet filters in human breast tissue at serial locations across the breast. *J. Appl. Toxicol.* 38, 1112–1120.
- Barr, L., Metaxas, G., Harbach, C.A.J., Savoy, L.A., Darbre, P.D., 2012. Measurement of paraben concentrations in human breast tissue at serial locations across the breast from axilla to sternum. *J. Appl. Toxicol.* 32, 219–232.
- Bens, G., 2014. Sunscreens. *Adv. Exp. Med Biol.* 810, 429–463.
- Berger, E., Potouridis, T., Haeger, A., Pittmann, W., Wagner, M., 2015. Effect-directed identification of endocrine disruptors in plastic baby teethers. *J. Appl. Toxicol.* 35, 1254–1261.
- Bernaer, U., Bodin, L., Chaudhry, Q., Coenraads, P., Dusinska, M., Ezendam, J., Gaffet, E., Galli, C., Granum, B. and Panteri, E. 2023a. SCCS OPINION on 4-Methylbenzylidene camphor (4-MBC)-SCCS/1640/21-Final version. Scientific Committee for Consumer Safety (European Commission).
- Bernaer, U., Bodin, L., Chaudhry, Q., Coenraads, P., Dusinska, M., Ezendam, J., Gaffet, E., Galli, C., Panteri, E. and Rogiers, V. 2023b. SCCS OPINION on Butylparaben (CAS No. 94-26-8, EC No. 202-318-7)-SCCS/1651/23-Final Opinion.
- Boberg, J., Axelstad, M., Svingen, T., Mandrup, K., Christiansen, S., Vinggaard, A.M., Hass, U., 2016. Multiple endocrine disrupting effects in rats perinatally exposed to Butylparaben. *Toxicol. Sci.* 152, 244–256.
- Bradley, E.L., Stratton, J.S., Leak, J., Lister, L., Castle, L., 2013. Printing ink compounds in foods: UK survey results. *Food Addit. Contam.: Part B* 6, 73–83.
- Buck Louis, G.M., Chen, Z., Kim, S., Sapra, K.J., Bae, J., Kannan, K., 2015. Urinary concentrations of benzophenone-type ultraviolet light filters and semen quality. *Fertil. Steril.* 104, 989–996.
- Campbell, J.L., Yoon, M., Clewell, H.J., 2015. A case study on quantitative in vitro to in vivo extrapolation for environmental esters: methyl-, propyl- and butylparaben. *Toxicology* 332, 67–76.
- Chan, M., Lonie, S., Mackay, S., MacGill, K., 2019. Reduction mammoplasty: what cup size will i be? *Plast. Reconstr. Surg. Glob. Open* 7, e2273.
- Chang, H.C., Miyamoto, H., Marwah, P., Lardy, H., Yeh, S., Huang, K.E., Chang, C., 1999. Suppression of Delta(5)-androstenediol-induced androgen receptor transactivation by selective steroids in human prostate cancer cells. *Proc. Natl. Acad. Sci. USA* 96, 11173–11177.
- Chen, J., Ahn, K.C., Gee, S.J., Hammock, B.D., Lasley, B.L., 2007. Antiandrogenic properties of parabens and other phenolic containing small molecules in personal care products. *Toxicol. Appl. Pharm.* 221, 278–284.
- Chetyrkin, S.V., Belyaeva, O.V., Gough, W.H., Kedishvili, N.Y., 2001a. Characterization of a novel type of human microsomal 3 $\alpha$ -hydroxysteroid dehydrogenase: unique tissue distribution and catalytic properties. *J. Biol. Chem.* 276, 22278–22286.
- Chetyrkin, S.V., Hu, J., Gough, W.H., Dumaul, N., Kedishvili, N.Y., 2001b. Further characterization of human microsomal 3 $\alpha$ -hydroxysteroid dehydrogenase. *Arch. Biochem. Biophys.* 386, 1–10.
- Commission, E. 2014. Commission Regulation (EU) No 358/2014 of 9 April 2014 Amending Annexes II and V to Regulation (EC) No 1223/2009 of the European Parliament and of the Council on Cosmetic Products. European Commission Brussels, Belgium.
- Commission, E. 2022. Commission Regulation (EU) No 1176/2022 of 7 July 2022 Amending Regulation (EC) No 1223/2009 of the European Parliament and of the Council as regards the use of certain UV filters in cosmetic products European Commission Brussels, Belgium.
- Commission, E. 2024. Commission Regulation (EU) No 996/2024 of 3 April 2024 amending Regulation (EC) No 1223/2009 of the European Parliament and of the Council as regards the use of Vitamin A, Alpha-Arbutin and Arbutin and certain substances with potential endocrine disrupting properties in cosmetic products. European Commission Brussels, Belgium.
- Darbre, P.D., 2006. Environmental oestrogens, cosmetics and breast cancer. *Best. Pr. Res. Clin. Endocrinol. Metab.* 20, 121–143.
- Darbre, P.D., Aljarrah, A., Miller, W.R., Coldham, N.G., Sauer, M.J., Pope, G.S., 2004. Concentrations of parabens in human breast tumours. *J. Appl. Toxicol.* 24, 5–13.
- Darbre, P.D., Harvey, P.W., 2008. Paraben esters: review of recent studies of endocrine toxicity, absorption, esterase and human exposure, and discussion of potential human health risks. *J. Appl. Toxicol.* 28, 561–578.
- Desai, A., Yassin, M., Cayetano, A., Tharakan, T., Jayasena, C.N., Minhas, S., 2022. Understanding and managing the suppression of spermatogenesis caused by testosterone replacement therapy (TRT) and anabolic-androgenic steroids (AAS). *Ther. Adv. Urol.* 14, 17562872221105017.
- Ding, K., Kong, X., Wang, J., Lu, L., Zhou, W., Zhan, T., Zhang, C., Zhuang, S., 2017. Side chains of parabens modulate antiandrogenic activity: in vitro and molecular docking studies. *Environ. Sci. Technol.* 51, 6452–6460.
- Downs, C.A., Amin, M.M., Tabatabaiean, M., Chavoshani, A., Amjadi, E., Afshari, A., Kelishadi, R., 2023. Parabens preferentially accumulate in metastatic breast tumors compared to benign breast tumors and the association of breast cancer risk factors with paraben accumulation. *Environ. Adv.* 11, 100325.
- EC, R. 2009. Regulation (EC) no 1223/2009 of the European Parliament on cosmetic products annex VI list of UV filters allowed in cosmetic products.
- El Hussein, S., Muret, P., Berard, M., Makkji, S., Humbert, P., 2007. Assessment of principal parabens used in cosmetics after their passage through human epidermis-dermis layers (ex-vivo study). *Exp. Dermatol.* 16, 830–836.
- Elder R, L., 1984. Final report on the safety assessment of methylparaben, ethylparaben, propylparaben, and butylparaben. *J. Am. Coll. Toxicol.* 3, 147–209.
- Farvid, M.S., Ng, T.W.K., Chan, D.C., Barrett, P.H.R., Watts, G.F., 2005. Association of adiponectin and resistin with adipose tissue compartments, insulin resistance and dyslipidaemia. *Diabetes, Obes. Metab.* 7, 406–413.
- FDA. 1999. Sunscreen Drug Products for Over-the-Counter Human Use. Subpart B§352.10 Sunscreen active ingredients. Federal Register.
- Flück, C.E., Meyer-Boni, M., Pandey, A.V., Kempna, P., Miller, W.L., Schoenle, E.J., Biason-Lauber, A., 2011. Why boys will be boys: two pathways of fetal testicular androgen biosynthesis are needed for male sexual differentiation. *Am. J. Hum. Genet.* 89, 201–218.
- Flück, C.E., Miller, W.L., Auchus, R.J., 2003. The 17, 20-lyase activity of cytochrome p450c17 from human fetal testis favors the delta5 steroidogenic pathway. *J. Clin. Endocrinol. Metab.* 88, 3762–3766.
- Fukami, M., Homma, K., Hasegawa, T., Ogata, T., 2013. Backdoor pathway for dihydrotestosterone biosynthesis: implications for normal and abnormal human sex development. *Dev. Dyn.* 242, 320–329.
- Fürstenberger, C., Vuorinen, A., Da Cunha, T., Kratschmar, D.V., Saugy, M., Schuster, D., Odermatt, A., 2012. The anabolic androgenic steroid fluoxymesterone inhibits 11 $\beta$ -hydroxysteroid dehydrogenase 2-dependent glucocorticoid inactivation. *Toxicol. Sci.* 126, 353–361.
- Gazin, V., Marsden, E., Marguerite, F., 2013. Oral propylparaben administration to juvenile male Wistar rats did not induce toxicity in reproductive organs. *Toxicol. Sci.* 136, 392–401.
- Geissler, W.M., Davis, D.L., Wu, L., Bradshaw, K.D., Patel, S., Mendonca, B.B., Elliston, K. O., Wilson, J.D., Russell, D.W., Andersson, S., 1994. Male pseudohermaphroditism caused by mutations of testicular 17 $\beta$ -hydroxysteroid dehydrogenase 3. *Nat. Genet.* 7, 34–39.
- Gough, W.H., VanOoteghem, S., Sint, T., Kedishvili, N.Y., 1998. cDNA cloning and characterization of a new human microsomal NAD<sup>+</sup>-dependent dehydrogenase that oxidizes all-trans-retinol and 3 $\alpha$ -Hydroxysteroids\*. *J. Biol. Chem.* 273, 19778–19785.
- Guerra, M.T., Sanabria, M., Leite, G.A.A., Borges, C.S., Cuciolo, M.S., Anselmo-Franci, J. A., Foster, W.G., Kempinas, W.G., 2017. Maternal exposure to butyl paraben impairs testicular structure and sperm quality on male rats. *Environ. Toxicol.* 32, 1273–1289.
- Harvey, P.W., Darbre, P., 2004. Endocrine disruptors and human health: could oestrogenic chemicals in body care cosmetics adversely affect breast cancer incidence in women? *J. Appl. Toxicol.* 24, 167–176.
- Harville, M.H., Voorman, R., Prusakiewicz, J.J., 2007. Comparison of paraben stability in human and rat skin. *Drug Metab. Lett.* 1, 17–21.
- Hawkins, P.C., Skillman, A.G., Warren, G.L., Ellingson, B.A., Stahl, M.T., 2010. Conformer generation with OMEGA: algorithm and validation using high quality structures from the Protein Databank and Cambridge Structural Database. *J. Chem. Inf. Model* 50, 572–584.
- Hayden, C.G.J., Roberts, M.S., Benson, H.A.E., 1997. Systemic absorption of sunscreen after topical application. *Lancet* 350, 863–864.
- He, X.-Y., Merz, G., Mehta, P., Schulz, H., Yang, S.-Y., 1999. Human Brain Short Chain 1-3-Hydroxyacyl Coenzyme A dehydrogenase is a single-domain multifunctional enzyme: characterization of a novel 17 $\beta$ -hydroxysteroid dehydrogenase\*. *J. Biol. Chem.* 274, 15014–15019.

- He, X.Y., Yang, Y.Z., Peehl, D.M., Lauderdale, A., Schulz, H., Yang, S.Y., 2003. Oxidative 3 $\alpha$ -hydroxysteroid dehydrogenase activity of human type 10 17 $\beta$ -hydroxysteroid dehydrogenase. *J. Steroid. Biochem. Mol. Biol.* 87, 191–198.
- Hoberman, A.M., Schreuer, D.K., Leazer, T., Daston, G.P., Carthew, P., Re, T., Loretz, L., Mann, P., 2008. Lack of effect of butylparaben and methylparaben on the reproductive system in male rats. *Birth Defects Res B Dev. Reprod. Toxicol.* 83, 123–133.
- Hofmann, L., Tsybovsky, Y., Alexander, N.S., Babino, D., Leung, N.Y., Montell, C., Banerjee, S., von Lintig, J., Palczewski, K., 2016. Structural insights into the drosophila melanogaster retinol dehydrogenase, a member of the short-chain dehydrogenase/reductase family. *Biochemistry* 55, 6545–6557.
- Horton, R., 1992. Dihydrotestosterone is a peripheral paracrine hormone. *J. Androl.* 13, 23–27.
- Huang, X.F., Luu-The, V., 2000. Molecular characterization of a first human 3 $\alpha$ ->3 $\beta$ -hydroxysteroid epimerase. *J. Biol. Chem.* 275, 29452–29457.
- Huang, Y., Wang, P., Law, J.C.-F., Zhao, Y., Wei, Q., Zhou, Y., Zhang, Y., Shi, H., Leung, K.S.-Y., 2020. Organic UV filter exposure and pubertal development: a prospective follow-up study of urban Chinese adolescents. *Environ. Int.* 143, 105961.
- Inderbinnen, S.G., Zogg, M., Kley, M., Smiesko, M., Odermatt, A., 2021. Species-specific differences in the inhibition of 11 $\beta$ -hydroxysteroid dehydrogenase 2 by itraconazole and posaconazole. *Toxicol. Appl. Pharm.* 412, 115387.
- Ishiwatari, S., Suzuki, T., Hitomi, T., Yoshino, T., Matsukuma, S., Tsuji, T., 2007. Effects of methyl paraben on skin keratinocytes. *J. Appl. Toxicol.* 27, 1–9.
- Janjua, N.R., Frederiksen, H., Skakkebaek, N.E., Wulf, H.C., Andersson, A.M., 2008a. Urinary excretion of phthalates and paraben after repeated whole-body topical application in humans. *Int. J. Androl.* 31, 118–130.
- Janjua, N.R., Kongshoj, B., Andersson, A.M., Wulf, H.C., 2008b. Sunscreens in human plasma and urine after repeated whole-body topical application. *J. Eur. Acad. Dermatol. Venereol.* 22, 456–461.
- Janjua, N.R., Mogensen, B., Andersson, A.M., Petersen, J.H., Henriksen, M., Skakkebaek, N.E., Wulf, H.C., 2004. Systemic absorption of the sunscreens benzophenone-3, octyl-methoxycinnamate, and 3-(4-methyl-benzylidene) camphor after whole-body topical application and reproductive hormone levels in humans. *J. Invest. Dermatol.* 123, 57–61.
- Janjua, N.R., Mortensen, G.K., Andersson, A.M., Kongshoj, B., Skakkebaek, N.E., Wulf, H.C., 2007. Systemic uptake of diethyl phthalate, dibutyl phthalate, and butyl paraben following whole-body topical application and reproductive and thyroid hormone levels in humans. *Environ. Sci. Technol.* 41, 5564–5570.
- Jeon, H.-K., Sarma, S.N., Kim, Y.-J., Ryu, J.-C., 2008. Toxicokinetics and metabolisms of benzophenone-type UV filters in rats. *Toxicology* 248, 89–95.
- Jewell, C., Prusakiewicz, J.J., Ackermann, C., Payne, N.A., Fate, G., Voorman, R., Williams, F.M., 2007. Hydrolysis of a series of parabens by skin microsomes and cytosol from human and minipigs and in whole skin in short-term culture. *Toxicol. Appl. Pharmacol.* 225, 221–228.
- Jones, G., Willett, P., Glen, R.C., Leach, A.R., Taylor, R., 1997. Development and validation of a genetic algorithm for flexible docking. *J. Mol. Biol.* 267, 727–748.
- Jumper, J., Evans, R., Pritzel, A., Green, T., Figurnov, M., Ronneberger, O., Tunyasuvunakool, K., Bates, R., Zidek, A., Potapenko, A., Bridgland, A., Meyer, C., Kohl, S.A.A., Ballard, A.J., Cowie, A., Romera-Paredes, B., Nikolov, S., Jain, R., Adler, J., Back, T., Petersen, S., Reiman, D., Clancy, E., Zielinski, M., Steinegger, M., Pacholska, M., Berghammer, T., Bodenstein, S., Silver, D., Vinyals, O., Senior, A.W., Kavukcuoglu, K., Kohli, P., Hassabis, D., 2021. Highly accurate protein structure prediction with AlphaFold. *Nature* 596, 583–589.
- Kang, K.S., Che, J.H., Ryu, D.Y., Kim, T.W., Li, G.X., Lee, Y.S., 2002. Decreased sperm number and motile activity on the F1 offspring maternally exposed to butyl p-hydroxybenzoic acid (butyl paraben). *J. Vet. Med. Sci.* 64, 227–235.
- Kim, S., Choi, K., 2014. Occurrences, toxicities, and ecological risks of benzophenone-3, a common component of organic sunscreen products: a mini-review. *Environ. Int.* 70, 143–157.
- Kingston, R.E., Moore, D., Seidman, J., Smith, J. and Struhl, K. 1987. **Current protocols in molecular biology.** Ausubel, F.M.
- Kley, M., Moser, S.O., Winter, D.V., Odermatt, A., 2023. In vitro methods to assess 11 $\beta$ -hydroxysteroid dehydrogenase type 1 activity. *Methods Enzym.* 689, 121–165.
- Kolšek, K., Gobec, M., Mlinarič Raščan, I., Sollner Dolenc, M., 2015. Screening of bisphenol A, triclosan and paraben analogues as modulators of the glucocorticoid and androgen receptor activities. *Toxicol. Vitr.* 29, 8–15.
- Krause, M., Klit, A., Blomberg Jensen, M., Søbørg, T., Frederiksen, H., Schlumpf, M., Lichtensteiger, W., Skakkebaek, N.E., Drzewiecki, K.T., 2012. Sunscreens: are they beneficial for health? An overview of endocrine disrupting properties of UV-filters. *Int. J. Androl.* 35, 424–436.
- Kunz, P.Y., Fent, K., 2006. Multiple hormonal activities of UV filters and comparison of in vivo and in vitro estrogenic activity of ethyl-4-aminobenzoate in fish. *Aquat. Toxicol.* 79, 305–324.
- Lu, L., Xiong, W., Li, X., Lv, S., Tang, X., Chen, M., Zou, Z., Lin, Z., Qiu, B., Chen, G., 2014. Determination of the migration of eight parabens from antibacterial plastic packaging by liquid chromatography-electrospray ionization-tandem mass spectrometry. *Anal. Methods* 6, 2096–2101.
- Ma, R., Cotton, B., Lichtensteiger, W., Schlumpf, M., 2003. UV filters with antagonistic action at androgen receptors in the MDA-kb2 cell transcriptional-activation assay. *Toxicol. Sci.* 74, 43–50.
- Mao, J.F., Li, W., Ong, C.N., He, Y., Jong, M.-C., Gin, K.Y.-H., 2022. Assessment of human exposure to benzophenone-type UV filters: a review. *Environ. Int.* 167, 107405.
- Matta, M.K., Florian, J., Zusterzeel, R., Pilli, N.R., Patel, V., Volpe, D.A., Yang, Y., Oh, L., Bashaw, E., Zineh, I., Sanabria, C., Kemp, S., Godfrey, A., Adah, S., Coelho, S., Wang, J., Furlong, L.-A., Ganley, C., Michele, T., Strauss, D.G., 2020. Effect of sunscreen application on plasma concentration of sunscreen active ingredients: a randomized clinical trial. *JAMA* 323, 256–267.
- Miller, W.L., Auchus, R.J., 2011. The molecular biology, biochemistry, and physiology of human steroidogenesis and its disorders. *Endocr. Rev.* 32, 81–151.
- Miyagi, S.J., Collier, A.C., 2011. The development of UDP-glucuronosyltransferases 1A1 and 1A6 in the pediatric liver. *Drug Metab. Dispos.* 39, 912–919.
- Mohler, J.L., Titus, M.A., Bai, S., Kennerley, B.J., Lih, F.B., Tomer, K.B., Wilson, E.M., 2011. Activation of the androgen receptor by intratumoral bioconversion of androstenediol to dihydrotestosterone in prostate cancer. *Cancer Res.* 71, 1486–1496.
- Molina-Molina, J.-M., Escandé, A., Pillon, A., Gomez, E., Pakdel, F., Cavaillès, V., Olea, N., Ait-Aissa, S., Balaguer, P., 2008. Profiling of benzophenone derivatives using fish and human estrogen receptor-specific in vitro bioassays. *Toxicol. Appl. Pharmacol.* 232, 384–395.
- Molins-Delgado, D., Olmo-Campos, M.D.M., Valeta-Juan, G., Pleguezuelos-Hernández, V., Barceló, D., Díaz-Cruz, M.S., 2018. Determination of UV filters in human breast milk using turbulent flow chromatography and babies' daily intake estimation. *Environ. Res.* 161, 532–539.
- Moos, R.K., Angerer, J., Dierkes, G., Brüning, T., Koch, H.M., 2016. Metabolism and elimination of methyl, iso- and n-butyl paraben in human urine after single oral dosage. *Arch. Toxicol.* 90, 2699–2709.
- Mustieles, V., Balogh, R.K., Axelstad, M., Montazeri, P., Márquez, S., Vrijheid, M., Draskau, M.K., Taxvig, C., Peinado, F.M., Berman, T., Frederiksen, H., Fernández, M. F., Marie Vinggaard, A., Andersson, A.M., 2023. Benzophenone-3: comprehensive review of the toxicological and human evidence with meta-analysis of human biomonitoring studies. *Environ. Int.* 173, 107739.
- Nakamura, N., Inselman, A.L., White, G.A., Chang, C.W., Trbojevič, R.A., Sefph, E., Voris, K.L., Patton, R.E., Bryant, M.S., Harrouk, W., McIntyre, B.S., Foster, P.M., Hansen, D.K., 2015. Effects of maternal and lactational exposure to 2-hydroxy-4-methoxybenzene on development and reproductive organs in male and female rat offspring. *Birth Defects Res. B Dev. Reprod. Toxicol.* 104, 35–51.
- Nakamura, N., Vijay, V., Desai, V.G., Hansen, D.K., Han, T., Chang, C.-W., Chen, Y.-C., Harrouk, W., McIntyre, B., Foster, P.M., Fuscoe, J.C., Inselman, A.L., 2018. Transcript profiling in the testes and prostates of postnatal day 30 Sprague-Dawley rats exposed prenatally and lactationally to 2-hydroxy-4-methoxybenzophenone. *Reprod. Toxicol.* 82, 111–123.
- Nashev, L.G., Schuster, D., Lagner, C., Sodha, S., Langer, T., Wolber, G., Odermatt, A., 2010. The UV-filter benzophenone-1 inhibits 17 $\beta$ -hydroxysteroid dehydrogenase type 3: virtual screening as a strategy to identify potential endocrine disrupting chemicals. *Biochem. Pharm.* 79, 1189–1199.
- Neumann, E., Mehboob, H., Ramírez, J., Mirkov, S., Zhang, M., Liu, W., 2016. Age-dependent hepatic UDP-glucuronosyltransferase gene expression and activity in children. *Front. Pharm.* 7, 437.
- O'Hara, L., Smith, L.B., 2015. Androgen receptor roles in spermatogenesis and infertility. *Best. Pr. Res. Clin. Endocrinol. Metab.* 29, 595–605.
- Oishi, S., 2001. Effects of butylparaben on the male reproductive system in rats. *Toxicol. Ind. Health* 17, 31–39.
- Oishi, S., 2002. Effects of propyl paraben on the male reproductive system. *Food Chem. Toxicol.* 40, 1807–1813.
- Okereke, C.S., Kadry, A.M., Abdel-Rahman, M.S., Davis, R.A., Friedman, M.A., 1993. Metabolism of benzophenone-3 in rats. *Drug Metab. Dispos.* 21, 788–791.
- O'Shaughnessy, P.J., Antignac, J.P., Le Bizet, B., Morvan, M.L., Svechnikov, K., Söder, O., Savchuk, I., Monteiro, A., Soffientini, U., Johnstone, Z.C., Bellingham, M., Hough, D., Walker, N., Filis, P., Fowler, P.A., 2019. Alternative (backdoor) androgen production and masculinization in the human fetus. *PLoS Biol.* 17, e3000002.
- Ozaki, H., Sugihara, K., Watanabe, Y., Fujino, C., Uramaru, N., Sone, T., Ohta, S., Kitamura, S., 2013. Comparative study of the hydrolytic metabolism of methyl-, ethyl-, propyl-, butyl-, heptyl- and dodecylparaben by microsomes of various rat and human tissues. *Xenobiotica* 43, 1064–1072.
- Pop, A., Drugan, T., Gutleb, A.C., Lupu, D., Cherfan, J., Loghin, F., Kiss, B., 2016. Individual and combined in vitro (anti)androgenic effects of certain food additives and cosmetic preservatives. *Toxicol. Vitr.* 32, 269–277.
- Poukka, H., Karvonen, U., Janne, O.A., Palvimo, J.J., 2000. Covalent modification of the androgen receptor by small ubiquitin-like modifier 1 (SUMO-1). *Proc. Natl. Acad. Sci. USA* 97, 14145–14150.
- Pugazhendhi, D., Pope, G.S., Darbre, P.D., 2005. Oestrogenic activity of p-hydroxybenzoic acid (common metabolite of paraben esters) and methylparaben in human breast cancer cell lines. *J. Appl. Toxicol.* 25, 301–309.
- Pycke, B.F., Geer, L.A., Dalloul, M., Abulafia, O., Halden, R.U., 2015. Maternal and fetal exposure to parabens in a multiethnic urban U.S. population. *Environ. Int.* 84, 193–200.
- Renfree, M.B., O, W.S., Short, R.V., Shaw, G., 1996. Sexual differentiation of the urogenital system of the fetal and neonatal tammar wallaby, *Macropus eugenii*. *Anat. Embryol. (Berl.)* 194, 111–134.
- Renfree, M.B., Wilson, J.D., Short, R.V., Shaw, G., George, F.W., 1992. Steroid hormone content of the gonads of the tammar wallaby during sexual differentiation. *Biol. Reprod.* 47, 644–647.
- Rodríguez-Bernaldo de Quirós, A., Paseiro-Cerrato, R., Pastorelli, S., Koivikko, R., Simoneau, C., Paseiro-Losada, P., 2009. Migration of photoinitiators by gas phase into dry foods. *J. Agric. Food Chem.* 57, 10211–10215.
- SAEZ, J.M., DE PERETTI, E., MORERA, A.M., DAVID, M., BERTRAND, J., 1971. Familial male pseudohermaphroditism with gynecomastia due to a testicular 17-ketosteroid reductase Defect. I. Studies in vivo. *J. Clin. Endocrinol. Metab.* 32, 604–610.

- Sarveiya, V., Risk, S., Benson, H.A.E., 2004. Liquid chromatographic assay for common sunscreen agents: application to in vivo assessment of skin penetration and systemic absorption in human volunteers. *J. Chromatogr. B* 803, 225–231.
- Satoh, K., Galli, I., Ariga, H., 1993. Effect of drugs on gene expression in mammalian cells: a highly efficient procedure to test large numbers of samples. *Nucleic Acids Res.* 21, 4429–4430.
- Schlecht, C., Klammer, H., Jarry, H., Wuttke, W., 2004. Effects of estradiol, benzophenone-2 and benzophenone-3 on the expression pattern of the estrogen receptors (ER) alpha and beta, the estrogen receptor-related receptor 1 (ERR1) and the aryl hydrocarbon receptor (AhR) in adult ovariectomized rats. *Toxicology* 205, 123–130.
- Schreurs, R., Lanser, P., Seinen, W., van der Burg, B., 2002. Estrogenic activity of UV filters determined by an in vitro reporter gene assay and an in vivo transgenic zebrafish assay. *Arch. Toxicol.* 76, 257–261.
- Scinicariello, F., Buser, M.C., 2016. Serum testosterone concentrations and urinary bisphenol A, benzophenone-3, triclosan, and paraben levels in male and female children and adolescents: NHANES 2011–2012. *Environ. Health Perspect.* 124, 1898–1904.
- Sharpe, R.M., Maddocks, S., Kerr, J.B., 1990. Cell-cell interactions in the control of spermatogenesis as studied using leydig cell destruction and testosterone replacement. *Am. J. Anat.* 188, 3–20.
- Shekhar, S., Sood, S., Showkat, S., Lite, C., Chandrasekhar, A., Vairamani, M., Barathi, S., Santosh, W., 2017. Detection of phenolic endocrine disrupting chemicals (EDCs) from maternal blood plasma and amniotic fluid in Indian population. *Gen. Comp. Endocrinol.* 241, 100–107.
- Shin, M.Y., Choi, J.W., Lee, S., Kim, S., Kho, Y., Choi, K., Kim, S., 2023. Pharmacokinetics of transdermal methyl-, ethyl-, and propylparaben in humans following single dermal administration. *Chemosphere* 310, 136689.
- Shin, M.Y., Shin, C., Choi, J.W., Lee, J., Lee, S., Kim, S., 2019. Pharmacokinetic profile of propyl paraben in humans after oral administration. *Environ. Int.* 130, 104917.
- Song, S., He, Y., Huang, Y., Huang, X., Guo, Y., Zhu, H., Kannan, K., Zhang, T., 2020. Occurrence and transfer of benzophenone-type ultraviolet filters from the pregnant women to fetuses. *Sci. Total Environ.* 726, 138503.
- Soni, M.G., Carabin, I.G., Burdock, G.A., 2005. Safety assessment of esters of p-hydroxybenzoic acid (parabens). *Food Chem. Toxicol.* 43, 985–1015.
- Soni, M.G., Taylor, S.L., Greenberg, N.A., Burdock, G.A., 2002. Evaluation of the health aspects of methyl paraben: a review of the published literature. *Food Chem. Toxicol.* 40, 1335–1373.
- Suzuki, T., Kitamura, S., Kkota, R., Sugihara, K., Fujimoto, N., Ohta, S., 2005. Estrogenic and antiandrogenic activities of 17 benzophenone derivatives used as UV stabilizers and sunscreens. *Toxicol. Appl. Pharm.* 203, 9–17.
- Thigpen, A.E., Davis, D.L., Milatovich, A., Mendonca, B.B., Imperato-McGinley, J., Griffin, J.E., Francke, U., Wilson, J.D., Russell, D.W., 1992. Molecular genetics of steroid 5 alpha-reductase 2 deficiency. *J. Clin. Invest* 90, 799–809.
- Tsachaki, M., Birk, J., Egert, A., Odermatt, A., 2015. Determination of the topology of endoplasmic reticulum membrane proteins using redox-sensitive green-fluorescence protein fusions. *Biochim. Et. Biophys. Acta (BBA) - Mol. Cell Res.* 1853, 1672–1682.
- Varadi, M., Bertoni, D., Magana, P., Paramval, U., Pidruchna, I., Radhakrishnan, M., Tsenkov, M., Nair, S., Mirdita, M., Yeo, J., Kovalevskiy, O., Tunyasuvunakool, K., Laydon, A., Židek, A., Tomlinson, H., Hariharan, D., Abrahamson, J., Green, T., Jumper, J., Birney, E., Steinegger, M., Hassabis, D., Velankar, S., 2024. AlphaFold Protein Structure Database in 2024: providing structure coverage for over 214 million protein sequences. *Nucleic Acids Res* 52, D368–D375.
- Vela-Soria, F., Jiménez-Díaz, I., Rodríguez-Gómez, R., Zafra-Gómez, A., Ballesteros, O., Fernández, M.F., Olea, N., Navalón, A., 2011. A multiclass method for endocrine disrupting chemical residue analysis in human placental tissue samples by UHPLC-MS/MS. *Analytical. Methods* 3, 2073–2081.
- Wang, L., Asimakopoulos, A.G., Kannan, K., 2015. Accumulation of 19 environmental phenolic and xenobiotic heterocyclic aromatic compounds in human adipose tissue. *Environ. Int* 78, 45–50.
- Wang, J., Chai, X., Eriksson, U., Napoli, J.L., 1999. Activity of human 11-cis-retinol dehydrogenase (Rdh5) with steroids and retinoids and expression of its mRNA in extra-ocular human tissue. *Biochem J.* 338 (Pt 1), 23–27.
- Wang, R.S., Yeh, S., Tzeng, C.R., Chang, C., 2009. Androgen receptor roles in spermatogenesis and fertility: lessons from testicular cell-specific androgen receptor knockout mice. *Endocr. Rev.* 30, 119–132.
- Wang, M., Yu, Y., Tang, Y., Pan, C., Fei, Q., Hu, Z., Li, H., Zhu, Y., Wang, Y., Ge, R.-s., 2023. Benzophenone-1 and -2 UV-filters potentially inhibit human, rat, and mouse gonadal 3β-hydroxysteroid dehydrogenases: structure-activity relationship and in silico docking analysis. *J. Steroid Biochem. Mol. Biol.* 230, 106279.
- Watanabe, Y., Kojima, H., Takeuchi, S., Uramaru, N., Sanoh, S., Sugihara, K., Kitamura, S., Ohta, S., 2015. Metabolism of UV-filter benzophenone-3 by rat and human liver microsomes and its effect on endocrine-disrupting activity. *Toxicol. Appl. Pharm.* 282, 119–128.
- Wei, F., Mortimer, M., Cheng, H., Sang, N., Guo, L.H., 2021. Parabens as chemicals of emerging concern in the environment and humans: a review. *Sci. Total Environ.* 778, 146150.
- Wilson, J.D., 2001. The role of 5alpha-reduction in steroid hormone physiology. *Reprod. Fertil. Dev.* 13, 673–678.
- Wilson, J.D., Griffin, J.E., Russell, D.W., 1993. Steroid 5 alpha-reductase 2 deficiency. *Endocr. Rev.* 14, 577–593.
- Xue, J., Liu, W., Kannan, K., 2017. Bisphenols, benzophenones, and bisphenol A diglycidyl ethers in textiles and infant clothing. *Environ. Sci. Technol.* 51, 5279–5286.
- Yamada, G., Suzuki, K., Haraguchi, R., Miyagawa, S., Satoh, Y., Kamimura, M., Nakagata, N., Kataoka, H., Kuroiwa, A., Chen, Y., 2006. Molecular genetic cascades for external genitalia formation: an emerging organogenesis program. *Dev. Dyn.* 235, 1738–1752.
- Yang, Y.-J., Hong, Y.-P., Chae, S.A., 2016. Reduction in semen quality after mixed exposure to bisphenol A and isobutylparaben in utero and during lactation periods. *Hum. Exp. Toxicol.* 35, 902–911.
- Ye, X., Bishop, A.M., Reidy, J.A., Needham, L.L., Calafat, A.M., 2006. Parabens as urinary biomarkers of exposure in humans. *Environ. Health Perspect.* 114, 1843–1846.
- Zhang, L., Dong, L., Ding, S., Qiao, P., Wang, C., Zhang, M., Zhang, L., Du, Q., Li, Y., Tang, N., Chang, B., 2014. Effects of n-butylparaben on steroidogenesis and spermatogenesis through changed E2 levels in male rat offspring. *Environ. Toxicol. Pharmacol.* 37, 705–717.
- Zhu, L.-J., Hardy, M.P., Inigo, I.V., Huhtaniemi, I., Bardin, C.W., Moo-Young, A.J., 2000. Effects of androgen on androgen receptor expression in rat testicular and epididymal cells: a quantitative immunohistochemical study. *Biol. Reprod.* 63, 368–376.

## Supplementary information

**Supplementary Table 1. Information on tested compounds and suppliers.**

<b>Test compound</b>	<b>CAS number</b>	<b>Supplier</b>	<b>Purity</b>
<i>p</i> -hydroxybenzoic acid	99-96-7	Merck	99%
Methylparaben	99-76-3	Merck	99%
Ethylparaben	120-47-8	Merck	99%
Propylparaben	94-13-3	Merck	98%
Isopropylparaben	4191-73-5	Merck	98%
Butylparaben	94-26-8	Merck	99%
Hexylparaben	1083-27-8	Merck	≥ 95%
Heptylparaben	1085-12-7	Merck	≥ 95%
Phenylparaben	17696-62-7	Merck	≥ 95%
Benzylparaben	94-18-8	Merck	99%
Benzophenone-1	131-56-6	Merck	99%
Benzophenone-2	131-55-5	Merck	97%
Benzophenone-3	131-57-7	Merck	98%
Benzophenone-6	131-54-4	Merck	98%
Benzophenone-7	85-19-8	Merck	99%
Benzophenone-8	131-53-3	Merck	98%
Benzophenone-9	76656-36-5	Carbosynth	99.9%
Benzophenone-10	1641-17-4	Carbosynth	99.5%
Benzophenone-12	1843-05-6	Merck	98%
4-Hydroxybenzophenone	1137-42-4	Merck	98%
4,4'-Dihydroxybenzophenone	611-99-4	Merck	99%
2,4,4'-Trihydroxybenzophenone	1470-79-7	Merck	95%
Avobenzone	70356-09-1	Merck	99%
3-Benzylidenecamphor	36275-29-3	Merck	≥ 95%
3-(4-Methylbenzylidene)camphor	36861-47-9	Merck	98%

**Supplementary Table 2. Regulatory status of the compounds analyzed.**

List of the regulatory status of the parabens and UV-filters tested in this study in the European Union (EU) and the United States of America (US). Legal limits are indicated as percentages according to the respective regulations. Because UV-filters when used as active ingredients in sun creams are regulated differently from cosmetics and body care products in the US, both limits are included in the list. NA, not approved; NR, not regulated.

Test chemical	European Union	
	Cosmetics (Commission 2014, 2022, 2024)	Active sunscreen ingredient (FDA 1999)
<i>p</i> -hydroxybenzoic acid	0.4% (as acid) for single ester 0.8% (as acid) for mixtures of esters	-
Methylparaben	0.4% (as acid) for single ester 0.8% (as acid) for mixtures of esters	-
Ethylparaben	0.4% (as acid) for single ester 0.8% (as acid) for mixtures of esters	-
Propylparaben	0.14% (as acid) for single ester 0.8% (as acid) for mixtures of esters individual concentrations of butyl- and propylparaben and their salts do not exceed 0.14%	-
Butylparaben	0.14% (as acid) for single ester 0.8% (as acid) for mixtures of esters individual concentrations of butyl- and propylparaben and their salts do not exceed 0.14%	-
Hexylparaben	NR	-
Heptylparaben	NR	-
Isopropylparaben	prohibited according to annex II	-
Phenylparaben	prohibited according to annex II	-
Benzylparaben	prohibited according to annex II	-
Benzophenone-1	NR	NA
Benzophenone-2	NR	NA
Benzophenone-3	6%	6%
Benzophenone-6	NR	NA
Benzophenone-7	NR	NA
Benzophenone-8	NR	NA
Benzophenone-9	NR	NA
Benzophenone-10	NR	NA
Benzophenone-12	NR	NA
4-Hydroxybenzophenone	NR	NA
4,4'-Dihydroxybenzophenone	NR	NA
2,4,4'-Trihydroxybenzophenone	NR	NA
Avobenzone	5%	3%
3-Benzylidene camphor	prohibited according to annex II	NA
3-(4-Methylbenzylidene)camphor	prohibited according to annex II	NA

**Supplementary Table 3. Human pharmacokinetic parameters of methyl-, ethyl-, propyl-, and butylparaben after dermal application in humans.** Numbers of assessed test subjects, applied dose, maximal plasma concentration ( $C_{max}$ ), the corresponding time to reach  $C_{max}$  ( $T_{max}$ ) and the respective terminal half-life ( $T_{1/2}$ ) of parabens. NA, not assessed; <sup>(1)</sup> (Shin et al. 2023); <sup>(2)</sup> (Janjua et al. 2007).

**Pharmacokinetic parameters of parabens after dermal application**

<b>Test compound</b>	<b>Test subjects</b>	<b>Applied dose</b>	<b><math>C_{max}</math> (plasma)</b>	<b><math>T_{max}</math> (h)</b>	<b><math>T_{1/2}</math> (h)</b>
<b>Methylparaben</b>	5 <sup>(1)</sup>	0.26%	37±52 nM	4.9±2.8	7.2±1.9
<b>Ethylparaben</b>	5 <sup>(1)</sup>	0.26%	42±44 nM	5.4±1.9	10.5±3.9
<b>Propylparaben</b>	5 <sup>(1)</sup>	0.28%	23±20 nM	5.3±2.2	21.8±20.2
<b>Butylparaben</b>	26 <sup>(2)</sup>	2%	695±57 nM	3	NA

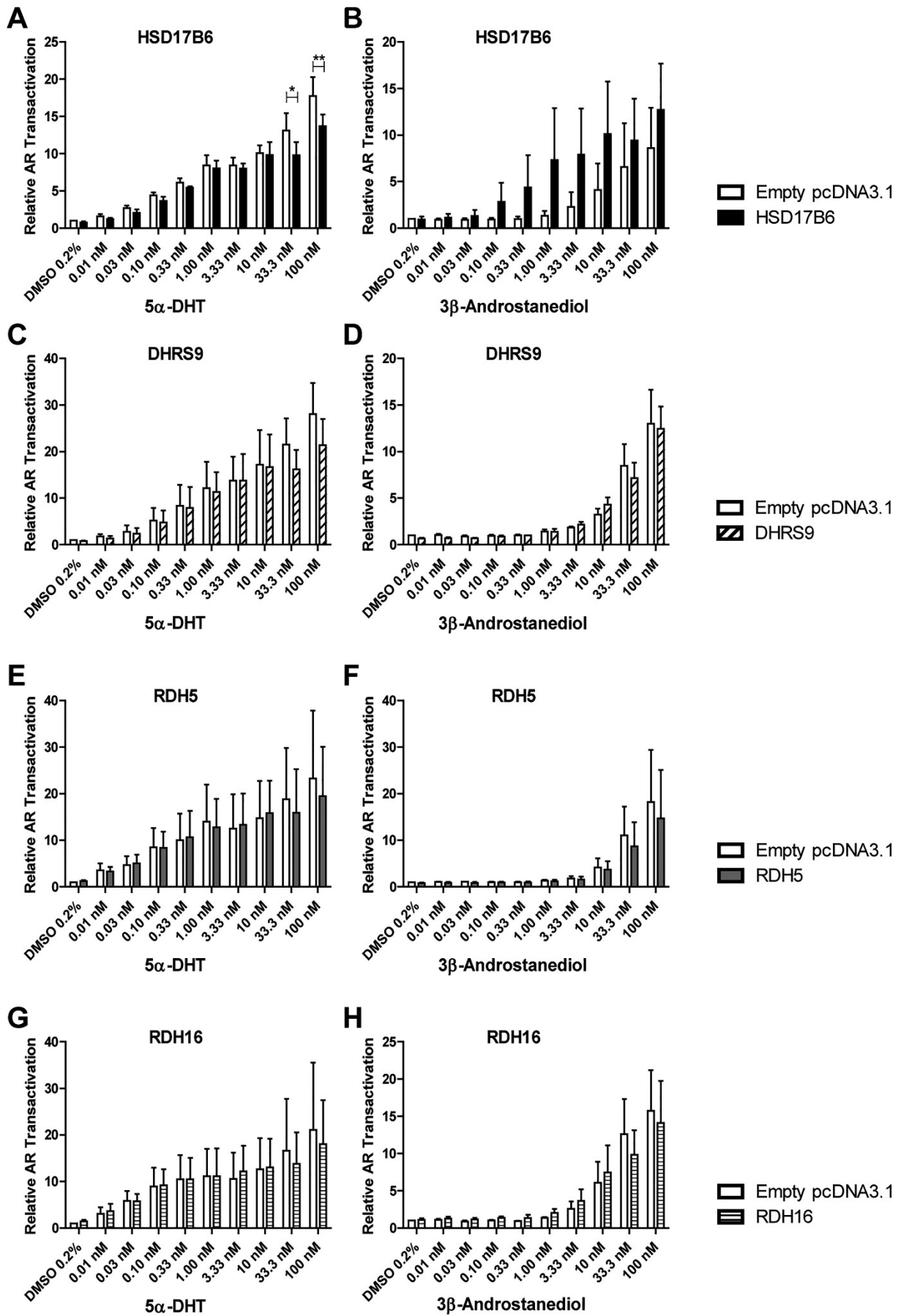
**Supplementary Table 4. Estimated concentrations of parabens in human breast and adipose tissues.** The amounts of methyl-, ethyl-, propyl-, and butylparaben in human tissues quantified in several studies were converted to tissue concentrations assuming the tissue densities indicated. Data represent either mean, geometric mean (GM) or median values measured in the respective studies as well as maximal measured amounts and calculated concentrations, respectively ( $C_{max}$ ) or the 75% percentile value (p75).

Tissue type	Breast cancer	Normal breast	Benign breast tumors (adenoma)	Malignant breast tumors (invasive)	Adipose tissue	
Assumed tissue density	0.98 g/mL (Farvid et al. 2005)				0.92 g/mL (Chan et al. 2019)	
	<u>Mean / <math>C_{max}</math></u> (ng/g) (nM)	<u>Median / <math>C_{max}</math></u> (ng/g) (nM)	<u>Mean / <math>C_{max}</math></u> (ng/g) (nM)	<u>Mean / <math>C_{max}</math></u> (ng/g) (nM)	<u>GM / <math>C_{max}</math></u> (ng/g) (nM)	<u>Mean / p75</u> (ng/g) (nM)
<b>Methylparaben</b>	12.8 / 29.3 82.4 / 189	16.6 / 5103 107 / 32868	150 / NI 965 / NI	173 / 239 1116 / 1537	- / 22.3 - / 135	0.57 / 0.71 3.4 / 4.3
<b>Ethylparaben</b>	2.0 / 7.4 11.8 / 43.6	3.4 / 500 20.1 / 2947	103 / NI 604 / NI	123 / 165 723 / 971	0.9 / 30.6 .0 / 169	0.08 / - 0.40 / -
<b>Propylparaben</b>	2.6 / 9.7 14.1 / 52.8	16.8 / 2053 91.4 / 11163	59.4 / NI 323 / NI	93.6 / 114 509 / 620	0.5 / 18.2 2.5 / 92.9	0.23 / 0.14 1.2 / 0.7
<b>Butylparaben</b>	2.3 / 11.5 11.6 / 58.0	5.8 / 95.4 29.3 / 481	45.2 / NI 228.3 / NI	82.9 / 115 418 / 579	- / 1.1 - / 5	-
<b>Reference</b>	(Darbre et al. 2004)	(Barr et al. 2012)	(Downs et al. 2023)		(Wang et al. 2015)	(Artacho-Cordón et al. 2019)

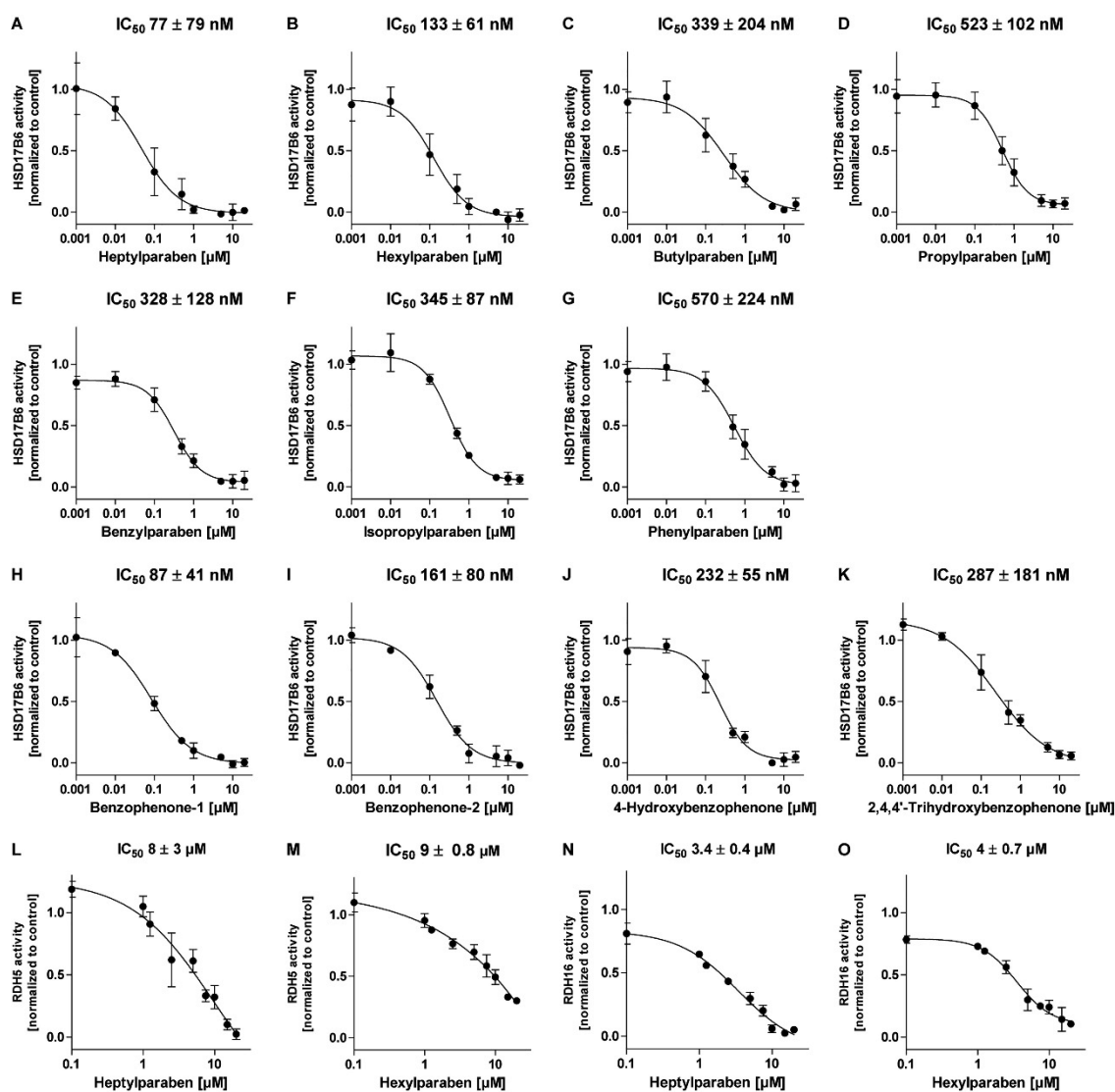


**Supplementary Table 5. Estimated concentrations of BP-3 in human breast and adipose tissue.** Amounts of BP-3 quantified in human tissues were converted to concentrations assuming the indicated tissue densities. Either mean or geometric mean (GM) values as well as maximal amounts and calculated concentrations ( $C_{max}$ ) or the 75% percentile value (p75) are indicated.

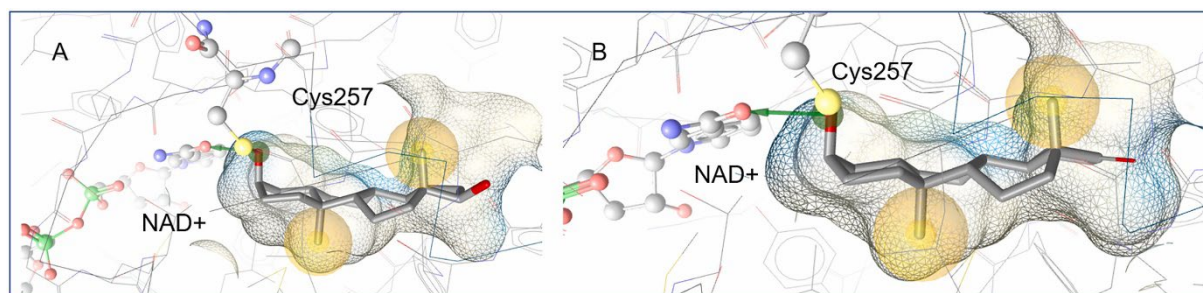
<b>Tissue type</b>	Normal breast tissue	Adipose tissue	
<b>Assumed tissue density</b>	0.98 g/mL (Farvid et al. 2005)	0.92 g/mL (Chan et al. 2019)	
	<u>Mean / <math>C_{max}</math></u> (ng/g) (nM)	<u>GM / <math>C_{max}</math></u> (ng/g) (nM)	<u>Mean / p75</u> (ng/g) (nM)
<b>Benzophenone-3</b>	2.4 / 26 10.3 / 112	43.4 / 4940 186 / 21211	1.1 / 0.6 4.5 / 2.4
<b>Reference</b>	(Barr et al. 2018)	(Wang et al. 2015)	(Artacho-Cordón et al. 2019)



**Supplementary Figure 1. Concentration-dependent AR transactivation by HSD17B6, DHRS9, RDH5, and RDH16 with DHT and 3 $\beta$ -androstenediol.** CV-1 cells were transfected with plasmids containing the genetic sequences of the human androgen receptor, a reporter gene construct expressed under an AR responsive promoter, and a plasmid for either HSD17B6 (A,B), DHRS9 (C,D), RDH5 (E,F) or RDH16 (G,H), or control vector pcDNA3.1, and a transfection control. Transfected cells were incubated with increasing concentrations of DHT (A,C,E,G) or 3 $\beta$ -androstenediol (B,D,F,H). AR transactivation was first normalized to the transfection control and then to the vector control treated with only 0.2% DMSO. Data represent mean  $\pm$  SD from three independent experiments. Statistical analysis was performed by two-way ANOVA. Significant statistical differences between tested enzyme and control vector are indicated. P values: \*, $<0.05$ , \*\*, $<0.01$ , \*\*\*, $<0.001$ , \*\*\*\*, $<0.0001$ .



**Supplementary Figure 2. Concentration-dependent inhibition of HSD17B6, RDH5 and RDH16 by parabens and BP UV-filters.** Lysates of HEK-293 cells expressing one of the three examined  $3\alpha$ -HSDs were incubated for 10 min (HSD17B6, RDH16) or 30 min (RDH5) at 37°C in the presence of 100 nM  $3\alpha$ -androsterone, containing 5.55 nCi of [9,11- $^3$ H(N)]- $3\alpha$ -androsterone, 500  $\mu$ M  $NAD^+$  and different concentrations of test compounds or vehicle control. The percentage of conversion of  $3\alpha$ -androsterone to  $5\alpha$ -androstanedione was analyzed by TLC separation of both steroids, on-plate derivatization and scintillation counting. Substrate conversion was normalized to vehicle control (0.1% DMSO). Concentration-response curves were fitted and analyzed by non-linear regression and data represent mean  $\pm$  SD from three independent experiments.



**Supplementary Figure 3. Binding poses of HSD17B6 substrates by the homology model.**

Predicted docking poses of **(A)** 3 $\alpha$ -androstanediol and **(B)** 3 $\alpha$ -androsterone in the binding site of the HSD17B6 homology model. Yellow spheres represent hydrophobic interactions and the green arrow indicate a hydrogen bond donor interaction.

### 5.3 Discussion

Parabens and UV-filters have been mainly analyzed for their direct effects on the AR while pre-receptor control by androgen biosynthesis was only partially considered. The effects of parabens on enzymes involved in androgen biosynthesis have not yet been investigated, whereas possible influences of certain benzophenones on the activities of enzymes involved in the classical DHT synthesis pathway, such as HSD3B1, HSD3B2, HSD17B3, and AKR1C3, have been studied previously. While 4-methoxylated BPs such as BP-3, -8 and -10 showed no significant effect on the steroidogenic enzymes studied, micromolar IC<sub>50</sub> values for HSD3B1, HSD3B2 and HSD17B3 have been demonstrated for BP-1 (7.55 μM, 5.66 μM and 1.05 μM, respectively) and BP-2 (5.90 μM, 5.84 μM and 18.1 μM) [247, 320]. AKR1C3, which similar to HSD17B3 converts androstenedione to testosterone, was not inhibited by either BP-1 or BP-2 [247].

In this project, we described parabens and UV-filters as the first xenobiotics that inhibit HSD17B6 in the backdoor pathway of DHT generation with IC<sub>50</sub> values in the medium and high nanomolar range. Similar to the steroidogenic enzymes in the classical pathway, 4-methoxylated BPs such as BP-3, -8 and -10 showed no inhibitory effects on HSD17B6. Using the HSD17B6 homology model generated for this project, we were able to predict that an additional methyl group probably prevents the formation of a hydrogen bond of the 4-hydroxy group with the cofactor NAD<sup>+</sup> in the active site of HSD17B6.

BP-3 has been described as inactive in several studies on steroidogenic enzymes of androgen biosynthesis, including the one completed in this project. BP-3, however, is metabolized in the human body to 4-hydroxylated BPs such as BP-1, BP-2, 4-hydroxy-BP and 4,4'-dihydroxy-BP, which show inhibitory effects against the steroidogenic enzymes in both the classical and backdoor pathways of DHT synthesis [228, 247, 249, 320-324]. Accordingly, a full safety assessment of BP-3 should also cover its metabolism. Available studies so far did not include simultaneous measurements of all known human BP-3 metabolites which should be addressed through further experimentation. In addition, BP-3 metabolism has been described as possibly age- and population-dependent, which should be taken into account [243]. Determination of the individual proportions of all BP-3 metabolites after topical or oral exposure could provide important information on its toxicokinetics and possibly serve as the starting point for a physiologically based toxicokinetic (PBTK) model (reviewed in [325]).

Parabens are continuously hydrolyzed in the skin and liver and, like BPs, are conjugated with glucuronide and sulfate for renal excretion [214, 218-222, 243, 326]. It is not yet known whether parabens and BPs can accumulate in tissues that are actively involved in androgen

biosynthesis, such as the testis, prostate and liver, or in what proportions they are present in their unconjugated forms. Further studies should quantify concentrations of parabens and UV-filters in several tissue types so that possible antiandrogenic effects during early male fetal development or during childhood and adolescence can be assessed.

Like the BPs identified in this project as HSD17B6 inhibitors, parabens have a 4-hydroxylated phenyl group with which they can form a hydrogen bond with the amide group of the cofactor NAD<sup>+</sup> in the binding pocket of the HSD17B6 homology model. This bond may be additionally stabilized by  $\pi$ -stacking of the aromatic ring of the phenyl group with the aromatic ring of Tyr208. However, this 4-hydroxy moiety of the phenyl group is not only relevant for the inhibitory capacity against HSD17B6, but has also been described as crucial for the inhibition of HSD3B1, HSD3B2 and HSD17B3 by BP-1 and BP-2 [247, 320]. Whether the structurally similar parabens have an antiandrogenic effect by inhibiting these three enzymes of the classic pathway of DHT biosynthesis could be addressed experimentally. Other, not yet assessed steroidogenic enzymes relevant for androgen biosynthesis, such as SRD5A1, SRD5A2 or AKR1C2 and AKR1C4, should also be investigated for possible inhibition by parabens and UV-filters.

Additive or synergistic effects through simultaneous inhibition of several enzymes in the classical and/or backdoor pathway could hypothetically arise after exposure towards the xenobiotics investigated in this project. However, such effects cannot be properly investigated with single enzyme activity assays. Endogenous cell models, which cover large parts of male androgen biosynthesis, may be better suited for this purpose.

The H295R cell line, which expresses genes encoding all the key enzymes for steroidogenesis, has so far been used as an *in vitro* screening model according to OECD guidelines to detect changes in estradiol and testosterone biosynthesis caused by xenobiotics [327]. However, H295R cells were isolated from an adrenal tumor, which is why they produce only low amounts of *de novo* testosterone from androstenedione by AKR1C3 instead of HSD17B3 [328, 329]. HSD17B3 is expressed exclusively in testicular Leydig cells and is essential for the male *in utero* development, especially for the normal formation of male external genitalia [89]. Except for the last enzymatic step, the reduction of testosterone to DHT, all reactions of the classical DHT synthesis pathway can be catalyzed *in vivo* by Leydig cells [87]. Establishment of a human Leydig model cell line may be useful for screening xenobiotics in future toxicological studies with regard to possible antiandrogenic effects that could affect early male development. So far, only murine Leydig cell lines are available commercially. However, several of these cell models, such as MA-10, BLTK1, and TM3, have been demonstrated to be

nearly incapable of producing testosterone [330]. Possible antiandrogenic activities of xenobiotics through inhibition of enzymes involved in androgen biosynthesis could be identified by quantifying testosterone synthesis in a novel human Leydig cell model. If a test substance affects testosterone synthesis, the overall steroid profile of androgens could be measured in treated and untreated cells. Similar to what has been done earlier with the H295R steroidogenesis cell model, the product to substrate ratios of the different enzymatic steps may then be calculated to pinpoint which enzymatic reaction steps of the androgen biosynthesis pathway are affected [331].

Certain prostate cancer model cell lines, such as vertebral cancer of the prostate (VCaP) cells express enzymes required for the backdoor pathway of DHT synthesis, such as CYP17A1, HSD3B1, HSD3B2, SRD5A1, SRD5A2, AKR1C2, AKR1C3, and HSD17B6 [332-335]. Hence, VCaP cells may be suitable in screenings for alterations in DHT biosynthesis via the backdoor pathway caused by chemicals. This cell line has been shown to convert both 3 $\alpha$ - and 3 $\beta$ -adiol to DHT, indicating HSD17B6 activity [336]. However, the functional redundancy of multiple expressed 3 $\alpha$ -HSDs in such prostate cancer cell lines may complicate a clear interpretation for the final step of DHT biosynthesis in the backdoor pathway. VCaP cells, for example, have been shown to express RDH5 and RDH16 in addition to HSD17B6 [335, 337]. To establish such a cell line as a model for the backdoor pathway, its 3 $\alpha$ -HSDs activity ought to be characterized in detail and it should be clarified if several 3 $\alpha$ -HSDs are expressed and whether the individual enzymes can compensate each other's activities. Knockout variants of such cell lines could be generated if necessary, so that only one 3 $\alpha$ -HSD is expressed at a time. Possible antiandrogenic effects of xenobiotics by specific HSD17B6 inhibition may be investigated through 3 $\beta$ -adiol conversion to DHT. HSD17B6 is so far the only described 3 $\alpha$ -HSD that accepts 3 $\beta$ -adiol as substrate [299, 338].

Treatment of prostate cancers with androgen deprivation therapy in human patients was associated with increased intratumoral HSD17B6 expression levels, an effect that is also observed after castration of orthotopic human prostate cancer xenograft models [334, 336]. This might be a compensatory mechanism that counteracts androgen deprivation. HSD17B6 was therefore proposed as a potential therapeutic target, in particular as a complementary measure to existing ADT approaches, which aim for inhibition of enzymes of the classical pathway of DHT synthesis [337].

Additionally, HSD17B6 is expressed in several regions of the brain and can convert the neurosteroids allopregnanolone, 3 $\alpha$ -androsterone and 3 $\alpha$ -adiol to their as neurosteroid inactive 3-keto forms through its oxidative 3 $\alpha$ -HSD activity [298, 299]. Allopregnanolone,



3 $\alpha$ -androsterone and 3 $\alpha$ -adiol act as direct allosteric modulators of  $\gamma$ -aminobutyric acid type A (GABA<sub>A</sub>) receptors. The binding of these neurosteroids to the GABA<sub>A</sub> receptor is dependent on the 3 $\alpha$ -hydroxyl group and leads to a greatly increased opening probability of the GABA<sub>A</sub> receptor chloride channel. This increased chloride flux through the channel results in a reduction in neuronal excitability [339-343]. Said three neurosteroids act primarily as anticonvulsants and may display anxiolytic effects, which is why they have been evaluated together with neurosteroid-like agents as potential treatments for various types of epilepsy and anxiety [341, 344-349]. Reduced levels of allopregnanolone in the human cerebrospinal fluid (CSF) have been associated with depression and posttraumatic stress disorder (PTSD) [350-352]. Antidepressant pharmacotherapy led to normalization of initially lower allopregnanolone levels in the CSF of depressed patients where the symptomatology improvement was correlated with the increased allopregnanolone levels [350]. Similar results were shown in a rat model for depression, where chronic treatment with antidepressants reversed the decline in cerebrocortical allopregnanolone levels [353].

Whether inhibiting 3 $\alpha$ -HSD activity of HSD17B6 in the brain, and the presumed higher neurosteroid levels associated with such an inhibition, could have a therapeutic benefit, has not yet been studied. The in this project established radiometric activity assay would allow screening to find specific HSD17B6 inhibitors. Subsequently, such inhibitors could be further assessed for potentially therapeutic effects in prostate cancer treatment or in neurological disorders such as epilepsy, anxiety and depression.

This project harbors strong potential for follow-up studies in which the established methodology for the assessment of 3 $\alpha$ -HSD activity and the HSD17B6 homology model may be of practical use.

## **6. Project 3: Activation of retinoic acid-related orphan receptor $\gamma(t)$ by parabens and benzophenone UV-filters**

### 6.1 Introduction

ROR $\gamma t$ , the shorter isoform ROR $\gamma$ , is a constitutively active nuclear receptor exclusively expressed in immune cells, including double-positive (CD4<sup>+</sup> CD8<sup>+</sup>) thymocytes, Th17 cells, and ILC3 [354]. It regulates the expression of pro-inflammatory cytokines like IL17A, IL17F, and IL22, among others [188, 189, 355, 356]. ROR $\gamma t$  is essential for the differentiation of naïve CD4<sup>+</sup> T cells into Th17 cells which protect hosts against infections by extracellular fungi and bacteria [188, 357]. ROR $\gamma t$  overactivation has been associated with enhanced inflammation in autoimmune diseases such as rheumatoid arthritis, psoriasis, glomerulonephritis, multiple sclerosis and Crohn's disease [190, 358].

Mouse ROR $\gamma$  null mutants were protected against the development of Th17-dependent inflammation in several autoimmune disease models, which is why ROR $\gamma t$  was considered a potential therapeutic target [188, 190, 191]. Several natural as well as artificially produced inverse agonists of ROR $\gamma t$  have been identified so far. Some, such as digoxin or SR2211 have been found to alleviate Th17-dependent inflammation in experimental rodent autoimmune disease models [359-365].

Possible beneficial uses of artificial ROR $\gamma t$  agonists such as SR1078, SR0987 or natural agonists such as genistein and digoxigenin are currently debated. In particular, possible improvements in host defense against fungal and bacterial infections through additional ROR $\gamma t$  activity as well as their potential in cancer treatment are discussed, where ROR $\gamma t$ -mediated lymphocyte stimulation could improve immune defense against tumors [366-370]. Whether excessive activation of ROR $\gamma t$ , for example through exposure to agonistic xenobiotics may exacerbate existing inflammatory conditions, such as autoimmune diseases has barely been looked at.

Additives used in cosmetics and body care products such as parabens and UV-filters have already been partially examined for possible ROR $\gamma(t)$ -modulating activity in the U.S. Tox21 program using high-throughput screenings [371]. Those screenings indicated possible ROR $\gamma(t)$  activity-altering effects for certain compounds, but the results were partly inconclusive due to technical limitations. Since a large proportion of the human population can be considered exposed to parabens and UV-filters, we investigated the influence of these compounds on ROR $\gamma(t)$  activity in more detail. Based on the ROR $\gamma(t)$  agonists identified in this study and those already known from the literature, we performed a computational similarity search in a database of body care constituents to identify additional agonists which we then also

assessed on their activity towards ROR $\gamma$ (t). Since several of such compounds may be used together in body care products, we also investigated compound mixtures and addressed the possibility of additive or synergistic effects. Finally, we used computational modeling to investigate the binding modes of the identified ROR $\gamma$ (t) agonists.

## 6.2. Published article: Activation of retinoic acid-related orphan receptor $\gamma(t)$ by parabens and benzophenone UV-filters

Silvia G. Inderbinen<sup>a,b,1</sup>, Manuel Kley<sup>a,b,1</sup>, Michael Zogg<sup>a</sup>, Manuel Sellner<sup>c</sup>, André Fischer<sup>c</sup>, Jacek Kędzierski<sup>b,c</sup>, Stéphanie Boudon<sup>b</sup>, Anton M. Jetten<sup>d</sup>, Martin Smieško<sup>b,c</sup>, Alex Odermatt<sup>a,b,\*</sup>

<sup>a</sup> Division of Molecular and Systems Toxicology, Department of Pharmaceutical Sciences, University of Basel, Klingelbergstrasse 50, 4056 Basel, Switzerland

<sup>b</sup> Swiss Centre for Applied Human Toxicology and Department of Pharmaceutical Sciences, University of Basel, Missionsstrasse 64, 4055 Basel, Switzerland

<sup>c</sup> Computational Pharmacy, Department of Pharmaceutical Sciences, University of Basel, Klingelbergstrasse 61, 4056 Basel, Switzerland

<sup>d</sup> Immunity, Inflammation, and Disease Laboratory, National Institute of Environmental Health Sciences, National Institutes of Health, 111. T.W. Alexander Drive, Research Triangle Park, NC 27709, USA

\* Corresponding author. e-mail address: alex.odermatt@unibas.ch

### Published article

**Personal contribution:** Completion and repetition of experimental screening experiments and concentration dependent activation of ROR $\gamma(t)$  by parabens and UV-filters (Figures 1 to 3). Experimental assessment of mixture effects of test compounds (Figure 5). Revision of pre-existing paper draft and data analysis.

**Aims:** Assessment of whether parabens and UV-filters alone or as mixtures may affect ROR $\gamma(t)$  activity.

**Conclusion:** Several parabens and benzophenone-type UV-filters have been identified as novel ROR $\gamma(t)$  agonists with EC<sub>50</sub> values in the nanomolar and lower micromolar range. Those newly identified agonists enhanced pro-inflammatory cytokine expression in the mouse EL4 T-lymphocyte cell model. Similarity search using a cosmetics database revealed additional additives with agonistic activity on ROR $\gamma(t)$ . Mixtures of the newly identified agonists displayed additive effects on ROR $\gamma(t)$  activity.



## Activation of retinoic acid-related orphan receptor $\gamma(t)$ by parabens and benzophenone UV-filters

Silvia G. Inderbinen<sup>a,b,1</sup>, Manuel Kley<sup>a,b,1</sup>, Michael Zogg<sup>a</sup>, Manuel Sellner<sup>c</sup>, André Fischer<sup>c</sup>, Jacek Kędzierski<sup>b,c</sup>, Stéphanie Boudon<sup>b</sup>, Anton M. Jetten<sup>d</sup>, Martin Smieško<sup>b,c</sup>, Alex Odermatt<sup>a,b,\*</sup>

<sup>a</sup> Division of Molecular and Systems Toxicology, Department of Pharmaceutical Sciences, University of Basel, Klingelbergstrasse 50, 4056 Basel, Switzerland

<sup>b</sup> Swiss Centre for Applied Human Toxicology and Department of Pharmaceutical Sciences, University of Basel, Missionsstrasse 64, 4055 Basel, Switzerland

<sup>c</sup> Computational Pharmacy, Department of Pharmaceutical Sciences, University of Basel, Klingelbergstrasse 61, 4056 Basel, Switzerland

<sup>d</sup> Immunity, Inflammation, and Disease Laboratory, National Institute of Environmental Health Sciences, National Institutes of Health, 111. T.W. Alexander Drive, Research Triangle Park, NC 27709, USA

### ARTICLE INFO

Handling Editor: Dr. Thomas Knudsen

#### Key words:

Retinoic acid-related orphan receptor gamma

Paraben

UV-filter

Th17 cell

Immune disease

Inflammation

### ABSTRACT

Retinoic acid-related orphan receptor  $\gamma t$  (ROR $\gamma t$ ) regulates immune responses and its impaired function contributes to inflammatory and autoimmune diseases and may promote skin cancer. Synthetic inverse ROR $\gamma t$  agonists block the production of Th17-associated cytokines including interleukin (IL)-17A and IL-22 and are under investigation for treatment of such pathologies. Unintentional ROR $\gamma t$  activation in skin, following exposure to environmental chemicals, may promote inflammatory skin disease. Parabens and UV-filters, frequently used as additives in cosmetics and body care products, are intensively inspected for endocrine disrupting properties. This study assessed whether such compounds can interfere with ROR $\gamma$  activity using a previously established tetracycline-inducible reporter gene assay in CHO cells. These transactivation experiments revealed hexylparaben, benzylparaben and benzophenone-10 as ROR $\gamma$  agonists (EC<sub>50</sub> values: 144 ± 97 nM, 3.39 ± 1.74 μM and 1.67 ± 1.04 μM, respectively), and they could restore ROR $\gamma$  activity after suppression by an inverse agonist. Furthermore, they enhanced ROR $\gamma t$ -dependent transcription of the pro-inflammatory IL-17A and/or IL-22 genes in the murine T-cell model EL4. Virtual screening of a cosmetics database for structurally similar chemicals and *in vitro* testing of the most promising hits revealed benzylbenzoate, benzylsalicylate and 4-methylphenylbenzoate as ROR $\gamma$  agonists (low micromolar EC<sub>50</sub> values). Moreover, an analysis of mixtures of the newly identified ROR $\gamma$  agonists suggested additive effects. This study presents novel ROR $\gamma(t)$  agonistic structural scaffolds. By activating ROR $\gamma(t)$  the identified parabens and UV-filters may potentially aggravate pathophysiological conditions, especially skin diseases where highest exposure of such chemicals can be expected. Follow-up studies should assess whether such compounds, either alone or as mixtures, can reach relevant concentrations in tissues and target cells to activate ROR $\gamma(t)$  *in vivo*.

### 1. Introduction

Retinoic acid-related orphan receptors (RORs) are nuclear receptors acting as ligand-dependent transcription factors. RORs are involved in multiple physiological functions, including lipid and glucose

metabolism, immune response, and circadian rhythm (Jetten, 2009). ROR $\gamma$  and its shorter isoform ROR $\gamma t$  share the same ligand binding domain (LBD) and are expressed in distinct cells and tissues, thereby exerting different biological functions (He et al., 1998; Villey et al., 1999). ROR $\gamma$  is widely expressed in peripheral tissues, including liver,

**Abbreviations:** 3-BC, 3-benzylidene camphor; 4-MBC, 4-methylbenzylidene camphor; DMSO, dimethyl sulfoxide; ECFP, Extended Connectivity Fingerprint; IL-17A, interleukin-17A; IL-22, interleukin-22; ILC3, innate lymphoid cells 3; LBD, ligand binding domain; PCR, polymerase chain reaction; PMA, phorbol 12-myristate 13-acetate; PPIA, peptidylprolyl isomerase A; ROR $\gamma$ , retinoic acid-related orphan receptor gamma; Th17, T helper 17.

\* Corresponding author at: Division of Molecular and Systems Toxicology, Department of Pharmaceutical Sciences, University of Basel, Klingelbergstrasse 50, 4056 Basel, Switzerland.

E-mail address: [alex.odermatt@unibas.ch](mailto:alex.odermatt@unibas.ch) (A. Odermatt).

<sup>1</sup> These authors contributed equally to the presented study.

<https://doi.org/10.1016/j.tox.2022.153159>

Received 3 December 2021; Received in revised form 9 March 2022; Accepted 17 March 2022

Available online 23 March 2022

0300-483X/© 2022 The Author(s). Published by Elsevier B.V. This is an open access article under the CC BY license (<http://creativecommons.org/licenses/by/4.0/>).

adipose tissue, skeletal muscle and kidney (Hirose et al., 1994; Jetten et al., 2013; Medvedev et al., 1996). In contrast, ROR $\gamma$ t is specifically expressed in a group of immune cells, including T helper 17 cells (Th17) and innate lymphoid cells 3 (ILC3) (Ivanov et al., 2006; Montaldo et al., 2015), and was found to be associated with enhanced inflammation in autoimmune disorders, such as psoriasis, rheumatoid arthritis, multiple sclerosis and Crohn's disease (Miossec and Kolls, 2012). For example, in mouse psoriasis models ROR $\gamma$ t positive ILC3 account for the production of the proinflammatory IL-17A and the potent keratinocyte growth factor IL-22 (Pantelyushin et al., 2012) and levels of this cell type are increased in human psoriatic skin (Cai et al., 2011; Villanova et al., 2014). Upregulation of ROR $\gamma$ t and elevated levels of IL-17A and IL-22 producing tissue-resident memory CD8 positive T cells have been observed in skin from patients with psoriatic arthritis (Leijten et al., 2021). Furthermore, chronic UV-radiation exposure induces a local immune shift toward ROR $\gamma$ t positive IL-17A/IL-22 producing ILC3 that are involved in mutant skin cell growth, thus promoting skin cancer (Lewis et al., 2021).

Mice lacking ROR $\gamma$ t were protected against the development of Th17-dependent inflammation in autoimmune disease models (Ivanov et al., 2006; Yang et al., 2008). This raised the interest for ROR $\gamma$ t as potential drug target to treat such disorders and several small molecules inhibiting ROR $\gamma$ t have been developed and were shown to ameliorate autoimmune and inflammatory pathologies in animal models (reviewed in Fauber and Magnuson, 2014; Jetten and Cook, 2020; Sun et al., 2019). For instance, treatment with ROR $\gamma$ t inhibitors reduced the expression of IL-17A and IL-22, which stimulated the release of proinflammatory cytokines and chemokines from primary human lung cells and in allergic airway inflammation in mice (Chung et al., 2006; Lamb et al., 2021; Pan et al., 2013; Zheng et al., 2007). Additionally, natural compounds such as ursolic acid and digoxin and some azole antifungals were found to inhibit ROR $\gamma$ t, thereby reducing IL-17A gene expression (Huh et al., 2011; Kojima et al., 2012; Xu et al., 2011).

RORs are thought to be constitutively active, suggesting that coactivators can activate ROR-mediated gene expression even in the absence of active ligands (Solt et al., 2010), or that they are constantly activated by endogenous (not yet identified) ligands present in cultured cells. Nevertheless, basal ROR $\gamma$ (t) activity can be further enhanced by agonists interacting with the LBD (Strutzenberg et al., 2019). In contrast to numerous inhibitors, only few studies described exogenous substances that activate ROR $\gamma$ (t), including the synthetic SR1078 (Wang et al., 2010) and SR0987 (Chang et al., 2016), and natural compounds such as digoxigenin (Karaš et al., 2018) and isoflavones (Kojima et al., 2015).

The effects of ROR $\gamma$ t activators have not been fully elucidated and are likely highly tissue- and context-dependent. Their benefit in the support of the host defense against bacterial and fungal infections that are defeated by Th17 cell-dependent mechanisms has been suggested (Kojima et al., 2015; Solt and Burris, 2012). Other reports postulated their potential in cancer treatment, with the strategy of using Th17 cells in adaptive immune cancer therapy (Bailey et al., 2014; Chang et al., 2016; Hu et al., 2016; Martin-Orozco et al., 2009). However, by enhancing Th17 cell-dependent pro-inflammatory mediators, ROR $\gamma$ t agonists may aggravate inflammatory and autoimmune diseases. Thus, it is important to identify xenobiotics that may lead to unintentional ROR $\gamma$ t activation.

Body care products and cosmetics contribute considerably to the exposure of humans to exogenous chemicals. Many of these products contain several paraben and UV-filter chemicals and their potential endocrine disrupting effects are of broad concern, widely studied but controversially discussed (Darbre and Harvey, 2014; Krause et al., 2012; Matwiejczuk et al., 2020; Nowak et al., 2018; Wang et al., 2016). In contrast, less is known on potential immune disrupting effects and xenobiotics-induced ROR $\gamma$  activation may disrupt immune responses. The U.S. Tox21 program included a quantitative high-throughput screening to detect small molecule antagonists of ROR $\gamma$  (PubChem, 2015), suggesting that some parabens and benzophenone UV-filters

might modulate the activity of this receptor. However, the data was inconclusive due to technical limitations of the high-throughput screening approach and some of the tested parabens and benzophenone UV-filters were cautiously suggested as potential ROR $\gamma$  agonists, without further elucidation.

Parabens have a broad spectrum of preservative effects and they are widely used as additives in cosmetics, medicines and processed foods to maintain long-term stability (CIR, 2008; Nowak et al., 2018). Parabens are esters of *p*-hydroxybenzoic acid (also described as 4-hydroxybenzoic acid) characterized by low production costs, excellent chemical stability and generally considered to be well tolerated (Matwiejczuk et al., 2020). Nevertheless, based on *in vitro* studies, parabens have been associated with disturbances of estrogen receptor function and estrogen metabolizing enzymes (Boberg et al., 2010; Darbre and Harvey, 2008; Engeli et al., 2017). Additionally, anti-androgenic properties of parabens were reported and a recent study described interferences with additional nuclear receptors (Chen et al., 2007; Ding et al., 2017; Fujino et al., 2019; Satoh et al., 2005). The relevance of these observations regarding human exposure scenarios remains to be investigated. Exposure to parabens mainly takes place through oral intake and transdermal absorption. Due to the rapid hepatic and intestinal hydrolysis, topical application of paraben containing cosmetic products is considered as the main route of human exposure, with a higher contribution to circulating levels compared to oral intake (Matwiejczuk et al., 2020).

Most sunscreens contain high levels of several UV-filter chemicals that can absorb and dissipate UV-radiation to protect the skin of the users from sunburn, ultimately preventing skin aging and skin cancer (Bens, 2014). Additionally, UV-filters are additives in multiple cosmetic products such as hair spray, shampoo, make-up, perfumes, and skin care products to protect ingredients from the effects of UV-radiation and consequently enhance product stability and durability (Liao and Kannan, 2014). An increasing number of human cell- and yeast-based *in vitro* studies and animal investigations suggest that some organic UV-filters can cause endocrine disrupting effects, including estrogenic and androgenic disturbances, as well as disturbances of thyroid hormone- and progesterone receptor-mediated signaling (reviewed in Krause et al., 2012; Kunz and Fent, 2006; Schlecht et al., 2004; Wang et al., 2016). Similar to parabens, the main route of human exposure to UV-filters is *via* dermal uptake after topical application of sunscreens and cosmetics, allowing direct entrance to the systemic circulation without first-pass effect in the liver (Krause et al., 2012; Sarveiya et al., 2004). Importantly, human exposure to UV-filters is not limited to summer and usage of sun cream, suggesting that a substantial exposure derives from other body care products (Calafat et al., 2008).

Considering its important function in skin and preliminary indications from Tox21 data, the present study further tested the hypothesis that ROR $\gamma$ (t) might be modulated by parabens and UV-filters, to which the majority of the human population is regularly exposed, by assessing the effect of such chemicals on ROR $\gamma$ (t) transcriptional activity. To detect additional ROR $\gamma$ (t) modulating chemicals, a computational similarity search was performed using the identified compounds and known ROR $\gamma$ (t) modulators analyzed against a database containing more than 6000 constituents of body care products. Since most cosmetic products contain several parabens and UV-filters, effects of mixtures of the examined compounds on ROR $\gamma$ (t) activity were assessed. Finally, the binding modes of methylparaben and hexylparaben were inspected by computational modeling to deduce structural elements responsible for their diverging activity towards ROR $\gamma$ (t).

## 2. Materials and methods

### 2.1. Chemicals and reagents

GSK2981278, SR2211, SR0987, phorbol 12-myristate 13-acetate (PMA), and ionomycin were purchased from Cayman Chemicals (Ann Arbor, MI, USA), benzophenone-9 and benzophenone-10 from

Carbosynth (Compton, UK), and the remaining benzophenone derivatives, 3-benzylidene camphor (3-BC) and 4-methylbenzylidene camphor (4-MBC) from Merck AG (Glattbrugg, Switzerland). All other chemicals were obtained from Sigma-Aldrich (Buchs, Switzerland). RPMI-1640 cell culture medium (R8758) was purchased from Sigma-Aldrich, Ham's F12 Nutrient Mix (21765-029) from Gibco (Thermo Fischer Scientific, Waltham, MA, USA), fetal bovine serum (FBS, S1810-500) from Biowest (Nuaille, France) and defined FBS for the use in Tet-on systems (HyClone, SH30070) from Cytiva (Marlborough, MA, USA).

## 2.2. Cell culture

Chinese hamster ovary (CHO) cells stably expressing a doxycycline-inducible ROR $\gamma$  Tet-on system (Slominski et al., 2014) were cultured in Ham's F12 Nutrient Mix medium supplemented with 10% defined FBS, 100 U/mL penicillin and 0.1 mg/mL streptomycin. RPMI-1640 medium supplemented with 10% FBS, 100 U/mL penicillin, 0.1 mg/mL streptomycin and 50  $\mu$ M  $\beta$ -mercaptoethanol was used to culture the murine EL4 T-cell line, in suspension in 75 cm<sup>2</sup> cell culture flasks from Falcon (Corning Inc., Corning, NY, USA). Both cell lines were cultured under standard conditions (37 °C, 5% CO<sub>2</sub>).

## 2.3. ROR $\gamma$ -reporter gene assays

The CHO ROR $\gamma$  Tet-on cell line used in this study is a well-established reporter gene system to assess ROR $\gamma$  agonists and antagonists. This cell model bears a tetracycline-inducible ROR $\gamma$  expression cassette and a ROR response element (RORE)-dependent luciferase reporter gene that is activated upon binding of ROR $\gamma$  to the RORE (Slominski et al., 2014). CHO ROR $\gamma$  Tet-on cells were seeded in 96-well plates at a density of 2000 cells/100  $\mu$ L culture medium, followed by incubation overnight. Subsequently, the medium was renewed, and the respective test compound dissolved in dimethylsulfoxide (DMSO) was added to the wells using a HP D300 Digital Liquid Dispenser with T8 dispense heads (HP Inc., Palo Alto, CA, USA). In experiments using ROR $\gamma$  inverse agonist, SR2211, was added at a final concentration of 1.25  $\mu$ M, simultaneously with the test compound. Two hours later, ROR $\gamma$  expression was induced by adding doxycycline at 1  $\mu$ M final concentration. All samples were adjusted to contain the same volume and concentration of DMSO. After 16 h of incubation, cells were washed with PBS, lysed with 20  $\mu$ L Tropix lysis solution (Applied Biosystems, Foster City, CA, USA) containing 1 mM dithiothreitol and frozen at -80 °C for at least 20 min. Luciferase activity was measured with a Cytation 5 reader (BioTek, Winooski, VT, USA) or SpectraMax L Microplate Reader (Molecular Devices, San Jose, CA, USA), injecting 100  $\mu$ L D-luciferin substrate solution [0.56 mM D-luciferin, 63 mM ATP, 0.27 mM CoA, 0.13 mM EDTA, 33.3 mM dithiothreitol, 8 mM MgSO<sub>4</sub>, 20 mM tricine (pH 7.8)] to 10  $\mu$ L of corresponding cell lysates, prepared on pure grade white 96-well micro-titration plates (BRAND, Wertheim, Germany). Measured values were normalized to values from control cells treated with DMSO vehicle control only and induced with doxycycline.

## 2.4. Measurement of IL-17A and IL-22 mRNA expression in EL4 cells

EL4 cells were transfected with plasmid encoding the human variant of ROR $\gamma$ t by electroporation and seeded into 12-well plates (500,000 cells and 1.6  $\mu$ g plasmid in 2 mL cultivation medium per well). Transfection was performed using the Neon<sup>TM</sup> transfection system (Invitrogen, Carlsbad, CA, USA) as follows:  $1.8 \times 10^6$  cells and 6  $\mu$ g plasmid in 100  $\mu$ L buffer R were exposed to one pulse (1080 V, 50 ms) utilizing a 100  $\mu$ L gold tip. After incubation for 16 h, the cells were treated for 5 h with the indicated test compounds as well as PMA and ionomycin at a total concentration of 0.253 nM and 31.3 nM, respectively. Subsequently, cells were centrifuged at 200 g for 3 min and total RNA was isolated from the pellet with the RNeasy Mini Kit according to the manufacturer's protocol (Qiagen, Venlo, Netherlands). Contamination

with genomic DNA was prevented by on-column DNA digestion using DNase I (RNase-free, Qiagen). RNA (1  $\mu$ g) was reverse transcribed to complementary DNA (cDNA) utilizing the Takara PrimeScript RT Reagent Kit, according to the manufacturer's protocol (Takara Bio Inc., Kusatsu, Japan). Finally, quantitative polymerase chain reaction (qPCR) was performed using Kapa SYBER<sup>®</sup> Fast qPCR Master Mix (KAPA Biosystems, Wilmington, MA, USA) as described earlier (Inderbinen et al., 2020). The following primers were used: peptidylprolyl isomerase A (PPIA): forward 5'-CAAATGCTGGACCAACACAAACG-3', reverse 5'-GTTTCATGCCTTCTTTACCTTCCC-3'; IL-17A: forward 5'-TCAAAGCTCAGCGTGT CCAA-3', reverse 5'-TCTTCATTGCGGTGGAGAGTC-3'; IL-22: forward 5'-GTGCGATCTCTGATGGCTGT-3', reverse 5'-TCCTTAGCACTGACTCCTCG-3'. Primer quality was verified by analysis of melting curves and inspection of the PCR product on an agarose gel (single band at the expected size of the amplified sequence). Resulting CT values were normalized to values of the endogenous control gene PPIA and compared to control according to the 2<sup>- $\Delta$ CT</sup> method (Schmittgen and Livak, 2008).

## 2.5. Computational similarity search

The computational similarity search was performed using the CosIng cosmetics database published by the European Commission (<https://ec.europa.eu/growth/tools-databases/cosing>) using several parabens, UV-filters and published ROR $\gamma$ (t) agonists as templates. The following template compounds were selected: hexylparaben (1083-27-8), benzylparaben (94-18-8), butylparaben (94-26-8), phenylparaben (17696-62-7), benzophenone-6 (131-54-4), and SR0987 (303126-97-8). All entries were retrieved from the CosIng database for which a unique CAS number was provided that were neither restricted nor banned. To obtain isomeric SMILES strings for these 10,754 CAS numbers, the Cactus web server of the National Cancer Institute (<https://cactus.nci.nih.gov>) as well as the PubChem database (Kim et al., 2019) were considered, resulting in 6715 entries. As some CAS numbers represented compound mixtures, their largest organic fragment was retained. A manual inspection was performed for entries that failed to produce unambiguous structural input. This revealed extracts with complex characteristic, entries with missing SMILES strings or incomplete structural information entries.

To compute the Extended Connectivity Fingerprints (ECFP), OpenBabel (v3.0.0) (O'Boyle et al., 2011) was employed and the library was compared to the templates by calculating the Tanimoto coefficient. Further, Extended Three-dimensional Fingerprints (E3FP) were generated using an open-source python package (Swain, 2013). The LigPrep routine within the Maestro Small-Molecule Drug Discovery Suite (Schrödinger LCC, 2019) was selected to assign protonation states with Epik at pH 7.4 and to obtain low-energy conformers using the OPLS3e force field. For each compound, a maximum of five conformers was retained and their highest Tanimoto coefficient was considered as similarity score.

## 2.6. Statistical analysis

Data were analyzed using the RStudio software (RStudio Team 2020: Integrated Development for R. RStudio, PBC, Boston, MA, <http://www.rstudio.com/>) using the one-way analysis of variance (ANOVA) followed by the Dunnett's post hoc test or Kruskal-Wallis test followed by Dunn's test to evaluate differences between control and treated cells in reporter-gene assays.

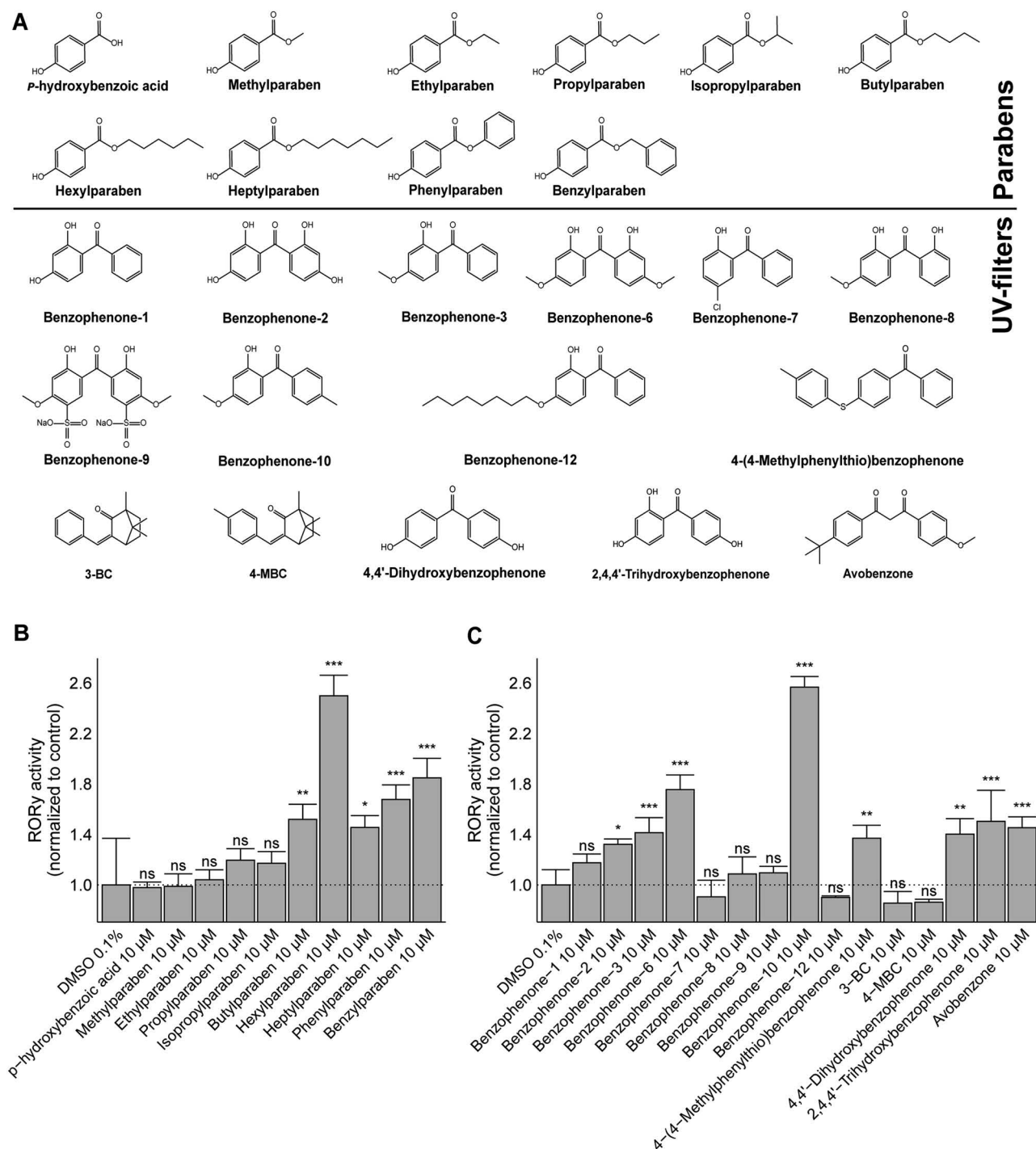
qRT-PCR experiments were analyzed with GraphPad Prism version 5 for Windows (GraphPad Software, San Diego, California USA, [www.graphpad.com](http://www.graphpad.com)) performing ANOVA and the Dunnett's post-hoc test. For estimation of EC<sub>50</sub> values, concentration-response curves were fitted and analyzed by non-linear regression and data was additionally analyzed by one-way analysis of variance (ANOVA) followed by Dunnett's post-hoc test using GraphPad Prism version 5 software as well.

### 3. Results

#### 3.1. Identification of parabens and benzophenone UV-filters that activate ROR $\gamma$

To assess whether parabens and UV-filters (for structures of examined chemicals see Fig. 1A) can interfere with ROR $\gamma$  activity, an already established doxycycline-inducible CHO ROR $\gamma$  Tet-on cell system was used in a transactivation assay (Slominski et al., 2014). A first screening

of parabens at a concentration of 10  $\mu$ M revealed that benzyl-, hexyl-, phenyl-, heptyl- and butylparaben activated ROR $\gamma$ -dependent transactivation by more than 1.5-fold compared to the DMSO vehicle control (Fig. 1B). The main paraben metabolite *p*-hydroxybenzoic acid and the short-chain length parabens methyl-, ethyl-, propyl- and isopropylparaben were inactive at this rather high concentration. The benzophenone-type UV-filters benzophenone-2, -3, -6 and -10, as well as 4-(4-methylphenylthio)benzophenone, 4,4'-dihydroxy- and 2,4,4'-trihydroxybenzophenone showed agonistic activity at 10  $\mu$ M.



**Fig. 1. Identification of parabens and UV-filters activating ROR $\gamma$ .** (A) Chemical structures of parabens and UV-filters tested. (B) Activation of ROR $\gamma$  by parabens and (C) benzophenone UV-filters. ROR $\gamma$  expression was induced by doxycycline and cells were treated with the test compounds at the concentrations indicated. Luciferase activity was determined and normalized to that of the vehicle control DMSO. Data represent mean  $\pm$  SD from three independent experiments. Statistical analysis was performed by one-way ANOVA followed by the Dunnett's post-hoc test. P values: \*\*\* < 0.001, ns (not significant).

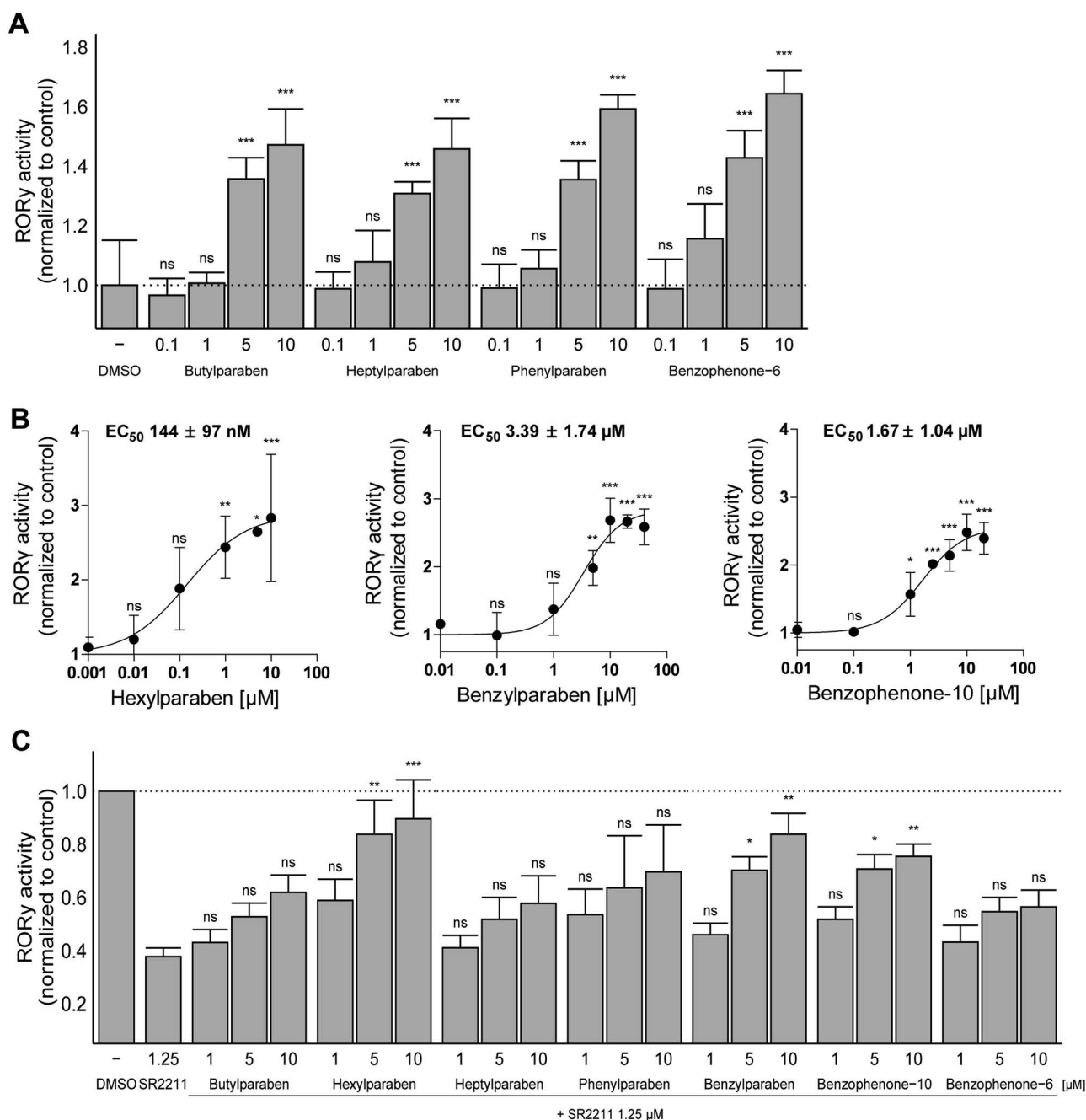


Concentration-dependence was then analyzed for compounds that activated ROR $\gamma$ -dependent transactivation by more than 1.5-fold compared to the DMSO vehicle control, namely butyl-, hexyl-, heptyl-phenyl- and benzylparaben as well as benzophenone-6 and -10 (Fig. 2A and B). Concentration-dependent increases were observed for all compounds, with EC<sub>50</sub> values for the three most potent ROR $\gamma$  agonists, i.e. hexylparaben, benzylparaben and benzophenone-10, of  $144 \pm 97$  nM,  $3.39 \pm 1.74$   $\mu$ M and  $1.67 \pm 1.04$   $\mu$ M, respectively (Fig. 2B). The ROR $\gamma$  active compounds were subjected to XTT assays to assess cell viability

and none of them showed any significant deviations from the vehicle control at the concentrations analyzed.

### 3.2. Competition of test compounds with the inverse agonist SR2211 and partial reversal of ROR $\gamma$ activity

ROR $\gamma$  typically shows constitutive activity due to the presence of endogenous agonists. This activity can be suppressed by inverse agonists, such as SR2211 (Kumar et al., 2012). To test whether the identified



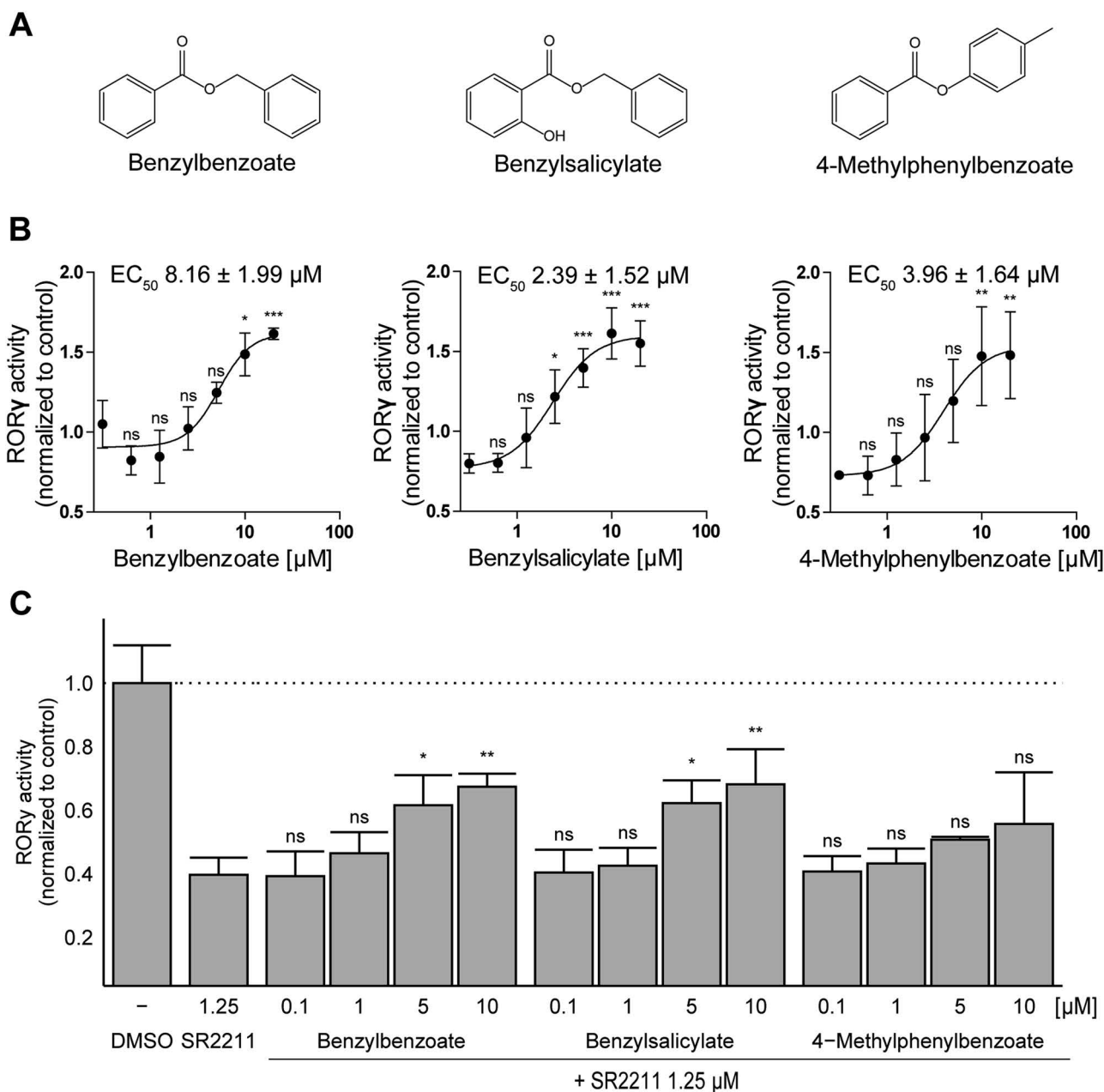
**Fig. 2.** Concentration-dependent agonist and antagonist activities of selected parabens and benzophenone UV-filters towards ROR $\gamma$ . (A, B) Concentration-dependent activation of ROR $\gamma$  by parabens and benzophenone UV-filters. ROR $\gamma$  expression was induced by doxycycline and cells were treated with the test compounds at the concentrations indicated. Luciferase activity was determined and normalized to that of the vehicle control DMSO. (B) Concentration-response curves were fitted and analyzed by non-linear regression. (C) Competition of parabens and benzophenone UV-filters with the ROR $\gamma$  inverse agonist SR2211. ROR $\gamma$  expression was initiated by doxycycline and basal ROR $\gamma$ -dependent transcriptional activity was suppressed by 1.25  $\mu$ M SR2211. Following incubation with the test compounds at the concentrations indicated, reactivation of the ROR $\gamma$ -dependent reporter gene signal was measured and normalized to that of the DMSO vehicle control. Data represent mean  $\pm$  SD from at least three independent experiments and were analyzed by (A, B) one-way ANOVA followed by the Dunnett's post-hoc test or (C) Kruskal-Wallis test with Dunn's post-hoc test, p values: \* < 0.05, \*\* < 0.01, \*\*\* < 0.001, ns (not significant).

ROR $\gamma$  agonists can compete with the inverse agonist SR2211, basal ROR $\gamma$  activity was suppressed to approximately 35% by 1.25  $\mu$ M SR2211. Cells were simultaneously exposed to SR2211 and a given test compound at different concentrations or vehicle control. All test compounds showed a concentration-dependent reversal of the SR2211-mediated inhibition of ROR $\gamma$  transactivation (Fig. 2C). A significant increase was obtained for hexylparaben, benzylparaben and benzophenone-10, consistent with our observations of the ROR $\gamma$  transactivation experiments in the absence of SR2211.

### 3.3. Structural similarity search to identify ROR $\gamma$ (t) modulators

To identify additional chemicals present in cosmetic products that

might interfere with ROR $\gamma$ (t) activity, a similarity search based on the structures of the newly identified parabens and benzophenone UV-filters and of the well-established ROR $\gamma$ t agonist SR0978 (Chang et al., 2016) as templates was conducted against the CosIng cosmetics database. Already tested compounds (and their salts) were removed from the hit list, and the remaining chemicals were visually inspected and checked for their commercial availability, followed by *in vitro* testing of the most promising compounds and their activities towards ROR $\gamma$  are displayed in Supplementary Fig. 1. Benzylbenzoate, benzylsalicylate and 4-methylphenylbenzoate showed significant agonistic activity towards ROR $\gamma$  (Fig. 3A, B), with a concentration-dependent activation and EC<sub>50</sub> values of  $8.16 \pm 1.99 \mu\text{M}$ ,  $2.39 \pm 1.52 \mu\text{M}$  and  $3.96 \pm 1.64 \mu\text{M}$ , respectively (Fig. 3B).



**Fig. 3.** Analysis of three compounds selected from the structural similarity search for effects on ROR $\gamma$  activity. (A) Chemical structures of the three ROR $\gamma$  activators identified by structural similarity search. (B) Concentration-dependent activation of ROR $\gamma$  by the selected compounds. Concentration-response curves were fitted and analyzed by non-linear regression. (C) Activation of ROR $\gamma$  by the three selected compounds in the presence of a ROR $\gamma$  inverse agonist. ROR $\gamma$  expression was induced by doxycycline in the absence (B) or presence (C) of 1.25  $\mu\text{M}$  SR2211. Cells were incubated with the test compounds at the concentrations indicated. Luciferase reporter activity was determined and normalized to that of the DMSO vehicle control. Data from three independent experiments represent mean  $\pm$  SD. Data were analyzed by one-way ANOVA with Dunnett's post-hoc test, p values: \* < 0.05, \*\* < 0.01, and ns (not significant).

Cytotoxicity was excluded for all active compounds at the concentrations applied by performing XTT assays. Additionally, the ability of these three compounds to reverse the inhibition of ROR $\gamma$  activity by SR2211 was assessed (Fig. 3C). Whilst benzylbenzoate and benzylsalicylate were able to restore the suppressed ROR $\gamma$  activity in a concentration-dependent manner, 4-methylphenylbenzoate failed to do so and only tended to restore ROR $\gamma$  activity at the highest concentration of 10  $\mu$ M.

### 3.4. Effect of hexylparaben, benzylparaben and benzophenone-10 on IL-17A and IL-22 mRNA expression in murine EL4 T-lymphocyte cells

The murine EL4 T-lymphocyte cell line is commonly used to study effects on ROR $\gamma$ -dependent target gene expression and known to produce the pro-inflammatory interleukins IL-17A and IL-22. Based on their ability to activate ROR $\gamma$  and reverse the inhibitory effect of the inverse agonist SR2211 and their frequent use in consumer products, hexylparaben, benzylparaben and benzophenone-10 were analyzed for their effects on ROR $\gamma$ -dependent target gene expression in EL4 cells stimulated with PMA and ionomycin. It needs to be noted that the endogenous ROR $\gamma$ t in the EL4 cells used in this study showed rather weak responsiveness and the increase of target gene transcription levels in the presence of known ROR $\gamma$ t agonists was less pronounced than described in earlier studies (Chang et al., 2016; Kojima et al., 2015). Furthermore, the cells did not respond to specific ROR $\gamma$ t inverse agonists; therefore, the human variant of ROR $\gamma$ t was overexpressed in the EL4 cells to generate a more sensitive system. These cells allowed an efficient modulation of IL-17A and IL-22 transcription levels in EL4 cells by the known inverse agonist GSK2981278 (1  $\mu$ M) and agonists SR0987 and genistein (10  $\mu$ M). Exposure of these cells to hexylparaben, benzylparaben or benzophenone-10 resulted in an elevated expression of IL-17A and IL-22 (Fig. 4). qRT-PCR analysis revealed that all tested compounds, except benzylparaben for which a trend was detected, significantly increased IL-17A transcription at a concentration of 10  $\mu$ M (Fig. 4A). With respect to IL-22, a significantly increased transcription was observed for the known ROR $\gamma$ t activators genistein and SR0987 and for hexylparaben, whereas benzylparaben and benzophenone-10 tended to increase the transcription of this ROR $\gamma$ t target gene (Fig. 4B). Benzylbenzoate, benzylsalicylate and 4-methylphenylbenzoate that were identified in the structural similarity search did not significantly

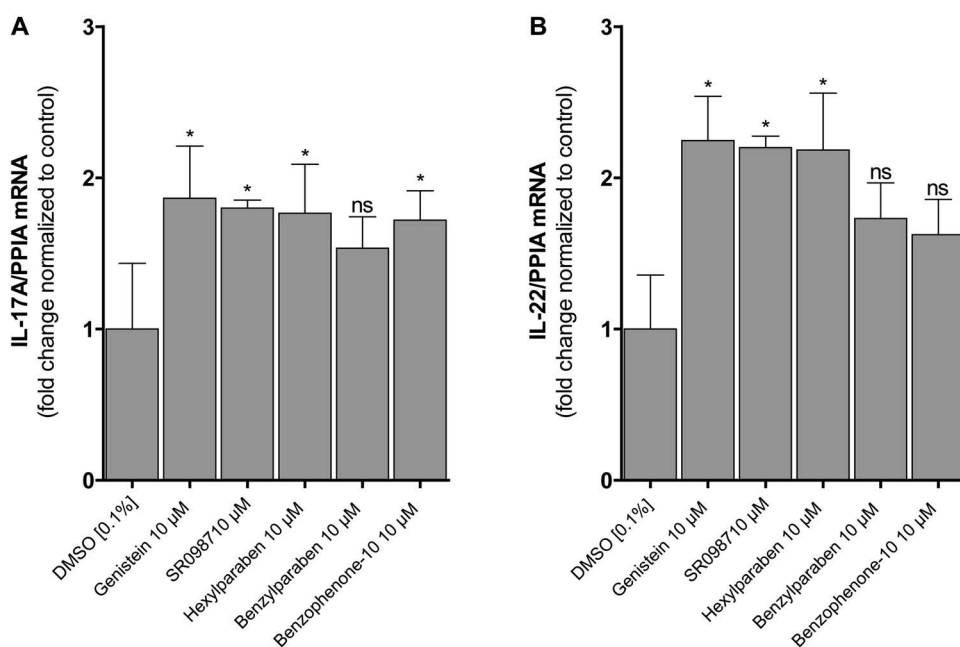
enhance IL-17A and IL-22 mRNA transcription levels.

### 3.5. Agonistic effects of mixtures of parabens and benzophenone UV-filters towards ROR $\gamma$

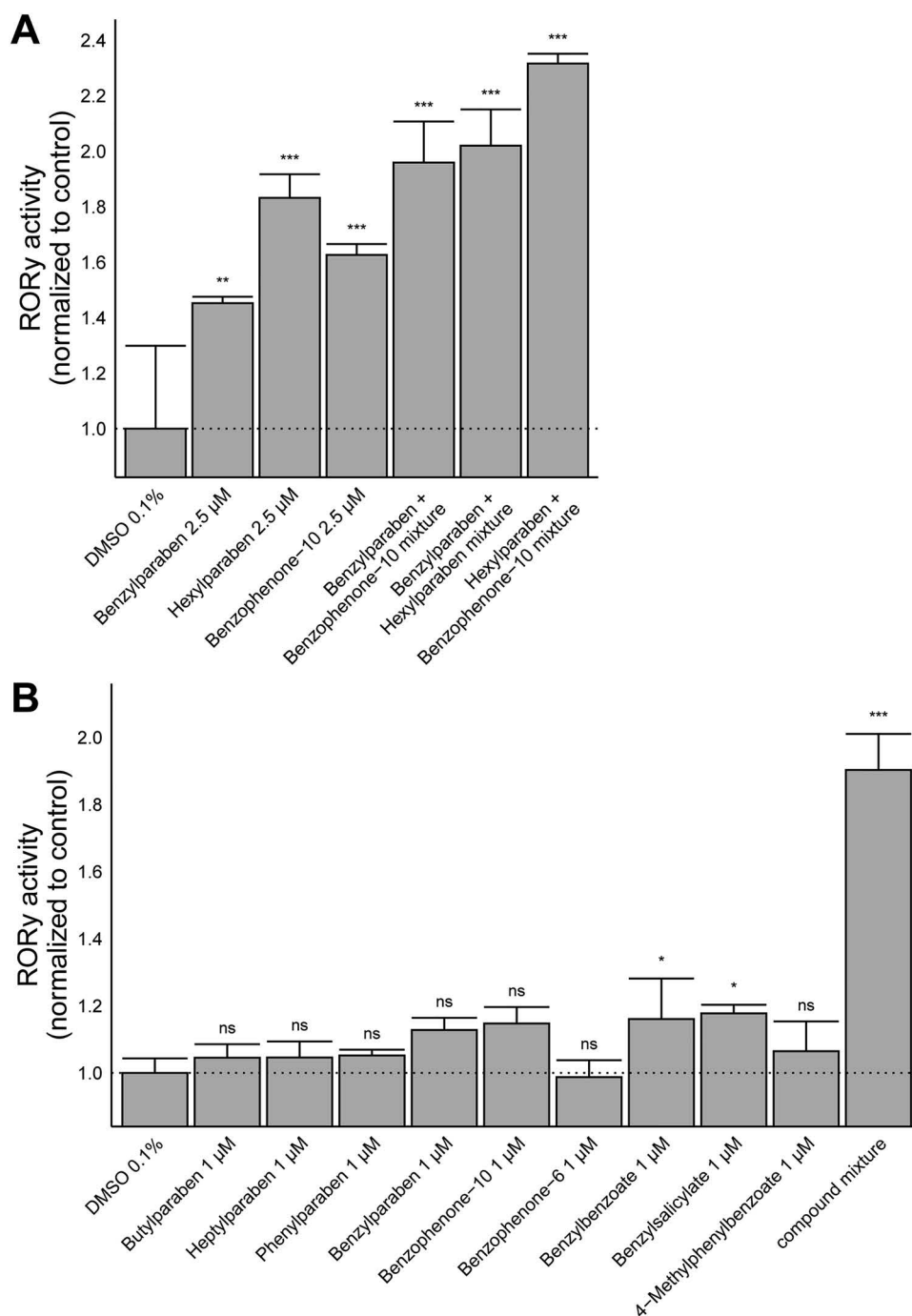
Parabens and UV-filters are usually added as mixtures of two or more compounds to cosmetics and sunscreens. To investigate whether mixtures of the identified parabens and benzophenone UV-filters exert more pronounced ROR $\gamma$  agonistic effects than the individual compounds, CHO ROR $\gamma$  Tet-on cells were exposed to either 2.5  $\mu$ M of the most potent ROR $\gamma$  agonists benzylparaben, hexylparaben and benzophenone-10 alone or mixtures of two of them each at a concentration of 2.5  $\mu$ M. As shown in Fig. 5A, all three mixtures led to a more pronounced activation of ROR $\gamma$  than the respective individual compounds. A comparison of the calculated sum of individual activities to the measured activity of the mixtures revealed no significant difference for two of the combinations (benzylparaben and benzophenone-10; benzophenone-10 and hexylparaben) while for one combination (benzylparaben and hexylparaben) the mixture showed somewhat lower effect than the calculated sum (Table 1). Additionally, to further explore mixture effects Tet-on cells were exposed to nine identified ROR $\gamma$  agonists alone at a concentration of 1  $\mu$ M or to a mixture of all compounds each at 1  $\mu$ M. It should be noted that the most active compound, hexylparaben, was excluded from this experiment as it may mask a possible additive effect of the other compounds due to its potent ROR $\gamma$  activation at concentrations well below 1  $\mu$ M. As shown in Fig. 5B, the individual compounds at a concentration of 1  $\mu$ M showed weak, *i.e.*, benzylbenzoate and benzylsalicylate, or no significant activation of ROR $\gamma$ . Importantly, treatment with the mixture containing each of these compounds at a concentration of 1  $\mu$ M resulted in a strong activation of ROR $\gamma$ , comparable with that seen for the most potent compounds at a concentration of 10  $\mu$ M (Fig. 2A, B and Fig. 3B). A comparison of the calculated sum of the nine individual agonistic effects to the effect of the mixture of the nine compounds revealed no significant difference, suggesting additive effects (Table 2).

## 4. Discussion

Parabens and UV-filters are major additives of cosmetics and body care products, enhancing product stability and shelf life, and these



**Fig. 4.** Effect of selected compounds on IL-17A and IL-22 mRNA levels in murine EL4 T-cells over expressing human ROR $\gamma$ t. EL4 cells transfected with ROR $\gamma$ t were stimulated with PMA/ionomycin to induce cytokine gene expression and exposed simultaneously to the compounds indicated. Subsequently, the mRNA expression of IL-17A (A) and IL-22 (B) were quantified by qRT-PCR and normalized to the expression of the housekeeping gene PPIA. Expression levels were normalized to vehicle control. Data represent mean  $\pm$  SD from three independent experiments. Data was analyzed by one-way ANOVA with Dunnett's post hoc test, p-value: \* < 0.05, ns (not significant).



**Fig. 5.** Mixture effects of parabens and benzophenone UV-filters on ROR $\gamma$  activity. ROR $\gamma$  expression was induced by doxycycline and cells were treated (A) with an individual test compound at a concentration of 2.5  $\mu$ M or with mixtures of two compounds each at 2.5  $\mu$ M, or (B) with an individual test compound at a concentration of 1  $\mu$ M or a mixture containing all nine individual compounds each at 1  $\mu$ M. Luciferase activity was measured and normalized to that of the DMSO vehicle control. Statistical analysis was performed by one-way ANOVA followed by the Dunnett's post-hoc test. P values: \* < 0.05, \*\*\* < 0.001, ns (not significant). Data represent mean  $\pm$  SD from three independent experiments.

chemicals have raised considerable interest regarding their potential to disrupt endocrine functions (reviewed in Matwiejczuk et al., 2020; Wang et al., 2016). Whilst considerable research focused on the potential effects of such compounds towards estrogen and androgen receptors (Boberg et al., 2010; Darbre and Harvey, 2008; Kunz and Fent, 2006; Satoh et al., 2005; Schlecht et al., 2004), the present study, to our knowledge, is the first to investigate more closely a series of parabens (including their main metabolite *p*-hydroxybenzoic acid) and UV-filters for their effects on ROR $\gamma$ (t). Of the nine parabens and 15 UV-filters initially tested, the two parabens hexylparaben and benzylparaben and the UV-filter benzophenone-10 were identified as the most active ROR $\gamma$  agonists, with estimated EC<sub>50</sub> values in the nano- and low micromolar range. Importantly, these substances were able to enhance the ROR $\gamma$ t-dependent transcriptional expression of the

pro-inflammatory cytokines IL-17A and IL-22, using the mouse T-lymphocyte cell model EL4.

IL-17A and IL-22 are produced by Th-17 cells and elevated levels of these cytokines are thought to be involved in the development and pathogenesis of autoimmune diseases, including psoriasis (Pan et al., 2013; Zheng et al., 2007). Due to the important role of ROR $\gamma$ t in autoimmune diseases, this receptor is considered to be a promising drug target and several studies describe inverse agonists suppressing ROR $\gamma$ t function, with the potential to treat patients suffering from such pathologies (Bronner et al., 2017; Fauber and Magnuson, 2014; Solt et al., 2010; Sun et al., 2019). In particular, autoimmune skin diseases are under investigation for the treatment with orally or dermally applied ROR $\gamma$ t suppressors (Ecoeur et al., 2019; Imura et al., 2019; Sasaki et al., 2018; Smith et al., 2016; Takaishi et al., 2017). Th17 cells and IL-17

**Table 1**

**Statistical comparison of the calculated sum and the measured effects of pairs of ROR $\gamma$  agonists of data shown in Fig. 5A.** ROR $\gamma$  activity was normalized to the vehicle control. The sums of ROR $\gamma$  activity of combinations of two agonistic compounds was calculated for each experimental replicate. Statistical analysis was performed by one-way ANOVA followed by the pairwise t-test with Bonferroni-adjusted *p* values. The calculated sums of ROR $\gamma$  activity of the two agonists were compared to the measured ROR $\gamma$  activity of their respective mixtures. *P* values: \* < 0.05, ns (not significant). Data represent mean  $\pm$  SD from three independent experiments.

Agonist [2.5 $\mu$ M]	% increase in ROR $\gamma$ activity (mean $\pm$ SD)	Calculated sum of % increase in ROR $\gamma$ activity (mean $\pm$ SD)	Measured % increase in ROR $\gamma$ activity of the mixture (mean $\pm$ SD)
Benzylparaben	45 $\pm$ 2	108 $\pm$ 15	96 $\pm$ 5 (ns)
Benzophenone-10	63 $\pm$ 4		
Benzylparaben	45 $\pm$ 2	128 $\pm$ 8	102 $\pm$ 13 (*)
Hexylparaben	83 $\pm$ 8		
Benzophenone-10	83 $\pm$ 8	146 $\pm$ 11	132 $\pm$ 4 (ns)
Hexylparaben	63 $\pm$ 4		

**Table 2**

**Statistical comparison of the calculated sum and the measured effects of nine ROR $\gamma$  agonists of data shown in Fig. 5B.** ROR $\gamma$  activity was normalized to the vehicle control. The sum of ROR $\gamma$  activity of all nine agonistic compounds was calculated for each experimental replicate. The calculated sum of ROR $\gamma$  activity of the nine agonists was compared to the measured ROR $\gamma$  activity of the respective mixture in a *t*-test. The two groups were not significantly different (ns). Data represent mean  $\pm$  SD from three independent experiments.

Agonist [1 $\mu$ M]	% increase in ROR $\gamma$ activity (mean $\pm$ SD)
Butylparaben	5 $\pm$ 4
Heptylparaben	5 $\pm$ 5
Phenylparaben	5 $\pm$ 2
Benzylparaben	13 $\pm$ 4
Benzophenone-10	15 $\pm$ 5
Benzophenone-6	-1 $\pm$ 5
Benzylbenzoate	16 $\pm$ 12
Benzylsalicylate	18 $\pm$ 3
4-Methylphenylbenzoate	6 $\pm$ 9
<b>Calculated sum of % increase in ROR<math>\gamma</math> activity (mean <math>\pm</math> SD)</b>	<b>81 <math>\pm</math> 2</b>
<b>Measured % increase in ROR<math>\gamma</math> activity of the mixture (mean <math>\pm</math> SD)</b>	<b>90 <math>\pm</math> 11 (ns)</b>

were also detected in skin biopsies of patients suffering from acne and have been associated with the development of this pathology (Agak et al., 2014; Kistowska et al., 2015). To our knowledge, there are currently no reports on effects of ROR $\gamma$ t overstimulation by xenobiotics in such skin diseases. However, it can be expected to be unfavorable, because an upregulation of ROR $\gamma$ t with elevated IL-17A and IL-22 levels has been proposed to play a role in immune disorders such as severe allergic asthma, psoriatic arthritis and UV-radiation induced promotion of skin cancer (Huang et al., 2020; Leijten et al., 2021; Lewis et al., 2021).

The consequences of human exposure to ROR $\gamma$ t activating parabens and benzophenone UV-filters remain unclear and need to be carefully addressed. In 2014, following studies describing endocrine disrupting properties of parabens, the European Union restricted the maximal concentrations allowed in cosmetic products and prohibited the use of isopropyl-, isobutyl-, phenyl-, benzyl- and pentylparaben (EC, 2014). Therefore, human exposure to the newly identified ROR $\gamma$  agonist benzylparaben after the use of cosmetic products can be expected to be rather low. Hexylparaben, which has not been banned, has a relatively long alkyl side chain, resulting in reduced solubility. For this reason, this compound is less frequently used in cosmetics compared to the better

soluble short-chain length parabens (CIR, 2008). Thus, due to the limited use, dermal exposure to hexylparaben (and the weakly active heptylparaben) can also be considered as low. Notably, butylparaben was detected in human plasma, seminal plasma, urine and breast cancer samples (Darbre et al., 2004; Frederiksen et al., 2011; Kang et al., 2016). However, the concentrations found in human samples were considerably lower than those found in the present *in vitro* study to activate ROR $\gamma$ . Nevertheless, the presence of unmetabolized parabens in human matrices demonstrated their uptake and exposure, despite the rapid hydrolysis to the ROR $\gamma$  inactive metabolite *p*-hydroxybenzoic acid. Parabens are metabolized by carboxylesterases that are highly expressed in the liver and intestine but also to a certain extent in the skin (Boberg et al., 2010; Jewell et al., 2007; Ozaki et al., 2013). Harville et al. (2007) showed by *in vitro* studies that the hydrolysis of parabens in human skin is much slower than in liver and the efficiency of hydrolysis was reduced with increased length of the alkyl chain. This suggests that longer chain parabens may accumulate in tissues such as subcutaneous fat. Whether extensive dermal application of cosmetics containing longer alkyl chain parabens might reach concentrations with the potential to disturb local ROR $\gamma$ t activity remains unclear. The most widely used parabens in cosmetic products, methyl- and propylparaben (reviewed in Matwiejczuk et al., 2020) as well as ethylparaben, did not interfere with ROR $\gamma$  activity in the present *in vitro* study at much higher concentrations than what has been measured in human plasma samples (Calafat et al., 2010; Sandanger et al., 2011) suggesting that they may not disturb ROR $\gamma$ t activity in the human skin.

Similar to parabens, maximal concentrations of UV-filters allowed in cosmetic products have been defined by the regulators as a consequence of the suspected endocrine disrupting effects of these substances (EC, 2009; FDA, 1999). Among the UV-filters tested in this study, benzophenone-10 showed the most potent ROR $\gamma$  agonistic effect. Allergic skin reactions have been reported after exposure to benzophenone-10 (Darvay et al., 2001; Goossens, 2016), furthermore a skin response involving Th17 cell activation (Peiser, 2013; Simon et al., 2014). Further investigations are required to test whether ROR $\gamma$ t activation contributes to this adverse effect of benzophenone-10.

The ROR $\gamma$  active benzophenone UV-filters identified in this study are added typically in small amounts as stabilizing and protecting agents to cosmetics or plastic materials to improve the product's shelf life (CIR, 2005). The expected exposure from contact with such products may well lie below the concentrations reported here to activate ROR $\gamma$ . However, it should be noted that for the ROR $\gamma$  agonistic compounds benzophenone-2 and -6 there are currently no studies in humans on plasma and/or urine levels available that would allow estimating bioavailability and potential activation of ROR $\gamma$  within skin after the use of cosmetics.

Amongst the benzophenone UV-filters showing agonistic ROR $\gamma$  effects, avobenzene and benzophenone-3 are allowed to be used as active UV-absorbing ingredients in sunscreens at high concentrations (up to 5% and 6%, respectively) (EC, 2009; FDA, 2019). Compared with avobenzene, which shows limited skin penetration and thus low bioavailability (Simeoni et al., 2004; Weigmann et al., 2001), benzophenone-3 has been reported to penetrate the human skin efficiently, and concentrations reaching the lower micromolar range in serum, urine and breast milk (304  $\mu$ g/l, 300  $\mu$ g/l, 779.9 ng/g milk) have been reported (Benson et al., 2005; Fernandez et al., 2002). Benzophenone-3 is metabolized in the human liver to benzophenone-1, benzophenone-8, 2,3,4-trihydroxybenzophenone, and 4,4'-dihydroxybenzophenone, which all were detected in human urine and breast milk samples (Janjua et al., 2008; Molins-Delgado et al., 2018; Tarazona et al., 2013; Watanabe et al., 2015; Yiin et al., 2015). While 4,4'-dihydroxybenzophenone was able to activate ROR $\gamma$ , benzophenone-1, showed only weak ROR $\gamma$  agonistic effect at micromolar concentrations. Whether other benzophenone-3 metabolites such as 2,3,4-trihydroxybenzophenone also can activate ROR $\gamma$ t has not yet been assessed. Importantly, parabens and UV-filters are usually used as mixtures and as shown in this study, they can

exert additive agonistic effects on ROR $\gamma$ (t). Whether benzophenone-3 and its metabolites may reach total concentrations within the skin and, less likely, within the body capable to activate ROR $\gamma$ t and whether the low level ROR $\gamma$ t overactivation by such xenobiotics impairs immune regulation and leads to adverse health effects requires further research.

4-(4-Methylphenylthio)benzophenone and 2,4,4'-trihydroxybenzophenone, included in the primary screening due to their structural similarity, are mainly used in printing inks (Bradley et al., 2013) and as UV stabilizers in plastic surface coatings of food packaging materials. 2,4,4'-trihydroxybenzophenone has been shown earlier to exhibit weak estrogenic activity (Suzuki et al., 2005). The present *in vitro* assessment found ROR $\gamma$  agonistic effects for both of these compounds at a concentration of 10  $\mu$ M. However, the currently limited data on distribution and migration of these benzophenone UV-filters into foods as well as missing plasma compound levels do not allow a clear assessment regarding the possible modulation of ROR $\gamma$  activity in the intestine or in other organs, warranting further investigations.

The computational similarity search based on the newly identified ROR $\gamma$  activating scaffolds, followed by *in vitro* evaluation, revealed additional cosmetic additives with agonistic ROR $\gamma$  activity. Benzylsalicylate is added to cosmetic products as perfuming agent and light stabilizer (de Groot, 2020). Benzylbenzoate and 4-methylphenylbenzoate are fragrance ingredients and preservatives in cosmetic products (de Groot, 2020; Johnson et al., 2017). Estrogenic activity was reported earlier for benzylsalicylate and benzylbenzoate (Charles and Darbre, 2009); however, only at high micromolar concentrations that are unlikely reached in realistic human exposure scenarios. Both of these chemicals need to be declared when exceeding 0.001% in leave-on and 0.01% in rinse-off cosmetic products (de Groot, 2020). Interestingly, cosmetics-induced dermatitis was found to be associated with benzylsalicylate and benzylbenzoate; however, only in rare cases (Goossens, 2016). Among other cosmetic additives, benzylsalicylate is currently subjected to further inspections to evaluate its potential for endocrine disruption in consumers (EC, 2019). Notably, benzylbenzoate is also employed as an active ingredient in topical treatments for scabies (Haustein and Hlawa, 1989). As side effects of the therapy, skin irritation and allergic reactions were described. Further experimental investigations are needed to assess whether a chronic activation of ROR $\gamma$ t might play a role in development of such side effects. It remains unclear whether dermal exposure to these chemicals can reach relevant systemic concentrations to activate ROR $\gamma$ t and cause adverse effects. Furthermore, as described for benzylbenzoate (Johnson et al., 2017), these chemicals may also be hydrolyzed in the skin.

A structure-activity comparison of the analyzed parabens revealed that compounds with short side chains, such as methyl- and ethylparaben as well as the main metabolite *p*-hydroxybenzoic acid do not activate ROR $\gamma$ . Interestingly, ROR $\gamma$ -active parabens exhibit higher clogP values than inactive compounds (clogP values listed in Engeli et al., 2017), indicating that hydrophobic interactions may stabilize ligand binding. Analysis of the potential binding modes of the active hexylparaben and the inactive methylparaben in the ROR $\gamma$  orthosteric pocket by molecular docking predicted the phenyl-cores of both parabens to bind in the same location, while the prolonged alkyl chain of hexylparaben protruded into a sub-pocket containing several hydrophobic residues. These additional hydrophobic interactions are absent in case of methylparaben, providing an explanation for the distinct activity of these two compounds (Suppl. Fig. 2). In contrast to these two parabens, the binding analysis of the benzophenones studied was inconclusive and the interactions responsible for the differences between active and inactive compounds remain unclear. The prediction of the binding mode of these relatively small compounds within the ligand binding pocket of ROR $\gamma$  remains challenging and only permits initial insights into the ligand-protein interactions.

Even if the individual compounds identified may not reach concentrations *in vivo* to activate ROR $\gamma$ (t), it needs to be kept in mind that parabens and UV-filters are mainly used as mixtures in cosmetics and

body care products. The agonistic mixture effects on ROR $\gamma$  identified in this study suggest additive effects of the newly identified compounds, which may be explained by their structural similarity and similar binding to the LBD of the receptor. However, because a cell-based assay was used, a contribution by synergistic action cannot be excluded. Follow-on studies using cell-free ROR $\gamma$ (t) assays should be performed to further corroborate the mechanism underlying the observed mixture effects.

The observed agonistic mixture effects on ROR $\gamma$ (t) emphasize the need for the development of extensive analytical methods to simultaneously quantify a larger number of relevant compounds in biological samples to assess exposure and test for correlations with biological functions. Additive and potentially also synergistic effects need to be taken into account in the safety considerations for the use of parabens and UV-filters. *In vivo* studies using animal models of autoimmune diseases may show whether the newly identified compounds and their metabolites alone or as mixtures can aggravate the pathophysiological effects by activating ROR $\gamma$ t.

In conclusion, the present study revealed new scaffolds of parabens and benzophenone UV-filters as novel ROR $\gamma$ (t) agonists, with the ability to enhance pro-inflammatory cytokine expression in a mouse EL4 T-lymphocyte cell model. Furthermore, a fingerprint-based similarity search identified additional cosmetic compounds with agonistic effects towards this receptor. Further research needs to address the toxicological relevance of the identified activities towards ROR $\gamma$ (t), considering the rapid metabolism of parabens and the additive and potentially synergistic effects of parabens, benzophenone UV-filters and structurally related chemical additives in body care products.

#### Declaration of Competing Interest

The authors declare that they have no known competing financial interests or personal relationships that could have appeared to influence the work reported in this paper.

#### Acknowledgement

This work was supported by the Swiss Centre for Applied Human Toxicology to AO and MS. We thank Anna Devaux, University of Basel, for support with the handling of EL4 cells.

#### Appendix A. Supporting information

Supplementary data associated with this article can be found in the online version at doi:10.1016/j.tox.2022.153159.

#### References

- Agak, G.W., Qin, M., Nobe, J., Kim, M.H., Krutzik, S.R., Tristan, G.R., Elashoff, D., Garbán, H.J., Kim, J., 2014. Propionibacterium acnes induces an IL-17 response in acne vulgaris that is regulated by vitamin A and vitamin D. *J. Invest. Dermatol.* 134, 366–373.
- Bailey, S.R., Nelson, M.H., Himes, R.A., Li, Z., Mehrotra, S., Paulos, C.M., 2014. Th17 cells in cancer: the ultimate identity crisis. *Front. Immunol.* 5, 276.
- Bens, G., 2014. Sunscreens. *Adv. Exp. Med. Biol.* 810, 429–463.
- Benson, H.A., Sarveiya, V., Risk, S., Roberts, M.S., 2005. Influence of anatomical site and topical formulation on skin penetration of sunscreens. *Ther. Clin. Risk Manag.* 1, 209–218.
- Boberg, J., Taxvig, C., Christiansen, S., Hass, U., 2010. Possible endocrine disrupting effects of parabens and their metabolites. *Reprod. Toxicol.* 30, 301–312.
- Bradley, E.L., Stratton, J.S., Leak, J., Lister, L., Castle, L., 2013. Printing ink compounds in foods: UK survey results. *Food Addit. Contam.: Part B* 6, 73–83.
- Bronner, S.M., Zbieg, J.R., Crawford, J.J., 2017. ROR $\gamma$  antagonists and inverse agonists: a patent review. *Expert Opin. Ther. Pat.* 27, 101–112.
- Cai, Y., Shen, X., Ding, C., Qi, C., Li, K., Li, X., Jala, V.R., Zhang, H.G., Wang, T., Zheng, J., Yan, J., 2011. Pivotal role of dermal IL-17-producing gammadelta T cells in skin inflammation. *Immunity* 35, 596–610.
- Calafat, A.M., Wong, L.Y., Ye, X., Reidy, J.A., Needham, L.L., 2008. Concentrations of the sunscreen agent benzophenone-3 in residents of the United States: National Health and Nutrition Examination Survey 2003–2004. *Environ Health Perspect.* 116, 893–897.

- Calafat, A.M., Ye, X., Wong, L.Y., Bishop, A.M., Needham, L.L., 2010. Urinary concentrations of four parabens in the U.S. population: NHANES 2005–2006. *Environ. Health Perspect.* 118, 679–685.
- Chang, M.R., Dharmarajan, V., Doebelin, C., Garcia-Ordóñez, R.D., Novick, S.J., Kuruvilla, D.S., Kamenecka, T.M., Griffin, P.R., 2016. Synthetic ROR $\gamma$ t agonists enhance protective immunity. *ACS Chem. Biol.* 11, 1012–1018.
- Charles, A.K., Darbre, P.D., 2009. Oestrogenic activity of benzyl salicylate, benzyl benzoate and butylphenylmethylpropional (Lilial) in MCF7 human breast cancer cells in vitro. *J. Appl. Toxicol.* 29, 422–434.
- Chen, J., Ahn, K.C., Gee, N.A., Gee, S.J., Hammock, B.D., Lasley, B.L., 2007. Antiandrogenic properties of parabens and other phenolic containing small molecules in personal care products. *Toxicol. Appl. Pharm.* 221, 278–284.
- Chung, Y., Yang, X., Chang, S.H., Ma, L., Tian, Q., Dong, C., 2006. Expression and regulation of IL-22 in the IL-17-producing CD $4^{+}$  T lymphocytes. *Cell Res.* 16, 902–907.
- CIR, C.I.R.E.P., 2005. Annual review of cosmetic ingredient safety assessments—2002/2003. *Int. J. Toxicol.* 24, 1–102.
- CIR, C.I.R.E.P., 2008. Final amended report on the safety assessment of methylparaben, ethylparaben, propylparaben, isopropylparaben, butylparaben, isobutylparaben, and benzylparaben as used in cosmetic products. *Int. J. Toxicol.* 27 (Suppl. 4), S1–S82.
- Darbre, P.D., Aljarrah, A., Miller, W.R., Coldham, N.G., Sauer, M.J., Pope, G.S., 2004. Concentrations of parabens in human breast tumours. *J. Appl. Toxicol.* 24, 5–13.
- Darbre, P.D., Harvey, P.W., 2008. Paraben esters: review of recent studies of endocrine toxicity, absorption, esterase and human exposure, and discussion of potential human health risks. *J. Appl. Toxicol.* 28, 561–578.
- Darbre, P.D., Harvey, P.W., 2014. Parabens can enable hallmarks and characteristics of cancer in human breast epithelial cells: a review of the literature with reference to new exposure data and regulatory status. *J. Appl. Toxicol.* 34, 925–938.
- Darvay, A., White, I.R., Rycroft, R.J., Jones, A.B., Hawk, J.L., McFadden, J.P., 2001. Photoallergic contact dermatitis is uncommon. *Br. J. Dermatol.* 145, 597–601.
- de Groot, A.C., 2020. Fragrances: contact allergy and other adverse effects. *Dermatitis* 31, 13–35.
- Ding, K., Kong, X., Wang, J., Lu, L., Zhou, W., Zhan, T., Zhang, C., Zhuang, S., 2017. Side chains of parabens modulate antiandrogenic activity: in vitro and molecular docking studies. *Environ. Sci. Technol.* 51, 6452–6460.
- EC, 2009. Regulation (EC) no 1223/2009 of the European Parliament on cosmetic products annex VI list of UV filters allowed in cosmetic products. *Off. J. Eur. Union.*
- EC, 2014. Regulation (EU) no 1004/2014 amending annex V to regulation (EC) no 1223/2009 of the European Parliament and the council on cosmetic products. *Off. J. Eur. Union.*
- EC, 2019. Call for data on ingredients with potential endocrine-disrupting properties used in cosmetic products. ([https://ec.europa.eu/growth/content/call-data-ingred-ients-potential-endocrine-disrupting-properties-used-cosmetic-products\\_en](https://ec.europa.eu/growth/content/call-data-ingred-ients-potential-endocrine-disrupting-properties-used-cosmetic-products_en)), (Accessed 13 August 2020).
- Ecoeur, F., Weiss, J., Kaupmann, K., Hintermann, S., Orain, D., Guntermann, C., 2019. Antagonizing retinoic acid-related-orphan receptor gamma activity blocks the T Helper 17/interleukin-17 pathway leading to attenuated pro-inflammatory human keratinocyte and skin responses. *Front. Immunol.* 10, 577.
- Engeli, R.T., Rohrer, S.R., Vuorinen, A., Herdlinger, S., Kaserer, T., Leugger, S., Schuster, D., Odermatt, A., 2017. Interference of paraben compounds with estrogen metabolism by inhibition of 17 $\beta$ -hydroxysteroid dehydrogenases. *Int. J. Mol. Sci.* 18, 2007.
- Fauber, B.P., Magnuson, S., 2014. Modulators of the nuclear receptor retinoic acid receptor-related orphan receptor- $\gamma$  (ROR $\gamma$  or RORc). *J. Med. Chem.* 57, 5871–5892.
- FDA, 1999. **Sunscreen Drug Products for Over-the-Counter Human Use (64 FR 27666, May 21, 1999) (now stayed) (stayed 1999 final monograph)**, Federal Register.
- FDA, 2019. **Sunscreen Drug Products for Over-the-Counter Human Use. A proposed rule by the Food and Drug Administration on 02/26/2019.**, Federal Register.
- Fernandez, C., Nielloud, F., Fortuné, R., Vian, L., Marti-Mestres, G., 2002. Benzophenone-3: rapid prediction and evaluation using non-invasive methods of in vivo human penetration. *J. Pharmaceut. Biomed. Anal.* 28, 57–63.
- Frederiksen, H., Jørgensen, N., Andersson, A.M., 2011. Parabens in urine, serum and seminal plasma from healthy Danish men determined by liquid chromatography-tandem mass spectrometry (LC-MS/MS). *J. Expo. Sci. Environ. Epidemiol.* 21, 262–271.
- Fujino, C., Watanabe, Y., Sanoh, S., Hattori, S., Nakajima, H., Uramaru, N., Kojima, H., Yoshinari, K., Ohta, S., Kitamura, S., 2019. Comparative study of the effect of 17 parabens on PXR-, CAR- and PPAR $\alpha$ -mediated transcriptional activation. *Food Chem. Toxicol.* 133, 110792.
- Goossens, A., 2016. Cosmetic contact allergens. *Cosmetics* 3, 5.
- Harville, H.M., Voorman, R., Prusakiewicz, J.J., 2007. Comparison of paraben stability in human and rat skin. *Drug Metab. Lett.* 1, 17–21.
- Haustein, U.F., Hlawka, B., 1989. Treatment of scabies with permethrin versus lindane and benzyl benzoate. *Acta Derm. Venereol.* 69, 348–351.
- He, Y.W., Deflos, M.L., Ojala, E.W., Bevan, M.J., 1998. ROR $\gamma$  agonists regulate multiple pathways in T cells. *Immunity* 9, 797–806.
- Hirose, T., Smith, R.J., Jetten, A.M., 1994. ROR gamma: the third member of ROR/RZR orphan receptor subfamily that is highly expressed in skeletal muscle. *Biochem. Biophys. Res. Commun.* 205, 1976–1983.
- Hu, X., Liu, X., Moisan, J., Wang, Y., Lesch, C.A., Spooner, C., Morgan, R.W., Zawadzka, E.M., Mertz, D., Bousley, D., Majchrzak, K., Kryczek, I., Taylor, C., Van Huis, C., Skalitzky, D., Hurd, A., Aicher, T.D., Toogood, P.L., Glick, G.D., Paulos, C. M., Zou, W., Carter, L.L., 2016. Synthetic ROR $\gamma$  agonists regulate multiple pathways to enhance antitumor immunity. *Oncoimmunology* 5, e1254854.
- Huang, M., Bolin, S., Miller, H., Ng, H.L., 2020. ROR $\gamma$  structural plasticity and druggability. *Int. J. Mol. Sci.* 21, 5329.
- Huh, J.R., Leung, M.W., Huang, P., Ryan, D.A., Krout, M.R., Malapaka, R.R., Chow, J., Manel, N., Ciofani, M., Kim, S.V., Cuesta, A., Santori, F.R., Lafaille, J.J., Xu, H.E., Gin, D.Y., Rastinejad, F., Littman, D.R., 2011. Digoxin and its derivatives suppress Th17 cell differentiation by antagonizing ROR $\gamma$ t activity. *Nature* 472, 486–490.
- Imura, C., Ueyama, A., Sasaki, Y., Shimizu, M., Furue, Y., Tai, N., Tsujii, K., Katayama, K., Okuno, T., Shichijo, M., Yasui, K., Yamamoto, M., 2019. A novel ROR $\gamma$ t inhibitor is a potential therapeutic agent for the topical treatment of psoriasis with low risk of thymic aberrations. *J. Dermatol. Sci.* 93, 176–185.
- Inderbinen, S.G., Engeli, R.T., Rohrer, S.R., Di Renzo, E., Aengenheister, L., Buerki-Thurnherr, T., Odermatt, A., 2020. Tributyltin and triphenyltin induce 11 $\beta$ -hydroxysteroid dehydrogenase 2 expression and activity through activation of retinoid X receptor  $\alpha$ . *Toxicol. Lett.* 322, 39–49.
- Ivanov, I.I., McKenzie, B.S., Zhou, L., Tadokoro, C.E., Lepelletier, A., Lafaille, J.J., Cua, D. J., Littman, D.R., 2006. The orphan nuclear receptor ROR $\gamma$  directs the differentiation program of proinflammatory IL-17+ T helper cells. *Cell* 126, 1121–1133.
- Janjua, N.R., Kongshoj, B., Andersson, A.M., Wulf, H.C., 2008. Sunscreens in human plasma and urine after repeated whole-body topical application. *J. Eur. Acad. Dermatol. Venereol.* 22, 456–461.
- Jetten, A.M., 2009. Retinoid-related orphan receptors (RORs): critical roles in development, immunity, circadian rhythm, and cellular metabolism. *Nucl. Recept. Signal.* 7, e003.
- Jetten, A.M., Cook, D.N., 2020. (Inverse) Agonists of retinoic acid-related orphan receptor  $\gamma$ : regulation of immune responses, inflammation, and autoimmune disease. *Annu. Rev. Pharm. Toxicol.* 60, 371–390.
- Jetten, A.M., Kang, H.S., Takeda, Y., 2013. Retinoic acid-related orphan receptors  $\alpha$  and  $\gamma$ : key regulators of lipid/glucose metabolism, inflammation, and insulin sensitivity. *Front. Endocrinol.* 4, 1.
- Jewell, C., Prusakiewicz, J.J., Ackermann, C., Payne, N.A., Fate, G., Voorman, R., Williams, F.M., 2007. Hydrolysis of a series of parabens by skin microsomes and cytosol from human and minipigs and in whole skin in short-term culture. *Toxicol. Appl. Pharm.* 225, 221–228.
- Johnson, W., Bergfeld, W.F., Belsito, D.V., Hill, R.A., Klaassen, C.D., Liebler, D.C., Marks, J.G., Shank, R.C., Slaga, T.J., Snyder, P.W., Andersen, F.A., 2017. Safety assessment of benzyl alcohol, benzoic acid and its salts, and benzyl benzoate. *Int. J. Toxicol.* 36, 5s–30s.
- Kang, H.S., Kyung, M.S., Ko, A., Park, J.H., Hwang, M.S., Kwon, J.E., Suh, J.H., Lee, H.S., Moon, G.I., Hong, J.H., Hwang, I.G., 2016. Urinary concentrations of parabens and their association with demographic factors: a population-based cross-sectional study. *Environ. Res.* 146, 245–251.
- Karaś, K., Salkowska, A., Walczak-Drzewiecka, A., Ryba, K., Dastych, J., Bachorz, R.A., Ratajowski, M., 2018. The cardenolides strophanthidin, digoxigenin and dihydroouabain act as activators of the human ROR $\gamma$ /ROR $\gamma$ T receptors. *Toxicol. Lett.* 295, 314–324.
- Kim, S., Chen, J., Cheng, T., Gindulyte, A., He, J., He, S., Li, Q., Shoemaker, B.A., Thiessen, P.A., Yu, B., Zaslavsky, L., Zhang, J., Bolton, E.E., 2019. PubChem 2019 update: improved access to chemical data. *Nucleic Acids Res.* 47, D1102–d1109.
- Kistowska, M., Meier, B., Proust, T., Feldmeyer, L., Cozzio, A., Kuendig, T., Contassot, E., French, L.E., 2015. Propionibacterium acnes promotes Th17 and Th17/Th1 responses in acne patients. *J. Invest. Dermatol.* 135, 110–118.
- Kojima, H., Muromoto, R., Takahashi, M., Takeuchi, S., Takeda, Y., Jetten, A.M., Matsuda, T., 2012. Inhibitory effects of azole-type fungicides on interleukin-17 gene expression via retinoic acid receptor-related orphan receptors  $\alpha$  and  $\gamma$ . *Toxicol. Appl. Pharm.* 259, 338–345.
- Kojima, H., Takeda, Y., Muromoto, R., Takahashi, M., Hirao, T., Takeuchi, S., Jetten, A. M., Matsuda, T., 2015. Isoflavones enhance interleukin-17 gene expression via retinoic acid receptor-related orphan receptors  $\alpha$  and  $\gamma$ . *Toxicology* 329, 32–39.
- Krause, M., Klit, A., Blomberg Jensen, M., Soeborg, T., Frederiksen, H., Schlumpf, M., Lichtensteiger, W., Skakkebaek, N.E., Drzewiecki, K.T., 2012. Sunscreens: are they beneficial for health? An overview of endocrine disrupting properties of UV-filters. *Int. J. Androl.* 35, 424–436.
- Kumar, N., Lyda, B., Chang, M.R., Lauer, J.L., Solt, L.A., Burris, T.P., Kamenecka, T.M., Griffin, P.R., 2012. Identification of SR2211: a potent synthetic ROR $\gamma$ -selective modulator. *ACS Chem. Biol.* 7, 672–677.
- Kunz, P.Y., Fent, K., 2006. Multiple hormonal activities of UV filters and comparison of in vivo and in vitro estrogenic activity of ethyl-4-aminobenzoate in fish. *Aquat. Toxicol.* 79, 305–324.
- Lamb, D., De Sousa, D., Quast, K., Fundel-Clemens, K., Erjefält, J.S., Sandén, C., Hoffmann, H.J., Kästle, M., Schmid, R., Menden, K., Delic, D., 2021. ROR $\gamma$ t inhibitors block both IL-17 and IL-22 conferring a potential advantage over anti-IL-17 alone to treat severe asthma. *Respir. Res.* 22, 158.
- Leijten, E.F., van Kempen, T.S., Olde Nordkamp, M.A., Pouw, J.N., Kleinrensink, N.J., Vincken, N.L., Mertens, J., Balak, D.M.W., Verhagen, F.H., Hartgring, S.A., Lubberts, E., Tekstra, J., Pandit, A., Radstake, T.R., Boes, M., 2021. Tissue-resident memory CD $8^{+}$  T cells from skin differentiate psoriatic arthritis from psoriasis. *Arthritis Rheumatol.* 73, 1220–1232.
- Lewis, J.M., Monico, P.F., Mirza, F.N., Xu, S., Yumeen, S., Turban, J.L., Galan, A., Girardi, M., 2021. Chronic UV radiation-induced ROR $\gamma$  agonist IL-22-producing lymphoid cells are associated with mutant KC clonal expansion. *Proc. Natl. Acad. Sci. USA* 118, e2016963118.
- Liao, C., Kannan, K., 2014. Widespread occurrence of benzophenone-type UV light filters in personal care products from China and the United States: an assessment of human exposure. *Environ. Sci. Technol.* 48, 4103–4109.

- Martin-Orozco, N., Muranski, P., Chung, Y., Yang, X.O., Yamazaki, T., Lu, S., Hwu, P., Restifo, N.P., Overwijk, W.W., Dong, C., 2009. T helper 17 cells promote cytotoxic T cell activation in tumor immunity. *Immunity* 31, 787–798.
- Matwiejczuk, N., Galicka, A., Brzóska, M.M., 2020. Review of the safety of application of cosmetic products containing parabens. *J. Appl. Toxicol.* 40, 176–210.
- Medvedev, A., Yan, Z.H., Hirose, T., Giguère, V., Jetten, A.M., 1996. Cloning of a cDNA encoding the murine orphan receptor RZR/ROR gamma and characterization of its response element. *Gene* 181, 199–206.
- Miossec, P., Kolls, J.K., 2012. Targeting IL-17 and TH17 cells in chronic inflammation. *Nat. Rev. Drug Discov.* 11, 763–776.
- Molins-Delgado, D., Olmo-Campos, M.D.M., Valeta-Juan, G., Pleguezuelos-Hernández, V., Barceló, D., Díaz-Cruz, M.S., 2018. Determination of UV filters in human breast milk using turbulent flow chromatography and babies' daily intake estimation. *Environ. Res.* 161, 532–539.
- Montaldo, E., Juelke, K., Romagnani, C., 2015. Group 3 innate lymphoid cells (ILC3s): origin, differentiation, and plasticity in humans and mice. *Eur. J. Immunol.* 45, 2171–2182.
- Nowak, K., Ratajczak-Wrona, W., Górska, M., Jabłońska, E., 2018. Parabens and their effects on the endocrine system. *Mol. Cell. Endocrinol.* 474, 238–251.
- O'Boyle, N.M., Banck, M., James, C.A., Morley, C., Vandermeersch, T., Hutchison, G.R., 2011. Open babel: an open chemical toolbox. *J. Cheminform.* 3, 33.
- Ozaki, H., Sugihara, K., Watanabe, Y., Fujino, C., Uramaru, N., Sone, T., Ohta, S., Kitamura, S., 2013. Comparative study of the hydrolytic metabolism of methyl-, ethyl-, propyl-, butyl-, heptyl- and dodecylparaben by microsomes of various rat and human tissues. *Xenobiotica* 43, 1064–1072.
- Pan, H.F., Li, X.P., Zheng, S.G., Ye, D.Q., 2013. Emerging role of interleukin-22 in autoimmune diseases. *Cytokine Growth Factor Rev.* 24, 51–57.
- Pantelyushin, S., Haak, S., Ingold, B., Kulig, P., Heppner, F.L., Navarini, A.A., Becher, B., 2012. Ror $\gamma$ mat+ innate lymphocytes and gammadelta T cells initiate psoriasis-like plaque formation in mice. *J. Clin. Invest.* 122, 2252–2256.
- Peiser, M., 2013. Role of Th17 cells in skin inflammation of allergic contact dermatitis. *Clin. Dev. Immunol.* 2013, 261037.
- PubChem, 2015. PubChem Bioassay Record for AID 1159523. National Library of Medicine (US), National Center for Biotechnology Information.**
- Sandanger, T.M., Huber, S., Moe, M.K., Braathen, T., Leknes, H., Lund, E., 2011. Plasma concentrations of parabens in postmenopausal women and self-reported use of personal care products: the NOWAC postgenome study. *J. Expo. Sci. Environ. Epidemiol.* 21, 595–600.
- Sarveiya, V., Risk, S., Benson, H.A., 2004. Liquid chromatographic assay for common sunscreen agents: application to in vivo assessment of skin penetration and systemic absorption in human volunteers. *J. Chromatogr. B Anal. Technol. Biomed. Life Sci.* 803, 225–231.
- Sasaki, Y., Odan, M., Yamamoto, S., Kida, S., Ueyama, A., Shimizu, M., Haruna, T., Watanabe, A., Okuno, T., 2018. Discovery of a potent orally bioavailable retinoic acid receptor-related orphan receptor-gamma-t (ROR $\gamma$ t) inhibitor, S18-000003. *Bioorg. Med. Chem. Lett.* 28, 3549–3553.
- Satoh, K., Nonaka, R., Ohya, K.-i., Nagai, F., 2005. Androgenic and antiandrogenic effects of alkylphenols and parabens assessed using the reporter gene assay with stably transfected CHO-K1 cells (AR-EcoScreen System). *J. Health Sci.* 51, 557–568.
- Schlecht, C., Klammer, H., Jarry, H., Wuttke, W., 2004. Effects of estradiol, benzophenone-2 and benzophenone-3 on the expression pattern of the estrogen receptors (ER) alpha and beta, the estrogen receptor-related receptor 1 (ERR1) and the aryl hydrocarbon receptor (AhR) in adult ovariectomized rats. *Toxicology* 205, 123–130.
- Schmittgen, T.D., Livak, K.J., 2008. Analyzing real-time PCR data by the comparative C (T) method. *Nat. Protoc.* 3, 1101–1108.
- Schrödinger LLC, 2019. Maestro Small-Molecule Drug Discovery Suite 2019-3.**
- Simeoni, S., Scalia, S., Benson, H.A.E., 2004. Influence of cyclodextrins on in vitro human skin absorption of the sunscreen, butyl-methoxydibenzoylmethane. *Int. J. Pharmaceut.* 280, 163–171.
- Simon, D., Aeberhard, C., Erdemoglu, Y., Simon, H.U., 2014. Th17 cells and tissue remodeling in atopic and contact dermatitis. *Allergy* 69, 125–131.
- Slominski, A.T., Kim, T.K., Takeda, Y., Janjetovic, Z., Brozyna, A.A., Skobowiat, C., Wang, J., Postlethwaite, A., Li, W., Tuckey, R.C., Jetten, A.M., 2014. ROR $\alpha$  and ROR $\gamma$  are expressed in human skin and serve as receptors for endogenously produced noncalcemic 20-hydroxy- and 20,23-dihydroxyvitamin D. *Faseb J.* 28, 2775–2789.
- Smith, S.H., Peredo, C.E., Takeda, Y., Bui, T., Neil, J., Rickard, D., Millerman, E., Therrien, J.P., Nicodeme, E., Brusq, J.M., Birault, V., Viviani, F., Hofland, H., Jetten, A.M., Cote-Sierra, J., 2016. Development of a topical treatment for psoriasis targeting ROR $\gamma$ : from bench to skin. *PLoS One* 11, e0147979.
- Solt, L.A., Burris, T.P., 2012. Action of RORs and their ligands in (patho)physiology. *Trends Endocrinol. Metab.* 23, 619–627.
- Solt, L.A., Griffin, P.R., Burris, T.P., 2010. Ligand regulation of retinoic acid receptor-related orphan receptors: implications for development of novel therapeutics. *Curr. Opin. Lipidol.* 21, 204–211.
- Strutzenberg, T.S., Garcia-Ordóñez, R.D., Novick, S.J., Park, H., Chang, M.R., Doebellin, C., He, Y., Patouret, R., Kamenecka, T.M., Griffin, P.R., 2019. Correction: HDX-MS reveals structural determinants for ROR $\gamma$  hyperactivation by synthetic agonists. *Elife* 8, e52847.
- Sun, N., Guo, H., Wang, Y., 2019. Retinoic acid receptor-related orphan receptor gamma-t (ROR $\gamma$ t) inhibitors in clinical development for the treatment of autoimmune diseases: a patent review (2016–present). *Expert Opin. Ther. Pat.* 29, 663–674.
- Suzuki, T., Kitamura, S., Khota, R., Sugihara, K., Fujimoto, N., Ohta, S., 2005. Estrogenic and antiandrogenic activities of 17 benzophenone derivatives used as UV stabilizers and sunscreens. *Toxicol. Appl. Pharmacol.* 203, 9–17.
- Swain, M., 2013. PubChemPy.** (<https://pypi.python.org/pypi/PubChemPy/1.0>).
- Takaishi, M., Ishizaki, M., Suzuki, K., Isobe, T., Shimozato, T., Sano, S., 2017. Oral administration of a novel ROR $\gamma$ t antagonist attenuates psoriasis-like skin lesion of two independent mouse models through neutralization of IL-17. *J. Dermatol. Sci.* 85, 12–19.
- Tarazona, I., Chisvert, A., Salvador, A., 2013. Determination of benzophenone-3 and its main metabolites in human serum by dispersive liquid-liquid microextraction followed by liquid chromatography tandem mass spectrometry. *Talanta* 116, 388–395.
- Villanova, F., Flutter, B., Tosi, I., Grys, K., Sreeneebus, H., Perera, G.K., Chapman, A., Smith, C.H., Di Meglio, P., Nestle, F.O., 2014. Characterization of innate lymphoid cells in human skin and blood demonstrates increase of Nkp44+ ILC3 in psoriasis. *J. Invest. Dermatol.* 134, 984–991.
- Villey, I., de Chasseval, R., de Villartay, J.P., 1999. ROR $\gamma$ mat, a thymus-specific isoform of the orphan nuclear receptor ROR $\gamma$ mat/TOR, is up-regulated by signaling through the pre-T cell receptor and binds to the TEA promoter. *Eur. J. Immunol.* 29, 4072–4080.
- Wang, J., Pan, L., Wu, S., Lu, L., Xu, Y., Zhu, Y., Guo, M., Zhuang, S., 2016. Recent advances on endocrine disrupting effects of UV filters. *Int. J. Environ. Res. Public Health* 13, 782.
- Wang, Y., Kumar, N., Nuhant, P., Cameron, M.D., Istrate, M.A., Roush, W.R., Griffin, P.R., Burris, T.P., 2010. Identification of SR1078, a synthetic agonist for the orphan nuclear receptors ROR $\alpha$  and ROR $\gamma$ . *ACS Chem. Biol.* 5, 1029–1034.
- Watanabe, Y., Kojima, H., Takeuchi, S., Uramaru, N., Sanoh, S., Sugihara, K., Kitamura, S., Ohta, S., 2015. Metabolism of UV-filter benzophenone-3 by rat and human liver microsomes and its effect on endocrine-disrupting activity. *Toxicol. Appl. Pharm.* 282, 119–128.
- Weigmann, H.J., Lademann, J., Schanzer, S., Lindemann, U., von Pelchrzim, R., Schaefer, H., Sterry, W., Shah, V., 2001. Correlation of the local distribution of topically applied substances inside the stratum corneum determined by tape-stripping to differences in bioavailability. *Skin Pharm. Physiol.* 14 (Suppl. 1), S98–S102.
- Xu, T., Wang, X., Zhong, B., Nurieva, R.I., Ding, S., Dong, C., 2011. Ursolic acid suppresses interleukin-17 (IL-17) production by selectively antagonizing the function of ROR $\gamma$  t protein. *J. Biol. Chem.* 286, 22707–22710.
- Yang, X.O., Pappu, B.P., Nurieva, R., Akimzhanov, A., Kang, H.S., Chung, Y., Ma, L., Shah, B., Panopoulos, A.D., Schluns, K.S., Watowich, S.S., Tian, Q., Jetten, A.M., Dong, C., 2008. T helper 17 lineage differentiation is programmed by orphan nuclear receptors ROR alpha and ROR gamma. *Immunity* 28, 29–39.
- Yiin, L.M., Tian, J.N., Hung, C.C., 2015. Assessment of dermal absorption of DEET-containing insect repellent and oxybenzone-containing sunscreen using human urinary metabolites. *Environ. Sci. Pollut. Res. Int.* 22, 7062–7070.
- Zheng, Y., Danilenko, D.M., Valdez, P., Kasman, I., Eastham-Anderson, J., Wu, J., Ouyang, W., 2007. Interleukin-22, a TH17 cytokine, mediates IL-23-induced dermal inflammation and acanthosis. *Nature* 445, 648–651.



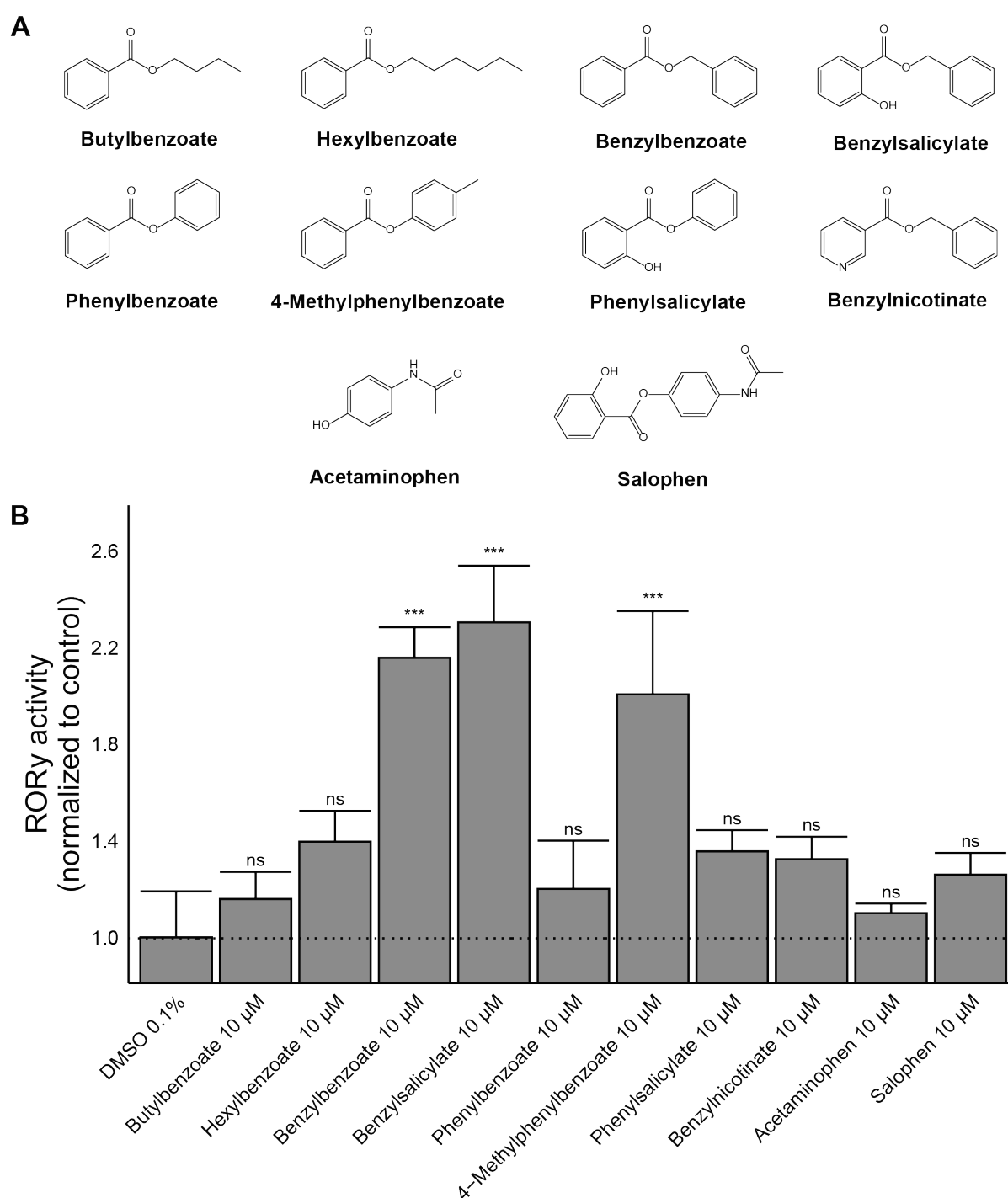
# 1 Supplementary information

## Computational Methods

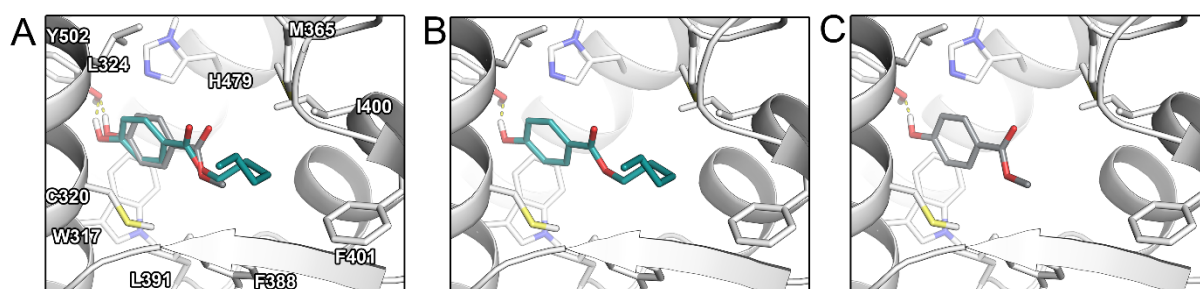
To investigate binding modes of parabens and benzophenones within the orthosteric pocket of ROR $\gamma$ , the standard-precision docking protocol of Glide [1] retaining default settings were selected. The respective crystal structure (PDB ID: 6FZU) was retrieved from the Protein Data Bank [2] and processed using the Protein Preparation Wizard [3] within Maestro. There, hydrogen atoms were added, bond orders assigned, the protonation states of ionizable groups at pH 7.4 predicted, the hydrogen bonding network reoriented, and the system subjected to a restrained minimization with the OPLS3e force field at a convergence threshold of 0.3 Å for protein heavy atoms. The ligand conformers for docking were available from the previously conducted similarity search.

**Supplementary Table 1.** Compounds selected for in vitro testing including the 2D and 3D Tanimoto score compared to the template structure.

Template	Substance	CAS Nr.	Similarity-2D	Similarity-3D
Benzylparaben	Benzylnicotinate	94-44-0	0.49	0.49
	Benzylbenzoate	120-51-4	0.66	0.60
	Benzylsalicylate	118-58-1	0.47	0.48
Hexylparaben	Hexylbenzoate	6789-88-4	0.64	0.62
Heptylparaben			0.60	0.49
Butylparaben	Butylbenzoate	136-60-7	0.61	0.59
Phenylparaben	Phenylbenzoate	93-99-2	0.63	0.56
	Phenylsalicylate	118-55-8	0.43	0.43
	4-Methylphenylbenzoate	614-34-6	0.44	0.29
SR0987	Salophen	118-57-0	0.19	0.21
	Acetaminophen	103-90-2	0.17	0.20



**Suppl. Fig. 1. Compounds selected from the similarity search.** (A) Chemical structures of investigated compounds from the similarity search. (B) ROR $\gamma$  activation by compounds selected from the similarity search. ROR $\gamma$  expression was induced by exposure of the Tet-on cells to doxycycline, and cells were incubated with 10  $\mu$ M of test compounds. Luciferase activity was determined and normalized to that of the vehicle control DMSO. Data represent mean  $\pm$  SD from three independent experiments. Data were analyzed by one-way ANOVA followed by the Dunnett's post-hoc test, p values: \* < 0.05, \*\* < 0.001, \*\*\* < 0.001, ns (not significant).



**Suppl. Fig. 2.** Predicted binding modes of **A)** methylparaben and hexylparaben together, **B)** hexylparaben, and **C)** methylparaben in the binding pocket of ROR $\gamma$ . Residues in the proximity of the ligand and hydrogen bonds to Y502 are depicted.

### Supplementary references

- [1] Halgren TA, Murphy RB, Friesner RA, Beard HS, Frye LL, Pollard WT, et al. Glide: A New Approach for Rapid, Accurate Docking and Scoring. 2. Enrichment Factors in Database Screening. *J Med Chem.* 2004;47(7):1750–9.
- [2] H.M. Berman, J. Westbrook, Z. Feng, G. Gilliland, T.N. Bhat, H. Weissig, I.N. Shindyalov, P.E. Bourne. (2000) *The Protein Data Bank Nucleic Acids Research*, 28: 235-242.
- [3] Madhavi Sastry G, Adzhigirey M, Day T, Annabhimoju R, Sherman W. Protein and ligand preparation: Parameters, protocols, and influence on virtual screening enrichments. *J Comput Aided Mol Des.* 2013;27(3):221–34.

### 6.3 Discussion

Parabens and UV-filters are used as additives in cosmetics and have so far mainly been investigated for their direct influence on androgen and estrogen receptors (reviewed in [372, 373]). Their influence on other nuclear receptors such as ROR $\gamma$ t, which controls the expression of pro-inflammatory cytokines such as IL-17 in T-helper cells, have been studied less thoroughly [188].

In this study we have shown that certain parabens and UV-filters are able to activate ROR $\gamma$ (t), where the strongest agonists, hexylparaben, benzylparaben and BP-10 displayed relatively low EC<sub>50</sub> values in the nanomolar or low micromolar range (144 nM, 3.39  $\mu$ M, and 1.67  $\mu$ M, respectively). Those three ROR $\gamma$ (t) agonists were able to reconstitute ROR $\gamma$ (t) activity after treatment with the potent inverse agonist SR2211 and increased the transcription of pro-inflammatory interleukins IL-17A and IL-22 in EL4 cells, a murine model for Th17 cells.

Computational similarity screening based on newly identified and already described ROR $\gamma$ (t) agonists allowed us to identify the body care constituents benzylbenzoate, benzylsalicylate, and 4-methylphenylbenzoate as ROR $\gamma$ (t) agonists. Those compounds displayed EC<sub>50</sub> values in the lower micromolar range (8.16  $\mu$ M, 2.39  $\mu$ M and 3.96  $\mu$ M, respectively) and also reconstituted ROR $\gamma$ (t) activity after treatment with the inverse agonist SR2211.

To date, only the LBD of ROR $\gamma$  has been successfully crystallized and over 100 co-crystallizations of the LBD and respective ligands have already been published (reviewed in [374]). The availability of such highly resolved crystal structures allowed us to address potential binding modes of some of the identified agonists to the orthosteric ROR $\gamma$  LBD, comparing them with inactive compounds [375]. According to the prediction of our computational model, both methyl- and hexylparaben appear to bind to the same location with their phenyl cores, but the binding may be additionally stabilized via interactions of the alkyl chain of the parabens with a hydrophobic sub-pocket in the LBD. Accordingly, binding interactions of hexylparaben to the ROR $\gamma$  LBD may be stronger than the ones from methylparaben due to its longer alkyl chain, which could be an explanation for their distinct influences on ROR $\gamma$  activity. Unfortunately, the binding analysis of agonistic benzophenone-type UV-filters was inconclusive and no clear binding modes of these ligands to ROR $\gamma$  could be estimated. This might also result from the plasticity of the orthosteric LBD of ROR $\gamma$ . Depending on the ligand, the ROR $\gamma$  LBD can adopt different conformations by means of induced-fit binding (reviewed in [374]). It is possible that ROR $\gamma$  adopted a suboptimal

conformation in the crystal structure on which we based our model, which might have complicated the determination of a possible binding mode of BPs. Future modeling of binding modes of parabens, UV-filters and other xenobiotics to the LBD of ROR $\gamma$ (t) should take induced-fit binding into account and should therefore be tested for different possible conformations of the LBD. Ideally, the binding modes of new ROR $\gamma$ (t) ligands should be determined via co-crystallization, if possible.

The identified parabens and UV-filters that act as ROR $\gamma$ t agonists may potentially exacerbate pre-existing inflammatory diseases by increasing ROR $\gamma$ t activity, especially in the skin where human exposure to these substances is expected to be the highest.

Notably, parabens are hydrolyzed relatively quickly in the skin, but so far it has not yet been elucidated what concentrations parabens could reach in the human skin after topical application [220]. Therefore, it is rather difficult to evaluate whether parabens are likely to cause a possible aggravation of inflammatory skin diseases such as psoriasis through ROR $\gamma$ (t) agonism. Of the UV-filters that we investigated, BP-3 can be expected to reach the highest concentrations in skin, since it is legally authorized in sunscreens as an active UV-absorbing ingredient in quantities of up to 6% and has been shown to penetrate skin efficiently [238, 376, 377]. BP-3 is itself able to increase ROR $\gamma$  activity and is metabolized in the human liver to BP-1 and 4,4'-dihydroxy-BP, among others, which both act as slightly weaker ROR $\gamma$ (t) agonists than their parent compound (reviewed in [242]).

Parabens and UV-filters are mostly used as mixtures in cosmetics and body care products which is why we examined mixture effects of the identified agonists on ROR $\gamma$  activity. Parabens, UV-filters as well as the identified similarity compounds showed additive effects towards ROR $\gamma$ (t) activity. Accordingly, individual low concentrations of multiple single agonistic parabens or UV-filters present within the human body may act in an additive or even synergistic manner to activate ROR $\gamma$ (t). Whether parabens, UV-filters, and their metabolites reach concentrations high enough in human tissues, such as the skin, to increase ROR $\gamma$ (t) activity has not yet been sufficiently investigated. Future experiments should therefore include simultaneous quantification of a broader spectrum of parabens and UV-filters, including their metabolites. Ideally, methods should be established to measure such a panel in different tissue backgrounds and bodily fluids, so that possible local ROR $\gamma$ (t) activation may be estimated more accurately. Establishment of experimentally validated pharmacokinetic models that simulate the metabolism of parabens and UV-filters within the human body would also facilitate the estimation of local paraben and UV-filter concentrations in tissues or bodily fluids after exposure.

In this project, we were able to show that certain parabens and UV-filters can increase the ROR $\gamma$ t-mediated transcription of pro-inflammatory interleukins, IL-17A and IL-22 in EL4 cells. However, this experimental setup had certain limitations. Although the EL4 cell model possesses an endogenously expressed ROR $\gamma$ t, this cellular system was not responsive enough on its own for efficient quantification of IL transcription levels. Therefore, we had to transiently transfect the cells with the human homolog of ROR $\gamma$ t first, before treating them with the previously identified ROR $\gamma$ (t) agonists. Additional experiments should be carried out with human primary Th17 cells or *in vitro* differentiated Th17 cells, which endogenously express ROR $\gamma$ t and also produce pro-inflammatory interleukins such as IL-17 [378]. In addition to the ROR $\gamma$ t mediated changes in mRNA levels of pro-inflammatory interleukins, the actual protein levels of the respective interleukins may be detected using immunoassays.

Whether parabens and UV-filters could exacerbate existing inflammatory skin diseases such as psoriasis by ROR $\gamma$ t activation requires further investigation using suitable models, such as one of the numerous rodent psoriasis models or a 3D immunocompetent psoriatic human skin model [379, 380]. Metabolism of parabens and UV-filters as well as additive or even synergistic effects of ROR $\gamma$ (t) agonists and their metabolites need to be taken into account when performing such experiments.

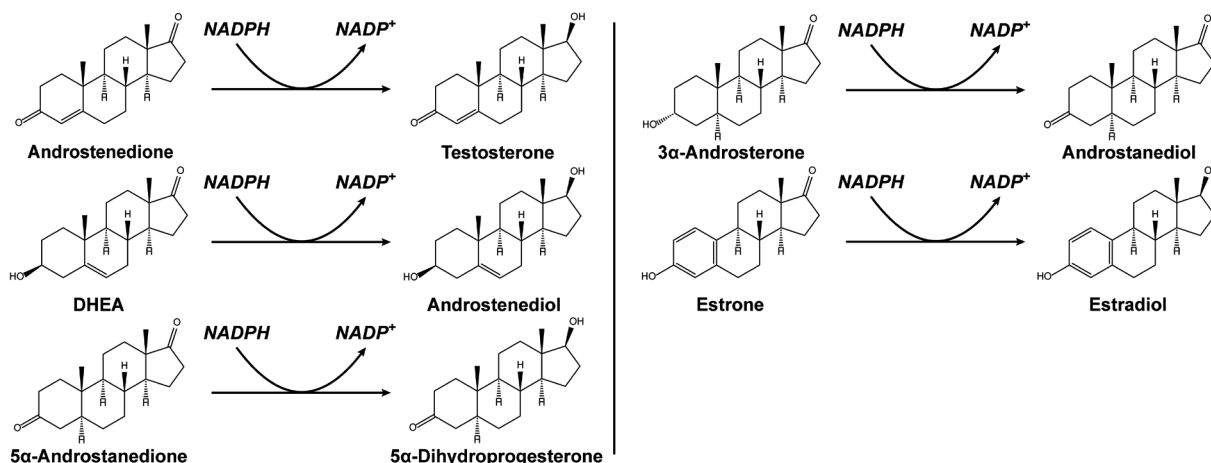
The outcomes of this project provide a good scientific basis for further studies in which a possible role of parabens and UV-filters in the aggravation of inflammatory skin diseases such as psoriasis could be investigated.

## 7. Additional project 4: Assessment of novel mutations in *HSD17B3* gene

### 7.1 Introduction

Human gonadal differentiation starts around six weeks after conception. The sex-determining region Y protein (SRY) encoded on the Y chromosome upregulates the expression of the SRY-Box Transcription Factor 9 (SOX9), which initiates the differentiation of bipotent gonads into testes [381-383]. During this process, primordial germ cells can differentiate into Sertoli and Leydig cells. Sertoli cells produce anti-Müllerian hormone (AMH), which inhibits the development of the female reproductive tract, while Leydig cells produce testosterone, which stabilizes the Wolffian ducts via AR activation, leading to formation of the vas deferens, epididymis, and seminal vesicles [31]. Secreted, systemic testosterone is further reduced by SRD5A2 to the more potent DHT in the respective target tissues, where localized AR activation leads to the masculinization of the external genitalia [384].

HSD17B3 localizes in the ER of Leydig cells and catalyzes the final enzymatic step of testosterone generation: the 17 $\beta$ -reduction of androstenedione to testosterone using NADPH as cofactor (Figure 12) [89, 385]. In addition to this reaction, the enzyme can also convert a variety of additional 17-ketosteroids, such as DHEA, 5 $\alpha$ -androstenedione, 3 $\alpha$ -androsterone and estrone to their 17 $\beta$ -forms: androstenediol, DHT, 3 $\alpha$ -adiol and estradiol, respectively, but with lower efficiency [89, 386].



**Figure 12. Enzymatic activities of HSD17B3.** HSD17B3 catalyzes the NADPH mediated 17 $\beta$ -reduction of various 17-ketosteroids such as androstenedione, dehydroepiandrosterone (DHEA), 5 $\alpha$ -androstenedione, 3 $\alpha$ -androsterone and estrone.

Partial or complete HSD17B3 deficiency results in 46,XY DSD characterized by a spectrum of clinical phenotypes [52, 387]. At birth, affected patients may present an underdevelopment of the external genitalia that often appears female, with a blind-ending vagina, with or without clitoromegaly and/or labial fusion, undescended testes and often with normal Wolffian duct derivatives [388]. HSD17B3 deficiency can be easily overlooked directly after birth, therefore patients are commonly raised as females. Primary amenorrhea and severe virilization of the patient during puberty may eventually lead to the correct diagnosis by a physician. The observed virilization is caused by extratesticular conversion of androstenedione to testosterone by AKR1C3 and could present as lack of breast development, hirsutism or deepening of the voice [52, 388-390]. HSD17B3 deficiency diagnosis is based on a decreased ratio of testosterone to androstenedione ( $< 0.8$ ) which reflects the enzymatic activity of HSD17B3 [388].

In this project, we analyzed three novel case reports of HSD17B3 deficiency from Tunisia, two of which originated from different consanguineous families. We identified and experimentally validated the molecular mechanism of two novel mutations in the *HSD17B3* gene: one turned out to be a pathogenic loss of function mutation in the catalytic tetrad of the enzyme, and the second was a splice site mutation.



## 7.2 Published article: Molecular mechanisms underlying the defects of two novel mutations in the HSD17B3 gene found in the Tunisian population

Bochra Ben Rhouma <sup>a,b,1</sup>, Manuel Kley <sup>c,d,1</sup>, Fakhri Kallabi <sup>a</sup>, Faten Hadj Kacem <sup>e</sup>, Thouraya Kammoun <sup>f</sup>, Wajdi Safi <sup>e</sup>, Leila Keskes <sup>a</sup>, Mouna Mnif <sup>e</sup>, Alex Odermatt <sup>c,d,\*,1</sup>, Neila Belguith <sup>a,g,1</sup>

<sup>a</sup> Human Molecular Genetics Laboratory, Faculty of Medicine, 3029 Sfax, Tunisia

<sup>b</sup> Higher Institute of Nursing, M. Ali Street, 4000 Gabes, Tunisia

<sup>c</sup> Division of Molecular and Systems Toxicology, Department of Pharmaceutical Sciences, University of Basel, Klingelbergstrasse 50, 4056 Basel, Switzerland

<sup>d</sup> Swiss Centre for Applied Human Toxicology and Department of Pharmaceutical Sciences, University of Basel, Missionsstrasse 64, 4055 Basel, Switzerland

<sup>e</sup> Department of Endocrinology, Hedi Chaker Hospital, 3029 Sfax, Tunisia

<sup>f</sup> Department of Pediatrics, Hedi Chaker Hospital, 3029 Sfax, Tunisia

<sup>g</sup> Department of Congenital and Hereditary Diseases, 1010 Charles Nicolle Hospital, Tunis, Tunisia

\* Corresponding author. e-mail address: alex.odermatt@unibas.ch

### Published article

**Personal contribution:** Establishment and execution of splicing assay (Figure 2). Cloning and expression control of the p.K202M mutant and functional analysis of wild type and mutant HSD17B3 variants by enzyme activity assay (Figure 3). Review of all described *HSD17B3* mutants known until August 2022 (Figure 4). Drafting and revision of the manuscript.

**Aims:** Genetic and molecular analysis of 3 novel cases of HSD17B3 deficiency found in Tunisian families.

**Conclusion:** Identification and molecular characterization of a novel null mutant of the *HSD17B3* gene (p.K202M) and a novel splice site mutant thereof may allow quicker diagnosis in future HSD17B3 deficiency cases with the same mutations.



## Molecular mechanisms underlying the defects of two novel mutations in the *HSD17B3* gene found in the Tunisian population

Bochra Ben Rhouma<sup>a,b,1</sup>, Manuel Kley<sup>c,d,1</sup>, Fakhri Kallabi<sup>a</sup>, Faten Hadj Kacem<sup>e</sup>,  
Thouraya Kammoun<sup>f</sup>, Wajdi Safi<sup>e</sup>, Leila Keskes<sup>a</sup>, Mouna Mnif<sup>e</sup>, Alex Odermatt<sup>c,d,\*,1</sup>,  
Neila Belguith<sup>a,g,1</sup>

<sup>a</sup> Human Molecular Genetics Laboratory, Faculty of Medicine, 3029 Sfax, Tunisia

<sup>b</sup> Higher Institute of Nursing, M. Ali Street, 4000 Gabes, Tunisia

<sup>c</sup> Division of Molecular and Systems Toxicology, Department of Pharmaceutical Sciences, University of Basel, Klingelbergstrasse 50, 4056 Basel, Switzerland

<sup>d</sup> Swiss Centre for Applied Human Toxicology and Department of Pharmaceutical Sciences, University of Basel, Missionsstrasse 64, 4055 Basel, Switzerland

<sup>e</sup> Department of Endocrinology, Hedi Chaker Hospital, 3029 Sfax, Tunisia

<sup>f</sup> Department of Pediatrics, Hedi Chaker Hospital, 3029 Sfax, Tunisia

<sup>g</sup> Department of Congenital and Hereditary Diseases, 1010 Charles Nicolle Hospital, Tunis, Tunisia

### ARTICLE INFO

#### Keywords:

HSD17B3

17beta-hydroxysteroid dehydrogenase

46,XY Disorders of Sex Development

Mutation

Alternative splicing

Testosterone

Androgen deficiency

### ABSTRACT

17 $\beta$ -hydroxysteroid dehydrogenase type 3 (17 $\beta$ -HSD3) converts  $\Delta$ 4-androstene-3,17-dione (androstenedione) to testosterone. It is expressed almost exclusively in the testes and is essential for appropriate male sexual development. More than 70 mutations in the *HSD17B3* gene that cause 17 $\beta$ -HSD3 deficiency and result in 46,XY Disorders of Sex Development (46,XY DSD) have been reported. This study describes three novel Tunisian cases with mutations in *HSD17B3*. The first patient is homozygous for the previously reported mutation p.C206X. The inheritance of this mutation seemed to be independent of consanguineous marriage, which can be explained by its high frequency in the Tunisian population. The second patient has a novel splice site mutation in intron 6 at position c.490 -6 T > C. A splicing assay revealed a complete omission of exon 7 in the resulting *HSD17B3* mRNA transcript. Skipping of exon 7 in *HSD17B3* is predicted to cause a frame shift in exon 8 that affects the catalytic site and results in a truncation in exon 9, leading to an inactive enzyme. The third patient is homozygous for the novel missense mutation p.K202M, representing the first mutation identified in the catalytic tetrad of 17 $\beta$ -HSD3. Site-directed mutagenesis and enzyme activity measurements revealed a completely abolished 17 $\beta$ -HSD3 activity of the p.K202M mutant, despite unaffected protein expression, compared to the wild-type enzyme. Furthermore, the present study emphasizes the importance of genetic counselling, detabooization of 46,XY DSD, and a sensitization of the Tunisian population for the risks of consanguineous marriage.

### 1. Introduction

17 $\beta$ -hydroxysteroid dehydrogenase type 3 (17 $\beta$ -HSD3) deficiency, a rare autosomal recessive cause of 46,XY Disorders of Sex Development (46,XY DSD), was first described in 1971 [1] and is caused by mutations in the *HSD17B3* gene (9q22) encoding 17 $\beta$ -HSD3 [2–5]. To date, more than 70 mutations in *HSD17B3* have been described, of which about one-third has been experimentally verified to cause 17 $\beta$ -HSD3

deficiency [6] (see also below, Fig. 4 and Supplementary Table 1). 17 $\beta$ -HSD3 is predominantly expressed in the testes and uses NADPH as cofactor to catalyze the conversion of  $\Delta$ 4-androstene-3,17-dione (androstenedione) to testosterone, which is essential for the normal fetal development of male genitalia [2]. 17 $\beta$ -HSD3 deficiency is characterized by a spectrum of clinical phenotypes due to a complete loss or residual activity of mutant 17 $\beta$ -HSD3 enzyme in the testes [3,4]. The onset of the extra-testicular conversion of androstenedione to testosterone by

\* Corresponding author at: Division of Molecular and Systems Toxicology, Department of Pharmaceutical Sciences, University of Basel, Klingelbergstrasse 50, 4056 Basel, Switzerland.

E-mail addresses: bochra.benrhouma@gmail.com (B. Ben Rhouma), manuel.kley@unibas.ch (M. Kley), fakhrikallabi@yahoo.fr (F. Kallabi), hadjkacemfaten@yahoo.fr (F.H. Kacem), thourayakammoun9@gmail.com (T. Kammoun), wajdisafi.zz@gmail.com (W. Safi), ammarkeskesl@gmail.com (L. Keskes), mnifmouna2020@gmail.com (M. Mnif), alex.odermatt@unibas.ch (A. Odermatt), neila.belguith@gmail.com (N. Belguith).

<sup>1</sup> These authors contributed equally to the presented study

<https://doi.org/10.1016/j.jsbmb.2022.106235>

Received 19 November 2022; Received in revised form 18 December 2022; Accepted 19 December 2022

Available online 20 December 2022

0960-0760/© 2022 The Authors. Published by Elsevier Ltd. This is an open access article under the CC BY license (<http://creativecommons.org/licenses/by/4.0/>).

17 $\beta$ -HSD5 (also known as AKR1C3) is mainly responsible for the observed virilization during puberty of patients with 17 $\beta$ -HSD3 deficiency [4]. The characteristic phenotype of such a patient at birth is an 46,XY individual with undervirilization of the external genitalia, which often appear female, with or without clitoromegaly and/or labial fusion and a blind-ending vagina [7]. Affected patients have testes and often normal Wolffian duct derivatives. The diagnosis of 17 $\beta$ -HSD3 deficiency is based on a decreased ratio of testosterone to androstenedione < 0.8 and can be suspected in case of inguinal hernia or sexual ambiguity at early childhood and in case of severe virilization and primary amenorrhea during puberty [4,7].

17 $\beta$ -HSD3 is a member of the short-chain dehydrogenase/reductase (SDR) superfamily (SDR12C2) [8]. SDR enzymes contain a conserved Rossmann-fold for NAD(P)(H) cofactor binding and a catalytic tetrad, with a tyrosine acting as acid/base catalyst, a lysine that together with the oxidized, positively charged nicotinamide cofactor lowers the tyrosine's hydroxyl pKa, a serine stabilizing and polarizing the carbonyl substrate group, and an asparagine that binds a water molecule with its main-chain carbonyl group, connecting the solvent with the active site tyrosine in form of a proton transfer system [9–12]. In human 17 $\beta$ -HSD3, the corresponding catalytic tetrad is composed of Asn157 Ser185, Tyr198, and Lys202, of which no known mutations had been identified in patients so far (Human Gene Mutation Database (HGMD), [13] accessed last August 2, 2022).

So far, three different mutations in *HSD17B3* causing 46,XY DSD have been identified in the Tunisian population: p.G133R, p.Q176P and p.C206X, with the latter representing a founder mutation within the Tunisian population [14–16]. In this work, we analyzed three novel cases of 17 $\beta$ -HSD3 deficiency, one patient from a non-consanguineous family and two patients from different consanguineous families. This led to the identification of two novel mutations in the *HSD17B3* gene. The effects of these mutations were assessed by a minigene-based splice assay and site-directed mutagenesis followed by enzyme activity measurements, respectively.

## 2. Materials and methods

### 2.1. Subjects and clinical history

Three Tunisian patients diagnosed with 46,XY Disorders of Sex Development (DSD) were studied. Patient P1 was initially examined at infant age due to hernia. Pelvic examination revealed bilateral inguinal masses consistent with testes, and magnetic resonance imaging (MRI) of the pelvis and the abdomen showed no visualization of the vagina or uterus. P2 was admitted to the hospital at the age of three months because of clitoral hypertrophy and inguinal hernia. Abdominal ultrasonography showed bilateral inguinal ovoid masses with testicular appearance. MRI of the pelvis and the abdomen showed no visualization of the vagina or uterus. Patient P3 was consulted at the age of 16 years for primary amenorrhea and virilization. Pelvic examination revealed vaginal agenesis, some vestiges of seminal vesicles in addition to bilateral inguinal masses consistent with testes and uterus. Karyotype analysis using standard G-banding technique revealed 46,XY for all patients. The results of hormonal baseline testing of all patients are listed in Table 1.

### 2.2. Sequencing of *HSD17B3*

DNA was extracted from whole blood samples of the patients and from their parents using phenol-chloroform standard procedures [17]. Sequencing was performed by PCR using previously reported primers [3], and the 11 encoding exons and their flanking intron regions were covered. The PCR was performed using a thermal cycler (GenAmp PCR System 9700, Applied Biosystem, Waltham, MA) in a final volume of 50  $\mu$ L containing 50 ng genomic DNA, 2  $\mu$ M of each primer, 1  $\times$  PCR buffer, 1.2 mM MgCl<sub>2</sub>, 0.5 mM dNTP, and 1 U Taq DNA polymerase (GoTaq

**Table 1**

Clinical, hormonal and genetic results of three patients with 46,XY disorder of sexual development.

	Patient 1 (P1)	Patient 2 (P2)	Patient 3 (P3)
Age	4 months	3 months	16 years
Height (cm)	na	na	168
Weight (kg)	na	na	68
Consanguinity	–	+	+
Masculinization score	1	3	3
Sex of rearing	na	na	female
Testosterone (ng/mL)	0.03 (<0.3 *)	0.86 (1.75–7.61 *)	2.89 (2.8–8 *)
Androstenedione (ng/mL)	11.9 (8–200 *)	79.6 (8–200 *)	9.6 (0.05–0.51 *)
LH (IU/L)	0.2 (0.1–0.4 *)	3.22 (0.1–4 *)	20.6 (1.7–8 *)
FSH (IU/L)	0.5 (1–5 *)	1 (1–5 *)	3 (1.5–12.4 *)
Karyotype analysis	46,XY	46,XY	46,XY
Referral reason	Hernia	Clitoral hypertrophy, inguinal hernia	Primary amenorrhea, virilization

Age corresponding reference values of measured hormones are shown in brackets with an asterisk. na, not analyzed.

DNA Polymerase, Promega, Fitchburg, WI). Direct sequencing of PCR products was performed on an ABI3730xl Genetic Analyzer using the Big Dye Terminator Cyclor Sequencing Ready Reaction Kit (Applied Biosystems). Both strands were sequenced to exclude PCR artefacts.

### 2.3. Sequence analysis and in silico pathogenicity prediction of novel *HSD17B3* gene variations

Sequencing data was analyzed using the software Chromas. A blast homology search was performed using the program BLAST2SEQ, available at the National Center for Biotechnology Information Website, to compare individual nucleotide sequences with the *HSD17B3* reference sequence (<http://blast.ncbi.nlm.nih.gov/Blast>). The human gene mutation database HGMD (<http://www.hgmd.cf.ac.uk/ac/index.php>, accessed last August 2, 2022, [13]) was used to confirm known and novel *HSD17B3* gene variations (see below, Fig. 4B).

Pathogenicity was investigated using the PolyPhen-2 program (Polymorphism Phenotyping v2), which estimates the probability that a missense mutation negatively affects the stability and function of a human protein. This program classifies a mutation based on a calculated score as benign, possibly damaging or probably damaging (<http://genetics.bwh.harvard.edu/pph2/>) [18]. Additionally, the PROVEAN program (Protein Variation Effect Analyzer) was used to predict whether an amino acid substitution or an indel mutation has an impact on the biological function of a protein. Calculated scores < 2.5 indicate that a polymorphism is possibly damaging, and scores > 2.5 indicate that the examined gene variation is likely benign (<http://provean.jcvi.org/seqs/ubmit.php>) [19].

Possible effects on splicing of the novel c.490 -6 T > C intronic mutation were analyzed using the ESEfinder software (<http://rulai.cshl.edu/tools/ESE/>). It predicts exonic splice enhancer (ESE) binding sites in RNA sequences, which are recognized by a specific splicing factor class, the so called serine/arginine-rich (SR) proteins. SR proteins promote splicing by recruiting spliceosomal components to the correct splice sites. The algorithm calculates a binding likelihood score for stretches of the input RNA bases and compares them with a threshold value of four of the SR proteins (SRSF1, SRSF2, SRSF5, SRSF6). If the threshold is exceeded, the sequence examined is predicted as putative ESE [20–22].

#### 2.4. Cloning of wild-type and mutant minigenes

The PCR amplification of exon 7 (35 base pairs) and its intron boundaries was performed using the following primers: forward: 5'-taggttaccatagttccccc-3', containing a mismatch to create a *Bst*II restriction site, and reverse primer R: 5'-ttgtctgtctgcagagtagcc-3' containing a mismatch to create a *Nhe*I endonuclease restriction site (restriction sites are marked in bold). PCR was performed on a thermal cycler (Biometra, Analytik Jena, Jena, Germany) with the iProof™ High-Fidelity PCR Kit (Bio-Rad Laboratories, Hercules, CA, USA) according to the manufacturer's protocol in a final reaction volume of 50 µL, using 0.5 µg genomic DNA of the patient P2's heterozygous mother (wt/c.490-6 T > C) as template. The total length of 631 bp of the expected PCR product, containing the 35 bp long exon 7 and its adjacent intron sequences, was confirmed by agarose gel electrophoresis. The amplified PCR product was inserted into the multiple cloning site (MCS) of a pRc/CMV plasmid, originally described by Deguillien et al. [23] and kindly provided by Dr. A. Ben Mahmoud [24]. This plasmid bears the exons 13 and 17 of the 4.1 gene including their downstream and upstream intron sequences, both flanking the multiple cloning site where the previously amplified exon 7 with its adjacent intron sequences was inserted using the restriction enzymes *Bst*II-HF and *Nhe*I as well as T4 ligase (New England Biolabs, NEB, Ipswich, MA). The newly generated plasmids were transformed into competent bacterial cells (*E. Coli*, *DH5α* strain) and subcloned, selecting for wild-type and mutant inserts. The generated minigenes were verified by Sanger sequencing (Microsynth, Balgach, Switzerland).

#### 2.5. Site-directed mutagenesis and construction of expression plasmid with p.K202M HSD17B3

An expression vector encoding FLAG-tagged, full-length human *HSD17B3* (reported earlier, [14]) was used as template to introduce the point mutation for p.K202M using the Stragene QuikChange® Site-Directed mutagenesis protocol and iProof™ High-Fidelity DNA polymerase (Bio-Rad Laboratories, Hercules, CA, USA) with the following primers: forward: 5'-tccatgactcagcttccatggcgtttgtgtgc-3', reverse: 5'-gcacacaacccatggaagctgagtagcatgga-3'. Template DNA was digested using *Dpn*I and the PCR product transformed into competent *DH5α E. Coli* cells for amplification. The plasmid was verified by Sanger sequencing (Microsynth).

#### 2.6. Cell culture

Human Embryonic Kidney-293 cells (HEK-293, ATCC, Manassas, VA) were cultured in Dulbecco's Modified Eagle Medium (DMEM, Sigma-Aldrich, St. Louis, MO) supplemented with 10% fetal bovine serum (FBS, Connectorate, Dietikon, Switzerland), 100 U/mL penicillin, 100 mg/mL streptomycin (Life Technologies, Grand Island, NY), 10 mM HEPES, pH 7.4 (Life Technologies, Grand Island, NY), and 1% MEM non-essential amino acid solution (Sigma-Aldrich). Cells were cultured under standard conditions (37 °C, 5% CO<sub>2</sub>).

#### 2.7. Transient transfection of HEK-293 cells and 17β-HSD3 activity assay

HEK-293 cells (2 × 10<sup>6</sup>) were seeded in 10 cm dishes, incubated for 24 h, and transiently transfected by the calcium phosphate precipitation method with 8 mg of plasmid for wild-type 17β-HSD3 [25,26] or mutant pK202M. At 48 h post-transfection, cells were washed with PBS, collected in 2 mL ice-cold PBS, aliquoted (200 µL) and centrifuged at 4 °C for 4 min at 300g. Cell pellets were snap-frozen in liquid nitrogen and stored at -80 °C. Cell pellets were suspended in 400 µL Tris-HCl buffer (10 mM Tris-HCl, pH 7.5, 150 mM KCl, 1 mM EDTA, 2 mM dithiothreitol, Sigma-Aldrich) and lysed by sonication (UP50H sonicator, Hielscher Ultrasonics).

The dilution of the cell lysate was adjusted to obtain 20–30% substrate to product conversion rate for wild-type 17β-HSD3 after 30 min of incubation. Lysates were incubated in the presence of 200 nM androstenedione, containing 11.1 nCi [1,2,6,7-<sup>3</sup>H] androstenedione (American Radiolabeled Chemicals, St. Louis, MO), and 500 µM NADPH in a total volume of 22.2 µL Tris-HCl, pH 7.4, at 37 °C. The total solvent concentration was kept at 0.1%. After 30 min, reactions were stopped by adding 10 µL methanol containing 2 mM each of unlabelled androstenedione and testosterone (Sigma-Aldrich). An amount of 10 µL per sample was loaded onto TLC plates (Macherey-Nagel, Oensingen, Switzerland), steroids were separated using chloroform/ethyl acetate (Sigma-Aldrich) at a ratio of 3:1. Substrate and product bands were excised and analyzed by scintillation counting (Tri-Carb 2900TR liquid scintillation analyzer, Packard, Connecticut).

#### 2.8. Western blotting

Cell pellets, described above, were lysed in 100 µL RIPA buffer (Sigma-Aldrich) containing protease inhibitor cocktail (Roche, Basel, Switzerland), and centrifuged at 14,000g for 2 min at 4 °C to remove debris. Protein concentration was determined using the Pierce™ BCA protein assay kit (Thermo Scientific, Rockford, IL), and 20 µg of total proteins were separated by SDS-PAGE, followed by transfer to Immobilon-Blot® polyvinylidene difluoride (PVDF) membranes (Bio-Rad Laboratories, Hercules, CA). For detection of the FLAG epitope, the membrane was blocked for 30 min using 5% non-fat milk in Tris-buffered saline (TBS, 140 mM NaCl, 20 mM Tris-HCl, pH 7.6) containing 0.1% Tween-20 and incubated with mouse monoclonal anti-FLAG M2 antibody (F1804, Sigma-Aldrich) at a dilution of 1:1000 in blocking solution overnight at 4 °C. After washing with TBS containing 0.1% Tween-20 (TBS-T), the membrane was incubated with horseradish peroxidase-conjugated goat anti-mouse secondary antibody at a dilution of 1:2000 (A0168, Sigma-Aldrich) in blocking solution for 1 h at room temperature. After washing with TBS-T, the Immobilon Western Chemiluminescent HRP substrate kit (Merck, Kenilworth, NJ, USA) was used for visualization on a FUSION FX (Vilber, Marne-la-Vallée, France). For the detection of the loading control β-actin, blocking was performed overnight at 4 °C and mouse anti-β-actin (C4) antibody (sc-47778, Santa Cruz Biotechnology, CA) at a dilution of 1:1000 was used as primary antibody. After washing with TBS-T, the secondary anti-mouse antibody mentioned above was used at a dilution of 1:2000, followed by chemiluminescence detection.

#### 2.9. Ex vivo splicing assays

HEK-293 cells were transfected as described above with 8 µg of wild-type or mutant minigene plasmids. After 48 h of transfection, total RNA was isolated using the RNeasy Mini Kit (Qiagen, Venlo, Netherlands) according to the manufacturer's protocol. Contamination with genomic DNA was prevented by on-column DNA digestion with DNase I (RNase-free, Qiagen). RNA (2 µg) was reverse transcribed to complementary DNA (cDNA) using the Takara PrimeScript RT Reagent Kit (Takara Bio Inc., Kusatsu, Japan). Subsequently, 10 ng of cDNA was subjected to PCR using Q5® Hot Start High-Fidelity DNA Polymerase (NEB). The forward (5'-CGCCTAGATGCCTCTGCTAA-3') and reverse primer (5'-AAGCGCTTGCTCCACTCGCT-3') used were located on exon 13 and 17, respectively, of the minigenes as shown in Fig. 2B. The splicing products were separated on a 3% agarose gel, visualized on a FUSION FX (Vilber) and extracted using the Wizard® SV Gel and PCR Clean-Up System (Promega). PCR products were analysed by Sanger sequencing (Microsynth).

### 3. Results

#### 3.1. Identification of novel 17β-HSD3 mutations in 46,XY DSD patients

The three patients were first sequenced for exon 9 of *HSD17B3*, a site for the founder mutation c.618 C > A that results in a stop codon instead of Cys206 and shows a high carrier frequency of about 1 in 40 in the Tunisian population [16].

Patient P1 was found to be homozygous for mutation p.C206X. Analysis of the family indicated that the parents were carriers of this mutation and that they were not related, at least for the last three generations (Fig. 1A).

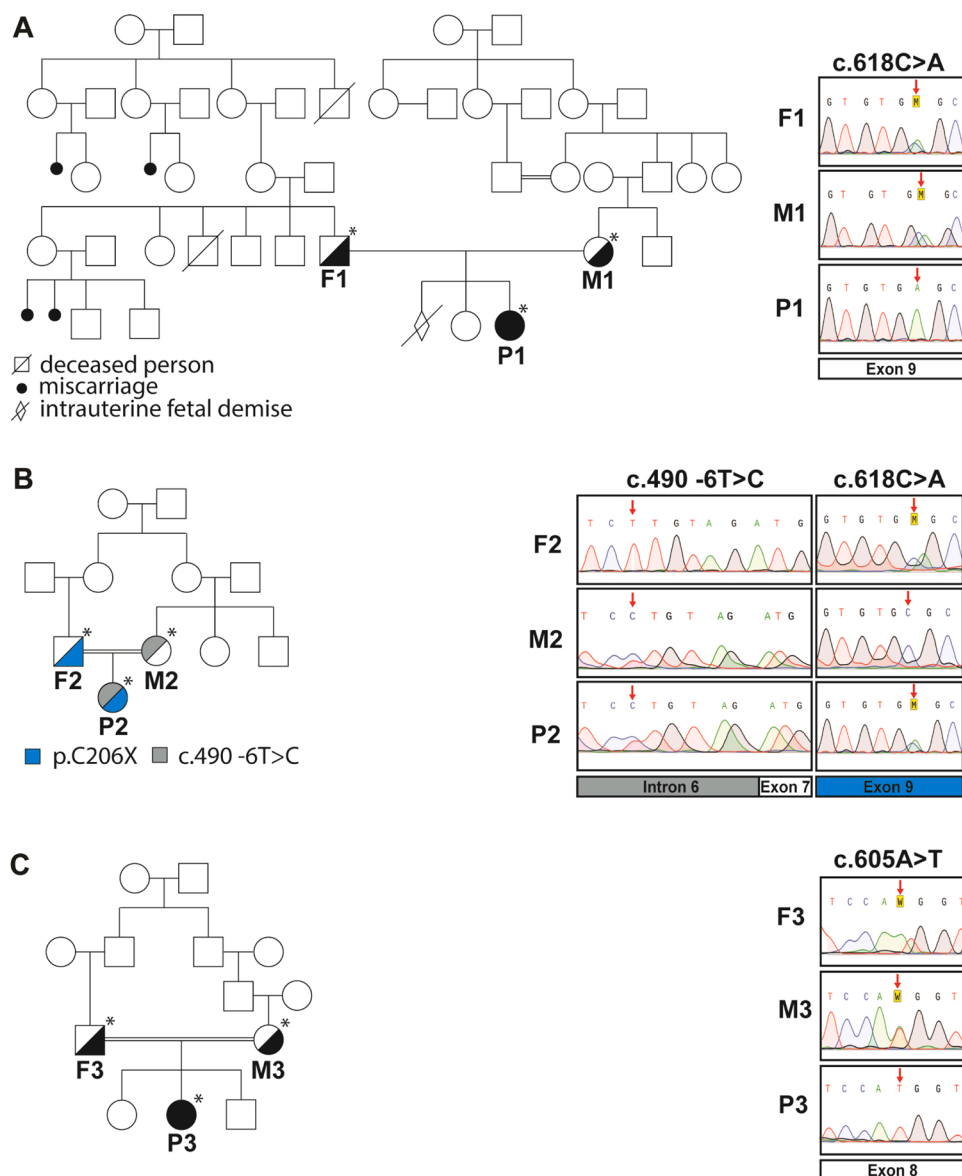
Patient P2 presented a heterozygous state of the mutation p.C206X. Sequencing of all exons and adjacent intron sequences of the *HSD17B3* gene revealed the novel mutation c.490 -6 T > C in intron 6, near the splice acceptor site of exon 7. Analysis of the parents revealed the presence of this novel splice site mutation in the mother in a heterozygous state as well as the known p.C206X mutation in the father, also in a heterozygous state (Fig. 1B).

For patient P3, none of the so far described and experimentally confirmed *HSD17B3* loss-of-function mutations in the Tunisian

population, i.e., p.G133R, p.Q176P or p.C206X, could be identified. Hence, the remaining *HSD17B3* exons were sequenced, revealing a novel substitution at position c.605 A > T in exon 8, resulting in the mutation p.K202M, in a homozygous state. Analysis of the transmission of this mutation in the family of P3 showed inheritance of p.K202M from consanguineous parents (Fig. 1C).

#### 3.2. In silico predictions for c.490 -6 T > C and p.K202M mutations

To test whether c.490 -6 T > C might affect splicing of the *HSD17B3* gene, an *in silico* splice site mutation analysis using the ESE finder 3.0 (<https://bio.tools/ese finder>) was conducted. The program's algorithm predicted two novel binding sites for splicing factors SRSF1 (IgM-BRCA1) and SRSF2 (SC35) in the intron 6 of the 490 -6 T > C mutant gene variant, in compared to the wild-type intron (Suppl. Fig. 1A-D). Additionally, an SRSF5 (SRp40) binding site in the wild-type intron is replaced in the 490 -6 T > C mutant gene by a new one, located two base pairs upstream of the original binding site and predicted to result in a more effective binding compared to the wild-type gene. The altered binding of the splicing factors might result in the displacement of the splicing machinery and an altered spliceosome assembly, resulting in an



**Fig. 1.** Mutational analysis of 46, XY DSD patients and their parents by automated DNA sequencing of the *HSD17B3* gene. (A) Patient P1 inherited a homozygous substitution (cDNA position 618, C > A) in exon 9 from heterozygous parents. (B) Patient P2 revealed to be compound heterozygote with the same substitution (cDNA position 618, C > A) in exon 9, inherited paternally, and a novel mutation in intron 6, in front of the exon 7 splice acceptor site (cDNA position 490, -6 T > C), which was transmitted from the heterozygous mother. (C) Patient P3 inherited a novel, homozygous substitution (cDNA position c.605 A > T) in exon 8 from heterozygous parents. Symbols indicate sex phenotype: females are represented by circles, squares represent males. Filled symbols indicate patients with two mutated *HSD17B3* alleles and half-filled symbols indicate one mutated allele. Consanguineous marriage is indicated by a double line. Individuals marked with an asterisk were genetically sequenced and analyzed. Additional symbols are indicated in legends below the respective pedigrees.

impaired splicing of exon 7 [20,27,28]. The possible pathogenicity of the p.K202M mutation was analyzed using PolyPhen-2 and PROVEAN software, which both predicted this novel mutation to be probably damaging or deleterious (Suppl. Fig. 1E and F) [18,19].

### 3.3. Functional analysis of the c.490 -6 T > C substitution

The substitution c.490 -6 T > C in intron 6 of the *HSD17B3* gene close to the exon 7 boundary was identified as the only change in the maternally inherited *HSD17B3* allele of patient P2. Based on *in silico* analyses, this substitution is predicted to affect the recruitment of various splicing factors; thus, a minigene approach was used to verify aberrant RNA splicing. For this purpose, the *HSD17B3* exon 7 and its flanking introns were cloned into the multiple cloning site (MCS) of a previously described plasmid [23,24]. This plasmid contains an expression cassette consisting of a cytomegalo virus promoter that induces the expression of an artificial gene consisting in this case of exon 13 of protein 4.1, the MCS with the introduced exon 7 of *HSD17B3*, and exon 17 of protein 4.1. The resulting minigene constructs containing either the wild-type variant or the c.490 -6 T > C mutation at the *HSD17B3* exon 7 boundary (Fig. 2A) were then transfected into HEK-293 cells and the expressed mRNA was subsequently extracted, amplified by RT-PCR and finally resolved by gel electrophoresis. While one major and one less abundant transcript were found for the wild-type minigene, only one transcript of lower size was detected in HEK-293 cells transfected with the plasmid for the c.490 -6 T > C minigene (Fig. 2B). In order to interpret this result conclusively, all bands were extracted from the gel, purified and analyzed by Sanger sequencing. The band with the higher size of the wild-type minigene was a non-specific band (not yielding a readable sequence) and the major band represented a transcript containing exon 7. The band of the wild-type minigene contained the sequences of exon 13 and exon 17 of protein 4.1, without exon 7 of *HSD17B3*, indicating that exon 7 was skipped during splicing of the c.490 -6T > C mutant minigene transcript (Fig. 2C). The presence of a faint band at this position for the wild-type minigene can be explained

by alternative splicing, where the relatively short exon 7 is partially skipped by the splicing machinery. Skipping of exon 7 in the mRNA of mutant *HSD17B3* is expected to cause a frameshift downstream of residue Lys163. This results in a truncated protein that lacks the catalytic center (encoded by exon 8) and therefore is most likely completely inactive (Fig. 2D and Fig. 4).

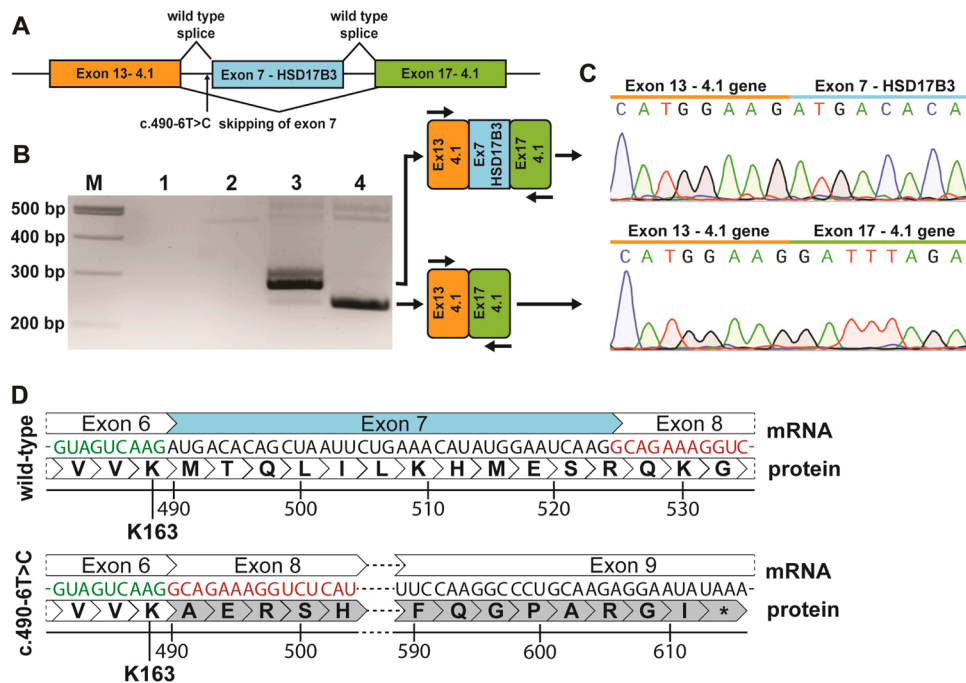
### 3.4. Functional analysis of the p.K202M mutation

The mutation of Lys202 to methionine in the catalytic center of 17β-HSD3 is expected to render the enzyme non-functional due to a loss of the acid/base catalyst function of the hydroxyl group of Tyr198 that is polarized by Lys202. Enzyme activity was assessed for wild-type and p.K202M 17β-HSD3 in whole cell lysates from transfected HEK-293 cells. Incubation with 200 nM of the substrate androstenedione in the presence of cofactor NADPH revealed a complete loss of activity for mutant p.K202M compared to wild-type 17β-HSD3 (Fig. 3A). Even after four times longer incubation time, *i.e.* 2 h, no activity could be detected for the mutant enzyme. Western blotting revealed that both enzyme variants were well expressed, with even higher expression levels obtained upon transient transfection for the mutant enzyme (Fig. 3B).

## 4. Discussion

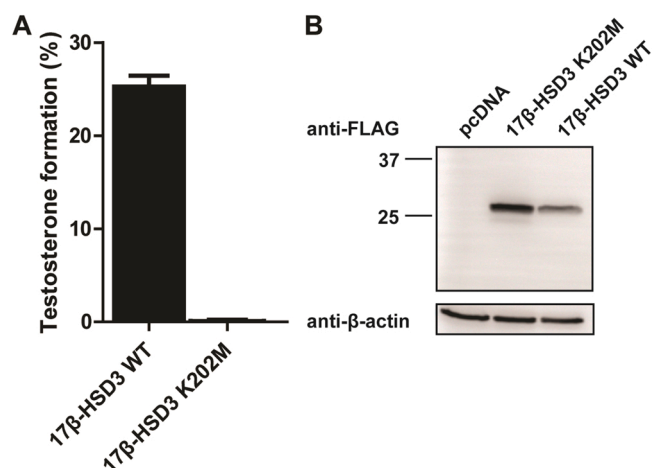
17βHSD3 deficiency due to mutations in *HSD17B3* is a rare autosomal form of 46,XY DSD that is frequently unnoticed at birth and misdiagnosed during childhood and puberty, especially in developing countries where 46,XY DSD often is tabooed. A complete hormonal profile including an hCG stimulation test needs to be conducted and correctly interpreted by the physician as it was the case for the three patients described in this study.

Patient P1 inherited the p.C206X mutation from unrelated parents. The truncated p.C206X mutant enzyme is inactive as it lacks part of the substrate binding pocket, the dimerization region and the C-terminal part (Fig. 4A) [14]. We previously calculated a frequency of 1/40 for the



**Fig. 2.** Minigene splice assay of exon 7 in wild-type and c.490 -6 T > C splice site mutated *HSD17B3*. **(A)** Schematic representation of the constructed wild-type and mutant minigenes used in the splice assay. Different exons are indicated in distinct colors. **(B)** Gel electrophoresis of the RT-PCR products spanning the exon 13 and exon 17 (primers indicated by small horizontal arrows) revealed two amplified products for wild-type minigene transcripts (column 3) and one single band for the c.490 -6T > C mutant minigene (column 4). No effective PCR amplification was detected in the negative control without RNA (column 1) and the background control of mock-transfected HEK-293 cells (2). The size marker (M) is indicated on the left. **(C)** Sanger sequencing of the major wild-type and mutant transcripts. Exon boundaries after splicing are shown and highlighted by colors above the sequence. Exon 7 was absent in the product from the transcript of the 490 -6 T > C splice site mutant. **(D)** Schematic representation of mRNA transcripts after splicing and the resulting expressed protein variants of wild-type and c.490 -6 T > C 17β-HSD3. Skipping of exon 7 (light blue) due to the intronic c.490 -6 T > C mutation results in a frame shift (grey marked amino acids), downstream of Lys163, which is the last encoded amino acid of exon 6 sequence (green). The frame shift starts with the begin of exon 8

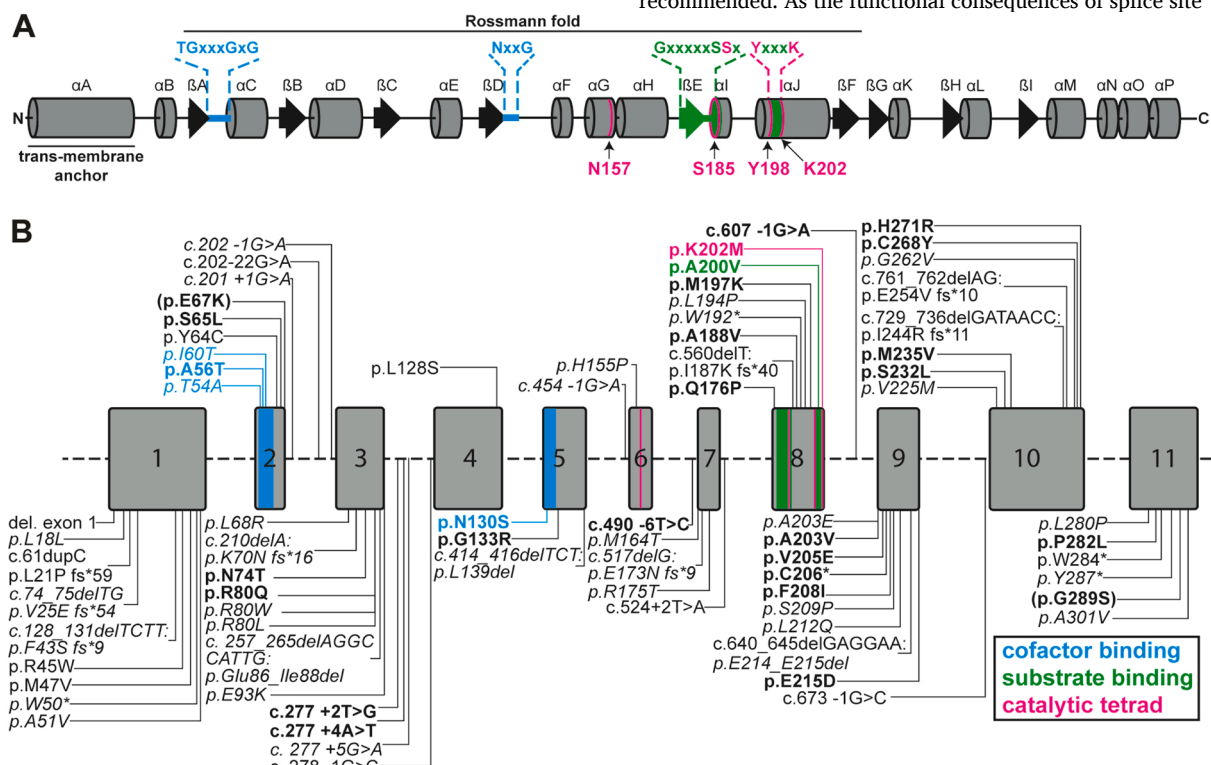
(mRNA sequence in red) and ends in a premature stop codon in exon 9.



**Fig. 3.** Activity and expression of wild-type and mutant 17β-HSD3 enzymes. **(A)** Enzyme activity of wild-type and mutant 17β-HSD3. Lysates of HEK-293 cells expressing wild-type 17β-HSD3 or mutant p.K202M were incubated for 30 min at 37 °C in the presence of 200 nM androstenedione, containing 11.1 nCi of [1,2,6,7-<sup>3</sup>H]-androstenedione, and 500 μM NADPH. Percentage of total conversion of androstenedione to testosterone was analyzed by TLC separation of both steroids and scintillation counting. Data are from three independent experiments and represent mean ± SD. **(B)** Western blot of FLAG-tagged wild-type 17β-HSD3 and mutant p.K202M. HEK-293 cells were transiently transfected with plasmids encoding C-terminally FLAG epitope-tagged wild-type or mutant enzyme. After incubation of 48 h, transfected cells were harvested and equal amounts of total protein were separated by SDS-PAGE and subjected to Western blotting using a mouse anti-FLAG antibody for detection. β-Actin was used as a loading control and analyzed using an anti-β-actin antibody.

p.C206X mutation in the population of Sfax, Tunisia, and concluded that the frequency of marriage between two carriers is 1/1600 and the frequency of p.C206X homozygosity is 1/6400 per new born child [16]. This frequency can be higher in consanguineous marriages in families where the mutation occurs. It appears that p.C206X is so frequent by now that despite non-consanguineous marriages over four generations in the family of P1 the mutation was inherited from unrelated parents. It is unknown when this mutation first appeared; however, it can be assumed that consanguineous marriages and geographic endogamy may have favored the spread and incidence of this autosomal recessive mutation, as has been shown in other studies conducted in Tunisia [29,30].

Patients P2 and P3 both originate from consanguineous families. Interestingly, P2 is a compound heterozygote and inherited two distinct defects in *HSD17B3*. P2 was initially examined due to clitoral hypertrophy and later on diagnosed based on a ratio of testosterone to androstenedione below 0.8. Sequence analysis revealed the deleterious p.C206X mutation on the paternal allele. Additionally, the novel splice site mutation c.490 -6 T > C was identified on the maternal *HSD17B3* allele. This splice site mutation is predicted by *in silico* tools to cause a complete skipping of exon 7, which was supported by the results from the splice assay involving artificial minigenes. Exon skipping can be caused by a rearrangement of binding sites for splicing factors, as predicted *in silico*. Skipping exon 7 in the *HSD17B3* mRNA transcript generates a frame shift downstream of Lys163 that affects the active site and leads to the loss of three out of four residues of the catalytic tetrad and further results in truncation of the protein in exon 9, thus leading to an inactive enzyme (Fig. 2D and Fig. 4). Compound heterozygosity may be overlooked in patients if the sequence analysis is not performed carefully or if not the entire gene including intron/exon boundaries is covered. Therefore, a manual check of the electropherograms following automated sequence analysis is recommended. As the functional consequences of splice site



**Fig. 4.** (A) Schematic representation of the secondary structure of the 17β-HSD3 protein. Cylinders depict α-helices and black arrows β-sheets. SDR typical Rossmann fold region as well as the transmembrane anchor are indicated. Cofactor- as well as the substrate binding motifs within the active site are highlighted in color. The catalytic tetrad is indicated in red. (B) Schematic representation of the *HSD17B3* gene, depicting all known *HSD17B3* mutations identified in patients until August 2022. Bold depicted mutations were experimentally verified to negatively impact enzyme activity, with the exception of (p.E67K) and (p.G289S), which are polymorphisms of *HSD17B3* with normal enzyme activity but that were initially suspected to cause 17β-HSD3 deficiency. Italic depicted mutations were computationally predicted to adversely affect 17β-HSD3 activity. References on the mutations depicted in this Figure can be found in Supplementary Table 1.

mutations often are unclear, experimental evaluation is needed.

For P3, 17 $\beta$ -HSD3 deficiency was proposed based on a testosterone to androstenedione ratio < 0.8 and on the observed signs of virilization during puberty. *HSD17B3* gene sequencing showed a novel mutation c.605 A > T in exon 8 encoding p.K202M, representing the first mutation in the catalytic tetrad of 17 $\beta$ -HSD3 described so far according to the HGMD and current literature ([13], accessed August 2, 2022; see Fig. 4B and Suppl. Table 2). Analysis of the recombinant 17 $\beta$ -HSD3 mutant p.K202M showed a complete loss of enzyme activity, whereas protein expression was not negatively affected. These findings highlight and confirm the central role that this conserved lysine residue plays in the electron transfer system within the active site of 17 $\beta$ -HSD3. Since the mutation c.605 A > T is located in the last codon of exon 8 close to the splice site, an additional influence of this mutation on mRNA splicing cannot be entirely excluded (Fig. 4B).

To date, 11 patients with 17 $\beta$ -HSD3 deficiency have been identified in Sfax, Tunisia. Four patients are homozygous for the most frequently found mutation p.C206X. Three patients are compound heterozygous carriers of p.C206X and p.G133R. One patient is compound heterozygous for p.C206X/p.Q176P. Another patient is compound heterozygous for p.C206X and the splice site mutation c.490 -6 T > C. A further patient is homozygous for p.K202M. Finally, one patient presenting with deficient testosterone synthesis and micropenis was diagnosed with 46, XY DSD and exhibits the polymorphism p.G289S and the silent polymorphism p.L18 = [14–16] (Suppl. Table 2). The cause of the testosterone synthesis defect in this latter patient still remains unclear; the G289S substitution did not affect 17 $\beta$ -HSD3 activity *in vitro* and the c.54 G > T substitution, predicted *in silico* to affect the splicing efficiency, requires experimental validation [16].

It should be noted that consanguinity and geographic endogamy represent two characteristics in Tunisia, especially in the region of Sfax. A marital model typical of choice is adopted in Sfax, where men prioritize to marry their first cousin, a distant cousin or a neighbour [30,31]. Generally, the natives of Sfax prefer the auto-unions within their geographically isolated community, which leads to a higher incidence of genetically recessive diseases and a higher probability of propagation of new mutations within the regional gene pool that may generate novel pathologies in the offspring. With respect to 17 $\beta$ -HSD3 deficiency, a delay until the age of diagnosis or an ignorance of this form of 46,XY DSD by clinicians as well as a tabooization of this subject in general within families likely contributes to the fact that the actual number of reported and confirmed patients with 17 $\beta$ -HSD3 deficiency is lower than estimated.

## 5. Conclusions

We report three novel 46,XY DSD cases with 17 $\beta$ -HSD3 deficiency in the Tunisian population. The fact that P1 is homozygous for p.C206X, inherited from unrelated parents, indicates that consanguinity is no longer a required factor for this frequent mutation to occur in a homozygous state. The mutation p.C206X was also found in P2 who is compound heterozygous with the novel, maternally inherited splice site mutation c.490 -6 T > C causing skipping of exon 7 during mRNA splicing and resulting in a truncated and inactive enzyme. Finally, a novel mutation, p.K202M, representing the first mutation within the catalytic tetrad of 17 $\beta$ -HSD3, was found in P3. Substitution of the highly conserved lysine, which ensures acid/base catalyst function of Tyr198, leads to a complete loss of 17 $\beta$ -HSD3 activity. The tabooization of XY,46 DSD and consanguineous marriages in the Tunisian population promote the emergence and establishment of deleterious mutations, not only in the *HSD17B3* gene. The Tunisian population needs to be sensitized to this issue and early diagnosis and genetic counselling can improve the quality of life of the affected patients.

## Funding

This work was supported by the Ministry of Higher Education and Scientific Research in Tunisia and the Swiss Centre for Applied Human Toxicology (SCAHT P3–2021–2024).

## CRediT authorship contribution statement

Conception and design, BBR, MK, AO, Patient recruitment and examination, FHK, TK, WS, MM, Performing experiments, BBR, MK, Data analysis and interpretation, BBR, MK, AO, NB, Writing manuscript draft, BBR, MK, LK, AO, Writing and revision of manuscript, BBR, MK, FK, FHK, TK, WS, LK, MM, AO, NB.

## Conflict of Interest

The authors declare no conflict of interest.

## Data Availability

Data will be made available on request.

## Acknowledgments

We thank the patients and their families for their cooperation in this study and for giving informed consent. Additionally, we are grateful to Dr. Afif Ben Mahmoud for providing the pRc/CMV plasmid used in the splice assay and Dr. Sana Kmiha for assisting with details for the clinical description of the patients.

## Appendix A. Supporting information

Supplementary data associated with this article can be found in the online version at doi:10.1016/j.jsbmb.2022.106235.

## References

- [1] J.M. Saez, E. De Peretti, A.M. Morera, M. David, J. Bertrand, Familial male pseudohermaphroditism with gynecomastia due to a testicular 17-ketosteroid reductase defect. I. Studies in vivo, *J. Clin. Endocrinol. Metab.* 32 (5) (1971) 604–610.
- [2] W.M. Geissler, D.L. Davis, L. Wu, K.D. Bradshaw, S. Patel, B.B. Mendonca, K. O. Elliston, J.D. Wilson, D.W. Russell, S. Andersson, Male pseudohermaphroditism caused by mutations of testicular 17 beta-hydroxysteroid dehydrogenase 3, *Nat. Genet.* 7 (1) (1994) 34–39.
- [3] S. Andersson, D.W. Russell, J.D. Wilson, 17beta-Hydroxysteroid dehydrogenase 3 deficiency, *Trends Endocrinol. Metab.* 7 (4) (1996) 121–126.
- [4] B.B. Mendonca, N.L. Gomes, E.M. Costa, M. Inacio, R.M. Martin, M.Y. Nishi, F. M. Carvalho, F.D. Tibor, S. Domenice, 46,XY disorder of sex development (DSD) due to 17beta-hydroxysteroid dehydrogenase type 3 deficiency, *J. Steroid Biochem. Mol. Biol.* 165 (Pt A) (2017) 79–85.
- [5] S. Andersson, W.M. Geissler, L. Wu, D.L. Davis, M.M. Grumbach, M.I. New, H. P. Schwarz, S.L. Blethen, B.B. Mendonca, W. Bloise, S.F. Witchel, G.B. Cutler Jr., J. E. Griffin, J.D. Wilson, D.W. Russel, Molecular genetics and pathophysiology of 17 beta-hydroxysteroid dehydrogenase 3 deficiency, *J. Clin. Endocrinol. Metab.* 81 (1) (1996) 130–136.
- [6] C.I. Goncalves, J. Carrico, M. Bastos, M.C. Lemos, Disorder of sex development due to 17-beta-hydroxysteroid dehydrogenase type 3 deficiency: a case report and review of 70 different HSD17B3 mutations reported in 239 patients, *Int. J. Mol. Sci.* 23 (17) (2022).
- [7] M.M. George, M.I. New, S. Ten, C. Sultan, A. Bhangoo, The clinical and molecular heterogeneity of 17betaHSD-3 enzyme deficiency, *Horm. Res Paediatr.* 74 (4) (2010) 229–240.
- [8] B. Persson, Y. Kallberg, J.E. Bray, E. Bruford, S.L. Dellaporta, A.D. Favia, R. G. Duarte, H. Jornvall, K.L. Kavanagh, N. Kedishvili, M. Kisiela, E. Maser, R. Mindich, S. Orchard, T.M. Penning, J.M. Thornton, J. Adamski, U. Oppermann, The SDR (short-chain dehydrogenase/reductase and related enzymes) nomenclature initiative, *Chem. Biol. Inter.* 178 (1–3) (2009) 94–98.
- [9] K.L. Kavanagh, H. Jornvall, B. Persson, U. Oppermann, Medium- and short-chain dehydrogenase/reductase gene and protein families: the SDR superfamily: functional and structural diversity within a family of metabolic and regulatory enzymes, *Cell Mol. Life Sci.* 65 (24) (2008) 3895–3906.
- [10] K.I. Varughese, N.H. Xuong, P.M. Kiefer, D.A. Matthews, J.M. Whiteley, Structural and mechanistic characteristics of dihydropteridine reductase: a member of the



- Tyr-(Xaa)<sup>3</sup>-Lys-containing family of reductases and dehydrogenases, *Proc. Natl. Acad. Sci. USA* 91 (12) (1994) 5582–5586.
- [11] C. Filling, K.D. Berndt, J. Benach, S. Knapp, T. Prozorovski, E. Nordling, R. Ladenstein, H. Jornvall, U. Oppermann, Critical residues for structure and catalysis in short-chain dehydrogenases/reductases, *J. Biol. Chem.* 277 (28) (2002) 25677–25684.
- [12] I. Hanukoglu, Proteopedia: Rossmann fold: a beta-alpha-beta fold at dinucleotide binding sites, *Biochem Mol. Biol. Educ.* 43 (3) (2015) 206–209.
- [13] P.D. Stenson, E.V. Ball, M. Mort, A.D. Phillips, J.A. Shiel, N.S. Thomas, S. Abeyasinghe, M. Krawczak, D.N. Cooper, Human gene mutation database (HGMD): 2003 update, *Hum. Mutat.* 21 (6) (2003) 577–581.
- [14] R.T. Engeli, B.B. Rhouma, C.P. Sager, M. Tsachaki, J. Birk, F. Fakhfakh, L. Keskes, N. Belguith, A. Odermatt, Biochemical analyses and molecular modeling explain the functional loss of 17beta-hydroxysteroid dehydrogenase 3 mutant G133R in three Tunisian patients with 46, XY Disorders of Sex Development, *J. Steroid Biochem. Mol. Biol.* 155 (Pt A) (2016) 147–154.
- [15] B. Ben Rhouma, N. Belguith, M.F. Mnif, T. Kamoun, N. Charfi, M. Kamoun, F. Abdelhedi, M. Hachicha, H. Kamoun, M. Abid, F. Fakhfakh, A novel nonsense mutation in HSD17B3 gene in a Tunisian patient with sexual ambiguity, *J. Sex. Med.* 10 (10) (2013) 2586–2589.
- [16] B. Ben Rhouma, F. Kallabi, N. Mahfoudh, A. Ben Mahmoud, R.T. Engeli, H. Kamoun, L. Keskes, A. Odermatt, N. Belguith, Novel cases of Tunisian patients with mutations in the gene encoding 17beta-hydroxysteroid dehydrogenase type 3 and a founder effect, *J. Steroid Biochem Mol. Biol.* 165 (Pt A) (2017) 86–94.
- [17] H.A. Lewin, J.A. Stewart-Haynes, A simple method for DNA extraction from leukocytes for use in PCR, *Biotechniques* 13 (4) (1992) 522–524.
- [18] I.A. Adzhubei, S. Schmidt, L. Peshkin, V.E. Ramensky, A. Gerasimova, P. Bork, A. S. Kondrashov, S.R. Sunyaev, A method and server for predicting damaging missense mutations, *Nat. Methods* 7 (4) (2010) 248–249.
- [19] Y. Choi, A.P. Chan, PROVEAN web server: a tool to predict the functional effect of amino acid substitutions and indels, *Bioinformatics* 31 (16) (2015) 2745–2747.
- [20] E.C. Ibrahim, T.D. Schaal, K.J. Hertel, R. Reed, T. Maniatis, Serine/arginine-rich protein-dependent suppression of exon skipping by exonic splicing enhancers, *Proc. Natl. Acad. Sci. USA* 102 (14) (2005) 5002–5007.
- [21] P.J. Smith, C. Zhang, J. Wang, S.L. Chew, M.Q. Zhang, A.R. Krainer, An increased specificity score matrix for the prediction of SF2/ASF-specific exonic splicing enhancers, *Hum. Mol. Genet.* 15 (16) (2006) 2490–2508.
- [22] L. Cartegni, J. Wang, Z. Zhu, M.Q. Zhang, A.R. Krainer, ESEfinder: A web resource to identify exonic splicing enhancers, *Nucleic Acids Res.* 31 (13) (2003) 3568–3571.
- [23] M. Deguillien, S.C. Huang, M. Moriniere, N. Dreumont, E.J. Benz Jr., F. Baklouti, Multiple cis elements regulate an alternative splicing event at 4.1R pre-mRNA during erythroid differentiation, *Blood* 98 (13) (2001) 3809–3816.
- [24] A. Ben Mahmoud, O. Siala, R.B. Mansour, F. Driss, S. Baklouti-Gargouri, E. Mkaouer-Rebai, N. Belguith, F. Fakhfakh, First functional analysis of a novel splicing mutation in the B3GALT1 gene by an ex vivo approach in Tunisian patients with typical Peters plus syndrome, *Gene* 532 (1) (2013) 13–17.
- [25] B. Legeza, Z. Balazs, L.G. Nashev, A. Odermatt, The microsomal enzyme 17beta-hydroxysteroid dehydrogenase 3 faces the cytoplasm and uses NADPH generated by glucose-6-phosphate dehydrogenase, *Endocrinology* 154 (1) (2013) 205–213.
- [26] L.G. Nashev, D. Schuster, C. Laggner, S. Sodha, T. Langer, G. Wolber, A. Odermatt, The UV-filter benzophenone-1 inhibits 17beta-hydroxysteroid dehydrogenase type 3: Virtual screening as a strategy to identify potential endocrine disrupting chemicals, *Biochem. Pharm.* 79 (8) (2010) 1189–1199.
- [27] X.B. Yan, C.H. Tang, Y. Huang, H. Fang, Z.Q. Yu, L.M. Wu, R.Y. Liu, Alternative splicing in exon 9 of glucocorticoid receptor pre-mRNA is regulated by SRp40, *Mol. Biol. Rep.* 37 (3) (2010) 1427–1433.
- [28] N.A. Patel, C.E. Chalfant, J.E. Watson, J.R. Wyatt, N.M. Dean, D.C. Eichler, D. R. Cooper, Insulin regulates alternative splicing of protein kinase C beta II through a phosphatidylinositol 3-kinase-dependent pathway involving the nuclear serine/arginine-rich splicing factor, SRp40, in skeletal muscle cells, *J. Biol. Chem.* 276 (25) (2001) 22648–22654.
- [29] S. Ben Arab, S. Masmoudi, N. Beltaief, S. Hachicha, H. Ayadi, Consanguinity and endogamy in Northern Tunisia and its impact on non-syndromic deafness, *Genet Epidemiol.* 27 (1) (2004) 74–79.
- [30] L. Romdhane, S. Abdelhak, D. Research, Unit on molecular investigation of genetic orphan, collaborators, genetic diseases in the Tunisian population, *Am. J. Med Genet A* 155A (1) (2011) 238–267.
- [31] N. Ben Halim, N. Ben Alaya Bouafif, L. Romdhane, R. Kefi Ben Atig, I. Chouchane, Y. Bouyacoub, I. Arfa, W. Cherif, S. Nouira, F. Talmoudi, K. Lasram, S. Hsouna, W. Ghazouani, H. Azaiez, L. El Matri, A. Abid, N. Tebib, M.F. Ben Dridi, S. Kachboura, A. Amouri, M. Mokni, S. Ben Arab, K. Dellagi, S. Abdelhak, Consanguinity, endogamy, and genetic disorders in Tunisia, *J. Community Genet* 4 (2) (2013) 273–284.

## Supplementary information



**Supplementary Figure 1. (A, B)** *In silico* splice site mutation analysis using ESE finder 3.0. Depiction of binding scores for different splice factors (see legend in graphs). Vertical black arrows indicate (A) wild-type and (B) 490 -6T>C splice site mutation. (B) Colored arrows indicate changes in predicted splice factor binding sites at the intron/exon boundary at the 490 -6T>C splice site mutant compared to the wild-type *HSD17B3* gene. (C, D) Tabular results of predicted binding sites and scores of the assessed splice factors of (C) wild-type and (D) 490 -6T>C splice site mutation. (E) PolyPhen-2 and (F) PROVEAN *in silico* prediction of the p.K202M mutation on 17 $\beta$ -HSD3 functionality. Red boxes mark the outcomes of the predictions.

**Supplementary Table 1. Known mutations in *HSD17B3* with references to Figure 4**

<b>Mutation</b>	<b>References</b>
deletion exon 1	[1]
p.L18L	[2]
c.61dupC: p.L21P fs*59	[3]
c.74_75 delTG: p.V25E fs*54	[1]
c.128_131 delTCTT: p. F43S fs*9	[4]
p.R45W	[5]
p.M47V	[5]
p.W50*	[6]
p.A51V	[7]
p.T54A	[7, 8]
p.A56T	[9]
p.I60T	[1]
p.Y64C	[5]
p.S65L	[10]
p.E67K	[11]
c.201 +1G>A	[12]
c.202 -22G>A	[13]
c.202 -1G>A	[12]
p.L68R	[12]
c.210delA: p.K70N fs*16	[5]
p.N74T	[11, 14]
p.R80Q	[15]
p.R80W	[16]
p.R80L	[17]
c.257_265delAGGCCATTG : p.(Glu86_Ile88del)	[18]
p.E93K	[19]
c.277 +2T>G	[20, 21]
c.277 +4A>T	[10, 14]
c.277 +5G>A	[12]
c.278 -1G>C	[10, 14, 15]
p.L128S	[5]
p.N130S	[9, 14]
p.G133R	[22]
c.414_416delTCT: p.L139del	[5]
c.454 -1G>A	[23]
p.H155P	[24]
c.490 -6T>C	Novel
p.M164T	[7, 8]
c.517delG: p.E173N fs*9	[7]

<b>Mutation</b>	<b>References</b>
p.R175T	[19]
c.524+2T>A	[25]
p.Q176P	[9, 10]
c.560delT: p.I187K fs*40	[26]
p.A188V	[11, 14]
p.W192*	[27]
p.L194P	[7, 8]
p.M197K	[11]
p.A200V	[11, 12]
p.K202M	Novel
c.607 -1G>A	[10, 14, 15]
p.A203E	[28]
p.A203V	[15, 29]
p.V205E	[10]
p.C206*	[22, 30]
p.F208I	[10]
p.S209P	[31]
p.L212Q	[28]
c.640_645delGAGGAA: p.E214_E215del	[32]
p.E215D	[10]
c.673 -1G>C	[33]
p.V225M	[12, 34]
p.S232L	[15]
p.M235V	[15]
c.729_736delGATAACC: p.I244R fs*11	[7, 10]
c.761_762delAG: p.E254V fs*10	[35]
p.G262V	[36]
p.C268Y	[37]
p.H271R	[11]
p.L280P	[17]
p.P282L	[10]
p.W284*	[4]
p.Y287*	[38]
p.G289S	[11, 14]
p.A301V	[39]

All mutations depicted in Figure 4 are listed here with their corresponding references. The references include mostly those publications where a mutation has been experimentally validated to be harmful or computationally predicted to adversely affect 17β-HSD3 activity.

**Supplementary Table 2. Reported Tunisian patients with 17 $\beta$ -HSD3 deficiencies**

	P1	P2	P3	P4	P5	P6	P7	P8	P9 (=P1)	P10 (=P2)	P11 (=P3)
Age	2 years	27 years	7 days	7 years	14 years	15 years	14 years	11 years	4 months	3 months	16 years
Height (cm)	85	-	-	155	-	-	148	155	-	-	168
Weight (kg)	11	-	-	45	-	-	-	-	-	-	68
Consanguinity	+	+	+	-	-	-	-	-	-	+	+
T (ng/mL)	0.9	-	0.15	0.8	3	4	3	-	0.03	0.86	2.89
A (ng/mL)	-	-	-	-	-	-	-	-	11.9	79.6	9.6
LH (IU/L)	8.5	18.9	0.1	12.5	-	-	5.7	2.3	0.2	3.22	20.6
FSH (IU/L)	0.98	28.9	0.58	4.7	40	42	8.2	0.2	0.5	1	3
Karyotype	46,XY	46,XY	46,XY	46,XY	46,XY	46,XY	46,XY	46,XY	46,XY	46,XY	46,XY
Masculinization Score	-	-	-	-	-	-	-	-	1	3	3
Sex of rearing	Female	Female	Female	Female	Female	Female	Female	Male	Female	Female	Female
Referral reason	Sexual ambiguity Prader IV	Primary amenorrhea, hirsutism	46, XY karyotype and female phenotype	Inguinal hernia	Primary amenorrhea, hirsutism	Primary amenorrhea, hirsutism	Primary amenorrhea, hirsutism	Micropenis	Hernia	Clitoral hypertrophy, inguinal hernia	Primary amenorrhea, hirsutism
Description	PE: bilateral inguinal masses consistent with testes, MRI: no vagina or uterus										
Tanner stage	P1B1	P5B4	-	P1B1	P4B1	P5B1	P4B1	-	-	-	-
Mutation type	C206*/C206C206*/C206*	C206*/C206*	C206*/C206*	C206*/G133R	C206*/G133R	C206*/G133R	C206*/Q176P	G289S/L18=	C206*/C206*	C206*/C206*/c.490-6T>A	K202M/K202M
Reference	[30]	[2]	[2]	[22]	[22]	[22]	[2]	[2]	New	New	New

All Tunisian patients with an identified 17 $\beta$ -HSD3 deficiency are listed and phenotypically described here with the corresponding references where they were mentioned the first time. Abbreviations of examination procedure: pelvic exam (PE), abdominal ultrasonography (AU), magnetic resonance imaging (MRI). Hormone abbreviations: testosterone (T),

androstenedione (A), follicle stimulating hormone (FSH), luteinizing hormone (LH). P9 to P11 correspond to P1 to P3 described in this paper (see brackets).

## References

- [1] B. Yu, Z. Liu, J. Mao, X. Wang, J. Zheng, S. Xiong, M. Cui, W. Ma, Q. Huang, H. Xu, B. Huang, M. Nie, X. Wu, Novel mutations of HSD17B3 in three Chinese patients with 46,XY Disorders of Sex Development, *Steroids* 126 (2017) 1-6.
- [2] B. Ben Rhouma, F. Kallabi, N. Mahfoudh, A. Ben Mahmoud, R.T. Engeli, H. Kamoun, L. Keskes, A. Odermatt, N. Belguith, Novel cases of Tunisian patients with mutations in the gene encoding 17beta-hydroxysteroid dehydrogenase type 3 and a founder effect, *J Steroid Biochem Mol Biol* 165(Pt A) (2017) 86-94.
- [3] L.J. Folsom, M. Hjaige, J. Liu, E.A. Eugster, R.J. Auchus, Germ cell neoplasia in situ complicating 17beta-hydroxysteroid dehydrogenase type 3 deficiency, *Mol Cell Endocrinol* 489 (2019) 3-8.
- [4] Z. Yang, L. Ye, W. Wang, Y. Zhao, W. Wang, H. Jia, Z. Dong, Y. Chen, W. Wang, G. Ning, S. Sun, 17beta-Hydroxysteroid dehydrogenase 3 deficiency: Three case reports and a systematic review, *J Steroid Biochem Mol Biol* 174 (2017) 141-145.
- [5] S. Eggers, S. Sadedin, J.A. van den Bergen, G. Robevska, T. Ohnesorg, J. Hewitt, L. Lambeth, A. Bouty, I.M. Knarston, T.Y. Tan, F. Cameron, G. Werther, J. Hutson, M. O'Connell, S.R. Grover, Y. Heloury, M. Zacharin, P. Bergman, C. Kimber, J. Brown, N. Webb, M.F. Hunter, S. Srinivasan, A. Titmuss, C.F. Verge, D. Mowat, G. Smith, J. Smith, L. Ewans, C. Shalhoub, P. Crock, C. Cowell, G.M. Leong, M. Ono, A.R. Lafferty, T. Huynh, U. Visser, C.S. Choong, F. McKenzie, N. Pachter, E.M. Thompson, J. Couper, A. Baxendale, J. Gecz, B.J. Wheeler, C. Jefferies, K. MacKenzie, P. Hofman, P. Carter, R.I. King, C. Krausz, C.M. van Ravenswaaij-Arts, L. Looijenga, S. Drop, S. Riedl, M. Cools, A. Dawson, A.Z. Juniarto, V. Khadilkar, A. Khadilkar, V. Bhatia, V.C. Dung, I. Atta, J. Raza, N. Thi Diem Chi, T.K. Hao, V. Harley, P. Koopman, G. Warne, S. Faradz, A. Oshlack, K.L. Ayers, A.H. Sinclair, Disorders of sex development: insights from targeted gene sequencing of a large international patient cohort, *Genome Biol* 17(1) (2016) 243.
- [6] H.A. Hassan, I. Mazen, Y.Z. Gad, O.S. Ali, M. Mekkawy, M.L. Essawi, A novel nonsense mutation in exon 1 of HSD17B3 gene in an Egyptian 46,XY adult female presenting with primary amenorrhea, *Sex Dev* 7(6) (2013) 277-281.
- [7] H.A. Hassan, I. Mazen, Y.Z. Gad, O.S. Ali, M. Mekkawy, M.L. Essawi, Mutational Profile of 10 Afflicted Egyptian Families with 17-beta-HSD-3 Deficiency, *Sex Dev* 10(2) (2016) 66-73.
- [8] R.T. Engeli, M. Tsachaki, H.A. Hassan, C.P. Sager, M.L. Essawi, Y.Z. Gad, A.K. Kamel, I. Mazen, A. Odermatt, Biochemical Analysis of Four Missense Mutations in the HSD17B3 Gene Associated With 46,XY Disorders of Sex Development in Egyptian Patients, *J Sex Med* 14(9) (2017) 1165-1174.
- [9] N. Moghrabi, I.A. Hughes, A. Dunaif, S. Andersson, Deleterious missense mutations and silent polymorphism in the human 17beta-hydroxysteroid dehydrogenase 3 gene (HSD17B3), *J Clin Endocrinol Metab* 83(8) (1998) 2855-2860.

- [10] S. Andersson, W.M. Geissler, L. Wu, D.L. Davis, M.M. Grumbach, M.I. New, H.P. Schwarz, S.L. Blethen, B.B. Mendonca, W. Bloise, S.F. Witchel, G.B. Cutler, Jr., J.E. Griffin, J.D. Wilson, D.W. Russel, Molecular genetics and pathophysiology of 17 beta-hydroxysteroid dehydrogenase 3 deficiency, *J Clin Endocrinol Metab* 81(1) (1996) 130-136.
- [11] T. Yazawa, Y. Imamichi, J. Uwada, T. Sekiguchi, D. Mikami, T. Kitano, T. Ida, T. Sato, T. Nemoto, S. Nagata, M.R. Islam Khan, S. Takahashi, F. Ushikubi, N. Suzuki, A. Umezawa, T. Taniguchi, Evaluation of 17beta-hydroxysteroid dehydrogenase activity using androgen receptor-mediated transactivation, *J Steroid Biochem Mol Biol* 196 (2020) 105493.
- [12] N. Phelan, E.L. Williams, S. Cardamone, M. Lee, S.M. Creighton, G. Rumsby, G.S. Conway, Screening for mutations in 17beta-hydroxysteroid dehydrogenase and androgen receptor in women presenting with partially virilised 46,XY disorders of sex development, *Eur J Endocrinol* 172(6) (2015) 745-751.
- [13] L.A. Hughes, K. McKay-Bounford, E.A. Webb, P. Dasani, S. Clokie, H. Chandran, L. McCarthy, Z. Mohamed, J.M.W. Kirk, N.P. Krone, S. Allen, T.R.P. Cole, Next generation sequencing (NGS) to improve the diagnosis and management of patients with disorders of sex development (DSD), *Endocr Connect* 8(2) (2019) 100-110.
- [14] A.L. Boehmer, A.O. Brinkmann, L.A. Sandkuijl, D.J. Halley, M.F. Niermeijer, S. Andersson, F.H. de Jong, H. Kayserili, M.A. de Vroede, B.J. Otten, C.W. Rouwe, B.B. Mendonca, C. Rodrigues, H.H. Bode, P.E. de Ruiten, H.A. Delemarre-van de Waal, S.L. Drop, 17Beta-hydroxysteroid dehydrogenase-3 deficiency: diagnosis, phenotypic variability, population genetics, and worldwide distribution of ancient and de novo mutations, *J Clin Endocrinol Metab* 84(12) (1999) 4713-4721.
- [15] W.M. Geissler, D.L. Davis, L. Wu, K.D. Bradshaw, S. Patel, B.B. Mendonca, K.O. Elliston, J.D. Wilson, D.W. Russell, S. Andersson, Male pseudohermaphroditism caused by mutations of testicular 17 beta-hydroxysteroid dehydrogenase 3, *Nat Genet* 7(1) (1994) 34-39.
- [16] J.R. Bilbao, L. Loridan, L. Audi, E. Gonzalo, L. Castano, A novel missense (R80W) mutation in 17-beta-hydroxysteroid dehydrogenase type 3 gene associated with male pseudohermaphroditism, *Eur J Endocrinol* 139(3) (1998) 330-333.
- [17] S. Wu, B. Zheng, T. Liu, Z. Zhu, W. Gu, Q. Liu, [17 beta-hydroxysteroid dehydrogenase 3 deficiency due to novel compound heterozygous variants of HSD17B3 gene in a sib pair], *Zhonghua Yi Xue Yi Chuan Xue Za Zhi* 38(8) (2021) 787-790.
- [18] C. Cocchetti, F. Baldinotti, A. Romani, J. Ristori, F. Mazzoli, L. Vignozzi, M. Maggi, A.D. Fisher, A Novel Compound Heterozygous Mutation of HSD17B3 Gene Identified in a Patient With 46,XY Difference of Sexual Development, *Sex Med* 10(4) (2022) 100522.
- [19] S. Ozen, H. Onay, T. Atik, A.E. Solmaz, F. Ozkinay, D. Goksen, S. Darcan, Rapid Molecular Genetic Diagnosis with Next-Generation Sequencing in 46,XY Disorders of Sex Development Cases: Efficiency and Cost Assessment, *Horm Res Paediatr* 87(2) (2017) 81-87.
- [20] C.C. Castro, G. Guaragna-Filho, F.L. Calais, F.B. Coeli, I.R. Leal, E.F. Cavalcante-Junior, I.L. Monlleo, S.R. Pereira, R.B. Silva, J.R. Gabiatti, A.P. Marques-de-Faria, A.T. Maciel-Guerra, M.P. Mello, G. Guerra-Junior, Clinical and molecular spectrum of patients with 17beta-hydroxysteroid dehydrogenase type 3 (17-beta-HSD3) deficiency, *Arq Bras Endocrinol Metabol* 56(8) (2012) 533-539.

- [21] F.L. de Calais, L.D. Smith, M. Raponi, A.T. Maciel-Guerra, G. Guerra-Junior, M.P. de Mello, D. Baralle, A study of splicing mutations in disorders of sex development, *Sci Rep* 7(1) (2017) 16202.
- [22] R.T. Engeli, B.B. Rhouma, C.P. Sager, M. Tsachaki, J. Birk, F. Fakhfakh, L. Keskes, N. Belguith, A. Odermatt, Biochemical analyses and molecular modeling explain the functional loss of 17beta-hydroxysteroid dehydrogenase 3 mutant G133R in three Tunisian patients with 46, XY Disorders of Sex Development, *J Steroid Biochem Mol Biol* 155(Pt A) (2016) 147-154.
- [23] O.T. Mueller, A. Coovadia, Novel human pathological mutations. Gene symbol: HSD17B3. Disease: 17 beta-hydroxysteroid dehydrogenase-3 deficiency, *Hum Genet* 125(3) (2009) 335.
- [24] K. Demir, M. Yildiz, O.N. Elmas, H.A. Korkmaz, S. Tunc, O. Olukman, F. Hazan, K.U. Ozkan, B. Ozkan, Two different patterns of mini-puberty in two 46,XY newborns with 17beta-hydroxysteroid dehydrogenase type 3 deficiency, *J Pediatr Endocrinol Metab* 28(7-8) (2015) 961-965.
- [25] M. Ellaithi, R. Werner, F.G. Riepe, N. Krone, A.E. Kulle, T. Diab, A.K. Kamel, W. Arlt, P.M. Holterhus, O. Sabir, O. Hiort, 46,XY disorder of sex development in a sudanese patient caused by a novel mutation in the HSD17B3 gene, *Sex Dev* 8(4) (2014) 151-155.
- [26] W. Twesten, P. Holterhus, W.G. Sippell, M. Morlot, H. Schumacher, B. Schenk, O. Hiort, Clinical, endocrine, and molecular genetic findings in patients with 17beta-hydroxysteroid dehydrogenase deficiency, *Horm Res* 53(1) (2000) 26-31.
- [27] A. Al-Sinani, W.A. Mula-Abed, M. Al-Kindi, G. Al-Kusaibi, H. Al-Azkawi, N. Nahavandi, A Novel Mutation Causing 17-beta-Hydroxysteroid Dehydrogenase Type 3 Deficiency in an Omani Child: First Case Report and Review of Literature, *Oman Med J* 30(2) (2015) 129-134.
- [28] S. Bertelloni, A. Balsamo, L. Giordani, R. Fischetto, G. Russo, M. Delvecchio, M. Gennari, A. Nicoletti, M.C. Maggio, D. Concolino, L. Cavallo, A. Cicognani, G. Chiumello, O. Hiort, G.I. Baroncelli, M.F. Faienza, 17beta-Hydroxysteroid dehydrogenase-3 deficiency: from pregnancy to adolescence, *J Endocrinol Invest* 32(8) (2009) 666-670.
- [29] B.B. Mendonca, N.L. Gomes, E.M. Costa, M. Inacio, R.M. Martin, M.Y. Nishi, F.M. Carvalho, F.D. Tibor, S. Domenice, 46,XY disorder of sex development (DSD) due to 17beta-hydroxysteroid dehydrogenase type 3 deficiency, *J Steroid Biochem Mol Biol* 165(Pt A) (2017) 79-85.
- [30] B. Ben Rhouma, N. Belguith, M.F. Mnif, T. Kamoun, N. Charfi, M. Kamoun, F. Abdelhedi, M. Hachicha, H. Kamoun, M. Abid, F. Fakhfakh, A novel nonsense mutation in HSD17B3 gene in a Tunisian patient with sexual ambiguity, *J Sex Med* 10(10) (2013) 2586-2589.
- [31] A. Khattab, T. Yuen, M. Yau, S. Domenice, E.M. Frade Costa, K. Diya, D. Muhuri, C.E. Pina, M.Y. Nishi, A.C. Yang, B.B. de Mendonca, M.I. New, Pitfalls in hormonal diagnosis of 17-beta hydroxysteroid dehydrogenase III deficiency, *J Pediatr Endocrinol Metab* 28(5-6) (2015) 623-628.
- [32] M.F. Faienza, F. Baldinotti, G. Marrocco, N. TyuTyusheva, D. Peroni, G.I. Baroncelli, S. Bertelloni, 17beta-hydroxysteroid dehydrogenase type 3 deficiency: female sex assignment and follow-up, *J Endocrinol Invest* 43(12) (2020) 1711-1716.



- [33] N. Ciftci, L. Kayas, E. Camtosun, A. Akinci, 46,XY Sex Development Defect due to a Novel Homozygous (Splice Site) c.673\_1G>C Variation in the HSD17B3 Gene: Case Report, *J Clin Res Pediatr Endocrinol* 14(2) (2022) 233-238.
- [34] F. Levy-Khademi, S. Zeligson, E. Lavi, T. Klopstock, B. Chertin, C. Avnon-Ziv, A. Abulibdeh, P. Renbaum, T. Rosen, S. Perlberg-Bengio, F. Zahdeh, D.M. Behar, E. Levy-Lahad, D. Zangen, R. Segel, The novel founder homozygous V225M mutation in the HSD17B3 gene causes aberrant splicing and XY-DSD, *Endocrine* 69(3) (2020) 650-654.
- [35] E. Sagsak, Z. Aycan, S. Savas-Erdeve, M. Keskin, S. Cetinkaya, K. Karaer, 17betaHSD-3 enzyme deficiency due to novel mutations in the HSD17B3 gene diagnosed in a neonate, *J Pediatr Endocrinol Metab* 28(7-8) (2015) 957-959.
- [36] R.L. de Omena Filho, R.J. Petroli, F.C. Soardi, D. de Paula Michelatto, T.N. Mazzola, H. Fabbri-Scallet, M.P. de Mello, S.V. Zanotti, I.C. Gubert, I. Monlleo, So, and if it is not congenital adrenal hyperplasia? Addressing an undiagnosed case of genital ambiguity, *Ital J Pediatr* 48(1) (2022) 89.
- [37] A. Lindqvist, I.A. Hughes, S. Andersson, Substitution mutation C268Y causes 17 beta-hydroxysteroid dehydrogenase 3 deficiency, *J Clin Endocrinol Metab* 86(2) (2001) 921-923.
- [38] H.U. Tuhan, A. Anik, G. Catli, S. Ceylaner, B. Dundar, E. Bober, A. Abaci, A novel missense mutation in HSD17B3 gene in a 46, XY adolescent presenting with primary amenorrhea and virilization at puberty, *Clin Chim Acta* 438 (2015) 154-156.
- [39] V. Ea, A. Bergougnoux, P. Philibert, N. Servant-Fauconnet, A. Faure, J. Breaud, L. Gaspari, C. Sultan, F. Paris, N. Kalfa, How Far Should We Explore Hypospadias? Next-generation Sequencing Applied to a Large Cohort of Hypospadiac Patients, *Eur Urol* 79(4) (2021) 507-515.

### 7.3 Discussion

HSD17B3 deficiency is a relatively rare recessive disorder which impairs testosterone production and can cause 46,XY DSD. Individual mutations in the *HSD17B3* gene can produce enzyme variants with different levels of activity. This results in a broad spectrum of phenotypes in affected patients, often presenting with varying degrees of undermasculinization. Accordingly, each patient should be considered and treated as an individual case [52, 387].

In this project, we analyzed three new case reports of diagnosed HSD17B3 deficiency for their molecular causes. We identified the first mutation in the catalytic tetrad of the *HSD17B3* gene, p.K202M, and experimentally confirmed the hypothesis of a complete loss of enzymatic activity. Furthermore, we were able to detect an already experimentally characterized mutation p.C206X in another patient [391]. This inactive gene variant had reached such a high frequency in the Tunisian population that the inheritance of this mutation no longer required consanguineous marriage to cause HSD17B3 deficiency. The last case turned out to be a compound heterozygote, with a paternally inherited p.C206X mutation and a maternally inherited splice site mutation in intron 6, that causes skipping of exon 7 in the resulting mRNA, which may result in the loss of parts of the catalytic tetrad as well as a truncation of the protein. Clear diagnosis including genetic analysis and the subsequent experimental confirmation of the mutations found in the *HSD17B3* gene provide an explanation for the observed phenotype of the examined patients.

To date, only about one third of the over 70 mutations in the *HSD17B3* gene described so far have been experimentally confirmed, our two novel mutations included. The remainder have been predicted to be potentially pathogenic using computational tools (reviewed in [392]). However, such formerly predicted as well as in the future identified mutations in the *HSD17B3* gene should be confirmed experimentally and described at the molecular level to rule out errors regarding a proposed influence of HSD17B3 functionality, as it has been done with the described p.E67K and p.G289S polymorphisms [390, 393].

Mutations in other genes involved in androgen production or AR activation can also lead to similar phenotypes that are clinically indistinguishable from HSD17B3 deficiency, such as mutations in the *SRD5A2* gene. The encoded protein SRD5A2 catalyzes the reduction of testosterone to DHT, which is required for complete masculinization of the external genitalia [384, 394]. Another possibility would be mutations in the *AR* gene itself (reviewed in [395]). If an *HSD17B3* mutation, that was suspected to be pathogenic, is experimentally disproven, mutations in genes involved in androgen biosynthesis or AR signaling should be considered as possible causes for the observed 46,XY DSD and analyzed accordingly.

A higher incidence of HSD17B3 deficiencies has been described in Arab countries with high frequencies of consanguineous marriages [396-400]. Segregated residential areas within those countries as well as socioeconomic and religious factors may favor this marriage type (reviewed in [401, 402]). Fully confirmed cases of HSD17B3 deficiency in affected families would allow genetic counseling, which would be particularly valuable for risk assessment within societies where consanguineous marriages are frequently practiced.

Sex-affirming surgeries can be performed after diagnosis of HSD17B3 deficiency, depending on how the patients may be raised. In the case of a female identity, this may include a gonadectomy to prevent further testosterone production by the testes, together with genitoplasty, vaginal dilation and estrogen treatment [403-405]. Penis reconstruction and orchidopexy may be performed to affirm male sexual identity [406, 407]. This project represents an important contribution to the public discourse of 46,XY DSD that may help to sensitize treating physicians to possible HSD17B3 deficiencies and enable a faster diagnosis of such cases. A more efficient early diagnosis of new HSD17B3 deficiency cases could lead to earlier determination of sexual identity and reduce potential future complications for affected patients.

## 8. Conclusion

In the context of this dissertation, three projects were conducted with the overall aim of identifying and characterizing substances that interfere with steroid metabolizing enzymes or ROR $\gamma$ (t) activity. In the first project, we revealed and characterized significant species-specific differences in the inhibition of human, mouse, rat and zebrafish homologs of HSD11B2 by the azole antifungals itraconazole and posaconazole. Using predictions based on homology modeling of HSD11B2 and analysis of chimeric enzymes, we were able to identify structural elements, such as the amino acid residues at position 170 and 172 and the C-terminal region, which appeared to be at least partially responsible for the species-specific differences between the mouse and the human homologs. This study highlights, as a further example, the problem of species-specific differences, which should generally be considered and taken into account in toxicological studies. The methods we applied to determine the enzyme activity of the various HSD11B2 homologs were summarized and together with additional methods, including several for HSD11B1, published as two chapters in the book series 'Methods in Enzymology'.

In the second project, we identified parabens and UV-filters as the first inhibitors of HSD17B6, which is part of the backdoor pathway of DHT biosynthesis. We analyzed the SAR of the individual inhibitors, which displayed IC<sub>50</sub> values in the nanomolar range, using an HSD17B6 homology model. The phenyl head group of parabens and BPs with a free 4-hydroxyl residue turned out to be essential for their inhibitory activities towards HSD17B6.

In the third project, we identified parabens, benzophenone-type UV-filters and structurally similar body care product constituents as novel ROR $\gamma$ (t) agonists that can enhance pro-inflammatory cytokine expression in a murine EL4 T-lymphocyte model. We observed agonistic additive mixture effects on ROR $\gamma$  activity by parabens, UV-filters and the identified similarity compounds. Whether parabens and UV-filters may reach high enough concentrations within different organs of the human body to exert antiandrogenic effects through HSD17B6 inhibition or aggravate already existing inflammatory and autoimmune diseases via further ROR $\gamma$ t activation remains to be determined by additional research.

As an additional, fourth project, we have described the molecular causes of two new *HSD17B3* mutations in the Tunisian population that have led to diagnosed HSD17B3 deficiencies. One mutation turned out to be a splice site mutation (c.490 -6 T > C), which causes skipping of exon 7 during mRNA splicing, resulting in a truncated and inactive enzyme, and the other, p.K202M is the first mutation within the catalytic tetrad of HSD17B3, which inactivates the enzyme. This project contributes to the sensitization towards the risks of consanguineous marriages, which can promote the emergence and establishment of deleterious mutations.

## 9. Acknowledgements

First and foremost, I would like to sincerely thank Prof. Dr. Alex Odermatt for his continuous support, valuable advices, stimulating scientific discussions and the opportunity to conduct my PhD thesis in the Molecular and Systems Toxicology group. Next, I would like to thank Prof. Dr. Jörg Huwyler for acting as my second supervisor and Prof. Dr. Michael Arand for taking on the role as external supervisor of my thesis committee. Further on I would like to express my gratitude to all our collaborators for all their work and input into the various projects. Special thanks go to the following contributors: Titularprof. Dr. Martin Smieško for establishing the human and mouse HSD11B2 homology models and supervising the computational similarity search for identification of additional ROR $\gamma$ (t) agonists, Dr. Veronika Temml for the establishment of the HSD17B6 homology model and the docking analysis, and Bochra Ben Rhouma for the genetical analysis of patient samples in the HSD17B3 project. Many thanks go to my former master student, Pamela Ruffiner who was a tremendous help in the 3 $\alpha$ -HSD project and to Dr. Cristina Gómez Castellà and Dr. Julien A. Allard for proofreading my thesis. I am also grateful to all members of the Molecular and Systems Toxicology group, for their support, the interesting discussions and the good times we had together. Finally, I would like to thank my family and friends for their unwavering support during all my endeavors.

### 9.1 Additional mentioning

Figures 2, 3, 6, and 7 of this thesis were partly generated using Servier Medical Art (Servier; <https://smart.servier.com/>), licensed under a Creative Commons Attribution 4.0 Unported License.

## 10. References

1. Evans, R.M., *The steroid and thyroid hormone receptor superfamily*. Science, 1988. 240(4854): p. 889-95.
2. Lagrange, A.H. and M.J. Kelly, *Neuroactive Steroids*, in *Encyclopedia of Hormones*, H.L. Henry and A.W. Norman, Editors. 2003, Academic Press: New York. p. 8-19.
3. Sánchez, E.P.G., *Mineralocorticoid modulation of central control of blood pressure*. Steroids, 1995. 60(1): p. 69-72.
4. Furman, B., *Androgens* ☆, in *Reference Module in Biomedical Sciences*. 2018, Elsevier.
5. Fukami, M., et al., *Backdoor pathway for dihydrotestosterone biosynthesis: Implications for normal and abnormal human sex development*. Developmental Dynamics, 2013. 242(4): p. 320-329.
6. Phung, J., J. Paul, and R. Smith, *Chapter 13 - Maintenance of Pregnancy and Parturition*, in *Maternal-Fetal and Neonatal Endocrinology*, C.S. Kovacs and C.L. Deal, Editors. 2020, Academic Press. p. 169-187.
7. Duax, W.L., J.F. Griffin, and D. Ghosh, *The fascinating complexities of steroid-binding enzymes*. Curr Opin Struct Biol, 1996. 6(6): p. 813-23.
8. Ha, C.E. and N.V. Bhagavan, *Chapter 23 - Regulation of gene expression*, in *Essentials of Medical Biochemistry (Third Edition)*, C.E. Ha and N.V. Bhagavan, Editors. 2023, Academic Press: San Diego. p. 527-546.
9. Gilad, Y., D.M. Lonard, and B.W. O'Malley, *Steroid receptor coactivators - their role in immunity*. Front Immunol, 2022. 13: p. 1079011.
10. JCBN, *IUPAC-IUB Joint Commission on Biochemical Nomenclature (JCBN). The nomenclature of steroids. Recommendations 1989*. Eur J Biochem, 1989. 186(3): p. 429-58.
11. Baker, M.E. and Y. Katsu, *Chapter Two - Evolution of the Mineralocorticoid Receptor*, in *Vitamins and Hormones*, G. Litwack, Editor. 2019, Academic Press. p. 17-36.
12. Fuller, P.J., *Aldosterone's effects and mechanism of action*. Current Opinion in Endocrinology, Diabetes and Obesity, 1997. 4(3): p. 218-224.
13. Krozowski, Z.S. and J.W. Funder, *Renal mineralocorticoid receptors and hippocampal corticosterone-binding species have identical intrinsic steroid specificity*. Proceedings of the National Academy of Sciences, 1983. 80(19): p. 6056-6060.
14. Byrd, J.B., A.F. Turcu, and R.J. Auchus, *Primary Aldosteronism: Practical Approach to Diagnosis and Management*. Circulation, 2018. 138(8): p. 823-835.
15. Gao, Q., et al., *Chapter 49 - Pathophysiological Roles and Disorders of Renin-Angiotensin-Aldosterone System and Nitric Oxide During Perinatal Periods*, in *Maternal-Fetal and Neonatal Endocrinology*, C.S. Kovacs and C.L. Deal, Editors. 2020, Academic Press. p. 869-889.
16. Weitzman, E.D., et al., *Twenty-four hour pattern of the episodic secretion of cortisol in normal subjects*. J Clin Endocrinol Metab, 1971. 33(1): p. 14-22.
17. Cockrem, J.F., *Individual variation in glucocorticoid stress responses in animals*. General and Comparative Endocrinology, 2013. 181: p. 45-58.
18. Timmermans, S., J. Souffriau, and C. Libert, *A General Introduction to Glucocorticoid Biology*. Frontiers in Immunology, 2019. 10: p. 1545.
19. Ramamoorthy, S. and J.A. Cidlowski, *Corticosteroids: Mechanisms of Action in Health and Disease*. Rheum Dis Clin North Am, 2016. 42(1): p. 15-31, vii.
20. Sopinka, N.M., et al., *Manipulating glucocorticoids in wild animals: basic and applied perspectives*. Conservation Physiology, 2015. 3(1).
21. Spiga, F., et al., *HPA Axis-Rhythms*, in *Comprehensive Physiology*. 2014. p. 1273-1298.

22. Burford, N.G., N.A. Webster, and D. Cruz-Topete, *Hypothalamic-Pituitary-Adrenal Axis Modulation of Glucocorticoids in the Cardiovascular System*. *Int J Mol Sci*, 2017. 18(10).
23. Hahner, S., et al., *Adrenal insufficiency*. *Nature Reviews Disease Primers*, 2021. 7(1): p. 19.
24. Lacroix, A., et al., *Cushing's syndrome*. *The lancet*, 2015. 386(9996): p. 913-927.
25. Feelders, R.A., et al., *The burden of Cushing's disease: clinical and health-related quality of life aspects*. *Eur J Endocrinol*, 2012. 167(3): p. 311-26.
26. Iwamoto, Y., et al., *Usefulness of cortisol/ACTH ratio (CAR) for diagnosis of cushing's syndrome: comparison of CAR with findings in dexamethasone suppression test*. *Sci Rep*, 2022. 12(1): p. 17680.
27. Barnes, P.J., *Glucocorticosteroids*. *Handb Exp Pharmacol*, 2017. 237: p. 93-115.
28. Coutinho, A.E. and K.E. Chapman, *The anti-inflammatory and immunosuppressive effects of glucocorticoids, recent developments and mechanistic insights*. *Mol Cell Endocrinol*, 2011. 335(1): p. 2-13.
29. Hopkins, R.L. and M.C. Leinung, *Exogenous Cushing's syndrome and glucocorticoid withdrawal*. *Endocrinol Metab Clin North Am*, 2005. 34(2): p. 371-84, ix.
30. Wang, Y., et al., *Steroidogenesis in Leydig cells: effects of aging and environmental factors*. *Reproduction*, 2017. 154(4): p. R111-R122.
31. Ostrer, H., *Sexual differentiation*. *Semin Reprod Med*, 2000. 18(1): p. 41-9.
32. McLachlan, R.I., et al., *Identification of specific sites of hormonal regulation in spermatogenesis in rats, monkeys, and man*. *Recent progress in hormone research*, 2002. 57(1): p. 149-179.
33. Penning, T.M., et al., *Identification of the molecular switch that regulates access of 5 $\alpha$ -DHT to the androgen receptor*. *Molecular and Cellular Endocrinology*, 2007. 265-266: p. 77-82.
34. Kaufman, F.R., et al., *Dehydroepiandrosterone and dehydroepiandrosterone sulfate metabolism in human genital skin*. *Fertility and sterility*, 1990. 54(2): p. 251-254.
35. Rainey, W.E., K.S. Rehman, and B.R. Carr. *The human fetal adrenal: making adrenal androgens for placental estrogens*. in *Seminars in reproductive medicine*. 2004. Copyright© 2004 by Thieme Medical Publishers, Inc., 333 Seventh Avenue, New ....
36. Jasuja, R., et al., *Delta-4-androstene-3,17-dione binds androgen receptor, promotes myogenesis in vitro, and increases serum testosterone levels, fat-free mass, and muscle strength in hypogonadal men*. *J Clin Endocrinol Metab*, 2005. 90(2): p. 855-63.
37. Handelsman, D.J., E.R. Cooper, and A.K. Heather, *Bioactivity of 11 keto and hydroxy androgens in yeast and mammalian host cells*. *The Journal of Steroid Biochemistry and Molecular Biology*, 2022. 218: p. 106049.
38. Flück, C.E. and A.V. Pandey. *Steroidogenesis of the testis—new genes and pathways*. in *Annales d'endocrinologie*. 2014. Elsevier.
39. Wilson, J.D., *The role of 5 $\alpha$ -reduction in steroid hormone physiology*. *Reproduction, Fertility and Development*, 2001. 13(8): p. 673-678.
40. Cui, J., Y. Shen, and R. Li, *Estrogen synthesis and signaling pathways during aging: from periphery to brain*. *Trends in Molecular Medicine*, 2013. 19(3): p. 197-209.
41. Handa, R.J. and T.R. Pak, *Androgen Action\**, in *Encyclopedia of Stress (Second Edition)*, G. Fink, Editor. 2007, Academic Press: New York. p. 171-175.
42. Stanczyk, F.Z., et al., *Androstenedione is an important precursor of dihydrotestosterone in the genital skin of women and is metabolized via 5 alpha-androstanedione*. *J Steroid Biochem Mol Biol*, 1990. 37(1): p. 129-32.
43. Naamneh Elzenaty, R., T. du Toit, and C.E. Flück, *Basics of androgen synthesis and action*. *Best Practice & Research Clinical Endocrinology & Metabolism*, 2022. 36(4): p. 101665.

44. Takayasu, S., et al., *Activity of Testosterone 5 $\alpha$ -Reductase in Various Tissues of Human Skin*. Journal of Investigative Dermatology, 1980. 74(4): p. 187-191.
45. Penning, T.M., et al., *Structure-function aspects and inhibitor design of type 5 17 $\beta$ -hydroxysteroid dehydrogenase (AKR1C3)*. Molecular and Cellular Endocrinology, 2001. 171(1): p. 137-149.
46. Dufort, I., et al., *Characteristics of a highly labile human type 5 17 $\beta$ -hydroxysteroid dehydrogenase*. Endocrinology, 1999. 140(2): p. 568-74.
47. Kim, H.-G., B. Bhagavath, and L.C. Layman, *Clinical manifestations of impaired GnRH neuron development and function*. Neurosignals, 2008. 16(2-3): p. 165-182.
48. Veldhuis, J.D., R.J. Urban, and M.L. Dufau, *Evidence that androgen negative feedback regulates hypothalamic gonadotropin-releasing hormone impulse strength and the burst-like secretion of biologically active luteinizing hormone in men*. The Journal of Clinical Endocrinology & Metabolism, 1992. 74(6): p. 1227-1235.
49. Rege, J., et al., *Liquid chromatography-tandem mass spectrometry analysis of human adrenal vein 19-carbon steroids before and after ACTH stimulation*. J Clin Endocrinol Metab, 2013. 98(3): p. 1182-8.
50. Reiter, E.O., V.G. Fuldauer, and A.W. Root, *Secretion of the adrenal androgen, dehydroepiandrosterone sulfate, during normal infancy, childhood, and adolescence, in sick infants, and in children with endocrinologic abnormalities*. The Journal of pediatrics, 1977. 90(5): p. 766-770.
51. Witchel, S.F., *Congenital adrenal hyperplasia*. Journal of pediatric and adolescent gynecology, 2017. 30(5): p. 520-534.
52. Mendonca, B.B., et al., *46,XY disorder of sex development (DSD) due to 17 $\beta$ -hydroxysteroid dehydrogenase type 3 deficiency*. The Journal of Steroid Biochemistry and Molecular Biology, 2017. 165: p. 79-85.
53. Mendonca, B.B., et al., *Steroid 5 $\alpha$ -reductase 2 deficiency*. The Journal of steroid biochemistry and molecular biology, 2016. 163: p. 206-211.
54. Yoshida, T., et al., *Circulating steroids and mood disorders in patients with polycystic ovary syndrome*. Steroids, 2021. 165: p. 108748.
55. Bulant, J., et al., *Changes of BMI, steroid metabolome and psychopathology in patients with anorexia nervosa during hospitalization*. Steroids, 2020. 153: p. 108523.
56. Belgorosky, A., et al., *Genetic and clinical spectrum of aromatase deficiency in infancy, childhood and adolescence*. Horm Res, 2009. 72(6): p. 321-30.
57. Mendonca, B.B., et al., *46,XY disorders of sex development (DSD)*. Clin Endocrinol (Oxf), 2009. 70(2): p. 173-87.
58. Witchel, S.F., *Disorders of sex development*. Best Pract Res Clin Obstet Gynaecol, 2018. 48: p. 90-102.
59. Hanukoglu, I., *Steroidogenic enzymes: structure, function, and role in regulation of steroid hormone biosynthesis*. J Steroid Biochem Mol Biol, 1992. 43(8): p. 779-804.
60. Penning, T.M., et al., *Structure and function of 3 $\alpha$ -hydroxysteroid dehydrogenase*. Steroids, 1997. 62(1): p. 101-111.
61. Persson, B., M. Krook, and H. Jörnvall, *Short-chain dehydrogenases/reductases*. Enzymology and Molecular Biology of Carbonyl Metabolism 5, 1995: p. 383-395.
62. Bauman, D.R., S. Steckelbroeck, and T.M. Penning, *The roles of aldo-keto reductases in steroid hormone action*. Drug news & perspectives, 2004. 17(9): p. 563-578.
63. Penning, T.M., *Human hydroxysteroid dehydrogenases and pre-receptor regulation: Insights into inhibitor design and evaluation*. The Journal of Steroid Biochemistry and Molecular Biology, 2011. 125(1): p. 46-56.
64. Jörnvall, H., et al., *Short-chain dehydrogenases/reductases (SDR)*. Biochemistry, 1995. 34(18): p. 6003-6013.



65. Kavanagh, K.L., et al., *Medium- and short-chain dehydrogenase/reductase gene and protein families : the SDR superfamily: functional and structural diversity within a family of metabolic and regulatory enzymes*. Cell Mol Life Sci, 2008. 65(24): p. 3895-906.
66. Filling, C., et al., *Critical Residues for Structure and Catalysis in Short-chain Dehydrogenases/Reductases\**. Journal of Biological Chemistry, 2002. 277(28): p. 25677-25684.
67. Hanukoglu, I., *Proteopedia: Rossmann fold: A beta-alpha-beta fold at dinucleotide binding sites*. Biochemistry and Molecular Biology Education, 2015. 43(3): p. 206-209.
68. Rao, S.T. and M.G. Rossmann, *Comparison of super-secondary structures in proteins*. J Mol Biol, 1973. 76(2): p. 241-56.
69. Miller, W.L. and R.J. Auchus, *The Molecular Biology, Biochemistry, and Physiology of Human Steroidogenesis and Its Disorders*. Endocrine Reviews, 2011. 32(1): p. 81-151.
70. Jefcoate, C.R., et al., *Regulation of cholesterol movement to mitochondrial cytochrome P450scc in steroid hormone synthesis*. J Steroid Biochem Mol Biol, 1992. 43(8): p. 751-67.
71. Thomas, J.L., R.P. Myers, and R.C. Strickler, *Human placental 3 $\beta$ -hydroxy-5-ene-steroid dehydrogenase and steroid 5 $\rightarrow$  4-ene-isomerase: purification from mitochondria and kinetic profiles, biophysical characterization of the purified mitochondrial and microsomal enzymes*. Journal of steroid biochemistry, 1989. 33(2): p. 209-217.
72. Lachance, Y., et al., *Characterization of human 3 beta-hydroxysteroid dehydrogenase/delta 5-delta 4-isomerase gene and its expression in mammalian cells*. Journal of Biological Chemistry, 1990. 265(33): p. 20469-20475.
73. Lorence, M.C., et al., *Human 3 $\beta$ -hydroxysteroid dehydrogenase/ $\Delta$ 5 $\rightarrow$  4isomerase from placenta: Expression in nonsteroidogenic cells of a protein that catalyzes the dehydrogenation/isomerization of C21 and C19 steroids*. Endocrinology, 1990. 126(5): p. 2493-2498.
74. Rhéaume, E., et al., *Structure and expression of a new complementary DNA encoding the almost exclusive 3 $\beta$ -hydroxysteroid dehydrogenase/ $\Delta$ 5- $\Delta$ 4-Isomerase in Human adrenals and gonads*. Molecular endocrinology, 1991. 5(8): p. 1147-1157.
75. Curnow, K.M., et al., *The product of the CYP11B2 gene is required for aldosterone biosynthesis in the human adrenal cortex*. Mol Endocrinol, 1991. 5(10): p. 1513-22.
76. Auchus, R.J., et al., *The enantiomer of progesterone (ent-progesterone) is a competitive inhibitor of human cytochromes P450c17 and P450c21*. Archives of Biochemistry and Biophysics, 2003. 409(1): p. 134-144.
77. White, P.C., K.M. Curnow, and L. Pascoe, *Disorders of Steroid 11 $\beta$ -Hydroxylase Isozymes\**. Endocrine Reviews, 1994. 15(4): p. 421-438.
78. Honour, J.W., *Chapter 1.3 - Steroid biosynthesis*, in *Steroids in the Laboratory and Clinical Practice*, J.W. Honour, Editor. 2023, Elsevier. p. 63-92.
79. Lisurek, M. and R. Bernhardt, *Modulation of aldosterone and cortisol synthesis on the molecular level*. Mol Cell Endocrinol, 2004. 215(1-2): p. 149-59.
80. Auchus, R.J., T.C. Lee, and W.L. Miller, *Cytochrome b5 augments the 17,20-lyase activity of human P450c17 without direct electron transfer*. J Biol Chem, 1998. 273(6): p. 3158-65.
81. Lee-Robichaud, P., et al., *Modulation of the activity of human 17 alpha-hydroxylase-17,20-lyase (CYP17) by cytochrome b5: endocrinological and mechanistic implications*. Biochem J, 1995. 308 ( Pt 3)(Pt 3): p. 901-8.
82. Flück, C.E., W.L. Miller, and R.J. Auchus, *The 17, 20-Lyase Activity of Cytochrome P450c17 from Human Fetal Testis Favors the  $\Delta$ 5 Steroidogenic Pathway*. The Journal of Clinical Endocrinology & Metabolism, 2003. 88(8): p. 3762-3766.

83. Brock, B.J. and M.R. Waterman, *Biochemical Differences between Rat and Human Cytochrome P450c17 Support the Different Steroidogenic Needs of These Two Species*. *Biochemistry*, 1999. 38(5): p. 1598-1606.
84. Lee, S.-G., et al., *Hydroxylation and lyase reactions of steroids catalyzed by mouse cytochrome P450 17A1 (Cyp17a1)*. *Journal of Inorganic Biochemistry*, 2023. 240: p. 112085.
85. Fevold, H.R., et al., *Rat P45017 $\alpha$  from Testis: Characterization of a Full-Length cDNA Encoding a Unique Steroid Hydroxylase Capable of Catalyzing Both  $\Delta$ 4- and  $\Delta$ 5-Steroid-17,20-Lyase Reactions*. *Molecular Endocrinology*, 1989. 3(6): p. 968-975.
86. Nicolaides, N.C., E. Charmandari, and G.P. Chrousos, *Overview of Glucocorticoids* ☆, in *Encyclopedia of Endocrine Diseases (Second Edition)*, I. Huhtaniemi and L. Martini, Editors. 2018, Academic Press: Oxford. p. 64-71.
87. Zirkin, B.R. and V. Papadopoulos, *Leydig cells: formation, function, and regulation* †. *Biology of Reproduction*, 2018. 99(1): p. 101-111.
88. Franks, S., *Androgen production and action in the ovary*. *Current Opinion in Endocrine and Metabolic Research*, 2021. 18: p. 48-53.
89. Geissler, W.M., et al., *Male pseudohermaphroditism caused by mutations of testicular 17 beta-hydroxysteroid dehydrogenase 3*. *Nat Genet*, 1994. 7(1): p. 34-9.
90. Nakamura, Y., et al., *Type 5 17beta-hydroxysteroid dehydrogenase (AKRIC3) contributes to testosterone production in the adrenal reticularis*. *J Clin Endocrinol Metab*, 2009. 94(6): p. 2192-8.
91. Matsuura, K., et al., *Identification of a principal mRNA species for human 3alpha-hydroxysteroid dehydrogenase isoform (AKRIC3) that exhibits high prostaglandin D2 11-ketoreductase activity*. *J Biochem*, 1998. 124(5): p. 940-6.
92. Penning, T.M., et al., *Human 3alpha-hydroxysteroid dehydrogenase isoforms (AKRIC1-AKRIC4) of the aldo-keto reductase superfamily: functional plasticity and tissue distribution reveals roles in the inactivation and formation of male and female sex hormones*. *Biochem J*, 2000. 351(Pt 1): p. 67-77.
93. Scaglione, A., et al., *Subcellular localization of the five members of the human steroid 5 $\alpha$ -reductase family*. *Biochim Open*, 2017. 4: p. 99-106.
94. Russell, D.W. and J.D. Wilson, *STEROID 5 $\alpha$ -REDUCTASE: TWO GENES/TWO ENZYMES*. *Annual Review of Biochemistry*, 1994. 63(Volume 63, 1994): p. 25-61.
95. Simpson, E.R., et al., *Aromatase cytochrome P450, the enzyme responsible for estrogen biosynthesis*. *Endocr Rev*, 1994. 15(3): p. 342-55.
96. Harada, N., *Cloning of a complete cDNA encoding human aromatase: immunochemical identification and sequence analysis*. *Biochem Biophys Res Commun*, 1988. 156(2): p. 725-32.
97. Wu, L., et al., *Expression cloning and characterization of human 17 beta-hydroxysteroid dehydrogenase type 2, a microsomal enzyme possessing 20 alpha-hydroxysteroid dehydrogenase activity*. *J Biol Chem*, 1993. 268(17): p. 12964-9.
98. Agarwal, A.K., et al., *Expression of 11 $\beta$ -Hydroxysteroid Dehydrogenase Using Recombinant Vaccinia Virus*. *Molecular Endocrinology*, 1990. 4(12): p. 1827-1832.
99. Agarwal, A.K., et al., *Cloning and Expression of Rat cDNA Encoding Corticosteroid 11 $\beta$ -Dehydrogenase\**. *Journal of Biological Chemistry*, 1989. 264(32): p. 18939-18943.
100. Mahendroo, M., et al., *Steroid 5 $\alpha$ -reductase 1 promotes 5 $\alpha$ -androstane-3 $\alpha$ , 17 $\beta$ -diol synthesis in immature mouse testes by two pathways*. *Molecular and Cellular Endocrinology*, 2004. 222(1-2): p. 113-120.
101. Wilson, J.D., et al., *5 $\alpha$ -Androstane-3 $\alpha$ , 17 $\beta$ -Diol Is Formed in Tammar Wallaby Pouch Young Testes by a Pathway Involving 5 $\alpha$ -Pregnane-3 $\alpha$ , 17 $\alpha$ -Diol-20-One as a Key Intermediate*. *Endocrinology*, 2003. 144(2): p. 575-580.

102. Flück, C.E., et al., *Why boys will be boys: two pathways of fetal testicular androgen biosynthesis are needed for male sexual differentiation*. Am J Hum Genet, 2011. 89(2): p. 201-18.
103. Gupta, M.K., O.L. Guryev, and R.J. Auchus, *5alpha-reduced C21 steroids are substrates for human cytochrome P450c17*. Arch Biochem Biophys, 2003. 418(2): p. 151-60.
104. Biswas, M.G. and D.W. Russell, *Expression cloning and characterization of oxidative 17beta- and 3alpha-hydroxysteroid dehydrogenases from rat and human prostate*. J Biol Chem, 1997. 272(25): p. 15959-66.
105. O'Shaughnessy, P.J., et al., *Alternative (backdoor) androgen production and masculinization in the human fetus*. PLoS Biol, 2019. 17(2): p. e3000002.
106. Gronemeyer, H., J.-Å. Gustafsson, and V. Laudet, *Principles for modulation of the nuclear receptor superfamily*. Nature reviews Drug discovery, 2004. 3(11): p. 950-964.
107. Kumar, R. and E.B. Thompson, *The structure of the nuclear hormone receptors*. Steroids, 1999. 64(5): p. 310-319.
108. Pratt, W.B. and D.O. Toft, *Steroid receptor interactions with heat shock protein and immunophilin chaperones*. Endocr Rev, 1997. 18(3): p. 306-60.
109. Goodman, H.M., *Chapter 1 - Introduction*, in *Basic Medical Endocrinology (Fourth Edition)*, H.M. Goodman, Editor. 2009, Academic Press: San Diego. p. 1-27.
110. Lonard, D.M. and B.W. O'malley, *Nuclear receptor coregulators: modulators of pathology and therapeutic targets*. Nature Reviews Endocrinology, 2012. 8(10): p. 598-604.
111. Roesler, W.J., et al., *Modulation of hormone response elements by promoter environment*. Trends Endocrinol Metab, 1990. 1(7): p. 347-51.
112. Beato, M. and A. Sánchez-Pacheco, *Interaction of Steroid Hormone Receptors with the Transcription Initiation Complex*. Endocrine Reviews, 1996. 17(6): p. 587-609.
113. Levin, E.R. and S.R. Hammes, *Nuclear receptors outside the nucleus: extranuclear signalling by steroid receptors*. Nat Rev Mol Cell Biol, 2016. 17(12): p. 783-797.
114. Krozowski, Z.S., et al., *Immunolocalization of renal mineralocorticoid receptors with an antiserum against a peptide deduced from the complementary deoxyribonucleic acid sequence*. Endocrinology, 1989. 125(1): p. 192-198.
115. Lombes, M., et al., *Immunohistochemical localization of renal mineralocorticoid receptor by using an anti-idiotypic antibody that is an internal image of aldosterone*. Proceedings of the National Academy of Sciences, 1990. 87(3): p. 1086-1088.
116. Lombes, M., et al., *Aldosterone binding in the human colon carcinoma cell line HT29: correlation with cell differentiation*. Journal of Steroid Biochemistry, 1984. 20(1): p. 329-333.
117. Sasano, H., et al., *Immunolocalization of mineralocorticoid receptor in human kidney, pancreas, salivary, mammary and sweat glands: a light and electron microscopic immunohistochemical study*. Journal of endocrinology, 1992. 132(2): p. 305-NP.
118. Cole, T.J. and D. Pearce, *Mineralocorticoid target genes*. Current Opinion in Endocrinology, Diabetes and Obesity, 2001. 8(3): p. 118-123.
119. Atlas, S.A., *The renin-angiotensin aldosterone system: pathophysiological role and pharmacologic inhibition*. J Manag Care Pharm, 2007. 13(8 Suppl B): p. 9-20.
120. Ruggiero, C. and E. Lalli, *Impact of ACTH Signaling on Transcriptional Regulation of Steroidogenic Genes*. Front Endocrinol (Lausanne), 2016. 7: p. 24.
121. Triebel, H. and H. Castrop, *The renin angiotensin aldosterone system*. Pflügers Archiv - European Journal of Physiology, 2024. 476(5): p. 705-713.
122. Edwards, C., et al., *Localisation of 11β-hydroxysteroid dehydrogenase—tissue specific protector of the mineralocorticoid receptor*. The Lancet, 1988. 332(8618): p. 986-989.

123. Funder, J.W., et al., *Mineralocorticoid action: target tissue specificity is enzyme, not receptor, mediated*. *Science*, 1988. 242(4878): p. 583-585.
124. Mune, T., et al., *Human hypertension caused by mutations in the kidney isozyme of 11 beta-hydroxysteroid dehydrogenase*. *Nat Genet*, 1995. 10(4): p. 394-9.
125. Ferrari, P., et al., *In vivo 11beta-HSD-2 activity: variability, salt-sensitivity, and effect of licorice*. *Hypertension*, 2001. 38(6): p. 1330-6.
126. Wilson, R.C., et al., *Several homozygous mutations in the gene for 11 beta-hydroxysteroid dehydrogenase type 2 in patients with apparent mineralocorticoid excess*. *J Clin Endocrinol Metab*, 1995. 80(11): p. 3145-50.
127. White, P.C., et al., *Molecular analysis of 11 beta-hydroxysteroid dehydrogenase and its role in the syndrome of apparent mineralocorticoid excess*. *Steroids*, 1997. 62(1): p. 83-8.
128. Ferrari, P., *The role of 11 $\beta$ -hydroxysteroid dehydrogenase type 2 in human hypertension*. *Biochim Biophys Acta*, 2010. 1802(12): p. 1178-87.
129. Cheek, D.B. and J.W. Perry, *A salt wasting syndrome in infancy*. *Arch Dis Child*, 1958. 33(169): p. 252-6.
130. Geller, D.S., et al., *Mutations in the mineralocorticoid receptor gene cause autosomal dominant pseudohypoaldosteronism type I*. *Nat Genet*, 1998. 19(3): p. 279-81.
131. Odermatt, A. and D.V. Kratschmar, *Tissue-specific modulation of mineralocorticoid receptor function by 11 $\beta$ -hydroxysteroid dehydrogenases: an overview*. *Mol Cell Endocrinol*, 2012. 350(2): p. 168-86.
132. Jaisser, F. and N. Farman, *Emerging Roles of the Mineralocorticoid Receptor in Pathology: Toward New Paradigms in Clinical Pharmacology*. *Pharmacol Rev*, 2016. 68(1): p. 49-75.
133. Huang, P., V. Chandra, and F. Rastinejad, *Structural Overview of the Nuclear Receptor Superfamily: Insights into Physiology and Therapeutics*. *Annual Review of Physiology*, 2010. 72(Volume 72, 2010): p. 247-272.
134. Galon, J., et al., *Gene profiling reveals unknown enhancing and suppressive actions of glucocorticoids on immune cells*. *The FASEB journal*, 2002. 16(1): p. 61-71.
135. Vandevyver, S., L. Dejager, and C. Libert, *Comprehensive overview of the structure and regulation of the glucocorticoid receptor*. *Endocrine reviews*, 2014. 35(4): p. 671-693.
136. Weikum, E.R., et al., *Glucocorticoid receptor control of transcription: precision and plasticity via allostery*. *Nature Reviews Molecular Cell Biology*, 2017. 18(3): p. 159-174.
137. Scheschowitsch, K., J.A. Leite, and J. Assreuy, *New insights in glucocorticoid receptor signaling—more than just a ligand-binding receptor*. *Frontiers in endocrinology*, 2017. 8: p. 16.
138. Miller, A.L., et al., *p38 Mitogen-activated protein kinase (MAPK) is a key mediator in glucocorticoid-induced apoptosis of lymphoid cells: correlation between p38 MAPK activation and site-specific phosphorylation of the human glucocorticoid receptor at serine 211*. *Molecular endocrinology*, 2005. 19(6): p. 1569-1583.
139. Wallace, A.D. and J.A. Cidlowski, *Proteasome-mediated glucocorticoid receptor degradation restricts transcriptional signaling by glucocorticoids*. *Journal of Biological Chemistry*, 2001. 276(46): p. 42714-42721.
140. Hua, G., L. Paulen, and P. Chambon, *GR SUMOylation and formation of an SUMO-SMRT/NCoRI-HDAC3 repressing complex is mandatory for GC-induced IR nGRE-mediated transrepression*. *Proceedings of the National Academy of Sciences*, 2016. 113(5): p. E626-E634.
141. Nader, N., G.P. Chrousos, and T. Kino, *Circadian rhythm transcription factor CLOCK regulates the transcriptional activity of the glucocorticoid receptor by acetylating its*

- hinge region lysine cluster: potential physiological implications.* The FASEB Journal, 2009. 23(5): p. 1572.
142. Cole, T.J., et al., *Targeted disruption of the glucocorticoid receptor gene blocks adrenergic chromaffin cell development and severely retards lung maturation.* Genes Dev, 1995. 9(13): p. 1608-21.
  143. Vingerhoeds, A., J. Thijssen, and F. Schwarz, *Spontaneous hypercortisolism without Cushing's syndrome.* The Journal of Clinical Endocrinology & Metabolism, 1976. 43(5): p. 1128-1133.
  144. Kino, T., et al., *Familial/sporadic glucocorticoid resistance syndrome and hypertension.* Annals of the New York Academy of Sciences, 2002. 970(1): p. 101-111.
  145. Charmandari, E., T. Kino, and G.P. Chrousos, *Familial/sporadic glucocorticoid resistance: clinical phenotype and molecular mechanisms.* Annals of the New York Academy of Sciences, 2004. 1024(1): p. 168-181.
  146. Charmandari, E., et al., *Generalized glucocorticoid resistance: clinical aspects, molecular mechanisms, and implications of a rare genetic disorder.* J Clin Endocrinol Metab, 2008. 93(5): p. 1563-72.
  147. Kino, T. and G.P. Chrousos, *Tissue-specific glucocorticoid resistance-hypersensitivity syndromes: multifactorial states of clinical importance.* Journal of allergy and clinical immunology, 2002. 109(4): p. 609-613.
  148. Rana, K., R.A. Davey, and J.D. Zajac, *Human androgen deficiency: insights gained from androgen receptor knockout mouse models.* Asian journal of andrology, 2014. 16(2): p. 169-177.
  149. Heemers, H.V. and D.J. Tindall, *Androgen receptor (AR) coregulators: a diversity of functions converging on and regulating the AR transcriptional complex.* Endocrine reviews, 2007. 28(7): p. 778-808.
  150. Van der Steen, T., D.J. Tindall, and H. Huang, *Posttranslational modification of the androgen receptor in prostate cancer.* International journal of molecular sciences, 2013. 14(7): p. 14833-14859.
  151. Mongan, N.P., et al., *Androgen insensitivity syndrome.* Best Pract Res Clin Endocrinol Metab, 2015. 29(4): p. 569-80.
  152. Mendonca, B.B., et al., *46,XY DSD due to impaired androgen production.* Best Pract Res Clin Endocrinol Metab, 2010. 24(2): p. 243-62.
  153. Morris, J.M., *The syndrome of testicular feminization in male pseudohermaphrodites.* American Journal of Obstetrics & Gynecology, 1953. 65(6): p. 1192-1211.
  154. Oakes, M.B., et al., *Complete Androgen Insensitivity Syndrome—A Review.* Journal of Pediatric and Adolescent Gynecology, 2008. 21(6): p. 305-310.
  155. Batista, R.L., et al., *Androgen insensitivity syndrome: a review.* Archives of endocrinology and metabolism, 2018. 62: p. 227-235.
  156. Hughes, I.A., et al., *Androgen insensitivity syndrome.* Semin Reprod Med, 2012. 30(5): p. 432-42.
  157. Audí, L., et al., *Novel (60%) and recurrent (40%) androgen receptor gene mutations in a series of 59 patients with a 46, XY disorder of sex development.* The Journal of Clinical Endocrinology & Metabolism, 2010. 95(4): p. 1876-1888.
  158. Delli Paoli, E., et al., *Androgen insensitivity syndrome: a review.* Journal of Endocrinological Investigation, 2023. 46(11): p. 2237-2245.
  159. Huggins, C. and C.V. Hodges, *Studies on prostatic cancer. I. The effect of castration, of estrogen and of androgen injection on serum phosphatases in metastatic carcinoma of the prostate.* Cancer research, 1941. 1(4): p. 293-297.
  160. Grossmann, M., A.S. Cheung, and J.D. Zajac, *Androgens and prostate cancer; pathogenesis and deprivation therapy.* Best Practice & Research Clinical Endocrinology & Metabolism, 2013. 27(4): p. 603-616.

161. Choi, E., et al., *Evolution of Androgen Deprivation Therapy (ADT) and Its New Emerging Modalities in Prostate Cancer: An Update for Practicing Urologists, Clinicians and Medical Providers*. Res Rep Urol, 2022. 14: p. 87-108.
162. Fujita, K. and N. Nonomura, *Role of Androgen Receptor in Prostate Cancer: A Review*. World J Mens Health, 2019. 37(3): p. 288-295.
163. Jetten, A.M., *Retinoid-related orphan receptors (RORs): critical roles in development, immunity, circadian rhythm, and cellular metabolism*. Nucl Recept Signal, 2009. 7: p. e003.
164. Giguère, V., *Orphan Nuclear Receptors: From Gene to Function\**. Endocrine Reviews, 1999. 20(5): p. 689-725.
165. Medvedev, A., et al., *Cloning of a cDNA encoding the murine orphan receptor RZR/ROR $\gamma$  and characterization of its response element*. Gene, 1996. 181(1-2): p. 199-206.
166. Carlberg, C., et al., *RZR $\alpha$ , a new family of retinoid-related orphan receptors that function as both monomers and homodimers*. Mol Endocrinol, 1994. 8(6): p. 757-70.
167. Giguère, V., L.D. McBroom, and G. Flock, *Determinants of target gene specificity for ROR alpha 1: monomeric DNA binding by an orphan nuclear receptor*. Mol Cell Biol, 1995. 15(5): p. 2517-26.
168. Hummasti, S. and P. Tontonoz, *Adopting new orphans into the family of metabolic regulators*. Molecular Endocrinology, 2008. 22(8): p. 1743-1753.
169. Solt, L.A., P.R. Griffin, and T.P. Burris, *Ligand regulation of retinoic acid receptor-related orphan receptors: implications for development of novel therapeutics*. Curr Opin Lipidol, 2010. 21(3): p. 204-11.
170. Sun, N., et al., *Molecular Mechanism of Action of ROR $\gamma$ t Agonists and Inverse Agonists: Insights from Molecular Dynamics Simulation*. Molecules, 2018. 23(12).
171. Rutz, S., et al., *Post-translational regulation of ROR $\gamma$ t—A therapeutic target for the modulation of interleukin-17-mediated responses in autoimmune diseases*. Cytokine & growth factor reviews, 2016. 30: p. 1-17.
172. Ermisch, M., B. Firla, and D. Steinhilber, *Protein kinase A activates and phosphorylates ROR $\alpha$ 4 in vitro and takes part in ROR $\alpha$  activation by CaMK-IV*. Biochemical and Biophysical Research Communications, 2011. 408(3): p. 442-446.
173. Singh, A.K., et al., *SUMOylation of ROR- $\gamma$ t inhibits IL-17 expression and inflammation via HDAC2*. Nature Communications, 2018. 9(1): p. 4515.
174. Solt, L.A. and T.P. Burris, *Action of RORs and their ligands in (patho)physiology*. Trends Endocrinol Metab, 2012. 23(12): p. 619-27.
175. Meyer, T., et al., *In vitro and in vivo evidence for orphan nuclear receptor ROR $\alpha$  function in bone metabolism*. Proceedings of the National Academy of Sciences, 2000. 97(16): p. 9197-9202.
176. Steinmayr, M., et al., *Staggerer phenotype in retinoid-related orphan receptor  $\alpha$ -deficient mice*. Proceedings of the National Academy of Sciences, 1998. 95(7): p. 3960-3965.
177. Wang, Y., et al., *Modulation of retinoic acid receptor-related orphan receptor alpha and gamma activity by 7-oxygenated sterol ligands*. J Biol Chem, 2010. 285(7): p. 5013-25.
178. Bitsch, F., et al., *Identification of natural ligands of retinoic acid receptor-related orphan receptor alpha ligand-binding domain expressed in Sf9 cells—a mass spectrometry approach*. Anal Biochem, 2003. 323(1): p. 139-49.
179. Mutemberezi, V., O. Guillemot-Legris, and G.G. Muccioli, *Oxysterols: From cholesterol metabolites to key mediators*. Progress in Lipid Research, 2016. 64: p. 152-169.

180. André, E., et al., *Disruption of retinoid-related orphan receptor beta changes circadian behavior, causes retinal degeneration and leads to vacillans phenotype in mice*. *Embo j*, 1998. 17(14): p. 3867-77.
181. Schaeren-Wiemers, N., et al., *The Expression pattern of the orphan nuclear receptor ROR $\beta$  in the developing and adult rat nervous system suggests a role in the processing of sensory information and in circadian rhythm*. *European Journal of Neuroscience*, 1997. 9(12): p. 2687-2701.
182. Stehlin-Gaon, C., et al., *All-trans retinoic acid is a ligand for the orphan nuclear receptor ROR beta*. *Nat Struct Biol*, 2003. 10(10): p. 820-5.
183. Jetten, A.M., S. Kurebayashi, and E. Ueda, *The ROR nuclear orphan receptor subfamily: critical regulators of multiple biological processes*. *Prog Nucleic Acid Res Mol Biol*, 2001. 69: p. 205-47.
184. He, Y.W., et al., *ROR $\gamma$ t, a novel isoform of an orphan receptor, negatively regulates Fas ligand expression and IL-2 production in T cells*. *Immunity*, 1998. 9(6): p. 797-806.
185. Villey, I., R. de Chasseval, and J.-P. de Villartay, *ROR $\gamma$ T, a thymus-specific isoform of the orphan nuclear receptor ROR $\gamma$  / TOR, is up-regulated by signaling through the pre-T cell receptor and binds to the TEA promoter*. *European Journal of Immunology*, 1999. 29(12): p. 4072-4080.
186. Hirose, T., R.J. Smith, and A.M. Jetten, *ROR- $\gamma$ : the third member of ROR/RZR orphan receptor subfamily that is highly expressed in skeletal muscle*. *Biochemical and biophysical research communications*, 1994. 205(3): p. 1976-1983.
187. Jetten, A.M., H.S. Kang, and Y. Takeda, *Retinoic acid-related orphan receptors  $\alpha$  and  $\gamma$ : key regulators of lipid/glucose metabolism, inflammation, and insulin sensitivity*. *Frontiers in endocrinology*, 2013. 4: p. 1.
188. Ivanov, I.I., et al., *The Orphan Nuclear Receptor ROR $\gamma$ t Directs the Differentiation Program of Proinflammatory IL-17+ T Helper Cells*. *Cell*, 2006. 126(6): p. 1121-1133.
189. Montaldo, E., K. Juelke, and C. Romagnani, *Group 3 innate lymphoid cells (ILC3s): Origin, differentiation, and plasticity in humans and mice*. *European Journal of Immunology*, 2015. 45(8): p. 2171-2182.
190. Steinmetz, O.M., et al., *The Th17-defining transcription factor ROR $\gamma$ t promotes glomerulonephritis*. *J Am Soc Nephrol*, 2011. 22(3): p. 472-83.
191. Yang, X.O., et al., *T helper 17 lineage differentiation is programmed by orphan nuclear receptors ROR $\alpha$  and ROR $\gamma$* . *Immunity*, 2008. 28(1): p. 29-39.
192. Jin, L., et al., *Structural basis for hydroxycholesterols as natural ligands of orphan nuclear receptor ROR $\gamma$* . *Molecular endocrinology*, 2010. 24(5): p. 923-929.
193. Wang, Y., et al., *A second class of nuclear receptors for oxysterols: Regulation of ROR $\alpha$  and ROR $\gamma$  activity by 24S-hydroxycholesterol (cerebrosterol)*. *Biochimica et Biophysica Acta (BBA)-Molecular and Cell Biology of Lipids*, 2010. 1801(8): p. 917-923.
194. Soroosh, P., et al., *Oxysterols are agonist ligands of ROR $\gamma$ t and drive Th17 cell differentiation*. *Proceedings of the National Academy of Sciences*, 2014. 111(33): p. 12163-12168.
195. Safety, I.P.o.C., *Global assessment on the state of the science of endocrine disruptors*. 2002, World Health Organization: Geneva.
196. Kahn, L.G., et al., *Endocrine-disrupting chemicals: implications for human health*. *Lancet Diabetes Endocrinol*, 2020. 8(8): p. 703-718.
197. Georgopapadakou, N.H. and T.J. Walsh, *Antifungal agents: chemotherapeutic targets and immunologic strategies*. *Antimicrob Agents Chemother*, 1996. 40(2): p. 279-91.

198. Saag, M.S., et al., *Treatment of fluconazole-refractory oropharyngeal candidiasis with itraconazole oral solution in HIV-positive patients*. *AIDS Res Hum Retroviruses*, 1999. 15(16): p. 1413-7.
199. Jennings, T.S. and T.C. Hardin, *Treatment of aspergillosis with itraconazole*. *Ann Pharmacother*, 1993. 27(10): p. 1206-11.
200. Keating, G.M., *Posaconazole*. *Drugs*, 2005. 65(11): p. 1553-1567.
201. Heykants, J., et al., *The Clinical Pharmacokinetics of Itraconazole: An Overview*. *Mycoses*, 1989. 32(s1): p. 67-87.
202. Poirier, J.M. and G. Cheymol, *Optimisation of itraconazole therapy using target drug concentrations*. *Clin Pharmacokinet*, 1998. 35(6): p. 461-73.
203. Courtney, R., et al., *Pharmacokinetics, Safety, and Tolerability of Oral Posaconazole Administered in Single and Multiple Doses in Healthy Adults*. *Antimicrobial Agents and Chemotherapy*, 2003. 47(9): p. 2788-2795.
204. Aronson, J.K., *Itraconazole*, in *Meyler's Side Effects of Drugs: The International Encyclopedia of Adverse Drug Reactions and Interactions (Fifteenth Edition)*, J.K. Aronson, Editor. 2006, Elsevier: Amsterdam. p. 1932-1946.
205. Thompson, G.R., III, et al., *Posaconazole-Induced Hypertension Due to Inhibition of 11 $\beta$ -Hydroxylase and 11 $\beta$ -Hydroxysteroid Dehydrogenase 2*. *Journal of the Endocrine Society*, 2019. 3(7): p. 1361-1366.
206. Thompson, G.R., 3rd, et al., *In Vivo 11 $\beta$ -Hydroxysteroid Dehydrogenase Inhibition in Posaconazole-Induced Hypertension and Hypokalemia*. *Antimicrob Agents Chemother*, 2017. 61(8).
207. Boughton, C., et al., *Mineralocorticoid hypertension and hypokalaemia induced by posaconazole*. *Endocrinol Diabetes Metab Case Rep*, 2018. 2018.
208. Barton, K., et al., *Posaconazole-induced hypertension and hypokalemia due to inhibition of the 11 $\beta$ -hydroxylase enzyme*. *Clinical Kidney Journal*, 2018. 11(5): p. 691-693.
209. Hoffmann, W.J., I. McHardy, and G.R. Thompson, 3rd, *Itraconazole induced hypertension and hypokalemia: Mechanistic evaluation*. *Mycoses*, 2018. 61(5): p. 337-339.
210. Wassermann, T., et al., *Refractory hypokalemia from syndrome of apparent mineralocorticoid excess on low-dose posaconazole*. *Antimicrobial Agents and Chemotherapy*, 2018. 62(7): p. 10.1128/aac. 02605-17.
211. Agarwal, N., et al., *Posaconazole-Induced Hypertension Masquerading as Congenital Adrenal Hyperplasia in a Child with Cystic Fibrosis*. *Case Rep Med*, 2020. 2020: p. 8153012.
212. Elder R, L., *Final report on the safety assessment of methylparaben, ethylparaben, propylparaben, and butylparaben*. *J. Am. Coll. Toxicol.*, 1984. 3: p. 147-209.
213. Soni, M.G., et al., *Safety assessment of propyl paraben: a review of the published literature*. *Food and Chemical Toxicology*, 2001. 39(6): p. 513-532.
214. Soni, M.G., I.G. Carabin, and G.A. Burdock, *Safety assessment of esters of p-hydroxybenzoic acid (parabens)*. *Food Chem Toxicol*, 2005. 43(7): p. 985-1015.
215. Darbre, P.D., *Environmental oestrogens, cosmetics and breast cancer*. *Best Pract Res Clin Endocrinol Metab*, 2006. 20(1): p. 121-43.
216. Ishiwatari, S., et al., *Effects of methyl paraben on skin keratinocytes*. *J Appl Toxicol*, 2007. 27(1): p. 1-9.
217. Wei, F., et al., *Parabens as chemicals of emerging concern in the environment and humans: A review*. *Sci Total Environ*, 2021. 778: p. 146150.
218. Jewell, C., et al., *Hydrolysis of a series of parabens by skin microsomes and cytosol from human and minipigs and in whole skin in short-term culture*. *Toxicology and Applied Pharmacology*, 2007. 225(2): p. 221-228.



219. Ozaki, H., et al., *Comparative study of the hydrolytic metabolism of methyl-, ethyl-, propyl-, butyl-, heptyl- and dodecylparaben by microsomes of various rat and human tissues*. *Xenobiotica*, 2013. 43(12): p. 1064-1072.
220. Harville, M.H., R. Voorman, and J.J. Prusakiewicz, *Comparison of Paraben Stability in Human and Rat Skin*. *Drug Metabolism Letters*, 2007. 1(1): p. 17-21.
221. Ye, X., et al., *Parabens as urinary biomarkers of exposure in humans*. *Environ Health Perspect*, 2006. 114(12): p. 1843-6.
222. Abbas, S., et al., *Metabolism of Parabens (4-Hydroxybenzoic Acid Esters) by Hepatic Esterases and UDP-Glucuronosyltransferases in Man*. *Drug Metabolism and Pharmacokinetics*, 2010. 25(6): p. 568-577.
223. Moos, R.K., et al., *Metabolism and elimination of methyl, iso- and n-butyl paraben in human urine after single oral dosage*. *Archives of Toxicology*, 2016. 90(11): p. 2699-2709.
224. Andersen, F.A., *Final amended report on the safety assessment of methylparaben, ethylparaben, propylparaben, isopropylparaben, butylparaben, isobutylparaben, and benzylparaben as used in cosmetic products*. *Int J Toxicol*, 2008. 27(Suppl 4): p. 1-82.
225. Chen, J., et al., *Antiandrogenic properties of parabens and other phenolic containing small molecules in personal care products*. *Toxicol Appl Pharmacol*, 2007. 221(3): p. 278-84.
226. Ding, K., et al., *Side Chains of Parabens Modulate Antiandrogenic Activity: In Vitro and Molecular Docking Studies*. *Environ Sci Technol*, 2017. 51(11): p. 6452-6460.
227. Kolšek, K., et al., *Screening of bisphenol A, triclosan and paraben analogues as modulators of the glucocorticoid and androgen receptor activities*. *Toxicol In Vitro*, 2015. 29(1): p. 8-15.
228. Suzuki, T., et al., *Estrogenic and antiandrogenic activities of 17 benzophenone derivatives used as UV stabilizers and sunscreens*. *Toxicol Appl Pharmacol*, 2005. 203(1): p. 9-17.
229. Kang, K.S., et al., *Decreased sperm number and motile activity on the F1 offspring maternally exposed to butyl p-hydroxybenzoic acid (butyl paraben)*. *J Vet Med Sci*, 2002. 64(3): p. 227-35.
230. Oishi, S., *Effects of butylparaben on the male reproductive system in rats*. *Toxicol Ind Health*, 2001. 17(1): p. 31-9.
231. Oishi, S., *Effects of propyl paraben on the male reproductive system*. *Food and Chemical Toxicology*, 2002. 40(12): p. 1807-1813.
232. EC, R., *No 1004/2014 amending Annex V to Regulation (EC) No 1223/2009 of the European Parliament and the Council on cosmetic products.(2014)*. Official Journal of the European Union, 2014.
233. Lester, C., et al., *Metabolism and plasma protein binding of 16 straight- and branched-chain parabens in in vitro liver and skin models*. *Toxicology in Vitro*, 2021. 72: p. 105051.
234. Xue, J., W. Liu, and K. Kannan, *Bisphenols, Benzophenones, and Bisphenol A Diglycidyl Ethers in Textiles and Infant Clothing*. *Environmental Science & Technology*, 2017. 51(9): p. 5279-5286.
235. Asimakopoulos, A.G., M. Elangovan, and K. Kannan, *Migration of Parabens, Bisphenols, Benzophenone-Type UV Filters, Triclosan, and Triclocarban from Teethers and Its Implications for Infant Exposure*. *Environmental Science & Technology*, 2016. 50(24): p. 13539-13547.
236. Bens, G., *Sunscreens*. *Adv Exp Med Biol*, 2014. 810: p. 429-63.
237. Rodríguez-Bernaldo de Quirós, A., et al., *Migration of Photoinitiators by Gas Phase into Dry Foods*. *Journal of Agricultural and Food Chemistry*, 2009. 57(21): p. 10211-10215.

238. EC, R., *Regulation (EC) no 1223/2009 of the European Parliament on cosmetic products annex VI list of UV filters allowed in cosmetic products*. 2009.
239. FDA, *Sunscreen Drug Products for Over-the-Counter Human Use. A proposed rule by the Food and Drug Administration on 02/26/2019*. Vol. 84. 2019: Federal Register
240. Hayden, C.G.J., M.S. Roberts, and H.A.E. Benson, *Systemic absorption of sunscreen after topical application*. *The Lancet*, 1997. 350(9081): p. 863-864.
241. Janjua, N.R., et al., *Systemic Absorption of the Sunscreens Benzophenone-3, Octyl-Methoxycinnamate, and 3-(4-Methyl-Benzylidene) Camphor After Whole-Body Topical Application and Reproductive Hormone Levels in Humans*. *Journal of Investigative Dermatology*, 2004. 123(1): p. 57-61.
242. Mao, J.F., et al., *Assessment of human exposure to benzophenone-type UV filters: A review*. *Environment International*, 2022. 167: p. 107405.
243. Wang, L. and K. Kannan, *Characteristic Profiles of Benzophenone-3 and its Derivatives in Urine of Children and Adults from the United States and China*. *Environmental Science & Technology*, 2013. 47(21): p. 12532-12538.
244. Kunz, P.Y. and K. Fent, *Multiple hormonal activities of UV filters and comparison of in vivo and in vitro estrogenic activity of ethyl-4-aminobenzoate in fish*. *Aquat Toxicol*, 2006. 79(4): p. 305-24.
245. Ma, R., et al., *UV Filters with Antagonistic Action at Androgen Receptors in the MDA-kb2 Cell Transcriptional-Activation Assay*. *Toxicological Sciences*, 2003. 74(1): p. 43-50.
246. Molina-Molina, J.-M., et al., *Profiling of benzophenone derivatives using fish and human estrogen receptor-specific in vitro bioassays*. *Toxicology and Applied Pharmacology*, 2008. 232(3): p. 384-395.
247. Nashev, L.G., et al., *The UV-filter benzophenone-1 inhibits 17beta-hydroxysteroid dehydrogenase type 3: Virtual screening as a strategy to identify potential endocrine disrupting chemicals*. *Biochem Pharmacol*, 2010. 79(8): p. 1189-99.
248. Schreurs, R., et al., *Estrogenic activity of UV filters determined by an in vitro reporter gene assay and an in vivo transgenic zebrafish assay*. *Archives of Toxicology*, 2002. 76(5): p. 257-261.
249. Watanabe, Y., et al., *Metabolism of UV-filter benzophenone-3 by rat and human liver microsomes and its effect on endocrine-disrupting activity*. *Toxicol Appl Pharmacol*, 2015. 282(2): p. 119-28.
250. Schlecht, C., et al., *Effects of estradiol, benzophenone-2 and benzophenone-3 on the expression pattern of the estrogen receptors (ER) alpha and beta, the estrogen receptor-related receptor 1 (ERR1) and the aryl hydrocarbon receptor (AhR) in adult ovariectomized rats*. *Toxicology*, 2004. 205(1): p. 123-130.
251. Schlumpf, M., et al., *In vitro and in vivo estrogenicity of UV screens*. *Environ Health Perspect*, 2001. 109(3): p. 239-44.
252. Yamasaki, K., et al., *Immature rat uterotrophic assay of 18 chemicals and Hershberger assay of 30 chemicals*. *Toxicology*, 2003. 183(1-3): p. 93-115.
253. Huang, Y., et al., *Organic UV filter exposure and pubertal development: A prospective follow-up study of urban Chinese adolescents*. *Environment International*, 2020. 143: p. 105961.
254. Scinicariello, F. and M.C. Buser, *Serum Testosterone Concentrations and Urinary Bisphenol A, Benzophenone-3, Triclosan, and Paraben Levels in Male and Female Children and Adolescents: NHANES 2011-2012*. *Environ Health Perspect*, 2016. 124(12): p. 1898-1904.
255. Buck Louis, G.M., et al., *Urinary concentrations of benzophenone-type ultraviolet light filters and semen quality*. *Fertil Steril*, 2015. 104(4): p. 989-996.

256. Persson, B., et al. *The Short-Chain Dehydrogenase/Reductase (SDR) Nomenclature Initiative*. in *VII European Symposium of The Protein Society*. 2007.
257. Odermatt, A., et al., *The N-terminal anchor sequences of 11 $\beta$ -hydroxysteroid dehydrogenases determine their orientation in the endoplasmic reticulum membrane*. *J Biol Chem*, 1999. 274(40): p. 28762-70.
258. Atanasov, A.G., et al., *Direct protein-protein interaction of 11 $\beta$ -hydroxysteroid dehydrogenase type 1 and hexose-6-phosphate dehydrogenase in the endoplasmic reticulum lumen*. *Biochimica et Biophysica Acta (BBA) - Molecular Cell Research*, 2008. 1783(8): p. 1536-1543.
259. Zhang, Y.L., et al., *H6PDH interacts directly with 11 $\beta$ -HSD1: implications for determining the directionality of glucocorticoid catalysis*. *Arch Biochem Biophys*, 2009. 483(1): p. 45-54.
260. Atanasov, A.G., et al., *Hexose-6-phosphate dehydrogenase determines the reaction direction of 11 $\beta$ -hydroxysteroid dehydrogenase type 1 as an oxoreductase*. *FEBS Letters*, 2004. 571(1-3): p. 129-133.
261. Draper, N., et al., *Mutations in the genes encoding 11 $\beta$ -hydroxysteroid dehydrogenase type 1 and hexose-6-phosphate dehydrogenase interact to cause cortisone reductase deficiency*. *Nat Genet*, 2003. 34(4): p. 434-9.
262. Bánhegyi, G., et al., *Cooperativity between 11 $\beta$ -hydroxysteroid dehydrogenase type 1 and hexose-6-phosphate dehydrogenase in the lumen of the endoplasmic reticulum*. *J Biol Chem*, 2004. 279(26): p. 27017-21.
263. Beck, K.R., et al., *11 $\beta$ -Hydroxysteroid dehydrogenases control access of 7 $\beta$ ,27-dihydroxycholesterol to retinoid-related orphan receptor  $\gamma$* . *J Lipid Res*, 2019. 60(9): p. 1535-1546.
264. Beck, K.R., et al., *Enzymatic interconversion of the oxysterols 7 $\beta$ ,25-dihydroxycholesterol and 7-keto,25-hydroxycholesterol by 11 $\beta$ -hydroxysteroid dehydrogenase type 1 and 2*. *J Steroid Biochem Mol Biol*, 2019. 190: p. 19-28.
265. Schweizer, R.A., et al., *Rapid hepatic metabolism of 7-ketocholesterol by 11 $\beta$ -hydroxysteroid dehydrogenase type 1: species-specific differences between the rat, human, and hamster enzyme*. *J Biol Chem*, 2004. 279(18): p. 18415-24.
266. Odermatt, A., et al., *Hepatic reduction of the secondary bile acid 7-oxolithocholic acid is mediated by 11 $\beta$ -hydroxysteroid dehydrogenase 1*. *Biochem J*, 2011. 436(3): p. 621-9.
267. Hult, M., et al., *Human and rodent type 1 11 $\beta$ -hydroxysteroid dehydrogenases are 7 $\beta$ -hydroxycholesterol dehydrogenases involved in oxysterol metabolism*. *Cellular and Molecular Life Sciences CMLS*, 2004. 61(7): p. 992-999.
268. Zhou, H.-Y., et al., *The metabolism of steroids, toxins and drugs by 11 $\beta$ -hydroxysteroid dehydrogenase 1*. *Toxicology*, 2012. 292(1): p. 1-12.
269. Whorwood, C.B., et al., *Increased glucocorticoid receptor expression in human skeletal muscle cells may contribute to the pathogenesis of the metabolic syndrome*. *Diabetes*, 2002. 51(4): p. 1066-75.
270. Wyrwoll, C.S., M.C. Holmes, and J.R. Seckl, *11 $\beta$ -hydroxysteroid dehydrogenases and the brain: from zero to hero, a decade of progress*. *Front Neuroendocrinol*, 2011. 32(3): p. 265-86.
271. Bujalska, I.J., S. Kumar, and P.M. Stewart, *Does central obesity reflect "Cushing's disease of the omentum"?* *Lancet*, 1997. 349(9060): p. 1210-3.
272. Rask, E., et al., *Tissue-specific dysregulation of cortisol metabolism in human obesity*. *J Clin Endocrinol Metab*, 2001. 86(3): p. 1418-21.
273. Paulmyer-Lacroix, O., et al., *Expression of the mRNA coding for 11 $\beta$ -hydroxysteroid dehydrogenase type 1 in adipose tissue from obese patients: an in situ hybridization study*. *J Clin Endocrinol Metab*, 2002. 87(6): p. 2701-5.

274. Csernansky, J.G., et al., *Plasma cortisol and progression of dementia in subjects with Alzheimer-type dementia*. Am J Psychiatry, 2006. 163(12): p. 2164-9.
275. Peskind, E.R., et al., *Increased CSF cortisol in AD is a function of APOE genotype*. Neurology, 2001. 56(8): p. 1094-8.
276. Gregory, S., et al., *11 $\beta$ -hydroxysteroid dehydrogenase type 1 inhibitor use in human disease-a systematic review and narrative synthesis*. Metabolism, 2020. 108: p. 154246.
277. Chapman, K., M. Holmes, and J. Seckl, *11 $\beta$ -hydroxysteroid dehydrogenases: intracellular gate-keepers of tissue glucocorticoid action*. Physiol Rev, 2013. 93(3): p. 1139-206.
278. Arriza, J.L., et al., *Cloning of human mineralocorticoid receptor complementary DNA: structural and functional kinship with the glucocorticoid receptor*. Science, 1987. 237(4812): p. 268-75.
279. Hollenberg, S.M., et al., *Primary structure and expression of a functional human glucocorticoid receptor cDNA*. Nature, 1985. 318(6047): p. 635-41.
280. Benediktsson, R., et al., *Placental 11 beta-hydroxysteroid dehydrogenase: a key regulator of fetal glucocorticoid exposure*. Clin Endocrinol (Oxf), 1997. 46(2): p. 161-6.
281. Pearson Murphy, B.E., *Ontogeny of cortisol-cortisone interconversion in human tissues: A role for cortisone in human fetal development*. Journal of Steroid Biochemistry, 1981. 14(9): p. 811-817.
282. Stewart, P.M., C.B. Whorwood, and J.I. Mason, *Type 2 11 beta-hydroxysteroid dehydrogenase in foetal and adult life*. J Steroid Biochem Mol Biol, 1995. 55(5-6): p. 465-71.
283. Seckl, J.R., et al., *Placental 11 beta-hydroxysteroid dehydrogenase and the programming of hypertension*. J Steroid Biochem Mol Biol, 1995. 55(5-6): p. 447-55.
284. Rääkkönen, K., et al., *Maternal Licorice Consumption During Pregnancy and Pubertal, Cognitive, and Psychiatric Outcomes in Children*. American Journal of Epidemiology, 2017. 185(5): p. 317-328.
285. Farese, R.V., Jr., et al., *Licorice-induced hypermineralocorticoidism*. N Engl J Med, 1991. 325(17): p. 1223-7.
286. Stewart, P., et al., *MINERALOCORTICOID ACTIVITY OF LIQUORICE: 11-BETA-HYDROXYSTEROID DEHYDROGENASE DEFICIENCY COMES OF AGE*. The Lancet, 1987. 330(8563): p. 821-824.
287. Beck, K.R., et al., *Inhibition of 11 $\beta$ -hydroxysteroid dehydrogenase 2 by the fungicides itraconazole and posaconazole*. Biochemical Pharmacology, 2017. 130: p. 93-103.
288. Beck, K.R., et al., *Molecular mechanisms of posaconazole- and itraconazole-induced pseudohyperaldosteronism and assessment of other systemically used azole antifungals*. J Steroid Biochem Mol Biol, 2020. 199: p. 105605.
289. Brown, R.W., et al., *Purification of 11 beta-hydroxysteroid dehydrogenase type 2 from human placenta utilizing a novel affinity labelling technique*. Biochem J, 1996. 313 ( Pt 3)(Pt 3): p. 997-1005.
290. Thonghin, N., et al., *Cryo-electron microscopy of membrane proteins*. Methods, 2018. 147: p. 176-186.
291. von Holst, D., *The Concept of Stress and Its Relevance for Animal Behavior*, in *Advances in the Study of Behavior*, A.P. Møller, M. Milinski, and P.J.B. Slater, Editors. 1998, Academic Press. p. 1-131.
292. Tsachaki, M., et al., *Absence of 11-keto reduction of cortisone and 11-ketotestosterone in the model organism zebrafish*. Journal of Endocrinology, 2017. 232(2): p. 323-335.
293. Tokarz, J., et al., *Discovery of a novel enzyme mediating glucocorticoid catabolism in fish: 20 $\beta$ -hydroxysteroid dehydrogenase type 2*. Molecular and Cellular Endocrinology, 2012. 349: p. 202-213.

294. Tokarz, J., et al., *Zebrafish and steroids: what do we know and what do we need to know?* Journal of Steroid Biochemistry and Molecular Biology, 2013. 137: p. 165-173.
295. Russell, W.M.S., R.L. Burch, and C.W. Hume, *The principles of humane experimental technique*. Vol. 238. 1959: Methuen London.
296. EP, *European Parliament and Council Directive 2010/63/EU of the European Parliament and of the Council of 22 September 2010 on the Protection of Animals Used for Scientific Purposes*. 2010.
297. Horton, R., *Dihydrotestosterone is a peripheral paracrine hormone*. J Androl, 1992. 13(1): p. 23-7.
298. Chetyrkin, S.V., et al., *Further characterization of human microsomal 3alpha-hydroxysteroid dehydrogenase*. Arch Biochem Biophys, 2001. 386(1): p. 1-10.
299. Huang, X.F. and V. Luu-The, *Molecular characterization of a first human 3(alpha-->beta)-hydroxysteroid epimerase*. J Biol Chem, 2000. 275(38): p. 29452-7.
300. He, X.-Y., et al., *Type 10 17beta-hydroxysteroid dehydrogenase catalyzing the oxidation of steroid modulators of gamma-aminobutyric acid type A receptors*. Molecular and Cellular Endocrinology, 2005. 229(1): p. 111-117.
301. He, X.-Y., et al., *Function of human brain short chain L-3-hydroxyacyl coenzyme A dehydrogenase in androgen metabolism*. Biochimica et Biophysica Acta (BBA) - Molecular and Cell Biology of Lipids, 2000. 1484(2): p. 267-277.
302. Du Yan, S., et al., *An intracellular protein that binds amyloid-beta peptide and mediates neurotoxicity in Alzheimer's disease*. Nature, 1997. 389(6652): p. 689-695.
303. Chetyrkin, S.V., et al., *Characterization of a novel type of human microsomal 3alpha-hydroxysteroid dehydrogenase: unique tissue distribution and catalytic properties*. J Biol Chem, 2001. 276(25): p. 22278-86.
304. Markova, N.G., et al., *Expression pattern and biochemical characteristics of a major epidermal retinol dehydrogenase*. Mol Genet Metab, 2003. 78(2): p. 119-35.
305. Soref, C.M., et al., *Characterization of a Novel Airway Epithelial Cell-specific Short Chain Alcohol Dehydrogenase/Reductase Gene Whose Expression Is Up-regulated by Retinoids and Is Involved in the Metabolism of Retinol\**. Journal of Biological Chemistry, 2001. 276(26): p. 24194-24202.
306. Gamble, M.V., et al., *Biochemical properties, tissue expression, and gene structure of a short chain dehydrogenase/ reductase able to catalyze cis-retinol oxidation*. J Lipid Res, 1999. 40(12): p. 2279-92.
307. Lidén, M., et al., *Biochemical Defects in 11-cis-Retinol Dehydrogenase Mutants Associated with Fundus Albipunctatus\**. Journal of Biological Chemistry, 2001. 276(52): p. 49251-49257.
308. Mertz, J.R., et al., *Identification and Characterization of a Stereospecific Human Enzyme That Catalyzes 9-cis-Retinol Oxidation: A POSSIBLE ROLE IN 9-cis-RETINOIC ACID FORMATION\**. Journal of Biological Chemistry, 1997. 272(18): p. 11744-11749.
309. Simon, A., et al., *The retinal pigment epithelial-specific 11-cis retinol dehydrogenase belongs to the family of short chain alcohol dehydrogenases*. J Biol Chem, 1995. 270(3): p. 1107-12.
310. Wang, J., et al., *Activity of human 11-cis-retinol dehydrogenase (Rdh5) with steroids and retinoids and expression of its mRNA in extra-ocular human tissue*. Biochem J, 1999. 338 ( Pt 1)(Pt 1): p. 23-7.
311. Gough, W.H., et al., *cDNA cloning and characterization of a new human microsomal NAD+-dependent dehydrogenase that oxidizes all-trans-retinol and 3alpha-hydroxysteroids*. J Biol Chem, 1998. 273(31): p. 19778-85.

312. Jurukovski, V., et al., *Cloning and characterization of retinol dehydrogenase transcripts expressed in human epidermal keratinocytes*. Mol Genet Metab, 1999. 67(1): p. 62-73.
313. Lapshina, E.A., et al., *Differential recognition of the free versus bound retinol by human microsomal retinol/sterol dehydrogenases: characterization of the holo-CRBP dehydrogenase activity of RoDH-4*. Biochemistry, 2003. 42(3): p. 776-84.
314. Mustieles, V., et al., *Benzophenone-3: Comprehensive review of the toxicological and human evidence with meta-analysis of human biomonitoring studies*. Environ Int, 2023. 173: p. 107739.
315. Berger, E., et al., *Effect-directed identification of endocrine disruptors in plastic baby teethers*. Journal of Applied Toxicology, 2015. 35(11): p. 1254-1261.
316. Golden, R., J. Gandy, and G. Vollmer, *A Review of the Endocrine Activity of Parabens and Implications for Potential Risks to Human Health*. Critical Reviews in Toxicology, 2005. 35(5): p. 435-458.
317. Darbre, P.D. and P.W. Harvey, *Paraben esters: review of recent studies of endocrine toxicity, absorption, esterase and human exposure, and discussion of potential human health risks*. J Appl Toxicol, 2008. 28(5): p. 561-78.
318. Harvey, P.W. and P. Darbre, *Endocrine disruptors and human health: could oestrogenic chemicals in body care cosmetics adversely affect breast cancer incidence in women?* J Appl Toxicol, 2004. 24(3): p. 167-76.
319. Janjua, N.R., et al., *Sunscreens in human plasma and urine after repeated whole-body topical application*. J Eur Acad Dermatol Venereol, 2008. 22(4): p. 456-61.
320. Wang, M., et al., *Benzophenone-1 and -2 UV-filters potently inhibit human, rat, and mouse gonadal 3 $\beta$ -hydroxysteroid dehydrogenases: Structure-activity relationship and in silico docking analysis*. The Journal of Steroid Biochemistry and Molecular Biology, 2023. 230: p. 106279.
321. Jeon, H.-K., et al., *Toxicokinetics and metabolisms of benzophenone-type UV filters in rats*. Toxicology, 2008. 248(2): p. 89-95.
322. Okereke, C.S., et al., *Metabolism of benzophenone-3 in rats*. Drug Metab Dispos, 1993. 21(5): p. 788-91.
323. Sarveiya, V., S. Risk, and H.A.E. Benson, *Liquid chromatographic assay for common sunscreen agents: application to in vivo assessment of skin penetration and systemic absorption in human volunteers*. Journal of Chromatography B, 2004. 803(2): p. 225-231.
324. Molins-Delgado, D., et al., *Determination of UV filters in human breast milk using turbulent flow chromatography and babies' daily intake estimation*. Environ Res, 2018. 161: p. 532-539.
325. Chen, M., et al., *The Application of a Physiologically Based Toxicokinetic Model in Health Risk Assessment*. Toxics, 2023. 11(10).
326. Ye, X., et al., *Quantification of urinary conjugates of bisphenol A, 2,5-dichlorophenol, and 2-hydroxy-4-methoxybenzophenone in humans by online solid phase extraction-high performance liquid chromatography-tandem mass spectrometry*. Anal Bioanal Chem, 2005. 383(4): p. 638-44.
327. OECD, *Test No. 456: H295R Steroidogenesis Assay*. 2023.
328. Strajhar, P., et al., *Steroid profiling in H295R cells to identify chemicals potentially disrupting the production of adrenal steroids*. Toxicology, 2017. 381: p. 51-63.
329. Xing, Y., et al., *The effects of ACTH on steroid metabolomic profiles in human adrenal cells*. Journal of Endocrinology, 2011. 209(3): p. 327-335.
330. Engeli, R.T., et al., *Currently available murine Leydig cell lines can be applied to study early steps of steroidogenesis but not testosterone synthesis*. Heliyon, 2018. 4(2): p. e00527.

331. Jäger, M.C., et al., *Extended steroid profiling in H295R cells provides deeper insight into chemical-induced disturbances of steroidogenesis: Exemplified by prochloraz and anabolic steroids*. Mol Cell Endocrinol, 2023. 570: p. 111929.
332. Mei, Z., et al., *Management of prostate cancer by targeting 3 $\beta$ HSD1 after enzalutamide and abiraterone treatment*. Cell Rep Med, 2022. 3(5): p. 100608.
333. Knuutila, M., et al., *Antiandrogens Reduce Intratumoral Androgen Concentrations and Induce Androgen Receptor Expression in Castration-Resistant Prostate Cancer Xenografts*. Am J Pathol, 2018. 188(1): p. 216-228.
334. Knuutila, M., et al., *Castration induces up-regulation of intratumoral androgen biosynthesis and androgen receptor expression in an orthotopic VCaP human prostate cancer xenograft model*. Am J Pathol, 2014. 184(8): p. 2163-73.
335. Cheng, J., et al., *The transcriptomics of de novo androgen biosynthesis in prostate cancer cells following androgen reduction*. Cancer Biol Ther, 2010. 9(12): p. 1033-42.
336. Ishizaki, F., et al., *Androgen deprivation promotes intratumoral synthesis of dihydrotestosterone from androgen metabolites in prostate cancer*. Sci Rep, 2013. 3: p. 1528.
337. Fiandalo, M.V., et al., *Inhibition of dihydrotestosterone synthesis in prostate cancer by combined frontdoor and backdoor pathway blockade*. Oncotarget, 2018. 9(13): p. 11227-11242.
338. Muthusamy, S., et al., *Estrogen receptor  $\beta$  and 17 $\beta$ -hydroxysteroid dehydrogenase type 6, a growth regulatory pathway that is lost in prostate cancer*. Proc Natl Acad Sci U S A, 2011. 108(50): p. 20090-4.
339. Timby, E., et al., *Pharmacokinetic and behavioral effects of allopregnanolone in healthy women*. Psychopharmacology, 2006. 186(3): p. 414-424.
340. Lambert, J.J., et al., *Neurosteroids and GABAA receptor function*. Trends in pharmacological sciences, 1995. 16(9): p. 295-303.
341. Reddy, D.S. and K. Jian, *The testosterone-derived neurosteroid androstanediol is a positive allosteric modulator of GABAA receptors*. J Pharmacol Exp Ther, 2010. 334(3): p. 1031-41.
342. Twyman, R. and R. Macdonald, *Neurosteroid regulation of GABAA receptor single-channel kinetic properties of mouse spinal cord neurons in culture*. The Journal of physiology, 1992. 456(1): p. 215-245.
343. Majewska, M.D., et al., *Steroid hormone metabolites are barbiturate-like modulators of the GABA receptor*. Science, 1986. 232(4753): p. 1004-1007.
344. Kaminski, R.M., et al., *Anticonvulsant activity of androsterone and etiocholanolone*. Epilepsia, 2005. 46(6): p. 819-827.
345. Frye, C.A. and L.E. Bayon, *Seizure Activity Is Increased in Endocrine States Characterized by Decline in Endogenous Levels of the Neurosteroid 3 $\alpha$ ,5 $\alpha$ -THP*. Neuroendocrinology, 1998. 68(4): p. 272-280.
346. Reddy, D.S., *Role of anticonvulsant and antiepileptogenic neurosteroids in the pathophysiology and treatment of epilepsy*. Front Endocrinol (Lausanne), 2011. 2: p. 38.
347. Nohria, V., et al., *Ganaxolone in progress report on new antiepileptic drugs: a summary of the Tenth Eilat Conference (EILAT X)*. Epilepsy Res, 2010. 92: p. 104-107.
348. Frye, C.A., K. Edinger, and K. Sumida, *Androgen Administration to Aged Male Mice Increases Anti-Anxiety Behavior and Enhances Cognitive Performance*. Neuropsychopharmacology, 2008. 33(5): p. 1049-1061.
349. Finn, D.A., et al., *Neurosteroid consumption has anxiolytic effects in mice*. Pharmacol Biochem Behav, 2003. 76(3-4): p. 451-62.

350. Uzunova, V., et al., *Increase in the cerebrospinal fluid content of neurosteroids in patients with unipolar major depression who are receiving fluoxetine or fluvoxamine*. Proceedings of the National Academy of Sciences, 1998. 95(6): p. 3239-3244.
351. Rasmusson, A.M., et al., *Decreased Cerebrospinal Fluid Allopregnanolone Levels in Women with Posttraumatic Stress Disorder*. Biological Psychiatry, 2006. 60(7): p. 704-713.
352. Rasmusson, A.M., et al., *Relationships between cerebrospinal fluid GABAergic neurosteroid levels and symptom severity in men with PTSD*. Psychoneuroendocrinology, 2019. 102: p. 95-104.
353. Uzunova, V., et al., *Chronic antidepressants reverse cerebrocortical allopregnanolone decline in the olfactory-bulbectomized rat*. European Journal of Pharmacology, 2004. 486(1): p. 31-34.
354. Li, X., et al., *Structural studies unravel the active conformation of apo ROR $\gamma$ t nuclear receptor and a common inverse agonism of two diverse classes of ROR $\gamma$ t inhibitors*. J Biol Chem, 2017. 292(28): p. 11618-11630.
355. Eberl, G. and D.R. Littman, *Thymic origin of intestinal  $\alpha\beta$  T cells revealed by fate mapping of ROR $\gamma$ t+ cells*. Science, 2004. 305(5681): p. 248-251.
356. Sun, Z., et al., *Requirement for ROR $\gamma$  in thymocyte survival and lymphoid organ development*. Science, 2000. 288(5475): p. 2369-73.
357. Jetten, A.M. and D.N. Cook, *(Inverse) Agonists of Retinoic Acid-Related Orphan Receptor  $\gamma$ : Regulation of Immune Responses, Inflammation, and Autoimmune Disease*. Annu Rev Pharmacol Toxicol, 2020. 60: p. 371-390.
358. Miossec, P. and J.K. Kolls, *Targeting IL-17 and TH17 cells in chronic inflammation*. Nat Rev Drug Discov, 2012. 11(10): p. 763-76.
359. Guendisch, U., et al., *Pharmacological inhibition of ROR $\gamma$ t suppresses the Th17 pathway and alleviates arthritis in vivo*. PLoS One, 2017. 12(11): p. e0188391.
360. Chang, M.R., et al., *Pharmacologic repression of retinoic acid receptor-related orphan nuclear receptor  $\gamma$  is therapeutic in the collagen-induced arthritis experimental model*. Arthritis Rheumatol, 2014. 66(3): p. 579-88.
361. Khan, P.M., et al., *Small molecule amides as potent ROR- $\gamma$  selective modulators*. Bioorganic & medicinal chemistry letters, 2013. 23(2): p. 532-536.
362. Smith, S.H., et al., *Development of a Topical Treatment for Psoriasis Targeting ROR $\gamma$ : From Bench to Skin*. PLoS One, 2016. 11(2): p. e0147979.
363. Xiao, S., et al., *Small-molecule ROR $\gamma$ t antagonists inhibit T helper 17 cell transcriptional network by divergent mechanisms*. Immunity, 2014. 40(4): p. 477-89.
364. Xu, T., et al., *Ursolic acid suppresses interleukin-17 (IL-17) production by selectively antagonizing the function of ROR $\gamma$  t protein*. J Biol Chem, 2011. 286(26): p. 22707-10.
365. Xue, X., et al., *Pharmacologic modulation of ROR $\gamma$ t translates to efficacy in preclinical and translational models of psoriasis and inflammatory arthritis*. Sci Rep, 2016. 6: p. 37977.
366. Karaś, K., et al., *The cardenolides strophanthidin, digoxigenin and dihydroouabain act as activators of the human ROR $\gamma$ /ROR $\gamma$ T receptors*. Toxicol Lett, 2018. 295: p. 314-324.
367. Chang, M.R., et al., *Synthetic ROR $\gamma$ t Agonists Enhance Protective Immunity*. ACS Chem Biol, 2016. 11(4): p. 1012-8.
368. Kojima, H., et al., *Isoflavones enhance interleukin-17 gene expression via retinoic acid receptor-related orphan receptors  $\alpha$  and  $\gamma$* . Toxicology, 2015. 329: p. 32-9.
369. Wang, Y., et al., *Identification of SR1078, a synthetic agonist for the orphan nuclear receptors ROR $\alpha$  and ROR $\gamma$* . ACS Chem Biol, 2010. 5(11): p. 1029-34.



370. Pastwińska, J., et al., *ROR $\gamma$ T agonists as immune modulators in anticancer therapy*. *Biochimica et Biophysica Acta (BBA) - Reviews on Cancer*, 2023. 1878(6): p. 189021.
371. PubChem. *PubChem Bioassay Record for AID 1159523*. 2015 2022 Jan. 23 [cited 2024 02.07.].
372. Nowak, K., et al., *Parabens and their effects on the endocrine system*. *Mol Cell Endocrinol*, 2018. 474: p. 238-251.
373. Wang, J., et al., *Recent Advances on Endocrine Disrupting Effects of UV Filters*. *Int J Environ Res Public Health*, 2016. 13(8).
374. Huang, M., et al., *ROR $\gamma$  Structural Plasticity and Druggability*. *Int J Mol Sci*, 2020. 21(15).
375. Carcache, D.A., et al., *Optimizing a Weakly Binding Fragment into a Potent ROR $\gamma$ t Inverse Agonist with Efficacy in an in Vivo Inflammation Model*. *Journal of Medicinal Chemistry*, 2018. 61(15): p. 6724-6735.
376. Benson, H.A.E., et al., *Influence of anatomical site and topical formulation on skin penetration of sunscreens*. *Therapeutics and Clinical Risk Management*, 2005. 1(3): p. 209-218.
377. Fernandez, C., et al., *Benzophenone-3: rapid prediction and evaluation using non-invasive methods of in vivo human penetration*. *Journal of pharmaceutical and biomedical analysis*, 2002. 28(1): p. 57-63.
378. Bedoya, S.K., et al., *Isolation and th17 differentiation of naïve CD4 T lymphocytes*. *J Vis Exp*, 2013(79): p. e50765.
379. Rioux, G., et al., *Development of a 3D psoriatic skin model optimized for infiltration of IL-17A producing T cells: Focus on the crosstalk between T cells and psoriatic keratinocytes*. *Acta Biomaterialia*, 2021. 136: p. 210-222.
380. Gangwar, R.S., J.E. Gudjonsson, and N.L. Ward, *Mouse Models of Psoriasis: A Comprehensive Review*. *J Invest Dermatol*, 2022. 142(3 Pt B): p. 884-897.
381. Sandberg, D.E. and M. Gardner, *Differences/Disorders of Sex Development: Medical Conditions at the Intersection of Sex and Gender*. *Annu Rev Clin Psychol*, 2022. 18: p. 201-231.
382. Sinclair, A.H., et al., *A gene from the human sex-determining region encodes a protein with homology to a conserved DNA-binding motif*. *Nature*, 1990. 346(6281): p. 240-244.
383. Warr, N. and A. Greenfield, *The molecular and cellular basis of gonadal sex reversal in mice and humans*. *Wiley Interdiscip Rev Dev Biol*, 2012. 1(4): p. 559-77.
384. Wilson, J.D., F.W. George, and J.E. Griffin, *The hormonal control of sexual development*. *Science*, 1981. 211(4488): p. 1278-84.
385. Engeli, R.T., et al., *Biochemical analyses and molecular modeling explain the functional loss of 17 $\beta$ -hydroxysteroid dehydrogenase 3 mutant G133R in three Tunisian patients with 46, XY Disorders of Sex Development*. *J Steroid Biochem Mol Biol*, 2016. 155(Pt A): p. 147-54.
386. Mindnich, R., et al., *Androgen metabolism via 17 $\beta$ -hydroxysteroid dehydrogenase type 3 in mammalian and non-mammalian vertebrates: comparison of the human and the zebrafish enzyme*. *Journal of Molecular Endocrinology*, 2005. 35(2): p. 305-316.
387. Andersson, S., D.W. Russell, and J.D. Wilson, *17 $\beta$ -Hydroxysteroid dehydrogenase 3 deficiency*. *Trends in Endocrinology and Metabolism*, 1996. 7(4): p. 121-126.
388. George, M.M., et al., *The clinical and molecular heterogeneity of 17 $\beta$ HSD-3 enzyme deficiency*. *Hormone Research in Paediatrics*, 2010. 74(4): p. 229-240.
389. Lee, Y.S., et al., *Phenotypic variability in 17 $\beta$ -hydroxysteroid dehydrogenase-3 deficiency and diagnostic pitfalls*. *Clinical Endocrinology*, 2007. 67(1): p. 20-28.

390. Moghrabi, N., et al., *Deleterious missense mutations and silent polymorphism in the human 17beta-hydroxysteroid dehydrogenase 3 gene (HSD17B3)*. J Clin Endocrinol Metab, 1998. 83(8): p. 2855-60.
391. Ben Rhouma, B., et al., *A Novel Nonsense Mutation in HSD17B3 Gene in a Tunisian Patient with Sexual Ambiguity*. The Journal of Sexual Medicine, 2013. 10(10): p. 2586-2589.
392. Gonçalves, C.I., et al., *Disorder of Sex Development Due to 17-Beta-Hydroxysteroid Dehydrogenase Type 3 Deficiency: A Case Report and Review of 70 Different HSD17B3 Mutations Reported in 239 Patients*. International Journal of Molecular Sciences, 2022. 23(17): p. 10026.
393. Yazawa, T., et al., *Evaluation of 17β-hydroxysteroid dehydrogenase activity using androgen receptor-mediated transactivation*. The Journal of Steroid Biochemistry and Molecular Biology, 2020. 196: p. 105493.
394. Boettcher, C. and C.E. Flück, *Rare forms of genetic steroidogenic defects affecting the gonads and adrenals*. Best Practice & Research Clinical Endocrinology & Metabolism, 2022. 36(1): p. 101593.
395. Yuan, S.M., et al., *Phenotypic and molecular characteristics of androgen insensitivity syndrome patients*. Asian J Androl, 2018. 20(5): p. 473-478.
396. Rösler, A., S. Silverstein, and D. Abeliovich, *A (R80Q) mutation in 17 beta-hydroxysteroid dehydrogenase type 3 gene among Arabs of Israel is associated with pseudohermaphroditism in males and normal asymptomatic females*. J Clin Endocrinol Metab, 1996. 81(5): p. 1827-31.
397. Ben Rhouma, B., et al., *Novel cases of Tunisian patients with mutations in the gene encoding 17β-hydroxysteroid dehydrogenase type 3 and a founder effect*. J Steroid Biochem Mol Biol, 2017. 165(Pt A): p. 86-94.
398. Mazen, I., et al., *Screening of genital anomalies in newborns and infants in two egyptian governorates*. Horm Res Paediatr, 2010. 73(6): p. 438-42.
399. Hassan, H.A., et al., *A novel nonsense mutation in exon 1 of HSD17B3 gene in an Egyptian 46,XY adult female presenting with primary amenorrhea*. Sex Dev, 2013. 7(6): p. 277-81.
400. de Vries, A.L.C., T.A.H. Doreleijers, and P.T. Cohen-Kettenis, *Disorders of sex development and gender identity outcome in adolescence and adulthood: understanding gender identity development and its clinical implications*. Pediatric endocrinology reviews : PER, 2007. 4(4): p. 343-351.
401. Hamamy, H., *Consanguineous marriages : Preconception consultation in primary health care settings*. J Community Genet, 2012. 3(3): p. 185-92.
402. Bittles, A., *Consanguinity and its relevance to clinical genetics*. Clinical Genetics, 2001. 60(2): p. 89-98.
403. Sircili, M.H., et al., *Anatomical and functional outcomes of feminizing genitoplasty for ambiguous genitalia in patients with virilizing congenital adrenal hyperplasia*. Clinics (Sao Paulo), 2006. 61(3): p. 209-14.
404. Dénes, F.T., et al., *The laparoscopic management of intersex patients: the preferred approach*. BJU Int, 2005. 95(6): p. 863-7.
405. Costa, E.M., et al., *Management of ambiguous genitalia in pseudohermaphrodites: new perspectives on vaginal dilation*. Fertil Steril, 1997. 67(2): p. 229-32.
406. Migeon, C.J., et al., *Ambiguous genitalia with perineoscrotal hypospadias in 46,XY individuals: long-term medical, surgical, and psychosexual outcome*. Pediatrics, 2002. 110(3): p. e31.
407. Nihoul-Fékété, C., et al., *Long-term surgical results and patient satisfaction with male pseudohermaphroditism or true hermaphroditism: a cohort of 63 patients*. J Urol, 2006. 175(5): p. 1878-84.